Epigenetic Characterisation of Chronic Lymphocytic Leukaemia with Frequently Altered DNA Damage Response Genes



UNIVERSITY OF BIRMINGHAM

Sael Musallam Alatawi

MSc, SUNY Upstate Medical University, USA
BSc, University of Tabuk, KSA

A thesis submitted to the
University of Birmingham for the degree of
Doctor of Philosophy

Institute of Cancer and Genomic Sciences
College of Medical and Dental Sciences
University of Birmingham
March 2022

UNIVERSITY OF
BIRMINGHAM

University of Birmingham Research Archive

e-theses repository

This unpublished thesis/dissertation is copyright of the author and/or third parties. The intellectual property rights of the author or third parties in respect of this work are as defined by The Copyright Designs and Patents Act 1988 or as modified by any successor legislation.

Any use made of information contained in this thesis/dissertation must be in accordance with that legislation and must be properly acknowledged. Further distribution or reproduction in any format is prohibited without the permission of the copyright holder.

لوالدي العزيز

To dear dad

1940-2000

ABSTRACT

Chronic lymphocytic leukaemia (CLL) is a neoplasm of mature B cells and it is considered the most common type of leukaemia in the western world. CLL is an extremely heterogeneous disease in which patients show a diverse clinical course driven among other factors by driver mutations. The most common CLL cytogenetic aberration are deletions in the 13q14 and 11q22.3 which are associated with early and later events during disease progression, respectively. Interestingly, these cytogenetic alterations affect genes encoding for DNA damage response proteins members. *RNASEH2B* gene resides in 13q14 region and it is a member of RNase H2 complex involved in Ribonucleotide excision repair (RER). *ATM* on the other hand is located to 11q22.3 regions and it is an essential kinase in the DNA double-strand break (DSB). While the consequences of ATM and RNASEH2B dysfunction on DNA repair in cancer cells are reasonably well understood, their impact on the epigenetic landscape remains to be elucidated.

The frequent alterations in these DDR genes suggests that CLL cells use cellular addictions in form of alternative pathways and mechanisms to maintain their survival. Thus, identifying different levels of these cellular addictions is the first step towards the design of personalized, targeted therapy.

Here, I generated chromatin accessibility, histone modifications and variants, and gene expression profiles using genome-wide methodologies on CLL cell lines that harbour defects in *RNASEH2B* and *ATM*. CLL cells harboring defects in *ATM* showed a unique pattern of chromatin accessibility, which was correlated with changes in gene expression. Global histone modification changes were observed and the epigenetic regulator KDM5B, a histone demethylase, were found to be upregulated in *ATM*-defective cells demonstrating a potential vulnerability that can be targeted therapeutically. On the other hand, *RNASEH2B*- defective CLL cells showed a unique transcriptional program associated with increased DNA-RNA hybrid levels. The results suggest that, RUNX Transcription Factors (TF) were required to maintain

the proliferation of RNASEH2B defective cells and this was confirmed by CRISPR KO screen. Together, these results provide novel insights into the mechanisms underlying CLL cells survival and pave the way for therapeutic agents targeting tumours cells harbouring mutations in *ATM* and *RNASEH2B* genes.

ACKNOWLEDGEMENTS

I would like to thank my lead supervisor, Prof. Tatjana Stankovic and co-supervisor Prof. Constanze Bonifer for their assistance and supervision at every element of my research since the beginning of my doctoral research. I thank them for their valuable feedback and suggestions; that really meant a lot to me. Thanks for giving me a chance to conduct scientific research in such an outstanding research environment.

I would give enormous thanks also to Dr. Ceri Oldreive, Dr. Angelo Agathanggelou, Dr. Nicholas Davies, Dr. Sophie Kellaway, Edward Smith, Jordan Wilson, and Ann-Marie Hewitt for sharing their outstanding scientific expertise, thank you all for the wonderful experience I encountered with you.

I want to express my appreciation to Dr. Peter Keane for inspiring me to learn bioinformatics. Peter helped me to understand genomic data science and then apply this knowledge on my own data. Peter was truly a generous teacher. Without Peter help, I would not expect to do a bioinformatic analysis on my data for my PhD dissertation. Thank you, Peter.

I would like to thank my sponsor, the University of Tabuk, Saudi Arabia, for offering me such an opportunity to pursue my graduate studies in the USA previously and the UK currently. Many thanks to the Saudi Cultural Bureau and Saudi Embassy in London for their guidance during studying in the UK. I thank Ministry of Education in Saudi Arabia for their support during the COVID19 global pandemic.

I would like to thank my teachers at Uqba ibn Nafi elementary school in Tabuk, KSA who worked hard to teach the essential elements of practical science despite limitations at that time. I thank you for telling amazing stories that led to scientific discoveries, which motivated me to continue my graduate studies and do scientific research. I also would thank my teacher Dr. Margaret Maimone who helped me during my Master graduate study in the USA to acquire and build new learning skills and to maintain an active learning approach.

I would also like to thank my dear friends Bassam Zaki, Mohammed Alshaker, and Yasser Alhejji who have offered constant help and inspiration not only during my PhD but also during the English language course and graduate studies.

I thank my family, including my mother Fatma, sisters, and brothers, for their encouragement and support to continue graduate studies abroad. Finally, my deepest and heartfelt thanks is to my dear wife Asma for her love and support to pursue my PhD as well as my little angels Lama and Khalid who supplied me with the energy and power to continue my graduate research.

TABLE OF CONTENTS

Contents

Chapter 1: Introduction 21

1.1 Chronic lymphocytic leukaemia nature and background 22

1.1.1 Clinical manifestations of CLL **23**

1.1.2 Clinical stages in CLL **23**

1.1.3 CLL development, progression and evolution **24**

1.1.4 CLL clinical and biological prognostic factors **26**

1.1.4.1 Epidemiology 26

1.1.4.2 Family history 27

1.1.4.3 Biological factors 27

1.1.4.4 CLL treatment options **30**

1.1.4.5 Genomic aberrations in CLL **35**

1.2 11q deletion and *ATM* **38**

1.2.1 ATM is a major component of DNA damage response 39

1.2.2 ATM Protein structure and function 39

1.2.3 ATM protein role in DNA double-strand break signalling 41

1.2.4 ATM involvement in remodelling the chromatin landscape 44

1.3 13q14 deletion and *RNASEH2B* **47**

1.3.1 RNASEH2B is a member of RNase H2 enzymatic complex 48

1.3.2 RNase H2 enzymatic complex structure 48

1.3.3 The functional role of RNase H2 complex 49

1.3.4 Defective ribonucleotide excision repair activates cGAS-STING pathway 51

1.3.5 Unrepaired rNMPs' influence on chromatin 52

1.4 Chromatin architecture **53**

1.4.1 Chromatin 53

1.4.2 Nucleosomes 54

1.4.3 Histone Variants and exchange 55

1.4.4 Histone post-translational modifications (PTMs) 56

1.4.5 Chromatin conformation 62

1.4.6 Transcription Regulation in Eukaryotic 64

1.4.6.1 Cis-regulatory elements (CREs) 64

1.4.6.2 Trans-regulatory elements (TREs) 67
1.4.6.2.2 Transcription Regulation by Long non-coding RNAs (lncRNAs) 68
1.4.6.2.3 Transcriptional Initiation 69
1.4.6.2.4 Transcriptional Elongation 70
1.4.6.2.5 Transcriptional Termination 72
1.4.7 DNA methylation **73**
1.5 Cross-talk between DNA damage response genes and epigenetic regulation **76**
1.5.1 Defective DNA damage response establishes a dependency on the remaining functional pathways 76
1.6 Specific aims and objectives **81**
Chapter 2: METHODS **84**
Cell line culture 90
CLL cell lines 90
Western blotting 91
Treatment of CLL cells with proteasome inhibitor 92
RNA-seq 93
Assay for transposase-accessible chromatin using sequencing (ATAC-seq) 94
Chromatin immunoprecipitation (ChIP) 96
DNA/RNA immunoprecipitation (DRIP) 97
NGS library preparation 99
Lentiviral transduction of ATM-defective MEC1 CLL cells 100
Genome-scale CRISPR screening 100
Bioinformatic analysis 101
Statistical Analysis 109
Chapter 3: Chromatin Landscape in ATM-deficient CLL cells 112
3.2 ATM loss is correlated with global gene expression deregulation in CLL cells **113**
3.3 ATM loss in CLL cells is correlated with the upregulation of pro-inflammatory genes **118**
3.4 Characterisation of histone post-translational changes in correlation with ATM loss **127**
3.5 Characterisation of chromatin cis-regulatory elements alterations in accordance with ATM loss status **133**
3.6 Integration analysis of ATAC-seq, ChIP-seq and RNA-seq data demonstrate the chromatin landscape changes in correlation with ATM loss **141**
3.7 The upregulation of KDM5B gene expression is correlated with ATM loss in CLL cells **146**
3.8 Genome-wide KDM5B localization in ATM-defective MEC1 CLL cells **148**

3.9 Generation of Dox-inducible KDM5B shRNA KD CLL cells derived from MEC1 ATM-defective cells 155

3.10 Discussion..... 157

Chapter 4: Chromatin landscape of RNASEH2B-deficient CLL cells 164

4.2 RNASEH2B loss is correlated with a global gene expression deregulation 165

4.2.1 Activated pro-inflammatory response transcriptional signatures are in correlation with RNASEH2B loss..... 167

4.3 RNASEH2B loss is correlated with increased RNA–DNA hybrid formation (R-loops)..... 177

4.4 Characterisation of histone post-translational modifications, histone variant H2AZ and Pol II changes correlated with RNASEH2B biallelic and monoallelic loss..... 180

4.4.2 RNASEH2B loss is correlated with genome-wide H3K4me3 deregulation 182

4.4.3 Genome-wide H3K27ac histone marks are increased in correlation with RNASEH2B KO cells183

4.4.4 RNASEH2B KO cells are correlated with upregulation of the histone variants H2A.Z..... 184

4.4.5 The H3K4me3 epigenetic mark is associated with a reduction at genes involved in RNA biology in correlation with RNASEH2B KO cells..... 187

4.5 Characterisation of the chromatin accessibility changes correlated with RNASEH2B monoallelic and biallelic loss 189

4.5.2 Observation of increased accessibility for RUNX, AP-1, and IRF motifs in correlation with RNASEH2B defective CLL cells 192

4.5.3 RUNX, AP1 and IRF co-localization is correlated with monoallelic and biallelic RNASEH2B loss 193

4.6 Integration analysis of ATAC-seq, ChIP-seq and RNA-seq data show cis-regulatory elements correlated with RNASEH2B monoallelic and biallelic loss 196

4.6.1 Integration analysis shows common chromatin alteration changes in correlation with biallelic and monoallelic RNASEH2B loss in CLL cells..... 196

4.6.2 Identification of transcription factor network correlated with monoallelic and biallelic RNASEH2B loss in CLL cells..... 199

4.7 Genome-wide CRISPR screening identified synthetic lethal interactions correlated with monoallelic and biallelic RNASEH2B loss 202

4.7.1 CRISPR screen identified APEX2 as a synthetic lethal gene correlated with RNASEH2B biallelic KO cells..... 209

4.7.2 CRISPR screen identified a set of synthetic lethal genes involved in inflammatory response, RNA biology, and transcription coactivators that are correlated with RNASEH2B loss..... 209

4.7.3 *RUNX3* is identified as a synthetic lethal gene in correlation with RNASEH2B KO cells..... 210

4.7.4 RUNX binding sites are associated with synthetic lethal gene hits in correlation with both RNASEH2B KO cells..... 212

4.8 Discussion 214

Chapter 5: Overall Discussion and Conclusions 225

5.1 ATM defective CLL cells are correlated with KDM5B upregulation and deregulated gene expression related pro-inflammatory pathways **225**

5.2 RNASEH2B deficient CLL cells were correlated with a reliance on the transcription factor RUNX3 ..... **227**

5.4 Project limitations **229**

5.5 Future work **231**

Appendix 233

CRISPR Screen Final Gene Hits List **233**

List of Differentially Expressed Genes **235**

References 360

LIST OF FIGURES

Figure 1.1 CLL disease development and heterogeneity

Figure 1.2 B cell receptor signalling in CLL

Figure 1.3 Mutational landscape of CLL

Figure 1.4 ATM protein structure

Figure 1.5 Activation of ATM leads to various effects on cellular processes

Figure 1.6 Protein structure of RNAase H2 enzymatic complex

Figure 1.7 RNase H2 activates RER upon recognition of ribonucleotides

Figure 1.8 Defective RER activates cGAS-STING pathway

Figure 1.9 Nucleosome components and structure

Figure 1.10 Histone modification occupancies with respect to active enhancers and genes

Figure 1.11 Histone modifications alter chromatin accessibilities

Figure 1.12 Eukaryotic chromatin organization

Figure 1.13 Eukaryotic transcription steps

Figure 1.14 DNA methylation patterns are correlated with overall CLL clinical subgroups

Figure 1.15 The concept of synthetic lethality in cancer

Figure 1.16 DNA methylation patterns are correlated with overall CLL clinical subgroups

Figure 2.1 Overall QC of RNA-seq libraries

Figure 2.2 ATAC-seq libraries QC before sequencing

Figure 2.3 qPCR validation of DRIP libraries

Figure 2.4 RNA-seq libraries' read depth

Figure 2.5 Chip-seq libraries' read depths

Figure 2.6 A model that describes the strategy used for the integration of three data sets

Figure 3.1 Western blots confirmed the absence of ATM protein expression in CLL cell lines

Figure 3.2 Linear regression analysis shows a positive correlation between RNA-seq replicates

Figure 3.3 Correlation clustering of gene expression profiles of ATM-deficient isogeneic CLL cells

Figure 3.4 Validation of RNA-seq data by measuring the expression of selected genes by qPCR

Figure 3.5 Differentially expressed genes in accordance with ATM loss status in CLL cells

Figure 3.6 Gene Ontology analysis on differentially expressed up-and down-regulated genes in correlation with ATM loss in CLL cells

Figure 3.7 Gene set enrichment analysis (GSEA) of differentially expressed genes correlated with ATM defective status in CLL cells

Figure 3.8 Common differentially expressed genes in correlation with ATM loss status and their role biological role

Figure 3.9 Heatmap of supervised clustering reveals a common gene expression profile in correlation with ATM loss in CLL cells

Figure 3.10 Chromatin immunoprecipitation data suggest a genome-wide alterations in histone PTM in correlation with ATM loss

Figure 3.11 Analysis of genomic regions associated with the observed changes in H3K4me3 epigenetic mark in correlation with ATM loss

Figure 3.12 Genome-wide changes in the chromatin accessibility landscape of distal regulatory elements are in correlation with ATM loss status in CLL cells

Figure 3.13 Validation of the defined sets of gained and lost chromatin accessible sites in correlation with ATM loss status

Figure 3.14 Sites that were lost in accordance with ATM status showed a decrease in H3K27ac levels

Figure 3.15 Motif enrichment analysis at gained and lost sites associated with ATM loss status (distal peaks only, MEC1 cells only)

Figure 3.16 ATM-defective CLL cells transcriptional landscape is correlated mainly with the transcription factors AP-1 and RUNX

Figure 3.17 Several members of AP-1 transcription factor family showed a differential gene expression pattern in line with ATM loss status in CLL cells

Figure 3.18 Integrative analysis of chromatin accessibility, gene expression, histone modifications and motif enrichment alterations in correlation with ATM loss in CLL cells

Figure 3.19 Identification of transcription factor networks driving gene expression in accordance with ATM loss status

Figure 3.20 Protein structure and function of KDM5B

Figure 3.21 KDM5B is up-regulated in CLL cells in correlation with ATM loss status

Figure 3.22 Analysis of KDM5B chromatin immunoprecipitation (ATM KD MEC1 cells)

Figure 3.23 The gene expression of genes identified as being associated with KDM5B peaks (ATM KD MEC1 cells)

Figure 3.24 Motif analysis of KDM5B significant summit peaks (ATM KD MEC1 cells)

Figure 3.25 Generation of Dox-inducible KDM5B shRNA KD CLL cells derived from MEC1 ATM-defective cells

Figure 3.26 A proposed model for the role of KDM5B in ATM defective CLL cells

Figure 4.1 Protein structure of RNAase H2 enzymatic complex

Figure 4.2 Western blots confirming RNASEH2B KO status in MEC1 cell line

Figure 4.3 Positive correlation between RNA-seq replicates samples were observed as suggested by linear regression analysis

Figure 4.4 Correlation clustering of gene expression profiles of RNASEH2B KO isogeneic cells

Figure 4.5 Differentially expressed genes in accordance with RNASEH2B monoallelic and biallelic loss status in CLL cells

Figure 4.6 Gene set enrichment analysis (GSEA) of differentially expressed genes correlated with RNASEH2B loss

Figure 4.7 Gene Ontology analysis on differentially expressed up-and down-regulated genes in correlation with RNASEH2B loss in CLL cells

Figure 4.8 Common differentially expressed genes in correlation with RNASEH2B loss and their role biological role

Figure 4.9 Heatmap of supervised clustering reveals common gene expression profile in correlation with RNASEH2B monoallelic and biallelic loss

Figure 4.10 RNASEH2B loss is correlated with increased RNA–DNA hybrid formation (R-loops).

Figure 4.11 Chromatin immunoprecipitation data suggest genome-wide alterations in histone PTM, histone variant, and Pol II in correlation with RNASEH2B loss

Figure 4.12 Analysis of associated with histone modifications, Pol II and histone variant H2AZ in correlation with RNASEH2B KO cells

Figure 4.13 Genomic annotations of H3K4m3 condition-specific peaks

Figure 4.14 Genome-wide changes in the chromatin accessibility landscape of distal regulatory elements are correlated with RNASEH2B status in CLL cells

Figure 4.15 Validation of the defined sets of gained and lost chromatin accessible sites in correlation with RNASEh2B loss status

Figure 4.16 Transcriptional landscape in RNASEH2B KO CLL cells is correlated with the increased activity transcription factors RUNX and AP-1

Figure 4.17 Integrative analysis of chromatin accessibility, gene expression, chromatin-bound proteins and motif enrichment correlated with RNASEH2B loss

Figure 4.18 The transcription factor networks driving gene expression in accordance with RNASEH2B loss status

Figure 4.19 The experimental design of genome-scale CRISPR screening

Figure 4.20 Quality control of CRISPR screen libraries

Figure 4.21 The applied workflow for analyzing CRISPR screening data

Figure 4.22 Examples of linear regression models for each time point comparison (Mono-KO vs WT cells)

Figure 4.23 Overlap analysis of CRISPR screen hits resulting from two algorithms used (BAGEL and JACKS)

Figure 4.24 RUNX3 is classified as synthetic lethal in correlation with RNASEH2B monoallelic and biallelic loss in CLL cells

Figure 4.25 The expression profile of genes identified as synthetic lethal and correlated with the presence of RUNX motifs

Figure 4.26 *USP18* locus shows enrichment for H3K4me3 and H3K27ac in correlation with RNASEH2B KO cells

Figure 4.27 A provisional model for the role of RUNX3 in RNASEH2B defective CLL cells

LIST OF TABLES

Table 1.1 A summary of major histone post translational modifications (mammalian)

Table 2.1 Instruments

Table 2.2 Reagents and suppliers

Table 2.3 Oligonucleotides

Table 2.4 Antibodies

Table 2.5 Buffer compositions

Table 2.6 Specialist software used for bioinformatics analysis

Table 2.7 qPCR thermal cycling conditions

Table 2.7 DRIP digestion reaction

Table 4.1 Motif enrichment analysis at gained and lost correlated with RNASEh2B monoallelic and biallelic loss (distal peaks only)

LIST OF ABBREVIATIONS

53BP1	p53-binding protein 1
AGS	Aicardi–Goutières syndrome
AP-1	Activator protein 1
ATAC-seq	Assay for transposase-accessible chromatin using sequencing
ATM	Ataxia Telangiectasia Mutated
ATR	Ataxia Telangiectasia And Rad3-Related Protein
BAFF	B cell activator factor
Bcl-2	B-cell lymphoma-2
BCR	B-cell receptor
BER	Base Excision Repair
BRCA1	breast cancer type 1
BS	Bloom's syndrome
BTK	Bruton tyrosine kinase
CAN	Copy number aberrations
CART	Chimeric antigen receptor T-cell
CD	cluster of differentiation
CDK1	Cyclin Dependent Kinase 1
cGAS	cyclic GMP-AMP synthase
CGI	CpG island
ChIP-seq	Chromatin immunoprecipitation, followed by next-generation sequencing
CHK1	Checkpoint Kinase 1
CHK2	Checkpoint Kinase 2
CLL	Chronic lymphocytic leukaemia
CNV	Copy number variation
CPD	Cyclobutane Pyrimidine Dimers
CPSF	cleavage and polyadenylation specific factor
CREs	Cis-regulatory elements
CRISPR	Clustered regularly interspaced short palindromic repeats
CRP	C-reaction protein
CstF	cleavage stimulation factor
DDR	DNA Damage Response
DNMT	DNA methyltransferase
DRIP-seq	DNA/RNA immunoprecipitation (DRIP), followed by next-generation sequencing
DSBs	Double Strande Breaks
FA	Fanconi anaemia
FACT	FAcilitates Chromatin Transcription
FATC	Fat-C-terminal domain
FISH	Fluorescence in situ hybridization

GTFs	general transcription factors
GWAS	Genome-wide association studies
HAT	histone acetyltransferases
HDAC	Histone deacetylase
HEAT	Huntington, Elongation factor 3, A subunit of protein phosphatase 2A, TOR1
HNPCC	Hereditary Nonpolyposis Colorectal Cancer
HOTAIR	HOX transcript antisense RNA
HR	Homologous Recombinational Repair
IGHV	Immunoglobulin heavy chain variable
IR	Ionizing Radiation
KDM5B	Lysine Demethylase 5B
LCR	locus control region
LDH	Lactic dehydrogenase
LDT	lymphocyte doubling time
LFS	Li–Fraumeni syndrome
lncRNAs	Long non-coding RNAs
LPL	lipoprotein lipase
mAbs	monoclonal antibodies
MAPK	mitogen-activated protein kinase
MBL	Monoclonal B-cell lymphocytosis
MLPA	Multiplex ligation-dependent probe amplification
MMR	Mismatch Repair
MRD	Minimal residual disease
MSI	Microsatellite Instability
ncRNAs	non-coding RNAs
NDR	nucleosome-depleted region
NER	Nucleotide Excision Repair
NGS	Next-generation sequencing
NHEJ	Non-Homologous End Joining
OS	Overall survival
PARP	Poly(ADP-ribose) polymerase
PFS	Progression-free survival
PI3Ks	Phosphatidylinositol 3-kinase
PIC	protein initiating complex
PTM	post-translational modifications
RER	Ribonucleotide excision repair
rNMPs	Ribonucleotide monophosphates
ROS	Reactive Oxygen Species
SAM	S-adenosyl-L-methionine
SSBs	Single Strande Breaks
STING	stimulator of interferon genes
STR	Short tandem repeat
SYK	Spleen tyrosine kinase

TADs	topologically associated domains
TET	ten-eleven translocation
TFI	Treatment-free interval
TFs	Transcription factors
TK	Thymidine kinase
TLS	Translesion DNA Synthesis
TOPI	Topoisomerase I
TREs	Trans-regulatory elements
TRRAP	transactivation-transformation domain-associated protein
TSS	transcription start site
TTFT	Time to first treatment
TTS	transcription termination site
UV	Ultra-Violet
WES	Whole exome sequencing
WGS	Whole genome sequencing
WSTF	Williams syndrome transcription factor
ZAP-70	Zeta-chain-associated protein kinase-70
β2M	Beta2-microglobulin

CHAPTER 1

INTRODUCTION

Chapter 1: Introduction

Genomic DNA is under constant assault from various stressors that cause DNA lesions and trigger the DNA damage response (DDR), a complex network of events in which essential proteins and enzymes are recruited for sensing and repairing DNA damage. The activation of DDR encompasses machineries mediating DNA damage repair, cell cycle checkpoint regulation, replication stress, and programmed cell death (apoptosis). For example, the occurrence of DNA lesion induces checkpoint to cause cell cycle arrest to allow for more time necessary for DNA repair prior to cell division. Consequently, failure to resolve DNA damage activates apoptotic machinery to remove cells with unrepaired DNA damage. Collectively, these examples highlight the importance of DDR in maintaining genomic stability, cell viability, and early oncogenic events prevention. Therefore, DDR pathways permit the survival of cells in the presence DNA damage or coordinate cells to programmed cell death (Roos et al., 2016).

Cancer cells are characterised by the presence of genomic instability resulting from defects in DDR and/or a high level of replication stress. Mutations in DDR genes promote the growth of cancer cells through the acquisition of driver mutations that contribute to evasion of apoptosis (Tubbs and Nussenzweig, 2017). Nonetheless, alterations in DDR genes can increase the demand on other alternative DDR pathways to maintain cell viability. This situation creates vulnerabilities associated with specific mutation that consequently can be exploited for therapeutic purposes as DDR pathways balance cell survival versus cell death.

Chronic lymphocytic leukaemia (CLL) is known to have diverse genetic mutation burden diversification throughout the disease course (Landau et al., 2015). Interestingly, the most frequent alterations observed in CLL are associated with genes involved in DDR. The 13q14 deletion containing *RNASEH2B* gene and 11q deletion encompassing the *ATM* gene. *RNASEH2B* is involved in ribonucleotide excision repair pathway (RER) whereas *ATM* is involved in double-strand break repair pathway (DSB). It is known that genetic and

epigenetic alterations cooperate to form the evolutionary landscape of cancer and CLL is no exception (Flavahan et al., 2017, Beekman et al., 2018). Moreover, DNA repair components rely on extensive chromatin modifications carried out by epigenetic regulators to allow repair of DNA damage (Karakaidos et al., 2020) highlighting the important role of the epigenome to assess DDR machinery. Therefore, finding epigenetic vulnerabilities that are linked with mutations in *RNASEH2B* and *ATM* would reveal an additional layer of epigenetic dependency that can aid in the development of novel epigenetic treatments. Taken together, CLL is a highly informative model for the investigation of DDR mutation-specific vulnerabilities and this context will help uncover new insights into mechanistic interplays between epigenetic regulation and DNA repair.

1.1 Chronic lymphocytic leukaemia nature and background

Chronic lymphocytic leukaemia (CLL) is the most frequent form of leukaemia in the western world and is characterised by a clonal proliferation of mature B lymphocytes (Chiorazzi et al., 2021, Chiorazzi et al., 2005, Fabbri and Dalla-Favera, 2016). Moreover, there are approximately 3800 new CLL cases each year, according to Cancer Research UK. In addition, in Saudi Arabia among elderly patients, the highest percentage of newly diagnosed leukaemia was CLL (32.5%) (Bawazir et al., 2019). CLL is caused by the clonal expansion of mature B-lymphocytes triggered by factors not clearly known, similar to many other haematological malignancies. Several published reports have revealed the familial risk of CLL, highlighting the genetic inheritance predisposition role in disease pathogenesis (Slager and Kay, 2009, Berndt et al., 2016, Goldin et al., 2004). Circulatory CLL tumours cells show a distinctive pattern of cytoplasmic and cell surface markers, which help differentiate them from other B lymphocytes. CLL cells express the CD5, CD19, CD20, CD23 surface antigens and residual surface immunoglobulin, CD20 and CD79b, and each leukemic clone cell is restricted to immunoglobulin light chains—either Κ or λ (Hallek et al., 2018).

The overgrowth of CLL cells results in a clinical heterogeneity among patients. Some patients do not need treatment, and typically the diagnosis is incidental, whereas some patients do require immediate treatment and may die within 2–3 years of diagnosis. Moreover, variability in disease progression and development is observed in CLL along with variabilities in the responsiveness to therapeutic agents. The observed clinical variability in CLL patients is possibly due to genetic and epigenetic alterations (intrinsic constituents) and surrounding microenvironment interactions (extrinsic constituents) (Chiorazzi et al., 2021). The surrounding microenvironment fosters CLL cells survival by either interacting with cells in proximity or by the consumption of cytokines or chemokines secreted by neighbouring cells.

1.1.1 Clinical manifestations of CLL

The diagnosis of CLL is typically accidental in routine blood tests where peripheral lymphocytosis is detected because many CLL patients are asymptomatic. However, patients with symptoms will, on average, show a history of recurrent infections, general fatigue, night sweats and, in some cases, unintentional weight loss. Moreover, the enlargement of lymph nodes may be noted at the time of diagnosis. The presence of anaemia and thrombocytopenia symptoms in CLL patients suggests bone marrow infiltration by CLL tumour cells and correlates with a progressive form of disease. Splenomegaly is rarely detected at diagnostic stage and is associated with advanced disease (Hallek et al., 2018).

1.1.2 Clinical stages in CLL

The CLL clinical spectrum can be subclassified using widely accepted staging systems (Binet et al., 1981) and (Gale and Rai, 1987). Both systems rely on standard physical and laboratory assessments, and both

categorize CLL patients into 3 major subgroups with unique clinical outcomes. The revised Rai system describes mild-risk groups as patients with lymphocytosis with leukaemia cells in the blood and/or bone marrow. The middle-risk group comprises patients with marked lymphocytosis, enlarged lymph nodes, and splenomegaly and/or hepatomegaly. The high-risk group involves those patients with disease-related anaemia (haemoglobin level < 1 g/dL) or thrombocytopenia (platelet count < 100 x 10^9/L). The Binet system relies on assessing the involvement of lymphoid organs as well as whether thrombocytopenia or anaemia is present. Stage A is when haemoglobin level ≥ 10 g/dl and platelets ≥ 100x10^9/L and involvement of up to 2 lymphoid areas. Stage B is marked if haemoglobin level ≥ 10 g/dl and platelets ≥ 100x10^9/L and involvement of 3 or more lymphoid areas, and stage C is reported when haemoglobin level < 10 g/dl and platelets < 100x10^9/L (Hallek et al., 2018).

1.1.3 CLL development, progression and evolution

The overall clinical course of CLL is remarkably variable , in which some patients do not require treatment for their disease, and others do need multiple treatment regimes, suggesting an active progressive disease. CLL usually is preceded by a state known as high-count MBL where a clonal B-cell population is present in the peripheral blood fewer than 5x10^9 cells/L. High-count MBL patients known to carry mutations in *SF3B1, DDX3X, BIRC3*, and *ATM.* However, *NOTCH1*, *TP53*, and *XPO1* mutations are more commonly observed in CLL (Barrio et al., 2017, Winkelmann et al., 2015). Upon CLL diagnosis, the dynamic proliferation of tumour cells is remarkably heterogenous and can be classified into three clinical phases: spontaneous regression, logistic growth, and exponential growth. Each clinical phase is characterised according to lymphocyte doubling time, IGHV status, and driver mutations (Gruber et al., 2019). The transformation of CLL into diffuse large B-cell lymphoma (DLBCL) occur in more than 90% of CLL patients (Al-Sawaf et al., 2021). This transformation known as (Richter transformation) is characterised by the

presence of specific stereotyped subset 8 (IGHV4-39), *TP53* and *NOTCH1* mutations, *MYC* translocation and *CDKN2A* deletion (Rossi et al., 2018) (Figure 1.1).

As is the case in other tumours, CLL progression begins with the occurrence of diverse clones of tumour cells with underlying genetic alterations promoting uncontrolled proliferation and survival and, in many cases, treatment resistance. These events facilitate the imbalance between cell survival and apoptosis, leading to an increased burden of leukemic cells (Chiorazzi, 2007). These mutational events can be developed spontaneously or generated as biological processes found in normal cells or exclusive to tumour cells and/or external factors. The AID enzymes found in normal B lymphocytes take part in the adaptive immune response by creating mutations in the variable domain of Abs/IGs (IGHV, IGHD, IGHJ, IGLV, IGLJ). In CLL, however, AID enzymes can be hyperactive and behave aberrantly by inducing mutation and double-strand breaks out of the IG loci (Oppezzo et al., 2003, Yamane et al., 2011). In addition, as it is a characteristic feature of cancer cells, CLL cells are known to have increased levels of reactive oxygen species, which are reported to have a part in mutagenesis (Zhou et al., 2003, Nogueira and Hay, 2013). In addition, chemotherapy can contribute to changes in tumour mutational burden, in which new mutations could be generated and, thus, adding more fitness to tumour clones, which leads to expansion of tumour cells and consequently leading to drug resistance (Tan et al., 2015, Li et al., 2020a).

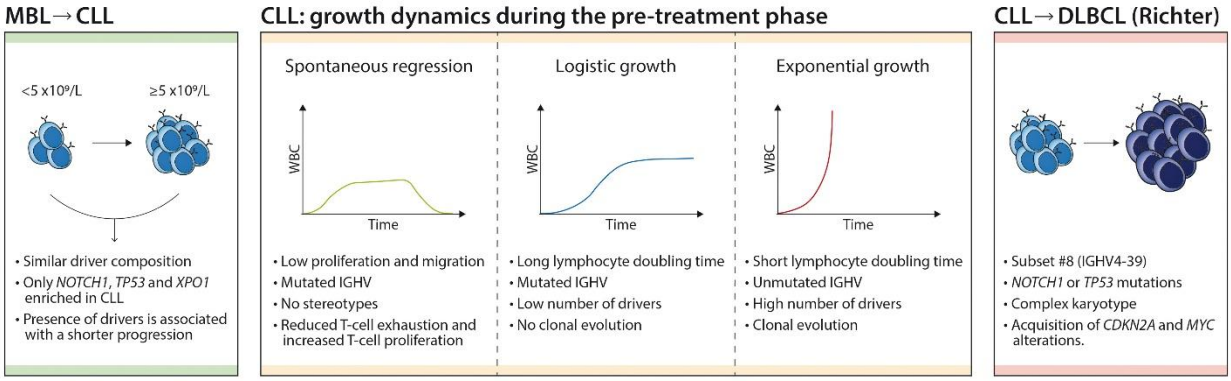


Figure 1.1 CLL disease development and heterogeneity
The development from monoclonal B-cell lymphocytosis MBL in (green) leads to different CLL disease course trajectories (orange). The acquisition of driver mutations associated with adverse prognosis is linked with advanced disease and Richter transformation to diffuse large B-cell lymphoma (DLBCL). Adapted from Delgado, Julio, et al. (2020).

Recurrent mutations in CLL identified by FISH and next-generation sequencing (NGS) have been utilized to construct a clonal evolution model for CLL disease (Landau et al., 2013, Nadeu et al., 2018). Therefore, the acquisition of genetic mutation variability, together with epigenetic heterogeneity, suggests a cooperative model that helps shape the evolutionary landscape of CLL progression (Flavahan et al., 2017, Gaiti et al., 2019). The sequential genetic and epigenetic alterations pave the way to further insights into the nature of disease progression and provide novel approaches for CLL treatment.

1.1.4 CLL clinical and biological prognostic factors

1.1.4.1 Epidemiology

Age, gender and race are factors that can predict the clinical prognosis and outcome of CLL patients. The highest groups of reported CLL cases are seen in the 65–74 age group of patients, and the median age at the diagnostic stage is 70 years. CLL is more frequent in males than females, with approximately a two-

fold increase in the former. The mechanisms that underlie the increased frequency of CLL in male patients are not fully understood. CLL incidences show variability among race/ethnicity (Chiorazzi et al., 2021).

1.1.4.2 Family history

Among other leukaemia, CLL has the highest occurrences of familial associations, with an eight-fold higher likelihood of developing disease seen in first-degree relatives (Goldin et al., 2004). This observation suggests a genetic inheritance link that is involved in disease predisposition. Genome-wide association studies (GWAS) have identified several genetic loci linked with familial CLL, and these loci are found in genes encoding for proteins that control human B-cell development and immune system signalling (Berndt et al., 2016, Law et al., 2017, Speedy et al., 2014). Familial CLL cases are correlated with an early disease onset and a likelihood of developing secondary malignancies when compared to sporadic cases of CLL (Ishibe et al., 2001). Moreover, the presence of monoclonal B-cell lymphocytosis (MBLs), a clonal B-cell expansion and precursor state of CLL, in relatives of CLL patients is associated with a four-fold increased prevalence in the general population, indicating a potential predisposition to this malignancy (Strati and Shanafelt, 2015, de Tute et al., 2006).

1.1.4.3 Biological factors

1.1.4.3.1 B-cell receptor signalling in CLL

The B-cell receptor (BCR) maintains survival and proliferation signals of mature B lymphocytes. BCR is a transmembrane protein located on the surface of B lymphocytes and comprises a complex of surface immunoglobulin (Ig) homodimer and the non-covalently bound heterodimer Igα/Igβ (CD79a/CD79b). Antibody production and cell proliferation are the main outcomes of BCR engagement in normal B lymphocytes. The BCR antigen ligation process initiates a series of kinase phosphorylate activation events,

such as spleen tyrosine kinase (SYK) and LYN. These phosphorylation events initiate activation processes, such as BTK and PI3K kinases (Longo et al., 2007), which subsequently activate other kinases including protein kinase C-β, mitogen-activated protein kinase ERK and mammalian target of rapamycin (Davids and Brown, 2012). These sequential activation events result in cell survival and proliferation via the activation of nuclear factor NF- κβ (Herishanu and Polliack, 2013) (Figure 1.2).

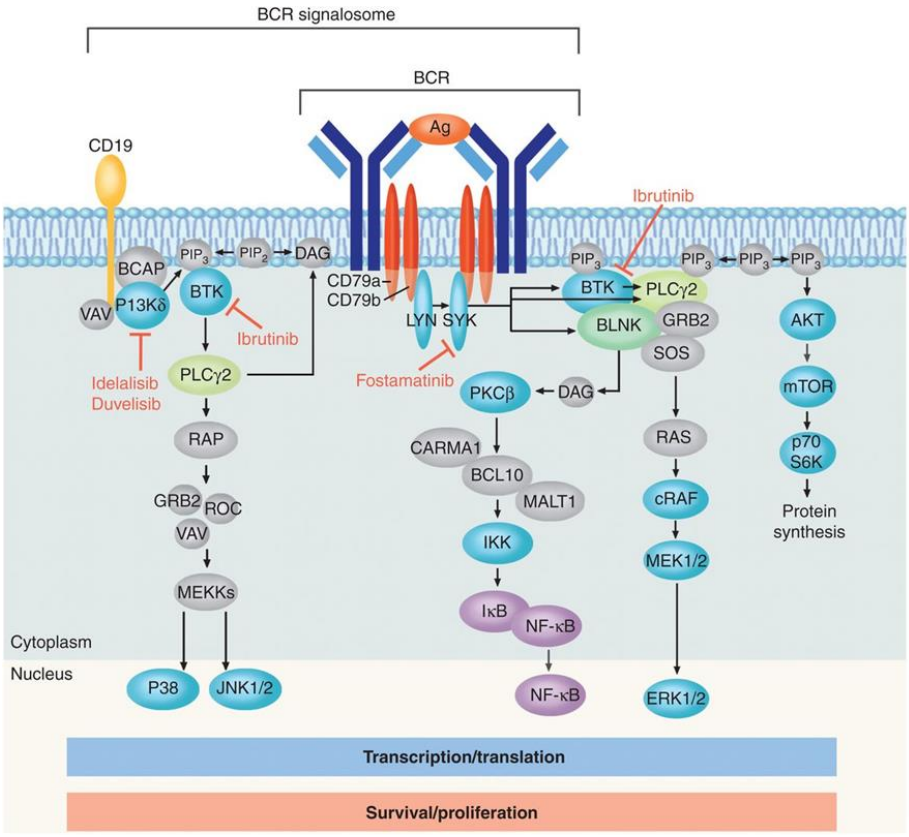


Figure 1.2 B cell receptor signalling in CLL
The engagement of IG member of BCR with an antigen leads to induction of a phosphorylation signalling cascade events initiated by phosphorylation of cytoplasmic tails of CD79a and CD79b. The outcome of these activation events is to maintain cell survival and proliferation. Targeted therapy is utilised to inhibit the activation of BCR signalling through kinase inhibitors (highlighted in red) SYK (fostamatinib), PI3Kδ (idelalisib), BTK (ibrutinib), and PI3Kδ+γ (duvelisib). Adapted from Chiorazzi, N., Chen, S. S., & Rai, K. R. (2021).

Mutations of genes coding for the immunoglobulin heavy chain variable region (IGHV), components of BCR, are well-established biomarkers in CLL prognosis (Damle et al., 1999). CLL patients were stratified according to the extent of similarity of genomic sequences of IGHV genes in tumour cells to that of their

closest germline counterpart. CLL patients demonstrating less than 98% homology to the *IGVH* gene germline in their tumour cells were categorized as having mutated *IGVH* genes (M-CLL) whereas CLL patients with at least 98% homology were categorized as having unmutated *IGVH* genes (U-CLL). In addition, there is a significant difference in terms of prognosis and disease severity between U-CLL and M-CLL groups (Hamblin et al., 1999). Moreover, it was described that CLL patients with unmutated IGHV (U-CLL) status were known to have inferior remission time and survival from the start of the treatment (Lin et al., 2009).

Furthermore, CLL patients show selective stereotypic usage of their IGVH genes, and this usage is associated with clinical prognosis. The use of VH1-69, VH3-21 is correlated with overall poor prognosis, whereas the usage of VH4-34 is linked with good prognosis (Ghia et al., 2005, Xochelli et al., 2017, Thorsélius et al., 2006). Moreover, a group of CLL patients (one-third) express stereotyped immunoglobulins (BcR IG) that can be allocated to unique subgroups with distinctive prognostic values, with subsets #1, #2 and #8 (poor outcome) and #4 (good outcome) (Jaramillo et al., 2020, Agathangelidis et al., 2012).

1.1.4.3.2 Flow cytometry and serum biomarkers

CLL flow-cytometric characterisation for immunophenotyping is essential for diagnosis and prognosis. CLL expresses a unique set of cluster of differentiation (CD) markers that help distinguish CLL cells from other leukaemia or lymphoma cells. CLL cells have the following immunophenotype demonstration: CD5, CD19, dim CD20, dim CD22, CD23, bright CD43, dim CD45, dim to null CD79b, dim CD81, CD200 and dim monoclonal cell surface immunoglobulin. Flow-cytometric assessments help in disease management and provide valuable prognostic information (Salem and Stetler-Stevenson, 2019). For example, the expression level of CD marker 38 (CD38), a cell surface glycoprotein of type II with NAD + glycohydrolase

and ADP-ribosyl cyclase enzymatic activities, has been found to add valuable clinical information in CLL in addition to its correlation with IGVH mutation status (Damle et al., 1999). Moreover, CD49d is another biomarker in CLL and is typically associated with an aggressive clinical course (Shanafelt et al., 2008). An additional CLL biomarker is ZAP-70, which is associated with an unfavourable clinical prognosis. The increased expression of ZAP-70 in CLL cells may have a role in enhancing their interactions and cross-talk within the tumour microenvironment and, thus, maintaining their survival (Chen et al., 2020).

In addition to flow cytometry biomarkers, standard serological tests are essential and routinely applied in the diagnosis and evaluation of CLL prognosis. Beta2-microglobulin (β2M) together with the enzymes thymidine kinase (TK) and lactic dehydrogenase (LDH) are frequently used as serum biomarkers in CLL and predict an inferior clinical disease course (Yun et al., 2020). Finally, the lymphocyte doubling time (LDT) is calculated by knowing the time (months) the absolute lymphocyte count takes to double. LDT reflects the accumulation rate and pace of neoplastic cells in CLL patients. The prognostic significance of LDT as an independent biomarker for disease progression and short survival has been confirmed in other independent and recent studies (Baumann et al., 2021, Molica and Alberti, 1987).

1.1.4.4 CLL treatment options

As mentioned previously, the subsequent disease course after initial diagnosis is remarkably variable. Some patients do not show any sign of symptoms (Rai low-risk, Binet A), whereas others do (Rai high-risk, Binet C), which prompts the initiation of a treatment regime. Generally, therapy for asymptomatic patients is not indicated, and they are monitored using a 'watch and wait' policy (Hallek et al., 2018). The landscape of therapeutic options for symptomatic CLL patients has been significantly changed in the last decade, with observed overall advancements in remission and survival rates (Burger and O'Brien, 2018). Treatment options in CLL target several biological aspects of the disease, including cytostatic agents,

monoclonal antibodies (mAbs), cell signalling, apoptosis, immune surveillance, CART cells, synthetic lethality, epigenetics and combinatory treatments.

Cytostatic drugs can inhibit tumour proliferation without direct toxicity by decreasing the birth rate of tumour cells (Anttila et al., 2019). Examples of this category include chlorambucil, fludarabine and bendamustine. mAb treatment is a type of targeted therapy in which mAbs target tumour cells overexpressing unique antigens and cause their death via blockade of survival signals (Zahavi and Weiner, 2020). Examples of this treatment type in CLL includes anti-CD20 antibodies including rituximab, ofatumumab, obinutuzumab and for anti-CD52 alemtuzumab. CLL treatments that target cell signalling work by inhibiting downstream kinases involved in the constitutive activation of B cell receptor signalling, which drives CLL pathogenesis (Muggen et al., 2016); examples include class I phosphatidylinositol 3-kinase (PI3Ks) PI3Kδ-isoform inhibitors (idelalisib), Bruton tyrosine kinase (BTK) inhibitors (ibrutinib) and irreversible BTK inhibitors (acalabrutinib).

CLL treatments that target apoptosis through the Bcl2 family, which consists of proapoptotic and prosurvival proteins. Tumour cells evade apoptosis by relying on prosurvival proteins of this family (Chao and Korsmeyer, 1998). An example of this type of treatment is venetoclax, which attaches to anti-apoptotic B-cell lymphoma-2 (Bcl-2) protein and prevents its functions, leading to programmed cell death induction.

T cells play an important role in immune active surveillance of tumour cells. T cells express the transmembrane programmed cell death 1 (PD-1) receptor, an immune checkpoint protein, which is involved in the negative regulation of tumour cell immune recognition. PD-1 primary ligands are PD-L1 (produced by tumour cells) and PD-L2 (produced by antigen-presenting cells) (Hamid et al., 2013). In the cancer context, tumour cells expressing PD-L1 interact with T-cells through ligation with the PD-1 receptor, and this process leads to T cell antitumor response inhibition. Pembrolizumab is a mAb used in

cancer immunotherapy in solid tumours and has been reported to be beneficial to CLL patients (Ding et al., 2017).

Chimeric antigen receptor (CAR)-T cell treatment introduced a new domain of cancer therapy. CART cells are patient autologous cells that have been engineered to produce synthetic receptors that coordinate lymphocytes (T cells) to distinguish and eliminate tumour cells showing a certain antigen. CART cell interactions with target antigen-presenting tumour cells cause a robust T-cell activation and remarkable anti-tumour activity (Sterner and Sterner, 2021). CART cell treatment has demonstrated a particularly impressive efficacy in the context of CLL (Porter et al., 2011, Turtle et al., 2017). However, because it is a relatively new type of treatment, more studies are required to gain further insights into its safety and tolerance.

Synthetic lethality treatment approaches take advantage of the existence of mutations in cancer cells. The acquisition of cancer cell genetic alterations causes the cells to heavily rely on relative pathways of that altered gene to maintain their survival or antiapoptotic nature. Therefore, using inhibitors to block remaining pathways will consequently induce cancer cell death while sparing normal cells because they do not rely on that pathway (O'Neil et al., 2017). Synthetic lethal approaches have shown promising results in CLL. ATM-deficient CLL cells were sensitive to PARP inhibitor (Olaparib) (Weston et al., 2010). PARP protein is a component of the DNA single-strand break (SSB) repair machinery (Dantzer et al., 1999), and ATM-deficient CLL cells show dependency on this protein to cope with the accumulating DNA damage. Similarly, the inhibition of ataxia telangiectasia and Rad3-related (ATR) in TP53 or ATM-defective CLL cells leads to hyper cytotoxicity and chemosensitization, which subsequently cause selective tumour cell death (Kwok et al., 2016). Moreover, mutations in genes encoding for the RNase H2 complex sensitize CLL cells to the PARP inhibitor Olaparib by creating PARP-trapping DNA lesions caused by TOP1, which, in turn, exacerbates DNA damage and causes cell death (Michal Zimmermann and Olga Murina and Martin, 2018).

Early preclinical studies showed that a combinatory treatment approach demonstrated synergistic effects between fludarabine and cyclophosphamide in CLL patients (Bellosillo et al., 1999, Bosch et al., 2002). The German CLL Study Group (GCLLSG) trial, in which rituximab was combined with fludarabine on previously treated and untreated CLL patients, showed 87% complete and partial remission (Schulz et al., 2002). Moreover, combining obinutuzumab, an anti-CD20 mAb, with chlorambucil provided overall improvements in CLL patients with coexisting conditions (Goede et al., 2014). Furthermore, adding the anti-CD20 antibody ofatumumab in addition to chlorambucil improved the clinical outcome for treatment-naive CLL patients (Hillmen et al., 2015). The use of idelalisib, a PI3K delta inhibitor, with rituximab showed an improved overall outcome of 81% and overall survival (OS) of 92% in CLL patients not fit for chemotherapy (Furman et al., 2014). In addition, in a long-term clinical trial, the administration of ibrutinib to rituximab provided an overall response rate of 95% and resulted in remarkable remissions in CLL patients with advanced stages (Jain et al., 2017). Using a combined treatment of venetoclax with rituximab improved the progression-free survival to 84.9% in CLL patients after a median follow-up of two years (Seymour et al., 2018). Moreover, combining ibrutinib with venetoclax for high-risk and older CLL patients showed complete remission in 88% of the patients with MRD negativity percentage of 61%, highlighting the effectiveness of combining these treatments (Jain et al., 2019). Altogether, the combined use of different therapeutic agents resulted in an improved overall treatment efficacy and led to advancement in CLL treatment.

Epigenetic studies have demonstrated a correlation between DNA methylation landscape and CLL disease clinical subtypes and outcomes (Kulis et al., 2012, Oakes and Martin-Subero, 2018, Oakes et al., 2014, Landau et al., 2014). In addition, the dysregulation of epigenetic regulators by either via mutations or epigenetic silencing or deregulated expression is frequently observed in CLL (Xanthopoulos and Kostareli, 2019). Therefore, these observed alterations in epigenetic landscape promote the development of epigenetic-based therapy in CLL. Histone deacetylase (HDAC) inhibitors showed promising results in CLL

treatments. HDAC inhibition by valproic acid shows upregulation of both MS4A1 and CD20 in CLL cells with NOTCH1 mutation, suggesting HDAC enzymes may contribute in the repression of CD20 expression (Pozzo et al., 2016). Moreover, it was shown that HDAC6 and BTK inhibitor Ibrutinib combined treatment resulted in a cell death and survival improvement, possibly due to a synergistic effect of this combination (Maharaj et al., 2018). The inhibition of EZH2, a histone methyltransferase, with the histone methylation inhibitor DZNep resulted in a reduction in IGF1R expression levels, which subsequently reduced pAKT levels in an HG3 CLL cell line (Kosalai et al., 2019). The use of BTK inhibitors resulted in extensive chromatin changes in CLL patients and the decrease of NF-κB and BCR signalling as well as upregulation of protein degradation and autophagy pathways, which selectively sensitized cells for PLK1 and mTOR inhibitors (Schmidl et al., 2019).

The involvement of non-coding RNAs (ncRNAs) in CLL has also been reported. HDAC enzymes were recruited to repress a set of microRNAs that are involved in BTK gene expression downregulation, and using HDAC inhibitors helped in the expression of these miRNAs and, thus, repression of BTK (Bottoni et al., 2016). This finding may support the use of HDACi in ibrutinib-resistant CLL patients. The hypermethylation of miR-34b/c promoter is observed in half of CLL patients, and restoring the expression of this miRNA in HG3 CLL cells induced apoptosis, highlighting their role in tumour suppression (Deneberg et al., 2014). Taken together, CLL epigenomic treatment approaches represent an increasingly growing field that may help further understand the nature of the disease and, in the near future, could provide more personalized CLL treatment based on CLL patients' individual epigenetic profiles.

1.1.4.5 Genomic aberrations in CLL

The acquisition of genomic mutations is an important aspect of CLL pathogenesis, as similarly seen in other cancers. CLLs disease's prolonged clinical course allows for the accumulation of passenger and driver mutations. However, the disease initiating defining tumour-causing lesions is not recognized. Moreover, CLL patients undergo a diverse mutational landscape that distinguishes them from one patient to another and contributes to this disease's heterogenous nature.

Prognostic CLL cytogenetic abnormalities were first described in the seminal study by Döhner et al (Döhner et al., 2000). In this study, del(13q14) was found to be most common abnormality (55%), succeeded by del(11q22-23) (18%), trisomy 12 (16%), del(17p) (7%), del(6q15-21) (6%) and trisomy 8q (5%). Linking the clinical features associated with these aberrations showed that the most prevalent group del(13q14) had the longest treatment-free interval (TFI) and was correlated with overall good prognosis. The trisomy 12 group had an intermediate TFI, whereas del(17p) and del(11q22-23) both exhibited the lowest TFI and were found to be linked with rapid disease progression and worst prognosis (Döhner et al., 2000).

The application of next-generation sequencing methodologies, such as whole genome (WGS) or whole exome (WES) sequencing, has allowed more unbiased insights into copy number aberrations (CNAs) and the allelic composition at each genomic locus in CLL. WGS studies have confirmed the existence of known CNAs, including, 17p, 11q22-q23, 13q14, 6q15-q21 and trisomy 12 (+12) and identified novel potential CLL driver CNAs, such as deletion 6q15, deletions of 2q37, loss of 3p21 and loss of 10q24 (Xose, 2015). Another WES study showed that del(13q14), trisomy 12, del(11q) and del(17p) were present in more than 5% of 538 mainly progressive CLL patients (Dan, 2015). Furthermore, the application of CNA analysis allowed the assessment of the clonality of these frequent CNAs within tumour cells. Del(13q14) and trisomy 12 mutations were observed as predominantly clonal consistent with being an initial event,

whereas del(11p) and del(17p) were observed as subclonal as they were present in a small fraction of CLL cells suggesting their role in disease progression rather than initiation. Notably, the occurrence of subclonal aberrations was considered to be an unbiased predictor of rapid disease progression and poor prognosis (Landau et al., 2013).

Genetic mutations play an essential and important part CLL development as in other types of cancers. The mutational landscape in CLL is heterogenous, and characterised by the diverse acquisition of low-frequency driver mutations. This diversity could be explained by three primary factors: the cell of origin, disease onset and disease evolution. For example, Xose et al. found that the level of driver mutations in IGVH U-CLL was significantly greater than in the IGVH M-CLL group, although the latter group had a 44% higher mutational burden (Xose, 2015). In addition, some mutations were mostly detected in IGVH M-CLL, such as *MYD88* and *PAX5*, whereas *U1*, *NOTCH1* and *POT1* mutations are mainly observed in IGVH U-CLL (Delgado et al., 2020). Several studies have shown that *MYD88* mutations are significantly associated with a young age of CLL patients (Martínez-Trillos et al., 2016, Improgo et al., 2019). The occurrences of some mutations, such as *SF3B1*, *POT1* and *ATM*, are more frequently noted in patients with a progressive disease requiring treatment, while others were associated with an indolent disease. In addition, CLL patients with a history of chemoimmunotherapy (CIT) exhibited frequent mutations in *TP53, BIRC3, MAP2K1* and *NOTCH1* genes (Xose, 2015, Dan, 2015, Stilgenbauer et al., 2014).

The application of high-throughput, next-generation deep DNA sequencing have added new insights into CLL pathogenesis and unravelled novel CLL-specific mutations (Fabbri et al., 2011, Quesada et al., 2011, Ljungström et al., 2016, Puente et al., 2015, Landau et al., 2013) and provided a new understanding of disease pathogenesis. The presence of a cluster of mutations within a particular biological pathway suggests a mechanism by which mutations enhance the fitness of tumour cells. Recurrent CLL mutations were seen in pathways such as BCR and TLR signalling (*TLR2, IKZF3, EGR2, BCOR, MYD88*); MAPK pathway (*KRAS, NRAS*); NF-κB signalling pathway (*NFKBIE, TRAF2, TRAF3, BIRC3, NFKB2*); NOTCH1 signalling

(*NOTCH1, FBXW7*); chromatin modification (*KMT2D, ASXL1, CHD2, SETD2*); DDR pathway (*ATM, TP53, POT1, RNASEH2B*); RNA splicing and biology (*SF3B1, U1, DDX3X, RPS15, XPO1*); and cell cycle regulation (*ATM, TP53, CDKN2A, CCND2, CDKN1B*). Some of these recurrent mutations were associated with chromosomal aberrations. For example, *NOTCH1, BCOR, BIRC3* mutations were linked with Trisomy 12. Mutations in *ATM, SF3B1* and *XPO1*, were linked with del11q, whereas *CHD2* and *RNASEH2B*, which were linked with del13q (Chiorazzi et al., 2021).

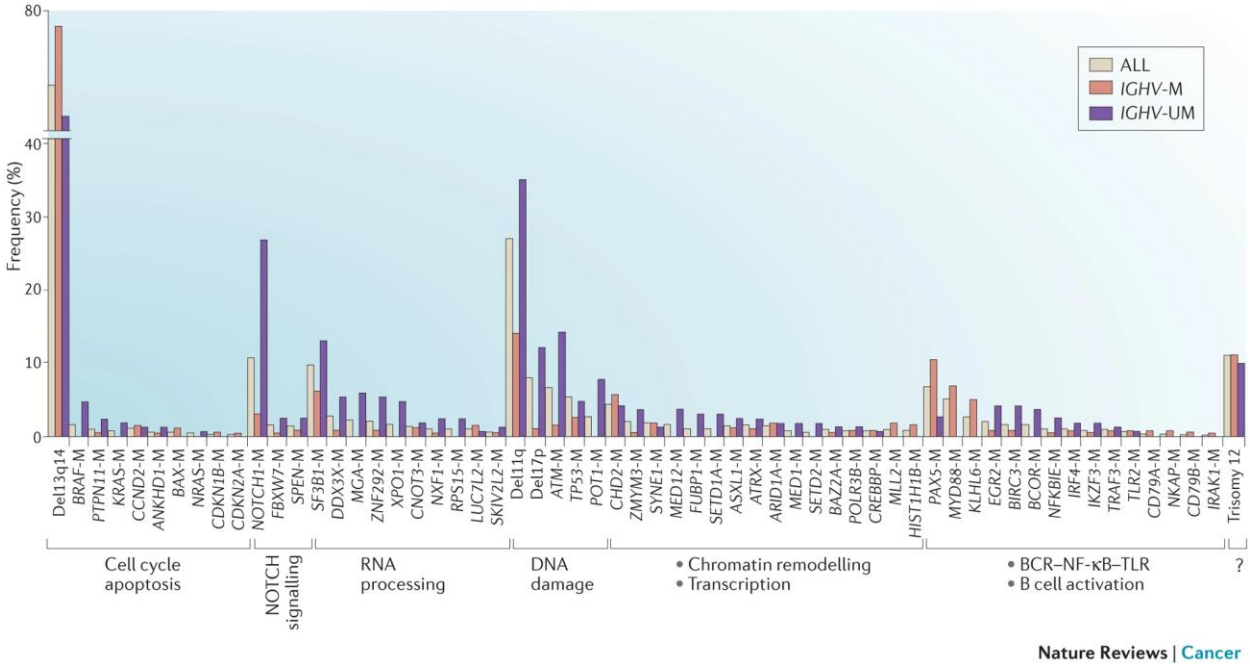


Figure 1.3 Mutational landscape of CLL
The percentage of CLL patients carrying recurrent CLL-linked genetic mutations along with IGHV status derived. The del13q14 genetic alteration is the most common genetic mutation seen in all CLL patients irrespective of IGHV status. This frequently altered region contains the RNASEH2B gene, a member of RER pathway. The del11q is the second most frequently altered genomic region in CLL which contains the ATM gene, a member of DSB pathway. Adapted from Fabbri, G., & Dalla-Favera, R. (2016).

1.1.4.5.1 CLL common mutations are components of DNA damage response

Two major chromosomal aberrations have a significant influence on CLL's overall clinical course. The first alteration is the del11 deletion, which includes the *ATM* gene, and is observed in nearly 20% of all CLL patients. The second aberration is the 13q14 deletion, which is seen in approximately 50% of CLL patients and is considered an early event in CLL pathophysiology (Figure 1.3) (Puente et al., 2015, Quesada et al., 2011, Angelo Agathaggelou and Olga Murina and Andrew, 2018, Fabbri et al., 2011, Edelmann et al., 2012). Notably, these deleted regions affect genes encoding for DNA damage response (DDR) pathways; *ATM* as a major player in double-strand break (DSB) repair and *RNASEH2B*, a subunit of the RNase H2 complex, is involved in the ribonucleotide excision repair (RER) pathway.

1.2 11q deletion and *ATM*

The *ATM* gene is located on chromosome 11q and codes for ataxia-telangiectasia mutated (ATM), a nuclear kinase that is activated in the presence of DSBs. Our group reported that in CLL mutations can occur in any part of the ATM gene without any preferential hotspots (Stankovic and Skowronska, 2014). *ATM* mutations not only cause a reduction in ATM phosphorylation levels in CLL cells but also a marked reduction in the phosphorylation levels p53, structural maintenance of chromosomes protein 1 (SMC1) and nibrin (NBS1) upon induction of DSBs via ionizing radiation (IR). This collectively leads to an inability of CLL cells to induce apoptosis (Austen et al., 2005).

ATM mutations are observed in 36–50% of CLL patients with 11q deletions, which results in inactivation of the remaining functional allele (Skowronska et al., 2012, Austen et al., 2007). Del11q, accompanied by a mutation in the remaining *ATM* allele is correlated with a progressive disease, resistance to chemotherapy and an poor survival (Austen et al., 2007). Furthermore, the findings by our group suggest

that the acquisition of *ATM* germline mutations accelerate the disease pace rather than initiating CLL onset (Skowronska et al., 2012).

1.2.1 ATM is a major component of DNA damage response

The ataxia-telangiectasia mutated (ATM) protein is encoded by a 160 kb gene on chromosome 11q22-23. The ATM gene, initially cloned in 1995 (Savitsky et al., 1995), and it contains an open reading frame of 9.138 kb, resulting in an enzyme comprising 3056 amino acids (Shiloh and Ziv, 2013). The ATM gene has 66 exons with exon 4 marking the translational start site. ATM protein kinase synchronises multiple complex signalling networks mainly involved in the reaction to DNA DSB. Germline mutations of ATM lead to a cancer predisposition syndrome referred to as ataxia telangiectasia, in which individuals have a 20–30% risk of lymphoid, breast, central nervous system and gastric tumours (Taylor et al., 1996, Choi et al., 2016).

1.2.2 ATM Protein structure and function

ATM is a member of the phosphoinositide 3-kinase-like kinase (PIKK) family of proteins, which is characterised by the presence of common domains, including the FRAP-ATM-TRRAP domain (FAT), the phosphoinositide 3-kinase catalytic domain – PI3K, the PIKK domain and the Fat-C-terminal domain (FATC). Members of this family include ATR, SMG-1, mTOR, DNA-PK , and TRRAP. These proteins are capable of activating various substrates through phosphorylation at serine and/or threonine residues (Daub, 2012).

In terms of domain localisation (Figure 1.4), a PI3K catalytic domain containing an ATP-binding site resides between 2715 to 3011 residues. FAT domain is found at the region between amino acid residues 1966 to 2566 and contains an autophosphorylation site (serine 1981). Furthermore, the FATC domain recognized

by the histone acetyltransferase Tip60 is located at the C terminal domain between amino acid residues 3034 to 3056 and contains an acetylation site (lysine 3016). Both FAT and FATC domains are necessary to regulate ATM kinase activity and function (Guo et al., 2010). The TAN domain, located in the N-terminal region, has been shown to have a role in telomeric length maintenance and DDR in the ATM ortholog in yeast; hence, the evolutionarily conserved TAN motif suggests that it may have an important role in the human ATM (Seidel et al., 2008). The N-terminal domain of ATM participates in DDR through interactions with other proteins including BLM, p53, LKB1, BRCA1,and NBS1 as well as nuclear localization and chromatin association (Beamish et al., 2002, Falck et al., 2005, Fernandes et al., 2005, Young et al., 2005). Huntington, Elongation factor 3, A subunit of protein phosphatase 2A, TOR1 (Heat repeats), are located upstream of PI3K domain allowing superhelical conformation of ATM to facilitate interactions with DNA and other proteins (Llorca et al., 2003).

In addition, the ATM protein also encloses domains that are described as proline-rich regions located between amino acid residues 1373–1382 and incomplete leucine zipper domain residues 1217–1238. Respectively, these middle-region domains are involved in the binding of ATM to c-ABL tyrosine kinase and help in producing an effective DDR through mediating protein–protein interactions (Chen et al., 2003, Shafman et al., 1997).

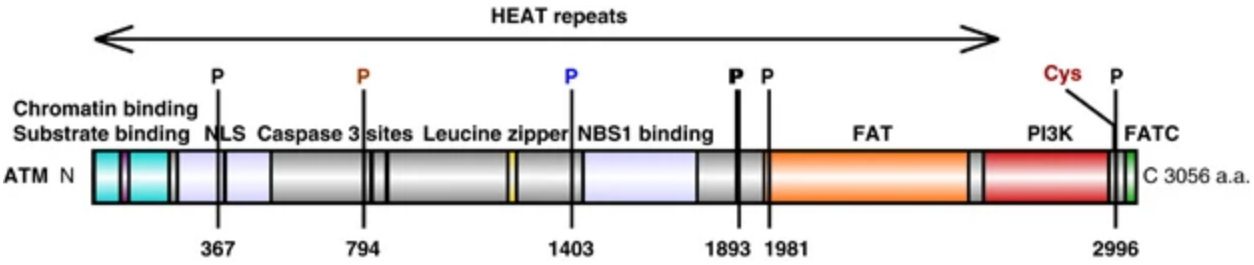


Figure 1.4 ATM protein structure schematic representation and sites of autophosphorylation The ATM protein contains a catalytic domain (PI3K), an autophosphorylation site (FAT), an acetylation site (FATC), an interaction domain (Tel-1/ATM N-terminal). The HEAT domain allows for proper ATM interaction through conformational change. Abbreviations: (PI3K) phosphoinositide-3 kinase, (FAT) FRAP, ATR, and TRRAP proteins, (FATC) FAT C-terminal domain, (NLS) nuclear localisation sequence, (HEAT) huntingtin, elongation factor 3.Adapted from Cremona, C. A., & Behrens, A. (2014).

1.2.3 ATM protein role in DNA double-strand break signalling

The activated ATM protein triggers the activation of several downstream targets in response to DSBs (Figure 1.5). ATM orchestrates the cellular response to DSBs by activating signalling that regulates DNA repair machinery, cell-cycle arrest and apoptosis. ATM is mainly confined to the nucleus, where it resides as an inactive homodimer under normal physiological conditions (Bakkenist and Kastan, 2003, Paull, 2015). The ATM post-translational modifications regulate its activity. For example, it has been determined that autophosphorylation of serine residue 1981 is necessary for ATM release from its inactive dimeric form to facilitate activation of the monomers (Bakkenist and Kastan, 2003, Kozlov et al., 2011). Consequently, the lysine 3016 residue is then acetylated by Tip60 (Sun et al., 2007). Under physiological conditions, protein phosphatase 2A (PP2A) is involved in the inhibition of ATM autophosphorylation by being constitutively associated with ATM (Goodarzi et al., 2004). Active ATM phosphorylates motifs (serine/threonine)-glutamine on downstream effector proteins, leading to widespread cellular responses, including DDR, cell cycle arrest and chromatin re-organization (Awasthi et al., 2015).

At the early stages of DSB response, the MRN complex, which contains Mre11, Rad50 and NBS-1 proteins, recruits ATM to the site of DSBs, leading to active ATM monomerization (Lee and Paull, 2005). Thereby,

the assembly of ATM/MRN complex add more fitness to ATM toward its substrates, assisting in robust network signalling and enhancing ATM accumulation at lesions. To assist and enhance this complex assembly, 53BP1 and BRCA1 sensor proteins participate in this process, which involves ubiquitylation of NBS1 by the E3 ubiquitin ligase SKP2 (Wu et al., 2012). In return, MRN complex is targeted for phosphorylation by ATM, thus allowing for the timely initiation of several DDR branches (Di Virgilio et al., 2009, Gatei et al., 2011). The phosphorylated active MRN complex contributes to homologous recombination repair (HRR) through the early processing of DNA broken ends (Williams et al., 2008, Hopfner et al., 2001).

In addition, ATM phosphorylates other DNA repair proteins and drives their activation. For example, Bloom syndrome protein (BLM) (threonine 99), endonuclease Artemis (serine 645) and RAD51 (tyrosine 315), BRCA1 (serine 988), and c-ABL kinase (serine 465) (Chen et al., 2005, Beamish et al., 2002, Shafman et al., 1997, Chen et al., 1999, Zhang et al., 2004). MDC1 mediated phosphorylation by ATM at the initial phase of DDR allows the recruitment of the RNF8 and RNF168 ubiquitin ligases and subsequently enhances H2AX ubiquitylation, increasing the accumulation of other repair proteins, including BRCA1 and 53BP1 at DNA lesion sites (Mailand et al., 2007, Stewart et al., 2001).

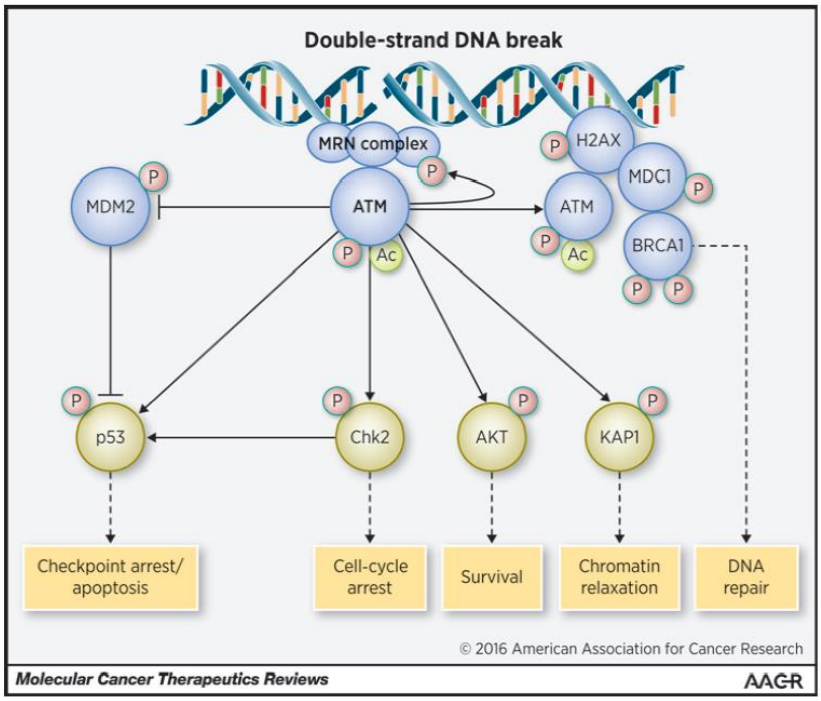


Figure 1.5 Activation of ATM leads to various effects on cellular processes
In the presence of DSBs, MRN complex induce the active form of ATM to enhance a high affinity of ATM to its substrates (MDC1, BECA1, and γH2AX) thereby activate a robust DNA repair machinery. Active form of ATM also phosphorylate other proteins allowing for chromatin relaxation for better DNA repair machinery (KAP1), cell survival (AKT), cell-cycle arrest (CHK2), and apoptosis/checkpoint arrest P53. Adapted from (Choi et al., 2016).

ATM influences cell cycle regulators, thereby activating cell cycle arrest at checkpoints G1, S or G2/M. In response to DNA damage, ATM interacts with p53 through phosphorylation (serine 15) and its negative regulator MDM2 (serine 395) together with CHK2 (threonine 68) checkpoint protein kinase, which, in turn, phosphorylates p53 (serine 20), allowing its stabilization (Barlow et al., 1997, Banin et al., 1998). This cascade of phosphorylation events initiated by ATM leads to upregulation of the cyclin-dependent kinase inhibitors p21 which consequently cause G1/S cell cycle to stop, allowing the cell to cope with the DNA damage that occurred. ATM phosphorylation of the BRCA1 affects cell cycle progress, and the type of cell cycle arrest depends on the phosphorylated residue. The G2/M arrest occurs in the case of serine 1423 phosphorylation and S-phase arrest in the case of serine 1387 phosphorylation (Xu et al., 2002). Moreover,

ATM can inhibit cell cycle progression to S-phase through phosphorylation of NBS1 (serines 343 and 278) directly. The same effect is observed through ATM-mediated phosphorylation of other cell cycle regulators, such as threonine 68 of CHK2, serine 222 of FANCD2, and serine residues 966, 957 of SMC1 (Buscemi et al., 2001, Falck et al., 2002, Ho et al., 2006, Yazdi et al., 2002).

1.2.4 ATM involvement in remodelling the chromatin landscape

Chromatin is a complex structure comprising DNA packaged with histone proteins to form the nucleosome structure. Based on the transcriptional activity potential, chromatin is classified into euchromatin and heterochromatin. Loosely packed chromatin that is typically transcriptionally active and gene rich is named euchromatin, whereas tightly packed chromatin associated with a gene-poor, inactive transcriptional profile is termed heterochromatin. Nucleosomes are subjected to post-translational modifications, allowing for the recruitment of specific enzymes that alter chromatin. The presence of DNA damage initiates the repair machinery in accordance with chromatin structure. The chromatin organization changes in the vicinity of DNA damage is necessary to minimize barriers, preclude interfering by physiological processes (transcription and replication) and permit repair DNA proteins to have access to the lesion. Together, these changes in the chromatin structure are taking place through epigenetic post-translational modification of nucleosomes, non-nucleosome proteins and ATP-dependent chromatin remodelling complexes (Price and D'Andrea, 2013).

One of the earliest events in DSB signalling is the formation of γH2AX foci at DSB lesions. ATM and DNA-PK phosphorylate H2AX at serine 139, whereas ATR contribution is strictly in situations where replication stress is triggered in S-phase or DSB termini resected in G2 (Bönisch and Hake, 2012, Bonner et al., 2008, Shiloh and Ziv, 2013). The magnitude of H2AX phosphorylation covers up to 30 megabases of DNA around the DSB lesion. In addition to ATM/DNA-PK/ATR, the formation of γH2AX is carried out through BRG1, a

subunit of the SWI/SNF chromatin remodelling machinery. Upon DNA damage, BRG1 is targeted by ATM for phosphorylation at serine 721, allowing for increased BRG1 affinity for acetylated histone 3 and H2AX-containing nucleosomes. Therefore, BRG1 localization to DNA damage sites enables the chromatin remodelling activity to enhance γH2AX spreading (Kwon et al., 2015, Rother and van Attikum, 2017). Moreover, the Williams syndrome transcription factor (WSTF) that belongs to WICH chromatin remodelling complex is involved in recruiting ATM and MDC1 to DNA damage lesions by phosphorylating H2AX at tyrosine 142 (Xiao et al., 2009). Further γH2AX regulation can be observed in quiescent cells where H2AX is constitutively observed, but it is subjected to proteasomal degradation by the E3 ubiquitin ligase HUWE1. However, upon DSB induction, HUWE1 is removed from chromatin to allow the incorporation of H2AX, leading to γH2AX formation (Atsumi et al., 2015). Taken together, these observations illustrate that γH2AX phosphorylation is regulated by ATM in multiple ways.

ATM kinase activity is required in DSBs at the heterochromatin region, and its disruption results in lesion repair failure. The transcription repressor (KAP-1) is targeted by ATM for phosphorylation at serine 824, allowing chromatin relaxation and decompaction to assist in recruiting repair factors to DSB lesions (Goodarzi et al., 2008). ATM hyperactivity in heterochromatin is vital to preclude the constitutive phosphatase activity of PP4 to KAP-1, thereby preserving KAP-1 phosphorylation status at serine 824. CHK2 protein, an ATM substrate, phosphorylates KAP-1 at serine 473, resulting in an effect on G2/M checkpoint signalling (Lee et al., 2012). Phosphorylated KAP-1 allows DSBs repair through interaction with CHD3 isoform 1, which belongs to the CHD-class chromatin remodellers (Rother and van Attikum, 2017, Klement et al., 2014). CHD3.1 is involved with the repression of gene expression and chromatin condensation as a essential factor of (NuRD) complexes, a mammalian nucleosome remodelling and deacetylase complex. The formation of the phosphorylated KAP-1 disrupts CHD3.1 activity by removing it from heterochromatin and eventually allowing chromatin relaxation (Ziv et al., 2006). In addition, ATM phosphorylation of the the RSF complex helps in recruiting SFN2H, a catalytic component of several

remodelling enzyme complexes. Upon DNA damage, RDF-1 enhances cell survival and checkpoint signalling, thereby promoting the build-up of homologous recombination (HR) repair proteins Rad51 and RPA at DSBs (Min et al., 2014).

In the euchromatin region, ATM coordinates transcriptional repression following DSBs to prevent DNA repair and transcription machinery collision. During DSBs, ATM mediates silencing of the primary rRNA polymerase RNA Pol I through NBS1 and MDC1 to establish its nucleolar exit (Kruhlak et al., 2007). However, global Pol II activity is not silenced during DSBs where ATM phosphorylation of BAF180 at serine 948 helps in precluding chromatin decompaction, allowing the PBAF complex to establish transcriptional repression and repair of DSBs via NHEJ (Kakarougkas et al., 2014). Moreover, the Polycomb repressive complexes PRC1 and PRC2 are recruited by ATM, and the depletion of PRC2 disrupts DSB repair and results in IR hypersensitivity (Campbell et al., 2013, Kakarougkas et al., 2014).

If the amount of DNA damage cannot be tolerated and repaired, ATM triggres the induction of apoptotic signalling through the activation of p53 (Bree et al., 2004). In this process, p53 protein, activated by ATM, interacts or affects the gene expression levels of the proapoptotic proteins BAX, PUMA, NOXA and BID (Joerger and Fersht, 2016). The activation of the transcription factor E2F1 can also trigger ATM-induced apoptosis through the upregulation of p53 functional homolog p73 (Carcagno et al., 2009, Yoshida et al., 2008).

In summary, given the fundamental role that ATM plays in DNA repair, cell cycle progression, chromatin remodelling, and apoptosis, the loss of ATM function in CLL leads to uncontrolled propagation of tumour cells with unresolved DNA damage and genomic instability (Stankovic et al., 2002, Lazarian et al., 2017).

1.3 13q14 deletion and *RNASEH2B*

RNASEH2B gene is located at 13q14 on chromosome 13, a frequently deleted region, and an early event of CLL pathogenesis (Agathaggelou et al., 2018). This deleted region also contains other well-studied tumour suppressor genes *DLEU2*, *MIR15A*, *MIR16A* and *RB1* (Klein et al., 2010). RNASEH2B is a subunit of the RNase H2 complex, which comprises RNASEH2A, RNASEH2B and RNASEH2C (Crow et al., 2006). The complex is involved in RNA degradation in R-loops, a type of RNA-DNA hybrids formed when co-transcriptionally nascent RNA transcript complements to nearby DNA template (Cerritelli and Crouch, 2009). In addition, RNase H2 complex removes misincorporated ribonucleotide monophosphates (rNMPs) by the ribonucleotide excision repair (RER) pathway (Williams et al., 2016). The occurrence of both R-loops and misincorporated rNMPs is a major source of DNA lesions that threatens genome stability (Nick McElhinny et al., 2010). Thus, RNase H2 maintains genomic integrity during transcription and replication.

The deletion of 13q14 is the most observed structural genetic alteration seen in CLL (Garg et al., 2012). Our laboratory has demonstrated that RNASEH2B deletions were observed in 43% of CLL patients, with 29% classified as monoallelic deletions and 14% as biallelic deletions using multiplex ligation-dependent probe amplification (MLPA) (Zimmermann et al., 2018). Clinically, 13q deletions as the sole mutation are associated with a favourable disease outcome, with an extended median survival among all CLL patients. However, in the light of the role of RNASEH2B in maintaining genome integrity, it is obvious that additional studies are required to understand its role in CLL pathogenesis and further assess its application as a predictive biomarker.

1.3.1 RNASEH2B is a member of RNase H2 enzymatic complex

Ribonuclease H2 Subunit B (RNASEH2B) is encoded by a gene of 114,443 bases encompassing 11 exons, producing a protein of 308 amino acids. The RNASEH2B gene encodes for a non-catalytic subunit of the RNase H2 complex, one of the major human endonucleases (Hyjek et al., 2019). RNase H2 is considered the dominant form of RNase H in humans (Eder and Walder, 1991, Frank et al., 1998). RNase H2 can degrade RNA-DNA hybrids through endonucleolytic cleavage of the complementary RNA engaging in the hybrid molecule. RNase H2 is also involved in the elimination and excision of DNA-embedded single ribonucleotides, whereby it facilitates ribonucleotide excision repair (RER), a unique feature that distinguish RNase H2 from RNase H1, another member of the RNase H family (Mackenzie et al., 2016). Disruption of any of the RNase H2 subunits (A,B or C) causes a loss of its enzymatic activity, highlighting the essential roles of the other subunits in maintain the complex stability (Agathaggelou et al., 2018, Reijns and Jackson, 2014, Zimmermann et al., 2018).

1.3.2 RNase H2 enzymatic complex structure

RNase H2 is heterotrimeric complex comprises three proteins encoded by *RNASEH2A*, *RNASEH2B* and *RNASEH2C* genes (Figure 1.6). RNase H2 complex stability is heavily dependent on the presence of all three proteins. The *RNASEH2A*, *RNASEH2B* and *RNASEH2C* genes encode for 301 amino acid , 308 amino acid , 166 amino acid respectively (Shaban et al., 2010). The RNase H2 complex structure shows that the H2C protein occupies the middle of the complex in between H2A and H2B proteins, possibly to maintain the complex cohesion. The subcomplex H2B-H2C of RNase H2 facilitates an interaction that creates a platform for H2A to exert its catalytic activity. Therefore, the existence of all three subunits is essential to create a stable, active enzyme (Shaban et al., 2010).

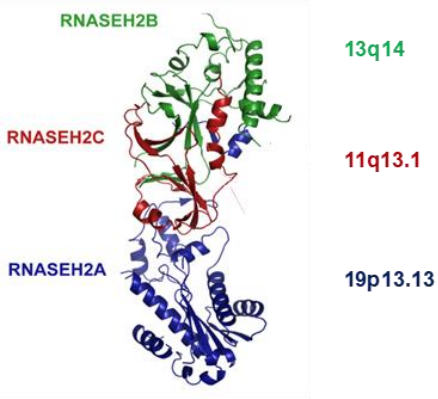


Figure 1.6 Protein structure of RNAase H2 enzymatic complex
RNase H2 complex consists of three proteins (RNAEH2A, RNASEH2B, RNASEH2C). The subcomplex H2A and H2B maintain complex structure whereas H2B and H2C maintain the catalytic activity. All three proteins are required to RNase H2 complex stability. The genomic locations of genes encoding for this complex are highlighted.

1.3.3 The functional role of RNase H2 complex

Similar to RNase H1, RNase H2 complex is involved in resolving R-loops through endonucleolytic hydrolysis of RNAs (Cerritelli and Crouch, 2009). Failure to remove these R-loops causes DNA lesions, leading to genomic instabilities, possibly caused by DNA replication collision (García-Muse and Aguilera, 2016). The RNase H2 enzyme complex also facilitates the ribonucleotide excision repair (RER) pathway, in which erroneously DNA-embedded rNMP are removed (Figure 1.7). Upon recognition of rNMP at the (5')RNA–DNA(3') junction, RNase H2 initiates RER by first making an incision at the adjacent DNA-RNA, producing a single-stranded DNA break edged by a 3' hydroxy group and a 5' phosphate. Next, DNA polymerases (Pol δ or Pol ε) carry out DNA synthesis, which leads to a tail of DNA strand containing the rNMP. This tail is then subjected to removal by single-stranded DNA endonuclease FEN1 or the exonuclease EXO1. Finally, DNA ligase is recruited to seal the remaining single-stranded DNA nick (Sparks et al., 2012, Eder et al., 1993, Rydberg and Game, 2002).

Failure to remove rNMPs via the RER pathway places the genomic stability at risk. Spontaneous single-stranded breaks occur in the DNA backbone as a consequence of rNMP hydrolysis due to the ribose-free 2'OH group (Li and Breaker, 1999). Lack of RNase H2 increases the rate of spontaneous mutations and gene conversion events in yeast (Ii et al., 2011). In addition, dual HRR/RNase H2 inactivation leads to synergistic increases of gross chromosomal rearrangements (GCRs) (Allen-Soltero et al., 2014). Short deletions, mostly up to five base pairs in length, in short tandem repeat (STR) regions are the most frequent type of mutation observed in the context of RER defects (Nick McElhinny et al., 2010). Moreover, complete absence of RNase H2 enzymatic activity leads to replication stress, spontaneous activation of cell cycle checkpoint, increased recombination rates and increased frequency of copy number variation (CNV) (Potenski et al., 2014, Williams et al., 2013, Kim et al., 2011). Furthermore, the presence of defective RER promotes TOP-dependent genomic instabilities, as seen in RNASEH2B-defective human cells that are sensitive to PARP inhibitors (Zimmermann et al., 2018).

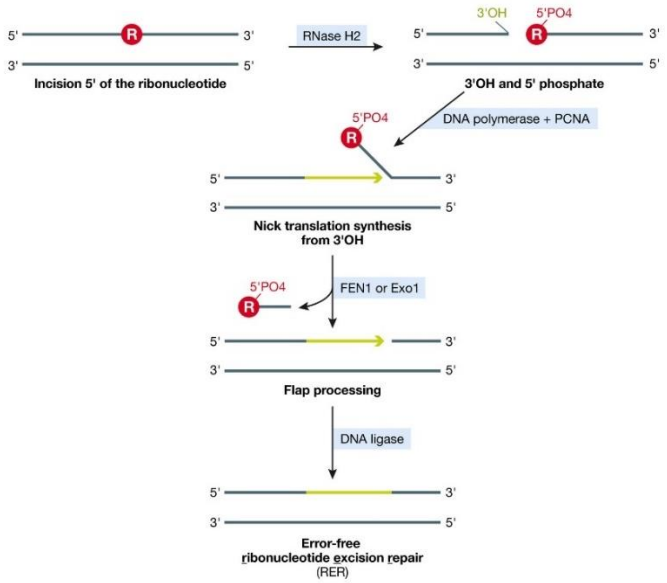


Figure 1.7 RNase H2 activates RER upon recognition of ribonucleotides
Upon recognition of rNMPs, RNase H2 activate RER by making a single-strand break at the adjacent DNA-RNA. DNA polymerases (Pol δ or Pol ε) carry out DNA production, which leads to a flanking tail strand containing the rNMP. DNA endonuclease (FEN1) or the exonuclease (EXO1) carry out the removal of rNMP containing tail structure. The remaining single-stranded DNA nick is resolved by DNA ligase. Adapted from Kellner, V., & Luke, B. (2020).

The increased mutation rate is a consequence of inefficient rNMP processing performed by TOP1 in the absence of RNase H2 activity (Williams et al., 2017). TOP1 is a critical enzyme for resolving DNA supercoils that occur in both transcription and replication (Pommier et al., 2016). In the absence of RNase H2 and upon rNMPs presence, the TOP1-cleavage complex creates random incisions at ribonucleotides sites, causing single-strand DNA breaks with DNA ends containing a 5'-OH and a 2'-3'-cyclic phosphate. DNA ligases are unable to seal this DNA structure, but they can be reversed by TOP1 (Sparks and Burgers, 2015, Huang et al., 2015). Nonetheless, the occurrence of this process at STR sequences leads to another TOP1-mediated cleavage, resulting in loss of the repeated sequences, thus, contributing to mutagenesis (Cho et al., 2015). Furthermore, the accumulation of unresolved rNMPs can lead to to replication stress that activates the ATR-Chk1 pathway, with the consequent sensitivity to ATR inhibitors (Wang et al., 2019b).

1.3.4 Defective ribonucleotide excision repair activates cGAS-STING pathway

High levels of DNA damage observed in RNase H2 cells elevates the frequency of micronuclei arising from unresolved DNA damage occurring during replication, and these micronuclei are found to colocalize with cyclic GMP-AMP synthase (cGAS), a cytosolic DNA sensor protein (Mackenzie et al., 2017, Pizzi et al., 2015). The cGAS interaction with the adaptor protein stimulator of interferon genes (STING) is involved in the induction of type I interferon signalling. The cGAS-STING pathway activates the innate immune reaction when cGAS recognition of cytoplasmic DNA derived from mitochondrial DNA, pathogens, endogenous retroviral elements or endogenous nuclear DNA (Dhanwani et al., 2018). Therefore, rNMP accumulation, together with the aberrant processing of stalled replication forks, contributes to the activation of the IFN response (Coquel et al., 2018, Kellner and Luke, 2020). Eventually, the cGAS-STING activation of type I IFN signalling leads to autophagy (Gui et al., 2019), which then helps eliminate the accumulating micronuclei (Bartsch et al., 2017) (Figure 1.8).

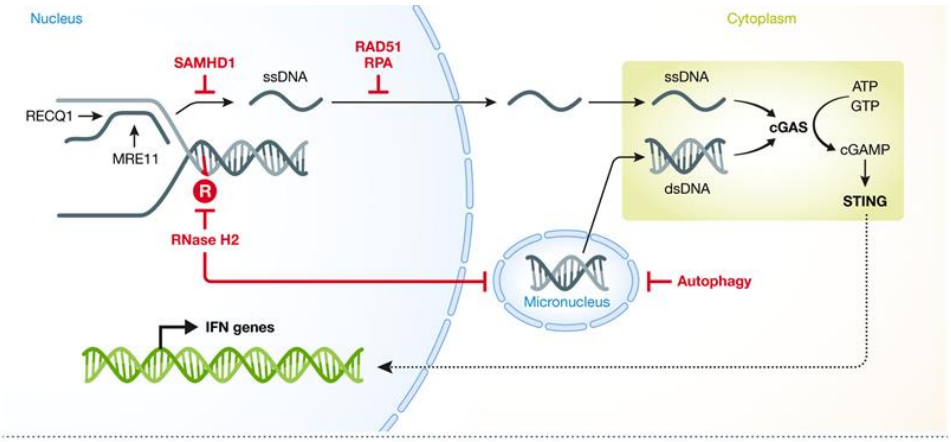


Figure 1.8 Defective RER activates cGAS-STING pathway
The presence of nuclear DNA fragments in cytoplasm leads to the induction of cGAS, which subsequently activates STING which consequently upregulate IFN genes. ssDNA (caused by replication stress) release into cytoplasm is under control of SAMHD1 through processing by RECQ1 and MRE11. RAD51 and RPA both are involved in prevention of ssDNA leakage to cytoplasm. RNase H2 is involved in rNMPs clearance from DNA to inhibit micronuclei formation. Autophagy can also resolve micronuclei. Adapted from Kellner, V., & Luke, B. (2020).

1.3.5 Unrepaired rNMPs' influence on chromatin

Early studies showed that the presence of ribonucleotide-containing DNA within the nucleosome structure has a negative impact on nucleosome assembly (Dunn and Griffith, 1980, Hovatter and Martinson, 1987). Defects in nucleosome assembly negatively affect cell fitness, exemplified by globally low nucleosome density and aberrations in nucleosome occupancy patterns. Thus, these alterations consequently affect normal nuclear processes including transcriptional regulation and DNA repair. The presence of rNMPs within the nucleosome distorts the DNA duplex structure and invokes RER repair. The inward-facing rNMPs within the DNA-bound histone octamer are associated with an increase in the width of the DNA minor groove leading to DNA double strand base pairing disruption and induction of local unwinding of the DNA double strand structure (Fu et al., 2019). Therefore, the presence of rNMPs alters the chromatin building block, represented by nucleosomes, consequently affecting the DNA structure. In addition, these chromatin alterations potentially trigger chromatin-remodelling enzymes to facilitate chromatin relaxation and facilatete RER.

RNase H2-defective cells show high levels of γ-H2AX, potentially due to stalled replication forks (Wang et al., 2019b, Kinner et al., 2008). The accumulation of γ-H2AX, leading to foci formation, is the most common epigenetic modification occurring within minutes of DNA damage induction. The induction of γ-H2AX formation initiates the early chromatin response to DNA damage (Bao, 2011). As described with respect to the ATM function, the formation of γ-H2AX is considered the first element in a sequence of chromatin landscape alterations, including nucleosome changes and histone post-translational modifications, such as acetylation, methylation and ubiquitination of lysine residues (House et al., 2014). Depending on the DNA lesion type and the DDR pathway required, these chromatin alterations allow for correct DNA repair by creating a chromatin environment favouring DNA repair.

1.4 Chromatin architecture

1.4.1 Chromatin

Eukaryotic cells are characterised by nuclear organization, which is the spatial distribution of nuclear elements in an intricate manner. Within the nucleus, DNA is accompanied by a diverse variety of proteins, including histones, to form a complex of long multiple linear molecules, which ultimately form chromatin and chromosomes. Therefore, the eukaryotic genome, including proteins and RNA, is highly packaged to form a compact structure termed chromatin. Chromatin is divided into euchromatin and heterochromatin. Active transcription, accessible DNA and cell cycle DNA decondensation are the main features of euchromatin. In contrast, heterochromatin is characterised by inactive transcription, inaccessible DNA, condensation during the cell cycle and the presence of repetitive DNA sequences (Craig, 2005, Grewal and Elgin, 2002). Controlling the chromatin accessibility is achieved mostly by post-translation modifications at the nucleosome level.

1.4.2 Nucleosomes

A single nucleosome consists of 147 bp in length DNA coiled around histone-protein octamers. The single nucleosome comprises 4 different histones—H3, H4, H2A and H2B—with each type having two histones to form a histone octamer. In each histone, there is a structural domain consisting of three alpha helices divided by two rings, needed for DNA interactions (Kornberg and Lorch, 1999). The nucleosome central tetrameric axis is formed by H3 and H4 dimerization. Next, H2A and H2B dimers join H3 and H4 dimers to form the final nucleosome octamer (Figure1.9). The localization of histone H1 within the nucleosome helps with locking DNA movement and attaching to more nucleosome units to establish increased chromatin compaction. It is important to sustain accessibility of the underlying DNA regions for many biological processes, such as gene expression regulation, DNA replication and repair regulation. Therefore, post-translation modifications (PTMs) of histones' amino-terminal tails, histone variants/exchange and nucleosome remodelling enzymes are all mainly involved in facilitating region-specific DNA accessibility.

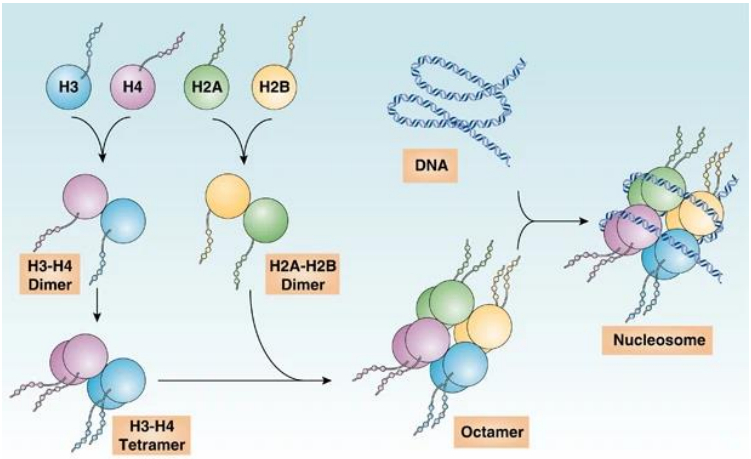


Figure 1.9 Nucleosome components and structure
The core histone is assembled by the association of 2 dimers of H3-H4 to form a tetramer complex, followed by association of dimers H2A-H2B to assemble the last octamer form of the nucleosome. Adapted from Chen, R., Kang, R., Fan, X. G., & Tang, D. (2014).

1.4.3 Histone Variants and exchange

Histone variants can replace the canonical histones that comprise the nucleosomes. These variants are similar to canonical histones, with the exception of the presence or absence of a few amino acids or an entire protein domain. The recruitment of histone variants into nucleosomes has an influence on chromatin and DNA-protein interactions (Kornberg and Lorch, 1999). For example, the histone variant H3.3 expression is cell cycle independent, in contrast to the canonical H3 histone, which is expressed in the S phase during replication only (Frank et al., 2003, Akhmanova et al., 1995). The incorporation of H3.3 leads to alterations in chromatin folding by counteracting linker histone H1 incorporation, subsequently resulting in an open chromatin conformation (Chen et al., 2013, Braunschweig et al., 2009). In addition to H3.3, other important histone variants also exist, such as H3.1 and H2A.Z. The histone variant H3.1 is often seen within heterochromatic regions and is associated with silenced genes (Tagami et al., 2004). H2A.Z incorporation leads to nucleosome destabilization to allow active gene expression and efficient DNA repair (Meneghini et al., 2003, Venkatesh and Workman, 2015).

Therefore, histone variants replacement is a biologically essential mechanism that allows the incorporation of histone variants to facilitate the dynamic nature of the chromatin environment. Histone exchange is carried out through a number of factors, such as chromatin remodellers and histone chaperones. Chromatin remodeller complexes translocase DNA by sliding or removing nucleosomes in an ATP-dependent manner to facilitate open DNA and allow contact with nucleosome assembly regulators and enable gene expression (Tsukiyama et al., 1994). The most well-studied chromatin remodellers are grouped into families according to their unique way of altering nucleosome positioning. These families include the SWI/SNF, IWSI and SWR1 families (Côté et al., 1994). The SWI/SNF large complexes are engaged in nucleosomes eviction, whereas IWSI complexes are more associated with sliding nucleosomes. Ultimately, in the context of active genes, both SWI/SNF and IWSI complexes create nucleosome-free DNA

regions that are accessible for transcription factors (Côté et al., 1994, Cockerill, 2011). Histone chaperones, on the other hand, are ATP independent and rely on DNA movement to perform their roles, including stabilization and organization of nucleosomes (Hondele et al., 2013). FACT (FAcilitates Chromatin Transcription) is a histone chaperon that functions in chromatin organization by removing or destabilizing chromatin to minimize barriers to RNA and DNA polymerase progression (Hsieh et al., 2013, Belotserkovskaya et al., 2003, Schwabish and Struhl, 2004). In addition, FACT function is important for maintaining histone PTM patterns during transcription (Jamai et al., 2009). Interestingly, CLL exhibits recurrent mutations in genes coding for proteins that have a role in chromatin remodelling, such as *CHD2*, *ZMYM3* and *ARID1A* (Ghamlouch et al., 2017) highlighting defective chromatin organization patterns in CLL that could potentially contribute to disease progression.

1.4.4 Histone post-translational modifications (PTMs)

Within the nucleosome, an amino acid N-termini tail is present and protrudes from the packed octamer, allowing for covalent enzymatic modifications (Bannister and Kouzarides, 2011). These modifications alter the histone N-termini by introducing or removing either methylation, acetylation, SUMOylation, phosphorylation, ribosylation or citrullination (Tan et al., 2011). Several research groups have reported that histone alterations are essential in the control of chromatin accessibility and, consequently, transcription (Bannister and Kouzarides, 2011, Kouzarides, 2007, Castillo et al., 2017). Moreover, histone post-translational modifications were recognized to have essential roles in facilitating normal biological activities including transcriptional activation, repression and elongation, euchromatin and heterochromatin maintenance (Lawrence et al., 2016) (Figure 1.10).

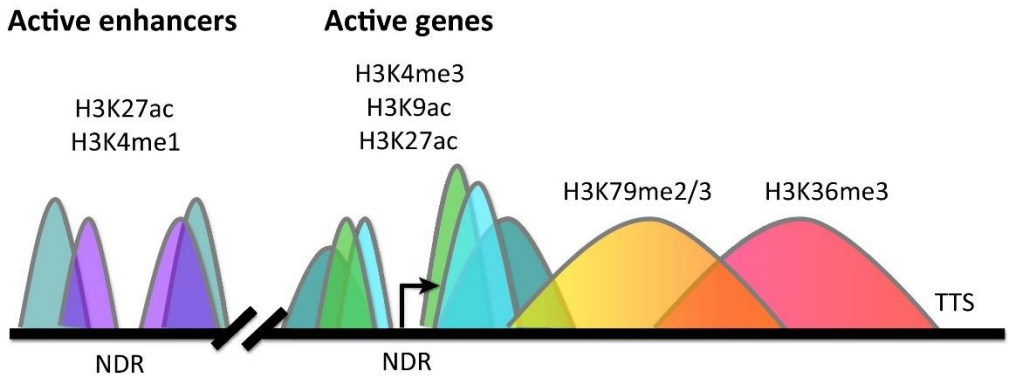


Figure 1.10 Histone modification occupancies with respect to active enhancers and genes
A simplified overview of the occupancy of histone modifications as reported by ChIP-seq assays. Sharp histone signals include H3K27ac and H3k4me1 (active enhancers), H3K4me3, H3K9ac, and H3K27ac (active promoters). Broad histone marks that mostly observed at gene body include H3K79me2/3 and H3K36me3. Arrow denotes the transcription start site (TSS). NDR, nucleosome-depleted region; TTS, transcription termination site. Adapted from Gates, L. A., Foulds, C. E., & O'Malley, B. W. (2017).

There are two potential mechanisms that alter chromatin and gene expression through histone tail modifications. First, through electrostatic interactions, the histone N-termini are positively charged, and DNA is negatively charged; therefore, the N-terminus may be either hidden or exposed depending on the histone tail modification. For example, the acetylation by histone acetyltransferases (HATs) of a lysine residue of the histone tail adds more negative charge to the histone tail and thereby inhibits DNA attraction (Figure 1.11). Consequently, this modification allows for more relaxed accessible chromatin, subsequently enabling transcription factors to interact with DNA at the promoters and enhancers (Zentner and Henikoff, 2013, Bannister and Kouzarides, 2011). Second, the presence of histone modifications attracts transcription factors, large transcriptional complexes and adaptor proteins, resulting in either transcriptional activation or repression. For example, the presence of histone tail modification H3K27me3 is identified by the chromodomain part of the Polycomb (Pc) member of PRC1-type complexes resulting in gene silencing (Schuettengruber et al., 2007).

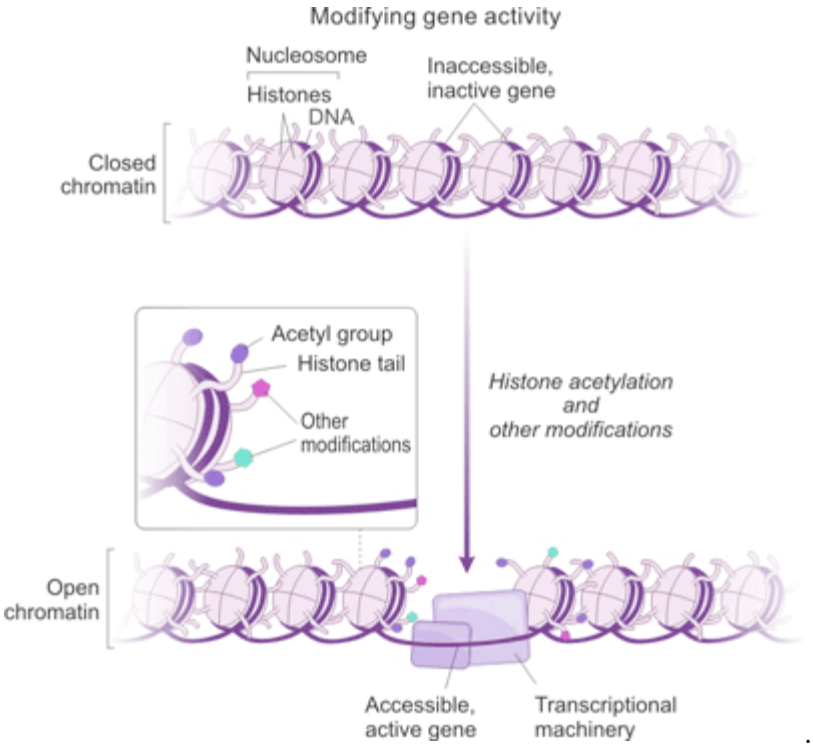


Figure 1.11 Histone modifications alter chromatin accessibilities
Histone post-translational modifications have a significant effect on altering the chromatin organization. These modifications permit the chromatin to be more open or closed to transcription factors. The histone N-termini are positively charged and modifications to this termini (acetylation for example) alter the electrostatic interactions resulting in a relaxed and open chromatin. In addition, histone N-termini modifications contribute in the recruitment of transcriptional complexes either transcriptional activation or repression which in turn affect the chromatin accessibility. Adapted from (CUSABIO and TECHNOLOGY, 2019)

The heterochromatin is subdivided into facultative and constitutive subentities (Saksouk et al., 2015) . The facultative heterochromatin is associated with H3K27me3 and H2AK119ub histone modifications and linked with genes required at specific developmental stages. Constitutive heterochromatin is correlated with permanently silenced genes and repeat regions of telomeres and centromeres, and it is associated with H3K9me2/3 histone modification.

Euchromatin represents transcriptionally active and relaxed chromatin. For example, the histone mark H3K4me3 is seen at the promoters of transcriptionally active genes (Guenther et al., 2007). The SETD1/MLL complex is engaged in trimethylation of the H3K4, which tends to localize this mark at histones

in proximity to CpG island (CGI) promoters (Deaton and Bird, 2011). The presence of the H3K4me mark induces RNA polymerase II (POL II) recruitment at gene promoters, attracting specific transcription factors to establish a positive feedback (Zhang et al., 2015b, Yokoyama et al., 2004). Another histone modification associated with euchromatin is H3K36me3, a mark that accumulates at the 3' boarder of the gene body (Pokholok et al., 2005). Moreover, the histone modifications H3K4me1, H3K4me2 and H3K27ac are associated with enhancer regulatory elements (Calo and Wysocka, 2013). Table 1.1 summarized mammalian major histone post translational modifications and their role in regulating the chromatin landscape.

Histone	Modification Residues	Modification Type	Modifying Enzyme	Associated with
H1	R54	Citrullination	PADI4	Cellular reprogramming, nucleosome binding
	K26	Methylation	EZH2	Transcriptional silencing
H2A	K5	Acetylation	Tip60, p300/CBP	Transcriptional activation
	Q105	Methylation	Nop1, Fibrillarin	Gene expression
	S1	Phosphorylation	MSK1	Mitosis, chromatin assembly, transcription repression
	T120	Phosphorylation	Bub1, VprBP	Mitosis, transcription repression
	T142	Phosphorylation	WSTF	Apoptosis, DNA repair
	S139	Phosphorylation	ATR, ATM, DNA-PK	DNA repair
	K13	Ubiquitylation	RNF168	DNA damage response
	K15	Ubiquitylation	RNF168	DNA damage response
	K63	Ubiquitylation	RNF8	DNA damage response
	K126	Biotinylation	Biotinidase	Cell proliferation, gene silencing, DNA damage response
	K127	Biotinylation	Biotinidase	Cell proliferation, gene silencing, DNA damage response
	K130	Biotinylation	Biotinidase	Cell proliferation, gene silencing, DNA damage response
H2B	K5	Acetylation	P300, ATF2	Transcriptional activation
	K12	Acetylation	P300/CBP, ATF2	Transcriptional activation
	K15	Acetylation	P300/CBP, ATF2	Transcriptional activation
	S36	Phosphorylation	AMPK	Transcriptional activation
	K120	Ubiquitylation	UBCH6	Meiosis
H3	K9	Acetylation	GCN5, SRC-1	Transcriptional activation, histone deposition
	K14	Acetylation	GCN5, PCAF, ESAI, Tip60, SRC-1, ELP3, HPA2, hTFIIIC90, TAF1,SAS2, SAS3, P300	Transcriptional activation, DNA repair, RNA Pol II and III transcription, histone deposition.
	K18	Acetylation	GCN5, P300/CBP	Transcriptional activation, DNA replication and repair
	K23	Acetylation	GCN5, P300/CBP, SAS3	Transcriptional activation, DNA repair
	K27	Acetylation	GCN5	Transcriptional activation
	K4	Methylation	Set1, Set7/9, MLL, ALL-1, ASH1	Transcriptional activation
	R2	Methylation	PRMT5, PRMT6	Transcriptional repression
	R8	Methylation	PRMT5, PRMT2/6	Transcriptional activation, Transcriptional repression
	K9	Methylation	SUV39h, CLR4, G9a, SETDB1, ASH1	Transcriptional silencing (me3), transcriptional repression
	R17, R26, R42	Methylation	CARM1	Transcriptional activation
	K27	Methylation	EZH2, G9a	Transcriptional silencing, chromosome X inactivation (me3)
	K36	Methylation	SET2	Transcriptional elongation
	K79	Methylation	DOT1	Transcriptional activation
	T3	Phosphorylation	Haspin/GSG2	Mitosis
	S10	Phosphorylation	MSK1, MSK2,IKK-α, SNF1	Mitosis, Meiosis, transcriptional activation
	T11	Phosphorylation	DLK/Zip	Mitosis
	S28	Phosphorylation	Aurora-B kinase, MSK1, MSK2	Mitosis
	K4	Biotinylation	Biotinidase	Gene expression
	K9	Biotinylation	Biotinidase	Gene expression

Table 1.1. A summary of major histone post translational modifications (mammalian)
Adapted from (Zhao and Garcia, 2015, Lawrence et al., 2016, Zhao et al., 2021, Technology, 2022)

Aberrant alternations of histone post-translational modifications have been linked to cancer (Audia and Campbell, 2016). These aberrant changes were observed at the genome-wide and at specific genes using ChIP-seq (chromatin immunoprecipitation, followed by high throughput next-generation sequencing) technology (Bannister and Kouzarides, 2011, Seligson et al., 2005). In addition, genes encoding for enzymes that add (writers) or remove (erasers) histone marks or proteins, acting as readers of such histone marks, were frequently mutated in cancer (Shen and Laird, 2013, French et al., 2001, French et al., 2008). These observations highlight the interplay between the epigenetic and genetic alterations in driving tumorigenesis.

Gene expression deregulation has also been observed for some of the aforementioned enzymes. For example, prostate cancer cells and gastric carcinomas overexpress the histone deacetylation enzymes HDAC1 and HDAC2, respectively, which correlate with lower levels of p21 expression (Halkidou et al., 2004, Song et al., 2005). In addition, histone demethylase enzymes KDM4C and KDM5B were overexpressed and associated with oncogenic potential and poor prognosis (Shigekawa et al., 2018, Young and Hendzel, 2013). In the CLL context, alterations of histone modification were observed in $CD19^{+}$ B cells demonstrated in global histone H3/H4 hypoacetylation and global histone H3K9 hypermethylation (Zhou et al., 2017). Moreover, increased HDAC expression in CLL cells was correlated with increased ZAP-70 and high CD44 expression, which, in turn, suggest more advanced disease and poor prognosis (Wang et al., 2011a). In addition, alterations of H3K4me3 and H3K4me1 epigenetic marks was found affect poised promoter status, which became the H3K27me3-associated repressed chromatin mark in CLL (Beekman et al., 2018). Collectively, histone PTM aberrant alterations lead to oncogenic potential through establishing a unique transcriptional program favouring the survival and proliferation of tumour cells.

1.4.5 Chromatin conformation

As mentioned above, histone post-translational modifications alter the chromatin conformation in proximity via the recruitment of chromatin modifying complexes. Therefore, depending on the histone modification, these changes allow for chromatin accessibly or condensation, which then enhance or preclude chromatin interactions, respectively. Chromatin's physical interactions between DNA regions were revealed in the last years via chromatin conformation capture (3C) and Hi-C techniques. These approaches provided new insights into how the chromatin conformational changes are essential for transcriptional regulation (Oluwadare et al., 2019). Topologically associated domains (TADs), representing significantly distinctive interactions between specific DNA regions of the three-dimensional (3D) nuclear organization were discovered using these techniques (Figure 1.12). TADs are involved in gene expression regulation because they are surrounded by boundary sequences that prevent interaction with neighbouring TADs (McArthur and Capra, 2021). TAD boundaries are recognized by the transcription factor CTCF, which acts as a guard involved in demarcating TAD boundaries. Interestingly, recent studies have demonstrated that CTCF inhibition disrupts transcription via enhancer blocking but not genomic compartmentalization, highlighting that CTCF is not the only player in TAD insulation (Nora et al., 2017).

Somatic alterations in TAD boundaries were reported in cancer and lead to oncogenic transformation. These mutations were mostly observed at CTCF-binding motifs, resulting in the activation of a proto-oncogene at the neighbouring TAD region (Kaiser and Semple, 2017). For example, in T-ALL, the disruption of CTCF-binding sites caused an upregulation of the neighbouring gene *TAL1*, a key oncogenic transcription factor that is overexpressed in most T-ALL patients, highlighting that *TAL1* silencing depends on the integrity of the neighbouring insulator (Hnisz et al., 2016). In CLL, CTCF binding was reported to be deregulated, and CTCF defective binding is linked with low gene expression of genes in the vicinity.

Moreover, CTCF is involved in enhancer rewiring, in which NFKB2 and FBXL15 genes proximal enhancers were reported to be bound by CTCF (Mallm et al., 2019).

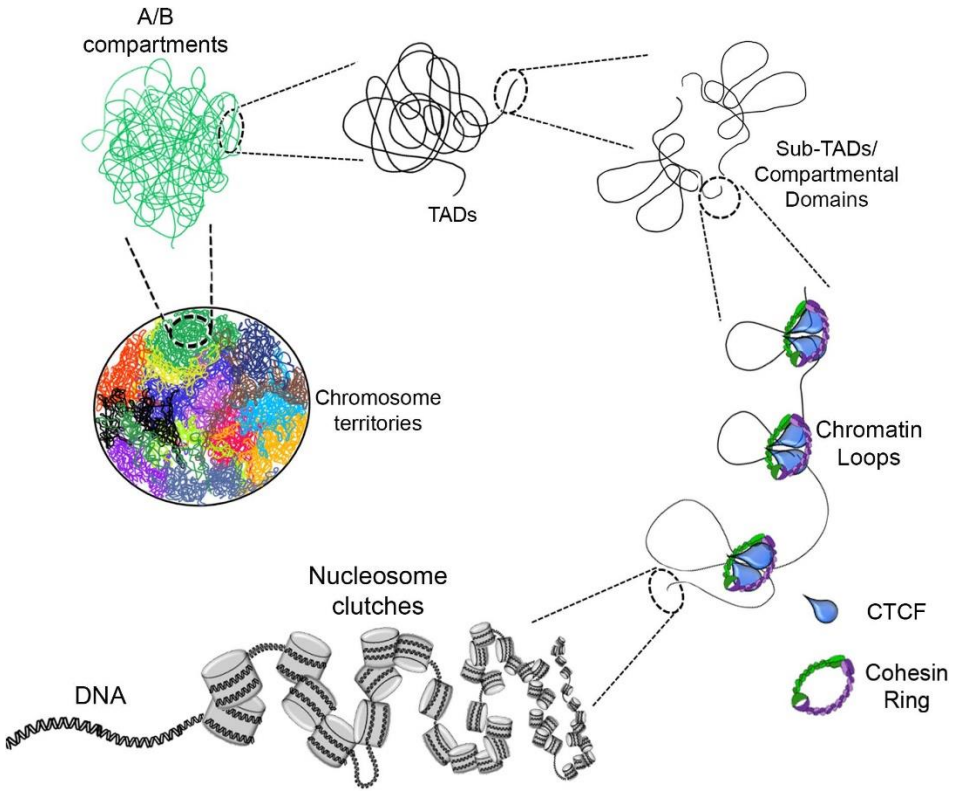


Figure 1.12 Eukaryotic chromatin organization
DNA interaction with histones to form nucleosome clutches. Chromatin loops which form a second level of compaction are formed by loop extrusion maintained by cohesion ring and CTCF. Formation of chromatin loops establish compartmental domains (sub-TADs and TADs) demarcating high level of interactions within these domains. A/B compartments can be defined by epigenetic marks, chromatin accessibility, gene content and nuclear localization. Finally, chromosome territories where chromosome localization is defined for each chromosome. Adapted from Magaña-Acosta, M., & Valadez-Graham, V. (2020).

1.4.6 Transcription Regulation in Eukaryotic

1.4.6.1 Cis-regulatory elements (CREs)

1.4.6.1.1 Promoters

Promoters are defined as cis-regulatory elements that participate in gene transcription regulation. Promoter regions are located upstream of the gene transcription site (TSS), where they are targeted to be bound by the protein initiating complex (PIC), a large protein complex comprising of RNA polymerase II and transcription factors that form the transcriptional machinery necessary for initiation of transcription. Eukaryotic promoters can be classified into three types based on transcription initiation pattern, present motifs and sequence composition as well as chromatin arrangement profile (Haberle and Stark, 2018).

First, promoters with sharp initiating patterns are associated with unorganized nucleosome positioning, the presence of TATA-box and initiator (Inr) motifs and display the active histone modifications H3K4me3 and H3K27ac. These promoters are commonly seen as active in terminally differentiated cells. Second, promoters with scattered initiation patterns have organized nucleosome-depleted regions and nucleosome positioning, are enriched in CpG islands (CGIs) and marked with histone modifications H3K4me3 and H3K27ac. These types of promoters are commonly observed in housekeeping genes. Third, a form of promoter is similar to the second type but different in terms of histone modification profile and associated genes. In this type of promoter, bivalent histone modifications of active (H3K4me3 and H3K27ac) and repressed (H3K27me3) marks are observed. These bivalent marks help create a ‘poised’ promoter status, which is involved in priming activation in the correct context and silencing otherwise. Notably, genes associated with this type are involved in key developmental transcription factors (Haberle and Stark, 2018).

1.4.6.1.2 Enhancers

Enhancers are positive transcriptional modular regulatory distal elements controlling the activation of gene expression. Enhancer elements play essential roles in maintaining tissue-specific gene expression. These regulatory elements are several hundred bp in length and are characterised by low nucleosome occupancy, creating an accessible chromatin region (Spitz and Furlong, 2012). Enhancer sequences contain motifs that are targeted by transcription factors, which consequently recruit cofactors. They are located at a distance ranging from approximately 200 bp up to 1 MB away from genes' TSS. Enhancers positively regulate transcription activation through looping the DNA, subsequently allowing enhancer-bound factors to interact with PIC at promoters. This enhancer looping feature was first discovered in the regulation of the β-globin gene, which is controlled by the locus control region (LCR) that is located away from the promoter (Carter et al., 2002). Enhancer elements can be found at exons of genes, at intra- and intergenic sites and introns (Birnbaum et al., 2012). Enhancer elements can positively regulate transcription, regardless of their positioning with respect to the target gene. Moreover, multiple enhancer elements can regulate the transcription of single or a group of genes (Smith and Shilatifard, 2014).

Enhancer elements are capable of positively regulating target genes through non-coding RNA transcripts described as enhancer RNA (eRNA) (Kim et al., 2010, De Santa et al., 2010). These eRNAs are classified into 2D-eRNA and 1D-eRNA. The 2D-eRNAs are short bidirectional, unspliced, non-polyadenylated and function in *cis*. The 1D-eRNAs are long unidirectional, spliced, polyadenylated and function in *trans* (De Santa et al., 2010). Enhancer aberrant function was identified as a key process in cancer pathogenesis (Herz et al., 2014). For example, in colorectal tumours, the oncogene c-MYC increased gene expression was regulated by an active enhancer that transcribes eRNA termed *CCAT1* (colon cancer-associated transcript 1) (McCleland et al., 2016). Ott, C. J. et al. showed that CLL core regulatory circuits consist of large enhancer clusters named super enhancers that are governed by the transcription factor PAX5. In

addition, these CLL enhancer-based core regulatory circuits can be pharmacologically blocked by BET bromodomain inhibition (Ott et al., 2018). Thus, this research highlights a novel therapeutic approach by taking advantage of enhancer specificity context.

1.4.6.1.3 Silencers and Insulators

Silencers are *cis*-regulatory distal elements that function in the negative regulation of gene expression, thereby opposing enhancer function. Silencers act in a similar manner to that of enhancers in which DNA is subjected to looping in order to interact with a specific promoter through cofactors to repress transcription. Moreover, silencers provide motifs that are targeted by regulatory factors known as 'transcription repressors'. Silencers could potentially repress transcription through two mechanisms. The first mechanism occurs via the recruitment of repression complexes, such as the PRC2 complex, and histone-modification enzymes, including as HDACs, KDMs and DNMTs, leading to PIC disassembly and chromatin state modifications at active promoters. The second mechanism occurs through silencing active enhancers by recruiting repressive TF that occludes activating TF factors at enhancers in the vicinity (Segert et al., 2021, Kolovos et al., 2012).

Insulators are another *cis*-regulatory distal element responsible for maintaining the target gene specificity of enhancers by preventing unspecific interactions between promoters and enhancers or silencers (Kolovos et al., 2012). Therefore, insulators act as important boundaries because their disruption results in unspecific and off-target promoter-enhancer interactions, as seen *in vivo* and *in vitro* (Hnisz et al., 2016). In addition, insulators can help prevent unspecific spreading of heterochromatin marks into euchromatin-containing transcriptionally active genes (Barkess and West, 2012). In TADs, the CTCF protein targets the activated mammalian insulator elements, where it interacts with cohesion and other proteins to form complexes. These complexes then act as mediators between insulator elements to translocate distant

DNA into the vicinity through DNA looping, thus creating domains referred to as 'insulated neighbourhoods' (Hnisz et al., 2016).

1.4.6.2 Trans-regulatory elements (TREs)

1.4.6.2.1 Transcription Factors

Transcription factors (TFs) are proteins with the capability of DNA binding at specific sequencing (motifs), and they play an essential role in gene expression regulation. TFs, in general, bind to proximal (promoter) or distal (enhancer) regulatory elements. TFs can also bind to DNA indirectly through interacting with other TFs regardless of their own DNA-binding domain. For example, PU.1 and GATA-1 TFs both bind to DNA directly, and both interact via the PU.1 ETS domain and GATA-1 C-terminal domain, leading to indirect PU.1 /DNA binding (Burda et al., 2010). Therefore, transcription factor interactions help in linking factors for specific chromatin state preservation as well as the recruitment of proteins involved in transcriptional activation or repression. In this way, these interactions define a cell's transcriptional program, which maintains its survival and maintenance.

The activity of transcription factor is dynamic and capable of responding to specific stimuli, such as genotoxicity, cytokines, growth factors or infection. For example, in a genotoxic stress context, the MAPK (mitogen-activated protein kinase) pathway is triggered by activated growth factor receptors or by DNA damage, which consequently activate transcription factors Activator protein 1 (AP-1). AP1 represents a TF family consisting of heterodimeric complexes including proteins of the Jun (c-Jun, JunB, JunD), Fos (c-Fos, FosB, Fra1, Fra2) and CREB/ATF (ATF1, ATF2) members (Christmann and Kaina, 2013). Moreover, NF-κB, a dimeric transcription factor, consisting of the proteins RelA (p65), RelB, c-Rel, p50/p105 (NF-κB1) as well as p52/p100 (NF-κB2), and is activated following genotoxic stress induced by anticancer drugs and ionizing radiation, leading to an induction of the inflammatory response in cells (Brasier, 2006, Christmann and Kaina, 2013).

Transcription factor function is altered in cancer (Bushweller, 2019). The first evidence showing the involvement of TF in driving tumorigenesis came from the fusion proteins observed in a variety of leukaemias, such as acute myeloid leukaemia 1 (AML1)–ETO, promyelocytic leukaemia protein (PML)–retinoic acid receptor α (RARα), TEL–AML1 and mixed-lineage leukaemia (MLL) fusions (Look, 1997). Moreover, alterations in TFs through fusions affect DNA repair genes, thereby establishing an environment that promotes genomic instability, tumour cell fitness and clonal heterogeneity (Alcalay et al., 2003). Consistent with this notion, CLL tumours cells were found to have increased TF-binding motifs associated with NFAT, FOX and TCF/LEF when compared to normal B cells (Beekman et al., 2018). Moreover, the transcription factor FOXO3a, often inactivated in CLL, is involved in regulation of both spontaneous and chemokine-induced B cell survival (Ticchioni et al., 2007). Finally, E2A, a TF and regulator of B-cell survival is overexpressed in CLL cells, and its inhibition correlates with spontaneous apoptosis and reduced CLL cells viability (Kardava et al., 2011).

1.4.6.2.2 Transcription Regulation by Long non-coding RNAs (lncRNAs)

Long non-coding RNAs (lncRNAs) are described as long RNA transcripts of at least 200 bp in length and do not encode for functional proteins. In general, lncRNAs are known to have similar transcription and maturation to that of mRNAs because they are transcribed by Pol II and 5'-end m^7G caps and 3'-end poly(A) tails, respectively. However, lncRNAs are considered to have fewer exons and inefficient splicing compared to mRNAs (Statello et al., 2021). Transcriptional regulation by lncRNAs is carried out at proximate and distal gene loci. Therefore, lncRNAs are involved in transcriptional regulation and chromatin remodelling either in *cis* and *trans.* Polycomb repressive complex 2 (PRC2) chromatin binding and spreading have been shown to be initiated by lnRNAs in *cis* and *trans.* For example, the lncRNA *ANRIL* is transcribed to facilitate PRC1 and PRC2 binding at neighbouring *CDKN2A* and *CDKN2B* genes and distant genes via Alu motifs, thereby keeping their expression under control (Yap et al., 2010, Holdt et al., 2013).

HOX transcript antisense RNA (HOTAIR) is a trans-acting lncRNA that recruits chromatin-modifying complexes to inactivate the distal *HOXD* gene expression. On the other hand, lncRNAs can promote gene expression via chromatin modifiers recruitment as it was observed for the lncRNA *HOTTIP*, which anchors the histone methyltransferase complex WDR5–myeloid/lymphoid or mixed-lineage leukaemia to gene TSS to facilitate active gene expression (Wang et al., 2011b, Luo et al., 2019).

Long non-coding RNAs (lncRNAs) were presumed to have functions in maintaining genome integrity. Homology-directed repair (HDR) and non-homologous end joining (NHEJ) DNA repair pathways can be initiated by ncRNAs. At sites of DNA lesions damage-induced long non-coding RNAs are transcribed by Pol II and involved in the efficient recruitment of DNA repair machinery (Statello et al., 2021, Michelini et al., 2017). As lncRNAs are involved in transcriptional regulation genome integrity, it is not surprising to observe that they are often deregulated in cancer. In fact, several key tumour suppressors and oncogenic genes, such as p53 and MYC, were regulated by lncRNAs (Statello et al., 2021). Notably, the lncRNA MALAT1, a well-known transcript that is linked to cancer progression, was significantly upregulated in CLL patients (Ahmadi et al., 2018). Moreover, lncRNAs profiling in early-stage CLL identified a set of lncRNAs whose deregulated expression is associated with clinical prognostic markers such as IGHV status and cytogenetic abnormalities (Ronchetti et al., 2016).

1.4.6.2.3 Transcriptional Initiation

The process of initiating transcription of genes encoding for proteins begins with the assembly of Pol II initiation complex (PIC) with the help of general transcription factors (GTFs) such as TFIIB, -D, -E, -F and -H that help in promoter recognition. Thus, the PIC complex contains Pol II, mediator and GTFs. The accessible promoter region is targeted for binding by TBP associated factors (TAFS), TFIID, and TATA box-binding protein (TBP) forming a complex with TFIIB to assemble the essential initiation complex (Kostrewa et al., 2009, Liu et al., 2013b). Transcription is initiated once PIC is established at promoters. It should be

noted that PIC is required for bidirectional transcription seen at enhancers in mammalian organisms (Schier and Taatjes, 2020).

PIC factors can recognize promoter DNA sequences. Hence, the promoter regions represent a platform that guides the early steps of transcription initiation. Promoters with TATA box motifs are recognized by TBP to initiate the PIC complex. However, a fraction of promoters do not have TATA box sequences, and these promoters were thought to be recognized by TAF members of the PIC (Basehoar et al., 2004). Upon binding to a DNA double-strand minor groove containing a promoter, TBP curves the DNA and wraps it around Pol II, highlighting a role for TBP other than DNA sequence recognition (Sainsbury et al., 2015). TFIIB is involved in assisting TBP-binding and DNA-bending capabilities by binding upstream and downstream of recognition elements. Upon formation of the core complex, Pol II and TFIIF are assembled in the complex, followed by TFIIE and TFIIH recruitment, resulting in complete PIC complex formation (Figure 1.13).

The formation of a heterodimer binding to Pol II near downstream DNA is carried out by the TFIIF member of the PIC complex. Non-specific contact of Pol II with DNA in the vicinity is prevented through TFIIB and TFIIF interactions via their winged-helix domain (Čabart et al., 2011). A transcriptional bubble is formed when double-strand DNA is unwound via TFIIE and TFIIH members of the PIC complex. In this process, TFIIE interacts with Pol II and functions as a docking site for TFIIH, which, in turn, behaves as a DNA double-strand opener forming a single-stranded DNA in an ATP-dependent manner (Grünberg et al., 2012). Finally, Pol II starts transcribing an mRNA, and the process of elongation is set to begin.

1.4.6.2.4 Transcriptional Elongation

The transcriptional elongation process is known to have two phases—an initial elongation phase and a productive elongation phase. In the initial elongation phase, RNA Pol II is moved from the promoter to perform the elongation phase. In this process, RNA Pol II is set to pause after transcribing 20–60

nucleotides of nascent RNA transcript to create 'promoter-proximal pausing', a phenomenon observed in approximately 30–60% of higher eukaryotic protein-coding genes (Kwak and Lis, 2013, Zhou et al., 2012). It is thought that transcriptional pausing is required to help the assembly of the capping complex required for the addition of a 5' cap on the nascent mRNA transcript (Pei and Shuman, 2002). Therefore, the pause and release of Pol II for elongation continuation is a critical stage in transcriptional regulation.

The regulation of promoter-proximal pausing is carried out via the transcription elongation members DSIF, NELF and P-TEFb. DSIF is known to induce transcriptional pausing via interactions with the NELF. Thus, the two factors—DSIF and NELF—bind to RNA Pol II and the nascent RNA transcript, causing transcription inhibition (Yamaguchi et al., 2013). In contrast, P-TEFb has been reported to induce transcription (Marshall and Price, 1995). The P-TEFb has two subunits—CDK9 and Cyclin T—and is involved in the phosphorylation of both NELF E and DSIF Spt5 subunits and the serine-2 residue of the carboxyl-terminal domain of RNA polymerase II. These phosphorylation events lead to RNA Pol II escaping from its paused state into a productive elongation state (Kwak and Lis, 2013) (Figure 1.13).

The productive elongation state is defined as the movement of RNA Pol II from an early paused state into a productive state, leading to the synthesis of a full-length transcript of a gene. Such a process requires factors to overcome Pol II pausing and then proceeding elongations. The elongation factor TFIIS is required to release arrested Pol II and maintain transcriptional fidelity during elongation. The elongins complex is also engaged in productive elongation of transcription by keeping RNA Pol II in an active state and by reducing pausing. During the elongation process, RNA Pol II may encounter blocking lesions that impede transcription, leading to transcription machinery stalling and activation of transcription-coupled repair (TCR). Cockayne Syndrome B protein (CSB) is required in TCR, and it has been demonstrated that CSB is a member of the transcriptional machinery. CSB is involved in RNA Pol II stabilization and direction upon DNA damage. Finally, the ELL-EAF family is also involved in transcriptional elongation by stimulating the catalytic transcriptional rate through reducing RNA Pol II pausing along the DNA template (Sharma, 2016).

After RNA Pol II successfully approaches the end of the gene being transcribed, the elongation process enters transcriptional termination.

1.4.6.2.5 Transcriptional Termination

Transcriptional termination occurs downstream of the 3' untranslated region end and involves three stages: cleavage, polyadenylation and termination of the newly synthesized RNA transcript (Richard and Manley, 2009). The 3'-end of nascent RNA establishes final mRNA maturation, which is coupled with transcription and splicing. Cleavage and polyadenylation take place upon recognition and binding to AAUAAA sequences by the CPSF complex composed of CPSF-30, CPSF-73, CPSF-100, CPSF-160 and Fip1. In addition, GU-rich sequences are targeted for binding by the cleavage stimulation factor (CstF) complex, which includes CstF-50, CstF-77 and CstF-64 subunits. These binding events occur at approximately 10–30 nucleotides downstream from AAUAAA sequences and upstream of U- or GU-rich sequences, respectively (Figure 1.13).

Two models were proposed to describe the termination mechanism allosteric and torpedo (Richard and Manley, 2009). In the former model, Poly A-enriched sites transcription causes a conformational change in the elongation complex due to dissociation and/or association of elongation factors of termination factors, respectively (Logan et al., 1987). In the later model, a rapid 3' RNA degradation rate at the poly A-enriched site via cleavage establishes active exonucleases, and this process causes RNA Pol II eviction (Connelly and Manley, 1988). The studies have suggested that transcriptional termination occurs by a combination of both proposed models. For example, it was observed that at β-globin gene mRNA termination processing, poly A recognition primed Pol II for termination, and exonucleolytic activity preceded Pol II DNA template eviction (West et al., 2008).

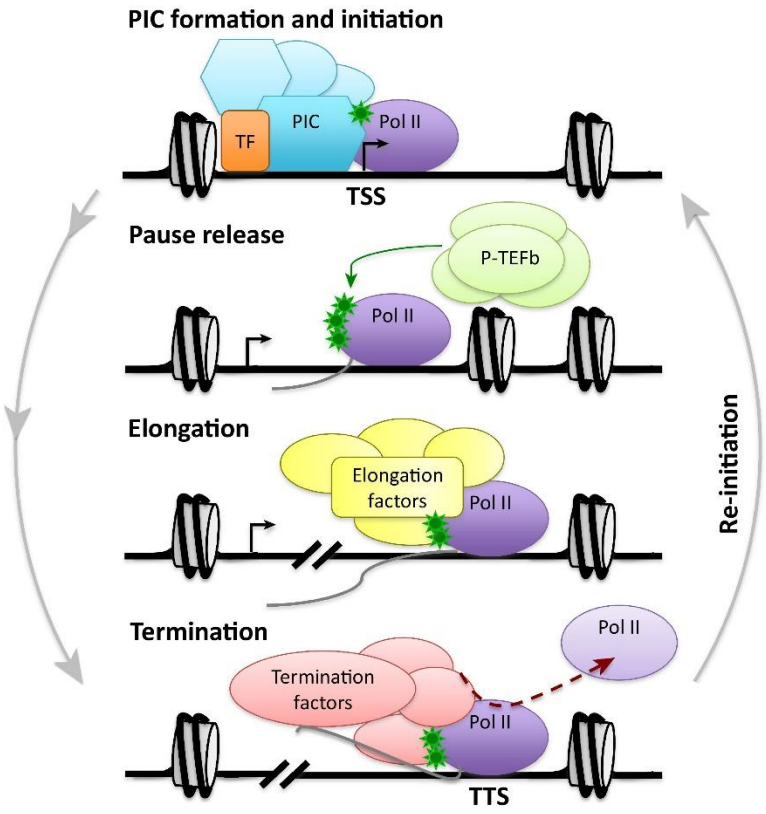


Figure 1.13 Eukaryotic transcription steps
A simplified illustration of eukaryotic transcription steps. The transcription begins at the TSS region by setting up the PIC, Pol II, and GTFs. Next, initiation of mRNA transcription occurs upon the creation of phosphodiester bonds by Pol II. Subsequently, after reaching about 8 nucleotides of the mRNA, Pol II often pauses and requires an additional activator. P-TEFb is responsible of Pol II escaping the pausing state and complete promoter release by phosphorylation of serine 2 of Pol II CTD together with factors. This step is required for Pol II to be able to generate a complete mRNA transcript. Transcription is terminated by mRNA cleavage and polyadenylation leading to Pol II release from the DNA. Adapted from Gates, L. A., Foulds, C. E., & O'Malley, B. W. (2017).

1.4.7 DNA methylation

DNA methylation is an epigenetic mechanism in which methyl groups are deposited on the DNA template, most commonly at CpG islands and intergenic regions. In this process, the cytosine position at carbon 5 (C5-methylcytosine, 5mC) is subjected to methylation by DNA methyltransferase enzymes. These enzymes catalyze the addition of a methylation residue from S-adenosyl-L-methionine (SAM) to C5 of cytosine. This reaction is carried out in mammalian cells by DNMT3a, DNMT3b and DNMT1 enzymes. The methylation enzymes DNMT3a and DNMT3b function in the establishment of DNA methylation and, therefore, are

termed a *de novo* DNA methyltransferases. On the other hand, DNMT1 functions in maintaining DNA methylation through cell cycle. DNA methylation can be read by proteins such as the MBD, UHRF and zinc-finger family of proteins. Such DNA modifications are also subjected to removal by ten-eleven translocation enzymes (TET1, TET2 and TET3) through the enzymatic oxidation of 5mC to 5hmC (5-hydroxymethylcytosine). DNA methylation, in general, is associated with the silencing of transcription through interfering with TF-binding sites. Alterations in DNA methylations and aberrant writer and eraser enzyme activity have been found to be closely associated with cancer (Greenberg and Bourc'his, 2019, Kinney and Pradhan, 2013).

Over the last decade, an extensive body of CLL research has suggested the link between DNA methylation and CLL pathogenesis. It was reported that IGHV UM cases were associated with a higher level of DNA methylation affecting PRC2 downstream genes in common with memory B cells (Oakes and Martin-Subero, 2018, Smith et al., 2015). Moreover, efforts have been made to classify CLL based on DNA methylation patterns into three groups: naive B cell-like, memory B cell-like and intermediate CLL (Kulis et al., 2012) (Figure 1.14). In addition, DNA methylation heterogeneity was found to be associated with a high subclonal mutational burden in a fraction of CLL cases harbouring IGHV UM status and other adverse prognostic clinical markers (Oakes et al., 2014). Furthermore, aberrant DNA methylation patterns are involved in the formation of intraclonal heterogeneity and correlate with poor clinical prognosis (Landau et al., 2014). Using a set of 18 loci methylation maturation score (MMS), Oakes and colleagues reported a CLL epigenetic signature that classified CLL cases into three programs termed high-, intermediate- and low-programmed CLL (Oakes et al., 2016).

Using DNA methylation high-throughput profiling, DNA methylation signatures were identified in CLL cases from 3 UK clinical trials. These methylation patterns were able to further divide IGHV mutated cases into clinically relevant groups, and established the memory-like m-CLL is to be an unbiased biomarker of prolonged survival for CLL patients treated with conventional chemotherapy (Wojdacz et al., 2019).

Finally, CLL DNA methylation and gene expression studies at the single-cell level revealed an increased CLL epimutation rate associated with high transcriptional dysregulation that was not seen in bulk CLL sequencing. Moreover, integration of the single-cell data allowed the construction of a CLL lineage tree, which revealed early and long branching of CLL cells in comparison to normal B-cells development (Gaiti et al., 2019). Although these studies demonstrated that epigenetic patterns are correlated with overall clinical disease course, correlation between these epigenetic patterns with disease-specific recurrent mutations remains to be elucidated.

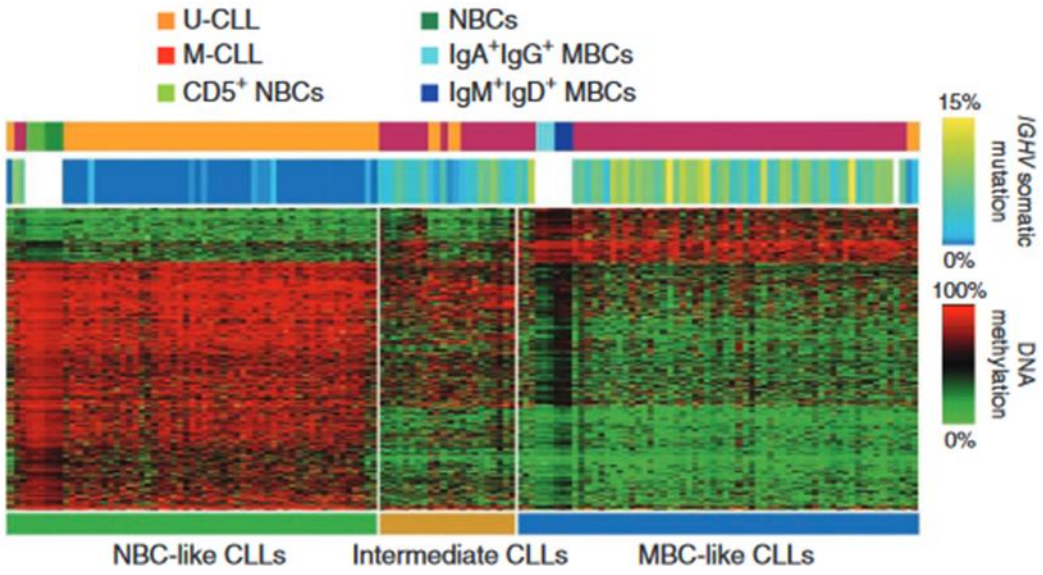


Figure 1.14 DNA methylation patterns are correlated with overall CLL clinical subgroups
DNA methylation profiling of CLL cells clustered CLL cells based on the IGHV gene status. In addition, these methylations clusters are of close resemblance to that of MBC-like CLLs in the case of U-CLLs whereas CD5+ NBCs and NBCs in the case of M-CLL. Therefore, CLL can be classified into, based on methylome, NBC-like CLLs, an MBC-like CLLs or CLL with an intermediate methylation profile. Abbreviations: (NBC) naive B cells, (MBC) memory B cells. Adapted from Kulis, M et al. (2012).

1.5 Cross-talk between DNA damage response genes and epigenetic regulation

The epigenetic inactivation of DDR genes is frequently observed in tumours without a link of mutation inheritance (Curtin, 2012). In addition, epigenetic silencing of DDR genes in cancer has been noted in several DDR pathways, including NER, BER and other DNA damage response mechanisms (Lahtz and Pfeifer, 2011). Epigenetic inactivation is carried out through gene promoter hypermethylation of key DDR genes. In fact, an increase in mutation burden and genomic instability can be caused by epigenetic inactivation of DDR genes such as FANCF, MLH1, BRCA1 and MGMT (Toyota and Suzuki, 2010). The MGMT gene, which participates in DNA direct repair, is commonly silenced epigenetically in cancers, including colon cancer, gastric carcinoma and glioblastoma (Esteller et al., 1999, Herfarth et al., 1999, Oue et al., 2001). The expression profile of the MLH1 gene, which is an MMR gene, is decreased and is correlated with promoter hyper methylation in sporadic colon cancer (Herman et al., 1998, Kane et al., 1997). Moreover, the MLH1 gene promoter has abnormal methylation patterns in gastric cancer and sporadic endometrial carcinoma (Fleisher et al., 1999, Esteller et al., 1998). Epigenetic silencing of KU70 and KU80, members of NHEJ, is associated with breast, lung and colorectal cancers (Lee et al., 2007, Willems et al., 2008). Epigenetic inactivation of the ataxia-telangiectasia-mutated (ATM) gene is reported in head and neck squamous cell carcinomas and is correlated with decreased overall survival (Ai et al., 2004).

1.5.1 Defective DNA damage response establishes a dependency on the remaining functional pathways

In cancer cells, the acquisition of loss of function mutations in more than one DDR pathway during their evolution creates a situation where the remaining pathways are in high demand or dependency (Jackson and Bartek, 2009). Early oncogenic events (replication stress) that lead to defective cell proliferation are involved in the initiation of DDR through a series of multistep activations of ATM and ATR signallings. This network of DDR is characterised by the active phosphorylation of p53, CHK2, H2AX and ATM (Bartkova et

al., 2010, Bartkova et al., 2005, Gorgoulis et al., 2005). This method of DDR activation in normal cells creates a barrier to uncontrolled cell growth. In tumour cells, however, this barrier no longer functions, allowing cells to have more genomic instability as well as an increased demand on the remaining functional DDR pathways to cope with DNA damage (Halazonetis et al., 2008, O'Connor, 2015). In cancer cells, frequent mutations in DDR genes significantly influence the overall prognosis of disease. For example, mutations in the *ATM* gene, a member of the HR pathway, result in the functional loss of the protein and tend to correlate with an aggressive disease course, whereas alteration of the *RNASEH2B* gene, a player in the RER pathway, caused by 13q14 deletions, demonstrates good overall prognosis in chronic lymphocytic leukaemia (Hallek, 2019). However, in other cancers, the situation is different because *RNASEH2B* depletion results in a progressive phenotype in intestinal carcinomas (Aden et al., 2019).

Synthetic lethality, first described in Drosophila in 1946 (DOBZHANSKY, 1946), is observed when the simultaneous disruption of two genes leads to a loss of cell viability, whereas single disruption in either gene does not affect cell viability (O'Neil et al., 2017). The remaining DDR pathway the cancer cell uses to survive and proliferate provides an opportunity to design an inhibitor to that particular pathway and, hence, induce cell death, also referred to as synthetic lethality, caused by the build-up of DNA damage that the cell cannot repair (Ashworth, 2008, Curtin, 2012) (Figure 1.15).

The use of Poly(ADP-ribose) polymerase inhibition (PARP) inhibitors in ovarian cancers with BRCA mutations provided clinical evidence regarding the efficacy of applying the synthetic lethality mechanism in a cancer context (Ashworth, 2008, Lord and Ashworth, 2017). Another example of synthetic lethality is the disruption of POLQ, an error-prone DNA polymerase, in BRCA1 and BRCA2 mutant cancers (Huang et al., 2020). POLQ is involved in an alternative non-homologous end-joining pathway, and its disruption affects cell viability on its own or paired with PARP inhibitors in a BRAC1 and BRCA2 mutant cancer background (Ceccaldi et al., 2015, Kent et al., 2015, Mateos-Gomez et al., 2015). The inhibition of ATR *in*

vivo and *in vitro* in a CLL-specific genetic context (TP53 and ATM defects) resulted in the induction of synthetic lethality, providing an additional example of how synthetic lethality is important in anticancer targeted therapy (Kwok et al., 2016). Our lab has also shown that defects in ribonuclease H2 complex, resulted in sensitivity toward PARP inhibitors. This increased sensitivity is caused by the accumulation of embedded rNMPs due to a lack of efficient RER in RNASEH2B-defective cells, which leads to an abundance of PARP-trapping lesions that interfere with DNA replication and consequently cause PARP-inhibitor-mediated cytotoxicity (Zimmermann et al., 2018). Several research groups have demonstrated that MTAP-null cancer cells are more susceptible to PRMT5 disruption (Kryukov et al., 2016, Mavrakis et al., 2016). Epigenetic cancer dependencies were observed in tumours harbouring BRG1/SMARCA4 mutations. In fact, defects in BRG1/SMARCA4 chromatin remodelling complex, resulted in an induction of cell cycle arrest, senescence and upregulation of global H3K9me3, suggesting a synthetic lethal interaction between SMARCA2 and SNARCA4 (Hoffman et al., 2014). In all instances, using the synthetic lethality strategy allows the sparing of normal cells and preferential killing of tumour cells. Taken together, synthetic lethal approaches provide a significant patient benefit compared to conventional cancer chemotherapeutic agents.

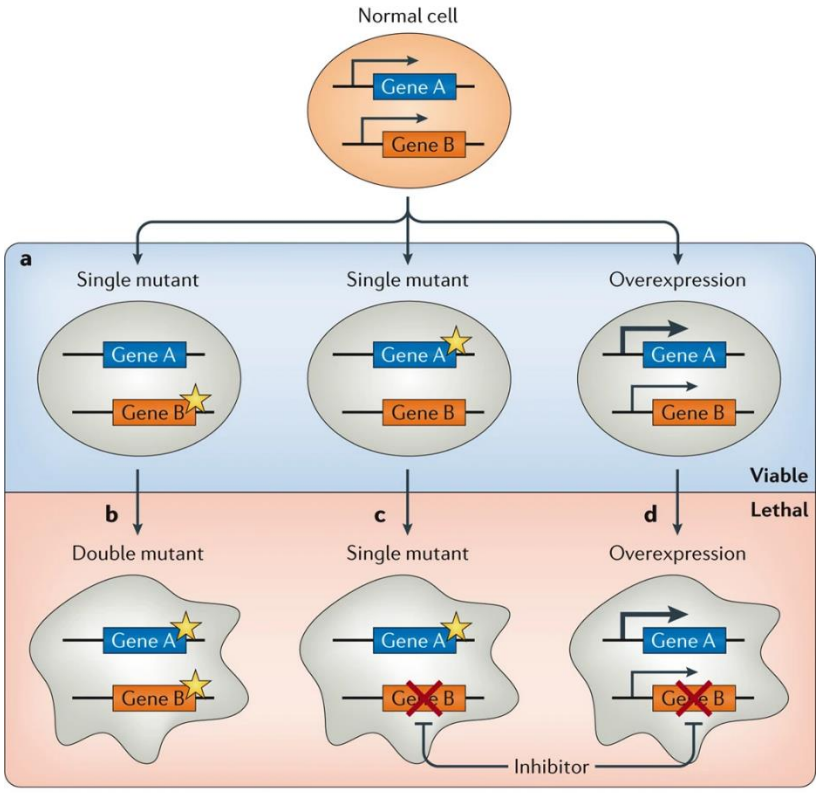


Figure 1.15 The concept of synthetic lethality in cancer
Cancer cells that have lost function in key genes (due to mutations or overexpression) tend to rely on other alternative genes. Synthetic lethality approaches exploit these dependencies to preferentially kill tumour cells and, at same time, spare normal cells. Adapted from O'Neil, N.J. et al. (2017).

Chronic lymphocytic leukaemia (CLL) is a very enlightening model of disease because its recurrent mutations of DDR genes significantly influence the disease outcome. CLL cells are capable of survival and proliferation in spite of alteration in genes encoding for proteins involved in genomic stability maintenance (*ATM* and *RNASEH2B*). Such mutations in important DNA repair pathways suggest the utilization of alternative secondary pathways that facilitate the survival of CLL cells. CLL cells carrying mutations in *ATM* or *RNASEH2B* are heavily dependent on alternative pathways specific to these alterations thereby providing an opportunity for novel therapeutic interventions using synthetic lethality approaches. Recent studies have shown the increased resistance level of CLL cells toward targeted therapy. For example, CLL cells were reported to resist the BCL-2 inhibitor venetoclax (Blombery et al.,

2019, Tausch et al., 2019). Moreover, CLL cells were known to develop a resistance to the BTK inhibitor ibrutinib and this process is characterised by a progressive disease and a high probability of Richter transformation (Kanagal-Shamanna et al., 2019, Ahn et al., 2017). Collectively, resistance to conventional targeted therapy brings the need toward finding novel therapeutic interventions. The use of PARP inhibitor Olaparib in ATM defective lymphoid tumors resulted in an induction of cell death thereby providing an example of targeting alternative pathway in cancer cells using synthetic approaches (Weston et al., 2010).

Therefore, finding mutation specific addictive pathways would pave the way for novel dimension of therapeutic strategies and for the development of a new layer of personalized medicine. Moreover, as *ATM* and *RNASEH2B* are known to influence the chromatin landscape, the consequences of such mutations at the epigenetic and genome-wide level remain to be investigated. Therefore, exploring the impact of these mutations in CLL could identify transcriptional and epigenetic dependencies that can be potentially targeted therapeutically.

1.6 Specific aims and objectives

DDR components ATM and RNASEH2B have been found to be involved in CLL pathogenesis. ATM and RNASEH2B are involved in maintaining genomic integrity through HRR and RER, respectively. The epigenomic landscape is poorly understood in the context of these frequent aberrations. The functional loss of ATM and RNase H2 in CLL is likely to be associated with the upregulation of alternative pathways that support tumour survival.

Previous studies of CLL reported an extensive epigenetic profiling of CLL cases using whole-genome mapping of DNA methylation, histone modifications, chromatin accessibility and conformation as well as gene expression. However, most of these studies did not report specific epigenetic profiles associated with recurrent CLL mutations such as *ATM* and *RNASEH2B*. Understanding the specific epigenomic landscape of ATM and RNase H2 deficient CLLs would add new dimensions of CLL pathogenesis and potentially identify transcriptional addiction CLL cell use to evade apoptosis

The work presented in this thesis aims to gain further insight into the epigenetic landscape associated with recurrent CLL DDR gene alterations and then identify cellular dependencies associated with such alterations. This aim is achieved by studying the impact of losing these genes in well-known CLL cell lines that mimic the tumour cells observed in patients. Therefore, the specific aims of this thesis were to:

1. Characterise the specific epigenetic landscape of CLL frequently altered DDR genes *ATM and RNASEH2B*.

To address this aim, I performed comprehensive epigenetic profiling using chromatin accessibility, histone modifications (H3K4me3, H3K4me1, H3K27ac) and gene expression in CLL isogenic cell lines (MEC1 and CII) containing *ATM*-knockdown. These aims are investigated in the third chapter of my thesis.

To characterise the epigenetic landscape of *RNASEH2B* loss, I performed chromatin profiling using chromatin accessibility, histone modifications (H3K4me3, H3K27ac), histone variant (H2A.Z), RNA Pol II, DNA RNA duplex formation (R-loops) and gene expression using CLL isogenic cell lines with heterozygous and homozygous *RNASEH2B* knock out. These aims are investigated in the forth chapter of my thesis.

2. Identify epigenetic and transcriptional dependencies associated with specific *ATM* or *RNASEH2B* loss.

Through integrative bioinformatic analysis of ATAC-Seq, ChIP-Seq and RNA-Seq, I investigated the genome-wide impact of *ATM* or *RNASEH2B* loss on CLL cells. I demonstrated the correlation level in the form of heatmaps of each data set and identified genes upregulated as a result of *ATM* or *RNASEH2B* loss. I then identified potential dependencies cells may rely on to maintain survival. Finally, I was able to construct transcriptional factor networks demonstrating the *ATM* or *RNASEH2B* specific regulatory networks driving the expression of CLL cells.

3. Functional validation of identified transcriptional dependencies obtained from our integrative analysis.

I performed an attempt using Dox-mediated inducible system to inhibit an epigenetic enzyme (KDM5B), the upregulation of which an effect are observed in CLL cells lacking the ATM protein which according to our results represent a potential dependency.

To validate the potential identified transcriptional dependencies identified in cells with RNASEH2B loss, our lab utilized genome-wide CRISPR-Cas9 knockout screens. I identified a set of synthetic lethal gene hits. Using this approach allowed me to confirm and validate the identified potential gene dependencies as well as the identification of other dependencies.

CHAPTER 2

METHODS

Table 2.1 Instruments

Instrument	Manufacturer
DynaMag™-2 magnetic rack	Thermo Fisher Scientific
MiniMACS™ column	Miltenyi Biotec
Qubit 3.0 fluorometer	Thermo Fisher Scientific
Mx3000P real-time PCR system	Agilent
ABI GeneAmp 9700 PCR - thermal cycler	Applied Biosystems
Bioruptor® Pico sonication device	Diagenode Diagnostics
2100 Bioanalyzer instrument	Agilent
iMark™ microplate absorbance reader	Bio-Rad
NextSeq 500/550 high-output kit v2.5 (150 cycles)	Illumina
NextSeq 500/550 high-output kit v2 (75 cycles)	Illumina
NextSeq 550 system	Illumina
Eppendorf Mastercycler Nexus PCR cycler	Eppendorf
G.Box Chemi 16 gel doc system UV transilluminator	Syngene
Spectrophotometer	GENEFLOW

Table 2.2 Reagents and suppliers

Product	Manufacturer
2100 high sensitivity DNA kit	Agilent
AMPure® XP beads	Beckman Coulter
cOmplete™ protease inhibitor cocktail	Roche
Ethanol	VWR
Ethidium bromide	Thermo Fisher Scientific
Ethylene-bis(oxyethylenenitrilo)tetraacetic acid (EGTA)	Sigma Aldrich
Ethylenedinitrilotetraacetic acid (EDTA)	Sigma Aldrich
Formaldehyde, 16%	Thermo Fisher Scientific
Glycerol	Sigma Aldrich
HEPES	Thermo Fisher Scientific
Glycine	Thermo Fisher Scientific
Hyper Prep Kit (Illumina)	KAPA Biosystems
Illumina library quantification kit	KAPA Biosystems
KAPA HyperPure beads	KAPA Biosystems
Lithium chloride	Sigma Aldrich
NEBNext® Library Quant Kit for Illumina	New England Biolabs
MACS® buffer	Miltenyi Biotec
Marvel dried skimmed milk powder	Premier Foods
MinElute® PCR purification kit	Qiagen
MiniMACS™column	Miltenyi Biotec

NP-40	Sigma Aldrich
Magna ChIP™ Protein A+G magnetic beads	Sigma Aldrich
Penicillin/streptomycin, 1%	Thermo Fisher Scientific
Dulbecco's phosphate-buffered saline	Sigma-Aldrich
Proteinase K	Sigma Aldrich
Invitrogen™ PureLink™ RNase A (20 mg/mL)	Invitrogen™
Purple gel loading buffer, 6X	New England Biolabs
SuperScript II reverse transcriptase kit	Thermo Fisher Scientific
Sodium deoxycholate	Sigma-Aldrich
Sodium bicarbonate ($NaHCO_3$)	Sigma-Aldrich
Sodium dodecyl sulphate (SDS)	Sigma-Aldrich
Sodium acetate (NaAc)	Sigma-Aldrich
Sodium chloride (NaCl)	Sigma-Aldrich
Sodium orthovanadate (Na3VO4)	Sigma-Aldrich
Sodium β-glycerophosphate(Na2 β-glycerophosphate)	Sigma-Aldrich
Sodium fluoride (NaF)	Sigma-Aldrich
SensiFAST™ SYBR® Lo-ROX Kit	Bioline
PowerUp™ SYBR™ Green Master Mix	Applied Biosystems
TE, 1X	Thermo Fisher Scientific
Tetramethylethylenediamine (TEMED)	Sigma-Aldrich
Tris base	Fisher Scientific
Triton™ X-100	Sigma-Aldrich
Trypan Blue Solution, 0.4%	Thermo Fisher Scientific
TWEEN® 20	Sigma-Aldrich
Whatman® 3MM blotting paper	Sigma-Aldrich
SDS Solution, molecular biology grade (10% w/v)	Promega
EDTA, 0.5M, pH 8.0 ethylenediaminetetraacetic acid	Promega
Acrylamide/bis-acrylamide, 40% solution	Sigma-Aldrich
NEBNext® Ultra™ II Directional RNA library prep kit for Illumina®	New England Biolabs
Monarch® Total RNA miniprep kit	New England Biolabs
NEBNext multiplex oligos for Illumina	New England Biolabs
NEBNext® rRNA depletion kit	New England Biolabs
Nextera DNA library prep kit	Illumina Cat #FC-121-1030
Digitonin	Promega
Nuclease-free H2O	Promega
NEBNext high-fidelity 2x PCR master mix	New England Biolabs
RPMI-1640 medium	Sigma-Aldrich
Dulbecco's modified Eagle medium	Sigma-Aldrich
Foetal bovine serum	Sigma-Aldrich
Lymphoprep™	STEMCELL Technologies
XbaI	NEB Cat # R0145S
EcoRI	NEB Cat # R0101S
HindIII	NEB Cat # R0104S
BsrGI	NEB Cat # R0575S
SspI	NEB Cat # R0132S

NEBbuffer 2	NEB Cat # B7002S
BSA	NEB Cat # B9000S
RNase H	NEB Cat # M0297S
Spermidine	Sigma Aldrich
phenol/chloroform/isoamyl alcohol (25:24:1)	Thermo Fisher Scientific
1x DPBS	Thermo Fisher Scientific

Table 2.3 Oligonucleotides

Name	Forward (5' -> 3')	Reverse (5' -> 3')
qPCR primers – gene expression (human)		
KDM5B	AATGGTGCGGCTCTGAAAGA	TAACACTGGCACACGTCCTC
MT1H	GCTCCTGCAAGTGCAAAAAG	CAGCAGCTGCACTTCTCTGA
MT1F	TCCTGCAAGTGCAAAGAGTG	AAAGGTTGTCCTGGCATCAG
E2F1	GCTGGACCACCTGATGAATATC	TCTGCAATGCTACGAAGGTCCTG
E2F2	TGGCAACTTTAAGGAGCAGACAG	GGGCACAGGTAGACTTCGATGG
CSNK2A1	AGAGGCAATGGAGCACCCCT	ATATTGGCGCTGCTGACGGG
BCL-2	TCACTGGCCACTGAGGAGCT	ATGCGGAATTGCCCAGGGAC
BRCA-1	GCCCTTCACCAACATGCCCA	GCATCTGGCTGCACAACCAC
KLF4	ACACCTGCGAACCCACACAG	TGTAAGGCGAGGTGGTCCGA
HCK	CTATGTCGCCCGCGTTGACT	TCACGGTATCTCCCTGCCGA
SATB2	AGGCCAAAACCTCGACACCG	CGGAGCAGTTCACACAGCCA
CDC42BPA	GCATTTTCTGGCCACCATCTGC	TGAGGTGGGACCAGCCGTAA
CORO2A	TTCAACACCAACGGCAGCCT	CCACCTGCCGGTTGTTCCAT
GAPDH	GAGTCAACGGATTTGGTCGT	GACAAGCTTCCCGTTCTCAG
qPCR primers – ATAC library validation (human)		
TBP (promoter region)	CTGGCGGAAGTGACATTATCAA	CCCGACCTCACTGAACCC
ACTB (gene body region)	GCAATGATCTGAGGAGGGAAGGG	AGCTGTCACATCCAGGGTCCTCA
B2M (gene body region)	TTTAGCACTGAACGAACATCTCAAG	TTATAGGATGCTAGGACAGCAGGAC
Chr18 (inaccessible region)	AGGTCCCAGGACATATCCATT	GTTCAAATTGTGTTTTGTGGTTA
qPCR primers – ATAC library validation (mouse)		
TBP (promoter region)	TGCAGTCAAGAGCGCAACTG	CACCGCTACCGGACTCGAT
ACTB (gene body region)	CAAGACAAGATGGTGAATGGTGAG	GTAAGCTAAGCATCCTTAGCTTGG
Chr1 (inaccessible region)	TGCTCCACAGTGTCCATGTACA	AGCAATTTCATGGGTGAGAGAAG
qPCR primers – ChIP library validation (human)		
TBP	CTGGCGGAAGTGACATTATCAA	CCCGACCTCACTGAACCC
PAX5 HS7	GCGGATCATCACTCATGAAA	CAAGAACGACGCTGAGGATT
IVL	GCCGTGCTTTGGAGTTCTTA	CCTCTGCTGCTGCCACTT
Chr18	AGGTCCCAGGACATATCCATT	GTTCAAATTGTGTTTTGTGGTTA
qPCR primers – DRIP library validation (human)		
RPL13A	AGGTGCCTTGCTCACAGAGT	GGTTGCATTGCCCTCATTAC
Chr18	AGGTCCCAGGACATATCCATT	GTTCAAATTGTGTTTTGTGGTTA

Table 2.4 Antibodies

Antibody	Manufacturer	Catalogue	Experimental Conditions
ChIP-seq			
H3K27ac	Diagenode	C15410196	1–2 µg per assay
H3K4me3	Diagenode	C15410003	1–2 µg per assay
H3K4me1	Diagenode	C15410194	1–2 µg per assay
H3K36me3	Diagenode	C15410192	1–2 µg per assay
H3K9me3	Diagenode	C15410193	1–2 µg per assay
H3K27me3	Diagenode	C15410195	1–2 µg per assay
Anti-KDM5B / PLU1 / Jarid1B	Abcam	ab181089	3 µg per assay
Histone H2A.Z	Abcam	ab4174	1–3 µg per assay
RNA polymerase II	Abcam	ab26721	1–3 µg per assay
Gamma H2A.X	Abcam	ab81299	1–3 µg per assay
Histone H3 (tri methyl K27)	Abcam	ab195477	1–3 µg per assay
Western blotting			
Total ATM	Santa Cruz Biotechnology	53173	1:1000 at 4 °C
Anti-phospho-ATM (Ser1981)	Millipore, USA	DR1002	1:1000 at 4 °C
Anti-β-Actin	Sigma-Aldrich	A2228	1:100000 at 4 °C
β-tubulin	Santa Cruz Biotechnology	sc-365791	1:2000 at 4 °C
KDM5B/ JARID1B	Cell Signaling	3273S	1:8000 at 4 °C
Anti-KDM5B / PLU1 / Jarid1B	Abcam	ab181089	1:8000 at 4 °C
RNASEH2B			
MCL-1			
S9.6	Sigma-Aldrich	MABE1095	10 µg per assay
Polyclonal swine anti-rabbit immunoglobulins/HRP	Dako, Denmark	P0217	1:3000, 1 hour at RT
Polyclonal goat anti-mouse immunoglobulins/HRP	Dako, Denmark	P0447	1:5000, 1 hour at RT

Table 2.5 Buffer compositions

Buffer	Composition
UTB buffer	9 M Urea 50 mM TRIS 150 mM β-mercaptoethanol
Western blot gel running buffer	0.1 M Tris/Bicine 0.1% SDS
Polyacrylamide gel (6%)	100 mM 1M Tris/Bicine 7.5% Acrylamide/bis-acrylamide 0.1% SDS 0.2% (v/v) TEMED

	0.05% APS
Transfer buffer	386 mM glycine 47.8 mM Tris 20% (v/v) methanol
TBST buffer (pH 7.6)	20 mM Tris 136.8 mM NaCl 0.1% (v/v) TWEEN
ChIP buffer A	10 mM Hepes pH 8.0 10 mM EDTA pH 8.0 0.5 mM EGTA pH 8.0 0.25% TritonX 100 1:100 (v/v) cOmplete™ protease inhibitor cocktail
ChIP buffer B	10 mM Hepes pH 8.0 200 mM NaCl 1 mM EDTA pH 8.0 0.5 mM EGTA pH 8.0 0.01% TritonX 100 1:100 (v/v) cOmplete™ protease inhibitor cocktail
IP buffer I	25 mM Tris pH 8.0 150 mM NaCl 2 mM EDTA pH 8.0 1% TritonX 100 0.5% SDS 1:100 (v/v) cOmplete™ protease inhibitor cocktail
IP buffer II	25 mM Tris pH 8.0 150 mM NaCl 2 mM EDTA pH 8.0 1% TritonX100 7.5% glycerol 1:100 (v/v) cOmplete™ protease inhibitor cocktail
Wash buffer 1	20 mM Tris pH 8.0 150 mM NaCl 2 mM EDTA pH 8.0 1% TritonX100 0.1% SDS
Wash buffer 2	20 mM Tris pH 8.0 500 mM NaCl 2 mM EDTA pH 8.0 1% TritonX100 0.1% SDS
LiCl buffer	10 mM Tris pH 8.0 250 mM LiCl 1 mM EDTA pH 8.0 0.5% NP40 0.5% Na- deoxycholate
TE/NaCl buffer	10 mM Tris pH 8.0

	50 mM NaCl 1 mM EDTA pH 8.0
Elution buffer (made fresh)	100 mM NaHCO3 1% SDS
1 x binding buffer (DRIP-seq)	10 mM NaPO4 pH 7 140 mM NaCl 0.05% Triton X-100
Elution buffer (DRIP-seq)	50 mM Tris pH 8 10 mM EDTA 0.5% SDS

Table 2.6 Specialist software used for bioinformatics analysis

Software	Version
BAGEL	2
BEDtools	2.27.1
Bowtie2	2.3.5.1
Cytoscape	3.8.2
DeepTools	3.3.2
featureCounts	2.0.1
HiSat2	2.2.1
Homer	4.11
Intervene	0.6.5
JACKS	0.2
Java	11.0.13
Java TreeView	1.2.0
MACS2	2.2.6
Mageck	0.5.9.2
Picard	2.25.5
R	4.1.0
R package: ChIPpeakAnno	3.26.2
R package: ChipSeeker	1.28.3
R package: clusterProfiler	4.0.2
R package: countToFPKM	1
R package: DESEQ2	1.32.0
R package: EdgeR	3.34.0
R package: EnhancedVolcano	1.10.0
R package: FGSEA	1.18.0
R package: GGplot2	3.3.5
R package: MAGeCKFlute	1.14.0
R package: Trackplot	1.3.5
R package: VennDiagram	1.6.20

SAMtools	1.9
Snakemake	6.4.1
Ubuntu	18.04

Cell line culture

CLL cell lines were cultured in RPMI-1640 medium augmented with 10% heat-inactivated foetal calf serum and 1% penicillin/streptomycin at 37 °C and 5% CO_2. The cells were maintained at a density of 0.5–2 x10^6 cells/ml prior to cell harvesting. The success of the experiment relied upon accurate cell counting along with cell viability of at least 90%. To count the cells, 100 µL was taken from the cell suspension and added to a 1.5 ml Eppendorf tube containing 400 µL Trypan blue stain used to stain dead cells; the final dilution of this mixture was 1:5. Next, 50 µL was applied to the haematocytometer, and using a 10 X objective lens, live and dead cells were counted in four sets of 16 squares. The average number of counted cells was multiplied by a dilution factor of 5 and 10^4 to obtain the cell number in ml. The total number of live cells only was divided by the total cell number (live and dead). Cell viability was approximately 90% prior to proceeding with any experiment.

CLL cell lines

The CII cell line was obtained from a CLL patient (47-year-old female) who had lymphadenopathy, hepatosplenomegaly, lymphocytosis and a high number of lymphocytes in the bone marrow. This cell line was generated by infecting patient's mononuclear cells with the of Epstein-Barr virus (Karande et al., 1980). This cell line displays typical mature B cell profile markers (CD5+, CD19+, CD20+ and CD23+). The cell line was characterised by high expression of ZAP-70, low CD38 and TCL1 expression in addition to trisomy 12. Furthermore, the CII cell line shows unmutated IGHV status (Lanemo Myhrinder et al., 2013). The MEC1 cell line was obtained from a CLL patient (58-year-old male) who was diagnosed with CLL at the stage of prolymphocytic transformation. The MEC1 cell line was generated by spontaneous outgrowth of

patient tumour B lymphocytes. This MEC1 cell line shows rescidual levels of CD38 and TCL1 but no CD5 expression. Moreover, MEC1 cells reveals mature B-cell profile markers (CD19+, CD20+ and CD23+). In addition, the MEC1 cell line has a loss of function mutation in TP53 that produces a truncation in the N-terminus, which, in turn, results in a smaller protein size (47 kDa in contrast to wild type p53 53 kDa). MEC1 reveals mutated IGHV status (Stacchini et al., 1999). To enable the investigation of the ATM loss associated cellular phenotype, our laboratory has generated a stable ATM shRNA KD isogeneic CLL cell lines and used western blotting to confirm the complete absence of ATM proteins in MEC1 and CII cell lines (Kwok et al., 2016). To study the impact of RNASEH2B loss on CLL cells, our laboratory has produced an isogenic CLL cell line (MEC1) with and without RNASEH2B CRSIPR knock out including biallelic and monoallelic KO of the RNASEH2B locus. Western blots and RNA-seq both confirmed the successful CRSIPR KO.

Western blotting

Whole-cell extracts were generated by lyses in UTB buffer (9 M Urea, 50 mM Tris, 150 mM b-mercaptoethanol) following by sonication and centrifugation. Protein concentration was determined using a Bradford assay according to manufacturers' instructions (Bio-Rad). Proteins were separated by 6–10% SDS-PAGE, transferred to a nitrocellulose membrane and incubated with primary antibody overnight. On the next day, the blots were washed with (TBST buffer ph 7.6) followed by incubation with HRP-linked secondary antibody for 1 h at room temperature. Next, Blots were subjected to three washes (15 minutes each) in TBST buffer. The antibody binding was detected using ECL western blotting substrate (Millipore) and autoradiography. The antibodies against β-Actin and β-tubulin were used as loading controls. For buffers used in western blotting, see Table 2.5. For antibody dilutions and incubation times, see Table 2.4

Treatment of CLL cells with proteasome inhibitor

Selected CLL cell lines (MEC1 and CII) with ATM wild type (WT) status confirmed by western blotting were cultured in RPMI-1640 media supplemented with 10% FCS and 1% penicillin/streptomycin at 37 °C and 5% CO_2. Cells were treated with 10 µM proteasome inhibitor MGT132 and incubated for 2, 6 and 16 h. Control cells (treated with DMSO) were incubated in the same manner as for treated cells. After each time point, cells were subjected to protein extraction, and protein lysates were stored at -80 °C for western blotting. As the positive control, MCL-1 antibody was used. JJN3 or HeLa cell lysates available in the laboratory were used as the positive control for KDM5B.

Determination of gene expression by quantitative polymerase chain reaction (qPCR)

Total cellular RNA extraction was done with a Monarch Total RNA miniprep kit (New England Biolabs (UK)) by following the manufacturer's instructions for cultured mammalian cells. Extracted RNA samples were subjected to DNase I treatment to digest genomic DNA. Surfaces were wiped down and cleaned with RNaseZap (Invitrogen, Lithuania) just before RNA extraction to minimize any source of contamination. RNA concentration and purity were measured with a NanoPhotometer® P 300 (IMPLEN). The cDNA synthesis reaction was performed using SuperScriptTM II Reverse Transcriptase (Invitrogen, California, USA), briefly, 10 nM dNTP (Thermo Scientific, Lithuania), 500 µg/mL Random Primers (Promega, USA) and 5 µg extracted RNA were mixed in a total volume of 20 µL. The newly synthesized cDNA samples were diluted 1:5 with nuclease-free water, and their concentration and purity were measured using a nanophotometer and then stored on ice or frozen at -20 °C. The qPCR reaction consisted of the following components: 1x SensiFAST SYBR Lo-ROX (Applied Biosystems, Lithuania), 0.4 µM of both forward and reverse primers, approximately 100 ng cDNA and nuclease-free water in a final volume of 20 µL. Each reaction was performed in triplicate in 96-well semi-skirted optical PCR plates sealed with MicroAmpTM Optical Adhesive Film (Applied Biosystems, USA) and briefly centrifuged to collect the component at the

bottom. qPCR was performed using a Stratagene Mx3005P (Agilent Technologies) with 2-step thermal cycling conditions that changed for each primer (Table 2.7). After qPCR, triplicate cycle threshold (Ct) values were analyzed for fold changes in the gene expression of KDM5B normalized to GAPDH (indigenous control), using the comparative Ct method (2-ΔΔCT) method (Livak and Schmittgen, 2001). Primer specificities were estimated by the dissociation curves generated.

Table 2.7 qPCR thermal cycling conditions.

Segment	Step	Cycles	Temperature (°C)	Temperature (°C)
1	Polymerase Activation	1	95	120
2	Denaturation	40	95	5
	Annealing	40	60–64	30
3	Dissociation Curve	1	95 55 95	60 30 30

RNA-seq

RNA samples were extracted from $3x10^6$ cells using a Monarch Total RNA miniprep kit (New England Biolabs (UK)), and the samples was then treated with DNase I to remove genomic DNA. Extracted RNAs were later submitted to quality control (QC), and a minimum of 9 RINs was used as the input for library preparation (Figure 2.1 A). Total RNAs (1 µg) were subjected to ribosomal depletion using a NEBNext® Poly(A) mRNA Magnetic Isolation Kit (New England Biolabs (UK)). The isolated mRNAs were then used as the input for making the RNA-seq libraries with a NEBNext Ultra II Directional RNA Library Prep Kit for Illumina (New England Biolabs (UK)). The library's yields was measured using a Qubit 4 fluorometer and checked for average size distribution with a Bioanalyzer (Figure 2.1 B); then, the concentration in nM for each library was calculated. Libraries were normalized and pooled at a concentration of 20 nM and submitted for paired-end NGS sequencing using NextSeq 500/550 sequencing kit on NextSeq platform (Illumina, USA).

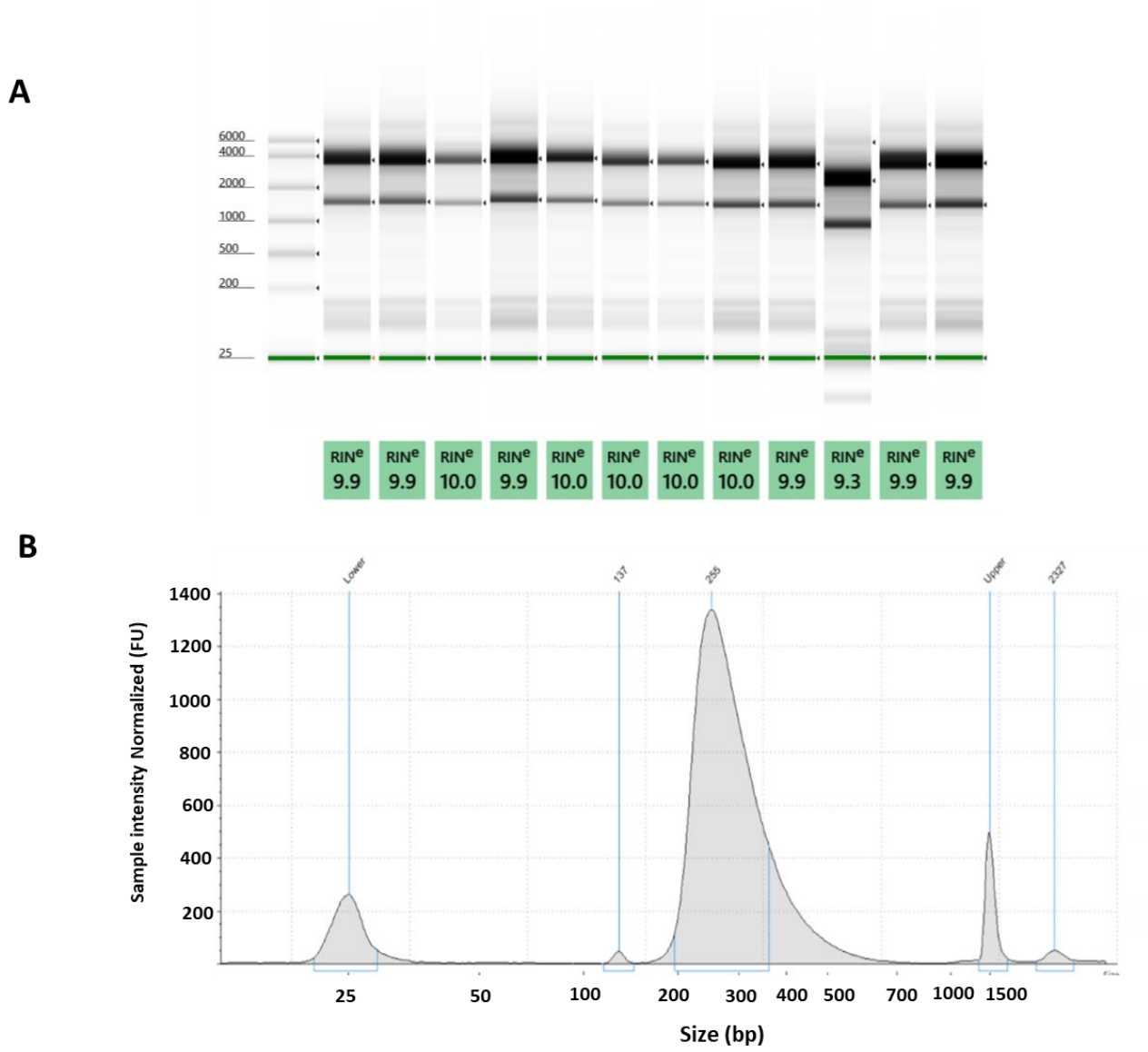


Figure 2.1 Overall QC of RNA-seq libraries
(A) Bioanalyzer QC results showing the RIN (RNA integrity number) for each RNA sample. (B) Final pool of RNA-seq libraries showing the expected size distribution of 300 bp.

Assay for transposase-accessible chromatin using sequencing (ATAC-seq)

The following components were added to the pelleted ($1x10^5$ cells) while it was set on ice: 12.5 µL 2X TD buffer, 2 µL Tn5 transposase enzyme, 0.25 µL digitonin and 10.25 µL nuclease-free water to achieve a total volume of 25 µL per tube. Each tube was subjected to gentle pipetting in order to resuspend the nuclei in

the transposition reaction mix. Next, transposition reaction tubes were incubated at 37 °C for 30 min in a thermal shaker (900 rpm). Subsequently, transposition reaction tubes were purified using a Qiagen MiniElute Kit. The transposed DNA was eluted in 20 µL. The purified tagged DNA was then subjected to PCR amplification, with barcodes being added. The PCR reaction was monitored by qPCR to prevent GC and size-biased PCR amplification. In this step, 5 µL was taken from the sample and was subjected to a qPCR assay for 20 cycles. Next, the optimum number of required cycles was determined by subtracting the bassline fluorescence (R) signal from saturation stage and then divide the resulted number by three then locate the cycle that is close to the fluorescence signal. After PCR reactions were complete, the products were purified with Ampure XP beads. To validate the ATAC libraries before submission for sequencing, qPCR was performed to check the enrichment of open regions (TBP) against gene-body (B2M) and closed (Chr18) regions (Figure 2.2).

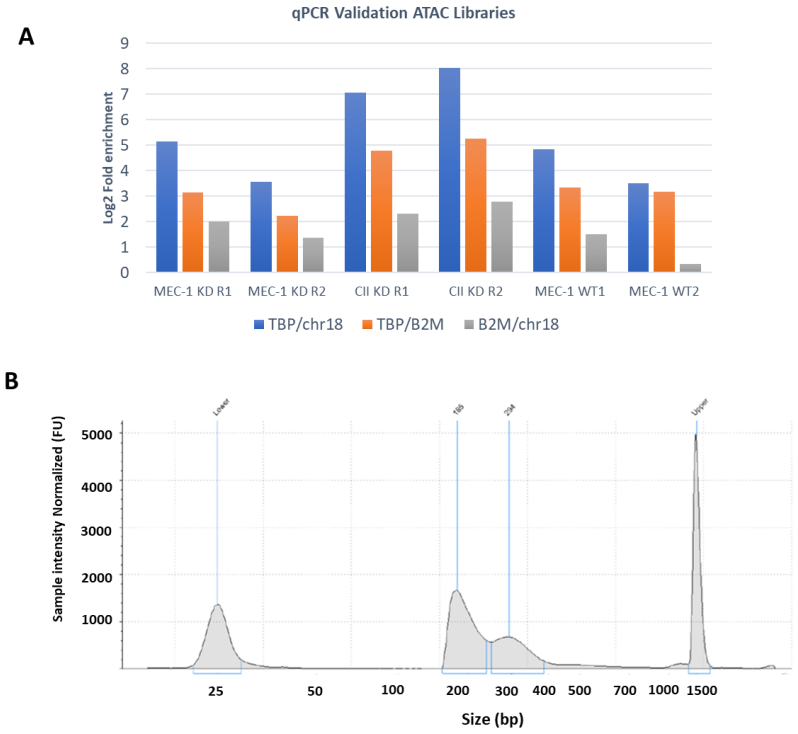


Figure 2.2 ATAC-seq libraries QC before sequencing
(A) Bar plots showing the log2 fold enrichment of accessible locus (TBP) over negative locus (Chr18) and the enrichment of gene body (B2M) over negative locus (Chr18). (B) Bioanalyzer track of a typical ATAC-seq library.

Chromatin immunoprecipitation (ChIP)

Chromatin preparation

Chromatin preparation was performed on 25 x 10^6 cells resuspended in phosphate-buffered saline (PBS). Sixteen per cent formaldehyde was added to produce a final concentration of 1%, and the combination was left at room temperature for 10 minutes on a roller. Next, 2M glycine was added and incubated for 5 minutes to stop the formaldehyde cross-linking effect, and the cells were then washed two times with ice-cold PBS. The cells then were resuspended in Buffer A (10 mM Hepes, 10 mM EDTA, 0.5 mM EGTA, 0.25% Triton, PIC) and kept on ice for 10 min and then centrifuged at 500 x g at 4 °C and resuspended in Buffer B (10 mM, 200 mM NaCl, 1 mM, EDTA, 0.5 mM EGTA, 0.01% Triton x 100) and kept on ice for 10 min. Next, the cells were centrifuged at 500 x g at 4 °C, and then 2 x 10^6 cells per each sonication tube were aliquoted in IP Buffer I (25 mM Tris-HCl, 150 mM NaCl, 2 mM EDTA, 1% Triton x 100, 10% SDS, PIC). The aliquoted cells were subjected to sonication using a Bioruptor Pico for 15 cycles of 30 seconds ON and 30 seconds OFF. Subsequently, the sonicated tubes were centrifuged at 16000 x g at 4 °C, and the supernatant was taken and added to two volumes of IP Buffer II (25 mM Tris-HCl, 150 mM NaCl, 2 mM EDTA, 1% Triton x 100, 7.5% Glycerol, PIC). Samples were taken from the sheared chromatin and subjected to reverse cross-linking by incubation of 10% chromatin with 1 ul of RNaseA (20 mg/ml) at 37^c thermoshaker for 30 minutes followed by incubation overnight at 65^c with 9 ul 10% SDS and 2 ul Proteinase K (50 mg/ml). Next day, samples were purified using Ampure XP beads with the use of 1.9X volume. To assess the chromatin shearing efficiency gel electrophoresis with 1.5% agarose gel was undertaken. Remaining tubes containing chromatin were snap-frozen in liquid nitrogen and then stored at -80 °C for Immunoprecipitation.

Immunoprecipitation

Immunoprecipitation was performed with 2 x 10^6 cells using Magna ChIP™ Protein A+G was resuspended in citrate-phosphate buffer, pH 5.0. One to two µg of antibodies were added to the beads blocked with 0.5 BSA and kept rotating at 4 °C for two hours. After incubation, the beads were washed with citrate-phosphate buffer to remove unbound antibodies. Chromatin was then added to the bead-bound antibody

mix and kept rotating at 4 °C overnight, 10% chromatin was saved and kept as an input control. On the following day, beads were washed with 1 x Wash Buffer 1, 2 x Wash Buffer 2, 1 x Wash with LiCl buffer, and 2 x Wash with TE/NaCl Buffer. Elution was performed by incubating beads with a freshly made Elution Buffer. Reverse cross-linking was carried out using NaCl (5 M) and Proteinase K (50 mg/ml) with an overnight incubation at 65 °C. Reversed cross-linked DNA was then purified using AmpureXP beads. To validate the ChIP experiment before library preparation, qPCR was performed using primers that served as positive and negative controls. Successful ChIP samples were then processed for NGS library preparation.

DNA/RNA immunoprecipitation (DRIP)

Two replicates of MEC1 CLL cells (4 million cells per replicate) were washed in 5 ml of 1 x DPBS and resuspended in TE buffer. One hundred µl of 10% SDS and 5 ul of 20 mg/ml proteinase K were added to the resuspended cells, and the tubes were inverted gently to allow the solution to become viscous. Samples were incubated at 37 °C overnight. On the next day, genomic DNA was extracted using phenol/chloroform/isoamyl alcohol (25:24:1), and the top aqueous phase (extracted DNA) was precipitated by adding a 1/10 volume of 3 M NaOAc, pH 5.2 and 2.5 volumes of 100% (vol/vol) ethanol. The precipitated DNA was then washed twice with 80% (vol/vol) ethanol and allowed to air-dry. The DNA pellet was then resuspended in 150 µl of TE buffer for an hour on ice. Fifty to one hundred µl of resuspended DNA was then digested with a cocktail of restriction enzymes (Table 2.1) using the supplier's instructions. The digestion reaction was Incubated overnight in a 37 °C. After overnight incubation, the viscosity of the mixture have disappeared. DNA was purified from the digestion reaction using phenol/chloroform/isoamyl alcohol (25:24:1) extraction; the DNA was precipitated as mentioned above, and the extracted DNA was measured with a nanodrop—the average yield was approximately 1.5–4 µg/µl.

Table 2.7 DRIP digestion reaction.

Component	Amount (µL)	Final concentration
DNA	100	
NEBbuffer 2 (supplied with restriction enzymes)	30	1 x
BSA	3	1 x
Restriction enzymes XbaI (1.5 ul), EcoRI (1.5 ul), HindIII (1.5 ul), BsrGI (3 ul), SspI (6 ul)	13.5 Repeat after 1 hour (SspI 3 ul)	30 U each
Water	37	
Spermidine (last to add)	3	0.5 x

For specificity control, 8 µg of digested RNA:DNA duplex were incubated overnight at 37 °C with 4 µL RNase H (5,000 units/ml), 10 µl Rnase H Reaction Buffer(10X), and nuclease-free water. On the following day, DNA was extracted and precipitated as previously mentioned and proceeded to s9.6 immunoprecipitation step. All samples, including specificity control ones, were diluted in 500 µl 1 x binding buffer. Ten µg S9.6 antibody was added and incubated at 4 °C with rotation overnight. On the next day, 20 µl of Magna ChIP beads was added and incubated for at least 2 hours at 4 °C with rotation. The beads were washed three times using 1 x binding buffer (while in tubes on magnets on ice), resuspended in 250 µl elution buffer + 3.1 µL Proteinase K 50 mg/ml and then incubated at 55 °C for 45 min with RPM 1000. The tubes were assembled on magnets, and once the solution became clear, 250 µl was taken from each tube and added to DNase-free tubes. DNA was subjected to phenol/chloroform/isoamyl alcohol extraction (as mentioned previously) and resuspended in 100 µl nuclease-free water. For qPCR validation, each sample was diluted 1:10. qPCR was performed using RPL13A (positive-control locus) and chr18 (negative-control locus).

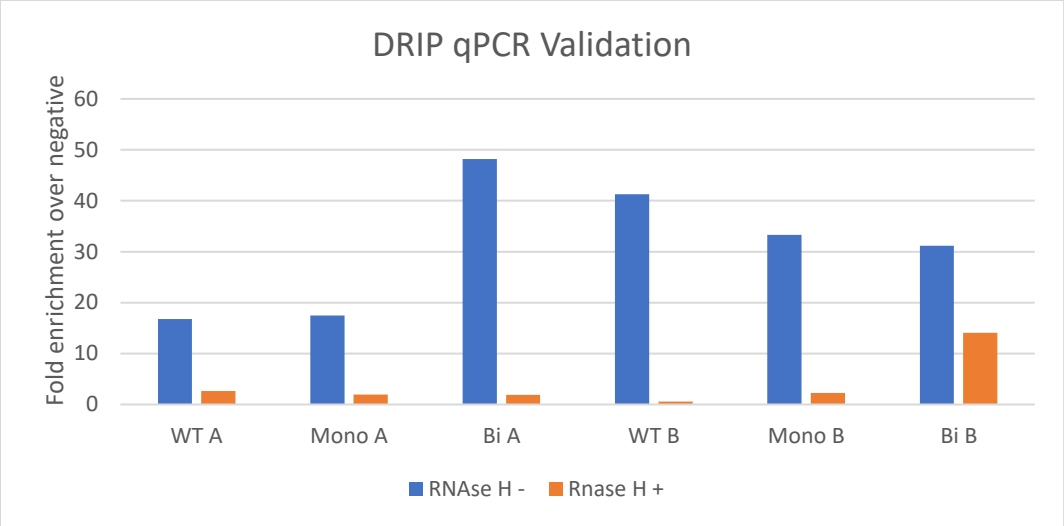


Figure 2.3 qPCR validation of DRIP libraries
Enrichment of each DRIP library using positive (RPL13A) versus negative (Chr18) locus.

NGS library preparation

All Chip and DRIP samples were prepared for NGS libraries using standard KAPA HyperPrep Kits for Illumina, according to the supplier's instructions. An average of 500 ng of each sample was used as the input. The generated NGS libraries were double-size selected to obtain an average size of 350 bp and to discard sequencing adaptors and primers using KAPA HyperPure Beads. Libraries were then quantified using Qubit and Bioanalyzer and pooled at a concentration of 20 nM. The final library pool (comprising 11 indexed libraries) was submitted for single-end sequencing using a Next-Seq 500/550 high-output kit v2 75 cycles (Illumina) at the Genomics Birmingham sequencing facility.

Lentiviral transduction of ATM-defective MEC1 CLL cells

MEC1 CLL cells (ATM-defective) were transduced in parallel with lentiviral vectors encoding short hairpin RNAs (shRNAs) targeting KDM5B and a non-targeting control in a Doxycycline (Dox)-inducible system. Lentiviral particles were purchased from (Horizon Discovery, Cambridge, United Kingdom). Cells were subcultured 1:2 the day before to keep cells actively cycling and minimise confluency levels. Frozen and viral particles were stored at 4 °C before lentiviral transduction. Transduction using a multiplicity of infection (MOI) of 5 was performed on $1x10^5$ cells in Dox-free DMEM media and the presence of 8 ug/ml polybrene. The next day, media was removed and replaced with a Dox-free RPMI containing 600 ng/ml puromycin for the selection of transduced cells. Cells were then incubated for four days. Transduced cells were treated with 1 ug dox, and the presence of TurbRFP positive cells were then confirmed under the fluorescent microscope. To establish a pure cell population expressing the TurboRFP, FACS-sorting was performed. To check the KD efficiency, cells lysates were extracted at 72 and 96 hours post the initiation of dox treatment and subjected to western blot validation.

Genome-scale CRISPR screening

CRISPR screening using Toronto KnockOut (TKO) CRISPR Library-Version 3 was executed as described (Addgene # 90294) (Mair et al., 2019, Hart et al., 2017). Dr. Angelo Agathanggelou transduced MEC1 CLL isogenic cell lines (RNASEH2B homozygous-KO, heterozygous-KO and WT) with the lentiviral TKOv3 (Hart et al., 2017) library at a low MOI (~0.2–0.3). Forty-eight hours later, the medium was removed and replaced with puromycin-containing medium, and selection was maintained until 96-hours post transduction, which was assigned as the initial time point (Day 0). At this time point, transduced cells were divided into technical replicates (A and B), and cells were subcultured every three days. Five samples were derived from each cell line that represented Day 0, one early time point from replicate A, one early time point from replicate B, one late time point from replicate A and one late time point from replicate B. Figure

4.19 summarizes the CRISPR screen experimental design. The number of cells used in the transduction ensured a 500x representation of the TKOv3 library (35 million cells) was propagated and harvested at each time point. Dr Agathanggelou maintained an equivalent population doubling between cell lines at each time point. Cell pellets (35 million cells) were frozen at each time point for genomic DNA (gDNA) extraction. Isolated gDNA samples were subjected to PCR amplification using the KAPA HiFi HotStart ReadyMix (Kapa Biosystems) to amplify genome-integrated sgRNA sequences. i5 and i7 multiplexing barcodes were added by a second PCR, and final gel-purified products were quantified by qPCR (KAPA Library Quantification Kit) and sequenced on an Illumina NextSeq500 to determine sgRNA redundancy in each sample. Next, I performed all downstream bioinformatic analysis.

Bioinformatic analysis

RNA-seq

Alignment of raw sequencing reads to the hg38 human genome was done using HISAT2 (Kim et al., 2019). Mapped reads were filtered to remove duplicate reads using Picard (Picard Toolkit, 2019). The filtered mapped reads were filtered further to remove multi-mapped and low-quality reads using samtools (Li et al., 2009). Figure 2.4 shows an example of RNA-seq data processing, with the filtered reads being highlighted. The final mapped reads were then used for downstream analysis. The fragments per kilobase of transcript per million mapped read (FPKM) values were obtained by normalizing the raw count matrix with feature effective length and library size (Trapnell et al., 2010) using the countToFPKM R package (Alhendi, A.S.N. 2019). Normalized genome bigwig tracks were produced using the bamCoverage tool in deepTools (Ramírez et al., 2014). A gene count matrix was generated using final filtered mapped reads annotated to the hg38 GTF annotation reference obtained from Gencode (Frankish et al., 2019) using the Featurecount tool (Liao et al., 2014). The count matrix was used as the input for differential gene expression analysis, which was carried out in R with the package DESEQ2 (Love et al., 2014). Pairwise Pearson correlation was produced from log2 normalized count matrix in R and depicted as a heatmap using the complexHeatmaps R package (Gu et al., 2016) with parameters of hierarchical clustering with

Euclidean distance and average linkage. Gene ontology assessment was achieved using the clusterprofiler package (Yu et al., 2012) on genes showing a log2 fold-change > 2 and adjusted p-value < 0.1 between conditions tested. Gene set enrichment analysis (GSEA) was performed on ranked differentially expressed genes showing a log2 fold-change > 2 and adjusted p-value < 0.1 using the packages fgsea (Sergushichev, 2016), Msigdb (Liberzon et al., 2015) and plotted using the package enrichplot (Yu et al., 2015b). The generation of a network of up- and down-regulated genes was carried out by taking common differentially expressed genes showing a log2 fold-change > 2 and adjusted p-value < 0.1 (MEC1 and CII for ATM project and Biallelic and Monoallelic KO for RNASEH2B project); the resulting gene list was subjected to gene enrichment analysis using the GO database (Jassal et al., 2020) and plotted as a network with the clusterprofiler package.

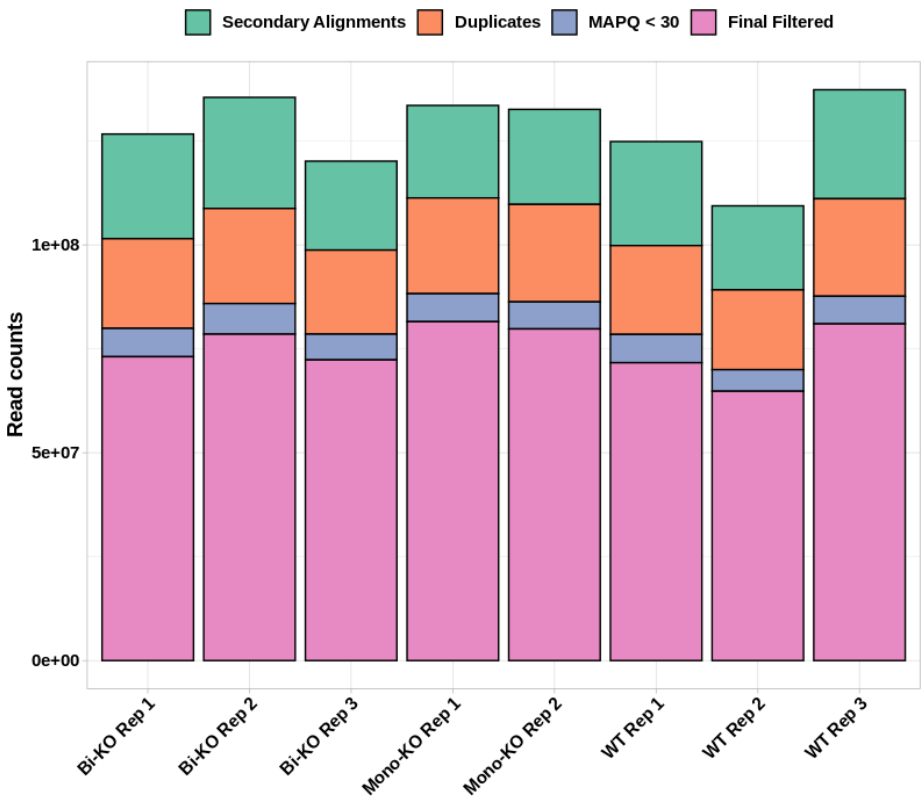


Figure 2.4 RNA-seq libraries' overall reads quality
RNA-seq sequencing reads were subjected for multiple assessments steps to insure the presence of high-quality reads for downstream analysis. Only pink-coloured reads which represent unique and high quality reads were considered for downstream analysis.

ATAC-seq

ATAC-seq raw reads were mapped to the hg38 human genome reference using Bowtie2 (Langmead and Salzberg, 2012) with the parameter --very-sensitive-local. Mapped reads were subjected to filtration to remove duplicates, low-quality alignments and mitochondrial DNA using Picard and samtools. ATAC accessible peaks were called on individual samples using the MACS2 peak caller (Zhang et al., 2008) with options -g hs –keep-dup all -B –trackline –nomodel –shift -100 –extsize 200. Peaks were called on merged bam files from all samples to generate a consensus peak list using the same options. Next, on individual samples, peaks summits were selected and extended 200 bp upstream and downstream of centre and were filtered on the following criteria: A) no overlap with hg38 blacklisted regions obtained from the encode project, B) peak height of a minimum of 10 tags, C) peaks that were also present in the consensus peaks list. featurecount was used to generate a count matrix on the final peak list, and the matrix was used as the input for differential chromatin accessibility, which was performed using the EdgeR package (Robinson et al., 2010). Peaks were defined as condition specific if they showed a fold-change > 1.5 and an adjusted p-value < 0.1. The obtained specific peaks were annotated and classified as a promoter region if the peak was within 1500 bp -/+ of TSS and distal otherwise using the ChIPseeker package (Yu et al., 2015a). ATAC heatmaps were produced by ranking differentially accessible peaks by fold change, and normalized tags were counted in a 2000 bp region centred on the peak summit using the annotatePeaks function in Homer software (Heinz et al., 2010) with the options -size 2000 -hist 10 -ghist. The obtained matrix was then plotted as a heatmap in Java TreeView (Saldanha, 2004). A gene expression heatmap of the ranked ATAC peaks list was developed by annotating each peak to the nearest gene using the ChIPseeker package, and then the log2 fold change for the obtained genes was extracted from differentially expressed RNA-seq data and plotted as a heatmap.

Motif co-occurrences analysis

Motif co-localization analysis was performed as previously described (Assi et al., 2019, Obier et al., 2016, Cauchy et al., 2015). De-novo discovered motifs in ATAC-specific defined sites was first carried out using Homer's algorithm findMotifsGenome (Heinz et al., 2010) using default settings. Motifs across all conditions were selected. Motif co-occurrences within 50 bp were computed with Homer's algorithm annotatePeaks (Heinz et al., 2010) and resulted in a motif co-occurrence count matrix. To examine the co-localization enrichments statistical significance, background co-localizations of selected motifs were processed using the reference condition peak populations. In the background reference population, I performed peaks' random subsampling of 1000 times equal in size to that of the specific population in focus, and in each subsample event, the motif co-occurrences count matrix was computed using bedtools (Quinlan and Hall, 2010) and annotatePeaks, respectively. The enrichment score was computed by means of motif co-localizations of the specific condition compared to the background as $Z = (x-\mu)/\sigma$, in which x is the co-occurrences in the specific set for a defined motif, and μ and σ are the mean and standard deviation computed from the background motif co-occurrences, respectively. The resulting enrichment score matrix was subjected to unsupervised clustering and plotted as a heatmap in R using the complexHeatmaps package (Gu et al., 2016).

Transcription factor network analysis

Transcription factor network analysis was carried as previously described (Assi et al., 2019). Briefly, condition-specific motifs were annotated to the nearest gene, and in each instance, the motif occurrence was counted using annotatePeaks.pl from Homer (Heinz et al., 2010). Genes encoding for transcription factors were obtained from AnimalTFDB (Hu et al., 2019). The calculated FPKM values for downstream TF genes were added to the TF network table along with the motif count occurrences. The final TF network table was loaded into Cytoscape for TF network visualization (Shannon et al., 2003). The significantly

enriched ATAC de-novo motifs were considered as major nodes. Minor nodes around a major node represent genes that share the same motif for that given motif. Minor node colour signifies the expression profile (FPKM) of the gene. A direct edge from a major to a minor node represents the motif occurrence at that given gene. The colour and size of the edge signify level of the motif count enrichment.

ChIP-seq and DRIP-seq

Mapping of raw ChIP reads to the hg38 human genome reference was done using Bowtie2 (Langmead and Salzberg, 2012), and mapped reads were filtered to remove duplicates and multi-low-quality reads using Picard and samtools. Figure 2.5 depicts an example of this data processing step in a group of Chip NGS libraries, highlighting the filtered reads. The resulting final filtered mapped reads were then used for downstream analysis. ChIP peaks were called using MACS2 (Zhang et al., 2008) with an FDR threshold of 0.01 using the default settings. Identification of common and unique peaks was performed using Bedtools (Quinlan and Hall, 2010). Peak annotation was carried out in R using the package ChIPseeker (Yu et al., 2015a). To generate normalized genome tracks for visualization, bigwig files were generated using the tool bamCoverage in deepTools (Ramírez et al., 2014). For DRIP-seq data processing, the same steps were followed except for peak calling where the epic2 (Stovner and Sætrom, 2019) peak caller was used because DRIP data contain mixed populations of narrow, broad and diffusely enriched peaks.

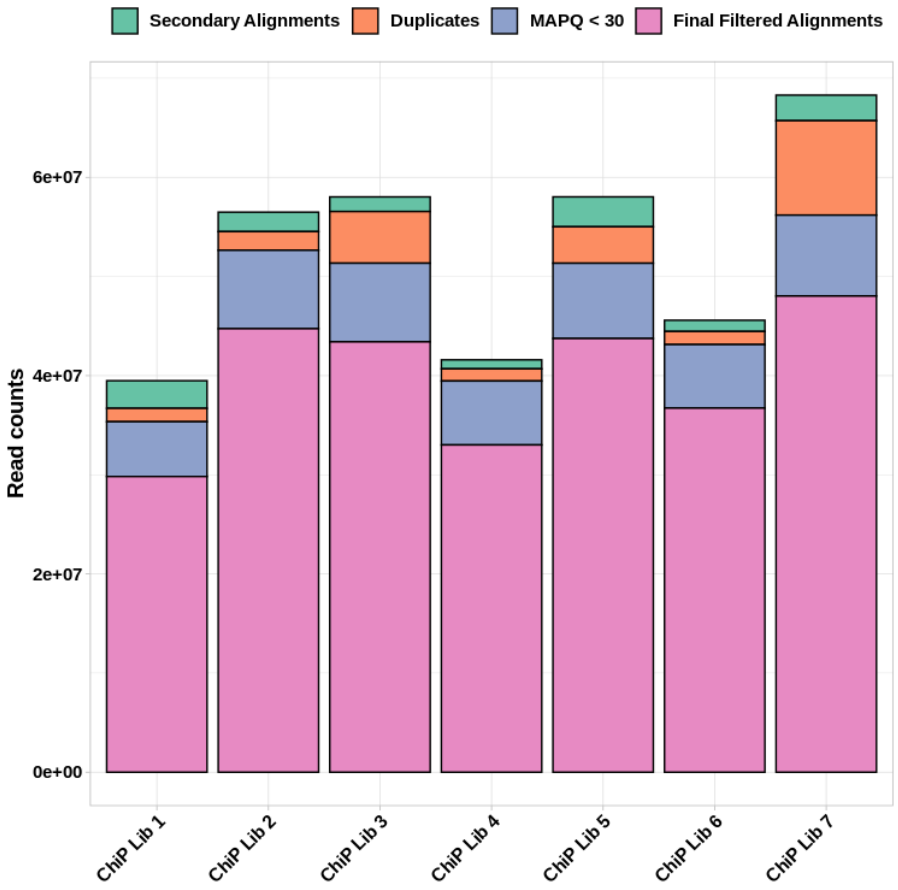


Figure 2.5 Chip-seq libraries' read depths
Sequencing reads were subjected for multiple filtration measures to insure the presence of high-quality reads to be used for downstream analysis. Only pink-coloured reads which represent unique and high quality reads were considered for downstream analysis.

Integrative analysis of gene expression, chromatin accessibility and chromatin immunoprecipitation

Integrative analysis of ATAC, RNA and ChIP-seq was achieved as previously described (Nafria et al., 2020, Kellaway et al., 2021, Gilmour et al., 2018). In short, consensus chromatin-accessible sites were ranked by the fold change obtained from differential accessibility analysis using edgeR (Robinson et al., 2010). The obtained ranked peaks bed file was used as the reference to construct heatmaps for ATAC, RNA and Chip-seq. To generate a gene expression heatmap correlated with the ranked peaks list, each peak was annotated to the nearest gene using ChIPseeker package (Yu et al., 2015a). Next, the log2 fold change for

the identified genes was extracted from RNA-seq differential gene expression analysis and then plotted as a heatmap using complexHeatmaps package (Gu et al., 2016). To generate an ATAC signal heatmap over ranked accessible sites, normalized tags were generated using makeTagDirectory from Homer (Heinz et al., 2010). A data matrix was produced for normalized tags over the ranked peak list using the tool annotatePeaks.pl from Homer with settings hg38 -size 2000 -hist 10 -ghist. This approach created a data matrix that covered a 2000 bp window centred on the peaks. Next, the data matrix was presented as a heatmap using Java TreeView (Saldanha, 2004). To generate a Chip signal over our previously determined ranked list, normalized tags were computed using makeTagDirectory from Homer, and a data matrix was created using the tool annotatePeaks.pl from Homer with settings hg38 -size 4000 -hist 10 -ghist -d, a strategy that created a data matrix that covered a 4000 bp window centred on the peak centre. The data matrix was then plotted as a heatmap using Java TreeView. Motif enrichment heatmaps were generated by producing a data matrix of motif enrichments in our previously determined ranked peak list using the function annotatePeaks.pl from Homer and the settings hg38 -size 2000 -hist 10 -ghist -m. The data matrix covered regions of 2000 bp centred on peaks and then plotted as a heatmap in Java TreeView. Figure 2.6 represents the overall strategy used to integrate the three data sets.

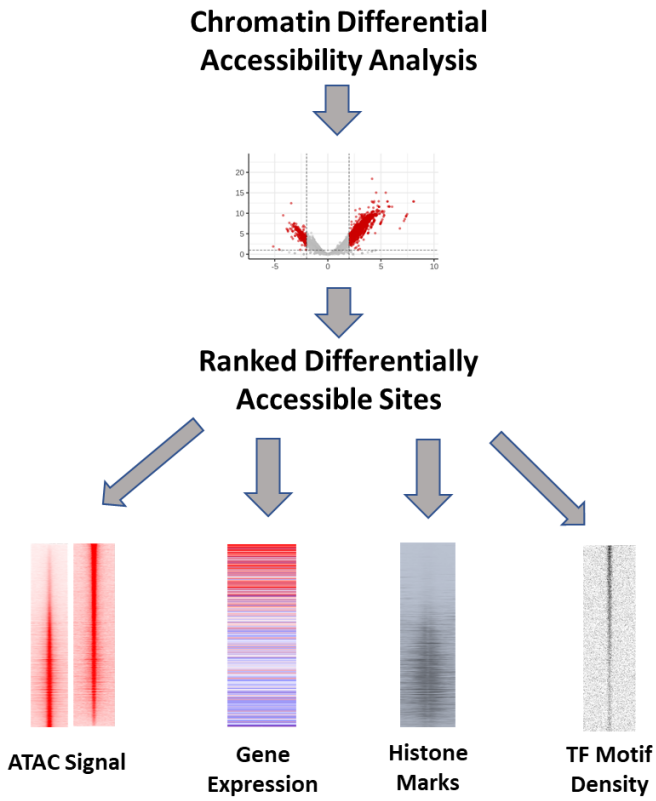


Figure 2.6 A model that describes the strategy used for the integration of three data sets
The differential accessible peak list was used as a reference to which all other data sets were aligned and integrated**.**

CRSIPR screen data analysis

CRSIPR screen library raw sequencing reads were aligned to Toronto KnockOut (TKO) CRISPR Library - Version 3 (Hart et al., 2017) using MAGeCK (Wang et al., 2019a). Raw sgRNA counts were subjected to copy-number variation (CNV) filtration, with the MEC1 cell line CNV data being obtained from the Depmap project (Ghandi et al., 2019). A raw sgRNA count matrix was used as the input for BAGEL and JACKS algorithms. Genes scores were computed using the aforementioned algorithms with their default settings. Identification of potential synthetic lethal hits was performed as described (Álvarez-Quilón et al., 2020). Briefly, reported scores from each algorithm from each condition were used to construct a linear regression model, where WT scores were treated as independent variables and KO scores as dependent

variables. I subsequently established a stringent cut-off of three standard deviations of the regression line. Hits that passed this cut-off were either classified as potentially synthetic lethal or potentially tumour suppressor hits. Subsequently, I defined the CRISPR screening final consensus hit list by only selecting hits that were common to two time points of the screen and common to the two algorithms used in the analysis.

Statistical Analysis

Gene expression count matrices were normalized and subjected to dispersion estimation using the DESeq2 package with default settings. Statistical analyses for differential gene expression were applied using the independent filtering algorithm provided by the DESeq2 package. To investigate the differential gene expression between conditions, a generalized linear model was made. The resulting p-values were adjusted for multiple testing by applying the Benjamini and Hochberg method (Love et al., 2014). For RNA-seq experiments, a minimum of two replicates (N=>2) per condition was used for the generation of a gene expression count matrix. Genes demonstrating an adjusted p-value (adj p-value) below 0.1 and an effect size of more than log2 fold change were considered differentially expressed.

ChIP-seq peaks were called using MACS2 software, where sample read counts were assumed to follow a Poisson distribution. After scaling the read counts of each condition versus its corresponding input sample, MACS2 begins peaks detection by shifting the read tags to predefined windows across the genome. Next overlapping peaks are then merged, and the location of the highest reads pileup is termed the summit. Since each peak is considered an independent test, the Benjamini-Hochberg correction was applied to correct for multiple testing (Zhang et al., 2008). For chromatin immunoprecipitation, one replicate (N=1) was used per condition. Summits peaks below an adjusted p-value of 0.01 were considered statistically significant and carried on for downstream analysis.

For chromatin accessibility analysis, the count matrix for the consensus summit peaks list that was identified previously was subjected to differential analysis using edgR package. The edgeR method utilizes the information from all consensus peaks and calculates the peakwise dispersion using conditional maximum likelihood on the total count for that peak. After normalization, using the trimmed mean of M-values, differential accessibility is examined for each peak using an adopted test for overdispersed data similar to Fisher's exact test. The resulting p-values were subjected to multiple testing corrections (Robinson et al., 2010). For ATAC-seq experiments, a minimum of two replicates (N=2) per condition was used to generate the consensus accessible peaks count matrix. Accessible chromatin peaks showing an adj p-value below 0.1 and a fold change of more than two were considered statistically significant and carried out for downstream analysis. For motif co-localization analysis, an enrichment score was computed to assess the significance of motif cooccurrence. The enrichment score was calculated by means of motif co-localization of the specific condition compared to the background as $Z = (x-\mu)/\sigma$, in which x is the co-occurrences in the particular set for a defined motif, and μ and σ are the mean and standard deviation computed from the background motif co-occurrences, respectively.

The qPCR gene expression analysis was performed on three replicates (N=3) per condition. ΔCt values for each condition were carried on for a statistical test (T-test) in Microsoft excel. Genes showing a p-value below 0.05 were considered statically significant. CRISPR screen analysis was performed using scores reported form BAGEL and JACKS algorithms using the default settings. Next, a linear regression model was made for each comparison (KO vs WT) at matched time points in which a p-value for each generated model was below 0.05. Genes passed a predetermined three standard deviations of the regression line were classified as synthetic lethal or tumour suppressor hits. The hit list were then intersected with the hit list generated by the other method to create a consensus hit list.

CHAPTER 3

The Epigenetic Landscape of ATM-defective CLL cells

Chapter 3: Chromatin Landscape in ATM-deficient CLL cells

Recent advances in genome-wide interrogation have enabled the accurate and precise characterisation of the CLL epigenome. New insights into understanding CLL clonal origin and evolution have been produced from the identification of CLL-specific DNA methylation profiles (Oakes and Martin-Subero, 2018, Oakes et al., 2016). In addition, efforts have been made to describe the chromatin landscape of CLL cells at the levels of the transcriptome, histone post-translational modifications and level of accessible chromatin (Beekman et al., 2018, Rendeiro et al., 2016). However, a CLL mutation-specific chromatin signature has yet to be established, and in particular, this is the case with respect to DDR defective genes that drive the disease progression.

Therefore, the main focus of this chapter is to address the transcriptional and epigenetic mechanisms in correlation with ATM loss status in CLL cells. To enable the investigation of the epigenetic landscape in accordance with ATM loss, our laboratory has generated a stable ATM shRNA KD isogeneic CLL cell line model (MEC1 and CII) (Figure 3.1) (Kwok et al., 2016). The ATM status, including protein expression, kinase activity, and effect on downstream target proteins, were validated in these cells in our lab.

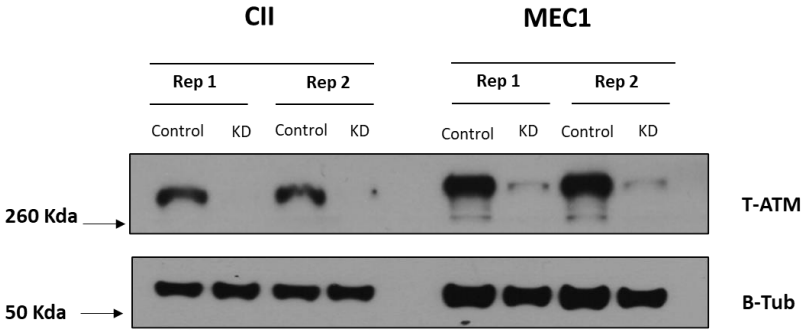


Figure 3.1 Western blots confirmed the absence of ATM protein expression in CLL cell lines
A western blot analysis was performed to confirm the ATM protein status in lysates derived from CLL cell lines (MEC1 and CII). In this analysis, an antibody was used for the detection of Total ATM (T-ATM) and an antibody for the detection of β-tubulin protein, which was used as loading control showing equal protein loading among samples.

To generate an epigenomic profile, these isogeneic cell lines were subjected to transcriptomic analysis using RNA-seq, histone post-translational modifications evaluation using ChIP-seq and chromatin accessibility landscape via ATAC-seq.

3.2 ATM loss is correlated with global gene expression deregulation in CLL cells

RNA sequencing (RNA-Seq) technology uses next-generation sequencing methods to allow for an accurate evaluation of cells' transcriptome profiles. RNA-seq delivers a high resolution and full coverage of cellular gene expression and compared to microarray-based methods, it is not biased toward a predefined set of target genes. Therefore, the RNA-seq method could potentially allow for the discovery of novel patterns of gene expression associated with a certain condition, disease or phenotype. In this method, mature polyadenylated mRNA is preferentially selected and subjected to fragmentations, cDNA synthesis, NGS adapter ligation, and finally, high-throughput next-generation sequencing.

To study the impact of ATM loss on the transcriptomic profile of CLL cells, RNA-seq was performed in duplicate on 2 ATM-deficient CLL cell lines in parallel with controls (GFP-KD). Linear regression analysis was carried out on the RNA-seq of all samples and produced an R^2 between 0.97 and 0.98 (Figure 3.2), suggesting a high degree of correlation between technical replicates. To demonstrate differences in gene expression variation between 4 conditions (MEC1 ATM KD, MEC1 ATM WT, CII ATM KD, CII ATM WT), a Pearson correlation analysis was calculated, resulting in a heatmap presented in (Figure 3.3). As expected, hierarchical unsupervised clustering shows that both MEC1 and CII isogenic cells cluster together, consistent with the genomic identity of the cell lines being a fundamental determinant of the transcriptome.

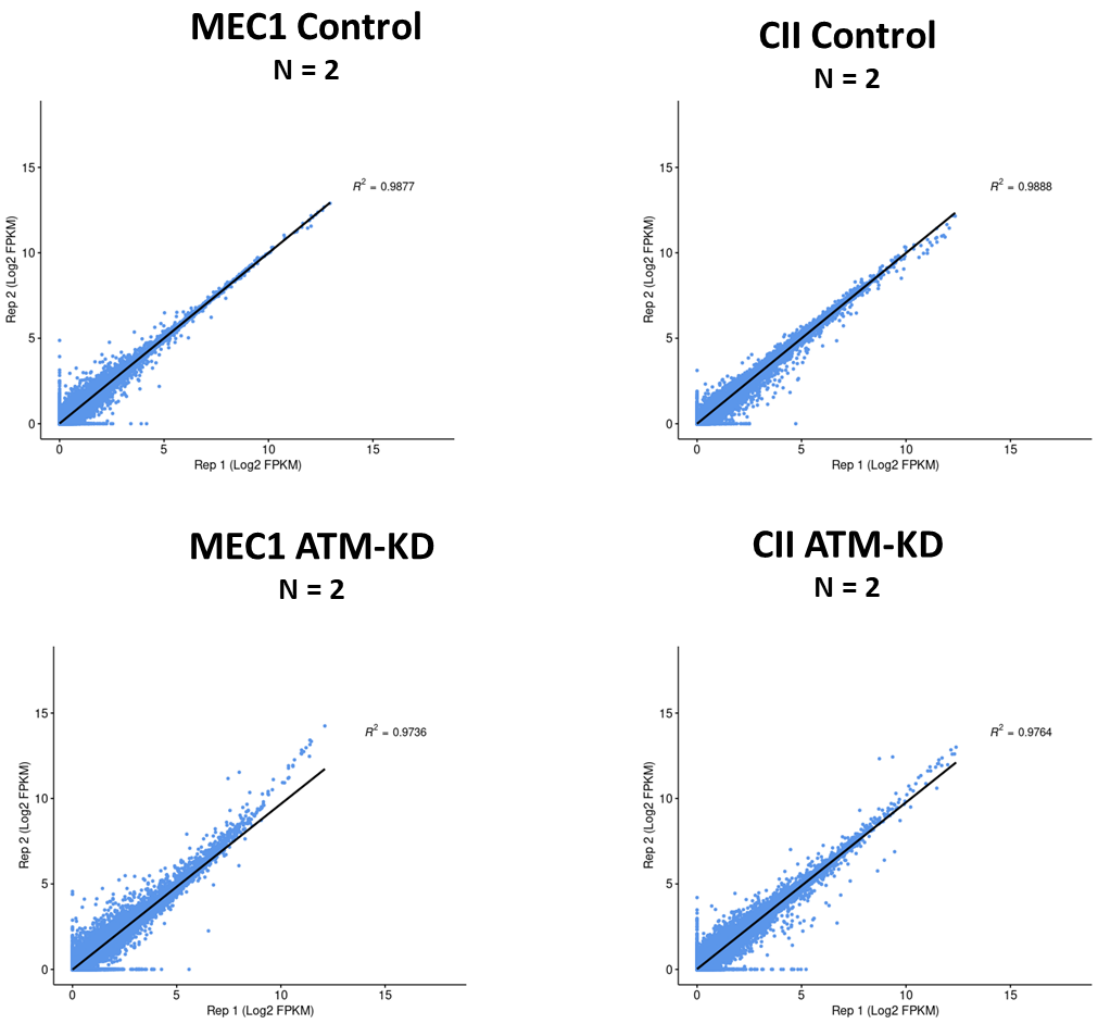


Figure 3.2 Linear regression analysis shows a positive correlation between RNA-seq replicates
Comparison of RNA-seq replicates of ATM-deficient and ATM WT (Control) isogeneic cell lines. Log2 FPKM+1 expression values were computed for each replicate (Two replicates for each condition). Next, a linear regression analysis was performed using Log2 FPKM+1 values. The resulted linear regression analysis shows a positive correlation between replicates and an R squared value above 97%, indicating high similarity between replicates.

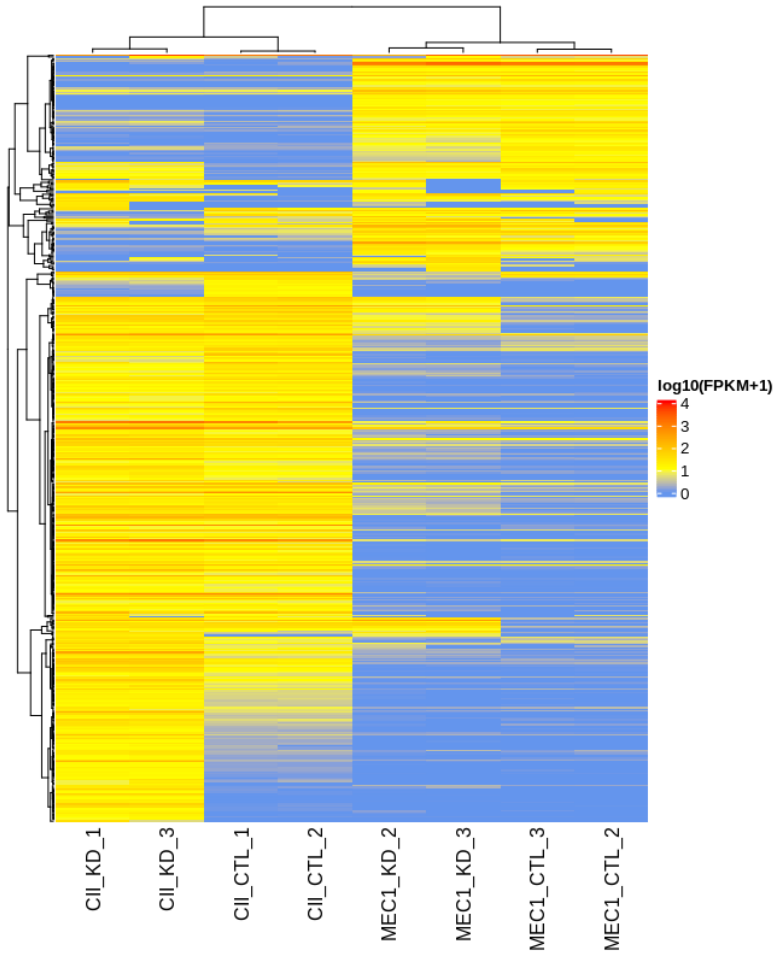


Figure 3.3 Correlation clustering of gene expression profiles of ATM-deficient isogeneic CLL cells
The expression values (Log10 FPKM+1) of all differentially expressed genes were computed for each RNA-seq sample replicate. Next, hierarchical unsupervised clustering of gene expression profiles is calculated by correlation analysis (1-Pearson correlation, average linkage) of expression values. The heatmap shows that each cell line is clustered away from the other cell line, and within each cell line, we see each condition replicates the cluster independently from its counterpart condition. (Abbreviation: FPKM : the fragments per kilobase per million fragments mapped).

To validate the global gene expression observed in RNA-seq data, I randomly selected a group of genes (*HCK, KLF4, SATB2*) that were up-regulated in the two KD cell lines in comparison to ATM WT counterpart. In MEC1 cells, the differential gene expression analysis of RNA-seq data showed that *HCK* gene has an adj p-value of 1.12×10^{-90}, *KLF4* gene has an adj p-value of 4×10^{-2}, and *SATB2* gene has an adj p-value of 2.25×10^{-46}. In CII cells, *HCK* has an adj p-value of 3.16×10^{-108}, *KLF4* has an adj p-value of 1.06×10^{-4}, and *SATB2*

has an adj p-value of 3.34×10^{-23}. All selected genes showed an upregulation of more than log2 fold change.

I designed primers to measure the expression of the selected genes independently using an independent method, qPCR. The qPCR showed a slightly variable expression but was consistent with RNA-seq data in terms of observed up-regulation, and increased gene expression was statistically significant (Figure 3.4). It is likely that this variation was affected by the type of normalization (small gene region vs entire transcript) and variable primer efficiency. Together, these validating experiments confirmed the acceptable quality of my RNA-seq data.

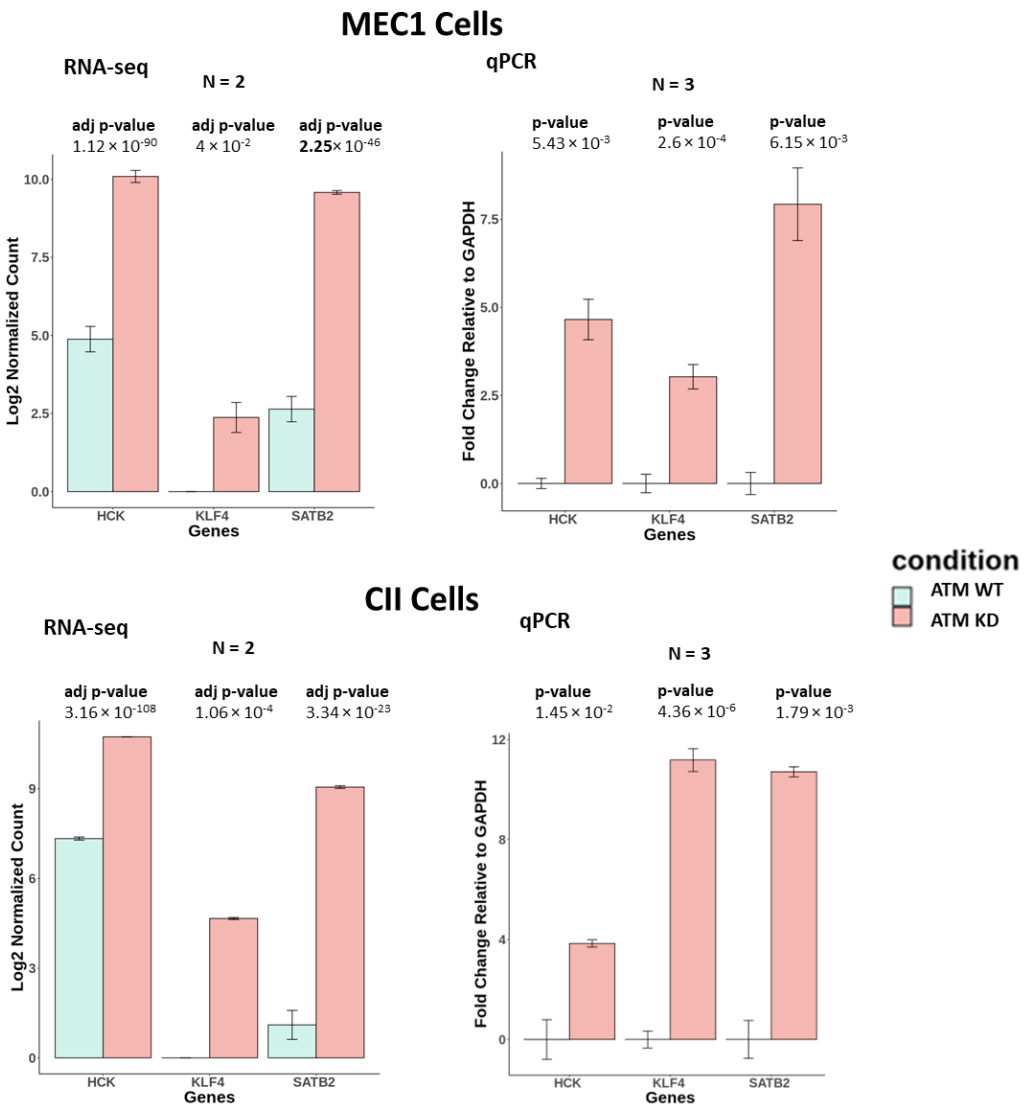


Figure 3.4 Validation of RNA-seq data by measuring the expression of selected genes by qPCR
Selected up-regulated genes in CII, and MEC1 cell lines from RNA-seq data were measured independently using qPCR. The normalized read count (Log2 normalized count) for each selected gene was extracted and plotted as a bar plot along with the adj p-value to establish a comparison with qPCR results. Results of the qPCR were plotted as mean plus/minus SE of three independent experiments. The resulted p-value derived from the t-test performed on each gene was labelled above the correspondent gene. qPCR gene expression was normalized to *GAPDH*. Results suggest that the expression of all genes were consistent with RNA-seq data in term of gene upregulation. The replicates for RNA-seq experiment (N=2), and the replicates for qPCR gene expression experiment (N=3). A p-value of cut off of 0.05 was used qPCR gene expression statistical test whereas an adjusted p-value cut off of 0.1 was used for differential gene expression analysis applied on RNA-seq data.

3.3 ATM loss in CLL cells is correlated with the upregulation of pro-inflammatory genes

Following successful validation experiments, I next conducted a differential gene expression analysis on each isogenic cell line using cells with the ATM wild type as controls. I decided to analyse the data first in the specific cellular context, by looking at the ATM loss correlated impact of in each individual cell line, and then irrespective of cellular context, by looking at the correlated effects of ATM loss common to both cell lines.

Differentially expressed genes were defined as statistically significant if they demonstrate an adjusted p-value below 0.1 (adj p-value < 0.1) and more than two log2 fold change (log2 FC > 2). Using this approach showed a number of differentially expressed genes correlated with ATM loss status between the two cell lines, suggesting that the cellular genetic background differences were reflected at the gene expression level (Figure 3.5). MEC1 cell line showed 947 differentially expressed genes, with 273 genes being downregulated and 674 genes being upregulated when comparing ATM KD cells to ATM WT cells. In contrast, the CII cell line showed 2236 differentially expressed genes, with 337 genes being downregulated and 1899 genes that are upregulated in ATM KD cells compared to ATM WT cells.

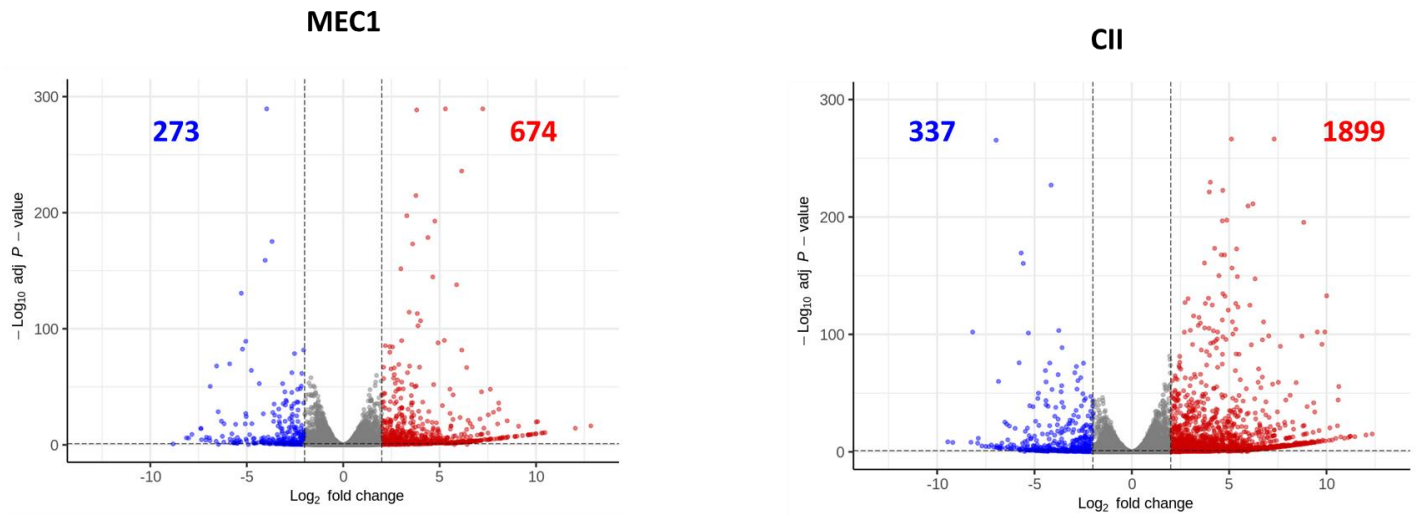


Figure 3.5 Differentially expressed genes in accordance with ATM loss status in CLL cells
Statically significant differentially expressed genes were highlighted. Differentially genes below adj p-values of 0.1 and showing upregulation (Log2FC >2) are coloured in red, whereas genes showing downregulation (Log2FC < -2) were coloured in blue (MEC1 cells on the left-hand side and CII cells on the right-hand side). MEC1 cells showed 674 genes that were upregulated and 273 genes that were downregulated, whereas CII cells showed 1899 genes that were upregulated and 337 genes downregulated. All comparisons were made against ATM WT counterpart cells.

Next, differentially expressed genes for each cell line were used as input for Gene Ontology (GO) pathway enrichment analysis to look for biological processes that are affected by ATM KD and were associated with each cell line individually. Gene ontology (GO) is a global standardized gene functional categorization resource that provides an updated definition of gene function. GO pathway analysis was performed to help in the detection of a set of genes involved in a specific biological pathway or process.

In MEC1 cells, the GO analysis demonstrated that the upregulated genes in accordance with ATM loss play a role in inflammatory (Genes count = 14, adj p-value= 8.21×10^{-5}) and immune responses (Genes count = 19, adj p-value= 3.19×10^{-4}), as well as cellular response to cytokines (Genes count = 27, adj p-value= 3.98×10^{-3}) whereas in CII cells ATM loss was correlated with the upregulation of the genes responsible for cell-cell adhesion (Genes count = 68, adj p-value= 5.30×10^{-23}) (Figure 3.6). It is well established that CLL cells reside in a pro-inflammatory environment which supports their survival and proliferation

(Rozovski et al., 2013). However, the observed differential upregulation of proinflammatory responses that were correlated with ATM loss in MEC1 cells that are also p53 deficient is likely to be related to the accumulation of unrepaired DNA damage. Namely, unrepaired DNA fragments could trigger activation of interferons (IFN) response, and in that respect, the relationship between DDR defects and immune activation is becoming a rapidly expanding area of cancer research (Rozovski et al., 2013, Ye et al., 2021).

Moreover, the two cell lines also showed variations in the type of down-regulated genes that were in accordance with ATM loss. In MEC1 cells, GO terms identified the down-regulation of genes correlated with ATM loss including WNT signalling (Genes count = 10, adj p-value= 5.66×10^{-2}) cell fate commitment (Genes count = 7, adj p-value= 3.57×10^{-3}), and JUN kinase pathway (Genes count = 9, adj p-value= 2.7×10^{-2}) In addition, I observed that genes encoding transcription factors, including *GATA3* (adj p-value = 1.29×10^{-2}) , *GATA4* (adj p-value = 7.18×10^{-2}) , *TCF7L2* (adj p-value = 2.08×10^{-2}) and the ZNF family of transcription factors were down-regulated. The observed *GATA4* downregulation in accordance with ATM inhibition is consistent with what is known about ATM involvement in the regulation of *GATA4* activation (Kang et al., 2015).

On the other hand, In CII cells, I observed that ATM KD cells were correlated with the downregulation of genes mainly involved in B-cell mediated immunity (Genes count = 11, adj p-value= 3.17×10^{-2}) and B-cell activation (Genes count = 12, adj p-value= 5.41×10^{-2}), consistent with CLLs representing functionally deficient B cells (Darwiche et al., 2018, Bartik et al., 1998). Moreover, in CII cells, I observed the down-regulation of transcription factors that were in accord with ATM loss, including *HOXD4* (adj p-value = 2.34×10^{-2}) , *FOXO3* (adj p-value = 7.05×10^{-102}) and *KLF2* (adj p-value = 2.86×10^{-6}) . The association of *FOXO3* downregulation in CII ATM defective cells is in line with the established cross-talk mediated by FOXO3 between ATM and p53 in response to DNA damage (Chung et al., 2012). The observed differences between transcription profiles of CII and MEC1 cell lines that were correlated with ATM loss detected by GO analysis (Figure 3.6) are likely to be related to cell-specific context and differences in the genetic

background of CII and MEC1 cell lines. Next, I will look for transcriptional alterations in parallel with ATM loss and are common to MEC1 and CII cell lines.

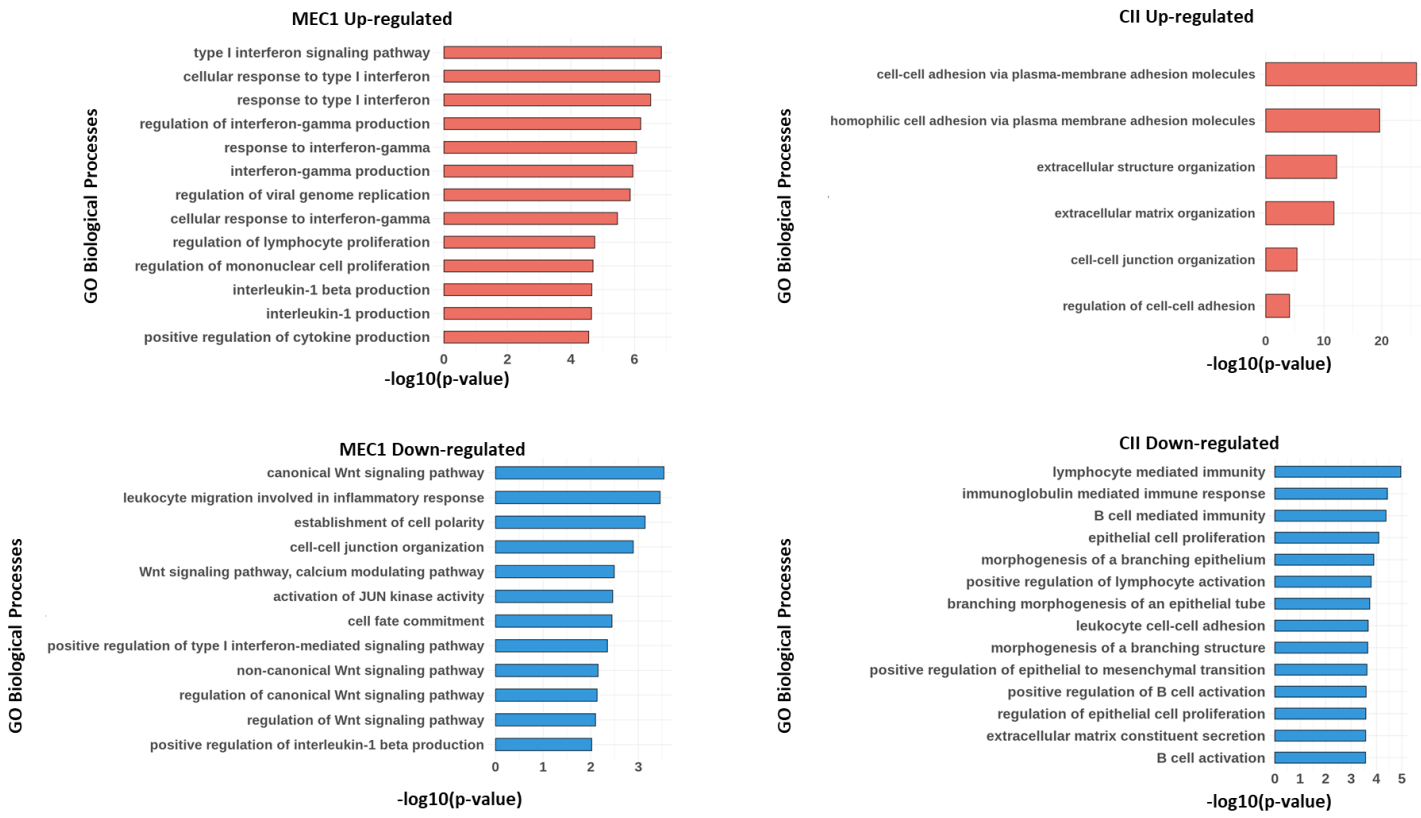


Figure 3.6 Gene Ontology analysis on differentially expressed up-and down-regulated genes in correlation with ATM loss in CLL cells

Gene ontology analysis was performed on genes that have an adjusted p-value below 0.1 and at least have a 2-log2 fold change up-or down-regulated in each cell line (ATM-deficient compared to ATM WT controls). The GO sets show the most significant GO terms in each cell line for both upregulation (red colour) and downregulation (blue colour) genes. The analysis highlights the up-regulation of inflammatory and immune response genes in line with ATM loss status

To gain more holistic insights on the overall differentially expressed genes in accord with ATM loss and link these genes with a biological phenotype, gene set enrichment analysis (GSEA) was performed. This analysis uses a set of differentially expressed genes, ranks them according to fold change and p-value and then compares the ranked list to a set of genes known for phenotype or disease. This analysis showed

common features correlated with ATM loss in CLL cells, such as pro-inflammatory response signature. In MEC1 cells, differentially expressed genes that were in line with ATM loss showed signatures of interferon-alpha (Genes count = 65, adj p-value = 3.90×10^{-3}) and gamma responses (Genes count = 108, adj p-value = 3.89×10^{-3}) whereas CII cells showed signatures of interferon-gamma response (Genes count = 105, adj p-value = 1.42×10^{-2}) and tumour necrosis factor-α (TNFA) signalling (Genes count = 53, adj p-value = 2.05×10^{-2}) (Figure 3.7 A).

To further check the expression status of the genes associated with the previously enriched signature in the GSEA analysis, selected genes related to each ATM loss correlated enriched hallmark signature were labelled in the volcano plot. Labelling the volcano plot clearly showed that these genes are associated with upregulated gene expression related to ATM loss (Figure 3.7 B). The GSEA analysis highlighted similarities in terms of upregulation of proinflammatory responses that were correlated with ATM loss in both cell lines (MEC1 and CII). These observed similarities suggest specific transcriptomic changes according to ATM loss changes that were upregulated in both cell lines despite their different genetic backgrounds. The upregulation of proinflammatory responses is likely to be an immune reaction toward the cytoplasmic build-up of DNA resulting from inefficient DNA damage clearance correlated with ATM loss in CLL cells.

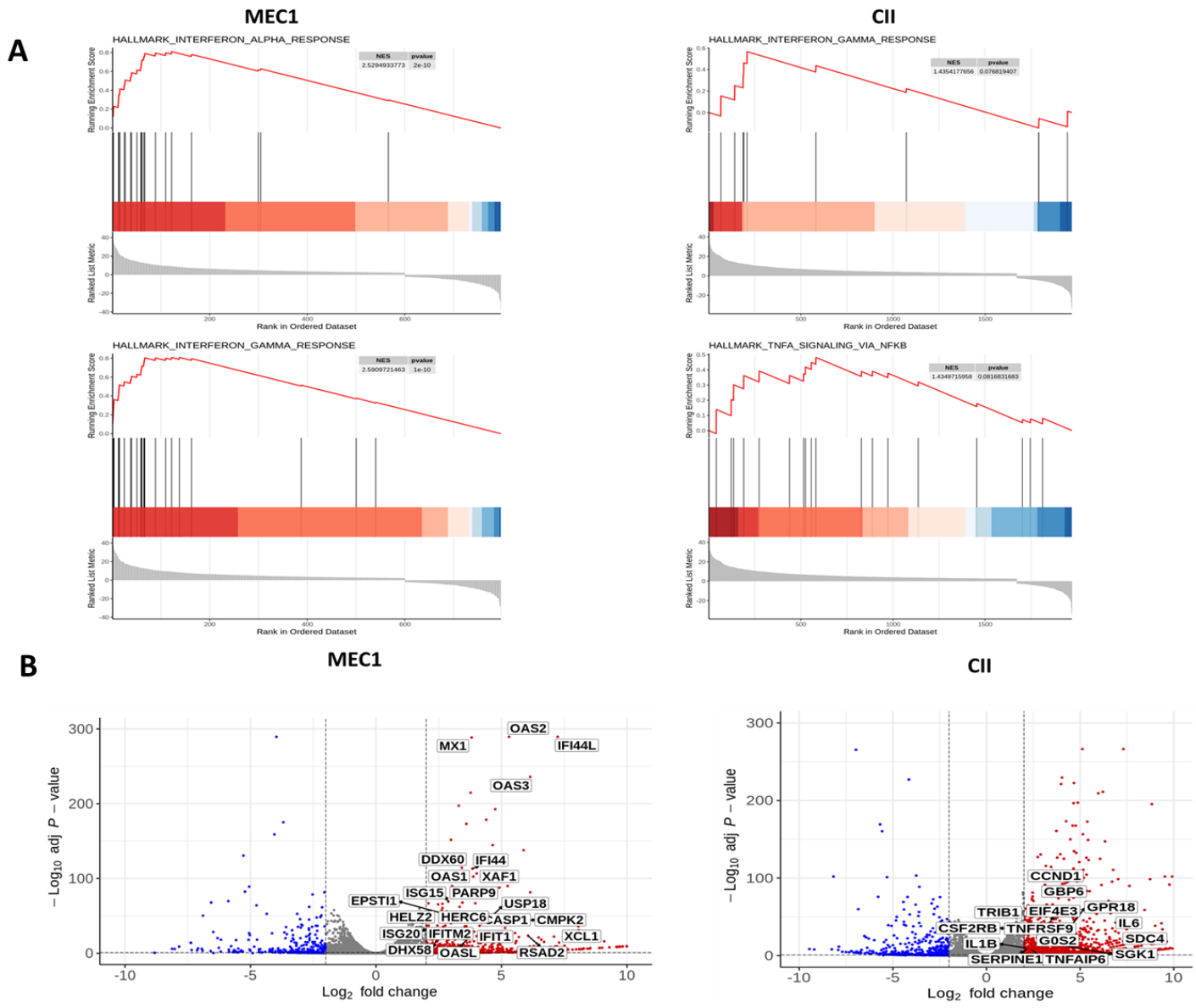


Figure 3.7 Gene set enrichment analysis (GSEA) of differentially expressed genes correlated with ATM defective status in CLL cells

(A) Gene set enrichment analysis (GSEA) shows enrichment for an inflammatory phenotype in line with ATM-deficient isogenic cell lines. In this analysis, differentially expressed genes are ranked according to p-value and log2 fold change and then compared to a set of genes known to have a role in certain biological phenotypes or diseases. Genes found in the set are coloured with black vertical lines. Enrichment score (ES) is the highest divergence from

the baseline (zero) as determined for each gene of the ranked list and denotes the extent of over-representation of a gene set. Coloured boxes at the bottom signify the extent of association of genes with the ATM-deficient phenotype (red for positive and blue for negative association). The GSEA threshold set at adj p-value < 0.1. (B) Volcano plots demonstrating genes associated with GSEA hallmarks are upregulated in correlation with ATM loss status in both CLL cell lines (MEC1 and CII).

To further identify transcriptomic signature and possible cellular dependencies in accordance with ATM loss despite cellular specific background, I next selected common up-regulated and down-regulated genes correlated with ATM loss in both cell lines (212 genes) and performed GO pathway analysis (Figure 3.8 A). Using this approach allowed identifying a network of up-and down-regulated genes pathway irrespective of cellular background. This analysis showed that ATM loss gene expression in CLL cells was mainly in correlation with positive regulation of proinflammatory pathways (interferon-gamma production (Genes count = 6, adj p-value = 4.41×10^{-4}) and cytokine production (Genes count = 10, adj p-value = 4.98×10^{-3}) as well as positive regulation of lymphocyte activation (Genes count = 9, adj p-value = 4.02×10^{-3})(Figure 3.8 B). The network shows the upregulation of the innate immunity activator (*INAVA*), which is also known to have roles in activating MAP kinases and NF-kappa-B signalling.

To demonstrate that common up-and down-regulated genes correlated with ATM loss between the two cell lines show a unique gene expression profile, a set of common differentially expressed genes was used as input for producing a supervised clustering heatmap. The resulting heatmap showed that ATM WT samples cluster together away from ATM KD samples that cluster together irrespective of cell line genetic background (Figure 3.9). This analysis highlights that differentially expressed genes that were correlated with ATM status and common between the two cell lines show a similar expression profile suggesting an ATM-specific change.

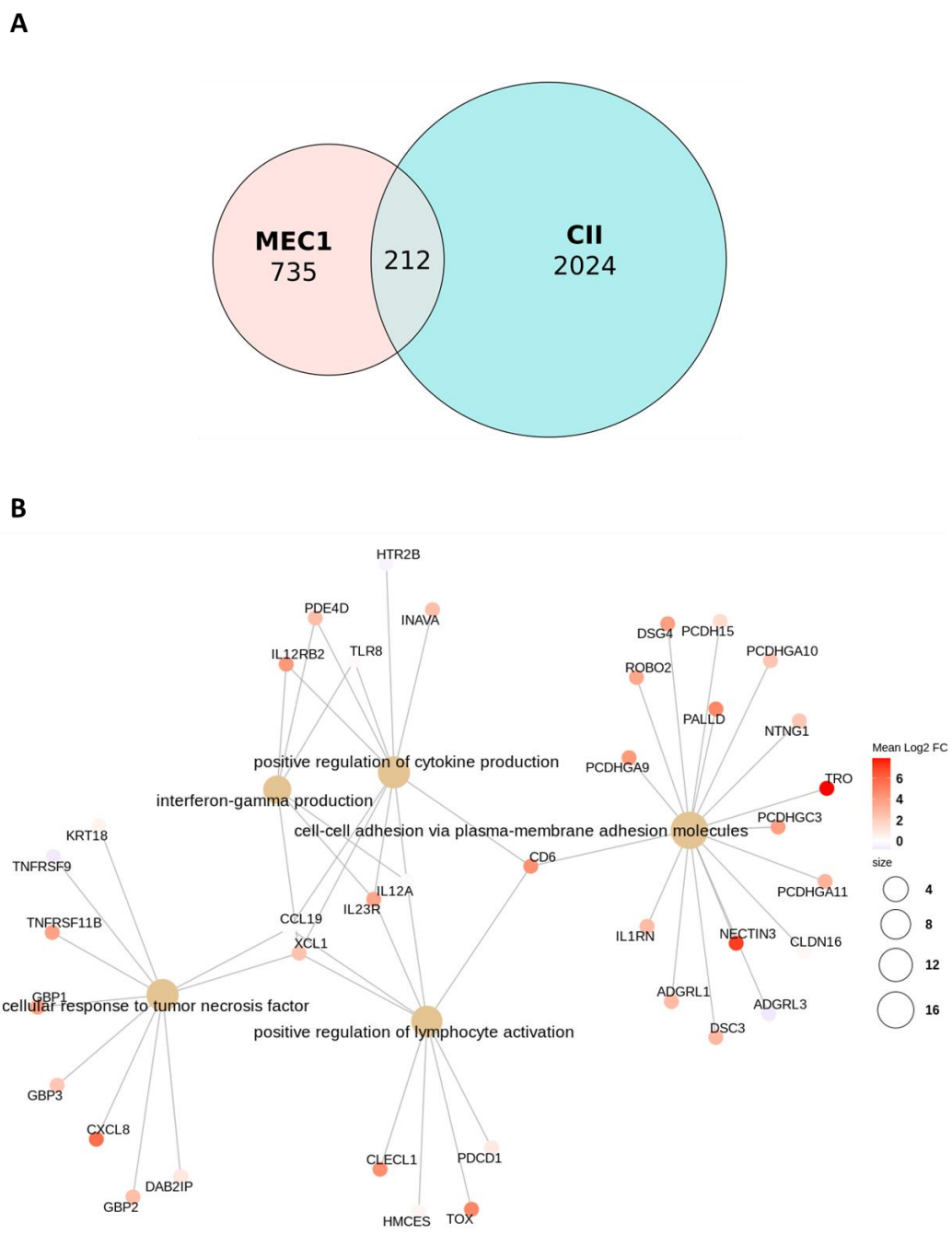


Figure 3.8 Common differentially expressed genes in correlation with ATM loss status and their role biological role

(A) Statistically significant differentially expressed genes lists correlated with ATM status resulting from each cell line were overlapped and resulted in a common gene (212 genes). These shared genes were then subjected to GO pathway enrichment analysis. (B)The results of GO pathway analysis connect commonly differentially expressed genes in accord with ATM loss status (MEC1 and CII) in contrast to control cells (ATM WT). The enriched GO terms include pathways such as positive regulation of lymphocyte activation and interferon-gamma production. The constructed network demonstrates interactions (grey lines) between individual genes grouped in multiple pathways. Red nodes represent up-regulated genes, and blue nodes indicate down-regulated genes in each particular pathway. The size of a node refers to the number of genes associated with that specific node.

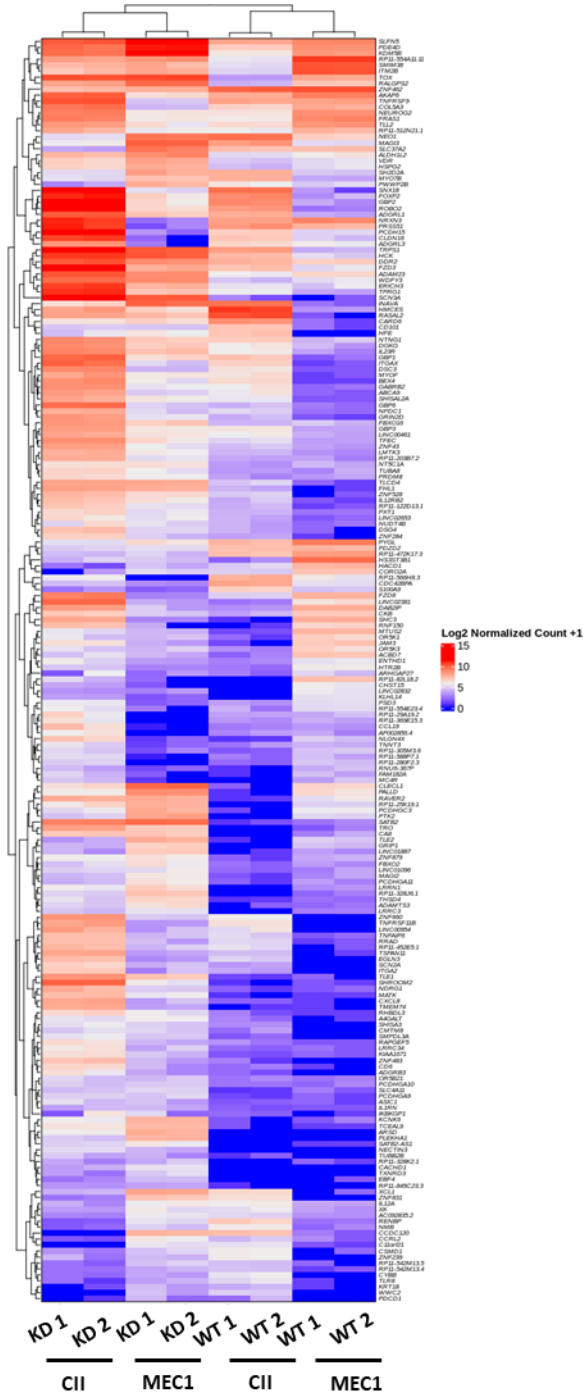


Figure 3.9 Heatmap of supervised clustering reveals a common gene expression profile in correlation with ATM loss in CLL cells

Common differentially expressed genes that were correlated with ATM loss for each cell line were identified. Next, normalized read counts for each gene were log2 transformed and subjected to supervised hierarchical clustering for each cell type. The heatmap shows that the common differentially expressed genes correlated with ATM loss have similar gene expression patterns related to the impact of ATM loss status.

In summary, by addressing ATM-specific transcriptome in CLL cell lines separately or in their combination, I identified a common pattern in accordance with ATM loss, which is the upregulation of pro-inflammatory pathways. This pattern of upregulation may provide cells with prolonged survival signals, including extensive transcriptional reprogramming coupled with active proinflammatory signalling that might be responsible for the proliferation of ATM-defective CLL cells. Therefore, identifying epigenetic alterations associated with changes in gene expression was the next logical step toward identifying transcriptional dependencies correlated with ATM loss in tumour cells.

3.4 Characterisation of histone post-translational changes in correlation with ATM loss

Chromatin immunoprecipitation followed by sequencing (ChIP–seq) methodology allows the detection of DNA binding proteins and chemical modifications associated with histone proteins in chromatin. Coupled with gene expression data, genome-wide evaluation of alterations in histone modifications and transcription factor binding sites enables a systematic assessment of how the epigenomic landscape contributes to transcriptional rewiring, cell development and identity. This method uses an antibody for a specific histone modification or DNA-binding protein to identify enriched loci within a genome associated with that protein of interest.

Beekman et al. in 2018 published an extensive CLL epigenome characterisation analysis where the epigenome profile of CLL samples was contrasted against the B-cell development lineage trajectory. The study demonstrated alterations in histone modifications in CLL compared to normal B-cells, highlighting global chromatin reconfiguration. However, this study lacked insights into CLL mutation-specific histone modification changes because normal B-cells were used to establish the comparison. Therefore, I performed chromatin immunoprecipitation followed by sequencing (ChIP-seq) in our isogenic CLL cell lines. I used histone post-translational modification marks associated with the active chromatin

(H3K4me3, H3K4me1, and H3K27ac) to understand the epigenomic layers correlated with ATM-defective cells proliferation nature.

In this experiment, immunoprecipitated DNA was used as input for validation with quantitative PCR (qPCR) using a set of primers targeting positive and negative loci. Samples that showed positive enrichment over negative loci were then selected for library generation and sequencing. Raw sequencing files were aligned to the human genome (hg38), and mapped files were filtered to remove duplicates, and low quality and multimap reads. Peaks were called for each sample with ChIP input as a control using MACS2 software with default parameters. Genome tracks were generated using deeptools software.

Only Summit peaks that represented the maximum ChIP intensity signal and were passed the FDR threshold of 0.01 were included in the analysis. The MEC1 cell line demonstrated histone PTM alterations in the form of H3K4me3 called peaks (ATM KD = 35774 peaks, ATM WT = 38909 peaks), H3K4me1 called peaks (ATM KD = 81482 peaks, ATM WT= 101990 peaks), H3K27ac (ATM KD = 54499 peaks, ATM WT = 56647 peaks). In agreement with MEC1 cells, CII cell line showed a similar pattern where H3K4me3 called peaks (ATM KD = 20540, ATM WT = 26134), and H3K27ac called peaks (ATM KD = 29030, ATM WT = 36143). The H3K4me1 CII samples were discarded as the ratio of signal to noise was low, which suggests the experiment has failed.

Pearson correlation analysis between the three histone marks was performed and showed that histone marks from the same type cluster together in MEC1 cells (Figure 3.10 A). The correlation analysis demonstrated the differences in histone marks in parallel with the condition (ATM defective vs control), suggesting ATM loss is in line with changes in histone PTM. To investigate further these changes, I analysed ChIP signals over transcriptional start sites (TSS) and generated a genome-wide meta profile for each histone mark (Figure 3.10 C–D).

The data show genome-wide down-regulation of histone marks associated with active gene transcription in correlation with ATM loss. These observations were also confirmed in ATM-defective CII cells, suggesting that down-regulation of histone marks is associated with ATM loss consequence. Various research groups have noted the down-regulation of H3K4me3 levels in the context of DNA damage (Gong et al., 2017, Li et al., 2014b). In addition, H3K4me3 demethylation is correlated with initiating DNA replication origins (Rondinelli et al., 2015), suggesting that alterations in histone marks may represent epigenomic cellular reprogramming as a response to biological stress.

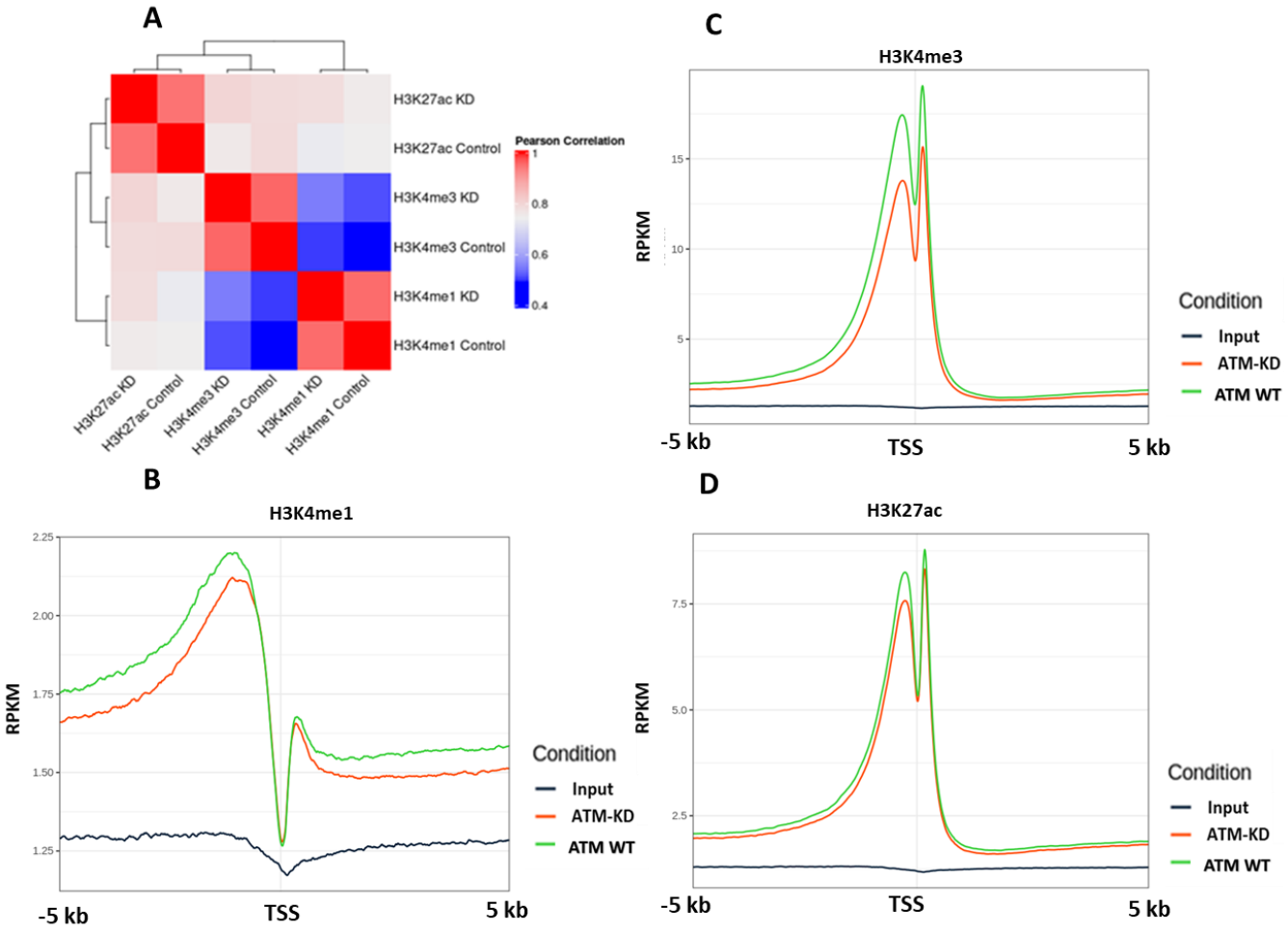


Figure 3.10 Chromatin immunoprecipitation data suggest a genome-wide alterations in histone PTM in correlation with ATM loss

(A) Pearson correlation heatmap of log2 transformed normalized count shows histone modification hierarchical unsupervised clustering; H3K4me3 and H3K4me1 histone marks cluster close to each other, whereas H3K27ac cluster further away. The heatmap highlights changes in histone PTM in line with ATM loss (B) Meta-profile of normalized ChIP samples centred 5 KB up- and downstream of the transcription start sites (TSS) of all annotated genes related to human genome version 38 (including expressing and not expressing genes TSS) for H3K4me1 for ATM-deficient, ATM- WT and input. (C) and (D) are meta-gene profiles for H3K4me3 and H3K27ac, respectively. Metagene profiles for the histone PTM indicated genome-wide changes in these histone PTM in accordance with ATM loss status. The number of replicates for each ChIP sample is one (N=1)

To investigate the biological pathways that were affected by either the loss or gain of the histone mark (H3K4me3) alongside the ATM loss status, GO functional pathway analysis for peaks with a cut-off of false discovery rate (FDR) of 0.01 was conducted. ATM KD and WT resulting summit peaks for each cell line were identified by intersecting the ATM KD summit peak set with the ATM WT summit peak set. Only peaks that did not show an overlap were termed unique peaks. These peaks were then annotated to the nearest gene, and the resulting gene list was used to perform the GO analysis. Consistent with RNA-seq data, the GO analysis revealed pathways that were common between the two cell lines were associated with the gain of the H3K4me3 mark in correlation with ATM loss. These included cell-cell adhesion (MEC1 cells: genes count = 152, adj p-value = 2.14×10^{-7}), (CII cells: genes count = 121, adj p-value = 5.17×10^{-7}), inflammatory and immune responses (MEC1 cells: genes count = 139, adj p-value = 2.78×10^{-12}), (CII cells: genes count = 164, adj p-value = 6.97×10^{-5}), and MAPK signalling pathway (MEC1 cells: genes count = 103, adj p-value = 3.31×10^{-7}), (CII cells: genes count = 113, adj p-value = 2.33×10^{-6}), (Figure 3.11).

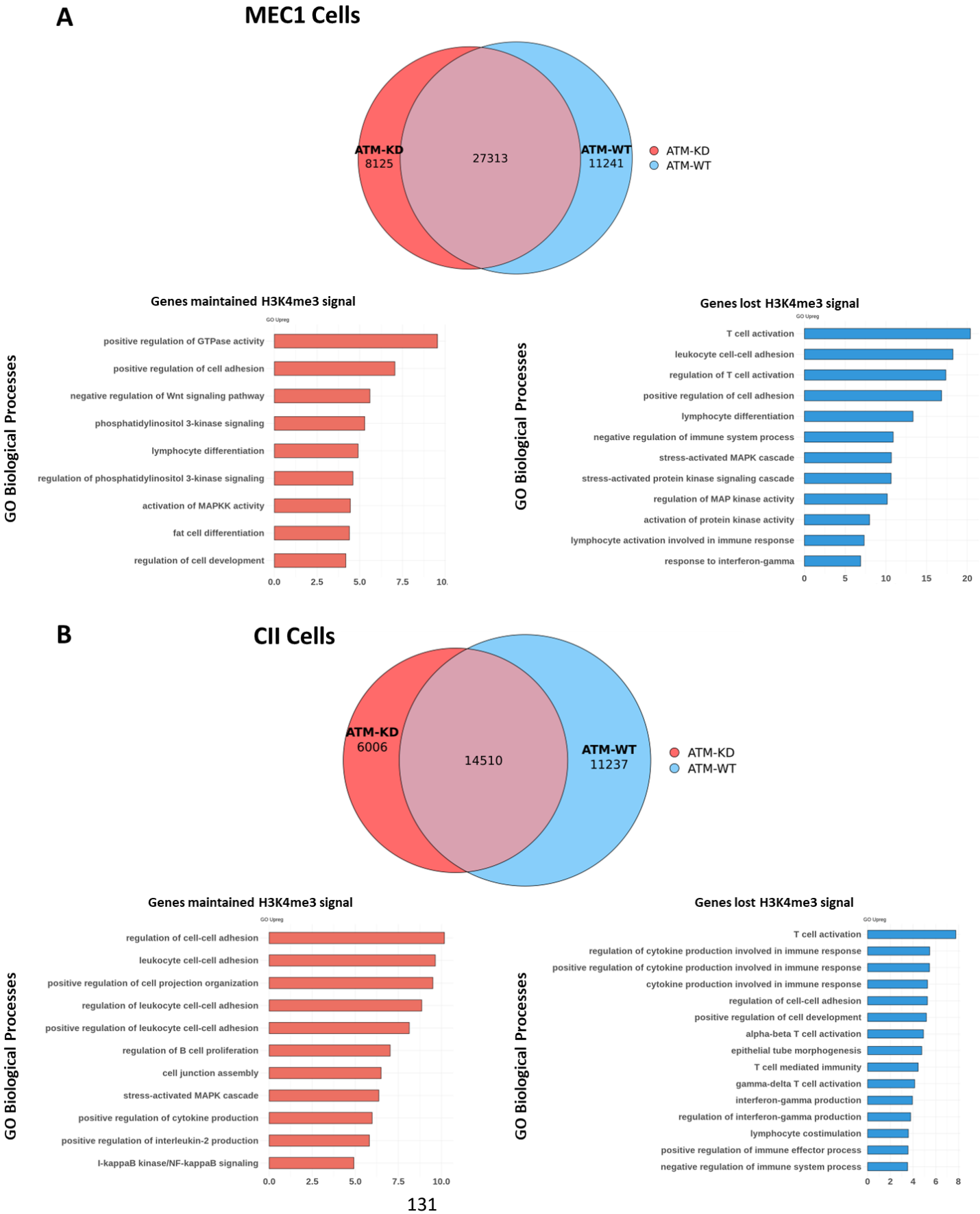

A
MEC1 Cells
ATM-KD
8125
27313
ATM-WT
11241
ATM-KD
ATM-WT
Genes maintained H3K4me3 signal
GO Biological Processes
GO Upreg
positive regulation of GTPase activity
positive regulation of cell adhesion
negative regulation of Wnt signaling pathway
phosphatidylinositol 3-kinase signaling
lymphocyte differentiation
regulation of phosphatidylinositol 3-kinase signaling
activation of MAPKK activity
fat cell differentiation
regulation of cell development
0.0
2.5
5.0
7.5
10.
Genes lost H3K4me3 signal
GO Biological Processes
GO Upreg
T cell activation
leukocyte cell-cell adhesion
regulation of T cell activation
positive regulation of cell adhesion
lymphocyte differentiation
negative regulation of immune system process
stress-activated MAPK cascade
stress-activated protein kinase signaling cascade
regulation of MAP kinase activity
activation of protein kinase activity
lymphocyte activation involved in immune response
response to interferon-gamma
0
5
10
15
20
B
CII Cells
ATM-KD
6006
14510
ATM-WT
11237
ATM-KD
ATM-WT
Genes maintained H3K4me3 signal
GO Biological Processes
GO Upreg
regulation of cell-cell adhesion
leukocyte cell-cell adhesion
positive regulation of cell projection organization
regulation of leukocyte cell-cell adhesion
positive regulation of leukocyte cell-cell adhesion
regulation of B cell proliferation
cell junction assembly
stress-activated MAPK cascade
positive regulation of cytokine production
positive regulation of interleukin-2 production
I-kappaB kinase/NF-kappaB signaling
0.0
2.5
5.0
7.5
10.0
Genes lost H3K4me3 signal
GO Biological Processes
GO Upreg
T cell activation
regulation of cytokine production involved in immune response
positive regulation of cytokine production involved in immune response
cytokine production involved in immune response
regulation of cell-cell adhesion
positive regulation of cell development
alpha-beta T cell activation
epithelial tube morphogenesis
T cell mediated immunity
gamma-delta T cell activation
interferon-gamma production
regulation of interferon-gamma production
lymphocyte costimulation
positive regulation of immune effector process
negative regulation of immune system process
0
2
4
6
8

Figure 3.11 Analysis of genomic regions associated with the observed changes in H3K4me3 epigenetic mark in correlation with ATM loss

H3K4me3 peaks from each condition were intersected to identify genomic regions unique for each condition (MEC1 ATM WT, MEC1 ATM KD, CII ATM WT, CII ATM KD) and Venn diagrams were generated for each cell line. Genomic regions not overlapping with cell line counterparts were termed (Unique). The red colour denotes H3K4me3 genomic regions correlated with ATM loss, whereas blue represents the genomic regions that lost this epigenetic mark. Unique peak sets for each condition were then annotated to the nearest gene, and GO analysis was carried out to determine the associated pathways with the identified set of genes. (A) The analysis was performed on the MEC1 cell line, (B) The analysis was performed on the CII cell line. Both cell lines show that the H3K4me3 epigenetic mark is associated with pathways such as MAPK and immune cell development in accordance with ATM loss.

Together, genes that maintained H3K4me3 epigenetic mark and correlated with ATM loss may potentially contribute to the proliferation of ATM defective CLL cells. With respect to genes that lost the H3K4me3 mark and in line with ATM loss, both cell lines showed GO terms related to T-cell activation (MEC1 cells: genes count = 204, adj p-value = 6.09×10^{-15}), (CII cells: genes count = 140, adj p-value = 1.66×10^{-6}), lymphocyte activation and co-stimulation (MEC1 cells: genes count = 80, adj p-value = 8.04×10^{-6}), (CII cells: genes count = 27, adj p-value = 1.52×10^{-4}), Several research groups have demonstrated the involvement of histone demethylases in immune system regulation (Li et al., 2014a, Wu et al., 2018) and tumour immunity (Qin et al., 2019), suggesting their role in tumorigenesis. Moreover, decreased H3K4 methylation levels were observed in drug-resistant cancer cells (Xu et al., 2018). Collectively, ATM loss was correlated with genome-wide deregulation of active histone marks. Further analysis of genomic regions affected by this observed deregulation revealed genes involved in immune regulation and inflammatory responses in agreement with RNA-seq results. Therefore, investigation of cis-regulatory elements associated with the observed changes in gene expression and histone post-translation modifications was the next step toward the identification of transcriptional dependencies correlated with ATM loss.

3.5 Characterisation of chromatin cis-regulatory elements alterations in accordance with ATM loss status

The Assay of Transposase Accessible Chromatin sequencing (ATAC-seq) methodology allows the assessment of chromatin accessibility at the genome-wide level. Knowing open chromatin regions helps reveal how chromatin landscape and transcription factors affect gene expression and regulation (Klemm et al., 2019). In principle, ATAC-seq uses a similar approach to DNase I hypersensitive sites analysis with high-throughput sequencing (DNase-seq). In ATAC-seq however, modified Tn5 transposase tags open DNA fragments with Illumina adapter sequences that removes the requirement for NGS libraries generation. The advantages of ATAC are the requirement for low input material compared to DNase-seq, and the avoidance of chemical treatment that might introduce bias compared to Formaldehyde-Assisted Isolation of Regulatory Elements followed by sequencing (FAIRE-seq).

Extensive research has been performed to characterise the chromatin-accessibility landscape in CLL (Beekman et al., 2018, Ott et al., 2018, Rendeiro et al., 2016, Pastore et al., 2017). The chromatin accessibility at the single-cell level was also reported following ibrutinib treatment in CLL (Rendeiro et al., 2020). It was subsequently reported that CLL cells rely on transcription factors (NFATc1, E2F5, and NR3C2) to facilitate disease progression and maintenance (Ott et al., 2015). However, the specific impact of ATM loss on chromatin alterations in CLL is still unclear.

Therefore, I performed assayed ATAC-seq to identify differentially accessible regions in both ATM KD and ATM WT cells. I then investigated the presence of regulatory regions at these differentially accessible sites bound by transcription factors in ATM KD and ATM WT cells. I subsequently integrated chromatin-accessible data with RNA-seq and ChIP-seq to generate a comprehensive picture of the chromatin landscape in ATM-deficient CLL cells.

Following the ATAC sequencing procedure as described in the method section, ATAC peaks were called using MACS2 software, and the resulted summit peaks were filtered to summit peaks that are common in both replicates and have at least a read pileup of 10. A consensus summit peak list was created and included peaks from both conditions (MEC1 cells: 28616 consensus summit peaks, CII cells: 39724 consensus summit peaks). FeatureCounts software was used to create a peak count matrix for downstream analysis. By employing duplicates from each condition in each cell line, I performed a differential chromatin-accessibility analysis (edgeR package) to identify ATM loss correlated lost and gained specific accessible sites. I defined peaks/sites as a specific site if it had an adj p-value below 0.1 and log2 fold change -/+ 1.5. A Volcano plot (Figure 3.12 A) shows significantly specific peaks that passed the predetermined cut-off.

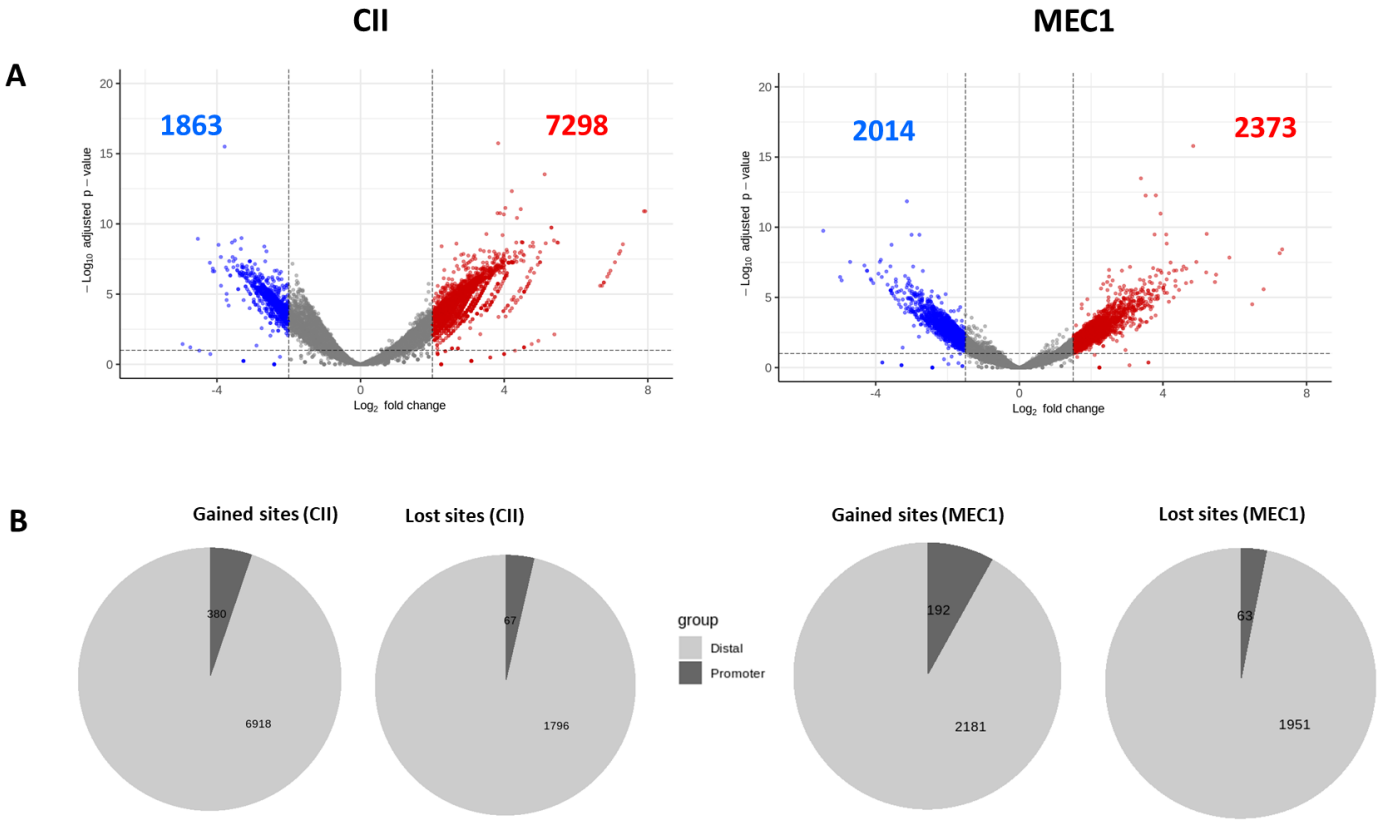


Figure 3.12 Genome-wide changes in the chromatin accessibility landscape of distal regulatory elements are in correlation with ATM loss status in CLL cells
(A) Volcano plots resulting from differential chromatin accessibility analysis performed on MEC1 and CII cell lines demonstrating statistically significant peaks (adj p-value < 0.1 and log2 fold change > 1.5) coloured in red for upregulated peaks and blue for downregulated peaks; up-regulated peaks were termed gained sites and down-regulated peaks termed lost sites. (B) Gained and lost sites were annotated to the nearest gene and considered to be in promoter regulatory regions if peaks fell within -/+ 1500 bp of TSS and distal regulatory regions otherwise. (MEC1 cells on the right-hand side and CII cells on the left-hand side). Overall, CLL cells with ATM loss are correlated with significant genome-wide changes at distal regulatory elements. The number of ATAC-seq replicates per condition is two (N=2)

From differential chromatin-accessibility analysis, I identified specific gained and lost accessible sites correlated with ATM loss. The analysis showed that MEC1 cells were correlated with 2373 upregulated and 2014 downregulated accessible sites, whereas CII cells were correlated with 7298 upregulated and 1863 downregulated accessible sites. I then annotated specific sites using the ChIPpeakAnno package and further sub-divided peaks as either a promoter or distal regulatory elements (Figure 3.12 B). A peak was considered to be in the gene promoter if it was found within 1500 bp upstream and downstream of the transcription start site (TSS) and as a distal element otherwise. From peak annotations, I observed that most chromatin alterations in line with ATM loss are located at distal elements, and the changes at promoter elements were minimal; therefore, downstream analysis is focused on peaks defined as distal elements.

To further validate that these identified specific sites are indeed sites associated with ATM loss and not in line with the control samples, I generated a meta profile of ATAC-normalized coverage at sites that were identified as specific sites in both isogenic cell lines (Figure 3.13). In ATM KD specific sites, ATAC coverage is correlated with both replicates of the ATM defective samples, whereas in the ATM WT specific sites, ATAC coverage is in accord with the ATM WT control samples, suggesting that these sites are related to ATAC condition-specific sites. To investigate the histone modification profiles at these regulatory sites in MEC1 cells, the H3K27ac coverage (because most changes occurred at distal elements) was plotted against gained and lost sites. From the results, it is apparent (Figure 3.14) that the sites in ATM-deficient

CLL cells were associated with a reduction of H3K27ac levels at defined lost sites, whereas no change was observed for the same histone mark at the gained sites suggesting that chromatin accessibility of some cis-regulatory elements was lost in parallel with ATM-deficient CLL cells.

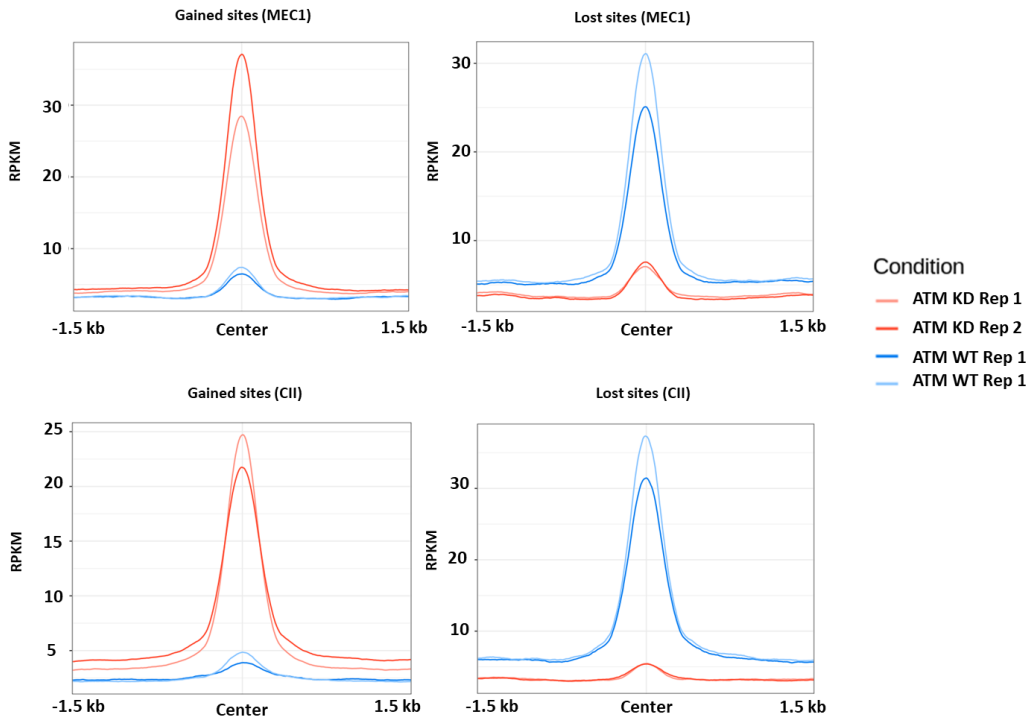


Figure 3.13 Validation of the defined sets of gained and lost chromatin accessible sites in correlation with ATM loss status.
Meta profile of gained and lost sites of a region that extends 1500 bp upstream and downstream of peak summit centres. Meta profile shows that gained sites are enriched in ATM-defective replicates, whereas lost sites show only enrichments for ATM WT control cells, suggesting that these sites are condition-specific sites.

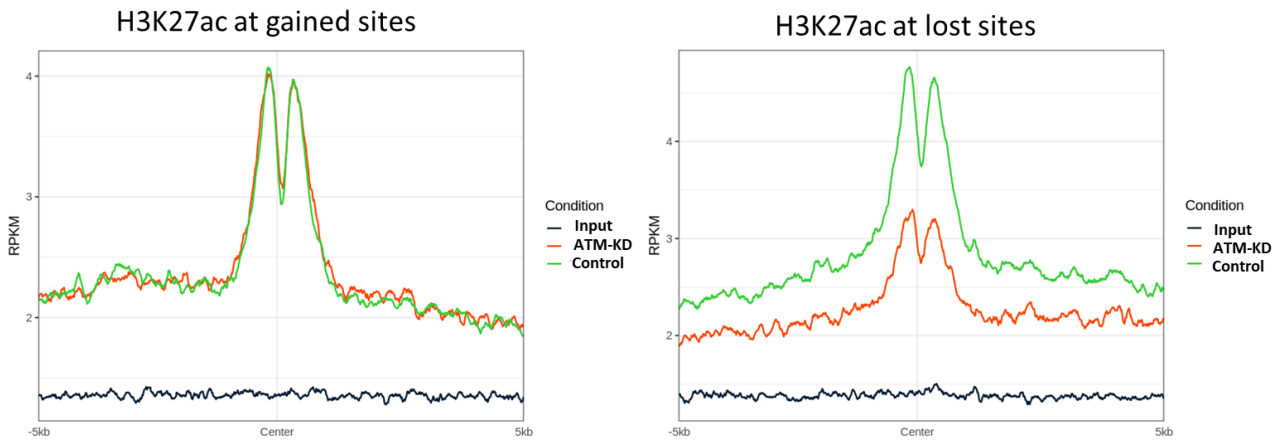


Figure 3.14 Sites that were lost in accordance with ATM status showed a decrease in H3K27ac levels
Meta profile of normalized H3K27ac ChIP counts centred on previously determined ATM-defective peaks of MEC1 CLL cells. The meta profile extends 5000 bp upstream and downstream of ATAC-specific peaks. The meta profile suggests that gained accessible sites are in line with H3K27ac levels in both conditions. In contrast, in lost sites, the levels of H3K27ac marks are reduced, suggesting a decreased chromatin accessibility in correlation with ATM loss status.

To investigate whether the identified ATAC-specific sites that were correlated with ATM loss contained motifs associated with transcription factors in MEC1 cells, I performed motif enrichment analysis in distal sites using HOMER software (Heinz et al., 2010). At the gained sites, de-novo motif discovery showed enrichment of RUNX, E-box, AP-1 and IRF, whereas, at the lost sites, an enrichment of ETS, HOX, IRF and NFkB was observed (Figure 3.15 A and B). These results suggest that ATM loss is in line with the enrichment of transcription factors AP-1, RUNX, Ebox and IRF and these TFs may have an important contribution in the transcriptional deregulation correlated with ATM absence in CLL cells and relate to the inflammatory signature observed in the GSEA analysis RNA-seq data (Figure 3.7).

A

ATM KD Specific

Motif	Match	% sites	p-value
	RUNX	36.77	1e-134
	E-Box	25.13	1e-49
	AP-1	22.42	1e-227
	IRF	18.66	1e-103

B

Control Specific

Motif	Match	% sites	p-value
	ETS	35.06	1e-178
	HOX	26.86	1e-70
	IRF	24.09	1e-55
	NFkB	13.79	1e60

Figure 3.15 Motif enrichment analysis at gained and lost sites associated with ATM loss status (distal peaks only, MEC1 cells only)

The defined gained and lost accessible sites obtained from chromatin accessibility analysis were subjected to motifs analysis to look for the enrichment of transcription factors associated with distal regulatory elements that were correlated with ATM loss. (A) Homer de novo motifs found at gained peaks (ATM KD specific) ranked by site percentage. (B) Homer de novo motifs found at lost peaks (ATM WT control specific) were ranked by site percentage. The analysis suggests that TF motifs of RUNX, AP-1, EBOX, and IRF are in correlation with ATM loss status

Transcription factors interact and cooperate to form large complexes that may reprogram the transcriptional landscape and create a transcriptional dependency (Edginton-White and Bonifer, 2022). Therefore, I performed bootstrapping analysis on ATAC distal-specific sites to seek significant co-localizing motifs within 50 bp. This analysis assesses the co-localization of motifs within 50 bp found in ATAC-specific sites by comparing motifs co-localization to the sample background. The analysis showed that the transcriptional landscape in ATM-defective cells is correlated with AP-1 and RUNX TFs, which have motifs co-localizing with each other along with additional transcription factors (Figure 3.16).

The AP-1 activity is known to be regulated by mitogen-activated protein kinases (MAPK), a subtype of enzymes conserved in eukaryotes that monitor cellular activities in reaction to surrounding environmental signals (oncogenes, cytokines and growth factors) (Atsaves et al., 2019). This result is in agreement with the results shown in figure 3.11), where the ChIP H3K4me3 data showed that genes maintaining their H3K4me3 signals that were in accordance with ATM loss were mainly involved in the MAPK activation cascade according to the GO analysis. Moreover, in agreement with RNA-seq data, a slight up-regulation of some of the AP-1 sub-families is correlated with ATM loss (Figure 3.17). The enrichment of AP-1 and RUNX motifs was also in parallel with ATM loss in CII cells.

In contrast, the co-localization analysis of ATAC lost specific sites demonstrated that ETS and HOX have motifs that co-occurred with each other along with other factors to maintain gene expression in ATM WT control cells, whereas this transcription signature is not observed in correlation with ATM loss status. ETS is required in B cells to maintain their quiescent state, and its loss leads to early pre-maturation into antibody-secreting cells (ASCs) (John et al., 2008, Wang et al., 2005). Therefore, this observation is consistent with the chronic immune stimulation as a well-known feature of CLL cells (Arruga et al., 2020) and may underlie the transcriptomic inflammatory signature observed in GSEA analyses (Figures 3.7).

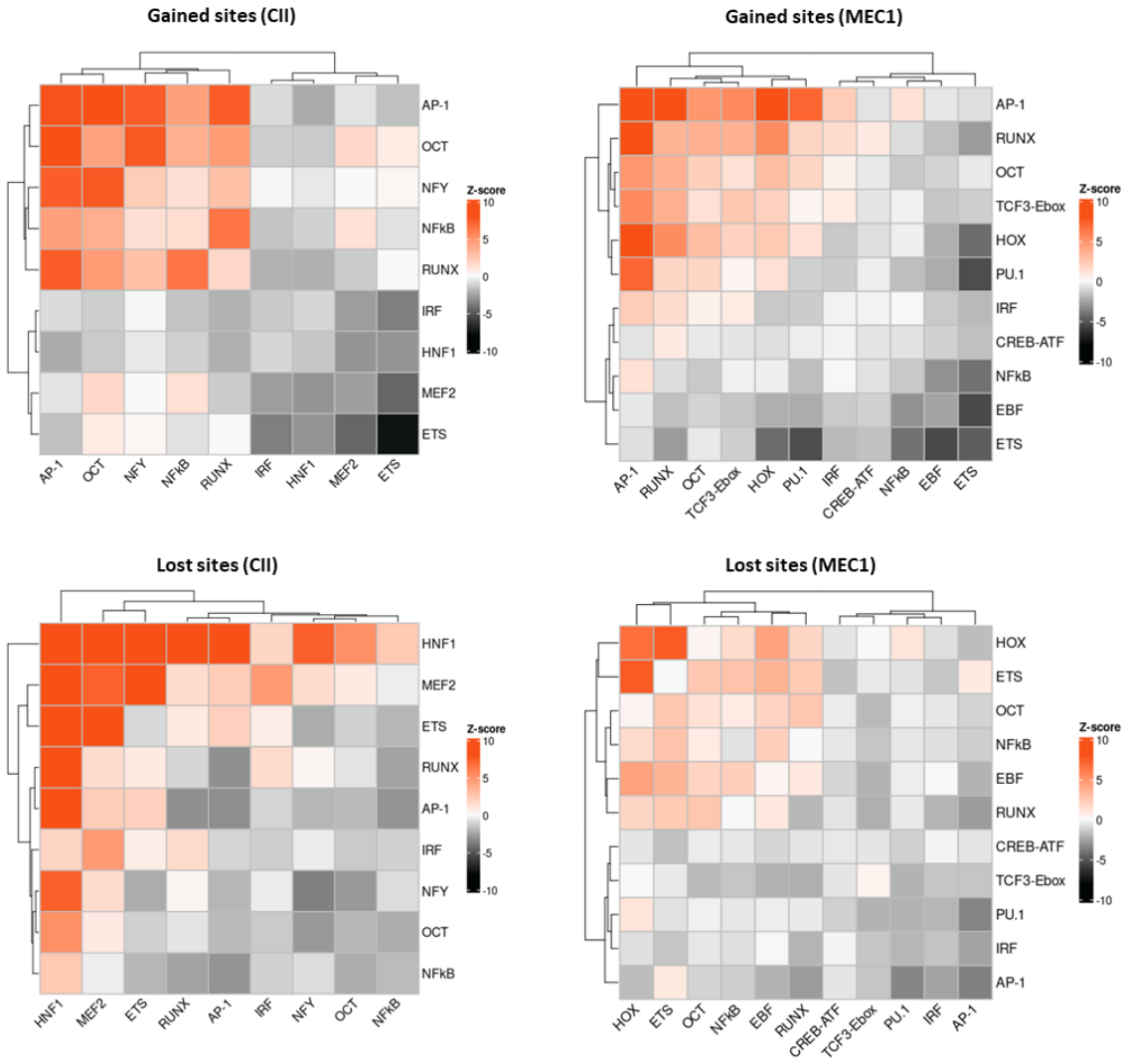


Figure 3.16 ATM-defective CLL cells transcriptional landscape is correlated mainly with the transcription factors AP-1 and RUNX

Bootstrapping analysis was computed on defined ATM-defective specific motifs in comparison to ATM WT control to examine the co-localization of binding motifs associated with transcription factors. This analysis revealed a significant co-localization of the AP-1 and RUNX motifs. The analysis highlighted that TFs AP-1 and RUNX are associated with transcriptional alterations in line with the loss of ATM.

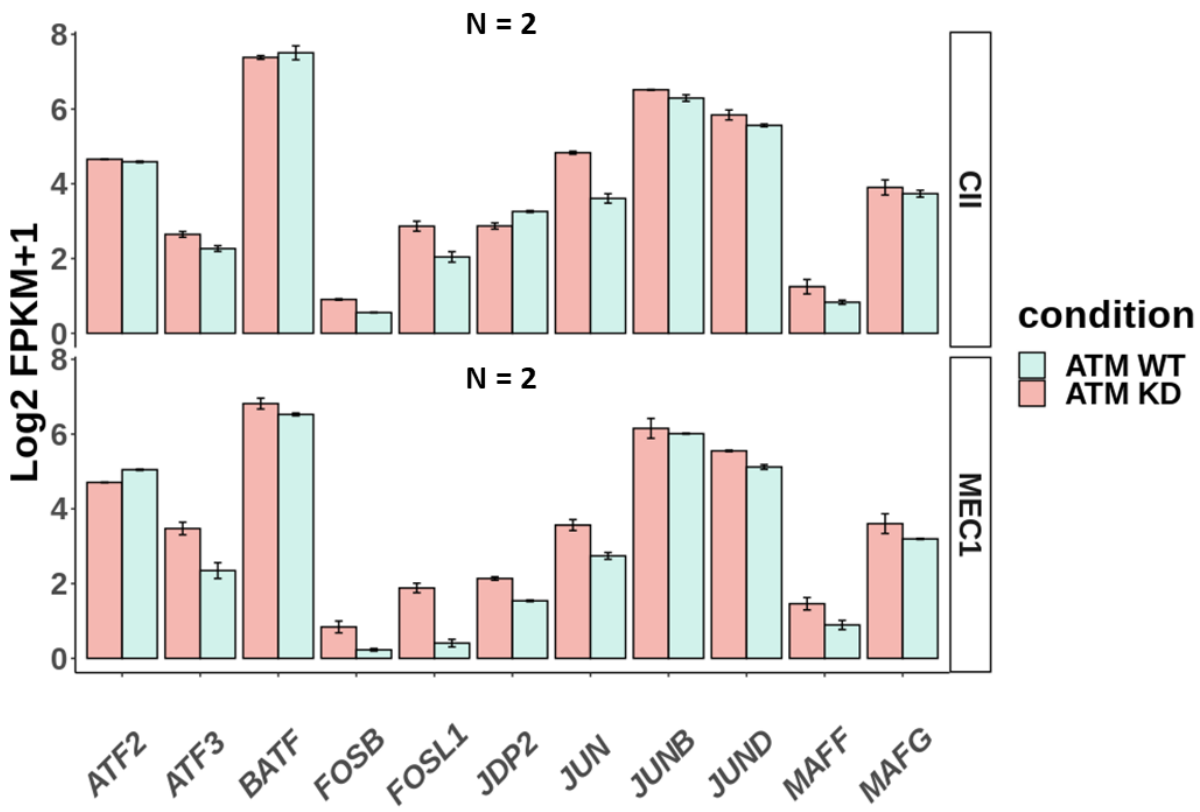


Figure 3.17 Several members of AP-1 transcription factor family showed a differential gene expression pattern in line with ATM loss status in CLL cells

The calculated Log2 normalized gene expression values (FPKM) for AP-1 family transcription factors were extracted and plotted as a bar plot. The expression pattern of some of the AP-1 family members showed an overall differential gene expression pattern (a slight upregulation) in both cell lines (MEC1 and CII) in line with ATM loss status.

3.6 Integration analysis of ATAC-seq, ChIP-seq and RNA-seq data demonstrate the chromatin landscape changes in correlation with ATM loss

To generate an overall picture of the chromatin landscape of ATM-defective cells, I performed an integrative analysis by correlating chromatin accessibility, histone modifications and transcriptomic data. This integration analysis allowed me to examine gained and lost sites and then study gene expression profiles at these sites together with histone modifications and transcription factor motif enrichment. I began the integration analysis by first ranking differential chromatin-accessibility distal sites by fold change (MEC1 cells: 28616 consensus summit peaks, CII cells: 39724 consensus summit peaks), where

gained sites (up-regulated) were at the top and lost sites (down-regulated) at the bottom. I then created a heatmap of ATAC-normalized counts at these sites using HOMER and used a window size of 1 KB before and after peak centres. For correlating ATAC with RNA-seq data, I used the same ATAC-ranked list, annotated each peak to the closest gene, extracted the gene expression log2 fold change for that annotated gene and plotted the gene expression profile as a heatmap. I selected the top four significant gained and lost de-novo motifs for the motif enrichment heatmap, examined their enrichment in my ATAC-ranked list, and created a heatmap with a 1-KB window around the peak centre. Finally, I used the same ATAC-ranked list for histone modifications and then created a heatmap with normalized ChIP counts in a 4-kb window around the peak centre.

The integration of the three data sets showed that ATM-defective specific gained sites were correlated with genes with an up-regulated gene expression profile (Figure 3.18). In contrast, ATM-defective lost sites were correlated with genes with a down-regulated gene expression profile. By linking chromatin-accessible data with transcriptomic data, I observed that accessible regions are correlated with an active transcription state, whereas closed or condensed regions are associated with an inactive transcriptomic state, in agreement with published research (Cao et al., 2018, Weintraub and Groudine, 1976, Hewish and Burgoyne, 1973, Kornberg, 1974). However, overall, all H3K4me3, H3K4me1, and H3K27ac signals were decreased in accordance with ATM loss status in MEC1 cells. The same was observed for histone PTMs H3K4me3 and H3K27ac in CII cells in agreement with ChIP data.

The integration analysis showed that ATM-defective gained sites were correlated with enrichment for motifs associated with AP-1, RUNX, IRF and E-box, suggesting that the up-regulated gene expression at these sites might be driven by these transcription regulators. In contrast, ATM-defective lost sites were in line with the enrichment of ETS, HOX, NFkB and IRF in parallel with reduced gene expression. The gene expression profiles of ETS and some HOX TFs were decreased slightly.

To further investigate and understand the stable regulatory network driving gene expression that is consistent with ATM loss, I analyzed ATAC defined gained and lost specific motifs and identified their enrichment at their downstream target TF genes. Enriched motifs correlated with ATM-defective specific sites (gained and lost) were considered as major nodes, and their border is coloured according to their expression values (FPKM). A direct edge from a major node (here representing an ATAC-enriched motif) to a minor node (here representing the locus of a downstream TF gene) indicates the enrichment of that motif at its target gene. The edge was coded by colour and width according to the motif count enrichment (Figure 3.19).

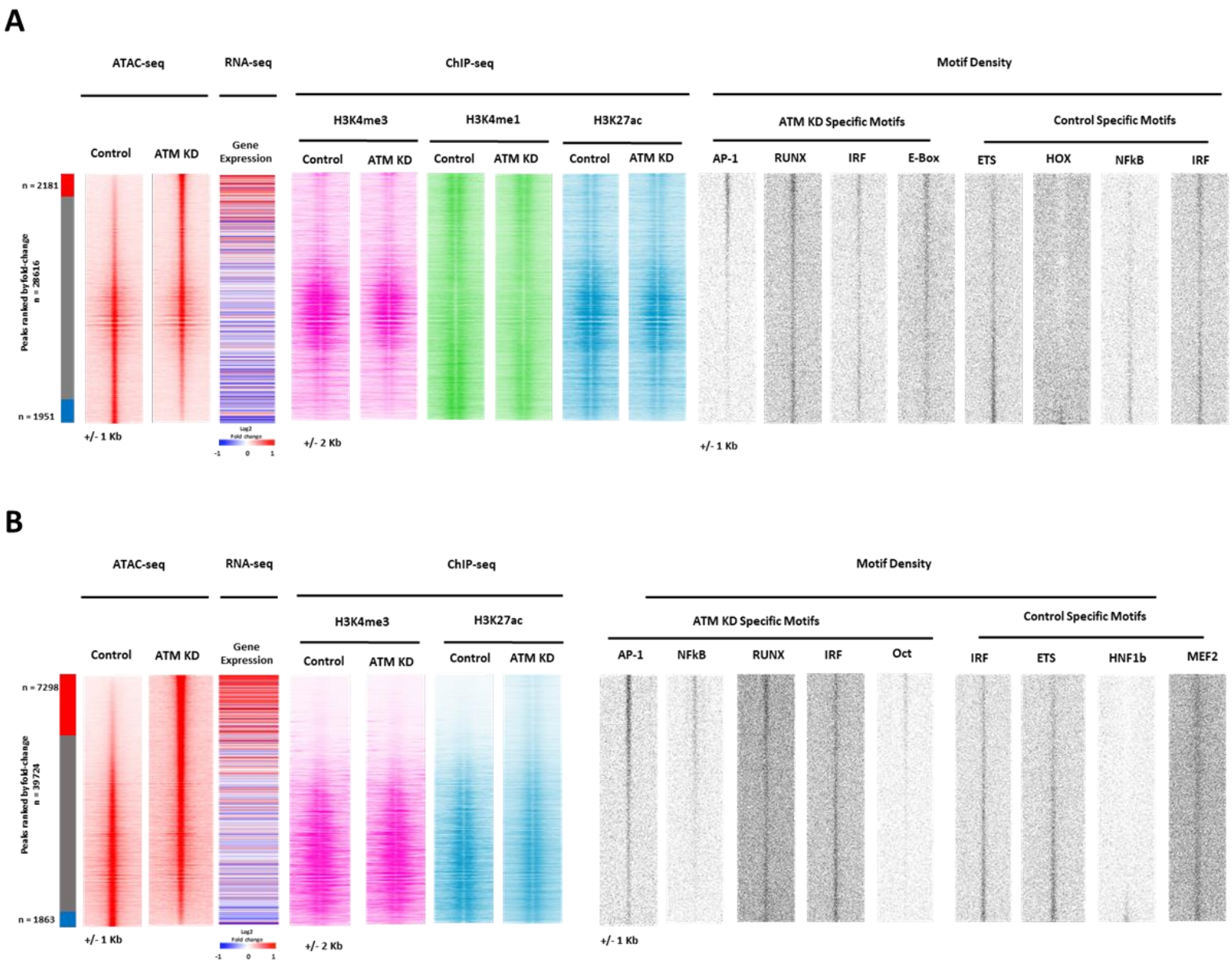

A
ATAC-seq
RNA-seq
ChIP-seq
Motif Density
H3K4me3
H3K4me1
H3K27ac
ATM KD Specific Motifs
Control Specific Motifs
Control
ATM KD
Gene Expression
AP-1
RUNX
IRF
E-Box
ETS
HOX
NFkB
IRF
n = 2181
Peaks ranked by fold-change
n = 28616
n = 1951
+/- 1 Kb
Log2 Fold change
-1
0
1
+/- 2 Kb
+/- 1 Kb
B
ATAC-seq
RNA-seq
ChIP-seq
Motif Density
H3K4me3
H3K27ac
ATM KD Specific Motifs
Control Specific Motifs
Control
ATM KD
Gene Expression
AP-1
NFkB
RUNX
IRF
Oct
IRF
ETS
HNF1b
MEF2
n = 7298
Peaks ranked by fold-change
n = 39724
n = 1863
+/- 1 Kb
Log2 Fold change
-1
0
1
+/- 2 Kb
+/- 1 Kb

Figure 3.18 Integrative analysis of chromatin accessibility, gene expression, histone modifications and motif enrichment alterations in correlation with ATM loss in CLL cells

The integration analysis began with ATAC-seq data (left), the consensus accessible sites were ranked according to fold change obtained from differential accessibility analysis. Next, ATAC-seq signals were plotted as heatmap above the defined peak list. The ATAC-seq heatmaps show that gained and lost sites are seen only in correlation with ATM loss conditions. Next, gene expression data were integrated by extracting the gene expression (log2 fold change) of genes linked with the defined peak list and plotting the expression results as a heatmap (upregulation coloured as red and downregulation coloured in blue). The gene expression heatmap shows that gained sites are linked with upregulated gene expression profile, whereas lost sites at the bottom are associated with downregulated gene expression profile. Next, histone PTM ChIP-seq signals for each condition were integrated and plotted over the defined ranked peak list. The ChIP-seq signals show marked signal intensity of histone PTM (H3K4me3, H3K4me1, and H3K27ac) in correlation with ATM loss status. Finally, the enriched TF motifs resulting from motifs analysis of ATAC-seq data were counted and plotted as a heatmap. The motif density heatmaps show the increased signal of AP-1, RUNX, and IRF motifs at gained sites in correlation with ATM loss status. (A) Integration analysis for MEC1 cell line. (B) Integration analysis for CII cell line.

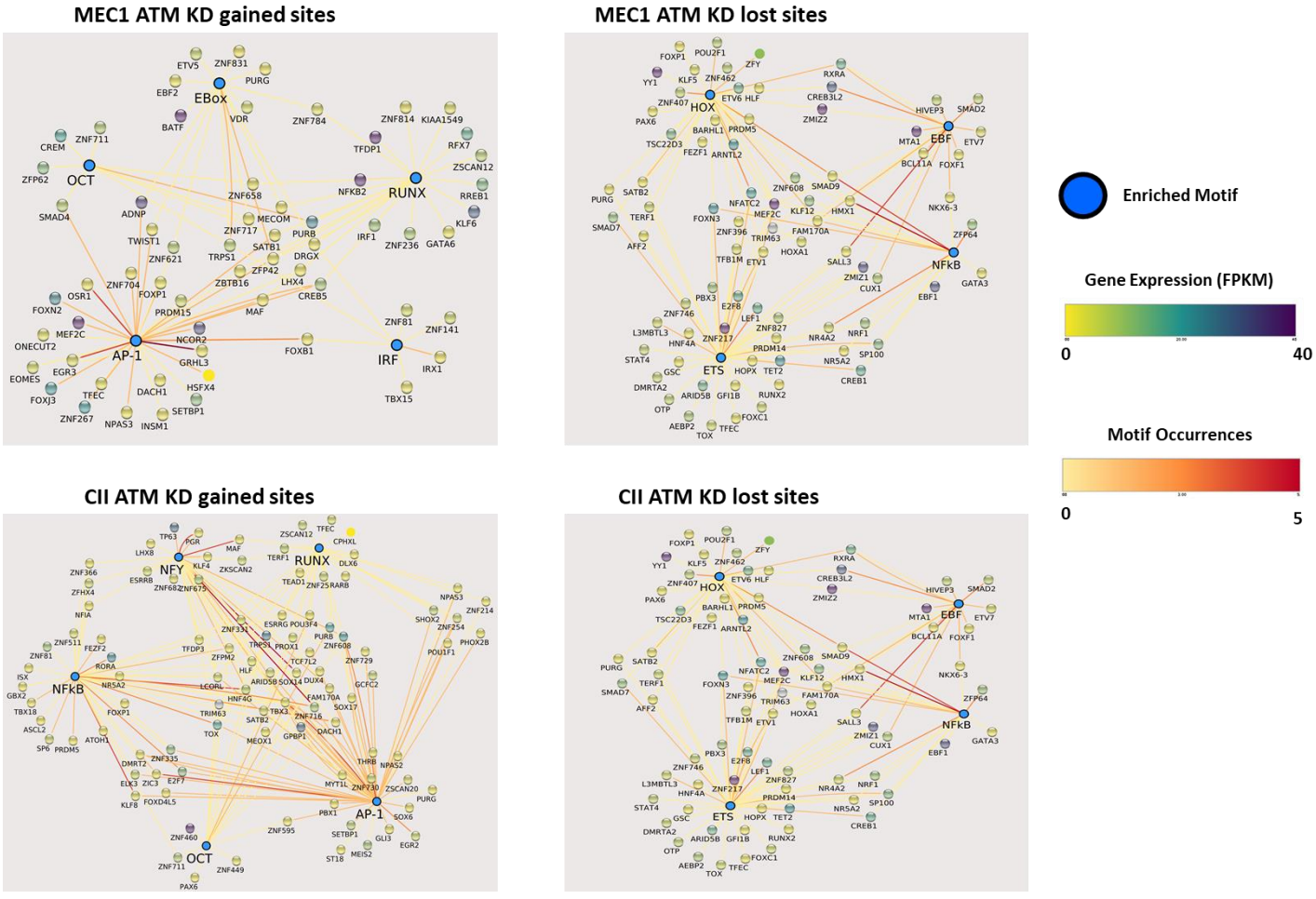


Figure 3.19 Identification of transcription factor networks driving gene expression in accordance with ATM loss status

The identified enriched ATAC motifs correlated with ATM-specific gained and lost sites were annotated to the nearest TF gene. The expression profile was extracted for each downstream gene as well as the motif occurrences. Together, the information on TF gene expression and ATAC motif occurrences at TF genes were used as an input for building the TF transcriptional network. Blue and black-bordered major nodes represent an enriched ATAC motif. Minor nodes represent downstream TF genes, and their colour represents the gene expression in FPKM. Edges emerging from major nodes toward minor nodes show the occurrence of a motif, and edge colour represents the number of motifs found at that TF gene. The analysis highlights that AP-1 and RUNX share a set of downstream TF target genes in line with defective ATM status.

The transcription factor network analysis identified the transcription factors that may be involved in driving the gene expression in accordance with ATM loss in CLL cells (Figure 3.19). The analysis demonstrated the high relevance of the AP-1 family network in correlation with ATM loss in the two cell lines (MEC1 and CII). The AP-1 and RUNX transcription factors both showed a common set of genes, suggesting that they potentially work with shared target genes to maintain a specific transcriptional signature, a result that is consistent with my co-localization analysis, where I demonstrated that the two transcription factors work in proximity of each other in line with ATM loss. In contrast, the TF network analysis of isogenic MEC1 and CII showed that the ETS transcriptional signature was lost in correlation with ATM loss. The ETS and Hox transcription factors share a set of genes responsible for maintaining a specific transcriptional program that has been lost in parallel with ATM loss CLL cells. This is consistent with the co-localization analysis, where the interaction between ETS and HOX interaction is lost in relation with ATM loss.

3.7 The upregulation of KDM5B gene expression is correlated with ATM loss in CLL cells

I reasoned that one potential cause for the observed down-regulation of H3K4me3 in correlation with ATM-defective CLL cells could be the significant upregulation of demethylase KDM5B found in RNA-seq analysis and was correlated with ATM loss. KDM5B is a histone demethylase that belongs to the KDM5 demethylase subfamily and is one of the Jumonji C (JmjC) KDMs. The protein structure (Figure 3.20) shows

three PHD domains; a C5HC2 zinc finger domain that guides this enzyme to its histone targets, a DNA binding domain ARID as well as JmjC and JmjN catalytic domains. The inclusion of ARID and PHD domains into the Jumonji domain results in two separate catalytic domains and makes this KDM5 family unique among the Jumonji histone demethylases (Pilka et al., 2015). This demethylase has an enzymatic activity that relies on 2-oxoglutarate-dependent dioxygenases, which need for their function Fe^{2+} and oxygen to remove histone tail methyl groups through a hydroxylation reaction (Figure 3.10) (Højfeldt et al., 2013). The observed up-regulation of KDM5B consistent with ATM-defective CLL cells was supported at both mRNA and protein levels (MEC1) (Figure 3.21). Emerging evidence suggests that KDM5B plays an essential part in cancer chemoresistance (Plch et al., 2019). This has the implications for potential therapeutic targeting of these enzymes. I set, therefore to interrogate the KDM5B status in ATM-defective CLL cells (MEC1) in more detail.

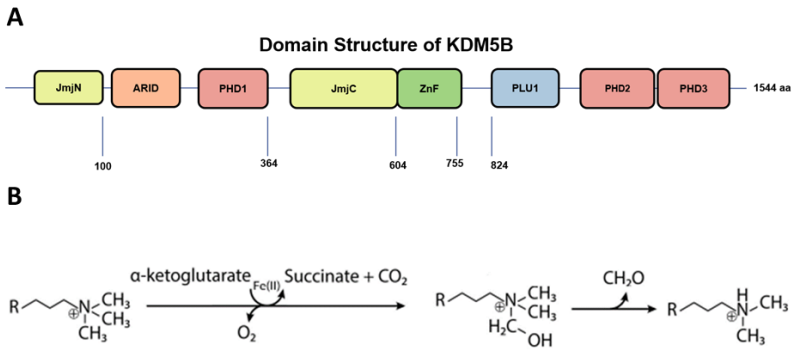


Figure 3.20 Protein structure and function of KDM5B
(A) Schematic plot showing KDM5B protein domains. (B) KDM5B demethylation reaction uses 2-oxoglutarate-dependent dioxygenases, which require Fe^{2+} and oxygen to undertake the hydroxylation reaction and remove methyl groups from histone tails.

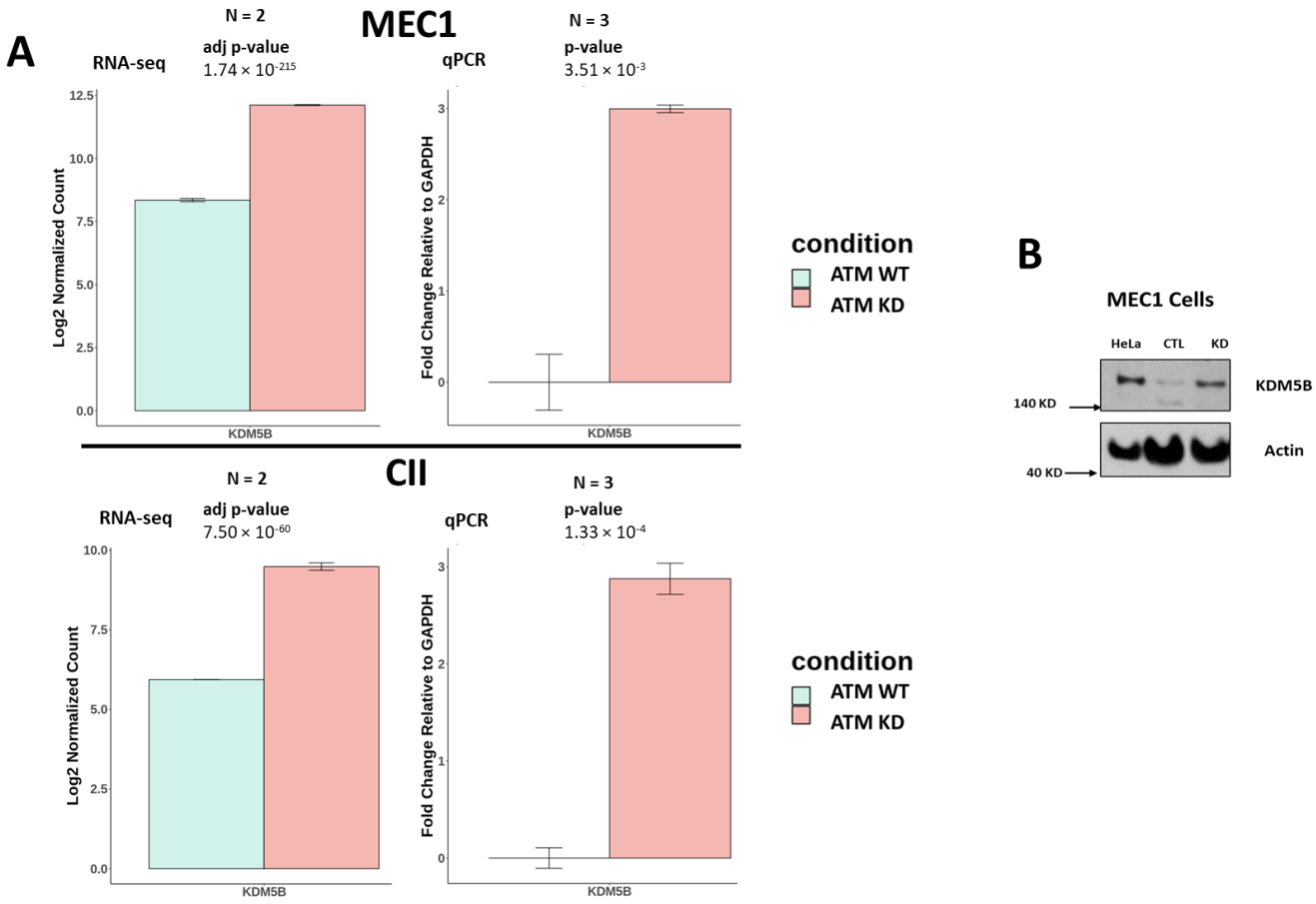


Figure 3.21 KDM5B is up-regulated in CLL cells in correlation with ATM loss status
(A) KDM5B is up-regulated in RNA-seq data in line with ATM loss status in both CLL cell lines (MEC1 and CII); the KDM5B up-regulation was validated in CLL cell lines using qPCR. (B) Western blot shows that KDM5B is also up-regulated at the protein level in ATM-defective CLL cells (MEC1). The replicates for RNA-seq experiment (N=2), and the replicates for qPCR gene expression experiment (N=3). A p-value of cut off of 0.05 was used qPCR gene expression statistical test whereas an adjusted p-value cut off of 0.1 was used for differential gene expression analysis applied on RNA-seq data.

3.8 Genome-wide KDM5B localization in ATM-defective MEC1 CLL cells

I hypothesised that the genome-wide changes of H3K4me3 and H3K4me1 correlated with ATM loss could be attributed to KDM5B up-regulation, that is also correlated with ATM loss. No information exists regarding the genome binding of KDM5B associated with changes in chromatin in the context of CLL. A previous CML study reported KDM5B genome-wide binding but was lacking a genetic context (Xue et al., 2020). Therefore, to determine the downstream targets of KDM5B that are regulated in an ATM defect-

specific manner, I carried out KDM5B chromatin immunoprecipitation followed by sequencing (ChIP-seq) in ATM defective MEC1 cells and used input as control as KDM5B expression was low in ATM WT CLL cells.

Raw sequencing data show a percentage of sequencing mapping quality (MAPQ=30) of more than 85%, indicating a low probability of calling wrong bases during the generation of sequencing reads (Figure 3.22 A). KDM5B summit peaks (3676) that passed an FDR of 0.01 were annotated to the nearest genes (Gene numbers) to determine what genomic regions are bound by KDM5B. I found that more than 50% of KDM5B peaks were in accord with promoter regions (Figure 3.22 B). KDM5B peaks were annotated to the nearest genes, and by observing the gene expression profile of these genes (adj p-value < 0.1), 829 and 546 genes were found to be up- and down-regulated, respectively (Figure 3.22 C). To further understand the biological impact of genes correlated with KDM5B peaks, I conducted a GO functional pathway analysis on upregulated and downregulated genes. This analysis showed that genes that were linked with KDM5B peaks and have upregulated gene expression profile were involved in pathways such as regulation of cell-cell adhesion (Genes count = 30, adj p-value = 1.23×10^{-2}), regulation of chromatin organization (Genes count = 17, adj p-value = 1.54×10^{-2}), regulation of cell cycle G1/S phase transition (Genes count = 17, adj p-value = 2.32×10^{-2}), and regulation of MAPK activity (Genes count = 17, adj p-value = 1.30×10^{-2})(Figure 3.22 D). On the other hand, genes related with KDM5B peaks that showed downregulation in gene expression were involved in pathways such as negative regulation of gene expression (Genes count = 23, adj p-value = 2.01×10^{-13}), regulation of gene silencing (Genes count = 19, adj p-value = 8.1×10^{-9}), chromatin assembly (Genes count = 23, adj p-value = 8.4×10^{-9}), and double-strand break repair (Genes count = 17, adj p-value = 1.23×10^{-3}), (Figure 3.22 E).

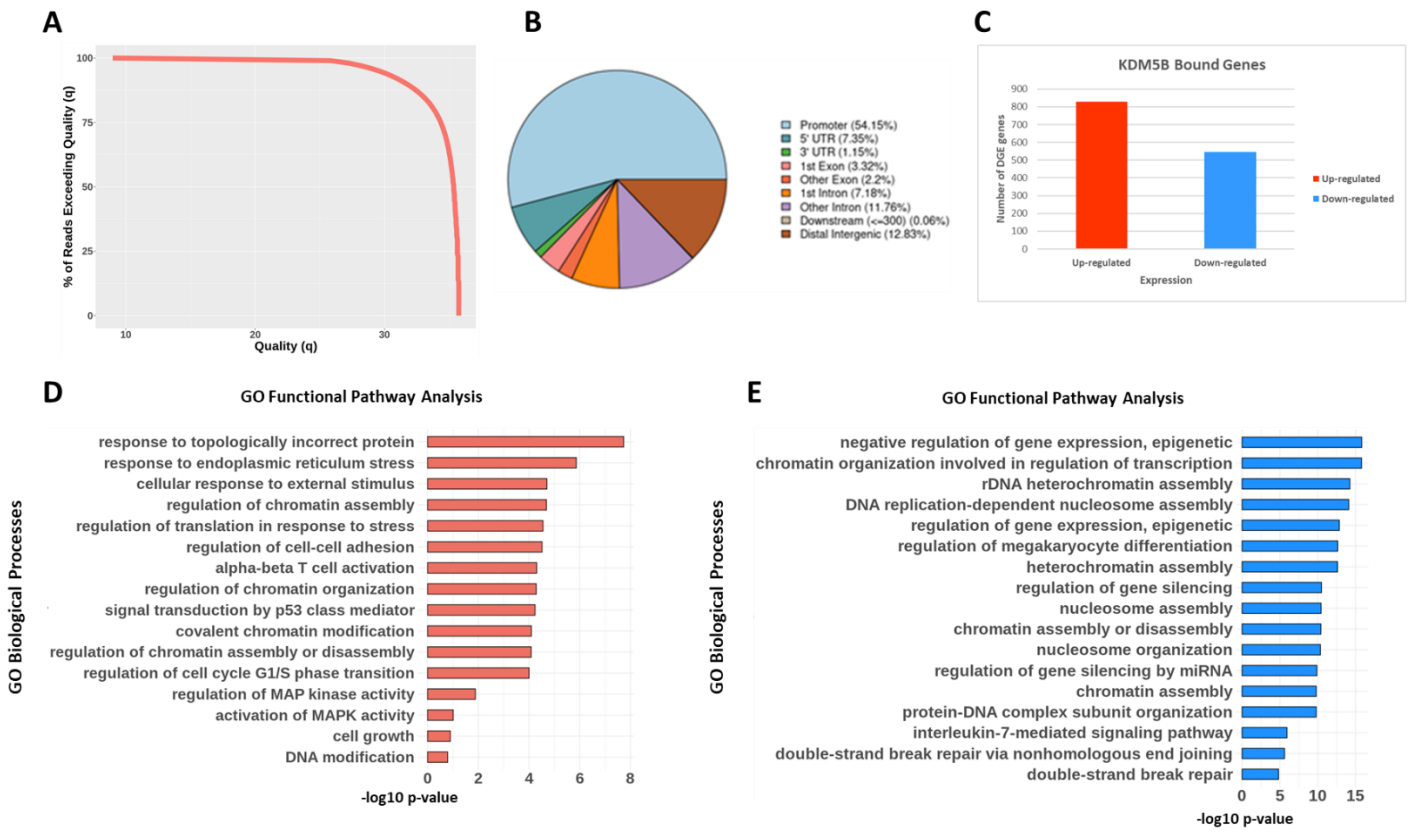


Figure 3.22 Analysis of KDM5B chromatin immunoprecipitation (ATM KD MEC1 cells)
(A) Line plot showing the percentage of sequencing mapping quality (MAPQ) of KDM5B ChIP raw data indicating a high percentage of primary alignments. (B) Genomic distribution of KDM5B peaks. (C) KDM5B peaks were annotated to the nearest genes; the gene expression fold change for KDM5B-bound genes was obtained and plotted as a bar plot (red for up-regulated and blue for down-regulated genes). (D) GO analysis was performed on KDM5B-bound upregulated genes, and the most significant GO terms were plotted. (E) GO analysis was performed on KDM5B-bound downregulated genes, and the most significant GO terms were plotted. Overall, KDM5B associated peaks are observed at promoters of genes that were differentially expressed in correlation with ATM loss. GO analysis of KDM5B associated differentially expressed genes show the enrichment of pathways of chromatin assembly and T-cell activation in relation to upregulated DGE, whereas regulation of gene silencing and DNA repair pathways were linked to downregulated DGE in accordance with ATM loss. Abbreviation: DGE: differentially expressed genes. The number of each ChIP replicates is one (N=1).

To further look into the expression profile of genes related to enriched GO pathways, selected genes associated with the previously enriched pathways were labelled on volcano plots derived from RNA-seq data. Genes that were related to MAP Kinase pathway showed variable log2 fold changes with *SYK* and *INAVA* genes both demonstrated a higher expression profile (Log2 fold change > 2). In contrast, genes

involved in chromatin covalent modifications showed upregulated log2 fold changes but were at the basal levels (Figure 3.23 Panel A).

On the other hand, genes correlated with KDM5B peaks linked with GO pathways and were associated with downregulated gene expression profiles were labelled on the volcano plot and those genes related to the regulation of gene silencing, and double-strand break pathways were indeed downregulated in RNA-seq data although the Log2 fold change was below 2 (Figure 3.23 Panel B).

The observed KDM5B upregulation in correlation with ATM defective CLL cells may contribute to gene expression downregulation by removing the epigenetic mark H3K4me3 using its demethylase property, thereby affecting the genes promoter activity. In contrast, it can be hypothesized that the observed upregulation of genes correlated with KDM5B peaks may be related to KDM5B influence on the transcription machinery activity. Reports have shown that KDM5B inhibition negatively affected RNA Pol II occupancy, transcriptional initiation and elongation in embryonic stem cells. This observation highlights a KDM5B role in enhancing the transcriptional machinery through positive Pol II activity regulation, thus maintaining an active gene expression profile (He and Kidder, 2017). Moreover, it was reported that KDM5B interacts with the epigenetic regulator Polycomb repressive complex 2 (PRC2) through its SUZ12 components. This interaction is correlated with active gene expression of retinoic acid signalling pathway associated genes (Zhang et al., 2014). Together, the previously published works show how KDM5B occupancy correlates with active gene expression as it was observed in ATM defective CLL cells. However, further work will be needed to evaluate KDM5B functional role in gene expression regulation.

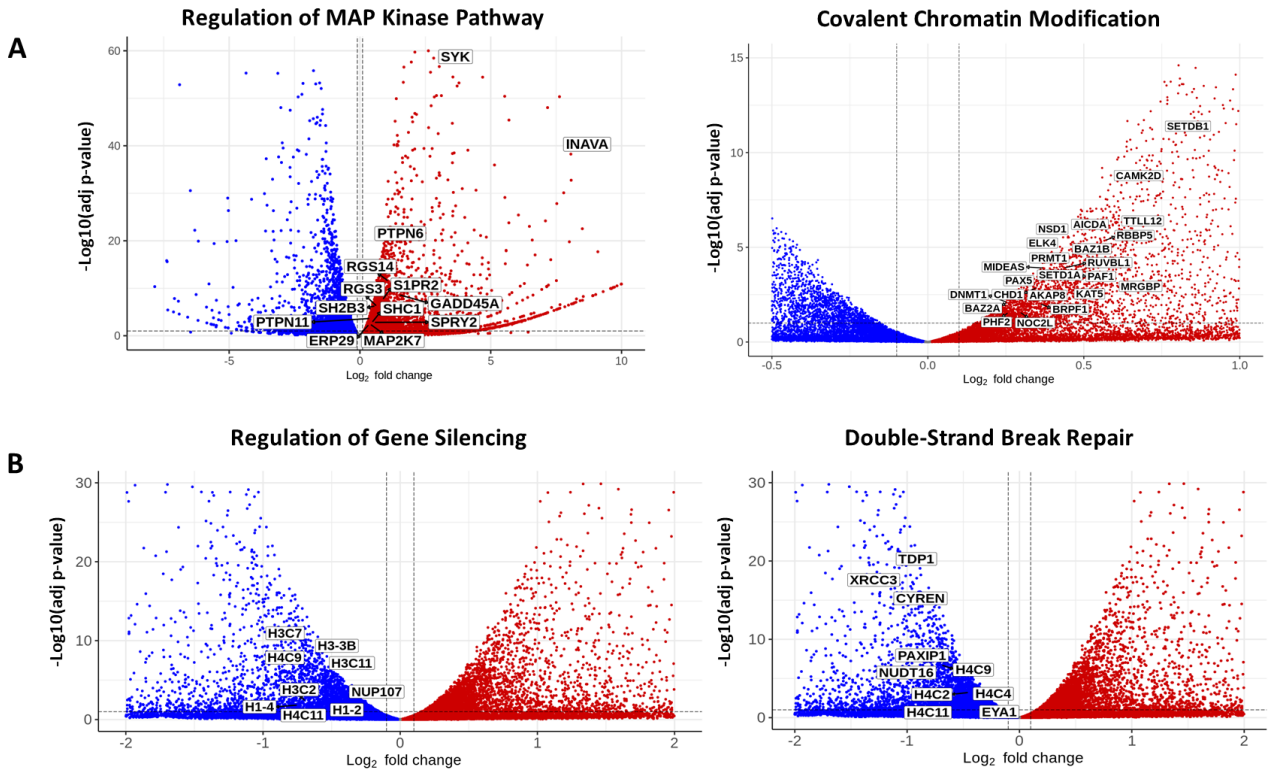


Figure 3.23 The gene expression of genes identified as being associated with KDM5B peaks (ATM KD MEC1 cells) Panel (A) selected enriched GO pathways of genes associated with KDM5B peaks that were in line with upregulated gene expression profile. Panel (B) selected GO pathways of genes linked with KDM5B peaks and were correlated with downregulated gene expression profile. Altogether, volcano plots support the gene expression pattern of KDM5B associated genes marked as upregulated and downregulated in accordance with ATM loss.

In my H3K4me3 ChIP data, I observed that genes that maintained the H3K4me3 epigenetic mark despite KDM5B upregulation correlated with pro-inflammatory pathways such as cytokine production and cell adhesion and MAPK pathways. The preservation of the activity of these pathways could be related to KDM5B activity. Collectively, I observed that KDM5B peaks sites were correlated with genes known to be involved in pathways such as re-organization of chromatin landscape that may establish an environment favouring the survival of ATM-defective MEC1 CLL cells.

To investigate whether KDM5B peaks could potentially be associated with transcription factor regulatory elements, I carried out a HOMER motif analysis on both peaks associated with the promoter and distal regulatory regions (Figure 3.24). The de-novo motif discovery in distal regions shows enrichments of

transcription factors motifs correlated with ETS, RUNX and AP-1 in agreement with de-novo motifs ATAC results. On the other hand, the de-novo motif discovery of promoter regions showed enrichment of transcription factors in line with ETS, SP2 and NFY.

A

Peaks assigned as distal sites

Motif	Match	% sites	p-value
	ETS	31.37	1e-71
	RUNX	26.15	1e-104
	AP-1	18.54	1e-65
	NFkB	12.83	1e-29

B

Peaks assigned as promoter sites

Motif	Match	% sites	p-value
	ETS	43.50	1e-123
	Sp2	40.28	1e-48
	NFY	23.23	1e-104

Figure 3.24 Motif analysis of KDM5B significant summit peaks (ATM KD MEC1 cells)
Statistically significant summit peaks associated with KDM5B were assigned to either promoter or distal regulatory elements according to their lab with TSS regions. Next, De-novo motif discovery analysis was performed to each peak set (A) De-novo motifs discovery showed that ETS, RUNX, AP-1, and NFkB were enriched at distal sites correlated with KDM5B summit peaks. (B) Promoter sites in accord with KDM5B summit peaks were enriched with motifs linked to ETS, Sp2, NFY.

Interestingly, genes that preserved their H3K4me3 signal in correlation with ATM loss and KDM5B associated genes show the association of the MAPK pathway, which regulates AP-1 at the transcriptional and post-translational levels (Karin, 1995). Thus, KDM5B could potentially interact with the AP-1 family of transcription factors to establish a chromatin environment favouring the proliferation of ATM defective

CLL cells. Therefore, the functional role of KDM5B in the ATM defective CLL cells is needed to test this hypothesis.

Several studies suggested that KDM5B is involved in maintaining genome integrity (Li et al., 2014b), replication stress and tolerance (Gaillard et al., 2021) and interaction with chromatin remodelers repressors ZMYND8-NuRD to facilitate DNA damage repair (Gong et al., 2017). Little is known regarding how KDM5B might be involved in driving the gene expression. There is a possibility that this association may provide a dependency pathway the cells potentially use to maintain survival. In a prostate cancer context, (Li et al., 2020b) showed that KDM5B is bound at the promoter of *PIK3CA*, resulting in increased *in vitro* and *in vivo* gene expression and highlighting a role in driving gene expression.

However, it is still unclear whether KDM5B interacts with other transcriptional regulators, including activators and repressors. The question to be answered here is what other players that interact with KDM5B to exert the observed active and repressing gene expression. Moreover, the impact of KDM5B on chromatin accessibility and cis-regulatory elements is still to be investigated. Therefore, studying KDM5B functional role in chromatin landscape will reveal insights into mechanisms underlying the involvement of KDM5B in transcriptional rewiring in ATM-defective CLL cells.

3.9 Generation of Dox-inducible KDM5B shRNA KD CLL cells derived from MEC1 ATM-defective cells

I demonstrated that ATM-defective cells were correlated with a unique transcriptional signature associated with an inflammatory and immune response. I also observed up-regulation of the epigenetic regulator and histone demethylase KDM5B correlated with ATM loss in both CLL cells with different backgrounds and confirmed its expression with qPCR and western blots. The genome-wide histone marks H3K4me3 and H3K4me1 were both down-regulated in accordance with ATM loss, yet the ATM-defective cells still maintained their proliferative state. The KDM5B chip data suggest that KDM5B peaks sites are correlated with enrichment of AP-1, RUNX and ETS motifs.

In agreement with the KDM5B ChIP data, the ATAC differential accessibility analysis showed enrichment of the same motifs as that KDM5B ChIP. The global H3K4 methylation levels showed that genes that had lost this histone mark and correlated with ATM loss were linked to immune activation. In contrast, genes that maintained this mark and linked with ATM loss were associated with MAPK signalling, which is known to control AP-1 activity, agreeing with the literature suggesting that AP-1 has an inhibitory effect on immune checkpoints (Atsaves et al., 2019).

Therefore, chromatin landscape changes correlated with KDM5B upregulation in ATM defective cells may facilitate AP-1 activity and reveal a potential transcriptional dependency that can be targeted for therapeutic purposes. Moreover, an increasing body of literature indicates that KDM5B is involved in tumour drug resistance in breast cancer and melanoma (Liu et al., 2019, Hinohara et al., 2019) as well as its identification as a drug target in B-ALL (Wang et al., 2016). Collectively, to validate and understand KDM5B's impact on ATM-defective cells, I transduced ATM-deficient MEC1 CLL cells with a Dox-inducible lentiviral vector encoding short hairpin RNAs (shRNAs) targeting KDM5B and a non-targeting control.

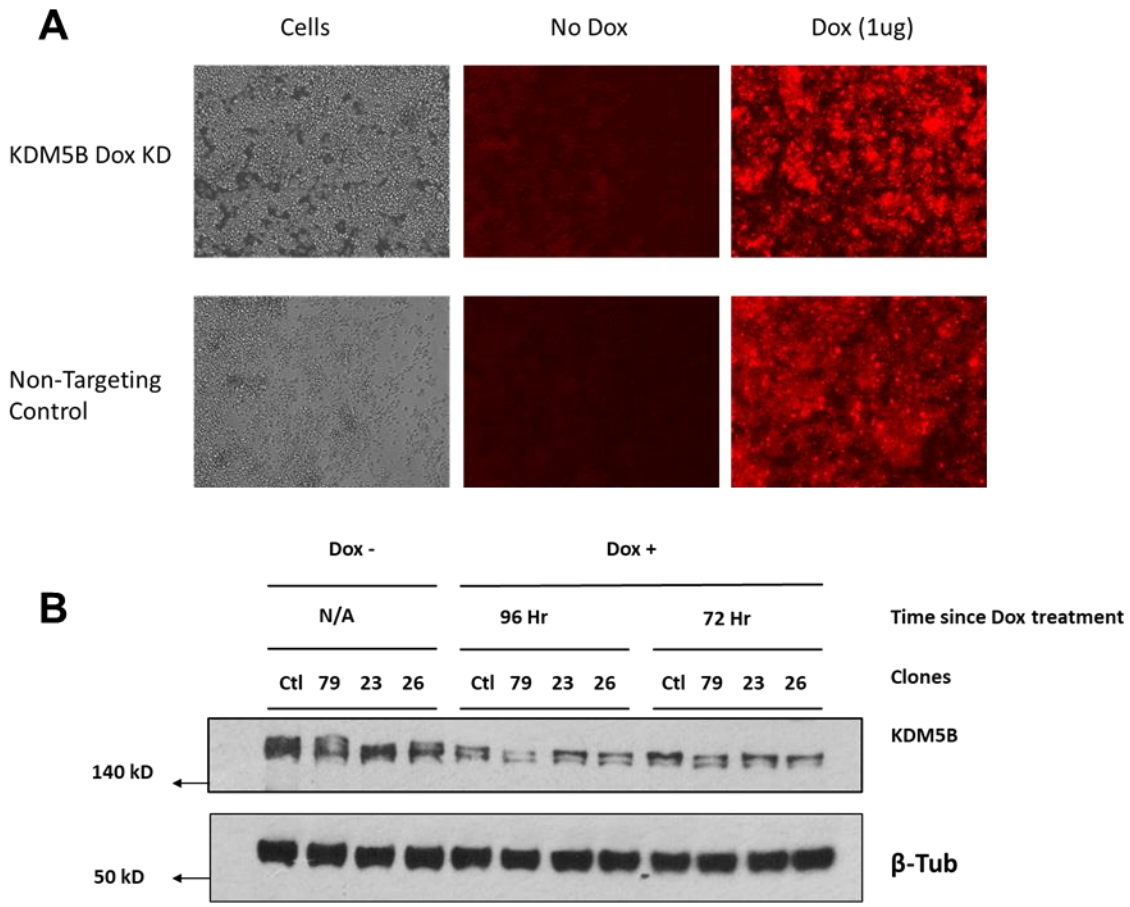


Figure 3.25 Generation of Dox-inducible KDM5B shRNA KD CLL cells derived from MEC1 ATM-defective cells
ATM defective CLL cells (MEC1) that were correlated with KDM5B upregulation were infected with lentiviral vectors encoding short hairpin RNAs (shRNAs) targeting KDM5B and a non-targeting control in a Doxycycline (Dox)-inducible system. (A) Transduced cells were imaged 96 hours post-initiation of doxycycline treatment (1 µg), showing induction of turboRFP. (B) Western blot result for three different clones in addition to a non-targeting control. Western blot confirmed the KDM5B KD in clone 79.

I treated transduced cells with 1 µg Dox and harvested cellular protein lysates at 72 and 96 hours to confirm the protein inhibition. The lentiviral vectors used to transduce cells encode for TurboRFP, a fluorescent protein that is transcribed upon Dox treatment and can be observed under a fluorescent microscope (Figure 3.25 A). Western blots showed that the clone coded 79 demonstrated optimal KDM5B inhibition at 96 hours post-Dox treatment (Figure 3.25 B). Therefore, cells with the clone coded 79 were used for downstream experiments. However, the dox-inducible KDM5B shRNA KD was not stable in subsequent experiments, although transduced cells showed a strong TurboRFP signal, as confirmed by

fluorescent microscopy and fluorescence-activated cell sorting (FACS). This observation suggests that KDM5B is associated with a potentially limited turnover and could resist rapid protein degradation. Indeed, it was reported recently that epigenetic regulatory enzyme proteins levels were stable for a prolonged time after blocking protein synthesis (Badreldin et al., 2021). For that reason, at this stage, subsequent experiments related to this project were stopped and are expected to be continued in future work. The assessment of KDM5B protein stability after inhibition of mRNA translation using cycloheximide is required to validate the observed results obtained from dox-inducible KDM5B shRNA KD. Moreover, the utilization of clustered regularly interspaced short palindromic repeats (CRISPR)-mediated KO will be necessary to validate the potential involvement of KDM5B in ATM-defective CLL cell survival.

3.10 Discussion

In this project, I characterised the epigenomic landscape of ATM-deficient CLL cells using gene expression, chromatin-accessibility assays, and chromatin immunoprecipitation assays. At the transcriptomic level, I showed that ATM-defective cells have transcriptomic signatures correlated with an inflammatory response signature. I then characterised the histone modification profile using three histone marks—H3K4me3, H3K4me1 and H3K27ac—and found a global down-regulation of H3K4me3 and H3K4me1 levels that were in line with ATM loss. I then examined whether the significant up-regulation of KDM5B, which was in parallel with ATM loss and validated by WB and qPCR, could be potentially responsible for the global deregulation of histone marks (H3K4me3 and H3K4me1) that were observed in accordance with ATM loss.

To investigate the chromatin-accessibility landscape in ATM-defective cells, I profiled the chromatin-accessibility landscape and found that specific gained accessible sites in accord with ATM loss status were correlated with motifs linked with RUNX and AP-1, whereas lost sites were linked to motifs linked with ETS and HOX transcription factors. Motif co-localization analysis suggested that AP-1 and RUNX co-localize

to drive the transcriptional network, and this observation was correlated with ATM loss status, whereas ETS and HOX co-localization absence was linked with ATM loss. Transcription factor network analysis further supported the finding seen in the motif co-localization analysis.

I performed chromatin immunoprecipitation for KDM5B to determine its genome-wide binding sites since its upregulation was correlated with ATM loss. I showed that KDM5B peaks sites were mainly associated with promoter cis-regulatory elements and demonstrated that sites occupied by KDM5B peaks are in accord with motifs related to RUNX, AP-1, ETS and NFkB. I hypothesized that the global chromatin alterations in line with ATM loss were a consequence of KDM5B up-regulation, that is also correlated with ATM loss, and its up-regulation could facilitate AP-1 activity, creating a potential transcriptional dependency. Therefore, I transduced ATM-defective cells with a lentiviral vector encoding for shRNA to functionally study the involvement of KDM5B in the chromatin landscape changes.

The transcriptional data from GSEA and GO analyses indicated that ATM loss is consistent with an inflammatory response signature. Interferons are vital to the response to pathogen invasion and immune response regulation (Dunn et al., 2006, Dunn et al., 2005). Activated interferon signalling recruits additional signalling cascades such as calcium/calmodulin-dependent protein kinase (CamK) II, mitogen-activated protein kinases (MAPKs), Janus kinases (JAKs), phosphatidylinositol 3-kinase (PI3K), and signal transducers and activators of transcription (STATs) (Ramana et al., 2002).

The observed enriched interferon response correlated with ATM loss status suggests a link between ATM activity and interferon signalling. It was reported that innate immune system inflammatory pathways were upregulated in response to the absence of ATM activity (Petersen et al., 2012, Härtlova et al., 2015). In addition, studies have shown that A-T patients and ATM-null mouse models both demonstrated upregulation in proinflammatory cytokines and high levels of serum inflammatory markers (Quek et al., 2017, Westbrook and Schiestl, 2010, Yang et al., 2014). Moreover, it was reported that ATM controls the

IFN-γ response in U20 cells highlighting ATM role in the regulation of cytokine responses (Watling et al., 2008, Wang et al., 2013). Furthermore, interferon signalling is stimulated as stress reaction in response to cytoplasmic DNA caused by the accumulation of DNA damage (Brzostek-Racine et al., 2011) and this is likely the case in ATM-deficient CLL cells in this study. In agreement with GSEA results, ATM inhibition led to an increase in interferon signalling in pancreatic cancer cells *in vitro* and *in vivo* (Zhang et al., 2019). Taken together, in consistent with other studies, ATM defective CLL cells were correlated with the upregulation of interferon signalling.

In addition, and as mentioned in the introduction, it has been documented that the activation of immune responses is a consequence of the build-up of nuclear DNA in the cytoplasm (Gasser et al., 2017, Gasser and Raulet, 2006). Moreover, the presence of high levels of cytoplasmic ssDNA and double-stranded (dsDNA) DNA is a hallmark of tumours and cancer and particularly those with defective DDR (Hong et al., 2019). Given that ATM-deficient CLL cells are defective in a major DNA repair pathway (double-strand repair), it is conceivable that an accumulation of DNA damage will eventually trigger a cellular immune response.

I have demonstrated a global downregulation of the histone marks H3K4me3 and H3K4me1 that were correlated with ATM loss, and I demonstrated that genes that maintained H3K4me3 were associated with pro-inflammatory pathways, lymphocyte differentiation and MAPK activation. In contrast, genes that lost the histone mark were linked with both T-cell and lymphocyte activation. The KDM5B ChIP data showed that KDM5B associated peaks were linked to genes associated with chromatin organization, DNA damage pathways and regulation of protein serine/threonine kinase activity. Moreover, KDM5B peaks were in line with AP-1, RUNX, ETS and NFkB motifs. It has been well documented that histone demethylases play a pivotal role in immune system regulation (Li et al., 2014a, Wu et al., 2018) and tumour immunity (Qin et al., 2019). Moreover, a significant global decrease in H3K4 methylation levels was observed in drug-resistant cells (Xu et al., 2018). Therefore, the global deregulation of H3K4 methylation levels correlated

with ATM loss could be a consequence of KDM5B activation. The enrichment of GO terms (MAPK pathway and the regulation protein serine/threonine kinase activity) in the KDM5B annotated peaks suggests a role in which KDM5B facilitates an alternative route when the cell needs to cope with the loss of ATM kinase activity.

In vivo, KDM5B overexpression is associated with enhanced PI3K/AKT signalling and its loss reverses the effect (Li et al., 2020b). As PI3K/AKT is a kinase family related to that of ATM (PIKK kinase family), it is reasonable to speculate that KDM5B could be involved in up-regulating alternative kinase pathways that can support cell survival in the absence of ATM kinase activity in a demethylase-independent manner. Similarly, the associated presence of KDM5B peaks at genes involved in DDR pathways (double-strand break repair, nonhomologous end joining and nucleotide-excision repair) implies a regulation role of alternative DDR pathways that repair DNA damage that was linked with ATM loss. In fact, it has been demonstrated that KDM5B increases the efficiency of the DSB repair machinery and is also required for the active recruitment of the component of homologous recombination nonhomologous end-joining BRCA1 and KU70, respectively (Li et al., 2014b).

In my ATAC-seq assay, I showed that sites gained that correlated with ATM loss were associated with AP-1 and RUNX motifs, consistent with the KDM5B chip data. It has been previously reported that both AP-1 and MAPK were activated in ATM-deficient brain cells (Weizman et al., 2003). In contrast, I found that ETS and HOX motifs were downregulated in correlation with ATM loss. Co-localization and TF network analyses revealed a transcriptional landscape that is correlated with ATM loss that is primarily controlled by AP-1 and RUNX, and not by the ETS- and Hox-driven transcription.

Interestingly, in correlation with ATM loss, genes that maintained H3K4me3 levels despite KDM5B up-regulation were associated with the MAPK pathway which is required to control AP-1 activity (Atsaves et al., 2019, Karin, 1995), implying a role for KDM5B in maintaining AP-1 signalling indirectly. Remarkably,

the activation of MAPK is correlated with an increase in the immune-compromised tumour microenvironment (Liu et al., 2013a). On the other hand, the AP-1 transcription factor members c-Jun, JunB, c-Fos and Batf were found to cooperate to induce the expression of PD-1 and PDL1 genes, which function as co-inhibitory immune checkpoints (Atsaves et al., 2019). It was also reported that the AP-1 inhibitory effects on immune checkpoint expression were mainly dependent on MAPK activity (Sumimoto et al., 2016, Jiang et al., 2013). Collectively, the preservation of the H3K4 methylation status of genes in line with MAPK signalling and the reduction of H3K4 methylation status of genes correlated to the immune response proposes a synergistic effect between KDM5B and AP-1.

Unfortunately, my dox-inducible KDM5B shRNA KD was not reproducible in subsequent experiments, and this experimental outcome could be related to limited KDM5B protein turnover levels, which may resist rapid protein degradation. Indeed, it was shown recently that epigenetic regulatory enzymes have the potential to maintain prolonged protein stability after blocking protein synthesis (Badreldin et al., 2021). Therefore, future experiments should address KDM5B protein stability after mRNA translation blocking. Moreover, another experiment in which KDM5B is subject to clustered regularly interspaced short palindromic repeats (CRISPR)-mediated gene KO is required to ensure the complete inhibition of KDM5B. Using a KDM5B CRISPR-mediated KO system will help to assess the viability of ATM-defective CLLs and validate its contribution to the survival of these cells.

In summary, in light of the obtained data, I propose a model (Figure 3.26) in which the impact of KDM5B in ATM-defective cells could be explained. First, ATM loss is correlated with DNA damage and inflammatory signalling upregulation. Second, KDM5B upregulation that is in line with ATM loss in return is involved in (A) genome-wide histone H3K4 methylation alteration and immune system modulation, (B) KDM5B could influence the expression of kinase genes (serin/threonine and MAPK genes). Third, the expression of the MAPK pathway is required to regulate the activity of AP-1. Forth, AP-1 in return, is involved in maintaining the transcription landscape of ATM-defective cells. Fifth, the AP-1 and KDM5B

work together in a feedback loop to create a transcriptional environment favouring the survival of ATM-deficient CLL cells. To validate the robustness of this model, a series of knockdown and complementation experiments with the components of this network will have to be undertaken in the future.

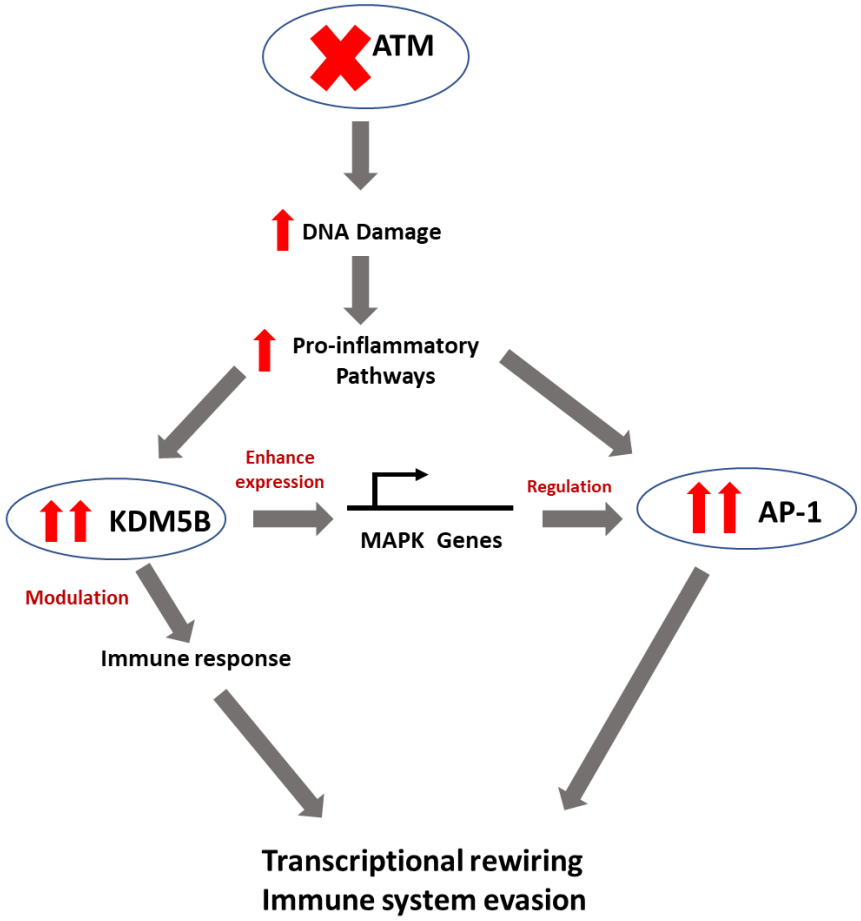


Figure 3.26 A proposed model for the role of KDM5B in ATM defective CLL cells
The loss of ATM is correlated with an increase in genomic instability, which in turn increases pro-inflammatory signalling. The observed upregulation of KDM5B in correlation with ATM loss status may have an influence on promoting the MAPK signalling pathway and modulating the immune response, which could be potentially involved in transcriptional rewiring and immune system evasion.

CHAPTER 4

The Epigenetic Landscape of RNASEH2B-defective CLL cells

Chapter 4: Chromatin landscape of RNASEH2B-deficient CLL cells

The incorporation of ribonucleotides into DNA during replication is the most frequent cause of DNA lesions in cycling cells. Genome-embedded ribonucleotides increase the rate of spontaneous DNA breaks and/or mutations and promote genomic instability. To reduce these potentially harmful effects, cells have developed a robust RER pathway initiated by the RNase H2 endoribonuclease, which contains a single catalytic subunit encoded by RNASEH2A and two non-catalytic subunits encoded by RNASEH2B and RNASEH2C Figure 4.1 (Shaban et al., 2010). The loss of any one of the three RNase H2 subunits disrupts the entire enzymatic complex and leads to an RNase H2 insufficiency as well as activation of an error-prone 'back-up' DNA repair pathway (Zimmermann et al., 2018).

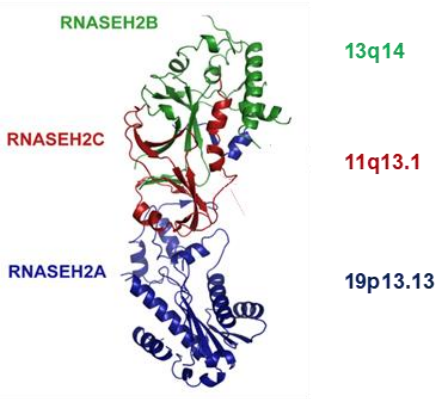


Figure 4.1 Protein structure of RNase H2 enzymatic complex
The RNase H2 complex is formed from three members encoded by three different genes named the RNASEH2A, the RNASEH2B and the RNASEH2C. The presence of the three members are essential for the integrity and stability of the RNase H2 complex.

As discussed in the introduction, recent evidence suggests a synthetic lethal interaction between RNASEH2B loss and inhibition of DDR proteins poly(ADP–ribose) polymerase (PARP) (Zimmermann et al., 2018), and Ataxia telangiectasia-mutated and RAD3-related (ATR) (Wang et al., 2019b). In addition to synthetic lethal interactions with DDR proteins, RNase H2 deficient cells are likely to develop a range of different cellular dependencies, including changes in gene expression or activation of lineage

inappropriate genes in order to survive. Therefore, the elucidation of these dependencies provides an opportunity for targeting tumours with this defect.

In this chapter, I will describe the chromatin landscape in RNASEH2B-deficient CLL cells using genome-wide methodologies, including RNA-seq, DRIP-seq, ChIP-seq and ATAC-seq. Subsequently, I used genome-wide CRISPR screen to validate the observed transcriptional dependencies as a means of functional validation. To enable the investigation of an RNASEH2B loss-specific chromatin signature, our laboratory has successfully generated a CLL isogenic cell line (MEC1) with an RNASEH2B monoallelic, and biallelic CRISPR knockout (KO) and the status of RNASEH2B was confirmed using western blot (Figure 4.2).

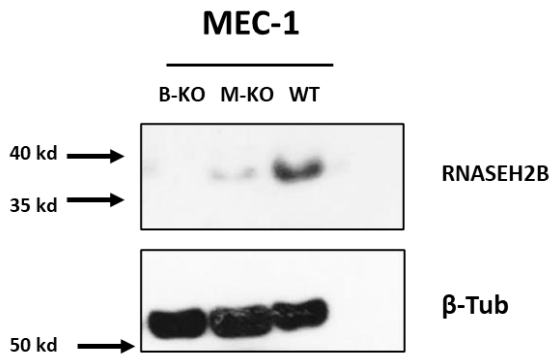


Figure 4.2 Western blots confirming RNASEH2B KO status in MEC1 cell line
Blots show that monoallelic KO cells produce RNASEH2B protein but less than WT cells. Biallelic KO cells show no traces of RNASEH2B protein. In this analysis, an antibody was used for the recognition of RNASEH2B protein and an antibody targeting B-tubulin was used as the loading control. Abbreviations: B-KO (biallelic KO), M-KO (monoallelic KO)

4.2 RNASEH2B loss is correlated with a global gene expression deregulation

To study the effect of RNASEH2B loss on the CLL transcriptomic profile, RNA-seq was performed in triplicate with RNASEH2B monoallelic KO and biallelic KO cells as well as WT controls. The third replicate for the monoallelic KO condition was discarded because it did not pass QC. To validate the consistency between replicates, linear regression analysis was performed and produced an R^2 of 0.991–0.994 (Figure 4.3), suggesting a high level of consistency between the three isogenic counterparts.

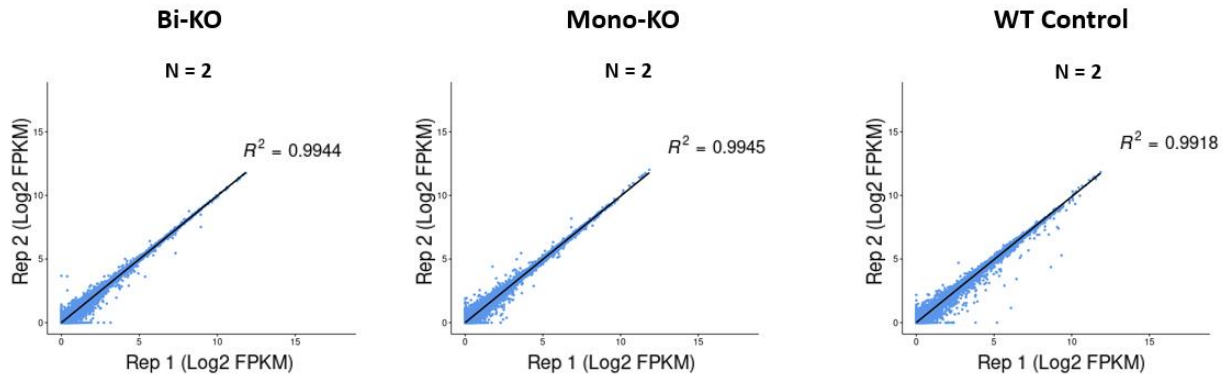


Figure 4.3 Positive correlation between RNA-seq replicates samples were observed as suggested by linear regression analysis

Comparison of RNA-seq replicates of RNASEH2B KO and WT (control) isogeneic cell lines. Log2 FPKM+1 expression values were calculated for each replicate (Two replicates for each condition). Next, a linear regression analysis was done using Log2 FPKM+1 computed values. The resulted linear regression analysis shows a positive correlation between replicates and an R squared value above 98%, suggesting high concordance between replicates.

To demonstrate gene expression (FPKM values) variation between all cell lines, a Pearson correlation analysis was computed and resulted in a heatmap (Figure 4.4). Hierarchical unsupervised clustering shows that MEC1 isogenic cells cluster together according to the RNASEH2B status condition. In addition, the heatmap indicates that RNASEH2B loss is correlated with deregulated gene expression in CLL cells.

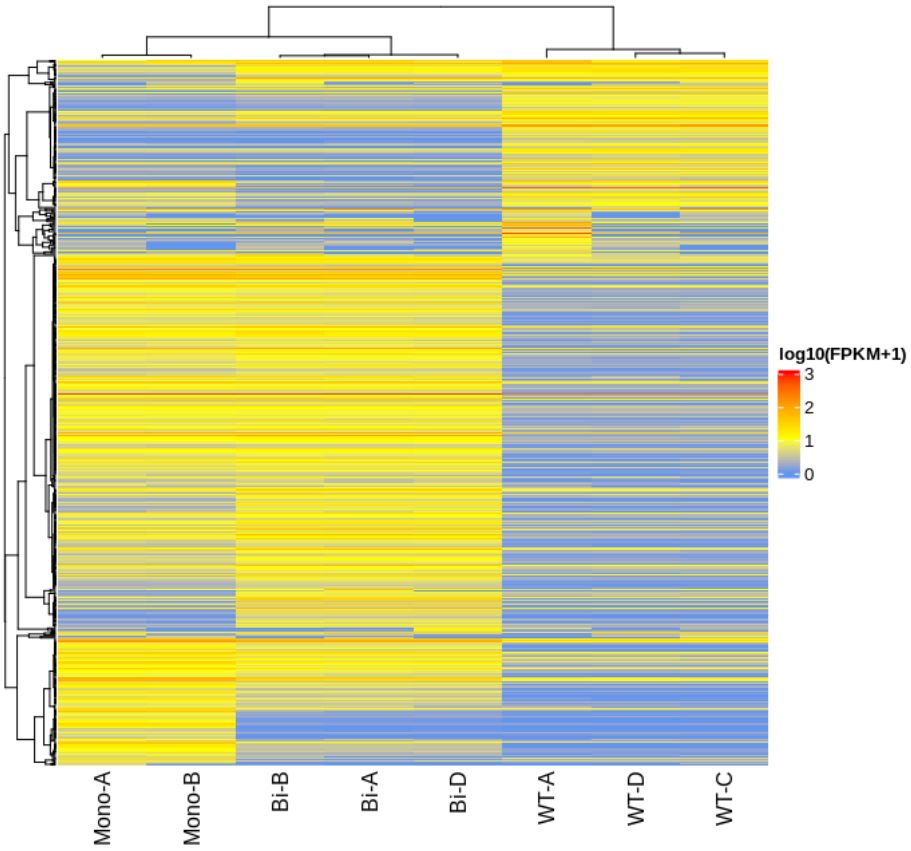


Figure 4.4 Correlation clustering of gene expression profiles of RNASEH2B KO isogeneic cells
The expression values (Log10 FPKM+1) of all differentially expressed genes were calculated for each RNA-seq sample. Next, hierarchical unsupervised clustering of gene expression profiles computed by correlation analysis (1-Pearson correlation, average linkage) of expression values was performed. The heatmap shows that each isogenic cell line is clustered away from the other cell line in correlation with RNASEH2B status. (Abbreviation: FPKM : the fragments per kilobase per million fragments mapped). Abbreviations: B-KO (biallelic KO), M-KO (monoallelic KO), WT (Wild type), FPKM : the fragments per kilobase per million fragments mapped. B-KO (N= 3), M-KO (N=2),WT (N=3).

4.2.1 Activated pro-inflammatory response transcriptional signatures are in correlation with RNASEH2B loss

To investigate the effect of RNASEH2B loss (biallelic or monoallelic) on global gene expression, I performed two differential gene expression comparisons— biallelic KO against WT control and monoallelic KO against WT control. I then set the differentially expressed gene significance level (adj p-value < 0.1 and log2 FC > 2), and genes passing this threshold were subsequently carried to downstream analysis. Applying this

significance threshold showed 2047 differentially expressed genes in correlation with monoallelic KO cells, with 1614 genes being upregulated and 433 genes being downregulated, whereas biallelic KO cells were correlated with a number of 1897 differentially expressed genes in which 1552 genes were upregulated and 345 were downregulated. To represent the overall differentially expressed genes in each comparison, volcano plots were generated (Figure 4.5), showing the significance and the log2 fold change. To determine whether differentially expressed genes correlated with RNASEH2B loss were associated with a disease phenotype or biological process, gene set enrichment analysis (GSEA) was performed. The GSEA showed common biological features in both isogenic cell lines in correlation with biallelic or monoallelic RNASEH2B loss by demonstrating an enrichment of the inflammatory response including interferon-alpha (Mo-KO: gene count: 20, adj p-value: 1.19×10^{-3}, Bi-KO: gene count: 20, adj p-value: 1.22×10^{-3}) and gamma (Mo-KO: gene count: 36, adj p-value: 1.2×10^{-3}, Bi-KO: gene count: 38, adj p-value: 1.23×10^{-3}) (Figure 4.6 A). Further investigation of genes associated with such signatures derived from GSEA analysis of differentially expressed genes indicated that these genes indeed show signs of gene expression upregulation in correlation with biallelic or monoallelic RNASEH2B loss (Figure 4.6 B).

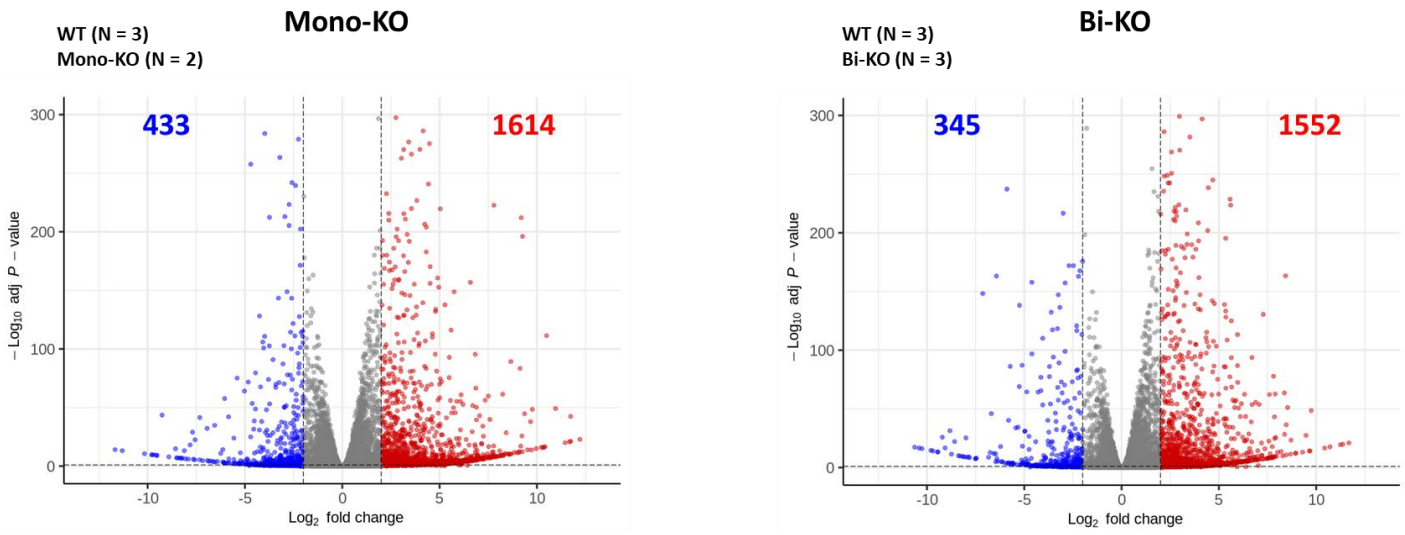


Figure 4.5 Differentially expressed genes in accordance with RNASEH2B monoallelic and biallelic loss status in CLL cells

Volcano plots demonstrate the significance and the log2 fold change of differentially expressed genes. Statistically significant differentially expressed genes were highlighted. Differentially genes below adj p-values of 0.1 and showing upregulation (Log2FC >2) are coloured in red, whereas genes showing downregulation (Log2FC < -2) were coloured in blue (Mo-KO MEC1 cells on the left-hand side and Bi-KO cells on right-hand side). Mo-KO MEC1 cells were correlated with 1614 genes that were upregulated and 433 genes that were downregulated, whereas Bi-KO MEC1 cells showed 1552 genes that were upregulated and 345 genes downregulated. All comparisons were made against RNASEH2B WT counterpart MEC1 cells

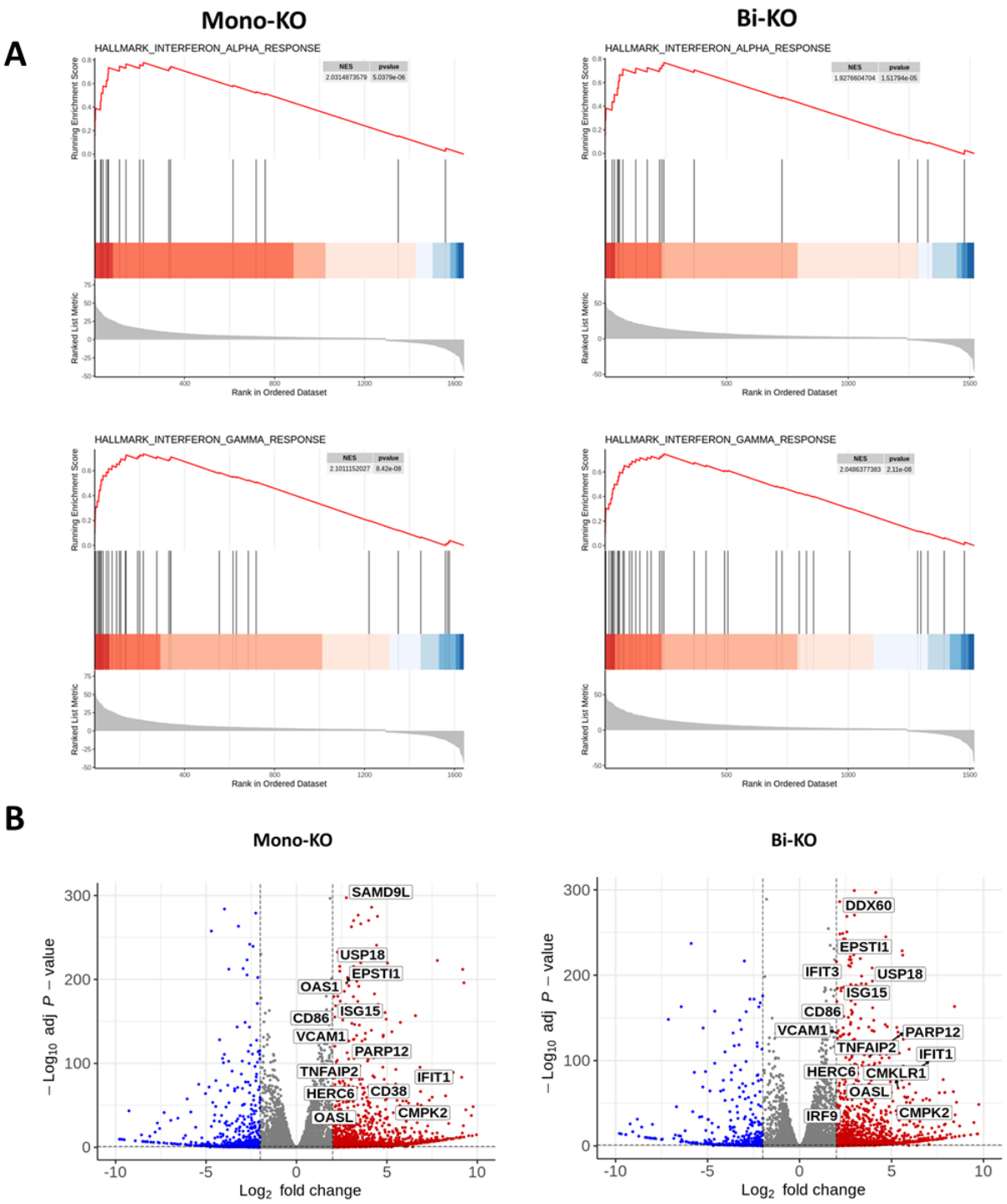

A
Mono-KO
Bi-KO
HALLMARK_INTERFERON_ALPHA_RESPONSE
NES
pvalue
2.0314873579
5.0379e-06
1.9276604704
1.51794e-05
HALLMARK_INTERFERON_GAMMA_RESPONSE
2.1011152027
8.42e-08
2.0486377383
2.11e-08
Running Enrichment Score
Ranked List Metric
Rank in Ordered Dataset
B
Mono-KO
Bi-KO
SAMD9L
USP18
EPSTI1
OAS1
ISG15
CD86
VCAM1
PARP12
TNFAIP2
IFIT1
HERC6
CD38
OASL
CMPK2
DDX60
IFIT3
CMKLR1
IRF9
– Log10 adj P – value
Log2 fold change

Figure 4.6 Gene set enrichment analysis (GSEA) of differentially expressed genes correlated with RNASEH2B loss. (A) Gene set enrichment analysis (GSEA) shows enrichment for an inflammatory phenotype signature in correlation with RNASEH2B monoallelic and biallelic KO cells isogenic cell lines. In this analysis, differentially expressed genes are ranked according to p-value and log2 fold change and then compared to a set of genes that are known to have a role in certain biological phenotypes or diseases. Genes that are found in the set are coloured with black vertical lines. Enrichment score (ES) is the highest divergence from the baseline (zero) as determined for each gene of the ranked list and denotes the extent of over-representation of a gene set. Coloured boxes at the bottom signify the extent of association of genes with the RNASEH2B loss phenotype (red for positive and blue for negative association). The GSEA threshold set at adj p-value < 0.1. (B) Volcano plots demonstrate genes associated with GSEA hallmarks are upregulated in correlation with RNASEH2B monoallelic and biallelic loss status in MEC1 CLL cell lines thus supporting the observed upregulation of inflammatory signalling.

To further investigate the correlated impact of RNASEH2B biallelic or monoallelic loss on cellular pathways and processes, gene ontology (GO) functional pathway analysis was performed on each set differentially expressed genes (Figure 4.7).

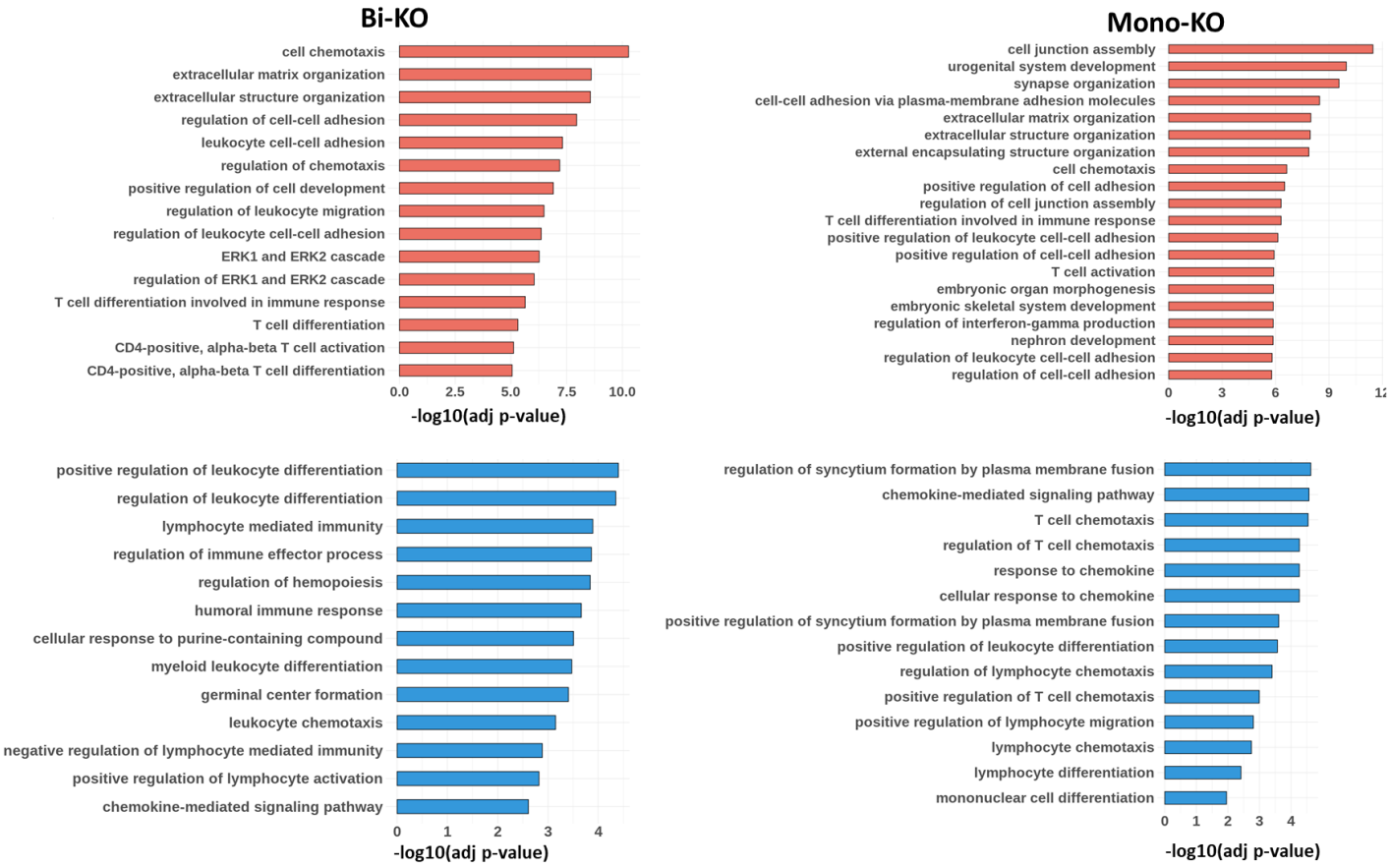


Figure 4.7 Gene Ontology analysis on differentially expressed up-and down-regulated genes in correlation with RNASEH2B loss in CLL cells

Gene ontology analysis was done on differentially expressed genes (adjusted p-value < 0.1 and log2 fold change >2) in each cell line. The GO sets show the most significant GO biological process in each cell line for upregulation (red colour) or downregulation (blue colour) changes. The analysis features the up-regulation of inflammatory and immune response genes in accordance with RNASEH2B loss status Abbreviations: B-KO (biallelic KO), M-KO (monoallelic KO), WT (Wild type)

Mono and biallelic cells with different RNASEH2B knockout CLL cells were in correlation with a commonality with respect to up- and down-regulated gene lists. GO pathways such as the activation of an immune response (Mo-KO: gene count: 49, adj p-value: 2.14×10^{-4}, Bi-KO: gene count: 17, adj p-value: 5.02×10^{-4}), cell chemotaxis (Mo-KO: gene count: 38, adj p-value: 6.89×10^{-5}, Bi-KO: gene count: 45, adj p-value: 1.01×10^{-7}), cell-cell adhesion (Mo-KO: gene count: 39, adj p-value: 2.81×10^{-6}, Bi-KO: gene count: 37, adj p-value: 8.05×10^{-6}) , leukocyte migration (Mo-KO: gene count: 21, adj p-value: 1.01×10^{-3}, Bi-KO: gene count: 29, adj p-value: 2.15×10^{-5}) and T cell regulation (Mo-KO: gene count: 31, adj p-value: 2.96×10^{-4}, Bi-KO: gene count: 30, adj p-value: 3.69×10^{-4}) , were enriched in correlation with the up-regulated gene lists. It is important to note that I observed in both mono and biallelic KO CLL cells an up-regulation of genes involved in unfolded protein response such as *CREB3L1* (Mo-KO adj p-value: 7.10×10^{-3}, Bi-KO adj p-value: 1.41×10^{-4}) and *CCL2* (Mo-KO adj p-value: 6.19×10^{-22}, Bi-KO adj p-value: 2.20×10^{-18})

. In addition, genes involved in the regulation of ribonuclease activity were also up-regulated, including *OAS2* (Mo-KO adj p-value: 1×10^{-2}, Bi-KO adj p-value: 5.61×10^{-303}), *OAS3* (Mo-KO adj p-value: 6.2×10^{-48}, Bi-KO adj p-value: 1.6×10^{-2}) *and OASL*(Mo-KO adj p-value: 6.19×10^{-22}, Bi-KO adj p-value: 9.95×10^{-55}). These genes participate in innate immunity and are activated in response to the presence of viral RNA. Moreover, inflammatory response pathways genes, such as *EDN1, PTGIR, IL1R1, AXL* and *IL12B*, were also up-regulated in both KO cells, agreeing with (Crow et al., 2006). Furthermore, T cell regulation- and activation-related genes, such as *IL27* (Mo-KO adj p-value: 8.50×10^{-2}, Bi-KO adj p-value: 8.98×10^{-2}) , *CCL19* (Mo-KO adj p-value: 4.09×10^{-8}, Bi-KO adj p-value: 2.67×10^{-5}), *IL1B* (Mo-KO adj p-value: 6.35×10^{-51}, Bi-KO adj p-value: 1.97×10^{-54}), *ANXA1* (Mo-KO adj p-value: 5.92×10^{-19}, Bi-KO adj p-value: 6.85×10^{-18})

and *RSAD2* (Mo-KO adj p-value: 1.92 x 10^{-23}, Bi-KO adj p-value: 1.90 x 10^{-24}) , were also in correlation with up-regulated gene expression correlated with RNASEH2B KO CLL cells suggesting a role in an induction of anti-tumour T cell responses possibly due to an increase in the genomic mutation burden (Riches et al., 2013).

Similarly, CLL cells demonstrated similarities in terms of down-regulated genes in accordance with RNASEH2B mono and biallelic loss. In general, there was a down-regulation of transcription factor genes, including *BCL6* (Mo-KO adj p-value: 7.05 x 10^{-33}, Bi-KO adj p-value: 9.83 x 10^{-24}), *PRDM5* (Mo-KO adj p-value: 8.65 x 10^{-5}, Bi-KO adj p-value: 3.89 x 10^{-6}), *MEIS1* (Mo-KO adj p-value: 3.87 x 10^{-2}, Bi-KO adj p-value: 1.54 x 10^{-2}), *KLF9* (Mo-KO adj p-value: 2.59 x 10^{-39}, Bi-KO adj p-value: 4.31 x 10^{-47}) and other ZNF family TF factors indicating a potential transcription reprogramming in correlation with RNASEH2B defective CLL cells.

To further elucidate global transcriptomic changes in correlation with both RNASEH2B monoallelic and biallelic KO cells, I selected the common up-and down-regulated significant differentially expressed genes associated with RNASEH2B KO cell lines conditions to create a consensus differentially expressed gene list (Common genes: 1277 gene) (Figure 4.8 A). This list was used as input for GO pathway analysis; a gene expression network was generated, highlighting pathways that are common in correlation with both RNASEH2B loss conditions. The analysis demonstrated that changes in the gene expression in correlation with RNASEH2B KO CLL cells mainly involved inflammatory signalling pathways such as regulation of inflammatory response (gene count: 32, adj p-value: 2.71 x 10^{-3}) and regulation of interferon-gamma production (gene count: 16, adj p-value: 8.29 x 10^{-4}) , in addition to T cell activation (gene count: 40, adj p-value: 1.05 x 10^{-3}), positive regulation of NIK/NF-kappa B signalling (gene count: 10, adj p-value: 9.28 x 10^{-3}), and Notch signalling pathway (gene count: 21, adj p-value: 1.52 x 10^{-3}) (Figure 4.8 B). Collectively, common differentially expressed genes correlated with RNASEH2B monoallelic and Bi allelic loss show signs of the enrichments of inflammatory and immune-related pathways. This observation is consistent

with the activation of immune signalling in response to defective nucleic acid processing observed in Aicardi–Goutières syndrome.

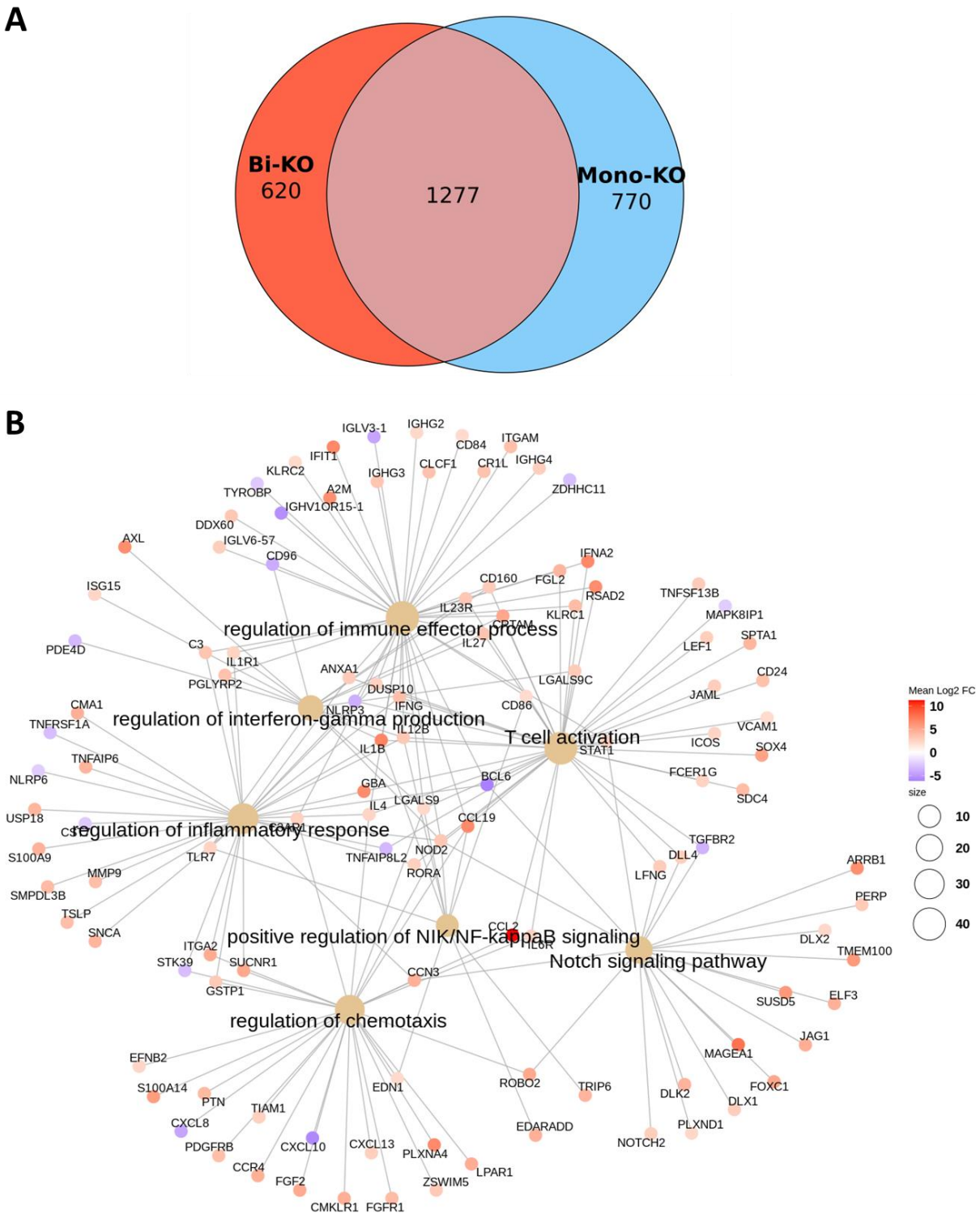


Figure 4.8 Common differentially expressed genes in correlation with RNASEH2B loss and their role biological role

(A) Statistically significant differentially expressed genes correlated with RNASEH2B monoallelic and biallelic loss status were overlapped and resulted in a common gene (1277 gene). These common genes were then subjected to GO pathway enrichment analysis. (B)The results of GO pathway analysis connecting commonly differentially expressed genes in accord with RNASEH2B loss status in contrast to control cells (RNASEH2B WT). The enriched GO terms contain pathways such as regulation of inflammatory response, positive regulation of NIK/NF-kappa B signalling, and T cell activation. The constructed network demonstrates interactions (grey lines) between individual genes grouped in multiple pathways. Red nodes represent genes that are up-regulated, and blue nodes indicate genes that are down-regulated in each particular pathway. The size of a node refers to the number of genes associated with that particular node.

I next investigated the gene expression pattern in correlation with RNASEH2B monoallelic and biallelic loss. To demonstrate that common up- and down-regulated genes associated with RNASEH2B biallelic and monoallelic KO show unique gene expression profile compared to WT control cells, a set of common differentially expressed genes was used in the previous analysis was used as input for producing a supervised clustering heatmap. The resulted heatmap showed that RNASEH2B WT samples cluster together away from RNASEH2B biallelic and monoallelic KO samples that are also cluster together (Figure 4.9). This analysis highlights that RNASEH2B biallelic and monoallelic KO associated common differentially expressed genes between the two cell lines show similar expression profiles, suggesting an RNASEH2B loss specific changes. Moreover, this analysis shows that the inactivation of one allele is sufficient to produce a gene expression similar to the inactivation of two alleles.

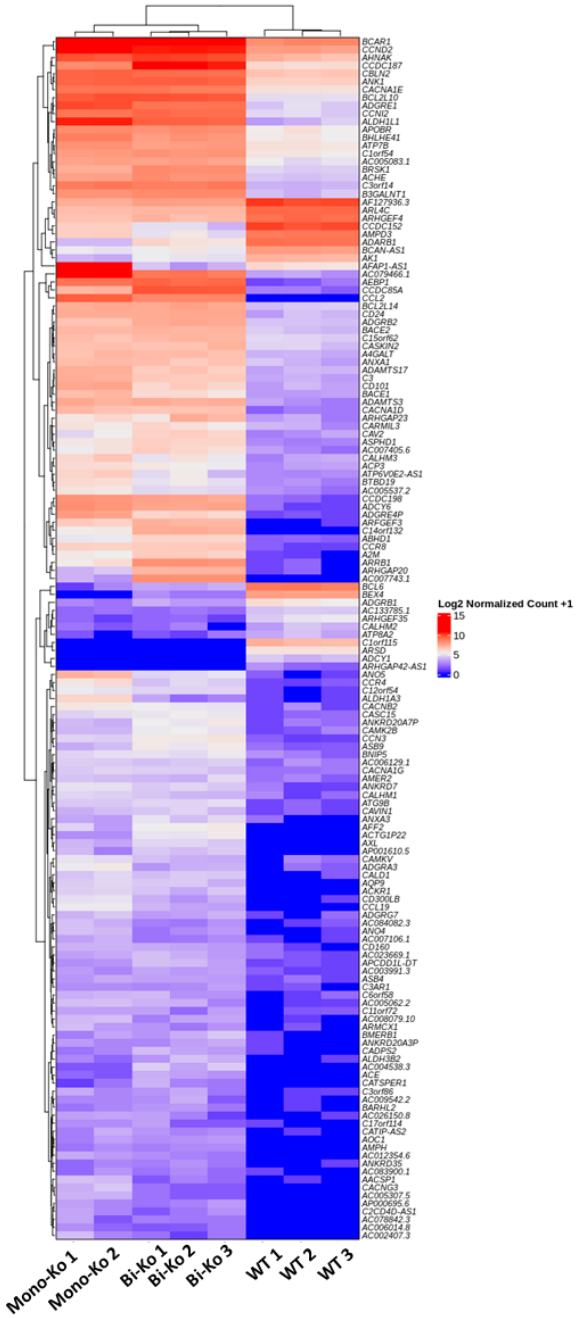


Figure 4.9 Heatmap of supervised clustering reveals common gene expression profile in correlation with RNASEH2B monoallelic and biallelic loss

Common differentially expressed genes that were correlated with RNASEH2B loss for each isogenic cell line were identified. Next, normalized read counts for each gene were derived, log2 transformed and subjected to supervised hierarchical clustering for each cell type. The heatmap shows that the common differentially expressed genes in accord with RNASEH2B loss were correlated with similar gene expression patterns thus suggesting that loss of one RNASEH2B allele could contribute to a gene expression pattern similar to that of biallelic loss. Only a number of 150 common genes were plotted for easy visualisation. Abbreviations: B-KO (biallelic KO), M-KO (monoallelic KO), WT (Wild type)

Taken together, the transcription data analysis suggests that RNase H2 functional loss in CLL cells is correlated with the upregulation of interferon signalling as well as activation of pro-inflammatory response, an observation that is seen in Aicardi–Goutières syndrome patients caused by a defect in nucleic acid processing. These alterations are likely to represent cellular response toward the misincorporation of ribonucleotides and the increased levels of RNA–DNA hybrid (R-loops) formation. In the next section, I will examine the impact of RNase H2 functional loss on RNA–DNA hybrid formation.

4.3 RNASEH2B loss is correlated with increased RNA–DNA hybrid formation (R-loops)

An R loop is a special nucleic acid structure formed of RNA–DNA hybrid and a single-stranded DNA (ssDNA) loop. This structure arises co-transcriptionally when the nascent RNA template complements to the template DNA strand. Several methods can be used to interrogate the biology of R loops. For example, DNA–RNA hybrid immunoprecipitation followed by high-throughput DNA sequencing (DRIP-seq) allows capturing these special nucleic structure locations at the genome-wide level. In this method, S9.6 monoclonal antibody (mAb) that specifically targets DNA-RNA hybrid is used to identify genomic regions where R loops are enriched. Other methods such as R-ChIP and RR-ChIP apply different principle for capturing R loops using an exogenous catalytically inactive RNase H1 that bind to R loops without resolving them. However, ectopic expression of mutant RNase H1 may influence the native R loops status. Thus, results obtained from such methods should be analyzed with that consideration in mind.

To examine the correlation between RNASH2B loss and DNA–RNA hybrid and R-loops formation in CLL cells, I began by carrying out a DNA–RNA immunoprecipitation with sequencing (DRIP-seq) on CLL MEC1 cells with RNASEH2B monoallelic KO, biallelic KO and WT control using the S9.6 antibody that binds to DNA–RNA hybrids (König et al., 2017, Boguslawski et al., 1986). A negative control sample of genomic DNA subjected to digestion with RNase H before S9.6 IP was included to control for nonspecific DNA duplex versus DNA–RNA hybrids. I observed an increase in the S9.6 signal correlated with monoallelic and biallelic

RNASEH2B loss compared to the control using EPIC2 peak caller (Stovner and Sætrom, 2019) with an FDR cut-off of 0.01 for peak calling. It is worth noting that the monoallelic KO cells demonstrated a higher S9.6 signal (Mo-KO:17960, Bi-KO:15108, WT:12856), suggesting that the resolution of RNA/DNA hybrids is differentially affected in those cells. At the genome-wide transcription start site (TSS), I found a higher DNA–RNA hybrid signal in correlation with monoallelic RNASEH2B KO and biallelic RNASEH2B KO (Figure 4.10 A), and the RNase H-treated sample (negative control) demonstrated a lower enrichment, as expected.

To further examine the genomic distribution of DNA–RNA hybrid peaks, I annotated the peaks to their nearest gene using ChIPpeakAnno (Zhu et al., 2010) and defined promoter regions if they were within 1500 +/- of the TSS. The annotation analysis showed that the majority of DNA–RNA hybrid signals were correlated within intron regions (Figure 4.10 B), consistent with other studies (Okamoto et al., 2018, Powell et al., 2013, Bonnet et al., 2017, El Hage et al., 2014). Moreover, the monoallelic KO cells were correlated with slightly higher DNA–RNA hybrid signals over promoter regions compared to biallelic KO and the WT control. I did not find other significant differences in terms of the genomic distribution of R-loop signals.

To get more insights on how DNA-RNA hybrids are processed, I further analysed the DNA–RNA hybrid peaks to determine whether the peaks correlated with the monoallelic and biallelic KO cells differed from those observed in the WT control in terms of peak width in base pair (bp). Within a defined genomic locus, sharp and narrow peaks correlated with effective R-loops processing, whereas broad and diffuse peaks correlated with an accumulation of R-loops, representing the formation of inefficient processing of DNA-RNA hybrids. I created a histogram in which I calculated the occurrences of each peak size in my data. It can be observed that the DNA–RNA hybrid signals are of similar width in correlation with the biallelic KO and WT control (Figure 4.10 C). However, I noted an increased number of broader peaks in correlation

with the monoallelic KO cells compared to biallelic KO and WT (Figure 4.10 C). This finding could be possibly explained by haploinsufficiency, wherein the remaining allele, the monoallelic KO cells is not sufficient to preserve normal RNASEH2B function (Morrill and Amon, 2019). Therefore, the amount of RNASEH2B protein produced in mono-KO cells is not enough to cope with DNA-RNA hybrids causing a disruption of RNase H2 complex formation and thus, cells cannot activate alternative pathways since RNASEH2B is produced in the first place. However, in the biallelic KO, where a complete absence of the RNASEH2B is observed, the cells may have developed an adaptation mechanism to manage DNA–RNA formation by opening alternate evolutionary routes (Helsen et al., 2020). Collectively, I showed that the impact of RNASEH2B loss is correlated with an increase in R-loop formation.

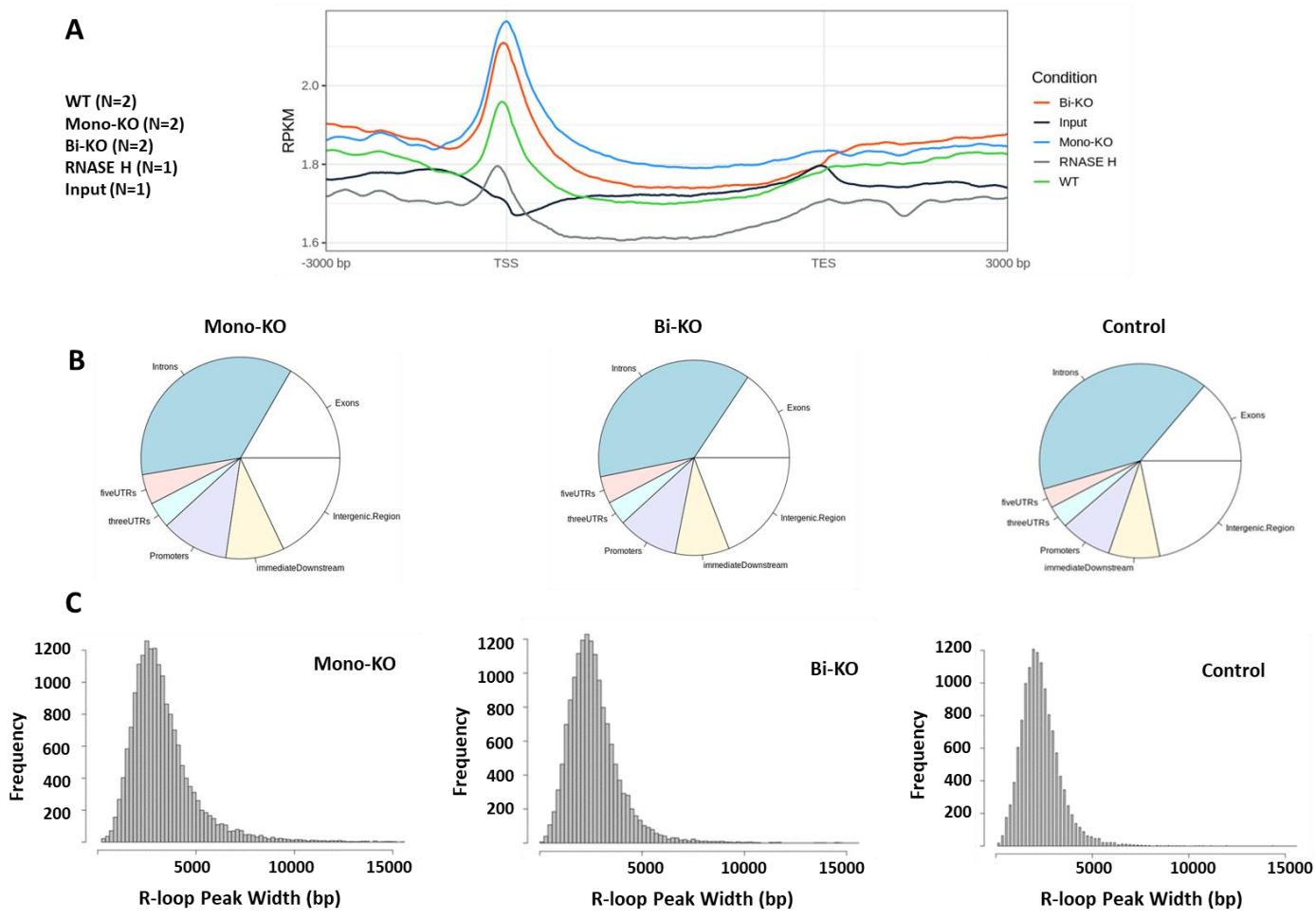


Figure 4.10 RNASEH2B loss is correlated with increased RNA–DNA hybrid formation (R-loops)
(A) Meta-profile of normalized DRIP read count in a scaled region containing 3000 bp upstream of the transcription start sites (TSS) of all annotated genes related to human genome version 38, 5000 bp across gene body, and 3000 bp downstream of TES. The result suggests an increase of S9.6 signal at TSS sites correlated with RNASEH2B loss. RNASE H treated sample (negative control) shows a reduced S9.6 signal. (B) Statistically significant peaks associated with S9.6 signal for each condition were annotated to look for the genome-wide distribution of R-loops correlated with RNSEH2B loss. The pie charts represent the annotations of R-loop peaks, and from the results, no major differences were seen in terms of R-loops distribution. (C) To examine the R-loop associated peaks width, peaks frequencies were counted and plotted as histograms showing the frequencies of R-loop peak widths (in bp). The result show a slight increase in the width of R-loop associated peaks correlated with RNASEH2B loss. Abbreviations: B-KO (biallelic KO), M-KO (monoallelic KO), WT (Wild type). The number of each DRIP-seq replicates is two per condition (N=2)

4.4 Characterisation of histone post-translational modifications, histone variant H2AZ and Pol II changes correlated with RNASEH2B biallelic and monoallelic loss

DNA–RNA hybrid (R-loop) formation is enriched at CpG islands (CGIs) and is consequently involved in chromatin state regulation (Ginno et al., 2012). In addition, R-loops at the promoters and terminators are linked with specific epigenomic signatures. At the promoters, R-loops are associated with relaxed open chromatin, active promoters and decreased DNA methylation, whereas at termination sites, these loops are more correlated with insulators and enhancers type of chromatin state and involved in transcription repression regulation (Sanz et al., 2016). Research into the CLL epigenome has demonstrated marked changes in the chromatin accessibility and H3K27ac level in CLL patients with 13q deletions (Beekman et al., 2018). However, the study did not assess the type of 13q deletion (biallelic or monoallelic), or RNASEH2B status. Therefore, RNASEH2B biallelic and monoallelic loss and R-loop formation impact on histone post-translational modifications in the context of CLL is still unknown.

I performed chromatin immunoprecipitation followed by sequencing (ChIP-seq) to profile the histone marks associated with active transcription (H3K4me3 and H3K27ac). I also included the histone variant H2A.Z because it is involved in transcription regulation (Draker et al., 2012, Vardabasso et al., 2015, Adam et al., 2001), chromatin organization (Greaves et al., 2007, Fan et al., 2004, Rangasamy et al., 2003) and DNA damage (Nishibuchi et al., 2014, Kalocsay et al., 2009, Xu et al., 2012) particularly in nucleotide excision repair (NER) (Yu et al., 2013). Finally, I integrated previous ChIP data measuring histone marks

and histone variants with RNA polymerase II to investigate and relate active transcription with the chromatin landscape. Together, using this approach, I generated an overall picture of the impact of RNASEH2B loss on the localization of active histones, genome-wide histone variants H2A.Z and RNA Pol II and their relation to gene expression and chromatin accessibility.

To illustrate the variation in histone modifications, H2A.Z and POL II occupancy in correlation with RNASEH2B monoallelic and biallelic loss, a pairwise Pearson correlation analysis was performed between the normalized counts (RPKM). Hierarchical unsupervised clustering of these correlation values revealed that the histone mark groups cluster together (Figure 4.11). In addition, the heatmap illustrated that the POL II and H2A.Z groups cluster individually but further away from the histone mark group, as expected, and the heatmap also revealed the differences in correlation with biallelic and monoallelic KO relative to the WT control. For example, I observed in the H2AZ group that cells labelled the biallelic and monoallelic KO cluster together but away from the WT control, suggesting changes in H2AZ occupancy in correlation with RNASEH2B loss status. Similarly, in the histone groups, both biallelic and monoallelic KO cells cluster together individually with respect to H3K4me3 and H3K27ac but are further away from the WT control, indicating alterations in the occupancy of these histone marks in correlation with RNASH2B loss status (Figure 4.11). Collectively, I observed an increased level of occupancy changes in H2A.Z, H3K4me3 and H3K27ac correlated with RNASEH2B biallelic and monoallelic KO relative to the WT control.

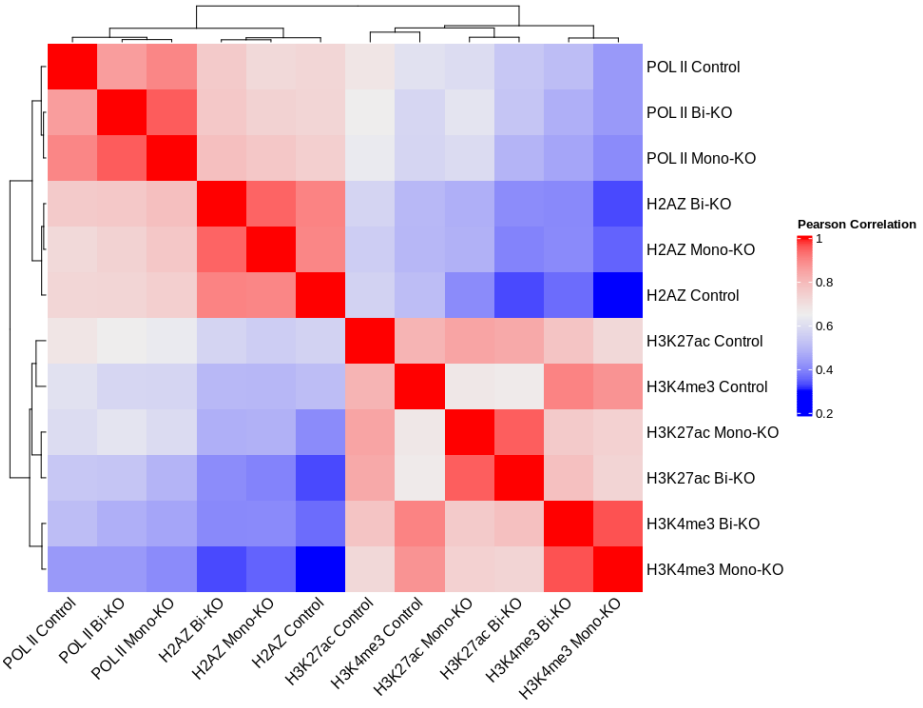


Figure 4.11 Chromatin immunoprecipitation data suggest genome-wide alterations in histone PTM, histone variant, and Pol II in correlation with RNASEH2B loss

Pearson correlation heatmap of log2 transformed normalized count of ChIP data show hierarchical unsupervised clustering; histone PTM marks cluster close to each other but away from the control sample, whereas histone variant H2A.Z samples cluster further away from the control sample. The Pol II ChIP data cluster solely and show a slight correlation reduction in comparison with the control sample. The heatmap highlight changes in histone PTM, histone variant, and Pol II in correlation with RNASEH2B loss. Abbreviations: B-KO (biallelic KO), M-KO (monoallelic KO), WT (Wild type). The number of each ChIP replicate per condition is one (N=1).

4.4.2 RNASEH2B loss is correlated with genome-wide H3K4me3 deregulation

To examine the genomic regions associated with my ChIP data, I called peaks using MACS2 and considered only summit peaks that passed the preset FDR cut-off (0.01). This analysis identified statistically significant summit peaks in correlation with RNASEH2B status for histone PTMs H3K4me3 (Mo-KO: 40771, Bi-KO:39637, WT: 22266) and H3k27ac (Mo-KO: 65347, Bi-KO: 68202, WT: 40505), Pol II (Mo-KO: 14493, Bi-KO: 11726, WT: 13982), and histone variant H2A.Z (Mo-KO: 32758, Bi-KO: 23117, WT: 17100). To assess the degree of overlapping between the detected statistically significant peaks associated with each condition, peaks were subjected to intersection analysis to report condition unique peaks. This analysis

allowed the assessment of similarities and differences of peaks with respect to genomic regions enriched with histone PTM, histone variant, and Pol II. The result shows that in correlation with RNASEH2B loss, histone PTM, histone variant, and Pol II show signs of increased occupancy at genomic regions not observed at WT control cells (Figure 4.12 A).

Next, peaks that passed this cut-off were annotated to genomic features using the ChIPseeker package on hg38 and defined promoter regions as 1500 bp before and after TSS. The annotated peaks were plotted as a horizontal bar plot, with the Y-axis representing the samples and the X-axis indicating the percentage; the genomic features were colour coded.

I observed an increased level of the H3K4me3 mark in correlation with KO cells (Figure 4.12 B). In addition, compared to WT control cells, the H3K4me3 mark was correlated with extended signal in promoter regions and towards the gene bodies. The observed increase in H3K4me3 levels may represent a response to ongoing transcription-replication stress. Consistent with this notion, several groups reported that H3K4 methylation is required to lower transcription–replication conflicts to prevent genomic instability (Chong et al., 2020, Higgs et al., 2018).

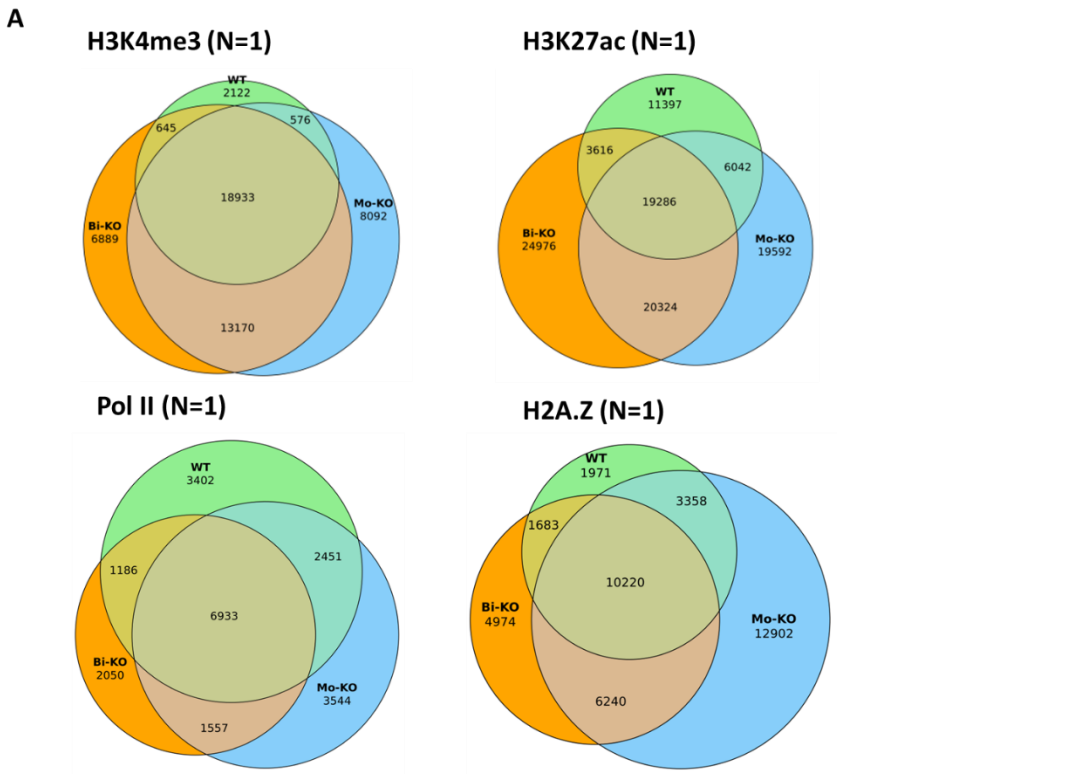
4.4.3 Genome-wide H3K27ac histone marks are increased in correlation with RNASEH2B KO cells

In agreement with H3K4me3, I observed an increased level of H3K27ac at gene bodies and a reduced level at gene promoters correlated with RNASEH2B monoallelic and biallelic loss (Figure 4.12 B). The H3K27ac mark was significantly enriched at the promoter regions in correlation with the WT control cells. However, a decreased H3K27ac levels at promoters and an increase in the gene bodies and distal regions observation were correlated with RNASEH2B monoallelic and biallelic loss. The Pol II genomic feature annotations showed no major differences in RNA POL II occupancy (mostly promoters) between monoallelic and biallelic KO and WT control cells (Figure 4.12 B). Therefore, POL II data suggest the

transcriptional machinery occupancy levels were not correlated with the status of RNASEH2B in CLL isogenic cell lines.

4.4.4 RNASEH2B KO cells are correlated with upregulation of the histone variants H2A.Z

The histone variant H2A.Z genomic feature annotation demonstrated a decrease at the promoter regions in correlation with RNASEH2B monoallelic and biallelic loss compared to WT controls. The analysis also showed an increase in H2A.Z occupancy at distal intergenic regions correlated with RNASEH2B loss (Figure 4.12 B). The histone variant H2A.Z is noted to be localized at promoter regulatory elements (Creyghton et al., 2008, Schones et al., 2008, Barski et al., 2007) and other regulatory elements, including enhancers and insulators (Johnson et al., 2018, Jin et al., 2009). The observed increase of the histone variant H2A.Z correlated with monoallelic and biallelic RNASEH2B loss is likely due to the increased levels of genomic impeded ribonucleotides which cause DNA structural and conformational alterations and negatively impact nucleosomes stability (Nick McElhinny et al., 2010, Meroni et al., 2017). Therefore, to maintain nucleosomes integrity and stability, the histone variant H2A.Z is known to be recruited to preserve nucleosomes functions and enhance interaction with DNA which explains the increased levels of H2A.Z correlated with monoallelic and biallelic RNASEH2B loss (Rudnizky et al., 2016, Jin and Felsenfeld, 2007, Adam et al., 2001, Wen et al., 2020)


A
H3K4me3 (N=1)
WT
2122
645
576
18933
Bi-KO
6889
Mo-KO
8092
13170
H3K27ac (N=1)
WT
11397
3616
6042
19286
Bi-KO
24976
Mo-KO
19592
20324
Pol II (N=1)
WT
3402
1186
2451
6933
Bi-KO
2050
Mo-KO
3544
1557
H2A.Z (N=1)
WT
1971
3358
1683
10220
Bi-KO
4974
Mo-KO
12902
6240

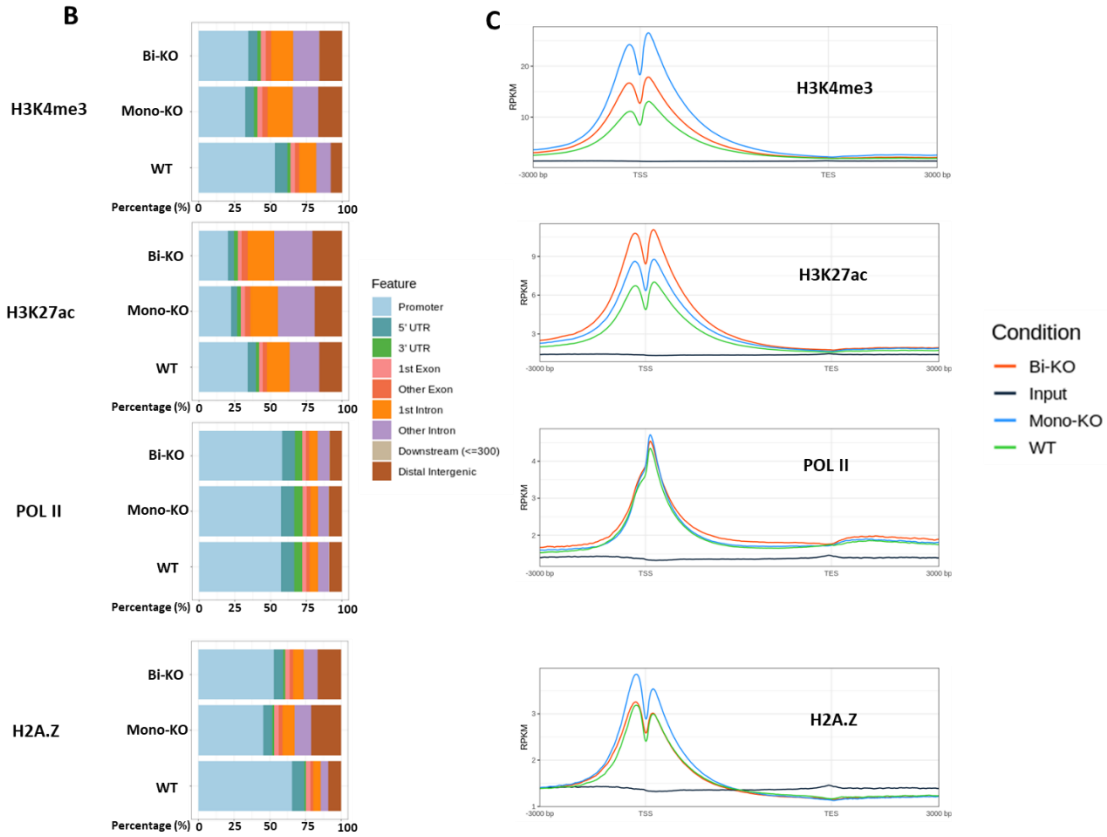

B
H3K4me3
H3K27ac
POL II
H2A.Z
Bi-KO
Mono-KO
WT
Percentage (%) 0 25 50 75 100
Feature
Promoter
5' UTR
3' UTR
1st Exon
Other Exon
1st Intron
Other Intron
Downstream (<=300)
Distal Intergenic
C
H3K4me3
H3K27ac
POL II
H2A.Z
RPKM
-3000 bp
TSS
TES
3000 bp
Condition
Bi-KO
Input
Mono-KO
WT

Figure 4.12 Analysis of associated with histone modifications, Pol II and histone variant H2AZ in correlation with RNASEH2B KO cells (A) Venn diagrams showing the degree of overlapping peaks correlated with RNASEH2B loss in comparison to WT control associated peaks. Overall, an increase in histone PTM and histone variant peaks in correlation with RNASEH2B loss was observed. (B) Genomic annotations of peaks associated with histone modifications, Pol II and H2AZ to assess their differential localization at regulatory elements. Histone PTM marks and histone variant show increased enrichments at regions other than promoters in correlation with RNASEH2B loss. (C) To assess the enrichment of ChIP signals across gene bodies, normalized ChIP-seq reads profiles were generated over a scaled region for H3K4me, H3K27ac, Pol II, H2AZ. The scaled region (x-axis) shows the distance of 3000 bp upstream of transcription start site (TSS) of all annotated genes related to human genome version 38, 5000 bp across gene body and 3000 bp downstream of transcription end site (TES). The (y-axis) represents the normalized ChIP signal. Abbreviations: B-KO (biallelic KO), M-KO (monoallelic KO), WT (Wild type)

I observed a positive correlation between H3K4me and H2A.Z occupancy correlated with RNASEH2B monoallelic and biallelic loss, in agreement with published research (Ku et al., 2012, Kim et al., 2013) where H2A.Z containing nucleosomes have high levels of H3K4me3. In addition, I noticed that in correlation with RNASEH2B monoallelic and biallelic loss, the level of both H3K4me3 and H2A.Z extended beyond the transcription start sites (TSS) region toward the gene body. The spread of H2A.Z beyond promoters is linked with global inhibition of transcription and heterochromatic regions (Xu et al., 2018, Hardy et al., 2009, Lashgari et al., 2017). Therefore, as a consequence of RNASEH2B loss, cells are likely to cope with this defection by reducing transcription to allow the resolution of DNA-RNA hybrids.

To better understand the occupancy patterns at the genome-wide level, I created metagene profiles of histone modifications, POL II and H2A.Z at the TSS across gene body transcription end sites (TES) (Figure 4.12 C). In this analysis, the normalized ChIP read counts were plotted against a scaled region that is divided into three parts. The metagene profile covers regions up to 3000 bp before TSS, 5000 bp across the gene body and 3000 bp after TES. In agreement with ChIP peak annotation analysis, the metagene profiles showed increased levels of H3K4me3, H3K27ac and H2A.Z enrichments across the gene body in correlation with monoallelic RNASEH2B loss status, whereas biallelic KO cells were correlated with higher levels of H3K27ac and H3K4me3 at gene bodies. I did not observe a significant difference in POL II occupancy in correlation with monoallelic and biallelic RNASEH2B KO cells compared to the WT control, consistent with the POL II peak annotation. Together, in agreement with the Person correlation analysis,

the data for H3K4me3 and H3K27ac demonstrated an extensive alteration in these histone marks correlated with monoallelic and biallelic RNASEH2B loss.

4.4.5 The H3K4me3 epigenetic mark is associated with a reduction at genes involved in RNA biology in correlation with RNASEH2B KO cells

Because I observed a significant amount of H3K4me3 occupancy alterations at genome-wide level in correlation with RNASEH2B defective cells (Figure 4.12 A and B), I further analysed the H3K4me3 peaks in all conditions (RNASEH2B monoallelic and biallelic KO and WT). I wanted to investigate the commonality and differences in occupancy patterns of this epigenetic mark between cells with different RNASEH2B statuses. Therefore, I created a Venn diagram (Figure 4.13 A) by intersecting all peaks from all conditions using Bedtools. In this analysis, overlapping genomic regions will be reported as common/shared regions, whereas non-overlapping regions will be defined as unique. The analysis showed a common peak set (18933 peaks) shared between all conditions. However, the analysis also demonstrated condition-specific peaks that are not shared with other conditions (WT=2112, mono-KO=8092 and bi-KO=6889). To determine whether these condition-specific peaks were of biological relevance, I further annotated these unique condition-specific peaks to the nearest gene and then carried out a GO analysis on the obtained gene list for each unique peak set (Figure 4.13 B).

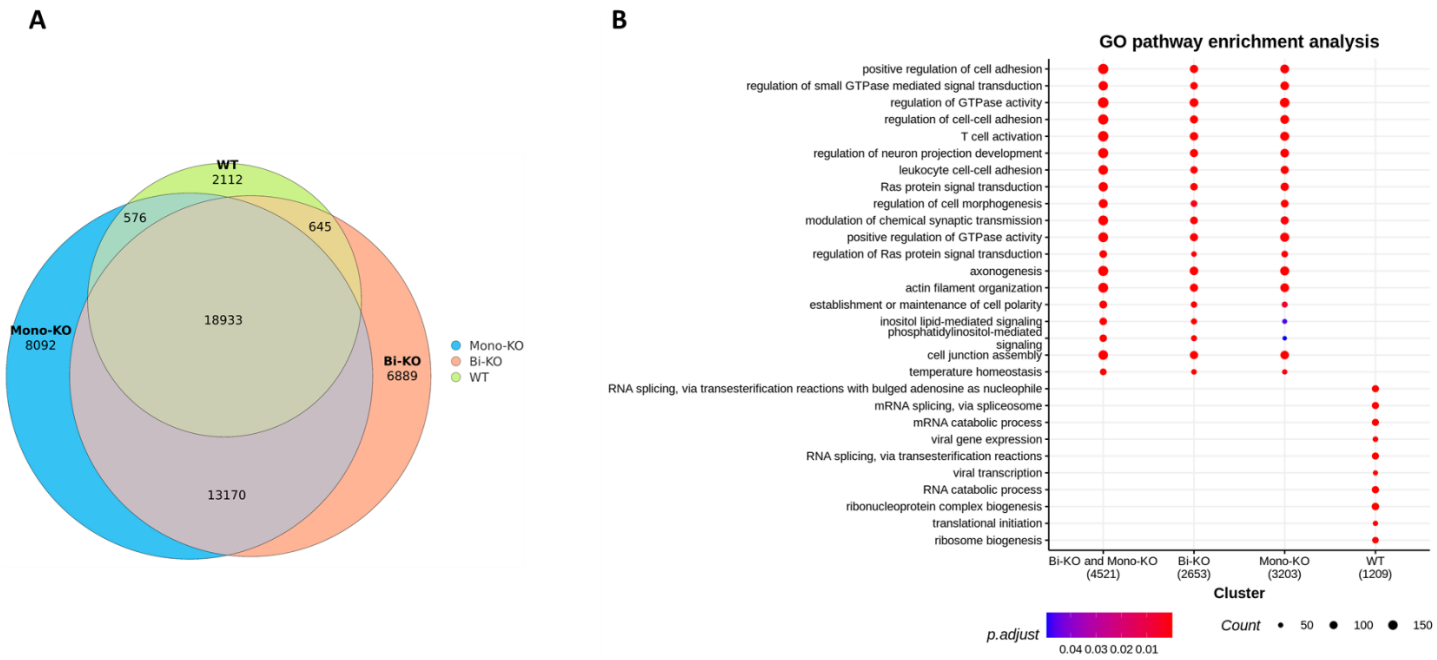


Figure 4.13 Genomic annotations of H3K4m3 condition-specific peaks
(A) A Venn diagram showing common and unique H3K4me3 peaks that were correlated with RNASEH2B status.(B) Peaks termed unique were annotated to the nearest gene and GO analysis was performed. Common H3K4me3 peaks between biallelic and monoallelic RNASEH2B KO cells were also plotted. The dot colour represents the significant level of the associated pathway, whereas the dot size shows the number of genes. The x-xis represents the number of total genes associated with peaks, whereas the y-axis represents the significant enriched GO pathways associated with the genes list for each condition. Abbreviations: B-KO (biallelic KO), M-KO (monoallelic KO), WT (Wild type)

The GO analysis on condition-specific unique peak sets demonstrated commonalities in terms of genes preserved H3K4me3 mark correlated with RNASEH2B monoallelic and biallelic loss status. The GO analysis showed that pathways such as regulation of GTPase activity (gene count: 200, adj p-value: 4.73×10^{-14}), cell adhesion (gene count: 182, adj p-value: 1.92×10^{-13}), T cell activation (gene count: 191, adj p-value: 1.48×10^{-12}), and lymphocyte differentiation (gene count: 147, adj p-value: 1.72×10^{-10}), were associated with genes encompassing H3K4me3 mark that have been annotated to be mutually observed in correlation with RNASEH2B monoallelic and biallelic loss status (Figure 4.13). This result is consistent with RNA-seq results where upregulated genes (log2 fold change > 2) were linked to immune and inflammatory regulatory pathways as well as cell-cell adhesion (Figure 4.7-4.8). This observation is possibly due to a

response to an increase in the genomic mutation burden in KO cells which may consequently activate anti-tumour T cell responses (Riches et al., 2013). Moreover, this observation correlates with the active inflammatory responses seen in patients with Aicardi–Goutières syndrome.

In contrast, WT condition-specific unique peaks were associated with genes relevant to RNA biology. The GO analysis showed that pathways such as RNA splicing (gene count: 77, adj p-value: 1.74×10^{-16}), ribonucleoprotein complex biogenesis (gene count: 86, adj p-value: 4.85×10^{-16}), regulation of mRNA metabolic process (gene count: 64, adj p-value: 6.48×10^{-13}), and translational initiation (gene count: 51, adj p-value: 6.96×10^{-16}), were enriched in genes associated with WT condition-specific unique peak sets (Figure 4.13). This observation is consistent with RNase H2-depleted cells showing a reduction in rRNA synthesis (El Hage et al., 2010). Moreover, RNA-seq data also demonstrated that monoallelic and biallelic RNASEH2B KO cells were correlated with overall down-regulation of genes related to RNA biology and translation (Figure 4.8).

4.5 Characterisation of the chromatin accessibility changes correlated with RNASEH2B monoallelic and biallelic loss

I performed chromatin profiling using an ATAC-seq essay, where I generated chromatin accessibility profiles of CLL cells correlated with RNASEH2B monoallelic and biallelic loss and compared them to chromatin accessibility profile correlated with RNASEH2B WT status. Using this approach allowed me to find a condition-specific chromatin accessible region from which regulatory regions were identified. I then performed an integrated analysis, where I linked chromatin profiles with gene expression data to gain an overall understanding of the chromatin landscape changes correlated with RNASEH2B-defective CLL cells.

MACS2 software was used to call peaks in ATAC BAM files using the settings –nomodel –nolambd --shift -100 --extsize 200. The resulting peaks were further filtered to keep only summit peaks with the following criteria: peaks should have at least 10 read pileup, peaks common to both replicates, peaks that were also

present in the consensus peak list and peaks not located to encode defined hg38-blacklisted regions. FeatureCounts software was used to create a peak count matrix that was used as the input for differential peak analysis. Using the WT control, I performed a differential peak analysis for both conditions (biallelic KO versus WT control and monoallelic KO versus WT control) using the EdgeR package. I defined a site as being specific if it had an adj p-value below 0.1 and least -/+ 1.5 logFC. As observed in the volcano plots (Figure 4.14 A), the peaks passing the defined significance level are highlighted in red.

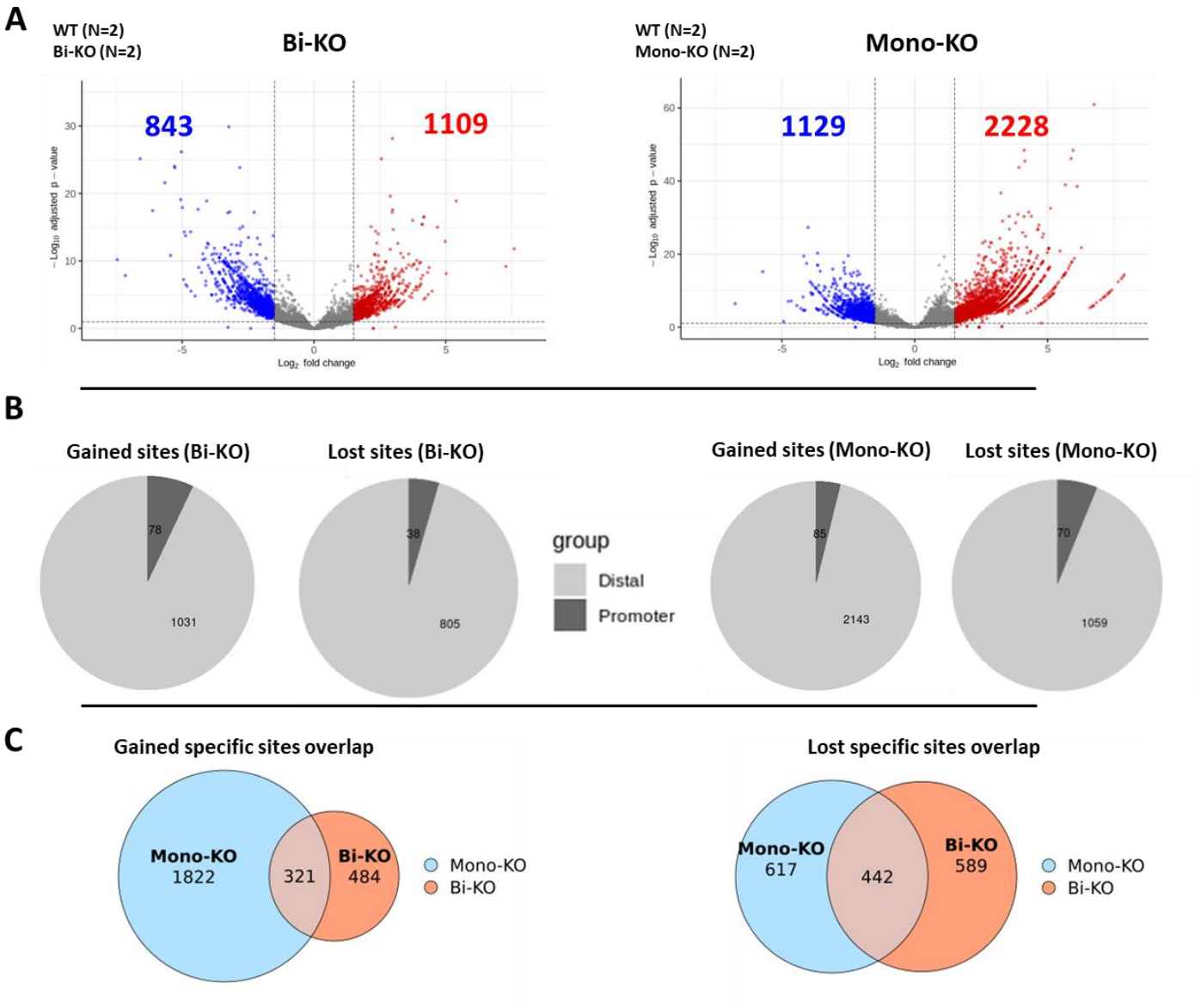


Figure 4.14 Genome-wide changes in the chromatin accessibility landscape of distal regulatory elements are correlated with RNASEH2B status in CLL cells

(A) Volcano plots resulting from differential chromatin accessibility analysis performed on RNASEH2B KO isogenic cell lines showing the statistical significant accessible peaks correlated with RNASEH2B status (adj p-value < 0.1 and log2FC > 1.5) coloured in red resulting from ATAC differential accessibility analysis; up-regulated peaks were termed gained sites and down-regulated peaks termed lost sites. (B) Gained and lost sites were annotated and considered to be in promoter regulatory regions if peaks fall within -/+ 1500 bp of TSS and distal regulatory regions otherwise. (C) Venn diagrams highlighting common sets of gained and lost specific accessible sites among RNASEH2B KO cells. Results suggest that RNASEH2B defective CLL cells are correlated with chromatin accessibility alterations at distal regulatory elements. Abbreviations: B-KO (biallelic KO), M-KO (monoallelic KO), WT (Wild type). The number of replicates per condition is two (N=2).

The differential accessibility analysis demonstrated that biallelic KO cells were correlated with gained 1109 specific accessible sites and lost 843 specific accessible sites. The monoallelic KO cells, on the other hand, were correlated with a gain of 2228 specific accessible sites and a loss of 1129 specific accessible sites. I further examined whether these sites were located at promoter or distal regulatory elements. A specific site was considered to be at a promoter region if it was within +/- 1500 bp of TSS region and distal otherwise. I created pie charts demonstrating specific site distributions with respect to the promoter and distal regions (Figure 4.14 B). I also noticed shared specific accessible sites between gained sites of both biallelic and monoallelic sites, and the same was observed for lost specific sites as well (Figure 4.14 C). Because minimal changes were observed at promoter regions, downstream analysis was focused on distal regions only. To further confirm that these specific sites were indeed seen at their corresponding condition, I created a metagene profile plot by calculating the normalized ATAC reads centred on our defined specific sites in a window 1.5 Kb above and below the peak centre (Figure 4.15). The metagene profile further supported the identified specific accessible sites; for example, I observed high enrichment of ATAC reads correlated with RNASEH2B biallelic KO in both replicates over biallelic KO defined gained specific accessible sites, whereas WT control replicates showed lower enrichment.

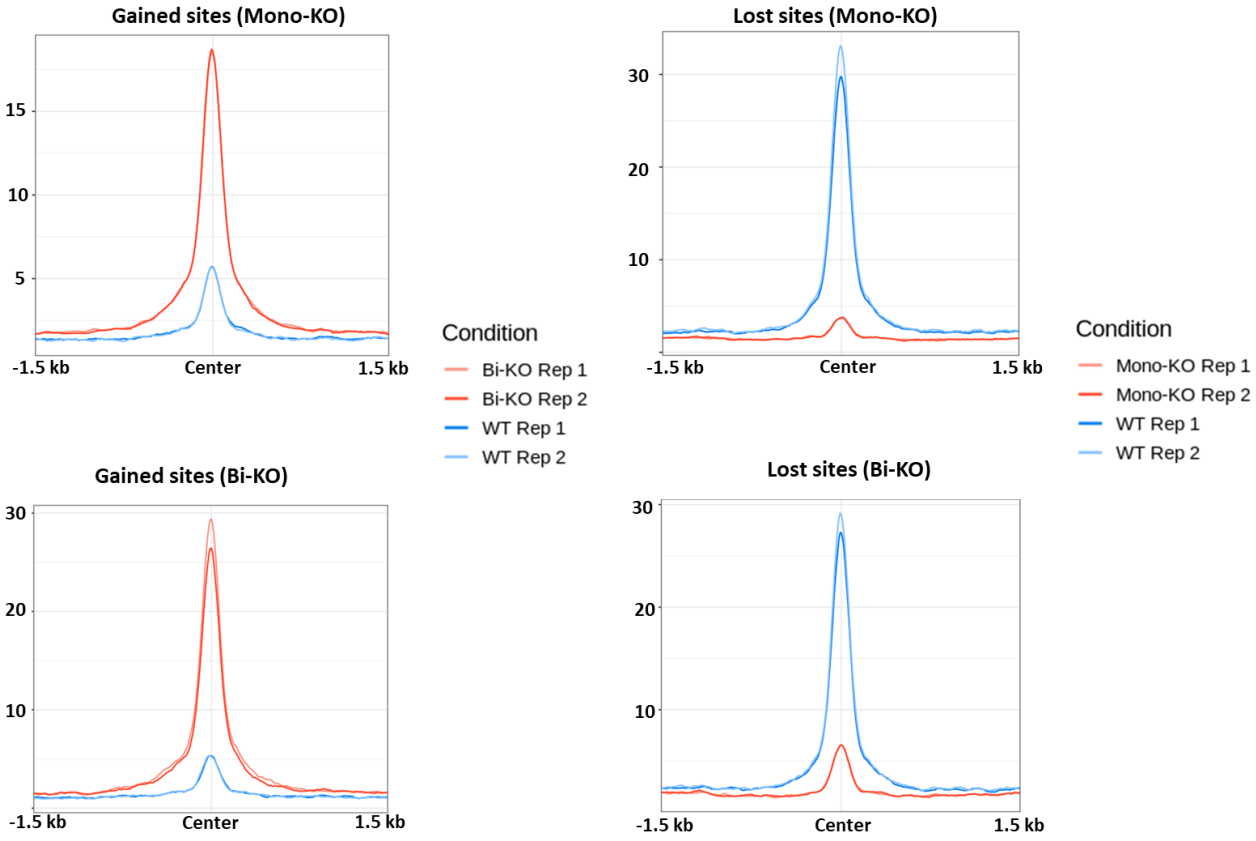


Figure 4.15 Validation of the defined sets of gained and lost chromatin accessible sites in correlation with RNASEh2B loss status.
Meta profile of gained and lost sites of a region that extends 1500 bp upstream and downstream of peak summit centres. The meta profile shows that gained sites are enriched in RNASEH2B KO replicates, whereas lost sites show only enrichments for RNASEH2B WT control cells. Thus, supporting that these gained and lost specific accessible sites are indeed correlated with RNSEH2B status. Abbreviations: B-KO (biallelic KO), M-KO (monoallelic KO), WT (Wild type)

4.5.2 Observation of increased accessibility for RUNX, AP-1, and IRF motifs in correlation with RNASEH2B defective CLL cells

Next, to examine whether these defined regulatory specific sites contained motifs associated with transcription regulatory elements, I performed a transcription factor motif analysis on these distal regulatory sites using HOMER (Heinz et al., 2010). Biallelic KO-specific gained sites were correlated with the enrichment of RUNX, AP-1, IRF, NFkB and PU.1 (Table 4.1 A), whereas lost specific sites were correlated with the enrichment of RUNX, ETS, NFkB, IRF and CREB/ATF in the de-novo motif discovery

analysis (Table 4.1 B). In contrast, the monoallelic KO cells gained specific sites were correlated with the enrichment of IRF, RUNX, AP-1, CTCF and ETS (Table 4.1 C). In monoallelic KO, lost sites were correlated with the enrichment of RUNX, E-box, Ap-1, NFkB and CREB/ATF (Table 4.1 D). Collectively, I observed that IRF, RUNX and AP-1 were among the highest enriched TF motifs at defined gained sites that are correlated with monoallelic and biallelic RNASEH2B loss in CLL cells.

A **Bi-KO Gained Sites**

Motif	Match	% Sites	p-value
	RUNX	24.84	1e-43
	AP-1	20.50	1e-85
	IRF	16.89	1e-49
	NFkB	7.20	1e-14
	PU.1	6.21	1e-26

C **Mono-KO Gained Sites**

Motif	Match	% Sites	p-value
	IRF	28.04	1e-70
	RUNX	25.90	1e-83
	AP-1	24.41	1e-82
	ETS	11.99	1e-47
	CTCF	4.81	1e-32

B **Bi-KO Lost Sites**

Motif	Match	% Sites	p-value
	RUNX	35.60	1e-67
	ETS	29.39	1e-26
	NFkB	17.07	1e-28
	IRF	8.73	1e-37
	CREB/ATF	8.44	1e-30

D **Mono-KO Lost Sites**

Motif	Match	% Sites	p-value
	RUNX	34.47	1e-75
	E-Box	28.80	1e-21
	AP-1	21.44	1e-34
	NFkB	15.86	1e-31
	CREB/ATF	15.86	1e-15

Table 4.1 Motif enrichment analysis at gained and lost correlated with RNASEh2B monoallelic and biallelic loss (distal peaks only)

The specified gained and lost accessible sites resulting from chromatin differential accessibility analysis were subjected to motifs analysis to look for the enrichment of transcription factors associated with distal regulatory elements that were correlated with RNASEH2B loss. (A) Homer De novo motifs were found at gained peaks (bi-KO specific). (B) Homer de novo motifs were found at lost peaks (bi-KO specific). (C) Homer de novo motifs were found at gained peaks (mono-KO specific). (D) Homer de novo motifs were found at lost peaks (mono-KO specific). All motifs were ranked by site percentage. Overall, RNASEH2B loss was correlated with the enrichment of RUNX, IRF, and AP-1, whereas RUNX, ETS, and NFkB were correlated with low enrichments. Abbreviations: B-KO (biallelic KO), M-KO (monoallelic KO), WT (Wild type).

4.5.3 RUNX, AP1 and IRF co-localization is correlated with monoallelic and biallelic RNASEH2B loss

To assess whether the observed enriched TF work together to form complexes that program the transcriptional landscape that is correlated with RNASEH2B monoallelic and biallelic KO cells, I performed

bootstrapping analysis. In this analysis, I examined the co-localization of motifs within 50 bp in ATAC-defined specific sites and compared it to what would be caused by random chance on the defined specific site background (reference cells). Correlated with biallelic KO cells, the analysis showed a co-localization between AP-1 and RUNX at the gained sites, whereas the lost sites revealed a co-localization between CREB/ATF, RUNX and ETS (Figure 4.16 A and B). This result indicated that in correlation with RNASEH2B biallelic KO cells, AP-1 works in proximity with RUNX to maintain the transcriptional landscape. In correlation with monoallelic KO cells, however, the analysis showed a co-localization between AP-1, RUNX and IRF at gained sites, whereas RUNX, Ebox and AP-1 demonstrated a co-localization at lost sites (Figure 4.16 C and D). The motif co-localization analysis suggests that monoallelic KO cells were correlated with the proximal activity of AP-1, RUNX, and ETS to maintain the transcription landscape. Collectively, I observed that RUNX, together with AP-1 and IRF are potential key players in maintaining the transcriptional landscape in correlation with CLL cells with RNASEH2B monoallelic and biallelic loss status.

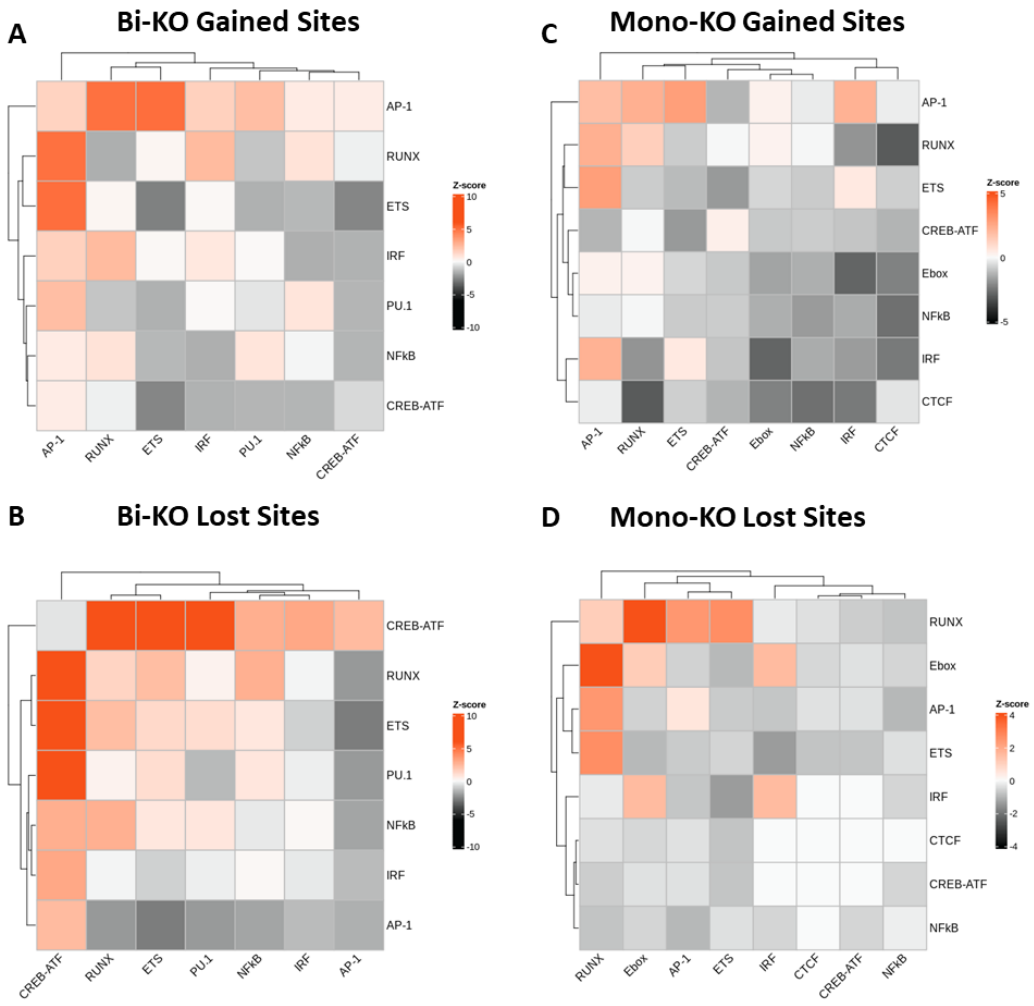


Figure 4.16 Transcriptional landscape in RNASEH2B KO CLL cells is correlated with the increased activity transcription factors RUNX and AP-1

Bootstrapping analysis was computed on specified RNASEH2B KO-specific motifs in comparison to RNASEH2B WT control to assess the co-localization of transcription factors motifs. Positive Z-scores suggest a high colocalization probability, whereas negative scores suggest a low probability. This analysis revealed a co-localization of the RUNX and AP-1 motifs in correlation with RNASEH2B loss in CLL cells. Abbreviations: B-KO (biallelic KO), M-KO (monoallelic KO), WT (Wild type).

4.6 Integration analysis of ATAC-seq, ChIP-seq and RNA-seq data show cis-regulatory elements correlated with RNASEH2B monoallelic and biallelic loss

To build an overall chromatin landscape in correlation with RNASEH2B monoallelic and biallelic KO cells, I began an integrative analysis involving the correlation of chromatin accessibility, ChIP and transcriptomic data. This type of analysis allowed me to examine chromatin accessible data in parallel with gene expression data and histone modifications/ variants, thereby building a comprehensive chromatin landscape. I started the integration analysis by first taking differential chromatin accessibility peaks sites and ranking them by fold change so that gained sites (up-regulated) were at the top and lost sites (down-regulated) at the bottom of the list. Next, I generated a heatmap of ATAC-normalized counts at these ranked sites using HOMER with a window size of 1 KB before and after the peak summit centre. To link transcriptomic data to these defined ranked sites, I annotated the ranked peaks summits to the closest gene and then extracted the gene expression log2 fold change for each annotated gene; hence, a heatmap was generated for all annotated peaks. For ChIP data, I used the previously defined ATAC-ranked peak list and generated a heatmap of normalized ChIP counts (H3K4me3, H3K27ac, Pol II and H2A.Z) within a 4 kb window of the ATAC peak centre. To further see the enrichment of TF motifs at our defined ranked ATAC peaks, I selected the most significant gained and lost de-novo motifs in correlation with RNASEH2B monoallelic and biallelic loss status and looked at their enrichment in the peak list and then generated a heatmap that covered a 2 kb window around the peaks' centre.

4.6.1 Integration analysis shows common chromatin alteration changes in correlation with biallelic and monoallelic RNASEH2B loss in CLL cells

The integration of the three data sets demonstrated a similar overall pattern between RNASEH2B monoallelic and biallelic KO cells. For example, when linking chromatin-accessible data with transcriptomic data, I see that the top-gained accessible sites were associated with active transcription,

whereas the sites that lost their accessibility were associated with an inactive transcription state (Figures 4.17 A and B), consistent with published research (Cao et al., 2018, Weintraub and Groudine, 1976, Kornberg, 1974). Linking ChIP data with chromatin accessibility data showed a similar pattern. Both monoallelic and biallelic KO cells were correlated with high enrichment of H3K4me3, H3K27ac and H2A.Z and no significant changes for Pol II, suggesting the presence of histone marks deregulation and histone variant incorporation at presumably actively transcribed accessible sites. Both monoallelic and biallelic KO cells (monoallelic KO in particular) were correlated with higher levels of H3K4m3, and H2A.Z at the defined ranked ATAC sites. The increased levels of H3K4me3 and H2A.Z are involved in global transcription inhibition and in the mitigation of transcription-replication conflicts (Chong et al., 2020, Higgs et al., 2018, Hardy et al., 2009, Lashgari et al., 2017).

The integration analysis showed that in correlation with RNASEH2B monoallelic and biallelic KO cells, the motifs for RUNX, AP-1, and IRF all gained and lost ATAC sites. However, monoallelic KO cells were correlated with the enrichment of the Ebox and NFkB motifs at lost sites, whereas biallelic KO cells were correlated with enrichment of ETS, NFkB and CREB/ATF motifs at lost sites. Collectively, the integration analysis demonstrated that in correlation with RNASEH2B monoallelic and biallelic loss, an up-regulation of H3K4me3, H3K27ac and H2A.Z levels at chromatin-accessible sites is noted, and this observation correlates with the occurrences of RUNX, AP-1 and IRF motifs. Moreover, the analysis highlights the observation of the inactivation of one RNASEH2B allele is enough to produce a phenotype similar to that of biallelic loss.

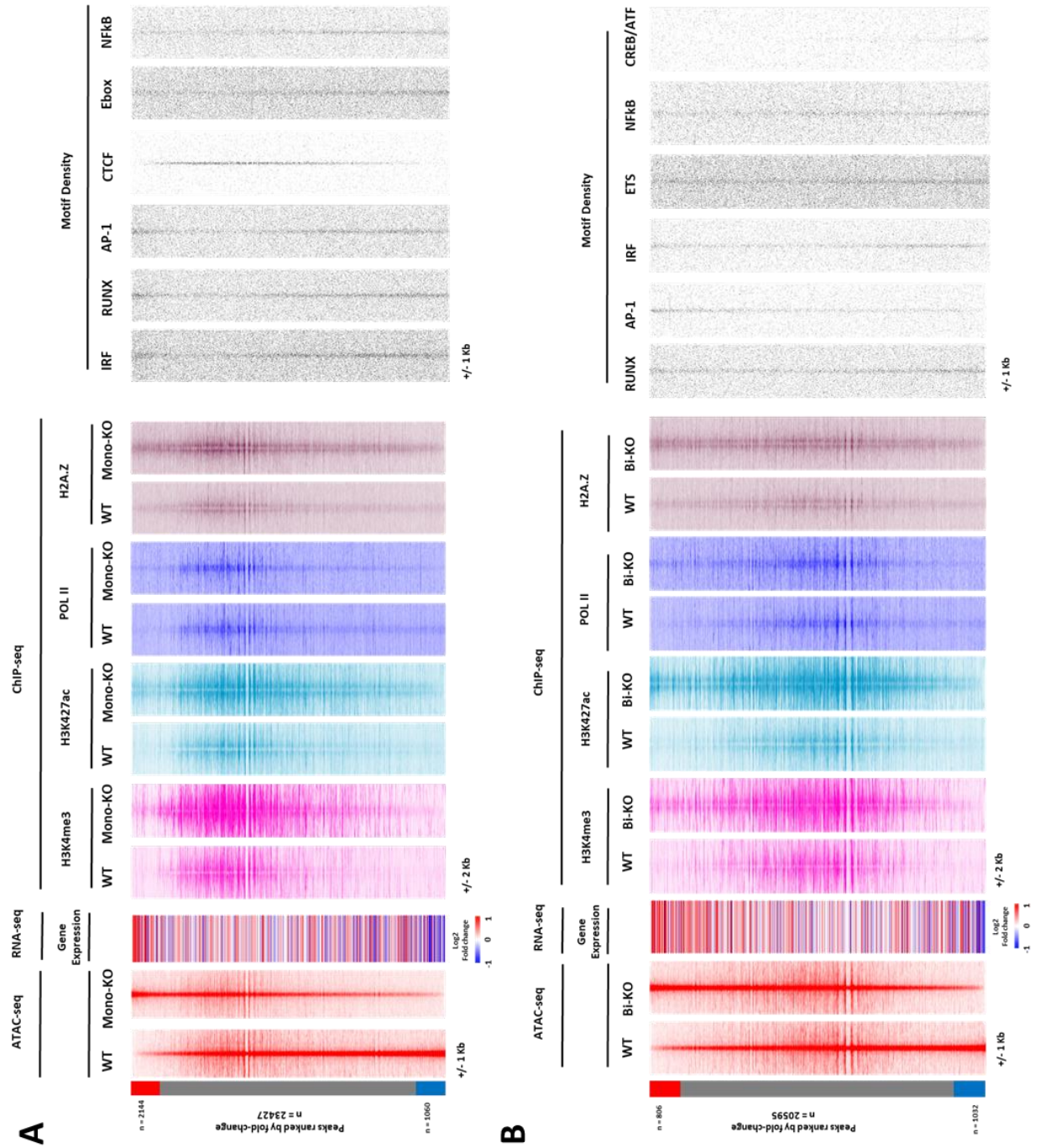


Figure 4.17 Integrative analysis of chromatin accessibility, gene expression, chromatin-bound proteins and motif enrichment correlated with RNASEH2B loss.

The integration analysis began with ATAC-seq data (left). Consensus accessible sites were ranked according to fold change obtained from differential accessibility analysis. Next, ATAC-seq signals were plotted as heatmap above the defined peak list. The ATAC-seq heatmaps show that gained and lost sites are seen only in correlation with RNASEH2B loss conditions. Next, gene expression data were integrated and the gene expression (log2 fold) of genes linked with the defined peak list was plotted as a heatmap (upregulation coloured as red and downregulation coloured in blue). The gene expression heatmap shows that gained sites are linked with upregulated gene expression profile, whereas

lost sites at the bottom are associated with downregulated gene expression profile. Next ChIP-seq signals for each condition were integrated and plotted over the defined ranked peak list. The ChIP-seq signals show marked signal intensity of histone PTM (H3K4me3, and H3K27ac), histone variant in correlation with RNASEH2B loss status. Finally, the enriched TF motifs resulting from motifs analysis of ATAC-seq data were counted and plotted as a heatmap. The motif density heatmaps show the increased signal of RUNX, IRF, and AP-1 motifs at gained sites in correlation with RNASEH2B loss status. (A) Integration analysis for RNASEH2B monoallelic KO CLL cell line. (B) Integration analysis for biallelic KO CLL cell line. Abbreviations: B-KO (biallelic KO), M-KO (monoallelic KO), WT (Wild type).

4.6.2 Identification of transcription factor network correlated with monoallelic and biallelic RNASEH2B loss in CLL cells

To further investigate and understand how RNASEH2B KO CLL cells maintain a stable regulatory network driving their gene expression, I examined ATAC gained and lost specific motifs and linked their enrichment at their downstream target TF genes. Enriched de-novo ATAC motifs correlated with RNASEH2B KO CLL-specific sites (gained and lost) were considered as major nodes, and their border is coloured according to their expression values (FPKM). A direct edge from a major node (represented here as an ATAC-enriched motif) to a minor node (represented here as the locus of a downstream TF gene) indicates the enrichment of that motif at its target gene. The edge was coded by colour and width according to the motif count enrichment.

The transcription factor network analysis (Figure 4.18) identified transcription factor regulatory networks correlated with RNASEH2B KO cells. The analysis demonstrated the correlation of RUNX, IRF and AP-1 in maintaining the transcriptional landscape correlated with RNASEH2B monoallelic and biallelic loss in CLL cells, in agreement with the co-localization analysis (Figure 4.16). The cooperation between RUNX, IRF and AP-1 in the co-localization analysis suggests that these factors work in proximity to regulate a set of genes. The network analysis showed a common set of TF genes shared by RUNX, IRF and AP-1 in correlation with monoallelic KO cells, in accordance with co-localization analysis, where I showed the three transcription factors work in proximity to each other.

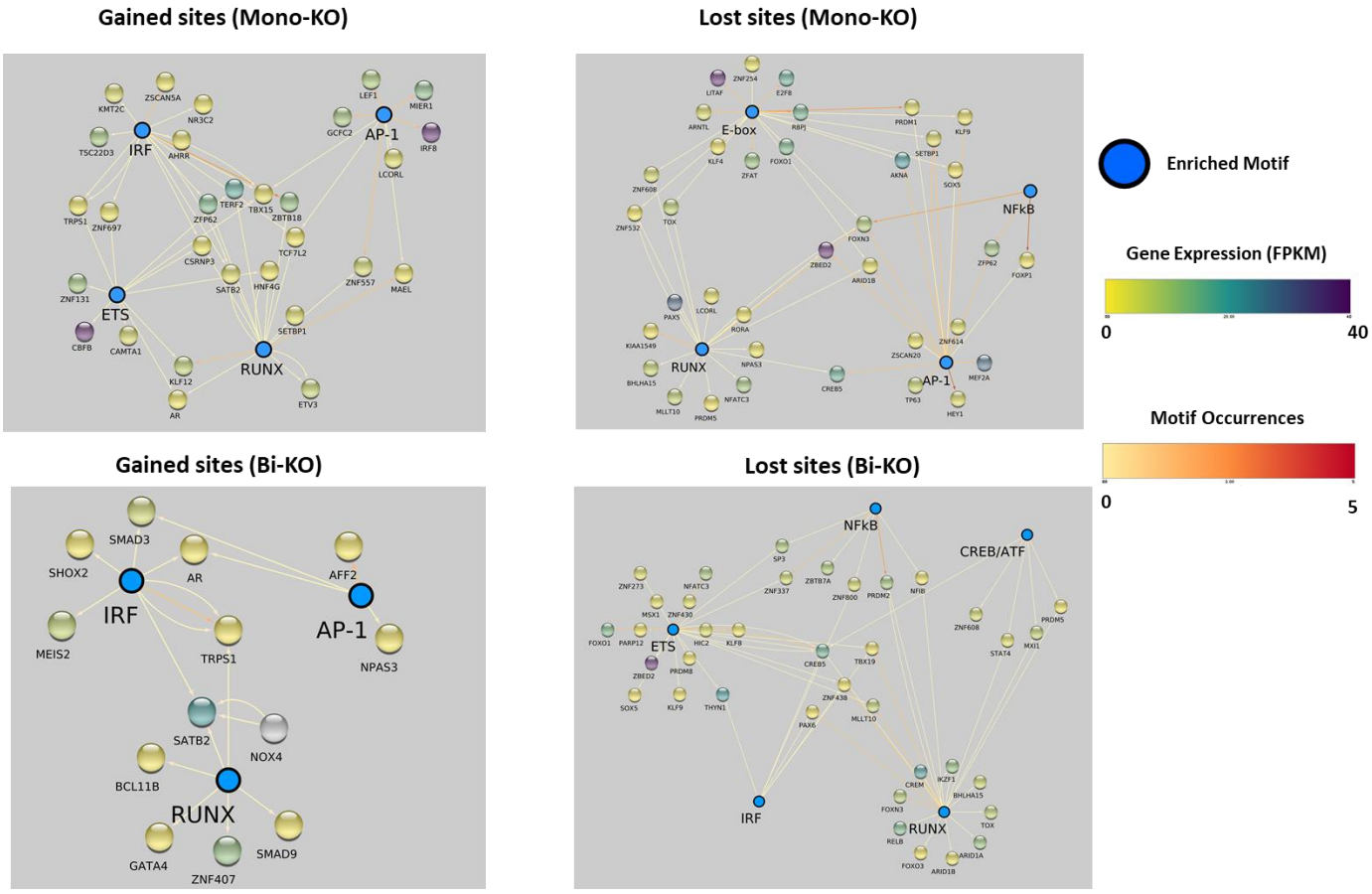


Figure 4.18 The transcription factor networks driving gene expression in accordance with RNASEH2B loss status
The expression profile was extracted for each downstream gene as well as the motif occurrences. Together, the information on TF gene expression and ATAC motif occurrences correlated with RNASEH2B loss at TF genes were used as an input for building the TF transcriptional network. Blue and black-bordered major nodes represent an enriched ATAC motif. Minor nodes represent downstream TF genes, and their colour represents the gene expression in FPKM. Edges emerging from major nodes toward minor nodes show the occurrence of a motif, and edge colour represents the number of motifs found at that TF gene. The analysis highlights that RUNX, IRF, and AP-1 share a set of downstream TF target genes in correlation with defective RNASEH2B status in CLL cells. Abbreviations: B-KO (biallelic KO), M-KO (monoallelic KO), WT (Wild type).

Furthermore, I observed that the association of RUNX, ETS and CREB/ATF was absent in correlation with RNASEH2B biallelic KO cells, whereas RUNX and Ebox cooperation was lost in correlation with monoallelic KO cells, in agreement with motif co-localization analysis (Figure 4.16). Together, from both co-localization and TF regulatory network analyses, I observed a reorganization of the transcriptional landscape

correlated with monoallelic and biallelic RNASEH2B loss, where RUNX is observed to have a major role in maintaining gene expression. It was noted that RUNX co-localize with IRF and AP-1 in correlation with RNASEH2B KO cells, whereas in WT cells, I observed that RUNX co-localize with different TF members (CREB/ATF and ETS in correlation with biallelic KO cells and Ebox in correlation with monoallelic KO cells). It is well established that RUNX proteins are linked with hallmarks of cancer initiation and tumour maintenance, as was reported in melanoma (Scheitz et al., 2012), breast cancer (Mendoza-Villanueva et al., 2010), and prostate cancer (Lim et al., 2010, Blyth et al., 2005). In my integrative analysis, CLL cells with monoallelic and biallelic RNASEH2B loss were correlated with signs of an active AP-1 signalling in parallel with increased RUNX activity which likely leads to cell proliferation and survival. Collectively, the data showed that RUNX TF could potentially play a pivotal role in driving and regulating the expression of TF genes correlated with monoallelic and biallelic RNASEH2B loss. However, the RUNX family of proteins share the DNA-binding motif, which adds an additional layer of complexity in identifying the exact RUNX protein role in this context. Therefore, functional studies are required to assess what member of the RUNX family is involved in the survival of RNASEH2B defective cells.

4.7 Genome-wide CRISPR screening identified synthetic lethal interactions correlated with monoallelic and biallelic RNASEH2B loss

Recently, CRISPR (clustered regularly interspersed palindromic repeats)-based methodologies have transformed the functional genomics laboratory tools. In addition, genome-wide CRISPR-Cas9 screens in tumour cell lines enable the systematic detection of potential genetic dependencies in cancers with specific genomic context (Zimmermann et al., 2018). RNASEH2B gene alterations are frequent in the context of CLL. However, the functional impact of RNASH2B loss in CLL is not fully understood. Therefore, to address the survival dependencies of RNASEH2B KO CLL cells, a colleague in my group (Dr Agathanggelou) undertook CRISPR screens, and I analysed the data. The purpose was to functionally validate data derived from the integration of multi-omics analyses (RNA-seq and ATAC-seq). Figure 4.19 summarizes the CRISPR screen experimental design.

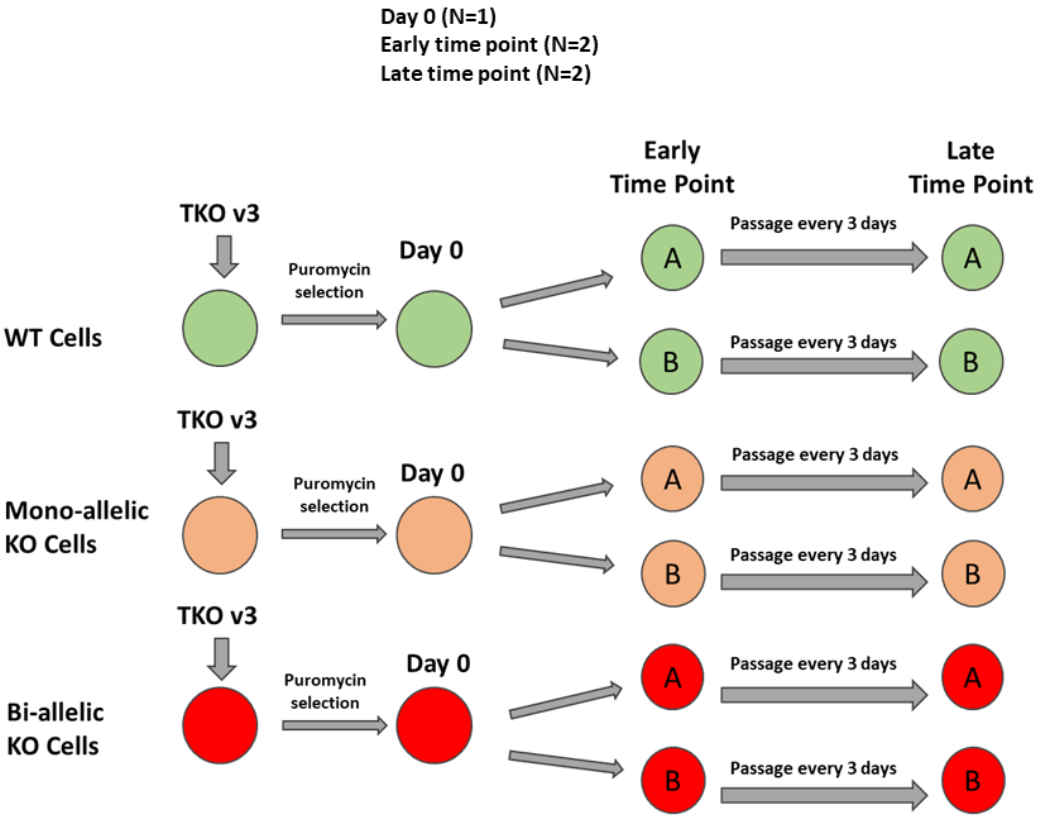


Figure 4.19 The experimental design of genome-scale CRISPR screening
MEC1 isogenic CLL cells with different RNASEH2B statuses were transduced with the TKOv3 sgRNA library. After 48 hours post-transduction, media was replaced with a puromycin containing media and this stage was considered (Day 0). Subsequently, samples were divided into two technical replicates per cell line (A and B), and cells were subcultured every three days. Samples were derived as follows: one sample at day 0, one sample at an early time point for replicate A, one sample at an early time point for replicate B, One sample at a later time point for replicate A, and one sample at the later time point for replicate B. This strategy was applied to all cell lines. Abbreviations: Bi-allelic KO (homozygous KO), Mono-allelic KO (heterozygous KO), WT (Wild type), Toronto KnockOut CRISPR Library-Version 3 (TKO v3). Replicates for the CRISPR screen day 0 (N=1), early time point (N=2), late time point (N=2).

Raw sequencing reads were aligned to Toronto KnockOut (TKO) CRISPR Library - Version 3 (Hart et al., 2017) using MAGeCK (Wang et al., 2019a). Raw sgRNA counts were subjected to copy-number variation (CNV) filtration because it is known that CNV may affect the results of the screen and generate false positive and false negative scores (Aguirre et al., 2016, Munoz et al., 2016). The MEC1 cell line CNV data were obtained from the Depmap project (Ghandi et al., 2019). All CRISPR screen libraries were subjected to quality control analysis in which I examined the average sequencing depth, the pairwise correlation between libraries, the correlation between replicates to check for consistency and the impact of CRISPR screening on core essential and non-essential genes.

The CRISPR screen libraries' sequencing depths were approximately 4–10 million reads per library, with a mapping percentage above 80% (Figure 4.20 A). Pairwise Pearson correlation was performed on log2 sgRNAs from all libraries and showed that Day 0 libraries clustered together, whereas early and later time point libraries clustered further away, indicating a reduced sgRNA redundancy (Figure 4.20 B). To further examine the agreement between library replicates, a scatter plot was generated for mono-KO Day 21 technical replicates and indicated a high correlation, in agreement with our Pearson pairwise correlation analysis (Figure 4.20 C). Finally, a density plot was generated to check the impact of the screening on core essential and non-essential genes (using JACKs scores on WT later time points), and I observed a minimal overlap indicating a non-marginal CRISPR screen (Figure 4.20 D). Overall, the CRISPR screen data demonstrated satisfactory QC results.

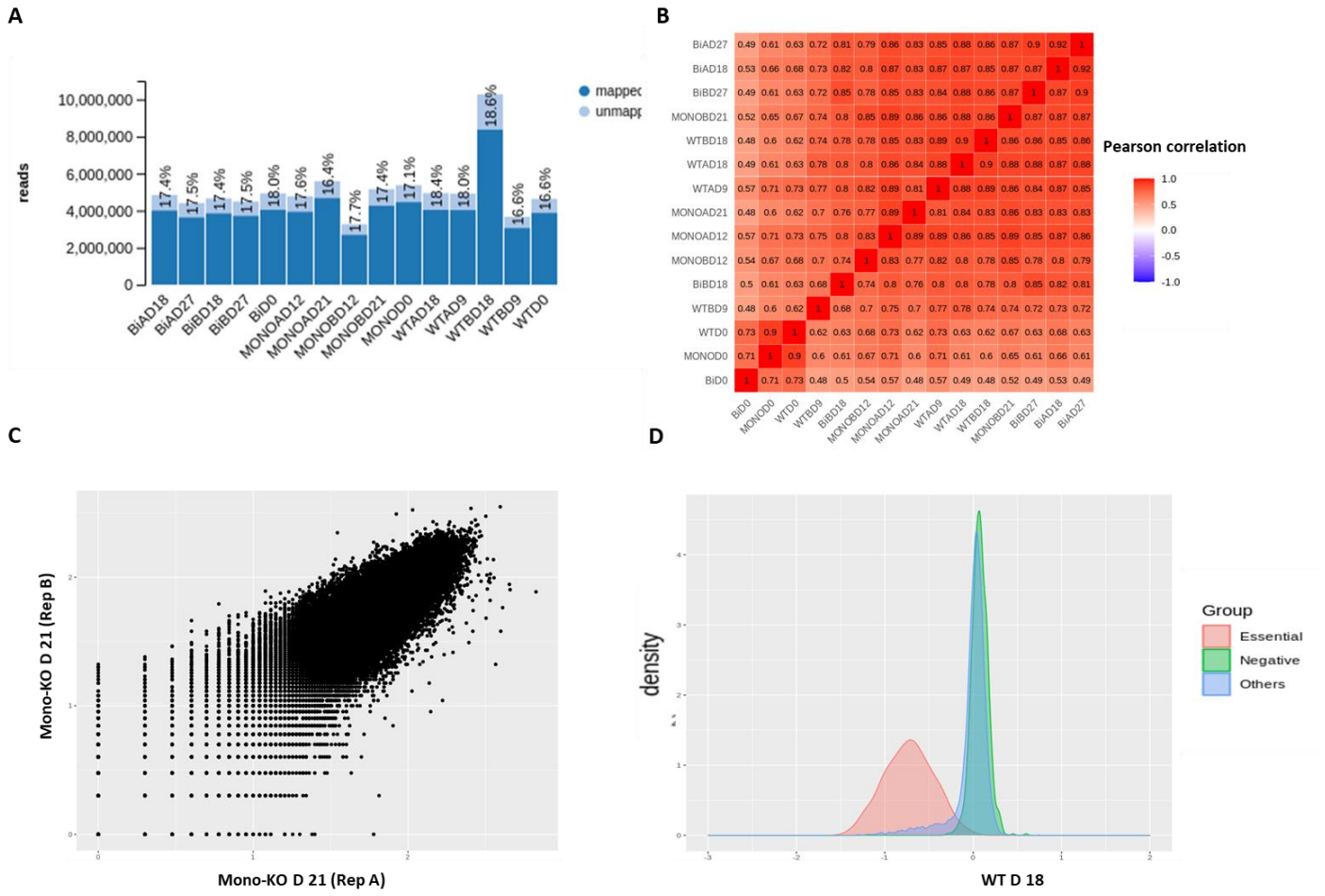


Figure 4.20 Quality control of CRISPR screen libraries
(A) Distribution of CRISPR library read depths. (B) Pearson correlation analysis on CRISPR screen libraries highlights that day 0 libraries clustered away from early and late time points. (C) Correlation between two selected replicates shows a high consistency. (D) Density plot showing the JACKS score for essential core genes and negative and other non-essential genes demonstrating a minimal overlap with essential core genes. Abbreviations: B-KO (biallelic KO), M-KO (monoallelic KO), WT (Wild type).

To analyse the CRISPR screen data, I integrated two known algorithms (BAGEL and JACKS) into my analysis to ensure obtaining high confidence set of CRISPR gene hits list and reduce false positives and false negatives hits. Each algorithm utilizes unique mathematical operations to return analysis scores. Bayesian analysis of gene essentiality (BAGEL) (Kim and Hart, 2021) calculates the log probability of a gene belonging to a 'non-essential' or 'essential' class and returns a log Bayes factor (BF), which is composed of biological effect size and a statistical significance. Joint analysis of CRISPR/Cas9 knockout screens

(JACKS) (Allen et al., 2019) is another Bayesian-based algorithm where the same gRNA library is jointly analysed across screens to allow for better modelling of gRNA efficiencies and enhancing inferences on treatment-specific effects. Together, applying two different algorithms for the CRISPR screen analysis helps identify a robust, high-confidence set of gene hits.

To establish a comparison between CRISPR screen libraries (KO and WT cells at matched time points), I created a linear regression model where I treated WT samples as the independent variable and KO samples as the dependent variable using each algorithm's final reported scores. I then set a stringent cut-off of three standard deviations of the regression line. The hits that passed this predefined cut-off were either classified as potential synthetic lethal hits or potential tumour suppressor hits. Finally, I created a consensus hits list by selecting only genes that passed predefined cut-off in all different algorithms at all time points. The CRISPR screen data analysis workflow is summarized in Figure 4.21.

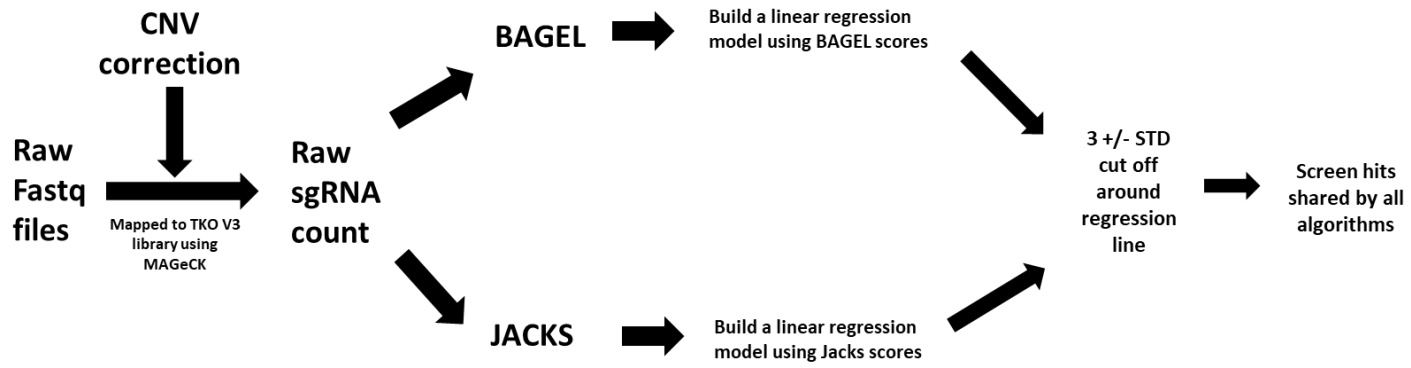


Figure 4.21. The applied workflow for analyzing CRISPR screening data
The workflow starts by mapping raw sequencing files to TKO v3 libraries using MAGeCK software. Next, the obtained sgRNA raw count matrix was filtered to remove genes associated with CNV alterations reported for the MEC1 cell line to remove potential artefacts that may influence the downstream analysis. Next, the raw sgRNA count matrix is loaded to BAGEL and JACKS algorithms using the default settings. Linear regression analysis is then performed for KO and WT samples at matched time points to classify hits as potential synthetic lethal or tumour suppressors if hits pass a preset 3 +/- standard deviation of the regression line. Finally, a hit list is derived and prepared for overlapping with a hit list obtained from the other algorithm's linear regression analysis.

I began the analysis by first evaluating CRISPR screen hits in KO cells against WT cells at early time points. I established the first comparison (monoallelic KO against WT) and generated linear regression plots for each algorithm used. Hits that passed our SD cut-off were overlapped with hits identified in the other method, and only shared hits among the two methods were kept. Similarly, I used the same approach in the second comparison (biallelic KO against WT at early time points) and created a list of common hits between the two methods. I applied the same approach in evaluating the CRISPR screen hits in KO cells against WT at later time points. Figure 4.22 depicts the linear regression models applied to all algorithm scores along with SD cut-off labels.

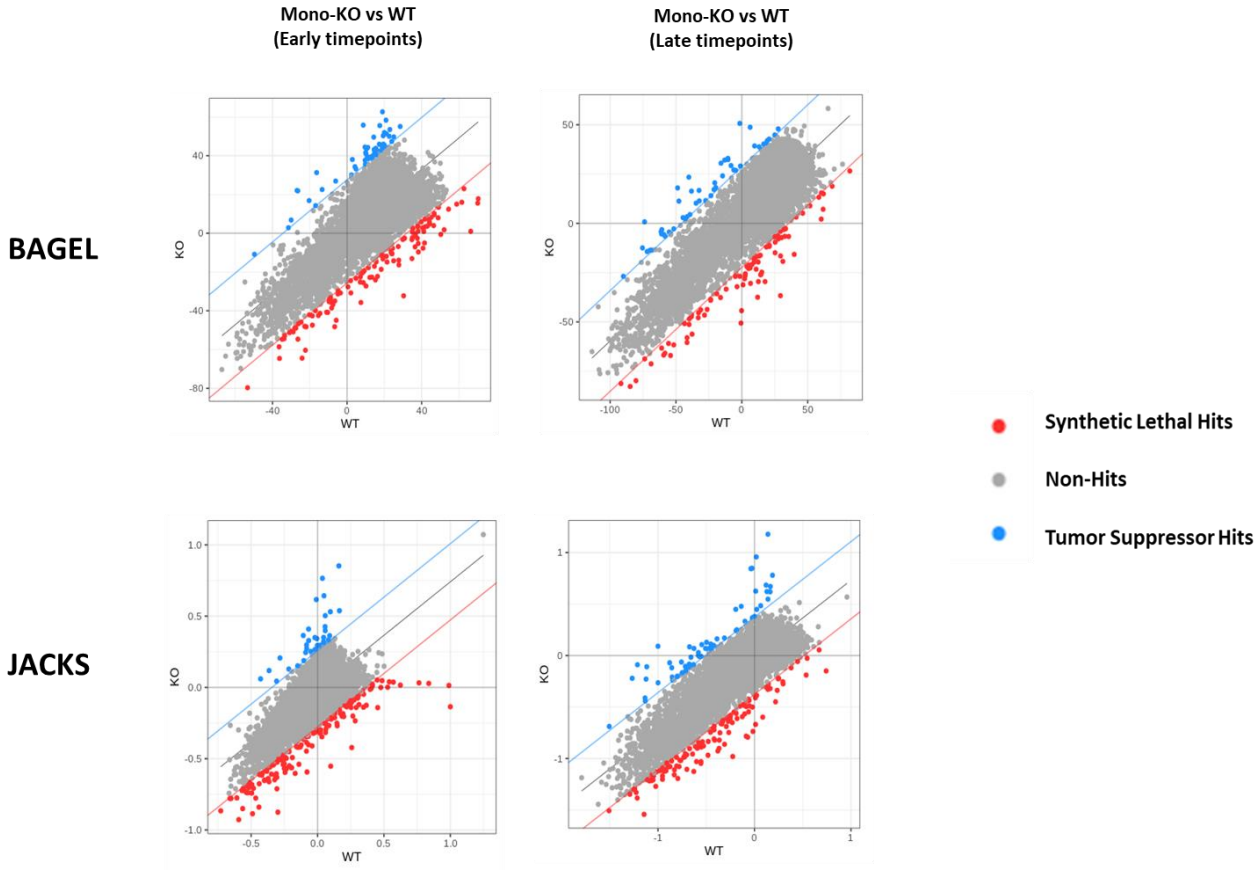


Figure 4.22 Examples of linear regression models for each time point comparison (Mono-KO vs WT cells)
In each linear regression model, WT was treated as the independent variable, whereas KO was treated as the dependent variable. A cut-off of three standard deviations was used to classify hits as potential synthetic lethal (red) or potential tumour suppressor (blue). Hits passed cut-off were then grouped for each time point and algorithm used in preparation for hist overlap analysis. Here are examples of the resulting linear regression models applied to RNASEH2B monoallelic loss vs WT cells. Abbreviations: B-KO (biallelic KO), M-KO (monoallelic KO), WT (Wild type).

I generated Venn diagrams, where the circle sizes correlate with the number of hits obtained from each method at each time point comparison, and the number of shared hits is highlighted (Figure 4.23). Next, the shared hits at each time point were overlapped, with a list of shared hits between the two methods at different time points being provided. The analysis showed that 109 gene hits (Early time point) and 99 gene hits (Late time point) were common between the two algorithms used and noted for RNASEH2B monoallelic KO CLL cells. Consequently, a final consensus hits list of 18 gene hits was correlated with RNASEH2B monoallelic loss CLL cells. On the other hand, 98 gene hits (Early time point) and 227 gene hits (Late time point) were common between the two algorithms and documented for RNASEH2B biallelic KO CLL cells. Accordingly, a final consensus hits list of 61 gene hits was correlated with RNASEH2B biallelic KO CLL cells. Taken together, I was able to identify CRISPR screen hits that may pose synthetic lethal interactions in correlation with RNASEH2B monoallelic and biallelic loss CLL cells using two different algorithms and two different time points.

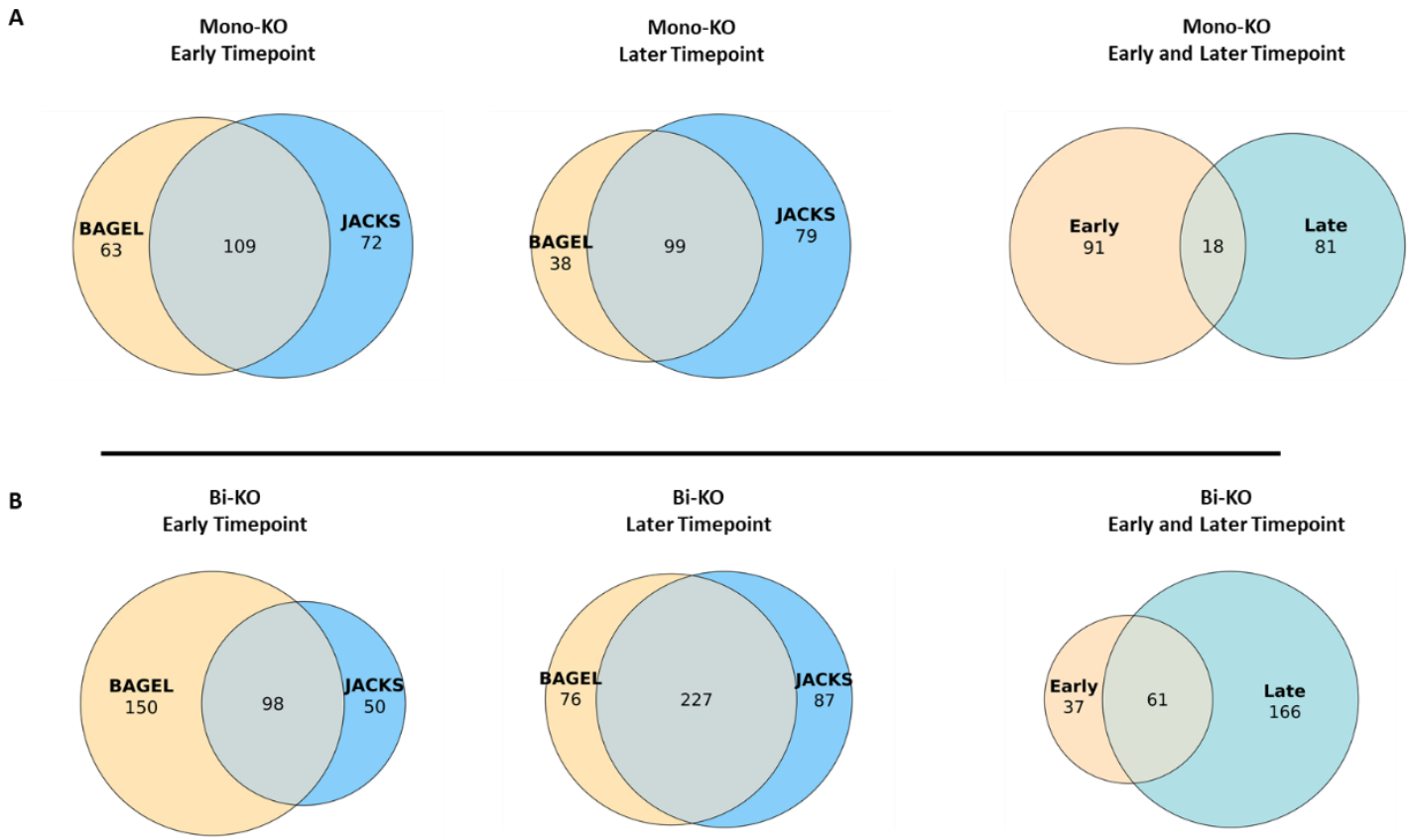


Figure 4.23 Overlap analysis of CRISPR screen hits resulting from two algorithms used (BAGEL and JACKS)
The analysis begins by overlapping hits resulting from BAGEL and JACKS algorithms at an early time point comparison. The common hits list was then overlapped with the common hits list derived from the two algorithms at a later time point to obtain a final consensus hits list that common among the algorithms and the two-time points at the given RNASEH2B condition. For each condition, hits shared between the two algorithms at both time points were considered in the final hit list. Abbreviations: B-KO (biallelic KO), M-KO (monoallelic KO), WT (Wild type).

4.7.1 CRISPR screen identified APEX2 as a synthetic lethal gene correlated with RNASEH2B biallelic KO cells

The final outcome of the two algorithms used to analyze the CRISPR screening data identified 18, and 61 gene hits in monoallelic and biallelic KO cells, respectively. The inactivation of these identified genes in correlation with monoallelic and biallelic RNASEH2B lass conditions in CLL cells had a profound effect on cell viability, indicating a dependency mechanism. Reassuringly, the final consensus hits list in biallelic KO cells contained an already established synthetic lethal interactor with the components of the RNase H2 complex the *APEX2* gene. *APEX2* encodes for the APE2 protein, which is related to the apurinic/apyrimidinic (AP) endonuclease APE1. APE2 possesses AP endonuclease activity that displays 3'phosphodiesterase and 3'-5'exonuclease reactions and participates in DNA damage and ATR activation (Wallace et al., 2017, Burkovics et al., 2009, Lin et al., 2018). Moreover, APE2 is involved in maintaining DNA integrity by preventing DNA lesions caused by genomic ribonucleotides and shows synthetic lethality with three genes coding for the RNase H2 complex (RNASEH2A, B and C) (Álvarez-Quilón et al., 2020). Therefore, in agreement with (Álvarez-Quilón et al., 2020), our CRISPR screen identified *APEX2* as synthetic lethal in biallelic KO RNASEH2B CLL cells. This finding is explained by the fact that cells need to reduce DNA damage caused by genomic ribonucleotides, and in the absence of RNASEH2B, the cells activate a secondary alternative repair pathway led by *APEX2*.

4.7.2 CRISPR screen identified a set of synthetic lethal genes involved in inflammatory response, RNA biology, and transcription coactivators that are correlated with RNASEH2B loss

The final consensus hits list correlated with monoallelic RNASEH2B KO cells included genes involved in interferon signalling regulation (*USP18*), ribosomal subunit protein (*RPL27A*) and transcriptional coactivators (*MED24* and *POU2AF1*). In correlation with biallelic RNASEH2B KO cells, consensus CRISPR hits list contained genes functioning in pre- (*RNF113A*) and post-mRNA splicing regulation of nonsense-mediated decay (*UPF2* and *SMG5*), G protein-coupled receptor signalling (*UTS2R, OR10H1* and *OR9Q2*)

and DNA damage repair (*CDCA5* and *APEX2*). The consensus hits lists correlated with monoallelic and biallelic RNASEH2B KO cells identified a number of other genes (appendix) that were found as potential synthetic lethal that may pose undiscovered dependency pathways in CLL with 13q deletions and pave the way for targeted therapy.

4.7.3 *RUNX3* is identified as a synthetic lethal gene in correlation with RNASEH2B KO cells

Both consensuses hit lists identified *RUNX3* as a potential synthetic lethal gene in correlation with monoallelic and biallelic RNASEH2B loss status (Figure 4.24 A). To further confirm this finding, I plotted the normalized sgRNAs counts for *RUNX3* and *APEX2* (as a positive control), and, indeed, I observed a reduction in RUNX3 sgRNA counts indicating a negative selection (Figure 4.24 B). I showed in the integration analysis of RNA-seq and ATAC-seq that the transcriptional landscape is cantered on the RUNX family of transcription factors. Therefore, our CRISPR screen data supported these findings suggesting a reliance of RNase H2 deficient cells on RUNX3 activity.

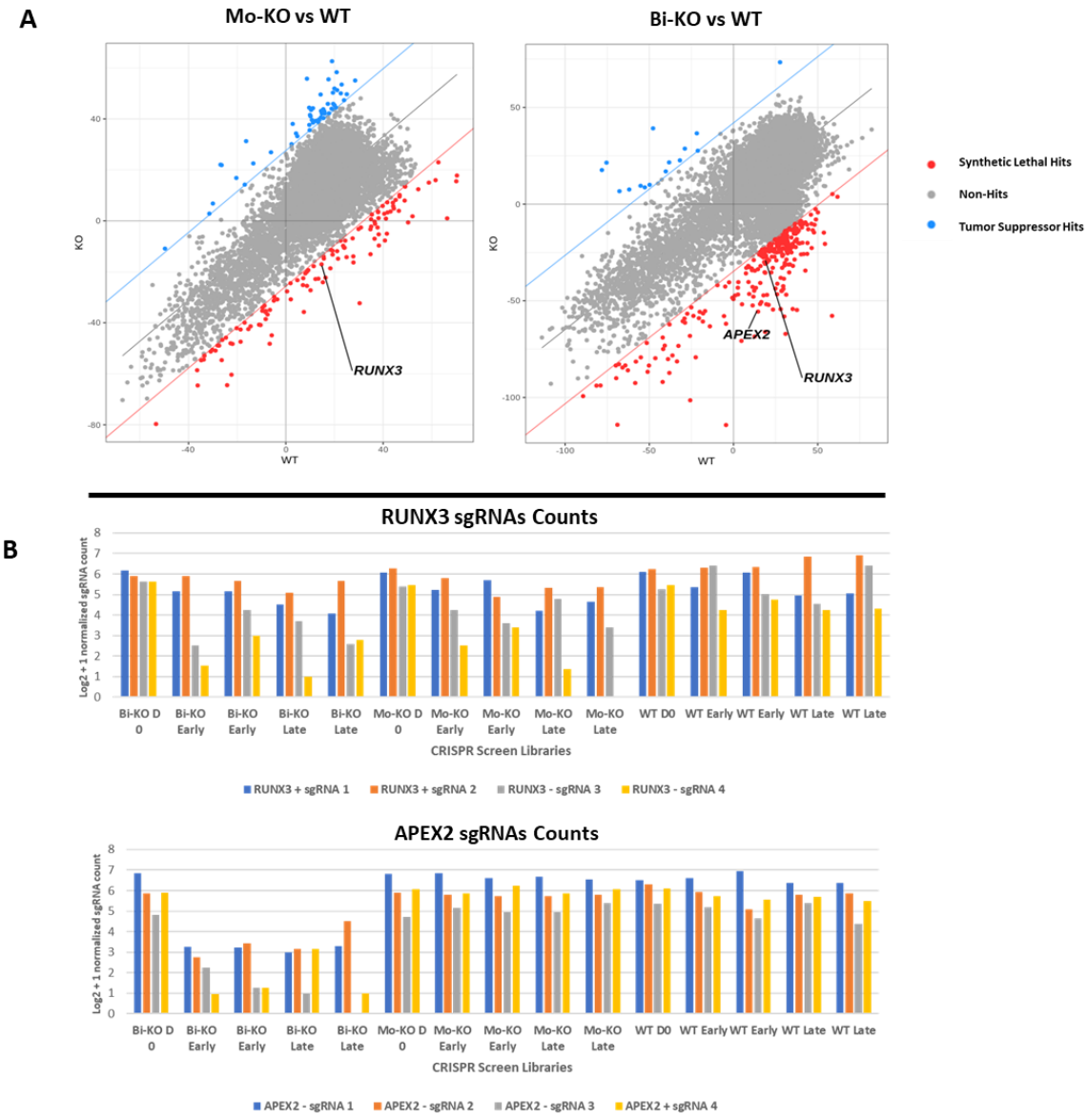


Figure 4.24 RUNX3 is classified as synthetic lethal in correlation with RNASEH2B monoallelic and biallelic loss in CLL cells

(A) The resulting linear regression plots of BAGEL scores in both RNASEH2B KO cells' comparisons classifying RUNX3 as a potential synthetic lethal interactor in correlation with RNASEH2B biallelic and monoallelic loss. The analysis also shows that *APEX2* is a synthetic lethal gene correlated with RNASEH2B biallelic loss in agreement with published research (B) Log2 transformed of normalized sgRNA counts targeting RUNX3 gene demonstrating a reduction in sgRNA count compared to WT, indicating a negative selection. APEX2 is used here as a positive control. Abbreviations: B-KO (biallelic KO), M-KO (monoallelic KO), WT (Wild type).

4.7.4 RUNX binding sites are associated with synthetic lethal gene hits in correlation with both RNASEH2B KO cells

Genome-wide data showed that the transcriptional landscape is cantered on the RUNX family of transcription factors and the CRISPR screen showed that RUNX3 is a synthetic lethal interactor in correlation with RNASEH2B KO cells. Therefore, I asked whether if RUNX family of transcription factors are involved in driving the expression of genes identified as synthetic lethal. To address this question, I annotated RUNX canonical motif (derived from (Assi et al., 2019)) to the nearest gene and then genes with RUNX binding sites were intersected with my CRISPR hits list. This analysis showed that nine genes out of 18 genes hits in the monoallelic KO CRISPR hit list were correlated with RUNX binding sites, whereas 11 genes out of 61 genes in the biallelic KO CRISPR hit list were correlated with RUNX binding sites.

Overall, genes identified as synthetic lethal show variable upregulation of expression in correlation with monoallelic and biallelic KO cells (Figure 4.25). Among the highest upregulated genes are *USP18* and *ERICH2* in monoallelic and biallelic KO cells, respectively. Taken together, the results suggest a potential mechanism in which RUNX transcription factors (RUNX3 in particular) are responsible not only for driving the transcription factor regulatory networks but also for driving the expression of other genes that are essential to maintain cell survival in correlation with monoallelic and biallelic RNASEH2B loss.

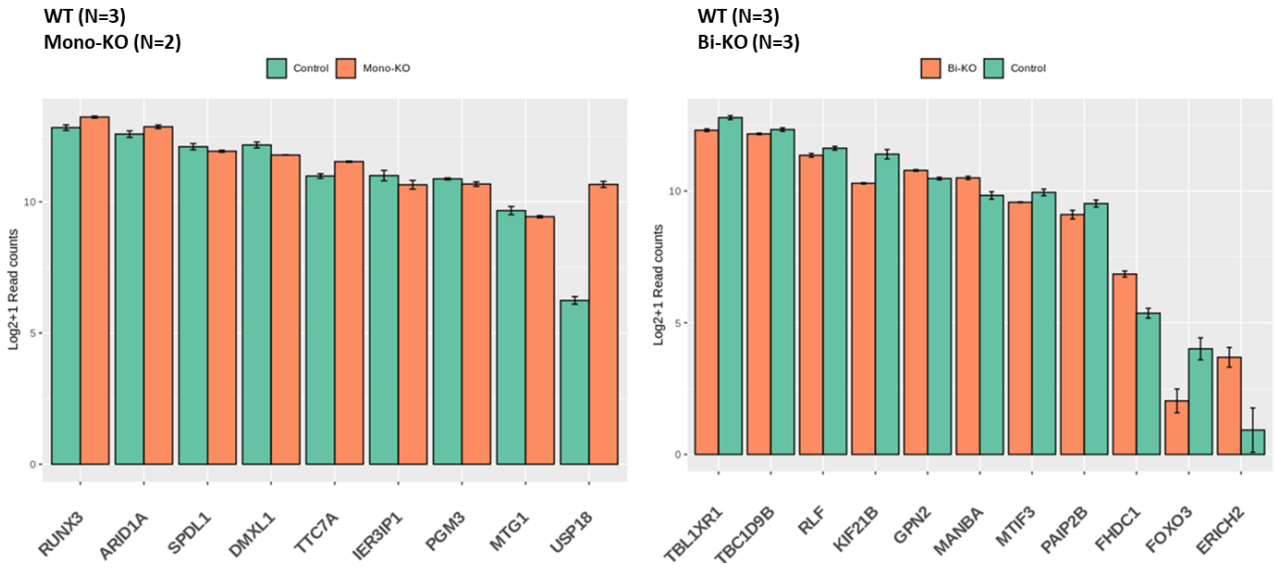


Figure 4.25 The expression profile of genes identified as synthetic lethal and correlated with the presence of RUNX motifs

RUNX motifs were annotated to the nearest gene, and the resulting gene list was overlapped with the CRISPR screen final consensus hits list for each condition. The normalised log2+1 read counts derived from Ranse data were extracted for genes correlated with RUNX motifs and were shared in the CRISPR screen hits. The normalised log2+1 read counts were plotted as bar plots for genes identified in Mono-KO cells (Left) and Bi-KO (Right). Abbreviations: B-KO (biallelic KO), M-KO (monoallelic KO), WT (Wild type).

4.8 Discussion

In this project, I profiled the epigenomic landscape correlated with RNASEH2B-defective CLL cells using gene expression, chromatin immunoprecipitation assays and chromatin accessibility profiles and applied CRISPR screen to validate potential cellular dependencies identified in multi-omics data. Starting with the transcriptomic profile, I observed that monoallelic and biallelic KO cells were correlated with the up-regulation of pro-inflammatory genes involved in pathways such as IFN α, IFN γ and NF-κB in addition to p53 signalling pathways. I next observed in the DRIP data an increase of DNA–RNA hybrid (R-loop) formation, as expected, which would result from a lack of an efficient mechanism to process R-loops in correlation with RNASEH2B KO cells. I also examined histone modification profiles for H3K4me3 and H3K27ac and the histone variant H2A.Z and observed genome-wide deregulation of these mentioned histone marks and variant. I subsequently characterised the chromatin accessibility landscape correlated with RNASEH2B monoallelic and biallelic loss in CLL cells and observed that gained accessible sites were enriched with motifs associated with RUNX, AP-1 and IRF transcription factors. Motif co-localization analysis showed that the transcriptional landscape correlated with RNASEH2B KO cells is mainly centred on RUNX and AP-1. Transcription factor network analysis supported that both RUNX and AP-1 as major TFs responsible for maintaining the gene expression of TF genes in correlation with RNASEH2B KO cells. Finally, CRISPR screening identified RUNX3 as a potential synthetic lethal gene in correlation with RNASEH2B monoallelic and biallelic loss in CLL cells, thereby further supporting my integration analysis, where I showed that the transcriptional landscape is mainly centred on RUNX.

The differential gene expression analysis demonstrated that RNASH2B KO cells were correlated with molecular signatures associated with the inflammatory response and p53 signalling. It is worth noting that the MEC1 CLL cell line carries a mutation in the p53 gene, producing a truncated version of the protein that is 47 kDa in size compared to the WT (53 kDa) (Kwok et al., 2016). Therefore, the MEC1 cell line may

develop an adaptation mechanism to compensate for the p53 mutation. However, cellular stresses, such as DNA damage, could allow the mutant p53 in MEC1 cells to alter the gene expression of its downstream genes because the mutant p53 is known to impact gene expression (Xu and El-Gewely, 2003). The marked inflammatory signature correlated with RNASEH2B KO cells could be a consequence of R-loop build-up, which is known to trigger inflammatory cascade signalling (Weinreb et al., 2021). Moreover, the loss of efficient mechanisms to process R-loops leads to R-loop-dependent DNA damage and eventually causes genomic instabilities and activates the immune response (Gasser et al., 2017).

Interestingly, CRISPR screen data identified *USP18* as a synthetic lethal gene in correlation with monoallelic RNASEH2B KO cells which happen to have RUNX binding sites. USP18 is an enzyme that belongs to ubiquitin-specific proteases (UBP) and is involved in the negative regulation of the inflammatory response (Arimoto et al., 2017, Meuwissen et al., 2016). is *USP18* gene is upregulated and marked with increased levels of chromatin accessibility and histone modifications H3K4me3 and H3K27ac (Figure 4.26)

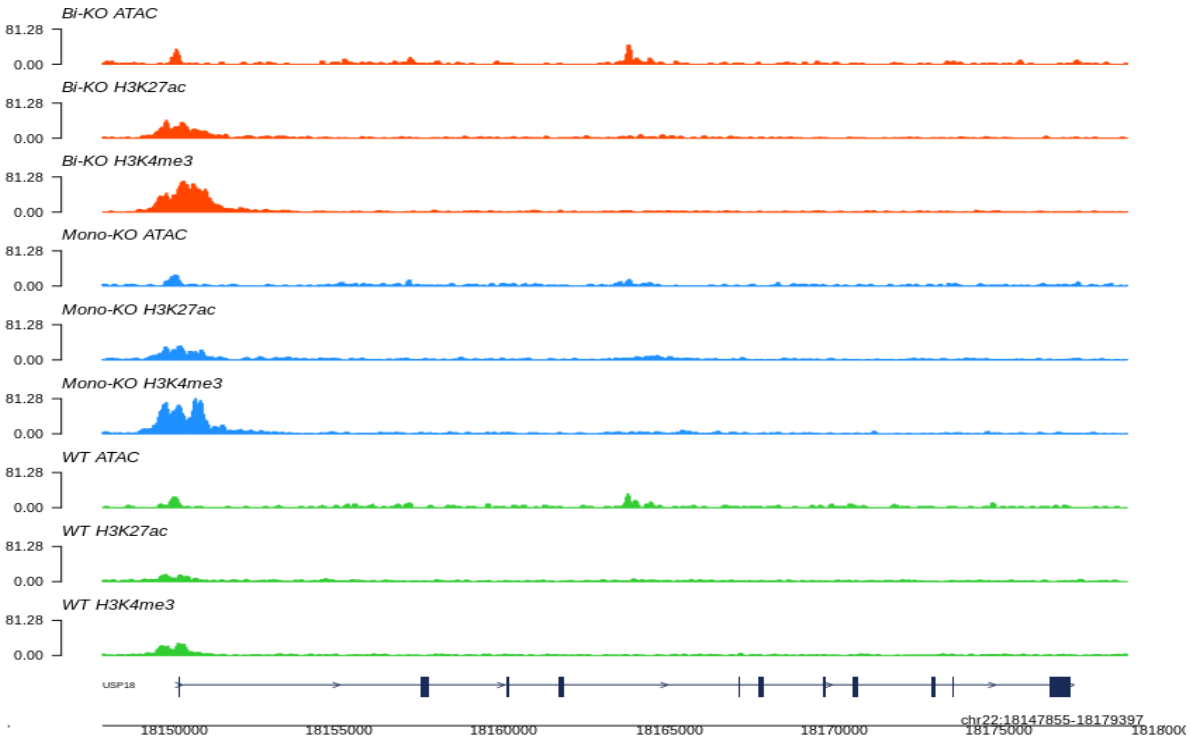


Figure 4.26 USP18 locus shows enrichment for H3K4me3 and H3K27ac in correlation with RNASEH2B KO cells Histone PTMs signals show a marked increase in correlation with monoallelic and biallelic RNASEH2B loss status in comparison with RNASEH2B WT cells. Biallelic tracks are coloured red, monoallelic tracks are coloured blue, and WT tracks are green. Abbreviations: B-KO (biallelic KO), M-KO (monoallelic KO), WT (Wild type).

I observed a marked increase in DNA–RNA hybrids (R-loops) correlated with RNASEH2B loss in both monoallelic and biallelic KO cells, as expected. However, I noted a higher R-loop signal in correlation with monoallelic KO cells compared to biallelic KO cells, which was unexpected. Thus, it appears that monoallelic KO cells do not develop a compensatory mechanism to deal with R-loops whereas biallelic cells, with a complete absence of RNASEH2B may have developed an adaptation mechanism to cope with DNA–RNA formation by opening alternative evolutionary routes (Helsen et al., 2020). The R-loop annotation analysis revealed that the majority of DNA–RNA hybrid signals were found within intronic regions (Figure 4.10 B), consistent with other studies (Okamoto et al., 2018; Powell et al., 2013; Bonnet et al. 2017; El Hage et al., 2014). This finding suggests that R-loops are generally formed on unmatured mRNA before splicing factors' processing engagement, and this is consistent with our CRISPR screen data showing that the pre-mRNA splicing factor (*RNF113A*) is synthetic lethal in correlation with RNASEH2B biallelic KO cells. Thus, my findings suggest that mRNA splicing machinery may have a role in R-loops clearance and therefore maintaining genome integrity.

The histone modifications ChIP data showed a significant increase of H3K4me3 mark levels in correlation with monoallelic and biallelic KO cells (Figure 4.12 A and B). Moreover, in contrast to the WT control cells, the H3K4me3 mark extended beyond the promoter regions toward the gene bodies, possibly in response to ongoing transcription–replication stress. Several groups have reported that H3K4 methylation is required to prevent genomic instability (Higgs et al., 2018). In fact, together with Rad53, an S-phase checkpoint kinase, H3K4me3, is needed to avoid collisions between transcription and replication machinery, thereby maintaining genome integrity (Chong et al., 2020). Moreover, reduced H3K4me3 levels by inhibiting *ASH2L*, a member of the SETD1A/B enzyme complex, result in low U2 snRNP

association with chromatin and consequently decreased pre-mRNA splicing machinery efficiency (Sims et al., 2007), highlighting a role of the H3K4me3 epigenetic mark in efficient mRNA splicing. Altogether, the marked increase in H3K4me3 in correlation with RNASEH2B monoallelic and biallelic KO cells may contribute to efficient splicing machinery recruitment as well as maintain genome integrity by mitigating transcription–replication conflict.

I observed an increased level of H3K27ac in correlation with RNASEH2B monoallelic and biallelic KO cells at gene bodies and a reduced level at the promoters (Figure 4.12 A). The H3K27ac was significantly enriched at the promoter regions that are correlated with WT control cells. In contrast, monoallelic and biallelic KO cells were correlated with a decreased H3K27ac level at promoters and an increase in the gene bodies as well as distal regions. It is known that H3K27ac undergoes genome-wide reprogramming (Schick et al., 2015) or genome-wide hyperacetylation (Yu et al., 2005) following induction of DNA damage, allowing for efficient repair of DNA damage. Moreover, acetylation of the histone H3 tail is involved in regulating the initial steps of base excision repair, where uracil excision by UDG and APE1 is dependent on histone tail acetylation (Banerjee et al., 2019). This is consistent with the results of our CRISPR screening, revealing the dependency of RNASEH2B KO cells on the BER repair pathway. Taken together, my data highlight a marked increase in the H3K27ac epigenetic mark and are consistent with previous research demonstrating this histone mark to be involved in the BER pathway. Therefore, BER might be one of the compensatory DDR pathways that operate in correlation with the absence of functional RNase H2.

The Pol II genomic feature annotations correlated with no major differences in RNA POL II occupancy between monoallelic, biallelic KO and WT control cells (Figure 4.12 A), suggesting transcription is not affected. The histone variant H2A.Z is known to be located at gene promoters (Creyghton et al., 2008, Schones et al., 2008, Barski et al., 2007) and other regulatory elements, including enhancers and insulators (Johnson et al., 2018, Jin et al., 2009). The histone variant H2A.Z genomic feature annotation in our data

revealed a decrease in the promoter regions in correlation with RNASEH2B monoallelic and biallelic KO cells in comparison to WT controls. The analysis also showed an increase in H2A.Z occupancy in distal intergenic regions (Figure 4.12 A). I observed a positive correlation between H3K4me and H2A.Z occupancy, in agreement with published research (Ku et al., 2012, Kim et al., 2013). In addition, I noticed that the level of both H3K4me3 and H2A.Z extend beyond the TSS region toward the gene body. The spread of H2A.Z over the gene body is linked with the global inhibition of transcription in heterochromatic regions (Xu et al., 2018, Hardy et al., 2009, Lashgari et al., 2017). In addition, the histone variant H2A.Z is required for efficient DNA repair by allowing chromatin relaxation, which, in turn, facilitates the recruitment of histone modification enzymes and DNA repair proteins (Xu et al., 2012, Adam et al., 2001). Therefore, results are consistent with inhibition of transcription in the light of engagement of compensatory DDR pathways in correlation with the absence of functional RNase H2.

I showed that RNASEH2B KO specific gained sites were correlated with the enrichment of motifs associated with RUNX, AP-1 and IRF and that RNASEH2B KO cells were correlated with a transcriptional landscape centred on RUNX and AP-1. Consistent with this finding, CRISPR analysis identified RUNX3 as a synthetic lethal interactor in correlation with RNASEH2B KO cells. RUNX3 belongs to the RUNX family of transcription factors responsible for many cellular and developmental processes, such as cell lineage commitment, cell proliferation and differentiation. RUNX proteins share the Runt homology domain (RHD), located near the N terminal end (Rennert et al., 2003). The RHD domain is required for DNA binding (Wang and Speck, 1992), interactions with other proteins (Lilly et al., 2016) and RUNX factor nuclear localization (Michaud et al., 2002). The RUNX protein's C terminal includes an activation and inhibitory domains named (AD and ID) respectively, and a five amino acid C-terminal motif (VWRPY) (Levanon and Groner, 2004).

RUNX family members act as transcriptional activators and repressors by forming a heterodimer with the core-binding factor beta (CBF-β) subunit. RUNX3 together with RUNX1 and RUNX2 are highly conserved

transcription factors that are involved in the regulation of lineage-specific genes, cell identities and functions during developmental stages. Moreover, all 3 factors were reported to have essential roles in haematopoiesis (Lotem et al., 2015, Blyth et al., 2010). Hematopoietic maturation toward B lymphopoiesis is mainly governed by the action of specific transcription factors such as PAX5, EBF1, IKZF1, E2A, and RUNX1 (Tijchon et al., 2013). These B-lineage transcription factors are frequently altered in haematological malignancies. Activation of RUNX1, but not RUNX3, was reported to be indispensable in early B cell development (Seo et al., 2012), suggesting that RUNX3 may not be a key player in early B cell development but rather a key player in later development stages and other cellular processes. The development of immune-related inflammatory disorders was associated with alterations in RUNX3 SNPs, which might contribute to RUNX3 activity in leukocytes (Levanon et al., 2014, Fainaru et al., 2004, Dicken et al., 2013), suggesting that RUNX3 may contribute to the regulation of autoimmunity and inflammation. This observation may give an explanation on why I see upregulation of pro-inflammatory genes in RNA-seq data.

In order for CLL cells with RNASEH2B loss to maintain a proliferative state, cells must maximize the usage of other DDR pathways to cope with spontaneous DNA lesions caused by rNMP misincorporation and R-loops formation. It is known that RUNX3 promote p53 dependent DDR (Samarakkody et al., 2020), and in the context of RNase H2 loss, this would cause cells to undergo apoptosis. However, MEC1 cells have a mutant p53 protein; therefore the effect of RUNX p53-dependent DDR regulation would be potentially insignificant. RUNX could be involved in positive regulation of DDR independent of p53 for RNase H2 defective cells survival as RUNX post-translational modifications through PARP-dependent poly(ADP-ribosyl)ation promotes Fanconi Anemia (FA) pathway of DNA repair (Tay et al., 2018). Thus, RUNX loss may potentially exacerbate DNA damage accumulation which leads to genomic instability and cell death.

Published research over the past decade has elucidated the roles of RUNX proteins in response to cellular stress and DNA damage. In addition, RUNX proteins are involved in the positive and negative regulation of DDR pathways (Samarakkody et al., 2020, Ozaki et al., 2013). Cells with defective RUNX1 and RUNX3 proteins show malfunctions in DNA repair, including interstrand crosslinking, homologous recombination and base excision repair (Bellissimo and Speck, 2017). Moreover, RUNX3 knockout (KO) mice models demonstrate bone marrow failure and myeloproliferative disorders, manifestations that are commonly seen in Fanconi anaemia (FA) patients (Wang et al., 2014).

In the previous study, researchers found that FANCI/FANCD2 chromatin involvement and foci formation in the occurrence of ICL was significantly defective when the RUNX3 protein was lost. FANCI/FANCD2 are important players in ICL repair by allowing the efficient recruitment of homologous recombination (HR) machinery through the unhooking of ICL lesions in collaboration with SLX4 and XPF-ERCC nucleases (Zhang et al., 2015a, Klein Douwel et al., 2014). FANCD2 maintains genomic integrity by opposing R-loop formation and accumulation (Aguilera and García-Muse, 2012). In addition, chromatin immunoprecipitation of FANCD2 binding sites was mainly associated with common fragile and active transcription regions (Okamoto et al., 2018), highlighting potential RUNX–FANCD2 cooperation. In conclusion, RUNX proteins could potentially be involved in the positive regulation of DDR pathways to resolve R-loop formation, rNMP misincorporation and deal with DNA lesions caused by these genomic instabilities.

Indeed, a growing body of evidence has demonstrated the functions of RUNX proteins in the DNA damage response. Upon DNA damage induction, RUNX proteins undergo PAPR-dependent PARylation, which enables their interaction with BLM to regulate FANCD2 recruitment at DNA lesions (Tay et al., 2018). Moreover, it was reported that cells lacking RUNX1 and RUNX3 proteins showed defects in homologous recombination, interstrand crosslinking and BER (Bellissimo and Speck, 2017).

CRISPR screening data showed that biallelic RNASEH2B KO cells were correlated with a dependency on the BER pathway, in which the cells required APEX2 to repair DNA lesions. This dependency was accompanied by an increased level of H3K27ac, which is required to initiate the BER pathway. Furthermore, APEX2 is a downstream target gene for RUNX (Rouillard et al., 2016). The observation that RUNX is also a potential synthetic lethal gene correlated with monoallelic KO cells raises a possibility of its involvement in maintaining cellular survival, possibly by regulating DNA damage response proteins, as seen in CRISPR data (Bi-KO) and other groups (Wang et al., 2014, Cai et al., 2015, Bellissimo and Speck, 2017). A further connection between RUNX and RNase H2 complex is highlighted by previous finding suggesting that RUNX proteins regulate RNASEH2B gene expression in myeloid precursor cells (Nafria et al., 2020).

The overlap between RUNX binding sites near genes identified as synthetic lethal in correlation with RNASEH2B KO cells suggests a role for RUNX in regulating the expression of essential genes other than TFs. Thus, the presence of RUNX binding sites at genes identified to be crucial for survival implies a potential mechanism where RUNX drive the expression of these genes to maintain cell survival in addition to its role in the transcription factor regulatory network. Taken together, my data suggest a pivotal role for RUNX proteins not only in driving the transcriptional landscape but also in maintaining genome integrity in correlation with monoallelic and biallelic RNASEH2B loss.

The RUNX proteins could be involved in the positive regulation of DDR pathways to resolve R-loop formation and rNMP misincorporation. Therefore, the identification of RUNX3 link with DNA damage from this study is a further confirmation that RUNX3 is indeed a player in DNA damage response (Samarakkody et al., 2020). Consequently, RUNX3 loss would be expected to exacerbate DNA damage accumulation significantly. This observation adds an additional layer of differentiation between RUNX proteins where a

member of RUNX proteins could substitute another member in regulating the transcriptional landscape but not in response to DDR. Taken together, results obtained from independent lines of investigations suggest that the inactivation of one RNASEH2B allele is sufficient to produce a similar phenotype to that observed in biallelic loss of the RNASEH2B gene. Therefore, CLL patients with monoallelic and biallelic 13q deletions could potentially benefit from treatment targeting RUNX proteins.

Based on my findings, I propose a model (Figure 4.27) where, in RNASEH2B KO cells, RUNX proteins have two roles: (A) RUNX1, and RUNX2 maintain the transcriptional landscape together with AP-1 for cell survival, and (B) RUNX3 is involved in the efficient recruitment of compensatory and alternative DNA damage members and the modulation of the immune response. The outcome of RUNX protein activity is to maintain efficient DNA repair (RUNX3) and transcriptional program (RUNX1 and 2) required for the survival of RNASEH2B KO cells.

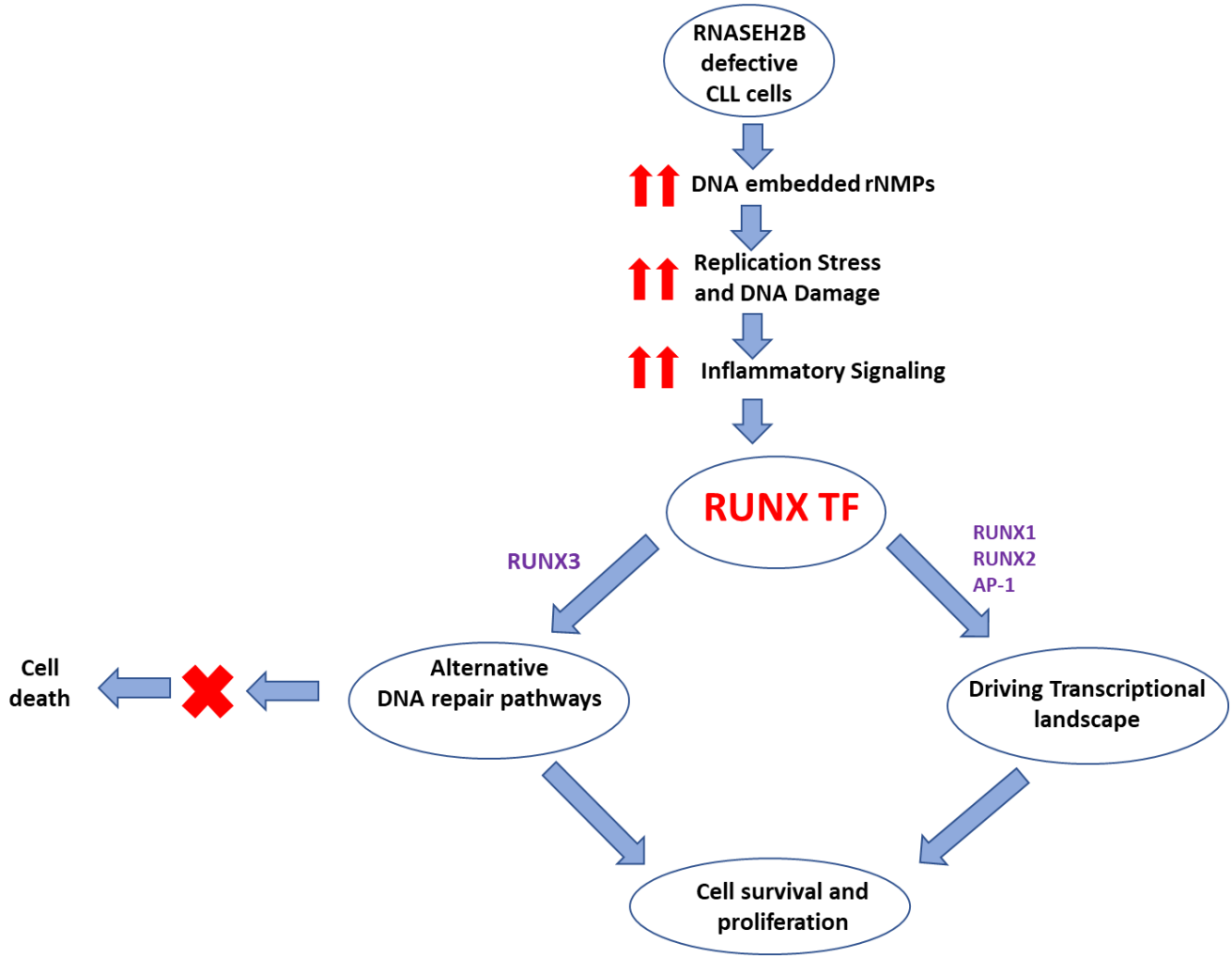


Figure 4.27 A provisional model for the role of RUNX3 in RNASEH2B defective CLL cells
The monoallelic and biallelic loss of RNASEH2B is correlated with elevated DNA embedded rNMPs and R-loops, which then contribute to replication stress and DNA damage. Thus, defective resolution of DNA embedded rNMPs and R-loops is correlated with an activation of the innate immune response, which in turn increases the levels of inflammatory signalling. RUNX TFs (RUNX1 and RUNX2) could be involved in maintaining the transcriptional landscape together with AP-1 whereas RUNX3 could be involved in efficient DDR and immune modulation. Thus, the outcome of cell survival and proliferation and immune evasion. Inactivation of RUNX3 is correlated with cell death which demonstrates that RNSEH2B defective CLL cells are correlated with reliance on RUNX3 activity.

CHAPTER 5

Overall Discussion

Chapter 5: Overall Discussion and Conclusions

The objectives of my thesis were to characterise the epigenetic landscape of CLL cells with frequently altered DDR genes *ATM* and *RNASEH2B* (heterozygous and homozygous loss), identify common epigenetic signatures and transcriptional dependencies correlated with those altered genes, and functionally validate the identified potential dependencies. These objectives were addressed through the use of well-known CLL isogeneic cell lines (CII and MEC1 in the ATM project) and (MEC1 monoallelic and biallelic KO in the RNASEH2B project). I have examined the chromatin landscape, including chromatin accessibility, histone modifications and variants, gene expression, and R-loop formation via genome-wide methodologies and obtained data that were subjected to a comprehensive bioinformatic analysis. A genome-wide CRISPR screen supported identified potential dependencies. My two major findings are that: a) ATM-deficient cells were correlated with an upregulation of the Histone demethylase KDM5B and b) CLL cells with monoallelic and biallelic RNASEH2B loss show synthetic lethal interaction with RUNX3

5.1 ATM defective CLL cells are correlated with KDM5B upregulation and deregulated gene expression related pro-inflammatory pathways

Although extensive research have been carried out to characterise the epigenetic landscape of CLL in primary samples (Xanthopoulos and Kostareli, 2019), specific transcriptional and epigenomic changes associated with *ATM* loss are still poorly examined.

In chapter 3 of my thesis, I have examined CLL cells with *ATM* inactivation using genome-wide methodologies. Starting with the transcriptomic level, I observed that *ATM* defective cells have transcriptomic profiles correlated with inflammatory response and showed enrichment for IFN γ molecular signature. In addition, common genes deregulated in ATM defective CLL cells irrespective of

genetic background and TP53 status were correlated with pathways such as interferon-gamma production, cytokine production, and positive regulation of lymphocyte activation. I then characterised the genome-wide histone modifications H3K4me3, H3K4me1, and H3K27ac. I found a global down-regulation of H3K4me3 and H3K4me1 levels in correlation with ATM loss status. Interestingly, I noted the upregulation of KDM5B at both mRNA and protein levels in correlation with ATM defective CLLs. I then carried a genome-wide mapping of KDM5B localizations and observed its peaks were correlated with promoter cis-regulatory elements. I also noted that KDM5B peaks sites were enriched in motifs associated with RUNX, AP-1, ETS, and NFkB TFs. Chromatin accessibility analysis supported the significant presence of the above-aforementioned motifs in correlation with ATM defective CLLs and showed that the transcriptional landscape program is associated with those TFs.

The correlation between KDM5B Chip and chromatin accessibility data suggested a link between KDM5B and AP-1. Indeed I found that KDM5B peaks were correlated with genes involved in MAPK signalling, and this was associated with gene expression upregulation (Figure 3.15). MAPK pathway is required to control AP-1 activity, and MAPK activation is seen in the immune-compromised tumour microenvironment (Liu et al., 2013a). It was reported that histone demethylases are involved in the regulation of tumour immunity (Qin et al., 2019). Furthermore, a recent study showed that KDM5B is involved in immune system evasion (Zhang et al., 2021). Therefore, the observed KDM5B upregulation and the deregulation in pro-inflammatory genes in correlation with ATM-deficient cells is in agreement with published research.

Taken together, my comprehensive analysis identified a potential dependency specific for ATM defective CLL cells. My results reveal a novel dependency correlated with ATM defective CLLs opening new insights for the development of novel epigenetic-based treatments targeting KDM5B to overcome conventional therapeutic treatment resistance and potentially enhance tumour immunogenicity.

5.2 RNASEH2B deficient CLL cells were correlated with a reliance on the transcription factor RUNX3

Deletions on chromosome 13q14 are common events in CLL patients, with an observed ratio of over 50% of cases (Zimmermann et al., 2018). *RNASEH2B* gene is located in this recurrently altered region which is considered an early event in CLL pathogenesis. *RNASEH2B* loss associated impact on chromatin landscape remains poorly understood in the context of CLL as the majority of CLL research reported 13q14 deletions without specifying the RNASEH2B mutation status.

In chapter 4, I profiled the chromatin landscape of *RNASEH2B* (monoallelic and biallelic) KO CLL cells using gene expression, chromatin immunoprecipitation assays and chromatin accessibility methodologies. Starting with the transcriptomic profile, I observed that heterozygous and homozygous KO cells that shared differentially expressed genes were correlated with the up-regulation of pro-inflammatory genes involved in pathways such as inflammatory signalling pathways (regulation of inflammatory response and regulation of interferon-gamma production), in addition to T cell activation, positive regulation of NIK/NF-kappa B signalling, and Notch signalling pathway. This deregulated inflammatory response is consistent with the observed hyperactive innate immune response seen in patients with Aicardi–Goutières syndrome. Next, I observed that RNASEH2B loss was correlated with an increase in DNA–RNA hybrid (R-loop) formation according to DRIP-seq data. Then, I also examined histone post-translational modification profiles for H3K4me3 and H3K27ac marks and the histone variant H2A.Z occupancy and observed global deregulation of these mentioned histone marks and variant in correlation with RNASEH2B loss. I next characterised the chromatin accessibility landscape of *RNASEH2B* monoallelic and biallelic KO cells and observed that gained accessible sites were enriched with motifs associated with RUNX, AP-1 and IRF transcription factors. Finally, using the CRISPR screen approach, I identified genes with synthetic lethal interactions with *RNASEH2B* and identified RUNX3 was identified as a synthetic lethal gene in *RNASEH2B* defective CLL cells. Interestingly, I found RUNX binding sites to overlap with genes identified as synthetic

lethal hits, which may provide a mechanistic link in which RUNX TF drives the expression of these essential genes to maintain cell survival.

Collectively, my comprehensive bioinformatic analysis showed that transcriptional rewiring in correlation with RNASEH2B defective CLL cells was mainly centred on the RUNX family of transcription factors. This finding was confirmed in our CRISPR screen as RNASEH2B KO cells were correlated with a reliance on RUNX3. Therefore, CLL patients carrying 13q14 deletion affecting RNASEH2B could potentially benefit from treatments targeting RUNX3 TF. Therefore, RUNX3 represent a novel therapeutic target in CLL cells harbouring RNASEH2B mutations.

To my knowledge, I have performed several independent approaches to genome-wide characterisation of the epigenetic landscape changes in correlation with alterations of specific DDR genes (*ATM* and *RNASEH2B*) that are novel not just in the context of CLL but indeed in any cancer. I have hypothesized from various lines of independent investigations that KDM5B and RUNX3 may represent potential dependencies that can be targeted therapeutically in *ATM* and *RNASEH2B* defective CLLs, respectively. I acknowledge that my analyses are not conclusive and that further studies are required to consolidate my findings. This is of potential importance to several malignancies in which roles for KDM5B and RUNX3 have appeared. KDM5B is linked with oncogenic potentials in several tumours, and it was associated with treatment resistance in breast cancer (Yamamoto et al., 2014), lung cancer (Lu et al., 2018), melanoma (Roesch et al., 2013), and gastric cancer (Xu et al., 2018). On the other hand, RUNX3 is also over expressed in several cancers, and its expression is linked to cell proliferation and viability in human epithelial ovarian cancer (Nevadunsky et al., 2009), head and neck cancer (Tsunematsu et al., 2009), and linked to treatment resistance in epithelial ovarian cancer (Barghout et al., 2015).

Taken together, my work has identified several potential therapeutic targets in CLL with specific DDR defects that are common across the range of different cancers. These observations should be validated in

other cancers with ATM and RNASEH2B defects, thereby motivating personalized medicine approaches toward the development of epigenetic based therapy for DDR defective tumours.

5.4 Project limitations

Unfortunately, as described in chapter 3, I did not obtain a consistent and reproducible dox-mediated KD of KDM5B; therefore, the role of KDM5B in ATM-defective CLL cells remains to be validated in further studies. In addition, It is important to mention that all lines of investigation in this thesis were carried out in CLL isogenic cell lines. Although they were derived from CLL patients and well-studied, they are not a complete, precise representation of primary CLL cells. It is essential, therefore, to replicate several lines of my investigations in primary CLL samples and determine the relevance of my findings. However, this is a challenging work as CLL is known for its heterogenic disease nature where mutational complexity and subclonal composition diversity may mask clear patterns. CLL research recently moved toward single-cell genomics, which helped understand disease heterogeneity by charting CLL lineage history and its evolution. Therefore, single-cell approaches have illuminated a new layer of biological complexity in cancer genomics.

The application of RNA-seq in my PhD project allowed for the evaluation of gene expressions of protein-coding genes. However, a set of non-coding RNAs such as micro-RNA and Long non-coding RNAs (lncRNA) which are known to have roles in gene expression and epigenetic regulation, were not captured using this approach. In addition, accurate and precise sequence annotation and data understanding depend on the reference genome. In my analysis, I followed published standardized analysis workflow protocols to ensure result reproducibility, but the annotation database used may vary from one analysis pipeline to another.

Investigation of the chromatin accessibility landscape using ATAC-seq enabled the assessment of transcription factors (TF) activity and epigenetic regulation. Although I was able to obtain a good

sequencing depth that allowed the investigation of TF activity, the sequencing approach was done in the single-end configuration. Thus, information about nucleosome positioning in the data was not available. Moreover, ATAC-seq methodology relies on the activity of the Tn5 transposase, which works on unprotected or accessible regions of DNA through fragmentation and tagmentation. This Tn5 activity is random, which may result in a high probability of having a DNA fragment with the same adaptor that is eventually unusable for PCR amplification and sequencing (Lu et al., 2017). In addition, the presence of mitochondrial DNA in ATAC-seq data is inevitable due to the openness of such DNA. However, using the updated ATAC-seq protocol (Omni-ATAC) (Corces et al., 2017) significantly minimized reads of mitochondrial DNA.

Chromatin immunoprecipitation followed by sequencing (ChIP-seq) is an important methodology in epigenetic research allowing for the assessment of histone post-translational modifications, transcription factor binding sites, and other DNA binding proteins. Such a method depends on the use of antibodies targeting specific DNA-binding proteins to look for enriched loci containing proteins of interest within the genome. Therefore, the data quality is heavily dependent on the quality of antibodies used. To mitigate this limitation aspect, I only used antibodies that were used in published CLL epigenetic studies to maintain good and reproducible data.

DNA:RNA Immunoprecipitation followed by sequencing (DRIP-seq) allowed for genome-wide mapping of R-loops for analysis and quantification. This method is dependent on the use of the S9.6 antibody that targets R-loops structure in cells. The target specificity of the S9.6 is questionable as it was reported that this antibody binds to RNA-RNA duplexes (Zhang et al., 2015c, Kinney et al., 1989). To maintain target specificity in this method, all samples were treated with Ribonuclease H enzyme that exclusively degrades RNA in DNA:RNA structures in vitro. Validation using qPCR showed that samples treated with Ribonuclease H enzyme do not show signs of enrichment for R-loops in contrast to untreated samples using positive and negative loci.

5.5 Future work

The results described from this project generate questions that pave the way for future work.

Firstly, in chapter 3 I showed that ATM-defective CLL cells are associated with KDM5B upregulation. This finding suggests a role for KDM5B in DDR and highlights a key link interaction between epigenetic regulation and DDR. It was reported that KDM5B is required for nonhomologous end-joining (NHEJ) and homologous recombination (HR) (Li et al., 2014b). However, its exact contribution to either of these DDR pathways is still unknown. Recent research suggests a role for KDM5B in replication stress response (Gaillard et al., 2021). Moreover, KDM5B is linked with transcriptomic heterogeneity to therapeutic resistance (Hinohara et al., 2018). Therefore, KDM5B apparently has functions other than its involvement in DDR, and it will be of interest to determine KDM5B interactors outside the context of DDR defects using CRISPR screen approaches in CLL cells where KDM5B is overexpressed. In addition, it would be interesting to determine whether KDM5B is overexpressed in primary CLL samples with 11q deletions and or samples associated with treatment resistance. This will help to consolidate KDM5B expression as a prognostic biomarker in CLL. Finally, KDM5B should be validated as a potential therapeutic target in primary ATM-deficient CLL cells. It would of interest to assess CLL patients known to have 11q deletions affecting ATM for clonal compositions using single-cell RNA-seq approach to screen for KDM5B gene expression associated with clones linked with defective ATM. This will be followed by cytotoxicity validation assays using KDM5B inhibitors (Pippa et al., 2019, Mitsui et al., 2019, Sayegh et al., 2013) both in vitro and in vivo in the relevant patient-derived xenografts (PDXs).

Secondly, in chapter 4 I demonstrated synthetic lethal interactions between RUNX3 and RNASEH2B. These observations suggest a potentially novel role for RUNX3 in the DDR pathway independent of its transcriptional regulation. Other groups showed that RUNX3 undergoes modifications such as PARP-

poly(ADP-ribosyl)ation which is essential for RUNX3 to facilitate DNA repair, and low RUNX3 levels are found to be correlated with high genomic instability (Tay et al., 2018). Work from our lab showed that CLLs with defects in RNASEH2B are highly sensitive to PARP inhibitors (Zimmermann et al., 2018). Thus, RUNX3 could be a key player in the processing of early lesions in CLL, given that 13q14 deletions are considered as early events in CLL pathogenesis. It will be of interest to determine whether RUNX3 is involved in initiating alterations that lead to CLL progression and evolution. After RUNX3 validation in vitro and in vivo as synthetic lethal in primary CLL samples, it would be of interest to understand the RUNX3 signalling in the context of RNASEH2B deletions observed in CLL. Therefore, targeting RUNX3 downstream target genes may influence cell survival and cause the induction of apoptosis. In fact, RNAi screen identified Cyclin D2 (CCNF2) as a downstream target of RUNX1, and the inhibition of CCND2 pharmacologically or by knockdown reduced the expansion of leukemic cells *in vivo* and *in vitro* (Martinez-Soria et al., 2018). In addition, RUNX1 induction was correlated with alteration in histone acetylation, formation of TF complexes, and increased CDK9 enrichments and using bromodomain inhibitor (JQ1) interfered with these changes highlighting the possibility of targeting RUNX mediated chromatin alterations through downstream target genes (Gilmour et al., 2018). Therefore, identifying RUNX3 downstream target genes that may pose a reliance point for cell survival and proliferation could potentially involve the disruption of RUNX3 circuits observed in monoallelic and biallelic RNASEH2B loss.

Thirdly, CLL is known for its heterogenic nature and the presence of subclonal variations within patients. Work by our group and others suggests that ATM or RNASEH2B alterations are often present at the subclonal level in primary CLL tumours. Thus, it would if interesting to assess primary CLL cells with ATM or RNase H2 dysfunction at the single-cell level using single-cell RNA-sequencing (scRNA-seq) and single-cell ATAC. Such methodologies in CLL primary samples validate and confirm the observations gained from using CLL isogenic cell lines in my study.

Appendix

CRISPR Screen Final Gene Hits List

RNASEH2B Mono-KO	**RNASEH2B Bi-KO**
ARID1A	*ABCF1*
ATP5A1	*ACBD4*
COX17	*ADSL*
DMXL1	*AHCY*
HDAC1	*ANHX*
IER3IP1	*APEX2*
MED24	*ASUN*
MTCH1	*C14orf180*
MTG1	*CDCA5*
NXF1	*CSDC2*
OSBPL7	*EGFLAM*
PGM3	*ERICH2*
POU2AF1	*FBXL17*
RPL27A	*FBXW12*
RUNX3	*FHDC1*
SPDL1	*FOXO3*
TMEM63A	*GABARAPL1*
TTC7A	*GPN2*
USP18	*HAUS8*
	IL13
	KCNB1
	KDSR
	KIF21B
	KRT83
	KRTAP4-12
	LEPREL1
	LIMCH1
	LIN54
	MANBA
	MED13
	MED23
	MGST3
	MTIF3
	NANP
	NEDD8

	OR10H1
	OR9Q2
	PAIP2B
	POLR1E
	RLF
	RNF113A
	RPN1
	RUNX2
	RUNX3
	SCNN1A
	SLC7A3
	SMG5
	STXBP3
	TBC1D22B
	TBC1D9B
	TBL1XR1
	TMEM14C
	TMEM159
	TMIE
	UPF2
	UTS2R
	WIF1
	ZC3H7A
	ZNF296
	ZNF354C
	ZNF444
	ZNF668

List of Differentially Expressed Genes

List of differentially expressed genes (padj < 0.1 and Log2 Fold change > 2)						
MEC1 ATM KD Vs ATM WT						
Gene Name	baseMean	log2FoldChange	lfcSE	stat	pvalue	padj
H4C6	723.949	12.838	1.451	8.846	9.08E-19	4.59E-17
SIT1	408.366	12.030	1.453	8.280	1.23E-16	5.11E-15
ZNF841	140.246	10.463	1.468	7.126	1.03E-12	2.96E-11
PKP2	129.138	10.355	1.469	7.049	1.80E-12	5.05E-11
NUDT12	121.962	10.283	1.470	6.995	2.66E-12	7.28E-11
SLFN13	579.841	10.082	1.032	9.774	1.45E-22	9.90E-21
SCN3A	549.730	10.006	1.032	9.699	3.04E-22	2.00E-20
ARSD	99.191	9.995	1.476	6.771	1.28E-11	3.21E-10
ARFGEF3	98.199	9.985	1.477	6.760	1.38E-11	3.43E-10
PLEKHA1	89.667	9.827	1.479	6.643	3.08E-11	7.36E-10
TEAD4	81.229	9.727	1.486	6.544	5.99E-11	1.38E-09
WASF3	78.959	9.673	1.485	6.515	7.26E-11	1.66E-09
TRIM61	74.636	9.613	1.492	6.442	1.18E-10	2.61E-09
ZNF506	75.950	9.586	1.485	6.453	1.09E-10	2.43E-09
RTL8A	75.376	9.581	1.485	6.451	1.11E-10	2.47E-09
ZNF831	60.920	9.297	1.495	6.216	5.09E-10	1.03E-08
ZNF711	290.399	9.093	1.039	8.754	2.05E-18	9.89E-17
TLCD5	50.665	9.012	1.504	5.991	2.09E-09	3.92E-08
ZKSCAN7	47.456	8.910	1.509	5.907	3.49E-09	6.38E-08
SLFN12L	47.038	8.895	1.509	5.894	3.76E-09	6.82E-08
FHL1	98.858	8.537	1.464	5.833	5.45E-09	9.67E-08
MNDA	34.443	8.508	1.541	5.521	3.37E-08	5.39E-07
SLFN11	289.057	8.501	0.856	9.935	2.92E-23	2.13E-21
HOOK1	34.174	8.418	1.534	5.486	4.11E-08	6.47E-07
MSRB3	83.428	8.277	1.469	5.634	1.77E-08	2.94E-07
CACNG6	30.095	8.256	1.544	5.348	8.89E-08	1.34E-06
FUNDC1	28.764	8.192	1.548	5.292	1.21E-07	1.78E-06
HFE	27.476	8.162	1.556	5.246	1.56E-07	2.25E-06
IMPACT	26.911	8.139	1.560	5.218	1.81E-07	2.59E-06
CNKSR2	27.025	8.088	1.555	5.200	1.99E-07	2.83E-06
FIRRE	361.140	8.074	0.670	12.058	1.77E-33	2.17E-31
INAVA	423.313	8.062	0.617	13.058	5.69E-39	9.17E-37
TMPRSS3	207.081	8.005	0.862	9.282	1.66E-20	9.37E-19
ZNF630	25.215	7.972	1.566	5.092	3.55E-07	4.84E-06
RP11-261A24.1	21.666	7.830	1.586	4.936	7.98E-07	1.02E-05
SERPINB1	293.789	7.789	0.675	11.543	8.05E-31	8.81E-29
FAM95C	54.742	7.649	1.490	5.133	2.86E-07	3.95E-06
MAP3K15	19.884	7.645	1.593	4.798	1.60E-06	1.92E-05
AC015969.3	476.556	7.628	0.507	15.030	4.67E-51	1.25E-48
CCDC152	19.327	7.597	1.598	4.754	2.00E-06	2.36E-05
CACHD1	18.474	7.557	1.603	4.714	2.43E-06	2.83E-05
DSG1	244.848	7.525	0.679	11.084	1.50E-28	1.42E-26
ARL14	18.570	7.512	1.610	4.666	3.08E-06	3.51E-05
CD276	95.678	7.509	1.072	7.005	2.47E-12	6.80E-11
RP11-29H23.8	16.578	7.416	1.621	4.575	4.77E-06	5.23E-05
OSTN-AS1	42.433	7.325	1.504	4.870	1.12E-06	1.39E-05
XCL1	126.068	7.295	0.878	8.308	9.77E-17	4.12E-15
IFI44L	4612.998	7.237	0.172	42.062	0.00E+00	0.00E+00
TCEAL9	79.554	7.205	1.076	6.695	2.16E-11	5.24E-10
RLN2	14.569	7.179	1.647	4.360	1.30E-05	1.29E-04
SATB2	385.531	7.172	0.489	14.676	9.14E-49	2.26E-46
RASAL2	73.924	7.139	1.086	6.576	4.83E-11	1.13E-09

TXNRD3	14.221	7.138	1.653	4.319	1.56E-05	1.52E-04
RP11-489G11.4	76.048	7.137	1.081	6.605	3.98E-11	9.38E-10
CMTM8	13.212	7.111	1.667	4.266	1.99E-05	1.88E-04
NFATC4	181.526	7.091	0.688	10.308	6.52E-25	5.10E-23
DUSP5P1	13.882	7.074	1.667	4.243	2.20E-05	2.07E-04
SHISA3	12.377	7.006	1.679	4.174	3.00E-05	2.73E-04
C8orf88	65.566	6.950	1.089	6.380	1.78E-10	3.84E-09
RP11-1094M14.5	11.751	6.922	1.689	4.098	4.16E-05	3.66E-04
SMPDL3A	11.899	6.915	1.685	4.103	4.08E-05	3.60E-04
ZNF660	11.403	6.872	1.695	4.054	5.04E-05	4.37E-04
GAS2L1	11.412	6.845	1.696	4.037	5.41E-05	4.66E-04
ACCS	10.977	6.838	1.707	4.006	6.18E-05	5.25E-04
ARX	10.707	6.769	1.710	3.958	7.56E-05	6.25E-04
NRG3	10.855	6.761	1.709	3.956	7.62E-05	6.29E-04
SLFN12	10.290	6.703	1.720	3.896	9.79E-05	7.87E-04
TLCD4	110.459	6.695	0.780	8.579	9.58E-18	4.43E-16
PTGFRN	10.220	6.691	1.722	3.885	1.02E-04	8.19E-04
NR1I2	9.933	6.676	1.730	3.859	1.14E-04	9.00E-04
PELI2	9.933	6.676	1.730	3.859	1.14E-04	9.00E-04
TOMM20P2	10.011	6.657	1.728	3.852	1.17E-04	9.24E-04
SYNGR1	26.986	6.654	1.542	4.315	1.60E-05	1.55E-04
CLIC6	51.198	6.615	1.112	5.947	2.74E-09	5.04E-08
SNX18P3	130.706	6.586	0.703	9.373	7.06E-21	4.18E-19
ZNF717	9.159	6.577	1.755	3.748	1.78E-04	1.35E-03
A4GALT	25.187	6.547	1.549	4.227	2.37E-05	2.22E-04
GRASLND	24.830	6.536	1.551	4.215	2.50E-05	2.32E-04
RP4-647C14.2	8.663	6.521	1.778	3.668	2.44E-04	1.78E-03
EPS8	144.427	6.478	0.645	10.048	9.42E-24	7.03E-22
SCN2A	8.829	6.443	1.768	3.644	2.68E-04	1.93E-03
ZNF239	8.393	6.436	1.778	3.619	2.96E-04	2.10E-03
BEND4	45.371	6.410	1.114	5.754	8.73E-09	1.52E-07
IGF2BP2	457.075	6.403	0.362	17.691	4.94E-70	2.47E-67
TESPA1	88.853	6.401	0.800	7.997	1.27E-15	4.83E-14
XXYLT1-AS2	7.471	6.323	1.832	3.452	5.56E-04	3.72E-03
WWC2	7.402	6.309	1.834	3.439	5.83E-04	3.86E-03
SALL2	7.550	6.303	1.816	3.472	5.17E-04	3.47E-03
TLE1	61.892	6.284	0.923	6.805	1.01E-11	2.56E-10
ZBED2	20.707	6.262	1.573	3.982	6.83E-05	5.72E-04
RP11-46H11.3	7.341	6.258	1.824	3.431	6.01E-04	3.97E-03
ZNF528	40.371	6.217	1.124	5.530	3.21E-08	5.14E-07
NECTIN3	7.132	6.212	1.833	3.389	7.03E-04	4.54E-03
ENAH	19.942	6.199	1.578	3.929	8.53E-05	6.95E-04
ZNF528-AS1	7.063	6.196	1.836	3.374	7.41E-04	4.76E-03
MPO	7.872	6.181	1.895	3.262	1.10E-03	6.70E-03
XCL2	7.359	6.173	1.828	3.378	7.31E-04	4.70E-03
ZNF483	6.776	6.172	1.861	3.316	9.13E-04	5.69E-03
TRPS1	534.358	6.148	0.314	19.556	3.68E-85	2.39E-82
LINC00954	7.437	6.146	1.842	3.336	8.50E-04	5.36E-03
OAS3	1903.113	6.145	0.186	33.095	3.52E-240	1.37E-236
AC002456.2	19.907	6.128	1.593	3.848	1.19E-04	9.38E-04
RIPK3	57.145	6.127	0.925	6.622	3.53E-11	8.39E-10
RP11-253E3.3	6.645	6.097	1.857	3.283	1.03E-03	6.30E-03
KHDRBS2	6.576	6.080	1.861	3.267	1.09E-03	6.60E-03
GUSBP5	7.159	6.080	1.863	3.263	1.10E-03	6.70E-03
RSAD2	144.700	6.058	0.573	10.577	3.81E-26	3.17E-24
RP5-827C21.2	6.654	6.050	1.858	3.255	1.13E-03	6.85E-03
RP11-412N9.1	6.654	6.050	1.858	3.255	1.13E-03	6.85E-03
DHRS9	6.080	6.002	1.898	3.163	1.56E-03	9.07E-03

GUCY1A1	35.065	5.996	1.140	5.261	1.44E-07	2.09E-06
ITGA2	6.741	5.975	1.902	3.142	1.68E-03	9.65E-03
MIXL1	5.941	5.965	1.906	3.129	1.75E-03	1.00E-02
ZNF233	6.019	5.934	1.895	3.132	1.74E-03	9.94E-03
MAP9	6.167	5.920	1.892	3.129	1.75E-03	1.00E-02
DSC1	6.167	5.920	1.892	3.129	1.75E-03	1.00E-02
RP11-845C23.3	5.949	5.915	1.899	3.114	1.85E-03	1.05E-02
RP11-876B24.1	5.949	5.915	1.899	3.114	1.85E-03	1.05E-02
ARHGEF35	5.732	5.908	1.919	3.078	2.08E-03	1.16E-02
CTSZ	910.757	5.880	0.232	25.343	1.06E-141	1.38E-138
RHOU	16.750	5.879	1.616	3.638	2.75E-04	1.97E-03
TUBB2B	5.445	5.876	1.959	3.000	2.70E-03	1.44E-02
GNAI1	5.593	5.869	1.929	3.042	2.35E-03	1.28E-02
PRSS16	5.741	5.855	1.914	3.058	2.23E-03	1.22E-02
RP11-305O6.3	5.741	5.855	1.914	3.058	2.23E-03	1.22E-02
CTC-559E9.5	5.454	5.828	1.939	3.006	2.65E-03	1.41E-02
PDCD1	5.088	5.814	2.026	2.869	4.11E-03	2.05E-02
KLF11	46.187	5.809	0.946	6.141	8.20E-10	1.63E-08
CYBB	5.384	5.807	1.944	2.987	2.82E-03	1.49E-02
RNLS	5.680	5.777	1.933	2.988	2.81E-03	1.48E-02
ZBTB47	42.280	5.717	0.954	5.995	2.03E-09	3.83E-08
RP11-344P13.6	5.471	5.711	1.954	2.922	3.47E-03	1.78E-02
CMPK2	262.718	5.696	0.399	14.259	3.91E-46	8.67E-44
PYHIN1	125.004	5.693	0.557	10.217	1.66E-24	1.28E-22
MBL1P	5.184	5.683	1.962	2.896	3.77E-03	1.91E-02
ADCY6	4.749	5.665	2.014	2.813	4.91E-03	2.37E-02
RP11-535M15.1	5.114	5.659	1.969	2.875	4.05E-03	2.02E-02
SATB2-AS1	26.679	5.653	1.175	4.809	1.51E-06	1.83E-05
B3GALNT1	12.618	5.634	1.700	3.315	9.18E-04	5.71E-03
NRIR	4.827	5.630	1.992	2.826	4.71E-03	2.30E-02
DPYSL4	4.827	5.630	1.992	2.826	4.71E-03	2.30E-02
RP11-705C15.5	4.610	5.619	2.027	2.772	5.58E-03	2.64E-02
CTC-471J1.2	4.610	5.619	2.027	2.772	5.58E-03	2.64E-02
ADGRB3	4.540	5.595	2.034	2.751	5.95E-03	2.79E-02
CCDC120	90.827	5.589	0.635	8.805	1.31E-18	6.49E-17
KCNK6	91.743	5.588	0.633	8.829	1.05E-18	5.31E-17
XIRP1	4.836	5.563	1.999	2.783	5.38E-03	2.57E-02
GS1-24F4.4	4.836	5.563	1.999	2.783	5.38E-03	2.57E-02
CCL28	75.583	5.557	0.688	8.072	6.94E-16	2.67E-14
VILL	12.949	5.546	1.651	3.360	7.80E-04	4.97E-03
STEAP2	4.401	5.546	2.048	2.708	6.78E-03	3.10E-02
ADAMTS12	151.691	5.541	0.488	11.347	7.65E-30	7.97E-28
ANKRD18A	294.262	5.533	0.368	15.043	3.84E-51	1.04E-48
TNFRSF11B	4.479	5.506	2.029	2.714	6.64E-03	3.05E-02
LINC01389	4.410	5.480	2.037	2.691	7.13E-03	3.23E-02
RP11-392E22.11	4.340	5.454	2.045	2.667	7.65E-03	3.43E-02
LA16c-349E10.1	4.123	5.443	2.080	2.617	8.86E-03	3.87E-02
H3C3	4.271	5.427	2.054	2.643	8.23E-03	3.65E-02
ANTXR2	34.523	5.424	0.986	5.503	3.74E-08	5.92E-07
SAMSN1-AS1	4.636	5.419	2.073	2.614	8.94E-03	3.90E-02
ZNF283	35.095	5.408	0.975	5.546	2.92E-08	4.71E-07
ZFPM2-AS1	4.567	5.392	2.087	2.584	9.77E-03	4.19E-02
IL12RB2	33.164	5.372	0.985	5.455	4.90E-08	7.67E-07
SATL1	4.132	5.371	2.072	2.592	9.53E-03	4.11E-02
MATK	22.870	5.366	1.195	4.491	7.09E-06	7.48E-05
ZNF284	10.738	5.355	1.700	3.150	1.63E-03	9.41E-03
BEX4	21.495	5.351	1.213	4.411	1.03E-05	1.05E-04
RP11-147L13.12	4.062	5.342	2.081	2.567	1.03E-02	4.38E-02

EGLN3	3.992	5.313	2.091	2.540	1.11E-02	4.64E-02
OAS2	2745.955	5.300	0.140	37.738	0.00E+00	0.00E+00
LPIN3	10.330	5.261	1.702	3.091	1.99E-03	1.12E-02
NEXN-AS1	4.071	5.260	2.110	2.493	1.27E-02	5.16E-02
MIR9-3HG	20.381	5.243	1.221	4.295	1.74E-05	1.67E-04
HCK	563.143	5.242	0.255	20.528	1.21E-93	1.12E-90
RHBDL3	20.034	5.237	1.221	4.289	1.79E-05	1.71E-04
MYOF	30.556	5.207	0.992	5.251	1.51E-07	2.19E-06
IKBKGP1	9.121	5.175	1.815	2.850	4.37E-03	2.16E-02
IFIT1	190.357	5.144	0.407	12.651	1.11E-36	1.60E-34
LONRF3	9.425	5.106	1.724	2.961	3.07E-03	1.60E-02
RTL5	9.573	5.094	1.723	2.957	3.11E-03	1.62E-02
NLRC4	9.138	5.091	1.735	2.935	3.34E-03	1.72E-02
RP11-686D22.10	9.503	5.082	1.725	2.945	3.23E-03	1.67E-02
PCDHGB5	27.232	5.065	1.010	5.015	5.30E-07	7.01E-06
CARD6	43.812	5.034	0.798	6.308	2.82E-10	5.92E-09
TNFAIP8L2	27.782	5.029	1.013	4.964	6.91E-07	8.95E-06
MYL9	17.163	5.017	1.252	4.006	6.18E-05	5.24E-04
ZNF844	17.894	5.010	1.235	4.056	5.00E-05	4.34E-04
RP11-79N23.1	8.868	5.001	1.741	2.872	4.08E-03	2.04E-02
RP11-147L13.13	8.452	4.985	1.760	2.833	4.62E-03	2.26E-02
EPHB2	60.483	4.958	0.672	7.381	1.57E-13	4.86E-12
LNX1	33.527	4.939	0.885	5.579	2.43E-08	3.96E-07
BRDT	7.937	4.933	1.790	2.755	5.87E-03	2.76E-02
ZNF572	16.712	4.923	1.255	3.922	8.78E-05	7.13E-04
MAGI3	505.865	4.918	0.242	20.284	1.78E-91	1.45E-88
RP11-328J6.1	65.802	4.914	0.634	7.757	8.73E-15	3.07E-13
MLC1	73.008	4.911	0.603	8.138	4.01E-16	1.58E-14
AC020951.1	7.965	4.887	1.775	2.753	5.90E-03	2.77E-02
CASP4LP	16.642	4.883	1.252	3.899	9.65E-05	7.78E-04
SHROOM2	23.648	4.881	1.039	4.700	2.60E-06	3.02E-05
DUXAP9	8.390	4.859	1.769	2.746	6.03E-03	2.82E-02
LOXL4	39.239	4.858	0.806	6.027	1.67E-09	3.19E-08
TRO	55.699	4.851	0.680	7.132	9.89E-13	2.84E-11
PITX1	23.152	4.839	1.050	4.610	4.03E-06	4.49E-05
LIPG	100.862	4.831	0.507	9.521	1.72E-21	1.06E-19
SHISAL2A	30.369	4.804	0.902	5.328	9.96E-08	1.49E-06
KRT18	7.242	4.786	1.814	2.638	8.34E-03	3.69E-02
CXCL8	8.042	4.782	1.787	2.676	7.46E-03	3.36E-02
POTEH	7.538	4.762	1.789	2.662	7.77E-03	3.48E-02
UTRN	1399.041	4.750	0.159	29.929	8.18E-197	1.99E-193
USP18	287.058	4.690	0.300	15.645	3.57E-55	1.16E-52
BMP6	28.402	4.679	0.928	5.042	4.60E-07	6.15E-06
ASPH	78.003	4.676	0.556	8.418	3.84E-17	1.66E-15
RP11-469G18.1	70.544	4.671	0.580	8.046	8.54E-16	3.28E-14
RP11-326C3.2	27.629	4.661	0.920	5.068	4.02E-07	5.44E-06
SHROOM3	936.207	4.645	0.179	25.954	1.63E-148	2.27E-145
VTRNA1-3	50.366	4.642	0.715	6.491	8.55E-11	1.93E-09
CTD-2008P7.8	6.981	4.627	1.816	2.548	1.08E-02	4.56E-02
HSBP1L1	101.546	4.612	0.480	9.600	8.03E-22	5.05E-20
GBP1	41.463	4.608	0.754	6.109	1.00E-09	1.97E-08
NAPSA	65.667	4.601	0.623	7.391	1.46E-13	4.54E-12
C11orf21	19.813	4.600	1.067	4.311	1.63E-05	1.57E-04
GRIN2D	20.178	4.596	1.062	4.329	1.50E-05	1.46E-04
CD6	6.259	4.594	1.878	2.447	1.44E-02	5.73E-02
RP11-310I9.2	6.643	4.579	1.830	2.503	1.23E-02	5.04E-02
TLR8	6.772	4.573	1.828	2.502	1.23E-02	5.05E-02
CSGALNACT1	6.416	4.535	1.843	2.460	1.39E-02	5.56E-02

RP11-122D13.1	19.135	4.531	1.072	4.227	2.37E-05	2.22E-04
THSD4	44.746	4.531	0.705	6.431	1.27E-10	2.81E-09
MICU3	6.651	4.524	1.834	2.467	1.36E-02	5.47E-02
LMCD1	25.142	4.492	0.931	4.825	1.40E-06	1.70E-05
AC023590.1	6.642	4.480	1.855	2.414	1.58E-02	6.16E-02
LINC02008	6.225	4.465	1.853	2.410	1.59E-02	6.22E-02
PROCR	6.137	4.457	1.859	2.397	1.65E-02	6.40E-02
CALD1	6.373	4.446	1.852	2.401	1.63E-02	6.35E-02
ILDR2	155.254	4.437	0.381	11.651	2.28E-31	2.58E-29
PCDHGA2	6.086	4.425	1.861	2.377	1.74E-02	6.68E-02
RP11-71G12.1	18.300	4.423	1.085	4.076	4.58E-05	4.00E-04
TMEM74	5.998	4.417	1.868	2.364	1.81E-02	6.87E-02
TRAT1	5.928	4.396	1.873	2.347	1.89E-02	7.13E-02
LRRTM4	1433.001	4.394	0.152	28.821	1.18E-182	2.55E-179
PEAK3	5.512	4.373	1.917	2.280	2.26E-02	8.22E-02
RP11-147L13.11	113.034	4.366	0.442	9.872	5.49E-23	3.92E-21
ABHD17AP5	5.424	4.365	1.925	2.268	2.33E-02	8.44E-02
GNB4	61.452	4.354	0.589	7.390	1.46E-13	4.54E-12
LINC01725	5.572	4.352	1.898	2.292	2.19E-02	8.03E-02
HEY2	28.132	4.344	0.854	5.088	3.62E-07	4.93E-06
TSPAN11	5.808	4.341	1.880	2.309	2.09E-02	7.74E-02
CTB-53D8.2	5.798	4.288	1.898	2.259	2.39E-02	8.61E-02
RP11-452E5.1	11.485	4.284	1.359	3.152	1.62E-03	9.37E-03
RP11-367L7.1	27.120	4.276	0.886	4.826	1.39E-06	1.69E-05
PCAT6	49.516	4.272	0.645	6.623	3.52E-11	8.36E-10
ADAMTS3	38.355	4.265	0.729	5.852	4.86E-09	8.68E-08
ZNF439	32.033	4.259	0.787	5.408	6.36E-08	9.76E-07
CTA-384D8.34	36.318	4.250	0.743	5.717	1.08E-08	1.85E-07
DSG4	15.750	4.235	1.135	3.732	1.90E-04	1.43E-03
FBXL2	21.122	4.234	0.990	4.279	1.88E-05	1.79E-04
SLC51A	5.460	4.229	1.907	2.218	2.66E-02	9.41E-02
HID1	30.884	4.223	0.799	5.288	1.23E-07	1.81E-06
STXBP6	9.962	4.218	1.390	3.034	2.41E-03	1.31E-02
MYL3	10.118	4.176	1.370	3.048	2.30E-03	1.26E-02
ZNF525	75.222	4.173	0.519	8.042	8.86E-16	3.39E-14
IGDCC4	20.403	4.164	0.976	4.266	1.99E-05	1.88E-04
ACP5	15.170	4.157	1.142	3.641	2.72E-04	1.96E-03
CASP1	209.816	4.126	0.312	13.203	8.48E-40	1.42E-37
SAMD4A	99.297	4.124	0.447	9.226	2.81E-20	1.58E-18
OXER1	18.957	4.089	0.994	4.116	3.86E-05	3.42E-04
EBF4	9.719	4.088	1.399	2.921	3.49E-03	1.79E-02
IL23R	76.942	4.085	0.505	8.081	6.40E-16	2.48E-14
LHX4	13.933	4.083	1.150	3.550	3.86E-04	2.67E-03
LMO3	48.053	4.067	0.630	6.451	1.11E-10	2.47E-09
VWA5A	40.817	4.058	0.688	5.902	3.59E-09	6.54E-08
ROBO2	41.932	4.055	0.666	6.091	1.12E-09	2.19E-08
ITGAX	13.595	4.053	1.162	3.487	4.89E-04	3.31E-03
CTD-2292N2.1	27.090	4.035	1.604	2.516	1.19E-02	4.89E-02
EIF3CL	212.747	4.024	1.827	2.202	2.77E-02	9.71E-02
MARK1	26.605	4.015	0.832	4.828	1.38E-06	1.68E-05
XAF1	835.080	4.010	0.179	22.344	1.38E-110	1.41E-107
CIART	9.431	4.009	1.397	2.869	4.11E-03	2.05E-02
FBXO6	134.370	4.007	0.383	10.467	1.22E-25	9.91E-24
AMIGO1	13.742	4.005	1.150	3.484	4.94E-04	3.33E-03
AC006129.1	9.422	3.989	1.437	2.775	5.52E-03	2.62E-02
TNFSF12	8.482	3.966	1.458	2.720	6.54E-03	3.02E-02
PARP9	422.629	3.957	0.223	17.731	2.40E-70	1.26E-67
CSMD1	13.718	3.952	1.177	3.358	7.85E-04	5.00E-03

LINC02009	13.195	3.949	1.159	3.408	6.53E-04	4.27E-03
LINC02653	22.357	3.935	0.903	4.358	1.31E-05	1.30E-04
CSPG4	180.436	3.911	0.334	11.717	1.04E-31	1.20E-29
RP11-542M13.5	12.888	3.905	1.195	3.268	1.09E-03	6.60E-03
KLHDC7B	96.133	3.902	0.444	8.788	1.52E-18	7.48E-17
OAS1	752.324	3.876	0.177	21.895	2.90E-106	2.83E-103
IFI44	861.145	3.843	0.167	22.983	6.93E-117	7.50E-114
MPEG1	15.799	3.835	1.042	3.681	2.33E-04	1.70E-03
ZNF829	57.226	3.830	0.553	6.920	4.50E-12	1.19E-10
CAMSAP3	27.673	3.823	0.788	4.854	1.21E-06	1.50E-05
HOXB2	8.180	3.820	1.460	2.617	8.87E-03	3.88E-02
LINC00674	24.511	3.816	0.841	4.537	5.70E-06	6.15E-05
VANGL2	31.922	3.813	0.732	5.209	1.89E-07	2.71E-06
MX1	6475.701	3.810	0.104	36.574	7.32E-293	3.57E-289
MAN1A1	318.558	3.785	0.245	15.467	5.81E-54	1.82E-51
LINC02870	7.300	3.776	1.513	2.495	1.26E-02	5.13E-02
KDM5B	2388.009	3.772	0.119	31.588	5.38E-219	1.75E-215
RP11-542M13.6	7.684	3.755	1.486	2.526	1.15E-02	4.79E-02
DUXAP10	14.521	3.753	1.090	3.444	5.73E-04	3.81E-03
FILIP1	91.283	3.742	0.437	8.560	1.12E-17	5.16E-16
ZNF320	23.032	3.736	0.853	4.381	1.18E-05	1.18E-04
LINC02609	42.421	3.723	0.635	5.863	4.55E-09	8.15E-08
NAPSB	364.360	3.715	0.242	15.370	2.60E-53	7.57E-51
SIGLEC10	22.795	3.714	0.857	4.335	1.46E-05	1.43E-04
KCNG2	18.764	3.711	0.935	3.969	7.22E-05	6.00E-04
LINC01887	59.869	3.704	0.531	6.970	3.17E-12	8.58E-11
TPD52L1	18.449	3.698	0.951	3.889	1.00E-04	8.07E-04
CACNA1A	7.623	3.692	1.488	2.482	1.31E-02	5.29E-02
CHSY3	7.100	3.689	1.498	2.463	1.38E-02	5.53E-02
ADCY4	7.100	3.689	1.498	2.463	1.38E-02	5.53E-02
H2AC19	156.546	3.665	1.667	2.199	2.79E-02	9.76E-02
RPSAP69	14.514	3.665	1.060	3.457	5.47E-04	3.66E-03
ZYG11A	157.031	3.658	0.333	10.987	4.40E-28	4.08E-26
GLS2	10.436	3.644	1.234	2.952	3.15E-03	1.64E-02
PLK2	126.941	3.639	0.373	9.746	1.92E-22	1.29E-20
LRRC1	84.888	3.630	0.441	8.221	2.01E-16	8.08E-15
DUXAP8	17.800	3.628	0.960	3.777	1.59E-04	1.21E-03
TLR4	60.354	3.622	0.521	6.948	3.72E-12	9.91E-11
CA8	59.706	3.618	0.538	6.729	1.70E-11	4.19E-10
PCSK6	14.009	3.613	1.061	3.405	6.63E-04	4.32E-03
RP11-297K8.2	7.317	3.605	1.526	2.362	1.82E-02	6.90E-02
SAMSN1	1919.675	3.602	0.127	28.365	5.39E-177	9.55E-174
HERC6	235.893	3.601	0.275	13.103	3.15E-39	5.16E-37
KLHL31	6.664	3.600	1.555	2.315	2.06E-02	7.66E-02
OASL	107.843	3.598	0.395	9.116	7.80E-20	4.16E-18
ESPNL	44.007	3.596	0.616	5.841	5.20E-09	9.27E-08
SMIM10	45.274	3.594	0.603	5.959	2.53E-09	4.68E-08
PCDHGA9	14.217	3.594	1.071	3.357	7.89E-04	5.02E-03
FAP	6.988	3.585	1.522	2.355	1.85E-02	7.00E-02
CRTAM	38.656	3.576	0.649	5.508	3.64E-08	5.78E-07
GNLY	195.578	3.570	0.309	11.560	6.55E-31	7.21E-29
A2M	13.790	3.566	1.075	3.317	9.12E-04	5.68E-03
RP11-46H11.11	26.965	3.558	0.762	4.666	3.07E-06	3.51E-05
CHFR	352.119	3.553	0.227	15.651	3.29E-55	1.09E-52
SESN3	152.336	3.552	0.331	10.746	6.17E-27	5.39E-25
SSTR3	162.318	3.547	0.337	10.540	5.66E-26	4.69E-24
WDFY3	238.257	3.537	0.270	13.079	4.34E-39	7.05E-37
CCRL2	29.412	3.537	0.745	4.746	2.07E-06	2.44E-05

IFITM2	221.639	3.535	0.278	12.735	3.76E-37	5.46E-35
DDX60L	313.731	3.532	0.250	14.150	1.87E-45	3.88E-43
FOXJ1	6.691	3.529	1.510	2.338	1.94E-02	7.28E-02
SULF2	6.603	3.529	1.551	2.276	2.28E-02	8.30E-02
TMEM273	62.559	3.529	0.507	6.964	3.31E-12	8.92E-11
CDH15	13.067	3.511	1.117	3.142	1.68E-03	9.64E-03
TBC1D30	6.187	3.505	1.565	2.239	2.52E-02	9.00E-02
SH2D2A	134.103	3.497	0.367	9.528	1.60E-21	9.91E-20
LRRN1	47.767	3.491	0.579	6.029	1.65E-09	3.15E-08
POTEG	6.770	3.487	1.512	2.306	2.11E-02	7.80E-02
GNAL	77.213	3.484	0.456	7.640	2.16E-14	7.40E-13
MGST1	9.708	3.482	1.288	2.702	6.89E-03	3.15E-02
CDH18	6.918	3.466	1.526	2.272	2.31E-02	8.37E-02
GABRB2	22.881	3.466	0.823	4.210	2.55E-05	2.36E-04
MYO7B	72.653	3.452	0.464	7.446	9.60E-14	3.05E-12
FCRL6	19.910	3.447	0.901	3.825	1.31E-04	1.02E-03
SPTBN2	602.801	3.443	0.193	17.855	2.66E-71	1.44E-68
TPRG1	70.185	3.439	0.474	7.249	4.19E-13	1.24E-11
KCNE5	9.166	3.430	1.311	2.616	8.89E-03	3.88E-02
DDX60	1049.853	3.420	0.148	23.099	4.68E-118	5.37E-115
ZNF347	68.304	3.416	0.480	7.116	1.11E-12	3.16E-11
PARD6G	12.636	3.412	1.100	3.102	1.92E-03	1.08E-02
RUSC2	30.073	3.397	0.709	4.788	1.68E-06	2.02E-05
AC008079.10	12.556	3.377	1.099	3.073	2.12E-03	1.17E-02
RP11-700A24.1	12.181	3.367	1.113	3.026	2.48E-03	1.33E-02
PAQR7	225.402	3.363	0.279	12.071	1.51E-33	1.86E-31
HAAO	50.195	3.355	0.548	6.121	9.31E-10	1.84E-08
CLECL1	482.112	3.333	0.195	17.100	1.48E-65	6.72E-63
RP11-712B9.2	12.028	3.308	1.155	2.864	4.18E-03	2.08E-02
ROBO3	17.343	3.304	0.915	3.612	3.04E-04	2.15E-03
GLUL	3307.616	3.297	0.109	30.288	1.64E-201	4.56E-198
LDLRAD2	22.477	3.292	0.806	4.084	4.43E-05	3.88E-04
ADGRL1	64.336	3.288	0.490	6.707	1.99E-11	4.85E-10
ABCA9	14.414	3.285	1.004	3.273	1.06E-03	6.49E-03
RALGPS2-AS1	8.271	3.273	1.312	2.494	1.26E-02	5.14E-02
HMCES	47.039	3.271	0.568	5.758	8.53E-09	1.49E-07
RRAD	8.141	3.271	1.332	2.457	1.40E-02	5.60E-02
GBP4	76.496	3.269	0.443	7.376	1.64E-13	5.04E-12
NSF	12.480	3.259	1.326	2.457	1.40E-02	5.59E-02
PLEKHG5	44.772	3.259	0.571	5.706	1.16E-08	1.98E-07
CDS1	18.923	3.249	0.880	3.692	2.23E-04	1.64E-03
NDRG1	13.937	3.241	1.013	3.201	1.37E-03	8.10E-03
FAM201A	41.078	3.231	0.595	5.431	5.61E-08	8.67E-07
CES3	57.156	3.228	0.514	6.278	3.43E-10	7.14E-09
ZNF222	13.303	3.223	1.064	3.029	2.45E-03	1.32E-02
RAB37	7.992	3.212	1.324	2.426	1.53E-02	5.99E-02
RP11-655C2.4	13.894	3.195	1.031	3.098	1.95E-03	1.09E-02
CLEC17A	173.112	3.183	0.300	10.612	2.61E-26	2.21E-24
PIFO	148.134	3.174	0.321	9.881	5.06E-23	3.64E-21
RMST	42.179	3.151	0.581	5.422	5.89E-08	9.07E-07
DUSP23	133.023	3.149	0.336	9.358	8.14E-21	4.79E-19
NEB	18.573	3.148	0.881	3.574	3.52E-04	2.46E-03
NUDT4B	17.810	3.142	0.891	3.528	4.18E-04	2.88E-03
EPCAM	71.923	3.138	0.451	6.961	3.38E-12	9.10E-11
SLA2	20.816	3.133	0.818	3.830	1.28E-04	1.00E-03
ZNF585A	83.271	3.121	0.418	7.466	8.26E-14	2.66E-12
PXT1	21.112	3.119	0.819	3.808	1.40E-04	1.09E-03
DBN1	432.517	3.114	0.207	15.064	2.77E-51	7.61E-49

PTK2	147.672	3.111	0.321	9.684	3.52E-22	2.29E-20
NOTUM	12.440	3.104	1.051	2.953	3.15E-03	1.63E-02
RENBP	19.755	3.076	0.834	3.688	2.26E-04	1.66E-03
LINC00665	96.507	3.074	0.392	7.834	4.74E-15	1.72E-13
ZNF227	206.003	3.073	0.294	10.444	1.57E-25	1.26E-23
CD101	12.291	3.060	1.068	2.867	4.15E-03	2.06E-02
LINC01762	10.460	3.058	1.165	2.624	8.70E-03	3.82E-02
SLC2A5	264.913	3.055	0.249	12.246	1.77E-34	2.27E-32
TLE2	112.086	3.048	0.362	8.413	3.98E-17	1.72E-15
CHIT1	33.981	3.046	0.642	4.744	2.09E-06	2.46E-05
FBP1	81.960	3.046	0.426	7.155	8.38E-13	2.42E-11
RP11-542M13.4	7.602	3.045	1.342	2.269	2.33E-02	8.43E-02
TYMP	217.322	3.045	0.274	11.113	1.09E-28	1.04E-26
RP11-328K2.1	10.303	3.044	1.185	2.570	1.02E-02	4.34E-02
KISS1R	11.527	3.039	1.118	2.718	6.56E-03	3.03E-02
PIGR	76.719	3.035	0.437	6.940	3.92E-12	1.04E-10
SYK	506.668	3.033	0.190	15.970	2.08E-57	7.64E-55
DTX3L	934.263	3.032	0.148	20.502	2.08E-93	1.84E-90
RETREG1	250.837	3.031	0.247	12.249	1.70E-34	2.21E-32
CPNE5	279.535	3.029	0.245	12.353	4.72E-35	6.30E-33
GAS8	199.703	3.020	0.275	10.975	5.02E-28	4.64E-26
RP5-1120P11.3	26.258	3.007	0.732	4.107	4.00E-05	3.53E-04
FOSL1	41.674	3.001	0.584	5.138	2.77E-07	3.85E-06
SLC4A11	16.529	2.999	0.911	3.294	9.87E-04	6.08E-03
MS4A6E	43.194	2.998	0.576	5.208	1.91E-07	2.73E-06
PECAM1	77.833	2.997	0.457	6.561	5.35E-11	1.24E-09
ZNF880	41.972	2.995	0.577	5.189	2.12E-07	3.00E-06
DNAH7	407.566	2.990	0.217	13.794	2.76E-43	5.39E-41
CHI3L2	3603.903	2.990	0.113	26.573	1.39E-155	2.09E-152
C5AR2	7.393	2.990	1.355	2.207	2.73E-02	9.61E-02
SLAMF8	20.847	2.985	0.806	3.704	2.12E-04	1.57E-03
PCDHGA11	34.578	2.977	0.637	4.672	2.98E-06	3.42E-05
ZNF486	12.169	2.972	1.085	2.739	6.16E-03	2.87E-02
RYR1	13.366	2.972	1.036	2.867	4.14E-03	2.06E-02
DGKG	61.167	2.962	0.492	6.027	1.67E-09	3.19E-08
ZAP70	53.154	2.961	0.513	5.777	7.63E-09	1.34E-07
ASIC1	8.798	2.961	1.246	2.376	1.75E-02	6.70E-02
EPB41L4A	32.275	2.959	0.672	4.401	1.08E-05	1.09E-04
FBXO39	21.281	2.951	0.806	3.661	2.51E-04	1.82E-03
CACNA1F	9.381	2.949	1.201	2.456	1.41E-02	5.61E-02
F12	30.918	2.943	0.693	4.244	2.20E-05	2.07E-04
TP73-AS1	72.374	2.940	0.447	6.577	4.79E-11	1.12E-09
CASKIN2	100.025	2.938	0.386	7.620	2.54E-14	8.63E-13
KIAA1671	11.109	2.931	1.090	2.689	7.17E-03	3.25E-02
HERC5	497.709	2.926	0.194	15.068	2.64E-51	7.35E-49
GJC1	267.857	2.923	0.241	12.138	6.63E-34	8.34E-32
ALDH1L2	260.282	2.921	0.258	11.308	1.20E-29	1.23E-27
RP1-239B22.5	9.565	2.911	1.204	2.417	1.56E-02	6.12E-02
MUC1	20.012	2.909	0.813	3.576	3.48E-04	2.44E-03
EEF1D	141.902	2.907	1.211	2.401	1.63E-02	6.34E-02
FBXO2	34.688	2.903	0.642	4.520	6.18E-06	6.63E-05
LINC00957	32.414	2.903	0.666	4.357	1.32E-05	1.31E-04
ABCC8	15.819	2.891	0.924	3.129	1.76E-03	1.00E-02
BMP3	39.847	2.890	0.596	4.853	1.22E-06	1.51E-05
TIMD4	152.963	2.887	0.308	9.360	8.01E-21	4.73E-19
ISG15	758.135	2.882	0.160	18.032	1.08E-72	6.22E-70
DSC3	8.903	2.882	1.205	2.391	1.68E-02	6.49E-02
PRAF2	52.632	2.879	0.516	5.582	2.38E-08	3.88E-07

LMTK3	30.434	2.862	0.659	4.341	1.42E-05	1.39E-04
PTPRJ	21.124	2.857	0.808	3.537	4.05E-04	2.79E-03
DDX24	80.733	2.856	0.424	6.731	1.68E-11	4.14E-10
FCGRT	12.785	2.848	1.006	2.830	4.66E-03	2.27E-02
NPDC1	14.643	2.843	0.948	2.999	2.71E-03	1.44E-02
SLC15A3	504.539	2.843	0.189	15.021	5.32E-51	1.38E-48
ACSL6	27.340	2.842	0.704	4.039	5.37E-05	4.63E-04
RP11-25K19.1	112.131	2.840	0.351	8.087	6.10E-16	2.36E-14
IL1RN	8.477	2.838	1.228	2.312	2.08E-02	7.71E-02
GBP2	39.592	2.832	0.602	4.703	2.56E-06	2.97E-05
RP11-403I13.4	15.050	2.832	0.962	2.945	3.23E-03	1.67E-02
CAPS2	19.395	2.828	0.818	3.457	5.46E-04	3.66E-03
NINL	10.876	2.828	1.110	2.547	1.09E-02	4.57E-02
KDF1	8.801	2.827	1.276	2.215	2.67E-02	9.46E-02
VDR	142.739	2.826	0.320	8.823	1.12E-18	5.61E-17
HIC1	50.389	2.825	0.524	5.388	7.11E-08	1.08E-06
LRRC3	21.488	2.824	0.777	3.634	2.79E-04	2.00E-03
RAPGEF5	8.407	2.823	1.231	2.294	2.18E-02	8.00E-02
LTF	128.485	2.821	0.328	8.602	7.81E-18	3.64E-16
APBB1IP	575.120	2.819	0.174	16.223	3.48E-59	1.33E-56
SMC1B	19.167	2.813	0.828	3.397	6.80E-04	4.42E-03
PPP2R2C	15.322	2.808	0.926	3.031	2.44E-03	1.32E-02
PCDHGC5	11.154	2.808	1.094	2.568	1.02E-02	4.37E-02
GALNT3	25.036	2.806	0.739	3.797	1.46E-04	1.13E-03
LRRK2	45.716	2.789	0.559	4.990	6.03E-07	7.88E-06
TFEC	40.906	2.787	0.576	4.838	1.31E-06	1.60E-05
LINC00654	100.258	2.775	0.372	7.454	9.03E-14	2.88E-12
JHY	238.565	2.772	0.258	10.741	6.51E-27	5.64E-25
TNFAIP6	10.727	2.772	1.099	2.523	1.17E-02	4.82E-02
KIF7	37.565	2.771	0.590	4.696	2.65E-06	3.07E-05
CST7	10.945	2.769	1.103	2.512	1.20E-02	4.94E-02
C1orf115	47.570	2.769	0.528	5.246	1.55E-07	2.25E-06
NEO1	366.221	2.760	0.208	13.262	3.84E-40	6.68E-38
RP11-284F21.10	237.335	2.758	0.253	10.913	9.95E-28	9.06E-26
PLAAT4	37.897	2.758	0.602	4.585	4.54E-06	5.00E-05
CARD16	63.225	2.748	0.456	6.020	1.75E-09	3.32E-08
PWWP2B	106.904	2.742	0.369	7.434	1.06E-13	3.35E-12
SNPH	67.309	2.732	0.442	6.180	6.42E-10	1.30E-08
AXIN2	10.014	2.724	1.121	2.430	1.51E-02	5.94E-02
SAA2	9.796	2.724	1.138	2.393	1.67E-02	6.45E-02
RALGPS2	472.125	2.722	0.185	14.737	3.73E-49	9.44E-47
RP3-413H6.3	51.473	2.715	0.506	5.365	8.10E-08	1.23E-06
SUGCT	20.217	2.711	0.795	3.409	6.52E-04	4.26E-03
LTBP4	232.766	2.708	0.261	10.363	3.66E-25	2.92E-23
PCDHGC4	10.379	2.705	1.113	2.431	1.51E-02	5.94E-02
EPSTI1	580.998	2.698	0.171	15.796	3.29E-56	1.15E-53
LINC00565	17.550	2.690	0.853	3.153	1.62E-03	9.34E-03
FOXP2	46.517	2.690	0.577	4.662	3.12E-06	3.56E-05
EMP3	356.935	2.679	0.206	12.978	1.63E-38	2.56E-36
MAGI2	33.542	2.678	0.627	4.273	1.92E-05	1.83E-04
TNFRSF10A	104.091	2.665	0.368	7.240	4.50E-13	1.33E-11
CTD-3247F14.3	53.708	2.662	0.495	5.373	7.75E-08	1.18E-06
RP11-284F21.7	81.858	2.650	0.411	6.455	1.08E-10	2.42E-09
TLR7	874.667	2.648	0.157	16.883	5.96E-64	2.52E-61
TOX	858.480	2.645	0.150	17.647	1.07E-69	5.22E-67
ANKRD50	42.540	2.645	0.561	4.714	2.43E-06	2.83E-05
PCDHGB6	13.112	2.639	0.974	2.710	6.73E-03	3.09E-02
ZNF568	35.862	2.637	0.601	4.390	1.14E-05	1.14E-04

RP11-1149O23.3	45.782	2.637	0.527	4.999	5.76E-07	7.58E-06
POGLUT3	502.511	2.624	0.187	14.002	1.52E-44	3.02E-42
SNX18	18.466	2.622	0.880	2.979	2.89E-03	1.52E-02
TRIM46	93.556	2.620	0.379	6.904	5.07E-12	1.33E-10
RAB3B	702.581	2.615	0.159	16.439	1.00E-60	3.99E-58
ZNF254	78.076	2.615	0.409	6.399	1.57E-10	3.41E-09
FHL3	18.035	2.596	0.840	3.091	1.99E-03	1.12E-02
GBP6	14.631	2.593	0.921	2.816	4.87E-03	2.36E-02
LINC01735	9.577	2.570	1.172	2.193	2.83E-02	9.88E-02
FZD3	125.556	2.567	0.335	7.666	1.78E-14	6.11E-13
PDE4D	1328.409	2.564	0.129	19.870	7.41E-88	5.35E-85
RASGRP2	128.022	2.557	0.328	7.793	6.53E-15	2.34E-13
MSH4	11.716	2.552	1.064	2.398	1.65E-02	6.38E-02
EPS8L2	84.441	2.552	0.395	6.454	1.09E-10	2.42E-09
TTC22	82.487	2.550	0.400	6.368	1.91E-10	4.11E-09
TRIM51	10.800	2.547	1.090	2.337	1.95E-02	7.30E-02
LINC01117	9.109	2.540	1.154	2.200	2.78E-02	9.74E-02
ZNF890P	17.844	2.531	0.827	3.061	2.21E-03	1.22E-02
C1orf54	21.192	2.523	0.781	3.233	1.23E-03	7.34E-03
LRRC34	11.401	2.518	1.079	2.334	1.96E-02	7.33E-02
FBXO16	67.196	2.514	0.456	5.520	3.40E-08	5.42E-07
HSPG2	122.051	2.508	0.333	7.540	4.71E-14	1.55E-12
NTNG1	65.395	2.505	0.448	5.592	2.25E-08	3.69E-07
HLX	14.745	2.504	0.921	2.719	6.55E-03	3.02E-02
LAMA3	70.178	2.504	0.427	5.857	4.73E-09	8.45E-08
ANXA1	12.138	2.491	0.995	2.502	1.23E-02	5.05E-02
MAST1	40.841	2.490	0.570	4.371	1.23E-05	1.23E-04
ERICH3	111.174	2.489	0.378	6.589	4.42E-11	1.04E-09
CAV2	48.647	2.488	0.523	4.758	1.95E-06	2.32E-05
LRRC46	16.463	2.482	0.892	2.783	5.38E-03	2.57E-02
IGFBP4	220.883	2.481	0.255	9.724	2.39E-22	1.59E-20
RUBCNL	941.084	2.477	0.141	17.530	8.44E-69	4.01E-66
SIRPA	11.249	2.477	1.107	2.238	2.52E-02	9.00E-02
MAP2K4P1	18.208	2.475	0.842	2.941	3.28E-03	1.69E-02
ABHD8	110.767	2.475	0.347	7.125	1.04E-12	2.97E-11
BCAN-AS1	43.752	2.467	0.531	4.644	3.43E-06	3.88E-05
TBC1D8B	232.724	2.464	0.243	10.132	4.00E-24	3.03E-22
GFI1	181.552	2.460	0.271	9.088	1.01E-19	5.32E-18
PALLD	238.809	2.459	0.248	9.936	2.90E-23	2.13E-21
LINC01531	96.225	2.452	0.384	6.390	1.66E-10	3.59E-09
RP11-385F5.5	13.916	2.452	0.983	2.494	1.26E-02	5.15E-02
FMO5	20.774	2.451	0.811	3.022	2.51E-03	1.35E-02
GZMM	97.908	2.449	0.406	6.035	1.59E-09	3.06E-08
APOL1	484.732	2.448	0.185	13.266	3.67E-40	6.44E-38
PLEKHN1	26.285	2.447	0.709	3.450	5.61E-04	3.74E-03
SYTL2	30.368	2.431	0.635	3.825	1.31E-04	1.02E-03
IFI6	191.029	2.427	0.283	8.571	1.03E-17	4.73E-16
SIGIRR	44.353	2.426	0.535	4.539	5.66E-06	6.12E-05
DHX58	218.483	2.424	0.251	9.641	5.36E-22	3.42E-20
TNK2-AS1	22.000	2.422	0.739	3.277	1.05E-03	6.41E-03
IL4I1	1572.106	2.419	0.121	19.923	2.58E-88	1.93E-85
SLFN5	1521.298	2.417	0.125	19.330	3.02E-83	1.90E-80
RUFY4	45.297	2.414	0.527	4.584	4.56E-06	5.02E-05
CD38	29.062	2.412	0.652	3.701	2.15E-04	1.59E-03
AC092835.2	25.047	2.411	0.693	3.480	5.01E-04	3.37E-03
KCNJ11	10.211	2.408	1.078	2.234	2.55E-02	9.09E-02
TBX6	37.563	2.406	0.583	4.129	3.65E-05	3.25E-04
DLX4	13.216	2.398	0.973	2.464	1.37E-02	5.51E-02

TBC1D10C	408.109	2.385	0.199	11.992	3.90E-33	4.66E-31
MED12L	72.455	2.375	0.424	5.602	2.12E-08	3.50E-07
BVES	121.731	2.364	0.324	7.290	3.10E-13	9.29E-12
LINC00461	38.683	2.353	0.560	4.202	2.65E-05	2.44E-04
MAP1B	14.762	2.344	0.925	2.535	1.13E-02	4.70E-02
GBP3	35.464	2.338	0.581	4.024	5.72E-05	4.90E-04
RP11-61G19.1	22.360	2.337	0.745	3.139	1.70E-03	9.74E-03
COL23A1	16.373	2.336	0.856	2.729	6.35E-03	2.95E-02
MAP3K21	291.649	2.336	0.227	10.271	9.49E-25	7.40E-23
PCDHGA10	14.604	2.331	0.909	2.565	1.03E-02	4.39E-02
RP11-83M8.1	14.534	2.321	0.910	2.550	1.08E-02	4.54E-02
RP11-404F10.6	27.921	2.320	0.664	3.492	4.79E-04	3.25E-03
SPINK2	29.870	2.315	0.633	3.660	2.53E-04	1.83E-03
NMB	14.030	2.314	0.929	2.491	1.27E-02	5.18E-02
ACTL10	35.098	2.313	0.627	3.691	2.24E-04	1.65E-03
ID1	19.860	2.310	0.783	2.951	3.17E-03	1.64E-02
GRIP1	58.744	2.304	0.456	5.047	4.48E-07	6.00E-06
ACVR1	44.552	2.294	0.522	4.399	1.09E-05	1.10E-04
IGFBP7	24.091	2.291	0.707	3.239	1.20E-03	7.21E-03
GPR82	19.109	2.290	0.789	2.901	3.71E-03	1.89E-02
XK	26.906	2.281	0.684	3.333	8.60E-04	5.41E-03
RAVER2	126.635	2.274	0.333	6.828	8.61E-12	2.21E-10
RP11-11N9.4	88.606	2.265	0.372	6.083	1.18E-09	2.30E-08
HCST	177.744	2.260	0.271	8.351	6.75E-17	2.90E-15
ADAM23	247.009	2.258	0.233	9.687	3.44E-22	2.24E-20
MINDY1	242.567	2.258	0.240	9.392	5.88E-21	3.50E-19
PLAUR	15.441	2.254	0.882	2.554	1.06E-02	4.50E-02
PAPLN	76.591	2.251	0.431	5.220	1.79E-07	2.58E-06
RTL3	12.857	2.249	0.971	2.315	2.06E-02	7.66E-02
RP11-763F8.1	14.482	2.246	0.927	2.421	1.55E-02	6.06E-02
STK39	18.821	2.237	0.797	2.808	4.98E-03	2.40E-02
NT5C1A	42.036	2.236	0.536	4.172	3.02E-05	2.75E-04
LINC01096	25.344	2.229	0.718	3.105	1.90E-03	1.07E-02
GGT4P	167.886	2.227	0.285	7.802	6.08E-15	2.19E-13
FOSB	41.341	2.221	0.540	4.112	3.92E-05	3.47E-04
AC104024.1	50.730	2.220	0.494	4.492	7.06E-06	7.46E-05
SPATA9	21.528	2.196	0.748	2.936	3.33E-03	1.72E-02
CABP4	19.181	2.195	0.779	2.816	4.86E-03	2.35E-02
AC010149.4	13.811	2.194	0.925	2.371	1.77E-02	6.76E-02
OSR2	30.788	2.189	0.617	3.549	3.87E-04	2.68E-03
AHNAK	2330.995	2.186	0.109	20.000	5.53E-89	4.31E-86
ZNF879	37.714	2.184	0.564	3.875	1.06E-04	8.48E-04
PCDHGC3	124.786	2.183	0.323	6.753	1.45E-11	3.61E-10
HES4	25.839	2.180	0.676	3.224	1.26E-03	7.54E-03
FILIP1L	19.037	2.178	0.798	2.731	6.32E-03	2.94E-02
ADGRG6	46.492	2.177	0.510	4.265	2.00E-05	1.89E-04
TUBB6	569.593	2.170	0.177	12.248	1.71E-34	2.21E-32
TNFRSF4	87.266	2.168	0.386	5.624	1.87E-08	3.10E-07
PPP1R13L	261.629	2.168	0.227	9.536	1.49E-21	9.25E-20
SCN4A	52.070	2.166	0.479	4.521	6.14E-06	6.59E-05
SPART	746.976	2.162	0.150	14.451	2.49E-47	5.77E-45
ODF3B	63.321	2.159	0.458	4.711	2.47E-06	2.87E-05
FAM167A	161.458	2.149	0.280	7.679	1.60E-14	5.53E-13
CFAP45	17.768	2.142	0.811	2.641	8.28E-03	3.67E-02
HDAC9	291.446	2.141	0.216	9.935	2.94E-23	2.14E-21
TESMIN	90.471	2.138	0.367	5.820	5.90E-09	1.04E-07
DNAJC12	27.833	2.136	0.656	3.258	1.12E-03	6.80E-03
PRDM8	28.652	2.127	0.636	3.342	8.33E-04	5.26E-03

PTK6	30.407	2.126	0.622	3.419	6.28E-04	4.12E-03
TCN2	19.499	2.121	0.774	2.741	6.12E-03	2.86E-02
RP11-960L18.1	43.360	2.118	0.521	4.063	4.85E-05	4.22E-04
TUBA8	26.448	2.109	0.688	3.065	2.18E-03	1.20E-02
GAS2	65.802	2.104	0.431	4.880	1.06E-06	1.33E-05
RP11-61J19.5	40.841	2.102	0.540	3.894	9.88E-05	7.94E-04
PSTPIP1	121.355	2.101	0.319	6.581	4.67E-11	1.09E-09
ZNF396	32.920	2.101	0.611	3.441	5.80E-04	3.85E-03
PRKD3	1219.946	2.101	0.128	16.401	1.88E-60	7.35E-58
CARD11	856.992	2.099	0.145	14.483	1.54E-47	3.66E-45
E2F3P2	23.235	2.098	0.718	2.924	3.45E-03	1.77E-02
RP11-203B7.2	22.624	2.097	0.728	2.882	3.95E-03	1.98E-02
SLC4A4	15.666	2.097	0.854	2.456	1.41E-02	5.61E-02
GPER1	679.818	2.096	0.158	13.246	4.78E-40	8.24E-38
CCNB3	19.851	2.090	0.762	2.743	6.08E-03	2.84E-02
LINC01134	55.904	2.088	0.468	4.461	8.17E-06	8.51E-05
ACSL4	1714.697	2.088	0.118	17.729	2.50E-70	1.28E-67
TTC39C-AS1	25.906	2.085	0.671	3.107	1.89E-03	1.07E-02
SLC37A2	383.534	2.081	0.209	9.978	1.90E-23	1.41E-21
NIBAN3	78.652	2.080	0.390	5.327	9.96E-08	1.49E-06
OR5B21	12.916	2.079	0.945	2.200	2.78E-02	9.74E-02
ISG20	678.746	2.075	0.166	12.501	7.39E-36	1.02E-33
LGALS9	312.849	2.075	0.216	9.623	6.40E-22	4.04E-20
ZNF43	25.660	2.074	0.674	3.077	2.09E-03	1.16E-02
IL12A	30.984	2.074	0.613	3.383	7.18E-04	4.62E-03
EML4-AS1	22.100	2.073	0.756	2.741	6.13E-03	2.86E-02
ARRB1	25.206	2.063	0.682	3.024	2.49E-03	1.34E-02
SOWAHD	44.385	2.050	0.521	3.932	8.44E-05	6.91E-04
PRICKLE1	47.579	2.047	0.507	4.037	5.41E-05	4.66E-04
IL6R	23.535	2.044	0.709	2.883	3.94E-03	1.98E-02
MYO1F	208.534	2.043	0.251	8.153	3.55E-16	1.41E-14
ADGRL2	30.011	2.035	0.616	3.301	9.62E-04	5.95E-03
EEPD1	83.754	2.029	0.375	5.406	6.43E-08	9.86E-07
ZNF426	78.657	2.024	0.393	5.146	2.65E-07	3.70E-06
PINLYP	14.234	2.024	0.917	2.208	2.72E-02	9.59E-02
NRIP1	1139.290	2.015	0.142	14.201	9.08E-46	1.92E-43
SYNGR3	140.417	2.014	0.300	6.709	1.96E-11	4.78E-10
HELZ2	1445.754	2.014	0.153	13.203	8.44E-40	1.42E-37
DDR2	255.003	2.011	0.230	8.744	2.26E-18	1.08E-16
P2RX7	210.003	2.004	0.247	8.129	4.32E-16	1.69E-14
RP11-327F22.6	14.753	2.002	0.871	2.298	2.15E-02	7.93E-02
KLF9	92.088	2.000	0.366	5.471	4.47E-08	7.00E-07
RIC3	87.439	-2.002	0.365	-5.490	4.03E-08	6.36E-07
ENTHD1	24.574	-2.008	0.672	-2.986	2.83E-03	1.49E-02
GNA15	61.719	-2.008	0.432	-4.644	3.41E-06	3.86E-05
RP11-512N21.1	113.489	-2.008	0.334	-6.016	1.79E-09	3.40E-08
RBM44	18.371	-2.018	0.777	-2.597	9.41E-03	4.06E-02
AC073043.1	70.046	-2.019	0.410	-4.923	8.54E-07	1.09E-05
EML6	61.804	-2.022	0.438	-4.615	3.93E-06	4.39E-05
RP11-87E22.2	135.576	-2.026	0.303	-6.681	2.38E-11	5.76E-10
C20orf194	170.441	-2.033	0.280	-7.269	3.63E-13	1.08E-11
CCDC136	188.150	-2.039	0.258	-7.901	2.76E-15	1.02E-13
FLACC1	29.329	-2.041	0.669	-3.051	2.28E-03	1.25E-02
CTD-2651B20.3	18.249	-2.043	0.785	-2.601	9.29E-03	4.02E-02
PCDH15	17.948	-2.045	0.810	-2.524	1.16E-02	4.80E-02
CTNND2	39.714	-2.045	0.550	-3.716	2.02E-04	1.51E-03
PLCG1-AS1	83.299	-2.046	0.374	-5.469	4.52E-08	7.08E-07
TTLL3	667.552	-2.049	0.157	-13.049	6.43E-39	1.03E-36

LGMNP1	22.718	-2.051	0.712	-2.881	3.97E-03	1.99E-02
OR5H2	156.112	-2.053	0.295	-6.952	3.61E-12	9.66E-11
RP11-386M24.5	20.429	-2.056	0.769	-2.672	7.54E-03	3.39E-02
RBM20	70.705	-2.056	0.406	-5.059	4.22E-07	5.71E-06
INSIG1	5596.933	-2.056	0.105	-19.561	3.35E-85	2.25E-82
ZBTB46	85.148	-2.058	0.381	-5.406	6.43E-08	9.86E-07
ZG16B	16.974	-2.063	0.820	-2.516	1.19E-02	4.89E-02
CORO2A	76.053	-2.068	0.394	-5.245	1.56E-07	2.26E-06
CTD-2017C7.2	36.481	-2.070	0.557	-3.717	2.02E-04	1.51E-03
PTK7	132.173	-2.081	0.317	-6.562	5.30E-11	1.23E-09
PTPRM	49.068	-2.081	0.487	-4.272	1.94E-05	1.84E-04
OR5K3	52.882	-2.084	0.496	-4.200	2.66E-05	2.46E-04
ATAD3C	106.632	-2.084	0.336	-6.200	5.65E-10	1.14E-08
HNRNPA1P39	13.616	-2.087	0.904	-2.310	2.09E-02	7.74E-02
GRIN2C	76.398	-2.098	0.414	-5.073	3.91E-07	5.31E-06
RP11-164H5.1	27.319	-2.115	0.714	-2.964	3.04E-03	1.59E-02
RP11-383G6.3	13.325	-2.116	0.915	-2.314	2.07E-02	7.68E-02
ASAP3	12.282	-2.118	0.961	-2.203	2.76E-02	9.68E-02
RP11-309L24.10	13.833	-2.124	0.913	-2.325	2.01E-02	7.49E-02
RP5-981O7.2	28.250	-2.136	0.655	-3.262	1.11E-03	6.71E-03
RP11-216B13.1	16.100	-2.140	0.833	-2.568	1.02E-02	4.37E-02
GRHL1	50.117	-2.140	0.546	-3.923	8.76E-05	7.12E-04
AC024084.1	85.770	-2.144	0.384	-5.583	2.36E-08	3.86E-07
LHX2	1411.422	-2.145	0.126	-17.007	7.24E-65	3.13E-62
RP11-381K20.5	42.354	-2.150	0.525	-4.095	4.21E-05	3.70E-04
KCNN2	236.748	-2.152	0.239	-8.997	2.32E-19	1.22E-17
CTD-2192J16.21	18.533	-2.153	0.863	-2.493	1.27E-02	5.15E-02
BHLHE41	147.545	-2.159	0.294	-7.355	1.91E-13	5.84E-12
RP11-1070N10.5	93.015	-2.160	0.358	-6.026	1.68E-09	3.20E-08
RHOXF1	14.200	-2.170	0.906	-2.396	1.66E-02	6.41E-02
RP11-554A11.11	1037.511	-2.175	0.141	-15.452	7.36E-54	2.24E-51
PLEKHG1	177.006	-2.206	0.268	-8.232	1.85E-16	7.44E-15
AC002044.3	12.910	-2.207	0.937	-2.356	1.85E-02	7.00E-02
GNAO1	99.908	-2.211	0.349	-6.338	2.33E-10	4.95E-09
CKB	69.438	-2.218	0.413	-5.370	7.87E-08	1.19E-06
SPARC	1017.941	-2.218	0.147	-15.106	1.48E-51	4.17E-49
PIP5KL1	79.221	-2.221	0.394	-5.639	1.71E-08	2.86E-07
RNY1P11	15.487	-2.255	0.865	-2.606	9.16E-03	3.98E-02
GATA4	12.256	-2.275	0.971	-2.343	1.91E-02	7.20E-02
RP11-165M1.2	26.979	-2.283	0.666	-3.426	6.13E-04	4.04E-03
FABP6	19.758	-2.294	0.796	-2.881	3.97E-03	1.99E-02
TDRD12	115.978	-2.299	0.328	-7.011	2.36E-12	6.54E-11
RP11-85O21.2	14.514	-2.303	0.962	-2.395	1.66E-02	6.43E-02
CBR3-AS1	23.859	-2.305	0.717	-3.215	1.31E-03	7.76E-03
MFGE8	128.780	-2.306	0.318	-7.254	4.04E-13	1.20E-11
GPR176	12.452	-2.313	1.019	-2.270	2.32E-02	8.40E-02
OR5K1	54.966	-2.314	0.475	-4.869	1.12E-06	1.39E-05
PDZD2	103.240	-2.315	0.347	-6.672	2.52E-11	6.06E-10
AASS	510.702	-2.334	0.177	-13.177	1.19E-39	1.98E-37
MPP7	13.444	-2.340	0.924	-2.531	1.14E-02	4.74E-02
EMID1	545.336	-2.343	0.196	-11.927	8.54E-33	1.00E-30
TLN2	247.728	-2.349	0.239	-9.813	9.87E-23	6.87E-21
RP11-141M1.3	25.120	-2.350	0.698	-3.367	7.60E-04	4.86E-03
CDC42BPA	21.173	-2.355	0.737	-3.195	1.40E-03	8.21E-03
ITM2B	718.073	-2.361	0.157	-15.023	5.16E-51	1.36E-48
ARHGAP27	15.222	-2.363	0.927	-2.549	1.08E-02	4.55E-02
LINC01091	23.346	-2.383	0.731	-3.261	1.11E-03	6.72E-03
FRY	520.752	-2.393	0.181	-13.214	7.28E-40	1.24E-37

ANK1	105.809	-2.394	0.342	-6.995	2.66E-12	7.28E-11
RP11-1430O6.2	18.160	-2.397	0.813	-2.947	3.21E-03	1.66E-02
RP11-507K2.6	120.723	-2.402	0.321	-7.490	6.90E-14	2.24E-12
FAM13A	372.084	-2.411	0.221	-10.884	1.38E-27	1.25E-25
LSM14A	42.827	-2.430	1.108	-2.193	2.83E-02	9.87E-02
TLL2	209.852	-2.436	0.286	-8.530	1.47E-17	6.66E-16
RP11-139E19.3	14.128	-2.455	0.915	-2.683	7.30E-03	3.30E-02
LRRC75A	11.239	-2.455	1.011	-2.429	1.51E-02	5.96E-02
AC002044.1	13.720	-2.459	0.986	-2.494	1.26E-02	5.15E-02
MYEOV	18.932	-2.464	0.804	-3.067	2.16E-03	1.19E-02
LINC02381	41.617	-2.492	0.545	-4.574	4.80E-06	5.25E-05
MAGED1	146.789	-2.495	0.301	-8.290	1.13E-16	4.72E-15
FRMPD3	136.019	-2.501	0.320	-7.816	5.45E-15	1.97E-13
SMIM38	679.229	-2.501	0.390	-6.408	1.48E-10	3.24E-09
PLPP3	14.934	-2.511	0.905	-2.775	5.53E-03	2.62E-02
BTBD7	22.608	-2.517	0.799	-3.152	1.62E-03	9.38E-03
SYNRG	45.315	-2.517	0.518	-4.862	1.16E-06	1.44E-05
TSPAN12	1278.726	-2.525	0.132	-19.196	3.99E-82	2.43E-79
LTBP2	157.512	-2.528	0.296	-8.553	1.20E-17	5.50E-16
NGB	26.394	-2.534	0.697	-3.636	2.76E-04	1.98E-03
RP1-65P5.3	11.332	-2.545	1.070	-2.378	1.74E-02	6.68E-02
GPC5	427.042	-2.545	0.197	-12.948	2.40E-38	3.71E-36
RP11-637C24.5	20.605	-2.569	0.756	-3.397	6.82E-04	4.43E-03
CLTCL1	78.086	-2.580	0.404	-6.390	1.66E-10	3.59E-09
GATA3	19.576	-2.582	0.850	-3.038	2.39E-03	1.29E-02
TACR1	25.306	-2.605	0.687	-3.790	1.51E-04	1.16E-03
RNY3	62.979	-2.612	0.531	-4.915	8.90E-07	1.13E-05
PMEPA1	20.881	-2.615	0.767	-3.407	6.56E-04	4.28E-03
LINC01977	44.232	-2.617	0.531	-4.928	8.31E-07	1.06E-05
STRIP2	258.025	-2.628	0.235	-11.165	6.02E-29	5.78E-27
CDK18	29.790	-2.631	0.652	-4.036	5.44E-05	4.68E-04
AC105760.3	11.137	-2.644	1.027	-2.576	1.00E-02	4.28E-02
NCR2	194.652	-2.646	0.268	-9.868	5.71E-23	4.06E-21
SERPINA9	162.720	-2.648	0.287	-9.215	3.12E-20	1.73E-18
WNT5A	13.460	-2.660	0.937	-2.838	4.54E-03	2.23E-02
ZNF462	731.336	-2.662	0.156	-17.090	1.75E-65	7.74E-63
DLX1	11.575	-2.664	1.073	-2.482	1.31E-02	5.28E-02
NOL4L	530.763	-2.665	0.183	-14.590	3.24E-48	7.79E-46
INA	336.129	-2.667	0.219	-12.193	3.37E-34	4.30E-32
NEUROG2	221.589	-2.671	0.250	-10.693	1.10E-26	9.41E-25
CUTALP	422.048	-2.673	0.213	-12.556	3.69E-36	5.17E-34
LINC02832	24.674	-2.699	0.713	-3.788	1.52E-04	1.17E-03
LMO2	9.237	-2.703	1.150	-2.351	1.87E-02	7.07E-02
RP11-1110F20.1	22.425	-2.712	0.733	-3.702	2.14E-04	1.58E-03
CHDH	153.687	-2.715	0.322	-8.421	3.75E-17	1.62E-15
ULBP1	17.121	-2.719	0.846	-3.214	1.31E-03	7.78E-03
RP11-487A2.1	48.161	-2.722	0.514	-5.297	1.17E-07	1.73E-06
CTC-303L1.1	7.866	-2.739	1.236	-2.216	2.67E-02	9.43E-02
LSAMP	91.984	-2.767	0.374	-7.399	1.37E-13	4.29E-12
ANKRD20A11P	193.502	-2.778	0.268	-10.358	3.83E-25	3.05E-23
SPRY4	16.265	-2.797	0.864	-3.236	1.21E-03	7.26E-03
DMRTA2	125.493	-2.807	0.332	-8.462	2.63E-17	1.16E-15
GTPBP6	23.145	-2.816	0.929	-3.032	2.43E-03	1.31E-02
CTA-984G1.5	12.442	-2.829	0.985	-2.871	4.09E-03	2.04E-02
LINC02470	10.630	-2.844	1.142	-2.491	1.27E-02	5.17E-02
PLXNA4	18.920	-2.856	0.868	-3.290	1.00E-03	6.17E-03
JPH4	49.025	-2.869	0.527	-5.444	5.22E-08	8.11E-07
AMN	85.297	-2.877	0.395	-7.276	3.43E-13	1.02E-11

RP5-850O15.3	8.656	-2.910	1.194	-2.437	1.48E-02	5.85E-02
TCF7L2	13.068	-2.924	1.022	-2.863	4.20E-03	2.09E-02
AKAP6	312.380	-2.936	0.221	-13.280	3.01E-40	5.33E-38
DLL4	45.974	-2.937	0.584	-5.031	4.88E-07	6.47E-06
RP11-681B3.4	15.577	-2.943	1.021	-2.884	3.93E-03	1.97E-02
ACBD7	72.231	-2.966	0.429	-6.910	4.86E-12	1.28E-10
PYGL	332.702	-2.969	0.220	-13.468	2.42E-41	4.53E-39
LRRC37A	17.336	-2.988	0.957	-3.123	1.79E-03	1.02E-02
FAM182A	8.275	-2.996	1.271	-2.357	1.84E-02	6.98E-02
RN7SL30P	8.293	-2.996	1.263	-2.372	1.77E-02	6.76E-02
CFAP70	266.044	-2.998	0.235	-12.745	3.32E-37	4.89E-35
OTP	162.692	-3.012	0.306	-9.843	7.37E-23	5.20E-21
ANKRD20A8P	11.186	-3.015	1.099	-2.745	6.06E-03	2.83E-02
FN1	364.611	-3.024	0.206	-14.676	9.17E-49	2.26E-46
S100A9	12.340	-3.055	1.008	-3.029	2.45E-03	1.32E-02
U91319.1	14.318	-3.058	0.936	-3.268	1.08E-03	6.58E-03
SLC14A1	49.580	-3.061	0.522	-5.863	4.55E-09	8.15E-08
RP11-305M3.6	13.181	-3.068	1.029	-2.980	2.88E-03	1.52E-02
RP11-883G10.1	21.074	-3.078	0.789	-3.903	9.49E-05	7.67E-04
YTHDC1	49.567	-3.080	0.581	-5.299	1.16E-07	1.71E-06
EML5	34.788	-3.094	0.638	-4.852	1.22E-06	1.51E-05
FRAS1	274.068	-3.109	0.240	-12.954	2.23E-38	3.48E-36
SNX18P13	21.041	-3.125	0.787	-3.970	7.20E-05	5.99E-04
RP4-584D14.7	14.083	-3.126	1.000	-3.126	1.77E-03	1.01E-02
RP11-554E23.4	18.039	-3.127	0.895	-3.495	4.73E-04	3.21E-03
CD200	415.957	-3.139	0.199	-15.764	5.49E-56	1.85E-53
CLDN16	12.197	-3.141	1.073	-2.929	3.41E-03	1.75E-02
GS1-146J4.4	6.246	-3.145	1.435	-2.191	2.84E-02	9.91E-02
HACD1	98.478	-3.167	0.387	-8.187	2.68E-16	1.07E-14
RP11-85O21.4	77.743	-3.170	0.424	-7.467	8.19E-14	2.64E-12
JAM3	67.217	-3.177	0.459	-6.921	4.48E-12	1.18E-10
CTB-92J24.2	7.382	-3.178	1.341	-2.370	1.78E-02	6.79E-02
HTR2B	29.890	-3.183	0.660	-4.826	1.39E-06	1.69E-05
CTC-359D24.5	11.631	-3.192	1.092	-2.923	3.47E-03	1.78E-02
ITGA5	6.540	-3.209	1.408	-2.280	2.26E-02	8.24E-02
RNY3P1	6.595	-3.222	1.414	-2.279	2.27E-02	8.25E-02
AC002519.8	7.694	-3.235	1.319	-2.452	1.42E-02	5.66E-02
TNNT3	8.223	-3.240	1.272	-2.547	1.09E-02	4.58E-02
DAB2IP	113.239	-3.243	0.389	-8.335	7.72E-17	3.30E-15
LINC02649	11.010	-3.248	1.127	-2.882	3.96E-03	1.99E-02
GPC5-IT1	11.796	-3.270	1.075	-3.043	2.34E-03	1.27E-02
ANKRD20A5P	115.902	-3.283	0.350	-9.375	6.91E-21	4.11E-19
RNU6-367P	9.708	-3.303	1.181	-2.796	5.17E-03	2.48E-02
CES4A	24.126	-3.307	0.748	-4.419	9.91E-06	1.01E-04
ZNF382	152.845	-3.307	0.307	-10.771	4.70E-27	4.13E-25
CALHM2	127.588	-3.317	0.338	-9.805	1.07E-22	7.39E-21
MAPK4	29.994	-3.338	0.731	-4.565	5.00E-06	5.46E-05
TRIM55	197.728	-3.340	0.276	-12.096	1.10E-33	1.37E-31
CYP4F29P	39.393	-3.360	0.593	-5.664	1.48E-08	2.49E-07
CTD-2207P18.2	6.176	-3.364	1.452	-2.317	2.05E-02	7.62E-02
GPRIN3	6.195	-3.367	1.447	-2.327	2.00E-02	7.46E-02
MTUS2	95.756	-3.374	0.383	-8.802	1.35E-18	6.67E-17
ZNF788P	20.874	-3.409	0.851	-4.005	6.20E-05	5.26E-04
OR2V2	52.099	-3.416	0.520	-6.565	5.21E-11	1.21E-09
RP11-346C20.4	5.390	-3.444	1.548	-2.224	2.61E-02	9.28E-02
PLA2G4E	8.117	-3.493	1.317	-2.652	8.00E-03	3.56E-02
RNF150	47.337	-3.505	1.454	-2.411	1.59E-02	6.21E-02
RP11-472K17.3	164.698	-3.550	0.322	-11.013	3.31E-28	3.09E-26

DYNLT3	214.678	-3.582	0.278	-12.887	5.33E-38	8.05E-36
RN7SL751P	12.940	-3.600	1.043	-3.451	5.58E-04	3.73E-03
ADGRL3	25.393	-3.606	0.794	-4.541	5.60E-06	6.07E-05
COL5A3	114.221	-3.607	0.367	-9.824	8.89E-23	6.23E-21
TNFRSF9	154.471	-3.648	0.317	-11.508	1.20E-30	1.31E-28
MMP15	30.952	-3.670	0.732	-5.016	5.27E-07	6.98E-06
RP11-48G14.2	5.007	-3.676	1.596	-2.303	2.13E-02	7.85E-02
CCND2	2275.108	-3.691	0.129	-28.543	3.39E-179	6.61E-176
RP11-5N11.2	9.426	-3.726	1.239	-3.007	2.64E-03	1.41E-02
PDGFRB	21.221	-3.798	0.867	-4.380	1.19E-05	1.19E-04
RP11-115N4.1	5.743	-3.880	1.538	-2.523	1.16E-02	4.81E-02
PSD3	18.926	-3.887	0.885	-4.394	1.11E-05	1.12E-04
RP11-95C14.1	32.771	-3.896	0.684	-5.695	1.24E-08	2.10E-07
ROBO1	5109.099	-3.965	0.105	-37.903	0.00E+00	0.00E+00
PLD1	13.284	-3.994	1.085	-3.683	2.30E-04	1.69E-03
TNK1	12.691	-4.004	1.115	-3.591	3.29E-04	2.31E-03
GSDMD	4.680	-4.017	1.669	-2.407	1.61E-02	6.26E-02
EPHA3	1227.835	-4.049	0.149	-27.196	7.18E-163	1.17E-159
ADSS1	81.113	-4.117	1.588	-2.593	9.51E-03	4.10E-02
RP11-334L9.2	28.217	-4.120	0.744	-5.537	3.08E-08	4.94E-07
KLHL14	19.904	-4.125	0.888	-4.643	3.43E-06	3.88E-05
USH1G	6.883	-4.139	1.436	-2.882	3.95E-03	1.98E-02
IL17RB	122.855	-4.141	0.367	-11.270	1.85E-29	1.81E-27
LINC02298	14.106	-4.186	1.073	-3.901	9.59E-05	7.73E-04
MRO	11.214	-4.207	1.183	-3.555	3.78E-04	2.62E-03
ACKR1	49.057	-4.218	1.106	-3.815	1.36E-04	1.06E-03
ZNRF2P2	11.343	-4.222	1.184	-3.567	3.61E-04	2.52E-03
RPL23P4	9.324	-4.229	1.275	-3.318	9.08E-04	5.66E-03
RP11-165N12.2	26.722	-4.233	0.821	-5.156	2.53E-07	3.54E-06
NLGN4X	12.364	-4.247	1.159	-3.664	2.48E-04	1.80E-03
OR2V1	250.593	-4.352	0.276	-15.771	4.96E-56	1.70E-53
MC4R	8.299	-4.410	1.377	-3.204	1.36E-03	8.02E-03
CCL19	4.317	-4.526	1.779	-2.544	1.10E-02	4.60E-02
RP11-542K23.7	4.556	-4.608	1.759	-2.620	8.79E-03	3.85E-02
CHST15	23.631	-4.612	0.885	-5.208	1.91E-07	2.72E-06
RP11-305F5.2	4.592	-4.620	1.746	-2.646	8.15E-03	3.62E-02
MYO18B	21.898	-4.664	0.916	-5.091	3.57E-07	4.86E-06
RP11-88I21.3	7.236	-4.665	1.481	-3.150	1.63E-03	9.42E-03
NID1	74.786	-4.737	0.507	-9.340	9.65E-21	5.66E-19
NCS1	328.985	-4.760	0.274	-17.359	1.68E-67	7.82E-65
RP11-214O1.2	38.290	-4.850	0.743	-6.530	6.60E-11	1.51E-09
RP11-795H16.3	12.527	-5.003	1.207	-4.144	3.41E-05	3.06E-04
FZD8	94.998	-5.026	0.466	-10.775	4.50E-27	3.97E-25
MTRNR2L12	24.799	-5.036	1.018	-4.949	7.45E-07	9.57E-06
HS3ST3B1	394.230	-5.051	0.247	-20.437	7.92E-93	6.71E-90
SHC3	104.845	-5.053	0.446	-11.322	1.02E-29	1.06E-27
ZDHHC22	69.845	-5.077	0.546	-9.293	1.49E-20	8.61E-19
STARD4-AS1	369.774	-5.219	0.266	-19.658	4.96E-86	3.45E-83
RIMBP2	606.990	-5.281	0.214	-24.674	2.03E-134	2.47E-131
RP11-463C8.7	7.222	-5.304	1.550	-3.422	6.22E-04	4.08E-03
AP000439.1	14.707	-5.375	1.238	-4.341	1.42E-05	1.39E-04
RP11-588P7.1	7.718	-5.404	1.534	-3.524	4.26E-04	2.92E-03
RP11-29A19.3	3.971	-5.486	2.020	-2.717	6.60E-03	3.04E-02
RP11-117L5.3	22.617	-5.486	0.994	-5.520	3.40E-08	5.42E-07
NPEPPSP1	23.862	-5.499	2.231	-2.464	1.37E-02	5.51E-02
RP11-82L18.2	70.425	-5.574	0.606	-9.190	3.92E-20	2.13E-18
NDUFB10P2	4.247	-5.586	1.981	-2.820	4.81E-03	2.33E-02
CTD-2367A17.1	8.784	-5.597	1.487	-3.765	1.66E-04	1.27E-03

RP11-117L5.4	14.223	-5.653	1.230	-4.596	4.31E-06	4.77E-05
AP002856.4	4.468	-5.662	1.972	-2.871	4.09E-03	2.04E-02
RP5-1097P24.1	4.578	-5.695	1.955	-2.914	3.57E-03	1.82E-02
DISC1FP1	37.805	-5.769	0.851	-6.776	1.23E-11	3.10E-10
AC114765.1	5.075	-5.851	1.894	-3.089	2.01E-03	1.12E-02
LINC02139	16.447	-5.864	1.195	-4.905	9.32E-07	1.18E-05
LINC00882	327.985	-5.883	0.325	-18.103	2.99E-73	1.77E-70
PHF21B	72.225	-6.176	0.663	-9.316	1.21E-20	7.08E-19
RP11-369E15.3	6.361	-6.188	1.801	-3.437	5.89E-04	3.90E-03
KCNK5	180.527	-6.262	1.046	-5.989	2.11E-09	3.95E-08
PRSS51	88.250	-6.312	0.640	-9.862	6.09E-23	4.32E-21
ADARB2	122.736	-6.482	0.557	-11.632	2.82E-31	3.16E-29
TMEM178B	293.391	-6.565	0.367	-17.865	2.20E-71	1.22E-68
RP11-29A19.2	8.329	-6.584	1.715	-3.840	1.23E-04	9.67E-04
NRXN3	232.955	-6.892	0.447	-15.411	1.39E-53	4.11E-51
RP11-280F2.3	10.351	-6.907	1.647	-4.194	2.74E-05	2.51E-04
ZNF30	21.728	-6.938	1.275	-5.440	5.32E-08	8.27E-07
RP11-214O1.3	24.082	-7.089	1.251	-5.666	1.46E-08	2.47E-07
RP11-425A6.6	12.024	-7.126	1.611	-4.423	9.75E-06	1.00E-04
C14orf132	13.973	-7.344	1.588	-4.625	3.74E-06	4.20E-05
ANO5	286.130	-7.369	0.899	-8.194	2.53E-16	1.01E-14
LINC02137	65.717	-7.385	0.895	-8.252	1.56E-16	6.38E-15
GNAQ	40.335	-7.843	1.191	-6.585	4.54E-11	1.06E-09
RP4-753M9.1	22.118	-8.017	1.506	-5.324	1.01E-07	1.51E-06
RP11-566H8.3	23.791	-8.124	1.503	-5.406	6.45E-08	9.87E-07
CII ATM KD Vs ATM WT						
Gene Name	baseMean	log2FoldChange	lfcSE	stat	pvalue	padj
HLA-DPB1	94.887	23.078	4.786	4.822	1.42E-06	1.48E-05
MAGI1	369.135	12.344	1.455	8.486	2.14E-17	6.87E-16
RPS18	295.993	12.027	1.457	8.256	1.51E-16	4.56E-15
TRIM48	198.689	11.454	1.462	7.833	4.77E-15	1.28E-13
ADGRF5	459.091	11.221	1.414	7.933	2.14E-15	5.89E-14
SHROOM2	456.355	11.210	1.415	7.924	2.30E-15	6.31E-14
MBOAT2	157.689	11.124	1.467	7.582	3.40E-14	8.58E-13
TRO	137.716	10.920	1.469	7.432	1.07E-13	2.57E-12
EYA1	1828.632	10.731	1.381	7.770	7.86E-15	2.06E-13
MOXD1	1517.164	10.630	0.659	16.133	1.50E-58	2.79E-56
SULF1	1188.791	10.596	0.736	14.391	5.87E-47	7.71E-45
GABRQ	579.529	10.560	1.033	10.227	1.50E-24	7.42E-23
MSR1	274.660	10.477	1.419	7.382	1.56E-13	3.66E-12
NLRP5	88.275	10.293	1.485	6.930	4.22E-12	8.50E-11
LINC01724	443.274	10.175	1.036	9.825	8.82E-23	3.92E-21
MID2	79.799	10.142	1.487	6.821	9.03E-12	1.77E-10
PTPRD	2764.042	10.008	0.402	24.867	1.69E-136	1.55E-133
RTL6	68.518	9.926	1.495	6.641	3.11E-11	5.73E-10
SCN3A	2026.402	9.912	0.455	21.804	2.15E-105	9.67E-103
PROX1	172.257	9.803	1.427	6.871	6.38E-12	1.26E-10
RORB	1672.240	9.768	0.473	20.658	8.19E-95	2.89E-92
CA8	60.123	9.730	1.499	6.491	8.54E-11	1.51E-09
EYA2	56.252	9.618	1.505	6.392	1.64E-10	2.80E-09
PI15	302.766	9.618	1.039	9.259	2.06E-20	7.83E-19
LINC02782	146.298	9.573	1.430	6.694	2.17E-11	4.07E-10
CD36	1692.523	9.525	0.437	21.807	1.99E-105	9.15E-103
CNTNAP3	51.683	9.496	1.510	6.290	3.18E-10	5.30E-09
FMN2	515.565	9.396	0.744	12.634	1.38E-36	1.20E-34
LANCL1-AS1	47.395	9.373	1.514	6.190	6.02E-10	9.86E-09
SYDE2	46.771	9.367	1.514	6.188	6.10E-10	9.98E-09

LINC02360	46.835	9.351	1.517	6.164	7.11E-10	1.15E-08
FABP4	619.369	9.341	0.668	13.991	1.77E-44	2.06E-42
F2R	242.769	9.314	1.049	8.875	6.98E-19	2.43E-17
SHC3	119.334	9.274	1.435	6.462	1.03E-10	1.81E-09
CTD-2291D10.4	42.519	9.229	1.520	6.070	1.28E-09	2.01E-08
TMEM74	113.387	9.201	1.436	6.408	1.48E-10	2.54E-09
ATRNL1	41.442	9.188	1.522	6.036	1.58E-09	2.47E-08
RCAN2	41.434	9.176	1.525	6.018	1.77E-09	2.74E-08
RP11-25K19.1	37.325	9.057	1.537	5.893	3.79E-09	5.65E-08
FAM182B	37.308	9.033	1.531	5.901	3.61E-09	5.39E-08
AC005387.3	37.462	9.032	1.532	5.895	3.75E-09	5.59E-08
RP11-19F9.2	36.711	9.008	1.532	5.879	4.13E-09	6.14E-08
BCHE	490.652	9.005	0.669	13.451	3.02E-41	3.13E-39
DPPA4	193.894	8.977	1.048	8.567	1.06E-17	3.44E-16
CTD-2272D18.1	93.813	8.941	1.446	6.185	6.22E-10	1.01E-08
LINC02555	34.449	8.921	1.537	5.803	6.51E-09	9.46E-08
MT1E	34.396	8.898	1.546	5.755	8.65E-09	1.23E-07
CD1D	181.002	8.883	1.050	8.460	2.68E-17	8.51E-16
MAP10	33.536	8.883	1.540	5.769	7.98E-09	1.14E-07
SATB2	266.680	8.853	0.859	10.308	6.45E-25	3.28E-23
RAB27B	32.821	8.852	1.542	5.742	9.36E-09	1.33E-07
CTD-2501M5.1	33.437	8.851	1.557	5.686	1.30E-08	1.82E-07
BMP4	88.156	8.839	1.444	6.120	9.36E-10	1.49E-08
COL22A1	2532.358	8.830	0.293	30.129	2.05E-199	3.92E-196
CD93	171.225	8.808	1.053	8.363	6.13E-17	1.89E-15
ADGRE4P	256.604	8.787	0.863	10.185	2.30E-24	1.13E-22
PCYT1B	84.302	8.774	1.446	6.068	1.29E-09	2.03E-08
CSPG4BP	31.492	8.765	1.561	5.615	1.96E-08	2.68E-07
ZNF835	30.161	8.735	1.550	5.635	1.75E-08	2.41E-07
ZEB2	1146.335	8.734	0.408	21.428	7.31E-102	2.95E-99
ZNF723	29.519	8.692	1.553	5.597	2.18E-08	2.95E-07
GAPT	29.592	8.684	1.558	5.574	2.49E-08	3.36E-07
GNAT3	28.261	8.654	1.562	5.541	3.00E-08	4.01E-07
MATK	76.752	8.645	1.451	5.958	2.55E-09	3.89E-08
SNX9	28.252	8.638	1.557	5.549	2.88E-08	3.86E-07
AKR1C2	76.300	8.626	1.451	5.946	2.74E-09	4.17E-08
RP11-432O12.1	27.031	8.593	1.569	5.478	4.31E-08	5.66E-07
PCDHB3	26.896	8.556	1.564	5.471	4.47E-08	5.85E-07
CCDC144A	71.891	8.534	1.452	5.876	4.20E-09	6.23E-08
ARSD	25.593	8.501	1.569	5.419	5.99E-08	7.67E-07
RNF150	69.584	8.485	1.454	5.835	5.37E-09	7.87E-08
YY1P2	24.760	8.458	1.574	5.374	7.72E-08	9.69E-07
RFLNB	598.313	8.440	0.508	16.613	5.63E-62	1.11E-59
BCL11A	372.717	8.433	1.375	6.131	8.74E-10	1.40E-08
RARB	24.390	8.408	1.578	5.328	9.92E-08	1.23E-06
SLC8A3	65.043	8.378	1.461	5.736	9.71E-09	1.37E-07
LRRN1	23.241	8.345	1.581	5.277	1.31E-07	1.59E-06
RP11-436H11.5	23.241	8.345	1.581	5.277	1.31E-07	1.59E-06
RP11-25E2.1	62.333	8.319	1.468	5.667	1.45E-08	2.02E-07
LINC02155	23.033	8.313	1.596	5.208	1.91E-07	2.28E-06
TLE1	182.125	8.307	0.869	9.555	1.24E-21	5.08E-20
RUNX2	118.829	8.273	1.065	7.771	7.76E-15	2.04E-13
PPM1E	234.976	8.257	0.755	10.933	8.03E-28	4.80E-26
AC005387.2	21.612	8.241	1.591	5.181	2.21E-07	2.61E-06
PAK3	21.377	8.233	1.591	5.174	2.29E-07	2.69E-06
CTSF	19.794	8.138	1.606	5.068	4.03E-07	4.54E-06
DPYSL3	430.613	8.133	0.541	15.027	4.89E-51	7.34E-49
USP32P1	20.256	8.133	1.608	5.056	4.27E-07	4.79E-06

TTLL7	105.928	8.113	1.069	7.588	3.25E-14	8.24E-13
SV2C	105.838	8.107	1.069	7.582	3.39E-14	8.57E-13
RP11-553L6.2	19.550	8.105	1.604	5.053	4.36E-07	4.88E-06
RP13-329D4.3	19.586	8.098	1.605	5.045	4.53E-07	5.06E-06
RP11-323C15.2	19.233	8.085	1.607	5.032	4.86E-07	5.40E-06
PTPRZ1	18.989	8.051	1.611	4.997	5.82E-07	6.41E-06
LINC00470	18.871	8.046	1.611	4.995	5.87E-07	6.47E-06
RAVER2	101.981	8.043	1.069	7.527	5.19E-14	1.29E-12
SCN8A	49.676	8.003	1.474	5.430	5.64E-08	7.26E-07
CCDC68	17.958	7.975	1.619	4.927	8.36E-07	9.02E-06
ZNF98	17.876	7.962	1.621	4.911	9.05E-07	9.72E-06
ZNF492	17.758	7.957	1.621	4.910	9.12E-07	9.77E-06
FAM71F1	94.038	7.928	1.072	7.397	1.40E-13	3.31E-12
PVR	94.038	7.928	1.072	7.397	1.40E-13	3.31E-12
PNMA2	93.825	7.926	1.077	7.359	1.85E-13	4.32E-12
BTNL9	371.201	7.906	0.550	14.384	6.54E-47	8.54E-45
RP11-13N12.1	17.161	7.905	1.628	4.856	1.20E-06	1.26E-05
CLIC5	180.745	7.870	0.762	10.333	4.98E-25	2.55E-23
NECTIN3	16.410	7.852	1.633	4.808	1.52E-06	1.58E-05
MAT1A	939.029	7.850	0.721	10.883	1.39E-27	8.11E-26
LINC01411	16.447	7.844	1.635	4.799	1.60E-06	1.65E-05
RP11-323P17.2	16.601	7.843	1.643	4.774	1.81E-06	1.86E-05
POTED	16.248	7.826	1.637	4.780	1.76E-06	1.81E-05
HOXA5	16.402	7.824	1.646	4.753	2.00E-06	2.04E-05
LINC01414	43.642	7.821	1.482	5.278	1.30E-07	1.59E-06
NCOR1P1	43.883	7.821	1.480	5.285	1.26E-07	1.53E-06
HUNK	16.049	7.806	1.640	4.760	1.94E-06	1.98E-05
BEND5	15.659	7.798	1.644	4.743	2.11E-06	2.13E-05
RP11-404O13.5	14.827	7.727	1.659	4.658	3.20E-06	3.12E-05
IL1RAPL2	40.421	7.708	1.488	5.180	2.21E-07	2.61E-06
ADCY9	39.757	7.687	1.488	5.165	2.40E-07	2.81E-06
MAGI1-IT1	14.420	7.653	1.660	4.610	4.02E-06	3.83E-05
UACA	39.065	7.650	1.493	5.125	2.98E-07	3.42E-06
RPF2P2	14.303	7.647	1.660	4.607	4.09E-06	3.89E-05
SV2B	685.563	7.629	0.373	20.474	3.65E-93	1.23E-90
SATB2-AS1	13.868	7.613	1.666	4.570	4.87E-06	4.57E-05
RP3-460G2.1	14.022	7.610	1.667	4.565	4.99E-06	4.68E-05
RP11-538D16.2	152.037	7.608	0.778	9.776	1.43E-22	6.23E-21
RP11-328I6.1	13.588	7.575	1.670	4.535	5.76E-06	5.33E-05
RP11-205M3.1	13.742	7.572	1.677	4.516	6.31E-06	5.82E-05
RP11-219A15.1	13.507	7.559	1.674	4.516	6.29E-06	5.80E-05
PRR32	13.389	7.552	1.674	4.512	6.41E-06	5.90E-05
ANKRD20A9P	13.543	7.549	1.681	4.490	7.12E-06	6.48E-05
ZNF99	13.117	7.549	1.683	4.485	7.30E-06	6.63E-05
MME	13.154	7.539	1.677	4.495	6.96E-06	6.35E-05
LINC02381	426.901	7.526	0.452	16.646	3.26E-62	6.56E-60
LIN28B	13.072	7.523	1.678	4.483	7.38E-06	6.69E-05
ABCC13	12.801	7.518	1.692	4.443	8.88E-06	7.94E-05
PPFIA4	176.966	7.511	0.716	10.486	1.00E-25	5.34E-24
NXF2	12.683	7.511	1.700	4.418	9.95E-06	8.81E-05
NECTIN2	35.057	7.500	1.500	5.001	5.71E-07	6.30E-06
ZNF208	241.257	7.478	0.591	12.643	1.22E-36	1.06E-34
RP11-107E5.3	33.899	7.443	1.506	4.943	7.68E-07	8.33E-06
PTK2	12.122	7.429	1.698	4.375	1.21E-05	1.05E-04
AC074391.1	67.162	7.426	1.096	6.777	1.23E-11	2.35E-10
KLF4	12.159	7.419	1.695	4.378	1.20E-05	1.04E-04
CTD-2015A6.2	12.114	7.390	1.705	4.335	1.46E-05	1.25E-04
LINC01249	32.520	7.387	1.504	4.911	9.07E-07	9.73E-06

SPHKAP	11.842	7.386	1.701	4.342	1.41E-05	1.21E-04
GRPEL2P1	11.761	7.368	1.703	4.327	1.51E-05	1.29E-04
NFYAP1	11.797	7.356	1.708	4.308	1.65E-05	1.39E-04
RP11-27P7.1	11.716	7.338	1.716	4.276	1.90E-05	1.59E-04
TNFRSF21	92.902	7.336	0.900	8.153	3.54E-16	1.03E-14
TCEAL2	123.035	7.319	0.779	9.393	5.82E-21	2.28E-19
RP11-82L18.2	11.517	7.311	1.722	4.245	2.18E-05	1.80E-04
ALDH1A1	3847.526	7.311	0.182	40.145	0.00E+00	0.00E+00
SERPINB7	122.393	7.309	0.780	9.370	7.23E-21	2.82E-19
BAALC	61.085	7.303	1.105	6.612	3.79E-11	6.90E-10
SEMA6B	90.405	7.300	0.902	8.096	5.66E-16	1.64E-14
PLEKHA1	11.164	7.287	1.717	4.245	2.19E-05	1.80E-04
SLC2A10	10.847	7.251	1.723	4.209	2.56E-05	2.08E-04
MTCO2P4	11.155	7.249	1.760	4.119	3.81E-05	2.97E-04
NAT8L	28.913	7.249	1.526	4.751	2.02E-06	2.06E-05
LINC00408	88.594	7.248	0.903	8.023	1.03E-15	2.93E-14
PCDHB4	10.729	7.243	1.726	4.197	2.70E-05	2.18E-04
NMBR	87.558	7.243	0.900	8.044	8.73E-16	2.48E-14
AC002383.2	10.611	7.235	1.730	4.181	2.90E-05	2.32E-04
MT1H	10.611	7.235	1.730	4.181	2.90E-05	2.32E-04
ZNF716	378.863	7.234	0.440	16.427	1.23E-60	2.40E-58
SCG2	10.648	7.223	1.728	4.180	2.91E-05	2.33E-04
MORN4	10.684	7.211	1.734	4.157	3.22E-05	2.55E-04
IGKV2OR22-4	10.684	7.211	1.734	4.157	3.22E-05	2.55E-04
ESRP1	28.462	7.199	1.520	4.736	2.18E-06	2.19E-05
ASB13	27.711	7.168	1.523	4.708	2.51E-06	2.49E-05
PCDHB6	10.132	7.156	1.741	4.111	3.95E-05	3.06E-04
NLGN4X	55.600	7.150	1.110	6.438	1.21E-10	2.09E-09
AKAP12	10.014	7.147	1.745	4.096	4.20E-05	3.24E-04
RP3-410C9.3	81.456	7.134	0.905	7.883	3.19E-15	8.66E-14
MC4R	10.051	7.134	1.745	4.088	4.34E-05	3.34E-04
LRRC3	10.051	7.134	1.745	4.088	4.34E-05	3.34E-04
PCDHB16	27.032	7.127	1.525	4.672	2.99E-06	2.93E-05
PALLD	26.915	7.123	1.526	4.669	3.03E-06	2.97E-05
SDC4	133.077	7.117	0.706	10.077	6.98E-24	3.38E-22
GS1-115G20.1	9.852	7.103	1.751	4.056	4.99E-05	3.77E-04
TEX13A	9.852	7.103	1.751	4.056	4.99E-05	3.77E-04
SVOPL	10.006	7.100	1.769	4.013	5.99E-05	4.43E-04
ATP1B2	26.830	7.091	1.527	4.643	3.44E-06	3.33E-05
TJP3	26.830	7.091	1.527	4.643	3.44E-06	3.33E-05
CFI	52.596	7.083	1.107	6.398	1.58E-10	2.70E-09
OR56A1	9.770	7.081	1.759	4.024	5.71E-05	4.25E-04
DGCR5	9.653	7.071	1.758	4.023	5.75E-05	4.28E-04
EYS	104.858	7.071	0.791	8.944	3.74E-19	1.32E-17
SLPI	25.458	7.069	1.544	4.578	4.69E-06	4.42E-05
RNVU1-23	9.381	7.066	1.769	3.994	6.49E-05	4.75E-04
TTLL7-IT1	9.535	7.062	1.759	4.016	5.92E-05	4.39E-04
CLEC12B	9.417	7.053	1.761	4.004	6.23E-05	4.58E-04
LINC02444	9.417	7.053	1.761	4.004	6.23E-05	4.58E-04
PCLO	180.331	7.051	0.600	11.746	7.44E-32	5.23E-30
RP11-622O11.6	9.571	7.049	1.767	3.989	6.64E-05	4.84E-04
AC002480.4	9.454	7.039	1.765	3.988	6.66E-05	4.85E-04
TOX	632.810	7.032	0.328	21.441	5.48E-102	2.25E-99
HOXA6	9.101	7.011	1.773	3.955	7.66E-05	5.50E-04
DSP	8.983	7.001	1.780	3.932	8.41E-05	5.99E-04
LINC02010	9.019	6.987	1.774	3.938	8.23E-05	5.87E-04
ZNF734P	8.748	6.980	1.804	3.868	1.10E-04	7.60E-04
MIR205HG	72.557	6.978	0.916	7.616	2.61E-14	6.67E-13

AC004160.4	8.938	6.962	1.780	3.912	9.15E-05	6.46E-04
ZNF722P	96.136	6.954	0.791	8.791	1.48E-18	5.05E-17
RP11-266N13.2	71.495	6.954	0.914	7.609	2.77E-14	7.06E-13
SEMG1	8.703	6.943	1.786	3.888	1.01E-04	7.06E-04
LINC00683	119.832	6.939	0.723	9.602	7.83E-22	3.27E-20
RP11-733O18.1	95.105	6.939	0.792	8.766	1.85E-18	6.26E-17
KRT8P4	8.739	6.927	1.788	3.875	1.07E-04	7.41E-04
RP11-91P17.1	8.504	6.907	1.793	3.853	1.17E-04	8.05E-04
TP53I11	8.812	6.903	1.838	3.755	1.73E-04	1.14E-03
TMEM71	8.386	6.897	1.800	3.833	1.27E-04	8.68E-04
IGSF10	278.576	6.888	0.487	14.131	2.43E-45	2.92E-43
MEIS3	8.268	6.886	1.809	3.806	1.41E-04	9.58E-04
IL6	182.833	6.880	0.566	12.164	4.86E-34	3.81E-32
LINC01748	8.305	6.871	1.800	3.817	1.35E-04	9.20E-04
GLI3	8.305	6.871	1.800	3.817	1.35E-04	9.20E-04
MTND5P10	8.459	6.866	1.808	3.797	1.46E-04	9.87E-04
LINC02839	8.187	6.860	1.807	3.797	1.46E-04	9.86E-04
LINC01580	8.187	6.860	1.807	3.797	1.46E-04	9.86E-04
LINC00944	22.382	6.850	1.549	4.422	9.77E-06	8.66E-05
RP11-208K4.1	44.572	6.844	1.121	6.106	1.02E-09	1.62E-08
LINC01674	8.106	6.834	1.808	3.779	1.57E-04	1.05E-03
LINC02261	22.066	6.833	1.551	4.406	1.05E-05	9.26E-05
GBP1P1	22.497	6.825	1.553	4.394	1.11E-05	9.74E-05
GTF2IP2	8.142	6.817	1.815	3.756	1.72E-04	1.14E-03
FA2H	108.751	6.799	0.714	9.517	1.78E-21	7.24E-20
OTULINL	7.907	6.796	1.817	3.741	1.83E-04	1.20E-03
RP11-1084E5.1	21.469	6.790	1.555	4.367	1.26E-05	1.09E-04
AEBP1	64.726	6.785	0.920	7.373	1.67E-13	3.92E-12
TRIQK	7.943	6.779	1.825	3.714	2.04E-04	1.32E-03
TMEM163	7.671	6.773	1.831	3.698	2.17E-04	1.40E-03
NMBR-AS1	7.825	6.767	1.824	3.711	2.07E-04	1.34E-03
KRTAP19-5	7.825	6.767	1.824	3.711	2.07E-04	1.34E-03
TACR3	21.429	6.766	1.554	4.355	1.33E-05	1.14E-04
C1orf21	671.733	6.763	0.298	22.704	4.08E-114	2.34E-111
ANKRD30BP1	21.230	6.751	1.555	4.341	1.42E-05	1.21E-04
PTPRD-AS1	7.626	6.727	1.834	3.668	2.45E-04	1.56E-03
LINC00856	42.018	6.724	1.132	5.940	2.85E-09	4.32E-08
RP11-45K10.2	206.477	6.723	0.523	12.851	8.45E-38	7.79E-36
STC1	40.763	6.721	1.130	5.950	2.69E-09	4.09E-08
TMEM114	7.355	6.721	1.853	3.628	2.86E-04	1.79E-03
LINC01181	81.430	6.719	0.804	8.353	6.64E-17	2.05E-15
C1QB	7.509	6.716	1.835	3.659	2.53E-04	1.61E-03
GRIP1	7.509	6.716	1.835	3.659	2.53E-04	1.61E-03
PHOX2B	7.237	6.708	1.870	3.587	3.34E-04	2.06E-03
GRIN2A	570.437	6.707	0.318	21.084	1.11E-98	4.19E-96
LINC02282	7.391	6.704	1.840	3.644	2.69E-04	1.69E-03
LINC01087	385.507	6.701	0.388	17.254	1.04E-66	2.35E-64
RP11-6J21.2	7.545	6.699	1.849	3.624	2.91E-04	1.82E-03
RBM11	7.545	6.699	1.849	3.624	2.91E-04	1.82E-03
MAMLD1	7.156	6.680	1.861	3.589	3.32E-04	2.04E-03
RORB-AS1	7.310	6.674	1.846	3.616	2.99E-04	1.86E-03
RP1-247E2.1	7.310	6.674	1.846	3.616	2.99E-04	1.86E-03
ARHGAP20	19.171	6.644	1.573	4.224	2.40E-05	1.96E-04
RNU4-38P	7.228	6.644	1.857	3.577	3.47E-04	2.13E-03
OR52N1	7.228	6.644	1.857	3.577	3.47E-04	2.13E-03
NDRG1	96.558	6.634	0.735	9.025	1.79E-19	6.48E-18
RP11-90N16.2	7.111	6.632	1.857	3.572	3.55E-04	2.17E-03
PCDHB2	57.229	6.630	0.931	7.119	1.08E-12	2.33E-11

LINC01344	329.091	6.628	0.414	15.998	1.32E-57	2.39E-55
KIAA1210	112.609	6.590	0.663	9.942	2.73E-23	1.25E-21
MYADM	18.851	6.589	1.571	4.196	2.72E-05	2.20E-04
IGSF9B	129.979	6.580	0.639	10.290	7.82E-25	3.95E-23
RYR3	6.794	6.575	1.871	3.513	4.42E-04	2.63E-03
CXCL8	127.708	6.562	0.617	10.639	1.97E-26	1.10E-24
RP11-397A16.1	6.676	6.562	1.879	3.493	4.77E-04	2.81E-03
CASC9	6.830	6.556	1.884	3.479	5.03E-04	2.94E-03
RP11-744K17.1	6.830	6.556	1.884	3.479	5.03E-04	2.94E-03
NPNT	18.181	6.553	1.581	4.145	3.40E-05	2.68E-04
RGS7BP	6.559	6.549	1.890	3.464	5.32E-04	3.09E-03
DYDC2	6.559	6.549	1.890	3.464	5.32E-04	3.09E-03
RP11-697C18.1	6.713	6.542	1.882	3.477	5.07E-04	2.96E-03
FLJ36000	6.713	6.542	1.882	3.477	5.07E-04	2.96E-03
PEG3	18.013	6.538	1.581	4.136	3.54E-05	2.78E-04
GCSAML	71.967	6.535	0.815	8.013	1.12E-15	3.15E-14
ZNF679	6.441	6.534	1.908	3.426	6.14E-04	3.50E-03
DAAM2	90.390	6.534	0.726	8.998	2.30E-19	8.26E-18
NCOR1P3	6.595	6.529	1.884	3.466	5.27E-04	3.07E-03
MAGEA6-DT	6.595	6.529	1.884	3.466	5.27E-04	3.07E-03
JAM3	35.311	6.522	1.152	5.662	1.50E-08	2.07E-07
OLFM3	388.770	6.515	0.359	18.160	1.06E-73	2.68E-71
ATP1A2	6.514	6.495	1.895	3.427	6.10E-04	3.48E-03
WDFY3-AS2	6.514	6.495	1.895	3.427	6.10E-04	3.48E-03
LINC02889	333.485	6.488	0.390	16.655	2.78E-62	5.66E-60
MGC27382	17.416	6.485	1.587	4.087	4.37E-05	3.35E-04
CRISPLD1	85.438	6.479	0.736	8.805	1.31E-18	4.51E-17
MTND2P16	17.797	6.478	1.641	3.948	7.88E-05	5.65E-04
CLU	17.340	6.464	1.584	4.081	4.48E-05	3.43E-04
INHBA	17.099	6.463	1.589	4.066	4.78E-05	3.62E-04
DUXAP1	6.432	6.462	1.916	3.373	7.45E-04	4.14E-03
RP11-134K1.3	6.432	6.462	1.916	3.373	7.45E-04	4.14E-03
MT1G	6.432	6.462	1.916	3.373	7.45E-04	4.14E-03
CACHD1	6.161	6.454	1.913	3.373	7.44E-04	4.14E-03
NKX3-2	6.161	6.454	1.913	3.373	7.44E-04	4.14E-03
RP11-400M8.1	17.413	6.448	1.591	4.052	5.09E-05	3.84E-04
RP11-513N24.1	6.315	6.447	1.911	3.374	7.40E-04	4.12E-03
RP11-319F12.3	6.043	6.439	1.930	3.336	8.50E-04	4.64E-03
JAZF1	16.936	6.436	1.594	4.037	5.41E-05	4.06E-04
AC009229.6	6.197	6.433	1.911	3.367	7.60E-04	4.22E-03
LINC02472	6.197	6.433	1.911	3.367	7.60E-04	4.22E-03
CA3	6.197	6.433	1.911	3.367	7.60E-04	4.22E-03
LINC00327	100.635	6.427	0.676	9.510	1.91E-21	7.73E-20
SCEL	16.701	6.426	1.594	4.032	5.52E-05	4.13E-04
MTCO1P4	33.870	6.422	1.160	5.534	3.13E-08	4.17E-07
RP11-33E12.2	6.079	6.419	1.916	3.351	8.06E-04	4.44E-03
CHRDL1	16.113	6.400	1.606	3.986	6.72E-05	4.89E-04
XXyac-YR38GF2.1	6.116	6.397	1.927	3.319	9.02E-04	4.88E-03
ANKRD30B	6.116	6.397	1.927	3.319	9.02E-04	4.88E-03
SLC16A10	16.031	6.387	1.603	3.983	6.80E-05	4.94E-04
AMOTL2	5.998	6.382	1.926	3.314	9.19E-04	4.97E-03
DIMT1P1	16.339	6.380	1.603	3.981	6.85E-05	4.97E-04
CYLC1	16.309	6.380	1.595	4.001	6.31E-05	4.63E-04
RP11-421N8.3	16.222	6.375	1.601	3.981	6.86E-05	4.98E-04
NELL2	80.568	6.370	0.737	8.649	5.21E-18	1.71E-16
GS1-34D21.1	16.228	6.366	1.595	3.990	6.60E-05	4.82E-04
RP3-410C9.2	143.439	6.366	0.554	11.488	1.51E-30	1.02E-28
DIP2C	173.137	6.341	0.508	12.471	1.08E-35	9.01E-34

RP11-621B23.1	5.645	6.337	1.956	3.239	1.20E-03	6.24E-03
ADAMDEC1	5.799	6.330	1.942	3.259	1.12E-03	5.89E-03
RP1-213J1P__B.1	5.799	6.330	1.942	3.259	1.12E-03	5.89E-03
AKR1C1	885.459	6.329	0.242	26.179	4.55E-151	4.55E-148
ITIH5	15.742	6.322	1.612	3.922	8.78E-05	6.23E-04
CHST15	5.681	6.314	1.946	3.246	1.17E-03	6.13E-03
ZNF648	231.369	6.311	0.433	14.564	4.78E-48	6.49E-46
SILC1	15.476	6.310	1.606	3.930	8.49E-05	6.04E-04
RP1-130L23.1	5.835	6.310	1.978	3.190	1.42E-03	7.27E-03
EPX	5.410	6.301	2.015	3.127	1.77E-03	8.74E-03
SLC8A1	15.272	6.300	1.609	3.914	9.07E-05	6.41E-04
CYP4X1	5.564	6.299	1.955	3.222	1.27E-03	6.58E-03
CHST9	5.564	6.299	1.955	3.222	1.27E-03	6.58E-03
THEG	5.718	6.292	1.965	3.202	1.37E-03	7.01E-03
SIX4	15.308	6.290	1.612	3.903	9.52E-05	6.68E-04
LINC01142	5.446	6.283	1.971	3.188	1.43E-03	7.31E-03
RP11-332K15.1	5.446	6.283	1.971	3.188	1.43E-03	7.31E-03
AP001601.2	5.446	6.283	1.971	3.188	1.43E-03	7.31E-03
RP11-875G18.1	5.600	6.275	1.960	3.201	1.37E-03	7.03E-03
RP11-564C24.2	5.636	6.256	2.004	3.121	1.80E-03	8.88E-03
AC005754.8	5.365	6.243	1.971	3.168	1.54E-03	7.76E-03
KLRD1	5.365	6.243	1.971	3.168	1.54E-03	7.76E-03
RP1-161N10.1	5.365	6.243	1.971	3.168	1.54E-03	7.76E-03
RPSAP33	5.519	6.236	1.987	3.138	1.70E-03	8.46E-03
GAPDHP71	5.519	6.236	1.987	3.138	1.70E-03	8.46E-03
ADAMTS17	5.519	6.236	1.987	3.138	1.70E-03	8.46E-03
LDOC1	29.002	6.228	1.170	5.324	1.01E-07	1.25E-06
RNF182	5.247	6.227	1.987	3.134	1.72E-03	8.56E-03
PDE9A	5.247	6.227	1.987	3.134	1.72E-03	8.56E-03
FSD1	14.168	6.223	1.638	3.800	1.45E-04	9.78E-04
GPR160	1338.899	6.216	0.198	31.322	2.36E-215	6.79E-212
SLC29A4	5.283	6.202	1.981	3.131	1.74E-03	8.63E-03
OAT	14.123	6.199	1.626	3.812	1.38E-04	9.36E-04
PRKAR2B	42.247	6.189	0.961	6.437	1.22E-10	2.11E-09
KIF6	70.930	6.186	0.745	8.304	1.01E-16	3.09E-15
OR2M3	5.166	6.186	1.988	3.111	1.87E-03	9.15E-03
AC098826.5	5.320	6.179	2.012	3.070	2.14E-03	1.03E-02
C2orf72	5.320	6.179	2.012	3.070	2.14E-03	1.03E-02
LINC02848	5.202	6.160	2.002	3.077	2.09E-03	1.01E-02
COL1A2	4.930	6.150	2.027	3.033	2.42E-03	1.14E-02
LINC01776	5.084	6.142	2.001	3.070	2.14E-03	1.03E-02
KMT5AP3	5.084	6.142	2.001	3.070	2.14E-03	1.03E-02
POTEKP	559.454	6.138	0.298	20.610	2.25E-94	7.71E-92
PCDHB5	13.680	6.128	1.633	3.752	1.76E-04	1.16E-03
ATP10B	4.967	6.125	2.007	3.051	2.28E-03	1.08E-02
KRT8P9	4.967	6.125	2.007	3.051	2.28E-03	1.08E-02
KLHL14	4.967	6.125	2.007	3.051	2.28E-03	1.08E-02
CTD-3046C4.1	13.568	6.112	1.630	3.750	1.77E-04	1.16E-03
FMO6P	4.849	6.107	2.022	3.020	2.52E-03	1.18E-02
RPL30P13	5.003	6.099	2.027	3.010	2.62E-03	1.22E-02
RP11-94M14.3	26.563	6.098	1.196	5.099	3.41E-07	3.87E-06
RP11-76E17.2	26.174	6.093	1.193	5.108	3.25E-07	3.71E-06
CD5L	4.885	6.080	2.023	3.006	2.65E-03	1.23E-02
FGF13	679.577	6.065	0.252	24.106	2.14E-128	1.49E-125
RP3-525N10.2	4.768	6.062	2.028	2.989	2.80E-03	1.29E-02
OR52N5	4.768	6.062	2.028	2.989	2.80E-03	1.29E-02
STEAP1B	65.321	6.060	0.752	8.060	7.61E-16	2.18E-14
RP11-472K22.1	4.922	6.057	2.074	2.921	3.49E-03	1.56E-02

ACOT11	13.360	6.050	1.646	3.676	2.37E-04	1.52E-03
ADAMTSL5	25.496	6.048	1.198	5.051	4.40E-07	4.92E-06
PTPRT	4.650	6.044	2.042	2.959	3.08E-03	1.40E-02
SEMG2	25.737	6.038	1.185	5.094	3.50E-07	3.97E-06
RP11-205M3.4	4.804	6.035	2.054	2.939	3.30E-03	1.49E-02
ME2P1	4.804	6.035	2.054	2.939	3.30E-03	1.49E-02
RP11-60G10.1	4.804	6.035	2.054	2.939	3.30E-03	1.49E-02
RP11-359D24.1	13.279	6.034	1.656	3.643	2.69E-04	1.70E-03
FRMD5	51.193	6.028	0.843	7.150	8.67E-13	1.88E-11
HOXA3	12.802	6.017	1.657	3.632	2.81E-04	1.76E-03
CFTRP3	4.686	6.015	2.047	2.938	3.30E-03	1.49E-02
RP11-557L19.1	4.415	6.002	2.102	2.855	4.30E-03	1.85E-02
RP11-94H18.1	4.569	5.996	2.051	2.923	3.46E-03	1.55E-02
IGSF1	74.755	5.987	0.692	8.651	5.12E-18	1.69E-16
KLHL13	159.880	5.982	0.480	12.467	1.13E-35	9.37E-34
RP11-13M3.1	4.451	5.977	2.064	2.896	3.78E-03	1.67E-02
LIPI	24.316	5.977	1.199	4.987	6.13E-07	6.73E-06
NSUN7	4.605	5.969	2.085	2.863	4.20E-03	1.82E-02
CTD-2176I21.2	4.605	5.969	2.085	2.863	4.20E-03	1.82E-02
KIAA1549L	1370.487	5.968	0.191	31.188	1.57E-213	4.00E-210
KRTAP6-1	12.133	5.964	1.657	3.599	3.19E-04	1.97E-03
TAFA1	12.256	5.960	1.652	3.609	3.08E-04	1.91E-03
RP11-720L8.1	4.333	5.957	2.087	2.854	4.32E-03	1.86E-02
ELAVL4	4.487	5.948	2.075	2.867	4.15E-03	1.80E-02
SCN7A	4.487	5.948	2.075	2.867	4.15E-03	1.80E-02
RP11-1E4.2	4.487	5.948	2.075	2.867	4.15E-03	1.80E-02
RP11-328K2.1	4.487	5.948	2.075	2.867	4.15E-03	1.80E-02
KRTAP19-6	4.487	5.948	2.075	2.867	4.15E-03	1.80E-02
ARHGAP39	47.864	5.938	0.849	6.997	2.62E-12	5.40E-11
CLDN10-AS1	4.216	5.934	2.124	2.794	5.21E-03	2.18E-02
VSNL1	4.370	5.927	2.076	2.855	4.31E-03	1.85E-02
RP11-634B22.4	4.370	5.927	2.076	2.855	4.31E-03	1.85E-02
SYNPR-AS1	11.852	5.919	1.665	3.555	3.77E-04	2.29E-03
CTD-2620I22.3	153.318	5.912	0.481	12.294	9.74E-35	7.76E-33
ERC2-IT1	11.889	5.908	1.674	3.529	4.17E-04	2.50E-03
RP11-33A14.1	4.252	5.907	2.088	2.829	4.67E-03	1.98E-02
HHIP	4.252	5.907	2.088	2.829	4.67E-03	1.98E-02
GMPR	4.252	5.907	2.088	2.829	4.67E-03	1.98E-02
RP11-486O13.2	4.252	5.907	2.088	2.829	4.67E-03	1.98E-02
KCNK13	4.252	5.907	2.088	2.829	4.67E-03	1.98E-02
SIM2	4.252	5.907	2.088	2.829	4.67E-03	1.98E-02
RP11-447N10.1	4.406	5.900	2.121	2.781	5.41E-03	2.25E-02
GAGE2A	4.406	5.900	2.121	2.781	5.41E-03	2.25E-02
CICP18	11.499	5.898	1.670	3.531	4.15E-04	2.48E-03
LINC02505	34.458	5.891	0.986	5.972	2.34E-09	3.59E-08
RP11-10E14.1	11.382	5.890	1.675	3.516	4.39E-04	2.61E-03
RP11-568G11.5	4.134	5.886	2.111	2.788	5.31E-03	2.21E-02
NTN4	34.531	5.883	0.986	5.965	2.44E-09	3.74E-08
CYP26B1	263.052	5.880	0.370	15.871	1.01E-56	1.75E-54
RP11-267L5.1	4.288	5.876	2.106	2.791	5.26E-03	2.19E-02
ATP1A3	4.288	5.876	2.106	2.791	5.26E-03	2.19E-02
LINC02888	81.150	5.865	0.656	8.946	3.68E-19	1.30E-17
MAGEB1	22.914	5.864	1.204	4.870	1.12E-06	1.18E-05
MISP	4.017	5.863	2.148	2.729	6.35E-03	2.56E-02
RP13-192B19.2	101.202	5.863	0.586	9.998	1.55E-23	7.34E-22
ARL2BPP4	4.171	5.855	2.104	2.782	5.40E-03	2.24E-02
RP11-203E8.1	3.899	5.836	2.210	2.641	8.27E-03	3.20E-02
HMGA2-AS1	3.899	5.836	2.210	2.641	8.27E-03	3.20E-02

GALNT17	4.053	5.834	2.115	2.758	5.81E-03	2.38E-02
NUGGC	4.053	5.834	2.115	2.758	5.81E-03	2.38E-02
RP11-181B11.1	4.053	5.834	2.115	2.758	5.81E-03	2.38E-02
RP11-257I14.1	4.053	5.834	2.115	2.758	5.81E-03	2.38E-02
RHOBTB1	4.053	5.834	2.115	2.758	5.81E-03	2.38E-02
RP11-415G4.1	4.053	5.834	2.115	2.758	5.81E-03	2.38E-02
RP11-256I9.2	4.053	5.834	2.115	2.758	5.81E-03	2.38E-02
GTF3C6P1	4.053	5.834	2.115	2.758	5.81E-03	2.38E-02
LPAR4	4.207	5.827	2.165	2.692	7.10E-03	2.82E-02
FAM182A	11.174	5.818	1.688	3.446	5.68E-04	3.27E-03
SAMMSON	3.935	5.812	2.138	2.719	6.55E-03	2.63E-02
LINC02619	3.935	5.812	2.138	2.719	6.55E-03	2.63E-02
GPC6	3.935	5.812	2.138	2.719	6.55E-03	2.63E-02
TRAV26-2	3.935	5.812	2.138	2.719	6.55E-03	2.63E-02
RGN	3.935	5.812	2.138	2.719	6.55E-03	2.63E-02
AC093843.1	4.089	5.802	2.140	2.711	6.72E-03	2.69E-02
CTD-2015A6.1	4.089	5.802	2.140	2.711	6.72E-03	2.69E-02
RP11-579O24.1	4.089	5.802	2.140	2.711	6.72E-03	2.69E-02
TCEAL9	32.028	5.797	1.006	5.761	8.36E-09	1.20E-07
KCTD8	22.359	5.797	1.210	4.792	1.65E-06	1.70E-05
RP11-8L2.1	3.818	5.788	2.175	2.661	7.78E-03	3.04E-02
ZNF676	3.818	5.788	2.175	2.661	7.78E-03	3.04E-02
PBX1	42.774	5.786	0.866	6.683	2.33E-11	4.35E-10
EFR3B	3.972	5.779	2.136	2.706	6.81E-03	2.72E-02
MRPL42P6	3.972	5.779	2.136	2.706	6.81E-03	2.72E-02
IGFBP3	3.972	5.779	2.136	2.706	6.81E-03	2.72E-02
GAPDHP54	3.972	5.779	2.136	2.706	6.81E-03	2.72E-02
RP13-57D9.3	3.972	5.779	2.136	2.706	6.81E-03	2.72E-02
TPPP	10.863	5.769	1.680	3.434	5.95E-04	3.40E-03
ZSCAN18	10.622	5.765	1.690	3.412	6.45E-04	3.65E-03
RP1-309H15.3	84.520	5.762	0.640	9.003	2.19E-19	7.91E-18
RP11-196G18.3	3.854	5.756	2.145	2.684	7.27E-03	2.88E-02
LINC02832	3.854	5.756	2.145	2.684	7.27E-03	2.88E-02
RP6-114E22.1	3.854	5.756	2.145	2.684	7.27E-03	2.88E-02
LINC02207	3.854	5.756	2.145	2.684	7.27E-03	2.88E-02
LLNLF-158E9.1	3.854	5.756	2.145	2.684	7.27E-03	2.88E-02
RP11-15A1.9	3.854	5.756	2.145	2.684	7.27E-03	2.88E-02
OR5BH1P	3.854	5.756	2.145	2.684	7.27E-03	2.88E-02
MAP2	10.356	5.744	1.721	3.338	8.43E-04	4.61E-03
DAB1-AS1	3.736	5.733	2.167	2.646	8.14E-03	3.16E-02
CTD-2143A15.1	3.736	5.733	2.167	2.646	8.14E-03	3.16E-02
CYP39A1	3.736	5.733	2.167	2.646	8.14E-03	3.16E-02
RP11-758M4.4	3.736	5.733	2.167	2.646	8.14E-03	3.16E-02
CLEC2B	124.991	5.733	0.506	11.335	8.79E-30	5.64E-28
RNU6-948P	10.577	5.731	1.709	3.355	7.95E-04	4.38E-03
FAM106C	3.890	5.723	2.181	2.624	8.69E-03	3.34E-02
NLRP2B	3.890	5.723	2.181	2.624	8.69E-03	3.34E-02
CDH7	20.330	5.719	1.238	4.621	3.81E-06	3.64E-05
EHF	204.250	5.717	0.402	14.239	5.27E-46	6.47E-44
IFITM8P	51.578	5.713	0.815	7.013	2.33E-12	4.82E-11
KCTD19	30.940	5.699	1.026	5.556	2.76E-08	3.71E-07
LRRIQ4	3.773	5.698	2.171	2.625	8.68E-03	3.33E-02
RP11-739P1.2	3.773	5.698	2.171	2.625	8.68E-03	3.33E-02
TARID	3.773	5.698	2.171	2.625	8.68E-03	3.33E-02
RP11-794P6.6	3.773	5.698	2.171	2.625	8.68E-03	3.33E-02
CLECL1	39.402	5.694	0.890	6.398	1.57E-10	2.69E-09
TRIM51HP	10.230	5.693	1.696	3.358	7.86E-04	4.34E-03
SYPL2	29.926	5.681	1.006	5.648	1.62E-08	2.23E-07

ZEB2-AS1	3.655	5.674	2.178	2.606	9.16E-03	3.48E-02
RP11-499O7.7	3.655	5.674	2.178	2.606	9.16E-03	3.48E-02
HMGN1P20	3.655	5.674	2.178	2.606	9.16E-03	3.48E-02
OPCML	3.655	5.674	2.178	2.606	9.16E-03	3.48E-02
HAUS6P2	3.655	5.674	2.178	2.606	9.16E-03	3.48E-02
RP11-115C10.1	39.127	5.669	0.882	6.431	1.27E-10	2.20E-09
KDM3AP1	19.974	5.661	1.228	4.611	4.01E-06	3.83E-05
WFDC2	9.789	5.658	1.711	3.308	9.41E-04	5.08E-03
AP001604.3	10.185	5.656	1.703	3.322	8.94E-04	4.85E-03
CAPNS1P1	3.537	5.650	2.199	2.570	1.02E-02	3.80E-02
ADAM18	3.537	5.650	2.199	2.570	1.02E-02	3.80E-02
NCOR1P2	3.537	5.650	2.199	2.570	1.02E-02	3.80E-02
ANKRD7	10.067	5.648	1.702	3.319	9.03E-04	4.89E-03
PCDHGC3	19.027	5.647	1.254	4.502	6.74E-06	6.17E-05
GPRC5A	98.127	5.646	0.559	10.099	5.57E-24	2.71E-22
RP11-385D13.3	3.691	5.641	2.230	2.530	1.14E-02	4.18E-02
GS1-115G20.2	9.708	5.634	1.713	3.289	1.01E-03	5.38E-03
C6	3.419	5.624	2.237	2.515	1.19E-02	4.33E-02
SNAI2	3.419	5.624	2.237	2.515	1.19E-02	4.33E-02
RNU1-108P	3.419	5.624	2.237	2.515	1.19E-02	4.33E-02
SLC47A1	18.475	5.617	1.272	4.417	1.00E-05	8.87E-05
TXNRD3	3.573	5.613	2.211	2.538	1.11E-02	4.10E-02
RP1-244F24.1	3.573	5.613	2.211	2.538	1.11E-02	4.10E-02
ZNHIT1P1	3.573	5.613	2.211	2.538	1.11E-02	4.10E-02
HAP1	3.573	5.613	2.211	2.538	1.11E-02	4.10E-02
ZNF479	9.633	5.598	1.711	3.272	1.07E-03	5.66E-03
LINC00355	65.743	5.592	0.671	8.340	7.46E-17	2.30E-15
AC010967.2	3.456	5.588	2.215	2.523	1.16E-02	4.25E-02
LINC01561	3.456	5.588	2.215	2.523	1.16E-02	4.25E-02
B3GALT5	3.456	5.588	2.215	2.523	1.16E-02	4.25E-02
AP001476.4	3.456	5.588	2.215	2.523	1.16E-02	4.25E-02
CALM1P1	3.456	5.588	2.215	2.523	1.16E-02	4.25E-02
GAS6	158.825	5.584	0.439	12.727	4.20E-37	3.75E-35
RP11-433A19.3	289.496	5.571	0.329	16.951	1.90E-64	4.03E-62
C4B	54.704	5.566	0.736	7.559	4.07E-14	1.02E-12
RPL12P40	9.464	5.564	1.744	3.191	1.42E-03	7.25E-03
ACTG1P25	3.338	5.562	2.235	2.489	1.28E-02	4.60E-02
GATA2	3.338	5.562	2.235	2.489	1.28E-02	4.60E-02
LINC02153	3.338	5.562	2.235	2.489	1.28E-02	4.60E-02
PADI2	167.602	5.562	0.430	12.920	3.48E-38	3.29E-36
DIPK1B	9.316	5.556	1.721	3.228	1.25E-03	6.47E-03
RP4-799O8.1	3.492	5.554	2.290	2.425	1.53E-02	5.32E-02
RP11-407P18.1	3.492	5.554	2.290	2.425	1.53E-02	5.32E-02
MTND1P5	28.645	5.544	1.032	5.375	7.66E-08	9.64E-07
KRTAP6-2	9.383	5.543	1.764	3.141	1.68E-03	8.39E-03
MMP17	3.220	5.535	2.273	2.436	1.49E-02	5.20E-02
LINC00351	3.220	5.535	2.273	2.436	1.49E-02	5.20E-02
AP000567.27	3.220	5.535	2.273	2.436	1.49E-02	5.20E-02
RP11-268G12.3	3.220	5.535	2.273	2.436	1.49E-02	5.20E-02
LINC02299	9.111	5.534	1.733	3.193	1.41E-03	7.19E-03
GRM7-AS3	8.839	5.532	1.749	3.163	1.56E-03	7.88E-03
RP11-281P23.2	9.265	5.531	1.754	3.154	1.61E-03	8.10E-03
AC013463.2	3.374	5.523	2.258	2.446	1.44E-02	5.07E-02
RNA5SP259	3.374	5.523	2.258	2.446	1.44E-02	5.07E-02
RP11-227G15.10	3.374	5.523	2.258	2.446	1.44E-02	5.07E-02
CLDN34	3.374	5.523	2.258	2.446	1.44E-02	5.07E-02
AC012593.1	9.117	5.522	1.727	3.197	1.39E-03	7.12E-03
DDX53	221.785	5.508	0.367	14.998	7.59E-51	1.13E-48

AC007099.2	3.103	5.503	2.339	2.353	1.86E-02	6.27E-02
SPTSSB	3.103	5.503	2.339	2.353	1.86E-02	6.27E-02
HCN1	3.103	5.503	2.339	2.353	1.86E-02	6.27E-02
RP11-717F1.1	3.103	5.503	2.339	2.353	1.86E-02	6.27E-02
GBP6	410.677	5.503	0.279	19.693	2.46E-86	7.54E-84
ITPRID1	3.257	5.495	2.257	2.435	1.49E-02	5.20E-02
RP11-318M2.3	3.257	5.495	2.257	2.435	1.49E-02	5.20E-02
RP11-134O15.3	3.257	5.495	2.257	2.435	1.49E-02	5.20E-02
KCNJ16	3.257	5.495	2.257	2.435	1.49E-02	5.20E-02
KRTAP19-9P	3.257	5.495	2.257	2.435	1.49E-02	5.20E-02
RP11-486O13.5	8.831	5.474	1.751	3.127	1.77E-03	8.74E-03
RP11-252I13.2	138.697	5.473	0.456	12.012	3.08E-33	2.34E-31
SPRR2E	3.139	5.468	2.275	2.404	1.62E-02	5.59E-02
RERG	3.139	5.468	2.275	2.404	1.62E-02	5.59E-02
LINC02693	3.139	5.468	2.275	2.404	1.62E-02	5.59E-02
RP11-363E6.4	3.293	5.464	2.376	2.300	2.15E-02	7.03E-02
GS1-122H1.1	26.100	5.456	1.039	5.249	1.53E-07	1.83E-06
UNC5C	642.057	5.453	0.228	23.954	8.30E-127	5.61E-124
RASSF8	52.184	5.452	0.730	7.474	7.79E-14	1.90E-12
CBR3	8.719	5.451	1.740	3.133	1.73E-03	8.58E-03
RP11-404O13.4	8.324	5.451	1.773	3.074	2.11E-03	1.02E-02
RASGEF1B	94.663	5.442	0.545	9.991	1.66E-23	7.83E-22
RP11-398A8.5	3.021	5.439	2.313	2.352	1.87E-02	6.27E-02
LZTS1	3.021	5.439	2.313	2.352	1.87E-02	6.27E-02
LINC00311	3.021	5.439	2.313	2.352	1.87E-02	6.27E-02
ARL2BPP10	3.021	5.439	2.313	2.352	1.87E-02	6.27E-02
RP1-138O17.1	3.021	5.439	2.313	2.352	1.87E-02	6.27E-02
CDH13	17.152	5.430	1.260	4.311	1.63E-05	1.38E-04
RECK	8.514	5.427	1.757	3.089	2.01E-03	9.74E-03
SPATA6	3.175	5.427	2.314	2.345	1.90E-02	6.36E-02
MIR4422HG	3.175	5.427	2.314	2.345	1.90E-02	6.36E-02
MIPEPP2	3.175	5.427	2.314	2.345	1.90E-02	6.36E-02
LINC01205	3.175	5.427	2.314	2.345	1.90E-02	6.36E-02
CACNA2D1-AS1	3.175	5.427	2.314	2.345	1.90E-02	6.36E-02
RP11-346I3.7	3.175	5.427	2.314	2.345	1.90E-02	6.36E-02
RP11-356B19.11	3.175	5.427	2.314	2.345	1.90E-02	6.36E-02
SMIM24	8.638	5.424	1.743	3.111	1.86E-03	9.13E-03
ERICH3	839.857	5.421	0.206	26.338	6.97E-153	7.27E-150
RP11-433J8.3	16.594	5.419	1.282	4.227	2.37E-05	1.94E-04
GXYLT2	25.554	5.417	1.029	5.266	1.40E-07	1.69E-06
RNF183	50.432	5.412	0.733	7.385	1.53E-13	3.59E-12
MAL2-AS1	42.697	5.411	0.812	6.664	2.67E-11	4.95E-10
IFTAP	24.674	5.411	1.054	5.136	2.81E-07	3.25E-06
HTRA3	2.904	5.406	2.382	2.270	2.32E-02	7.49E-02
IL6-AS1	2.904	5.406	2.382	2.270	2.32E-02	7.49E-02
PTPRQ	2.904	5.406	2.382	2.270	2.32E-02	7.49E-02
KRTAP19-10P	2.904	5.406	2.382	2.270	2.32E-02	7.49E-02
MGAT4C	133.629	5.404	0.456	11.855	2.02E-32	1.47E-30
RAB3C	33.485	5.400	0.898	6.016	1.79E-09	2.76E-08
CGNL1	172.860	5.399	0.404	13.375	8.46E-41	8.59E-39
RP11-520E6.1	3.058	5.397	2.305	2.342	1.92E-02	6.41E-02
EFNA1	3.058	5.397	2.305	2.342	1.92E-02	6.41E-02
ERFE	3.058	5.397	2.305	2.342	1.92E-02	6.41E-02
RNU6ATAC42P	3.058	5.397	2.305	2.342	1.92E-02	6.41E-02
RP11-4D11.1	3.058	5.397	2.305	2.342	1.92E-02	6.41E-02
TPRG1	981.736	5.383	0.190	28.341	1.07E-176	1.76E-173
CTD-2591A1.2	2.940	5.368	2.321	2.313	2.07E-02	6.83E-02
RP11-187K14.1	2.940	5.368	2.321	2.313	2.07E-02	6.83E-02

LINC00943	2.940	5.368	2.321	2.313	2.07E-02	6.83E-02
NUS1P2	2.940	5.368	2.321	2.313	2.07E-02	6.83E-02
POTEC	2.940	5.368	2.321	2.313	2.07E-02	6.83E-02
DNAJA1P5	7.962	5.359	1.772	3.024	2.49E-03	1.17E-02
WDFY3	408.083	5.356	0.272	19.718	1.51E-86	4.76E-84
AC012593.2	44.933	5.354	1.477	3.625	2.88E-04	1.80E-03
GSPT2	213.099	5.353	0.374	14.325	1.53E-46	1.95E-44
KCNK6	23.642	5.352	1.061	5.047	4.50E-07	5.02E-06
GUSBP7	15.761	5.351	1.292	4.143	3.43E-05	2.70E-04
ZNF483	70.036	5.343	0.627	8.529	1.48E-17	4.80E-16
CCND1	527.509	5.340	0.242	22.062	7.35E-108	3.75E-105
EFEMP1	15.680	5.337	1.295	4.121	3.78E-05	2.95E-04
LINC02785	2.822	5.337	2.359	2.263	2.37E-02	7.60E-02
RPS6P7	2.822	5.337	2.359	2.263	2.37E-02	7.60E-02
TMC5	2.822	5.337	2.359	2.263	2.37E-02	7.60E-02
SOX9	677.959	5.334	0.220	24.253	6.14E-130	4.55E-127
FRG2EP	8.004	5.327	1.766	3.016	2.56E-03	1.20E-02
CRLF3P2	2.976	5.325	2.383	2.234	2.55E-02	8.09E-02
KRTAP19-7	2.976	5.325	2.383	2.234	2.55E-02	8.09E-02
ZNF727	331.903	5.318	0.296	17.971	3.31E-72	8.09E-70
HDGFL1	23.639	5.314	1.052	5.049	4.44E-07	4.97E-06
PCAT19	8.348	5.311	1.902	2.792	5.24E-03	2.19E-02
GARNL3	22.810	5.305	1.067	4.972	6.62E-07	7.24E-06
CLRN1	2.705	5.302	2.429	2.183	2.90E-02	9.00E-02
ARRDC4	2.705	5.302	2.429	2.183	2.90E-02	9.00E-02
MILR1	2.705	5.302	2.429	2.183	2.90E-02	9.00E-02
LRRC4C	140.449	5.302	0.437	12.146	6.00E-34	4.67E-32
RP11-455G16.1	7.799	5.301	1.783	2.972	2.95E-03	1.35E-02
LUZP4	62.059	5.300	0.648	8.184	2.75E-16	8.09E-15
LINC01446	164.934	5.295	0.423	12.520	5.77E-36	4.87E-34
THSD4	15.759	5.294	1.285	4.122	3.76E-05	2.94E-04
AC024162.2	2.859	5.291	2.361	2.241	2.50E-02	7.98E-02
C8orf34	2.859	5.291	2.361	2.241	2.50E-02	7.98E-02
RP11-65D17.1	2.859	5.291	2.361	2.241	2.50E-02	7.98E-02
MIR548F1	2.859	5.291	2.361	2.241	2.50E-02	7.98E-02
RP11-137O10.1	2.859	5.291	2.361	2.241	2.50E-02	7.98E-02
CEACAM22P	2.859	5.291	2.361	2.241	2.50E-02	7.98E-02
GAL3ST1	2.859	5.291	2.361	2.241	2.50E-02	7.98E-02
MTCYBP11	7.805	5.287	1.774	2.980	2.88E-03	1.32E-02
RIN2	60.171	5.284	0.659	8.014	1.11E-15	3.14E-14
RTN1	31.046	5.283	0.911	5.798	6.73E-09	9.75E-08
LINC01257	45.110	5.281	0.756	6.984	2.87E-12	5.88E-11
SPOCK3	22.258	5.280	1.074	4.917	8.79E-07	9.46E-06
ERVV-1	60.036	5.266	0.654	8.051	8.19E-16	2.34E-14
ACTG1P22	105.163	5.261	0.496	10.604	2.87E-26	1.58E-24
RP11-433N2.1	2.741	5.259	2.373	2.216	2.67E-02	8.39E-02
RP11-565A3.1	2.741	5.259	2.373	2.216	2.67E-02	8.39E-02
MTCYBP22	2.741	5.259	2.373	2.216	2.67E-02	8.39E-02
PCDHGB9P	2.741	5.259	2.373	2.216	2.67E-02	8.39E-02
H1-6	2.741	5.259	2.373	2.216	2.67E-02	8.39E-02
ARC	2.741	5.259	2.373	2.216	2.67E-02	8.39E-02
ANKRD20A3P	2.741	5.259	2.373	2.216	2.67E-02	8.39E-02
SOHLH1	2.741	5.259	2.373	2.216	2.67E-02	8.39E-02
TMEM63C	2.741	5.259	2.373	2.216	2.67E-02	8.39E-02
TMEM59L	2.741	5.259	2.373	2.216	2.67E-02	8.39E-02
OXT	2.741	5.259	2.373	2.216	2.67E-02	8.39E-02
RP11-318N11.1	15.565	5.249	1.284	4.088	4.35E-05	3.34E-04
ATP4A	7.483	5.248	1.793	2.926	3.43E-03	1.54E-02

KIAA1671	37.190	5.246	0.819	6.403	1.52E-10	2.61E-09
OR9Q1	7.606	5.246	1.782	2.943	3.25E-03	1.47E-02
SERPINE2	37.615	5.246	0.823	6.375	1.82E-10	3.10E-09
HTR1F	7.488	5.234	1.790	2.924	3.46E-03	1.55E-02
TUBA3C	162.357	5.230	0.403	12.978	1.63E-38	1.56E-36
UBXN10	2.623	5.227	2.411	2.168	3.01E-02	9.27E-02
AC011752.1	2.623	5.227	2.411	2.168	3.01E-02	9.27E-02
ERVV-2	2.623	5.227	2.411	2.168	3.01E-02	9.27E-02
EBF4	2.623	5.227	2.411	2.168	3.01E-02	9.27E-02
PNPLA3	2.623	5.227	2.411	2.168	3.01E-02	9.27E-02
LPP	7.247	5.226	1.805	2.896	3.78E-03	1.66E-02
LINC02389	103.251	5.225	0.496	10.530	6.31E-26	3.40E-24
RNU6-367P	7.401	5.217	1.804	2.891	3.84E-03	1.69E-02
PHKA1	58.823	5.217	0.655	7.965	1.66E-15	4.61E-14
RASSF8-AS1	7.166	5.194	1.807	2.875	4.04E-03	1.76E-02
ZNF728	58.012	5.194	0.653	7.954	1.81E-15	5.01E-14
CTA-392E5.1	14.609	5.193	1.294	4.013	5.98E-05	4.43E-04
PTPRS	497.427	5.190	0.240	21.621	1.15E-103	4.79E-101
RP11-431M3.2	14.492	5.187	1.293	4.011	6.06E-05	4.47E-04
CTD-2007H18.2	7.320	5.187	1.823	2.846	4.43E-03	1.90E-02
PES1P1	7.443	5.183	1.799	2.882	3.95E-03	1.73E-02
RP13-122B23.8	7.443	5.183	1.799	2.882	3.95E-03	1.73E-02
CEBPA	7.048	5.183	1.814	2.858	4.27E-03	1.84E-02
OAF	206.347	5.177	0.354	14.627	1.88E-48	2.62E-46
UBL4B	14.206	5.177	1.335	3.879	1.05E-04	7.31E-04
AC016768.1	2.660	5.177	2.428	2.132	3.30E-02	9.97E-02
RP11-597D13.12	2.660	5.177	2.428	2.132	3.30E-02	9.97E-02
GLIS3-AS1	2.660	5.177	2.428	2.132	3.30E-02	9.97E-02
BTBD7P2	2.660	5.177	2.428	2.132	3.30E-02	9.97E-02
OR9Q2	2.660	5.177	2.428	2.132	3.30E-02	9.97E-02
RP11-1157N2__B.2	2.660	5.177	2.428	2.132	3.30E-02	9.97E-02
KLK11	2.660	5.177	2.428	2.132	3.30E-02	9.97E-02
RP11-63C8.1	28.395	5.172	0.922	5.612	2.00E-08	2.72E-07
LINC01579	592.424	5.166	0.227	22.712	3.39E-114	2.00E-111
ZNF702P	98.553	5.165	0.502	10.294	7.48E-25	3.78E-23
DAB2IP	148.926	5.165	0.412	12.551	3.90E-36	3.33E-34
AC002480.3	34.642	5.154	0.837	6.160	7.27E-10	1.17E-08
RP11-479O16.1	28.064	5.153	0.934	5.515	3.49E-08	4.64E-07
CD40LG	27.997	5.150	0.924	5.576	2.47E-08	3.33E-07
GPM6A	948.879	5.145	0.191	26.976	2.80E-160	3.21E-157
NKAIN2	14.094	5.142	1.301	3.953	7.72E-05	5.53E-04
LINC01709	89.375	5.129	0.523	9.804	1.08E-22	4.77E-21
RP1-35C21.2	34.880	5.123	0.830	6.174	6.67E-10	1.08E-08
CCN3	4088.588	5.119	0.124	41.222	0.00E+00	0.00E+00
KRTAP20-2	7.009	5.114	1.811	2.825	4.73E-03	2.00E-02
PPM1L	109.430	5.107	0.472	10.818	2.83E-27	1.62E-25
RP4-768P8.2	6.768	5.104	1.828	2.793	5.23E-03	2.19E-02
FCRL4	60.890	5.098	0.624	8.167	3.17E-16	9.27E-15
KRTAP20-3	7.045	5.093	1.823	2.793	5.22E-03	2.18E-02
ZNF733P	6.650	5.092	1.833	2.777	5.48E-03	2.27E-02
RP11-205M3.6	6.774	5.089	1.828	2.784	5.37E-03	2.23E-02
RP11-131K5.2	13.138	5.081	1.340	3.793	1.49E-04	1.00E-03
FEZ1	154.000	5.079	0.398	12.746	3.29E-37	2.97E-35
DLEC1	41.099	5.078	0.769	6.605	3.99E-11	7.23E-10
LINC02471	39.383	5.076	0.776	6.541	6.12E-11	1.10E-09
NRBP2	26.553	5.069	0.946	5.356	8.50E-08	1.06E-06
ZFHX4-AS1	72.209	5.065	0.572	8.863	7.78E-19	2.69E-17
SLIT2	13.584	5.063	1.315	3.851	1.18E-04	8.10E-04

LINC01821	45.832	5.056	0.716	7.057	1.70E-12	3.56E-11
RP11-274B21.9	6.692	5.055	1.827	2.767	5.66E-03	2.33E-02
LINC01213	13.620	5.053	1.315	3.843	1.21E-04	8.34E-04
SIGLEC6	52.412	5.045	0.665	7.587	3.27E-14	8.27E-13
RP11-357P18.3	6.451	5.044	1.845	2.735	6.24E-03	2.53E-02
ANKK1	6.451	5.044	1.845	2.735	6.24E-03	2.53E-02
BOLL	26.565	5.041	0.935	5.391	7.03E-08	8.90E-07
OR51I1	6.605	5.035	1.859	2.709	6.75E-03	2.70E-02
AKR1C3	63.802	5.035	0.609	8.262	1.43E-16	4.32E-15
RP11-352M15.1	6.334	5.031	1.855	2.713	6.67E-03	2.67E-02
LINC01474	122.761	5.026	0.440	11.427	3.05E-30	2.01E-28
SP6	159.577	5.024	0.391	12.856	7.94E-38	7.35E-36
MYH11	6.062	5.016	1.962	2.556	1.06E-02	3.92E-02
ANKRD45	18.830	5.007	1.120	4.471	7.79E-06	7.03E-05
LA16c-321D4.2	6.647	4.997	1.852	2.698	6.99E-03	2.78E-02
PDE11A	6.530	4.983	1.846	2.699	6.96E-03	2.77E-02
PCDHGA8	6.530	4.983	1.846	2.699	6.96E-03	2.77E-02
TMEM144	70.430	4.982	0.588	8.477	2.31E-17	7.39E-16
RP11-236B18.2	25.012	4.971	0.944	5.266	1.39E-07	1.69E-06
CYP1A2	136.573	4.971	0.414	12.009	3.17E-33	2.39E-31
HTR6	55.534	4.970	0.637	7.799	6.26E-15	1.66E-13
TSPEAR-AS1	12.107	4.969	1.361	3.652	2.60E-04	1.65E-03
LTBP1	18.841	4.967	1.086	4.572	4.82E-06	4.53E-05
LINC01916	111.808	4.965	0.454	10.936	7.76E-28	4.66E-26
DNAH6	721.307	4.953	0.209	23.702	3.47E-124	2.28E-121
CAV1	17.843	4.948	1.122	4.408	1.04E-05	9.18E-05
MMP13	6.053	4.944	1.869	2.645	8.17E-03	3.17E-02
LINC01761	6.177	4.942	1.859	2.658	7.86E-03	3.07E-02
RP4-550H1.4	6.177	4.942	1.859	2.658	7.86E-03	3.07E-02
RP11-10H3.1	115.261	4.936	0.448	11.022	2.99E-28	1.82E-26
ENPP5	42.771	4.935	0.726	6.803	1.03E-11	1.99E-10
RP1-305G21.1	6.207	4.935	1.895	2.605	9.19E-03	3.49E-02
RP1-79C4.1	96.041	4.935	0.487	10.125	4.26E-24	2.08E-22
DNAH11	127.223	4.925	0.446	11.043	2.36E-28	1.45E-26
NTS	71.116	4.921	0.562	8.753	2.07E-18	7.01E-17
PCDHGB4	6.090	4.919	1.884	2.611	9.03E-03	3.45E-02
LINC02862	5.700	4.901	1.915	2.559	1.05E-02	3.90E-02
GLT1D1	5.854	4.891	1.883	2.597	9.40E-03	3.56E-02
LINC01014	53.246	4.883	0.650	7.510	5.91E-14	1.46E-12
LINC01887	6.132	4.879	1.877	2.599	9.36E-03	3.55E-02
PCDH15	1587.003	4.877	0.161	30.274	2.48E-201	5.70E-198
SETD7	111.698	4.877	0.449	10.859	1.81E-27	1.05E-25
ROS1	69.403	4.871	0.560	8.694	3.49E-18	1.17E-16
L1CAM	11.428	4.870	1.384	3.520	4.32E-04	2.58E-03
AC010148.1	5.891	4.866	1.902	2.558	1.05E-02	3.91E-02
LINC01541	6.014	4.864	1.874	2.596	9.43E-03	3.57E-02
RP13-492C18.2	5.619	4.862	1.906	2.551	1.07E-02	3.97E-02
TLE2	5.619	4.862	1.906	2.551	1.07E-02	3.97E-02
LINC02293	17.683	4.853	1.108	4.382	1.18E-05	1.03E-04
CTSE	75.302	4.852	0.541	8.970	2.98E-19	1.06E-17
KRTAP22-1	5.773	4.850	1.897	2.557	1.06E-02	3.92E-02
RP11-268G12.1	5.501	4.847	1.928	2.514	1.19E-02	4.33E-02
ERC2	90.710	4.839	0.491	9.851	6.81E-23	3.05E-21
ACVR1C	5.625	4.838	1.940	2.493	1.26E-02	4.55E-02
TNS1	570.999	4.836	0.229	21.117	5.61E-99	2.15E-96
KLF15	5.779	4.836	1.884	2.566	1.03E-02	3.83E-02
RP3-468K18.6	5.655	4.836	1.898	2.548	1.08E-02	4.00E-02
MIR1295B	11.112	4.834	1.389	3.480	5.01E-04	2.93E-03

FER1L6	11.112	4.834	1.389	3.480	5.01E-04	2.93E-03
RP11-205A6.1	23.058	4.832	0.971	4.976	6.49E-07	7.11E-06
C2CD4D-AS1	5.661	4.820	1.899	2.538	1.11E-02	4.10E-02
MAL2	50.954	4.817	0.648	7.431	1.08E-13	2.60E-12
COLCA1	130.339	4.793	0.414	11.563	6.36E-31	4.31E-29
DAZL	11.630	4.792	1.370	3.499	4.68E-04	2.76E-03
SLC35F1	221.216	4.792	0.320	14.973	1.11E-50	1.64E-48
LINC02331	724.734	4.789	0.193	24.837	3.58E-136	3.16E-133
AC023669.1	5.456	4.778	1.914	2.496	1.26E-02	4.53E-02
EEF1A2	10.442	4.775	1.411	3.385	7.12E-04	3.98E-03
RP11-394J1.3	5.734	4.767	1.916	2.489	1.28E-02	4.60E-02
MTND4LP3	11.226	4.767	1.399	3.407	6.57E-04	3.71E-03
OSMR-AS1	95.953	4.764	0.476	10.019	1.25E-23	5.98E-22
RP1-122K4.2	5.339	4.763	1.921	2.480	1.32E-02	4.70E-02
FMO3	1113.512	4.761	0.171	27.922	1.44E-171	2.05E-168
CTB-12A17.2	5.493	4.753	1.945	2.443	1.46E-02	5.11E-02
RP11-53O19.2	5.221	4.748	1.935	2.454	1.41E-02	4.98E-02
SORT1	105.784	4.743	0.454	10.454	1.40E-25	7.43E-24
ZNF879	26.138	4.737	0.888	5.338	9.41E-08	1.17E-06
LINC02113	16.167	4.735	1.151	4.114	3.88E-05	3.02E-04
HPCAL4	5.375	4.735	1.935	2.448	1.44E-02	5.06E-02
LINC01522	5.381	4.720	1.914	2.466	1.36E-02	4.84E-02
ZNF725P	10.044	4.715	1.422	3.316	9.13E-04	4.93E-03
SLC4A11	10.403	4.709	1.380	3.412	6.46E-04	3.65E-03
RP11-274G22.1	15.102	4.706	1.167	4.034	5.48E-05	4.10E-04
TBC1D16	20.724	4.697	0.981	4.789	1.67E-06	1.73E-05
RP11-642C5.2	46.015	4.693	0.676	6.941	3.89E-12	7.85E-11
PCDH7	30.179	4.689	0.823	5.698	1.21E-08	1.70E-07
LINC02780	5.022	4.687	1.951	2.403	1.63E-02	5.59E-02
RPL23AP93	5.022	4.687	1.951	2.403	1.63E-02	5.59E-02
RP11-120I21.2	15.380	4.685	1.139	4.114	3.89E-05	3.02E-04
EMP2	61.488	4.683	0.575	8.144	3.83E-16	1.12E-14
PLSCR4	513.630	4.678	0.219	21.361	3.10E-101	1.23E-98
FAM171A1	5.299	4.675	1.925	2.428	1.52E-02	5.28E-02
HHLA2	784.738	4.672	0.187	25.037	2.45E-138	2.34E-135
NDRG4	10.358	4.671	1.388	3.364	7.69E-04	4.26E-03
CLIC2	2192.945	4.670	0.145	32.161	6.23E-227	2.39E-223
LINC01505	45.505	4.669	0.667	6.996	2.63E-12	5.41E-11
CHST4	34.758	4.664	0.760	6.135	8.52E-10	1.37E-08
PCAT18	24.196	4.664	0.932	5.004	5.63E-07	6.22E-06
ANK3	65.940	4.662	0.562	8.289	1.14E-16	3.48E-15
MINAR2	240.887	4.659	0.316	14.741	3.52E-49	4.99E-47
OR51K1P	5.058	4.657	1.952	2.385	1.71E-02	5.82E-02
ARHGAP44	424.002	4.652	0.236	19.693	2.46E-86	7.54E-84
LINC01365	14.967	4.651	1.252	3.715	2.03E-04	1.32E-03
ZNF608	1391.632	4.648	0.154	30.227	1.06E-200	2.21E-197
TWF1P2	46.066	4.648	0.669	6.948	3.69E-12	7.49E-11
ADAM23	607.757	4.647	0.203	22.871	8.97E-116	5.42E-113
RP11-149P24.2	5.336	4.646	1.964	2.366	1.80E-02	6.08E-02
SYNPO2	382.947	4.646	0.249	18.688	6.17E-78	1.69E-75
AC005077.14	20.640	4.644	0.994	4.674	2.95E-06	2.90E-05
CYP2AB1P	64.536	4.643	0.587	7.910	2.57E-15	7.02E-14
TSPAN7	4.941	4.640	1.956	2.372	1.77E-02	5.99E-02
RP11-94M14.2	132.211	4.636	0.417	11.118	1.03E-28	6.38E-27
STXBP1	14.541	4.634	1.183	3.918	8.94E-05	6.33E-04
RP3-357D13.5	34.402	4.633	0.756	6.125	9.05E-10	1.45E-08
NAV1	232.743	4.625	0.306	15.103	1.55E-51	2.37E-49
RP11-26L20.3	4.946	4.623	1.964	2.354	1.86E-02	6.26E-02

MGMT	86.757	4.621	0.495	9.340	9.67E-21	3.74E-19
SPSB1	20.001	4.619	0.999	4.625	3.75E-06	3.59E-05
ZNF521	5.100	4.611	1.944	2.371	1.77E-02	6.01E-02
NLGN1	67.504	4.611	0.557	8.272	1.32E-16	3.99E-15
RIMS1	1318.599	4.600	0.165	27.920	1.52E-171	2.05E-168
DAB1	44.042	4.599	0.668	6.882	5.92E-12	1.17E-10
LRRC36	9.842	4.598	1.401	3.281	1.03E-03	5.50E-03
SNTG1	18.936	4.596	1.010	4.548	5.41E-06	5.03E-05
PLPP4	28.609	4.593	0.839	5.474	4.40E-08	5.77E-07
RHBDL3	46.803	4.586	0.657	6.982	2.90E-12	5.95E-11
PCDHGA9	14.231	4.583	1.157	3.961	7.46E-05	5.36E-04
SNX19P2	63.737	4.578	0.605	7.567	3.82E-14	9.59E-13
RP11-572P18.2	4.742	4.574	1.976	2.315	2.06E-02	6.81E-02
RP11-408E5.4	75.897	4.569	0.508	8.993	2.41E-19	8.64E-18
SASH1	9.013	4.569	1.468	3.112	1.86E-03	9.11E-03
CASKIN1	14.354	4.568	1.153	3.962	7.45E-05	5.36E-04
RP11-175O15.1	9.167	4.561	1.450	3.145	1.66E-03	8.31E-03
RP11-337L12.1	18.963	4.561	1.026	4.446	8.74E-06	7.83E-05
RAI14	9.730	4.556	1.416	3.217	1.30E-03	6.69E-03
CAMK2B	9.730	4.556	1.416	3.217	1.30E-03	6.69E-03
EFNA2	9.049	4.553	1.455	3.129	1.76E-03	8.69E-03
LINC01866	4.901	4.544	1.966	2.312	2.08E-02	6.85E-02
RP11-1055B8.1	4.901	4.544	1.966	2.312	2.08E-02	6.85E-02
MTUS2	18.851	4.539	1.005	4.515	6.33E-06	5.83E-05
LINC00305	9.290	4.539	1.415	3.207	1.34E-03	6.90E-03
UBE2QL1	18.683	4.533	1.040	4.359	1.30E-05	1.13E-04
OR6A2	4.660	4.523	1.998	2.264	2.36E-02	7.58E-02
POTEI	18.381	4.521	1.008	4.484	7.33E-06	6.65E-05
LINC02575	13.362	4.513	1.186	3.805	1.42E-04	9.59E-04
ELOVL4	4.666	4.509	1.979	2.278	2.27E-02	7.35E-02
AKR1C6P	4.543	4.505	1.998	2.255	2.41E-02	7.74E-02
SHISA9	77.328	4.499	0.503	8.937	3.99E-19	1.40E-17
ZNF695	17.383	4.497	1.058	4.251	2.13E-05	1.76E-04
CD1C	13.280	4.496	1.181	3.806	1.41E-04	9.58E-04
AC006115.7	4.548	4.489	2.000	2.245	2.48E-02	7.92E-02
HHIP-AS1	4.425	4.487	2.008	2.235	2.54E-02	8.09E-02
RP11-93O17.1	4.425	4.487	2.008	2.235	2.54E-02	8.09E-02
LINC02055	1016.661	4.474	0.169	26.414	9.44E-154	1.03E-150
BHLHA15	8.533	4.473	1.478	3.025	2.48E-03	1.17E-02
ABI3BP	98.129	4.472	0.457	9.781	1.35E-22	5.94E-21
LARP1P1	4.307	4.469	2.028	2.203	2.76E-02	8.62E-02
ZNF385D-AS2	97.115	4.465	0.447	9.992	1.65E-23	7.77E-22
OR51B3P	4.461	4.452	2.025	2.198	2.79E-02	8.71E-02
SLC9A7P1	4.461	4.452	2.025	2.198	2.79E-02	8.71E-02
TMEM132A	47.780	4.448	0.628	7.088	1.36E-12	2.89E-11
TRIM36	26.673	4.436	0.837	5.298	1.17E-07	1.44E-06
CGREF1	8.334	4.436	1.487	2.984	2.85E-03	1.31E-02
UTS2	4.344	4.433	2.023	2.192	2.84E-02	8.84E-02
CACNA1B	4.344	4.433	2.023	2.192	2.84E-02	8.84E-02
ENSG10010139722.1	4.344	4.433	2.023	2.192	2.84E-02	8.84E-02
GALNT9	21.289	4.429	0.933	4.749	2.04E-06	2.07E-05
OBSCN	95.848	4.428	0.447	9.906	3.91E-23	1.77E-21
RP3-416J7.6	26.202	4.423	0.840	5.267	1.38E-07	1.68E-06
ENSG10010135702.1	4.349	4.418	2.020	2.187	2.87E-02	8.92E-02
FLRT3	12.837	4.417	1.186	3.723	1.97E-04	1.28E-03
GBGT1	16.777	4.415	1.083	4.078	4.54E-05	3.46E-04
LINC01115	4.226	4.414	2.031	2.173	2.98E-02	9.18E-02
AC005077.7	4.226	4.414	2.031	2.173	2.98E-02	9.18E-02

B4GALNT4	4.226	4.414	2.031	2.173	2.98E-02	9.18E-02
RP11-407A16.3	4.226	4.414	2.031	2.173	2.98E-02	9.18E-02
RP11-845C23.3	4.226	4.414	2.031	2.173	2.98E-02	9.18E-02
KIAA1217	765.803	4.406	0.202	21.811	1.83E-105	8.60E-103
LARGE2	17.428	4.406	1.026	4.293	1.76E-05	1.48E-04
ADGRB3	29.892	4.406	0.802	5.496	3.88E-08	5.12E-07
RP4-555D20.2	530.217	4.405	0.240	18.339	4.06E-75	1.05E-72
ADAMTS3	13.437	4.404	1.195	3.684	2.29E-04	1.47E-03
GUSBP8	119.968	4.404	0.403	10.917	9.51E-28	5.62E-26
HYDIN	4.503	4.401	2.017	2.182	2.91E-02	9.01E-02
CYCSP23	4.108	4.394	2.051	2.143	3.21E-02	9.76E-02
MYO3A	4.108	4.394	2.051	2.143	3.21E-02	9.76E-02
SLC7A2	172.341	4.391	0.339	12.968	1.87E-38	1.78E-36
LRRC34	33.264	4.387	0.738	5.945	2.77E-09	4.20E-08
TNFRSF19	600.886	4.385	0.207	21.161	2.20E-99	8.54E-97
RP11-351N6.1	4.386	4.382	2.014	2.176	2.96E-02	9.14E-02
RP11-286B14.2	8.171	4.379	1.497	2.925	3.45E-03	1.54E-02
EPB41L1	20.933	4.377	0.926	4.729	2.26E-06	2.27E-05
LINC01258	51.201	4.375	0.608	7.197	6.16E-13	1.36E-11
RP11-329N11.1	8.259	4.375	1.460	2.997	2.73E-03	1.26E-02
RP11-314C9.1	8.413	4.365	1.450	3.010	2.62E-03	1.22E-02
MEIOC	8.413	4.365	1.450	3.010	2.62E-03	1.22E-02
LRRC49	115.377	4.365	0.403	10.827	2.56E-27	1.47E-25
NKAIN3	70.242	4.364	0.531	8.216	2.10E-16	6.24E-15
FZD8	291.549	4.358	0.271	16.099	2.59E-58	4.73E-56
ARL14EPL	12.680	4.358	1.187	3.670	2.42E-04	1.54E-03
ZNF682	62.346	4.357	0.547	7.973	1.55E-15	4.33E-14
CTC-786C10.3	8.090	4.352	1.512	2.878	4.00E-03	1.75E-02
NCCRP1	8.090	4.352	1.512	2.878	4.00E-03	1.75E-02
PRDM1	528.437	4.346	0.214	20.313	9.80E-92	3.22E-89
LLfos-22E10.1	16.867	4.339	1.039	4.176	2.96E-05	2.37E-04
CCL19	58.391	4.338	0.603	7.199	6.06E-13	1.34E-11
GUCY1A2	16.391	4.336	1.036	4.185	2.85E-05	2.28E-04
IRAG1	8.060	4.336	1.467	2.955	3.13E-03	1.42E-02
FBXO16	175.113	4.335	0.331	13.085	4.02E-39	3.95E-37
GRIN2D	168.915	4.334	0.347	12.483	9.25E-36	7.75E-34
ASPA	153.908	4.328	0.350	12.374	3.62E-35	2.95E-33
NYNRIN	20.490	4.328	0.943	4.587	4.50E-06	4.25E-05
PNMA8B	15.592	4.327	1.089	3.974	7.07E-05	5.12E-04
PCDHGB7	12.635	4.326	1.209	3.578	3.46E-04	2.12E-03
MFAP2	8.214	4.326	1.460	2.963	3.05E-03	1.39E-02
PPP1R3G	8.214	4.326	1.460	2.963	3.05E-03	1.39E-02
CD6	44.512	4.314	0.633	6.811	9.68E-12	1.89E-10
SGK1	55.513	4.314	0.574	7.518	5.58E-14	1.38E-12
CCR4	20.224	4.313	0.932	4.627	3.71E-06	3.56E-05
TSPAN9	15.987	4.313	1.060	4.071	4.69E-05	3.56E-04
CCDC39	12.128	4.311	1.200	3.592	3.29E-04	2.02E-03
STAB2	12.554	4.308	1.225	3.516	4.38E-04	2.61E-03
RP11-454H19.2	8.183	4.305	1.493	2.883	3.94E-03	1.72E-02
SNORA35B	16.587	4.305	1.050	4.101	4.11E-05	3.18E-04
LINC02046	19.154	4.302	0.971	4.429	9.46E-06	8.41E-05
ABBA01000934.1	7.773	4.300	1.521	2.827	4.69E-03	1.99E-02
RP11-33M22.4	11.601	4.298	1.256	3.423	6.20E-04	3.53E-03
MUCL1	629.195	4.296	0.205	20.983	9.42E-98	3.49E-95
LINC01285	12.319	4.292	1.210	3.546	3.91E-04	2.36E-03
CASC15	142.973	4.292	0.365	11.753	6.82E-32	4.82E-30
PLEKHH1	30.710	4.290	0.774	5.541	3.00E-08	4.02E-07
MT1F	11.929	4.284	1.205	3.556	3.76E-04	2.28E-03

LINC00520	23.214	4.272	0.865	4.941	7.76E-07	8.40E-06
NOS1	51.573	4.270	0.592	7.211	5.54E-13	1.23E-11
RP11-642C5.1	35.099	4.265	0.706	6.043	1.51E-09	2.36E-08
DTHD1	27.832	4.263	0.808	5.278	1.31E-07	1.59E-06
CDH20	7.574	4.258	1.534	2.776	5.50E-03	2.28E-02
FZD3	1370.376	4.253	0.150	28.390	2.70E-177	4.77E-174
SMIM10L2A	7.457	4.246	1.533	2.771	5.59E-03	2.31E-02
MAGEC1	76.673	4.246	0.480	8.849	8.83E-19	3.05E-17
GPRC5B	19.224	4.244	0.947	4.480	7.46E-06	6.76E-05
FHL1	144.039	4.236	0.360	11.774	5.34E-32	3.83E-30
CSMD3	83.466	4.235	0.461	9.195	3.77E-20	1.41E-18
BBOX1	276.333	4.231	0.266	15.898	6.59E-57	1.16E-54
GPR18	140.669	4.228	0.360	11.755	6.67E-32	4.73E-30
NR2F1-AS1	15.278	4.228	1.054	4.010	6.08E-05	4.49E-04
RP11-378I13.1	23.612	4.217	0.885	4.767	1.87E-06	1.92E-05
TNFRSF11A	40.818	4.215	0.650	6.483	8.99E-11	1.59E-09
MAGEA3	59.947	4.201	0.553	7.595	3.08E-14	7.84E-13
SLC6A6P1	7.345	4.201	1.505	2.791	5.25E-03	2.19E-02
MMP16	275.373	4.200	0.264	15.911	5.30E-57	9.44E-55
PARN	44.319	4.199	0.664	6.321	2.59E-10	4.35E-09
FYB2	105.014	4.194	0.429	9.787	1.27E-22	5.61E-21
AC004538.3	33.916	4.192	0.717	5.848	4.97E-09	7.31E-08
ZFHX4	678.515	4.190	0.191	21.916	1.85E-106	8.84E-104
JCAD	48.658	4.189	0.608	6.895	5.37E-12	1.07E-10
GABRA6	7.858	4.189	1.502	2.789	5.29E-03	2.20E-02
NPAS3	11.728	4.183	1.244	3.362	7.73E-04	4.28E-03
MDGA1	33.066	4.183	0.725	5.773	7.81E-09	1.12E-07
TNIP3	537.611	4.176	0.201	20.827	2.47E-96	9.01E-94
ADGRB2	68.770	4.175	0.517	8.080	6.45E-16	1.85E-14
LINC02607	33.072	4.174	0.717	5.825	5.72E-09	8.36E-08
KCNA6	25.778	4.172	0.809	5.156	2.52E-07	2.94E-06
CASC6	7.176	4.171	1.563	2.669	7.62E-03	2.99E-02
LRIG3	14.886	4.167	1.069	3.898	9.68E-05	6.79E-04
ZNF467	14.681	4.162	1.067	3.903	9.52E-05	6.68E-04
SH3BGRL2	25.257	4.153	0.813	5.109	3.23E-07	3.70E-06
AJ006998.2	18.828	4.152	0.971	4.277	1.89E-05	1.58E-04
PDE5A	177.809	4.147	0.324	12.780	2.13E-37	1.94E-35
ARHGAP32	137.594	4.146	0.363	11.407	3.87E-30	2.52E-28
RP11-586K2.1	14.241	4.146	1.087	3.815	1.36E-04	9.25E-04
POU6F2	7.300	4.145	1.503	2.758	5.82E-03	2.38E-02
CTD-2561J22.5	7.300	4.145	1.503	2.758	5.82E-03	2.38E-02
CNTN1	50.443	4.138	0.582	7.111	1.15E-12	2.46E-11
AC027119.1	21.188	4.134	0.885	4.670	3.02E-06	2.96E-05
NKD1	17.231	4.132	1.026	4.027	5.64E-05	4.20E-04
RALGPS2	141.962	4.132	0.355	11.632	2.85E-31	1.96E-29
SLC12A8	885.447	4.131	0.171	24.123	1.44E-128	1.04E-125
TMEM132D	21.112	4.111	0.882	4.663	3.12E-06	3.05E-05
CADM4	6.470	4.098	1.625	2.522	1.17E-02	4.25E-02
CXCR2	51.477	4.088	0.573	7.135	9.65E-13	2.08E-11
CNTNAP5	6.624	4.088	1.580	2.586	9.70E-03	3.65E-02
OGDHL	6.983	4.088	1.517	2.695	7.04E-03	2.80E-02
C6orf58	42.059	4.080	0.636	6.420	1.37E-10	2.36E-09
PCDHGB1	10.178	4.079	1.257	3.245	1.17E-03	6.13E-03
RP11-203B7.2	109.396	4.078	0.396	10.303	6.85E-25	3.47E-23
GABARAPL1	136.314	4.077	0.359	11.359	6.71E-30	4.32E-28
RP11-396O20.1	9.906	4.077	1.296	3.146	1.65E-03	8.28E-03
MTCO1P22	6.865	4.076	1.523	2.677	7.43E-03	2.93E-02
LINC01545	6.661	4.065	1.590	2.556	1.06E-02	3.92E-02

SLC24A2	13.767	4.064	1.084	3.748	1.78E-04	1.17E-03
SLC40A1	27.176	4.064	0.777	5.233	1.67E-07	2.00E-06
RP11-424M21.1	128.066	4.062	0.373	10.901	1.14E-27	6.74E-26
CTC-273B12.13	23.900	4.054	0.832	4.870	1.12E-06	1.18E-05
RP11-1023P17.2	10.542	4.050	1.280	3.164	1.55E-03	7.84E-03
CYP1A1	573.555	4.048	0.195	20.765	9.04E-96	3.25E-93
MIR3945HG	43.182	4.042	0.621	6.508	7.62E-11	1.35E-09
PWWP2AP1	6.784	4.040	1.529	2.642	8.24E-03	3.20E-02
LUM	6.425	4.039	1.594	2.534	1.13E-02	4.15E-02
DACT3	40.402	4.037	0.640	6.306	2.87E-10	4.79E-09
TRPS1	2653.572	4.032	0.123	32.669	4.36E-234	2.51E-230
RP11-289F5.1	10.102	4.032	1.259	3.202	1.36E-03	7.00E-03
KBTBD7	66.489	4.032	0.516	7.819	5.32E-15	1.42E-13
SLC4A10	6.308	4.026	1.605	2.508	1.21E-02	4.39E-02
RP11-443B7.2	55.640	4.026	0.549	7.328	2.34E-13	5.43E-12
RP11-447M4.2	26.102	4.024	0.793	5.074	3.89E-07	4.38E-06
RP11-174C7.3	7.179	4.019	1.571	2.557	1.06E-02	3.91E-02
RP11-739N10.1	9.780	4.014	1.270	3.160	1.58E-03	7.93E-03
MOAP1	9.765	4.012	1.438	2.790	5.28E-03	2.20E-02
C4A	19.733	4.010	0.926	4.333	1.47E-05	1.25E-04
IL17B	9.575	4.009	1.329	3.017	2.55E-03	1.20E-02
LINC01242	49.044	4.004	0.590	6.787	1.15E-11	2.20E-10
RP11-14A10.1	12.775	4.002	1.116	3.586	3.36E-04	2.06E-03
SLC6A14	19.534	3.994	0.927	4.308	1.65E-05	1.39E-04
LRCH2	486.906	3.990	0.204	19.580	2.29E-85	6.91E-83
TKTL1	18.920	3.986	0.929	4.288	1.80E-05	1.51E-04
KRTAP22-2	13.294	3.979	1.102	3.609	3.07E-04	1.91E-03
LINC02446	3334.875	3.978	0.124	32.057	1.74E-225	5.70E-222
MALRD1	770.265	3.967	0.179	22.136	1.43E-108	7.45E-106
PRKAG2-AS1	29.588	3.966	0.758	5.234	1.66E-07	1.98E-06
MIR548AH	6.709	3.966	1.561	2.541	1.10E-02	4.07E-02
WFDC12	6.350	3.966	1.556	2.548	1.08E-02	4.00E-02
OR1N1	9.258	3.965	1.337	2.966	3.01E-03	1.38E-02
ZNF221	63.001	3.962	0.509	7.784	7.05E-15	1.86E-13
MAGEC2	117.033	3.955	0.377	10.484	1.03E-25	5.47E-24
CTB-111H14.1	39.724	3.955	0.679	5.828	5.61E-09	8.21E-08
LINC00303	6.145	3.950	1.622	2.435	1.49E-02	5.20E-02
GRTP1	18.405	3.947	0.937	4.214	2.51E-05	2.04E-04
AC009303.1	24.432	3.946	0.827	4.773	1.82E-06	1.87E-05
ZNF703	27.822	3.942	0.766	5.143	2.71E-07	3.14E-06
LINC02842	124.673	3.939	0.373	10.555	4.81E-26	2.61E-24
LINC01644	6.386	3.938	1.556	2.530	1.14E-02	4.18E-02
LINC00922	133.366	3.938	0.366	10.753	5.74E-27	3.25E-25
ACCSL	18.528	3.938	0.919	4.287	1.81E-05	1.52E-04
SLC2A13	1106.212	3.938	0.160	24.675	2.00E-134	1.70E-131
ZNF730	98.491	3.937	0.415	9.478	2.58E-21	1.03E-19
SMPDL3A	22.006	3.936	0.846	4.651	3.31E-06	3.22E-05
SORCS1	12.655	3.933	1.110	3.543	3.95E-04	2.38E-03
CPQ	49.831	3.918	0.565	6.935	4.07E-12	8.22E-11
RERGL	6.064	3.912	1.648	2.374	1.76E-02	5.97E-02
RP11-25O3.3	6.064	3.912	1.648	2.374	1.76E-02	5.97E-02
SFTPA1	9.183	3.911	1.293	3.025	2.48E-03	1.17E-02
EVC2	246.791	3.907	0.269	14.526	8.26E-48	1.10E-45
RP11-897M7.2	11.979	3.897	1.136	3.432	5.99E-04	3.43E-03
RP11-10A14.3	12.220	3.893	1.118	3.483	4.97E-04	2.91E-03
MTND6P6	12.287	3.890	1.176	3.307	9.44E-04	5.09E-03
CTA-250D13.1	6.187	3.885	1.572	2.472	1.35E-02	4.79E-02
SEC22B3P	9.101	3.884	1.301	2.984	2.84E-03	1.31E-02

ZCCHC24	5.828	3.882	1.642	2.364	1.81E-02	6.10E-02
A2M-AS1	5.828	3.882	1.642	2.364	1.81E-02	6.10E-02
FMN1	5.828	3.882	1.642	2.364	1.81E-02	6.10E-02
RP5-1016A21.1	15.171	3.879	1.010	3.841	1.23E-04	8.42E-04
VWA3B	21.436	3.857	0.868	4.443	8.89E-06	7.95E-05
CRPPA	11.545	3.856	1.151	3.350	8.07E-04	4.44E-03
LINC01612	8.989	3.852	1.300	2.962	3.05E-03	1.39E-02
RP6-99M1.3	23.726	3.849	0.802	4.797	1.61E-06	1.67E-05
HPSE2	8.902	3.847	1.311	2.934	3.35E-03	1.50E-02
RP11-673E1.1	119.860	3.846	0.386	9.958	2.33E-23	1.08E-21
LINC02338	78.140	3.844	0.465	8.259	1.47E-16	4.42E-15
CCDC73	570.424	3.840	0.192	19.963	1.15E-88	3.67E-86
PLXDC2	490.202	3.839	0.207	18.582	4.46E-77	1.21E-74
LINC02052	32.911	3.835	0.692	5.539	3.04E-08	4.06E-07
MIR325HG	13.784	3.834	1.099	3.487	4.88E-04	2.87E-03
RCAN3	63.670	3.832	0.497	7.704	1.31E-14	3.41E-13
MAFA	17.693	3.831	0.926	4.138	3.50E-05	2.76E-04
LINC00652	5.988	3.830	1.589	2.411	1.59E-02	5.50E-02
TRABD2A	125.784	3.826	0.372	10.284	8.32E-25	4.19E-23
LINC02301	51.531	3.823	0.552	6.922	4.47E-12	8.97E-11
YPEL5P1	6.229	3.822	1.602	2.386	1.70E-02	5.82E-02
ADGRF1	8.549	3.820	1.320	2.895	3.80E-03	1.67E-02
NDST4	323.790	3.819	0.235	16.255	2.06E-59	3.94E-57
CLCN1	5.870	3.816	1.589	2.401	1.63E-02	5.61E-02
ACE	34.146	3.815	0.681	5.605	2.09E-08	2.84E-07
PRKD1	67.329	3.811	0.504	7.567	3.81E-14	9.55E-13
RP11-38M8.1	5.512	3.811	1.668	2.285	2.23E-02	7.25E-02
UNC5D	5.512	3.811	1.668	2.285	2.23E-02	7.25E-02
GYPE	8.432	3.810	1.330	2.865	4.17E-03	1.81E-02
KRTAP20-4	14.543	3.810	1.019	3.738	1.85E-04	1.21E-03
RP11-73G16.2	19.850	3.804	0.877	4.339	1.43E-05	1.22E-04
C17orf107	34.486	3.800	0.675	5.631	1.79E-08	2.46E-07
RP11-398G24.2	11.147	3.799	1.161	3.272	1.07E-03	5.67E-03
AP000431.2	103.176	3.799	0.392	9.694	3.21E-22	1.37E-20
COL6A6	59.962	3.791	0.507	7.480	7.44E-14	1.81E-12
LINC00457	5.635	3.789	1.611	2.352	1.87E-02	6.27E-02
CTC-260E6.3	26.070	3.788	0.786	4.819	1.44E-06	1.50E-05
RASGRF2	17.090	3.786	0.949	3.988	6.67E-05	4.86E-04
TMEM100	384.071	3.780	0.248	15.223	2.51E-52	3.94E-50
PCDHB15	8.950	3.777	1.340	2.819	4.82E-03	2.04E-02
KLF3	962.218	3.776	0.156	24.258	5.42E-130	4.15E-127
SSX1	39.504	3.771	0.622	6.065	1.32E-09	2.07E-08
OR5K1	16.686	3.765	0.995	3.784	1.54E-04	1.03E-03
RP1-34B20.4	8.387	3.760	1.330	2.827	4.70E-03	1.99E-02
AP000431.1	64.373	3.759	0.491	7.652	1.98E-14	5.09E-13
RP11-342F21.2	5.671	3.758	1.606	2.340	1.93E-02	6.43E-02
RP11-279N8.1	5.671	3.758	1.606	2.340	1.93E-02	6.43E-02
KCNJ2	5.671	3.758	1.606	2.340	1.93E-02	6.43E-02
ISLR	8.628	3.757	1.316	2.855	4.30E-03	1.85E-02
PAX6	57.815	3.754	0.515	7.289	3.13E-13	7.16E-12
FNBP1L	19.253	3.754	0.886	4.238	2.25E-05	1.85E-04
WT1	80.215	3.751	0.442	8.482	2.22E-17	7.10E-16
THAP10	5.912	3.751	1.621	2.313	2.07E-02	6.83E-02
KRTAP6-3	8.510	3.747	1.318	2.843	4.46E-03	1.91E-02
VGLL2	5.554	3.745	1.612	2.323	2.02E-02	6.69E-02
ZNF43	153.025	3.744	0.326	11.473	1.80E-30	1.21E-28
CLDN16	853.499	3.743	0.169	22.180	5.41E-109	2.89E-106
ADGRB1	30.161	3.739	0.706	5.296	1.18E-07	1.45E-06

CNTN4	10.990	3.737	1.153	3.241	1.19E-03	6.21E-03
MYH10	1469.697	3.731	0.136	27.344	1.28E-164	1.63E-161
LINC00536	8.305	3.730	1.345	2.774	5.54E-03	2.29E-02
VEPH1	171.490	3.730	0.312	11.944	6.99E-33	5.16E-31
KLHL32	201.402	3.726	0.287	12.988	1.43E-38	1.38E-36
BCAN	16.462	3.724	0.944	3.943	8.04E-05	5.74E-04
TSPAN11	134.908	3.712	0.342	10.852	1.96E-27	1.13E-25
EPS15P1	7.798	3.710	1.380	2.689	7.16E-03	2.84E-02
IL36G	45.228	3.706	0.584	6.347	2.20E-10	3.70E-09
AC098872.3	13.870	3.705	1.052	3.522	4.28E-04	2.55E-03
COLGALT2	124.510	3.705	0.355	10.425	1.91E-25	1.00E-23
ETV3L	102.780	3.703	0.389	9.518	1.76E-21	7.17E-20
LINC01695	326.204	3.699	0.265	13.957	2.87E-44	3.31E-42
PAGE1	20.746	3.698	0.856	4.320	1.56E-05	1.32E-04
PYY	5.472	3.698	1.624	2.277	2.28E-02	7.38E-02
RP11-290F24.3	8.193	3.697	1.332	2.775	5.52E-03	2.28E-02
CCDC74B	52.987	3.695	0.535	6.910	4.85E-12	9.72E-11
RP11-430L3.2	5.713	3.692	1.640	2.251	2.44E-02	7.80E-02
RAB26	21.895	3.690	0.829	4.451	8.56E-06	7.68E-05
FAM9B	276.803	3.686	0.248	14.863	5.71E-50	8.30E-48
PCDHGA7	13.430	3.686	1.043	3.534	4.09E-04	2.46E-03
RP11-386D6.1	13.430	3.686	1.043	3.534	4.09E-04	2.46E-03
LINC01388	7.476	3.685	1.434	2.571	1.02E-02	3.80E-02
PCDHB10	5.355	3.683	1.629	2.261	2.37E-02	7.63E-02
RP11-236B18.5	8.588	3.681	1.370	2.686	7.23E-03	2.87E-02
ODAPH	7.717	3.680	1.369	2.689	7.17E-03	2.84E-02
SLC49A3	31.380	3.679	0.689	5.342	9.22E-08	1.14E-06
CLEC2D	39.553	3.679	0.620	5.929	3.04E-09	4.59E-08
AGMO	18.345	3.668	0.888	4.130	3.63E-05	2.85E-04
PKHD1	125.870	3.664	0.357	10.276	9.04E-25	4.54E-23
CTB-30L5.1	16.019	3.657	0.964	3.794	1.48E-04	9.98E-04
BEX5	178.958	3.656	0.329	11.110	1.12E-28	6.95E-27
BAMBI	323.787	3.651	0.241	15.157	6.81E-52	1.06E-49
TANC2	78.903	3.650	0.444	8.227	1.91E-16	5.71E-15
TFEC	214.079	3.648	0.278	13.132	2.16E-39	2.13E-37
CDK7	27.419	3.648	0.910	4.009	6.09E-05	4.50E-04
SPTA1	53.572	3.646	0.533	6.835	8.19E-12	1.61E-10
RP11-12A2.1	15.338	3.643	1.007	3.617	2.98E-04	1.86E-03
CSAG3	21.181	3.639	0.837	4.349	1.37E-05	1.17E-04
LINC01397	10.275	3.636	1.177	3.089	2.01E-03	9.76E-03
CAVIN3	10.275	3.636	1.177	3.089	2.01E-03	9.76E-03
NOS1AP	5.273	3.634	1.644	2.211	2.71E-02	8.49E-02
MIR548AG2	5.273	3.634	1.644	2.211	2.71E-02	8.49E-02
MTND4P16	39.948	3.633	0.644	5.645	1.65E-08	2.27E-07
JAM2	72.572	3.632	0.458	7.925	2.27E-15	6.23E-14
CTD-2374C24.1	9.916	3.630	1.208	3.006	2.64E-03	1.23E-02
RTKN2	13.156	3.624	1.070	3.386	7.10E-04	3.98E-03
RP5-1031J8.1	25.655	3.624	0.755	4.798	1.60E-06	1.66E-05
C4BPB	75.332	3.620	0.465	7.777	7.41E-15	1.95E-13
DIXDC1	19.838	3.619	0.870	4.161	3.17E-05	2.52E-04
RP11-108M9.4	5.397	3.614	1.666	2.170	3.00E-02	9.25E-02
RP11-705C15.3	35.322	3.612	0.662	5.461	4.75E-08	6.18E-07
OSBP2	12.864	3.610	1.070	3.374	7.40E-04	4.12E-03
RPLP0P2	10.435	3.609	1.182	3.054	2.26E-03	1.08E-02
DHRS3	35.532	3.609	0.640	5.639	1.71E-08	2.35E-07
RP11-167H9.4	30.346	3.606	0.691	5.219	1.80E-07	2.15E-06
RP11-25O3.2	22.135	3.606	0.852	4.234	2.30E-05	1.88E-04
MAGI2	9.835	3.605	1.205	2.993	2.76E-03	1.28E-02

RP4-555D20.4	5.038	3.604	1.659	2.172	2.98E-02	9.19E-02
RP11-545K2.1	321.726	3.603	0.242	14.880	4.44E-50	6.53E-48
LMTK3	107.788	3.600	0.376	9.567	1.10E-21	4.51E-20
OR5K4	22.208	3.598	0.880	4.091	4.29E-05	3.31E-04
MYBPC1	75.598	3.593	0.444	8.096	5.66E-16	1.64E-14
PHLDB1	27.815	3.589	0.726	4.946	7.59E-07	8.25E-06
GALNT13	25.145	3.587	0.755	4.752	2.01E-06	2.05E-05
RP11-346J10.2	5.192	3.585	1.676	2.139	3.24E-02	9.83E-02
C4BPAP1	9.754	3.580	1.206	2.967	3.00E-03	1.37E-02
MT1X	14.797	3.576	0.980	3.649	2.63E-04	1.66E-03
KDM5B	389.760	3.574	0.215	16.638	3.69E-62	7.36E-60
HOXB9	22.337	3.572	0.817	4.372	1.23E-05	1.07E-04
MAGEC3	7.355	3.570	1.378	2.592	9.55E-03	3.61E-02
FAM3D-AS1	7.868	3.570	1.397	2.555	1.06E-02	3.93E-02
CLVS1	714.823	3.569	0.177	20.109	6.19E-90	2.00E-87
COL25A1	5.074	3.568	1.666	2.141	3.22E-02	9.79E-02
CACNG8	22.461	3.567	0.805	4.432	9.35E-06	8.32E-05
IBSP	12.312	3.563	1.069	3.332	8.62E-04	4.70E-03
COL21A1	56.696	3.563	0.506	7.035	1.99E-12	4.14E-11
COL27A1	12.553	3.563	1.063	3.350	8.07E-04	4.44E-03
GTF2IP7	11.953	3.558	1.096	3.247	1.17E-03	6.11E-03
SYNM	17.633	3.554	0.912	3.897	9.74E-05	6.82E-04
RP11-657O9.1	24.542	3.554	0.766	4.640	3.49E-06	3.37E-05
FBLN2	9.913	3.553	1.190	2.987	2.82E-03	1.30E-02
RP11-30G13.1	9.555	3.545	1.214	2.920	3.50E-03	1.56E-02
KNOP1P3	10.067	3.545	1.214	2.919	3.51E-03	1.56E-02
CEP170B	41.172	3.542	0.599	5.908	3.46E-09	5.19E-08
CEACAM19	24.072	3.540	0.766	4.621	3.81E-06	3.64E-05
DSG4	78.301	3.534	0.441	8.017	1.08E-15	3.06E-14
ADGRE1	261.410	3.528	0.250	14.133	2.37E-45	2.86E-43
NTN1	494.905	3.526	0.201	17.575	3.80E-69	9.01E-67
ASIC1	14.825	3.525	0.999	3.529	4.18E-04	2.50E-03
LCAL1	20.925	3.524	0.839	4.199	2.68E-05	2.17E-04
SRGAP3	107.842	3.520	0.371	9.479	2.58E-21	1.03E-19
GLIS3	968.946	3.518	0.156	22.599	4.45E-113	2.49E-110
CNTNAP2	11.760	3.516	1.086	3.236	1.21E-03	6.30E-03
LINC02562	64.070	3.513	0.475	7.393	1.44E-13	3.40E-12
RP11-759A24.2	7.792	3.510	1.430	2.454	1.41E-02	4.98E-02
LINC02118	49.922	3.508	0.563	6.227	4.77E-10	7.89E-09
LINC01801	12.155	3.508	1.075	3.263	1.10E-03	5.82E-03
RP11-305M3.6	14.472	3.507	0.986	3.556	3.76E-04	2.28E-03
FSIP2	7.521	3.506	1.418	2.472	1.34E-02	4.78E-02
IKBKGP1	18.146	3.504	1.099	3.188	1.43E-03	7.30E-03
LRP1B	11.350	3.497	1.178	2.968	2.99E-03	1.37E-02
NGFR	6.562	3.492	1.500	2.328	1.99E-02	6.61E-02
AF241725.6	42.029	3.488	0.582	5.995	2.04E-09	3.13E-08
RP11-678G14.2	12.074	3.486	1.083	3.221	1.28E-03	6.61E-03
UNC5C-AS1	11.474	3.481	1.115	3.122	1.80E-03	8.86E-03
RAPGEF5	39.185	3.478	0.613	5.671	1.42E-08	1.97E-07
FAM66D	6.957	3.476	1.402	2.479	1.32E-02	4.71E-02
RP11-897M7.4	14.550	3.471	1.006	3.449	5.62E-04	3.24E-03
GORAB-AS1	200.658	3.467	0.279	12.436	1.66E-35	1.37E-33
TUBB2B	9.793	3.465	1.228	2.822	4.78E-03	2.02E-02
SPATA31D2P	166.427	3.460	0.347	9.984	1.79E-23	8.36E-22
PYCR3	7.148	3.460	1.550	2.233	2.56E-02	8.12E-02
FRMD7	6.481	3.456	1.495	2.312	2.08E-02	6.84E-02
SNAP91	9.434	3.455	1.220	2.832	4.62E-03	1.97E-02
DRAIC	50.278	3.454	0.530	6.515	7.27E-11	1.30E-09

EPPK1	40.880	3.449	0.586	5.883	4.02E-09	5.99E-08
TMTC1	46.428	3.449	0.558	6.176	6.58E-10	1.07E-08
RUNX1	1032.775	3.449	0.149	23.089	6.04E-118	3.75E-115
CHRNA6	199.372	3.449	0.289	11.952	6.31E-33	4.67E-31
LINC01206	24.915	3.435	0.751	4.575	4.76E-06	4.48E-05
STXBP5L	6.517	3.431	1.494	2.296	2.17E-02	7.09E-02
DPY19L2P1	19.675	3.429	0.879	3.900	9.63E-05	6.76E-04
CCNA1	25.526	3.423	0.761	4.501	6.76E-06	6.19E-05
RALYL	6.882	3.417	1.403	2.435	1.49E-02	5.20E-02
SLC2A4	6.640	3.416	1.420	2.405	1.62E-02	5.58E-02
KLHL4	121.463	3.415	0.349	9.781	1.36E-22	5.96E-21
TNFRSF14	37.457	3.412	1.481	2.305	2.12E-02	6.95E-02
HCK	934.565	3.409	0.152	22.384	5.67E-111	3.10E-108
RP11-281P23.1	8.876	3.409	1.252	2.722	6.50E-03	2.62E-02
SLIT1	38.952	3.405	0.620	5.495	3.91E-08	5.16E-07
RP11-15A1.8	6.405	3.392	1.448	2.342	1.92E-02	6.40E-02
KCTD12	266.758	3.391	0.251	13.486	1.90E-41	1.98E-39
DCBLD2	8.641	3.390	1.253	2.706	6.81E-03	2.72E-02
LINC02751	112.288	3.387	0.365	9.291	1.53E-20	5.82E-19
EIF4E3	277.892	3.385	0.240	14.113	3.17E-45	3.77E-43
RP11-89C3.6	7.041	3.377	1.450	2.329	1.99E-02	6.59E-02
ADCY2	6.559	3.376	1.431	2.359	1.83E-02	6.18E-02
FCER1A	8.647	3.373	1.245	2.710	6.73E-03	2.69E-02
ULK2	111.419	3.362	0.366	9.196	3.73E-20	1.40E-18
CCDC181	8.801	3.362	1.235	2.723	6.47E-03	2.61E-02
CRABP2	21.090	3.352	0.806	4.157	3.23E-05	2.56E-04
LINC01602	125.594	3.352	0.345	9.729	2.26E-22	9.74E-21
CAMK2N1	13.284	3.347	1.018	3.287	1.01E-03	5.41E-03
RMDN2-AS1	41.611	3.345	0.586	5.707	1.15E-08	1.62E-07
LRIG1	110.596	3.342	0.365	9.150	5.71E-20	2.11E-18
RP11-705C15.2	15.043	3.340	0.947	3.528	4.19E-04	2.51E-03
C21orf62-AS1	6.719	3.339	1.430	2.335	1.95E-02	6.51E-02
KCNMB3	50.013	3.334	0.538	6.201	5.60E-10	9.21E-09
TUBA8	50.988	3.333	0.519	6.419	1.37E-10	2.37E-09
NYX	10.448	3.329	1.127	2.955	3.13E-03	1.42E-02
FRAS1	298.115	3.326	0.237	14.030	1.02E-44	1.20E-42
CTD-2545G14.4	6.360	3.323	1.447	2.296	2.17E-02	7.09E-02
CPT1C	8.361	3.320	1.272	2.609	9.07E-03	3.46E-02
LINC01093	21.210	3.313	0.797	4.159	3.20E-05	2.54E-04
PDGFRA	43.426	3.312	0.566	5.855	4.77E-09	7.03E-08
AJ003147.11	6.001	3.312	1.533	2.160	3.08E-02	9.44E-02
CYP27B1	87.771	3.308	0.400	8.272	1.32E-16	3.99E-15
ESRRB	189.556	3.307	0.281	11.763	6.04E-32	4.29E-30
RP4-794I6.4	8.607	3.305	1.255	2.632	8.48E-03	3.27E-02
ITGA2	61.643	3.297	0.476	6.932	4.15E-12	8.37E-11
LINC02588	20.980	3.297	0.807	4.084	4.44E-05	3.40E-04
MTND5P5	10.280	3.295	1.167	2.823	4.76E-03	2.01E-02
SLC24A4	32.630	3.295	0.648	5.086	3.66E-07	4.14E-06
EGFEM1P	161.752	3.280	0.302	10.854	1.92E-27	1.11E-25
LINC01208	12.891	3.280	1.052	3.116	1.83E-03	9.01E-03
LINC00963	13.538	3.275	1.033	3.171	1.52E-03	7.70E-03
GABRA4	189.068	3.273	0.287	11.406	3.91E-30	2.53E-28
GULP1	20.095	3.270	0.819	3.993	6.51E-05	4.76E-04
SLC30A3	8.044	3.269	1.283	2.547	1.09E-02	4.01E-02
TLCD4	137.960	3.266	0.330	9.907	3.86E-23	1.76E-21
CMTM7	534.800	3.266	0.189	17.256	1.00E-66	2.28E-64
RP11-1137G4.4	14.328	3.265	0.961	3.399	6.77E-04	3.80E-03
LINC02840	20.131	3.262	0.822	3.968	7.25E-05	5.23E-04

HMGN1P31	12.569	3.260	1.036	3.148	1.65E-03	8.25E-03
RASD1	8.562	3.253	1.273	2.555	1.06E-02	3.93E-02
SPATA31D1	374.464	3.253	0.252	12.896	4.72E-38	4.42E-36
TPRXL	20.501	3.253	0.810	4.014	5.96E-05	4.42E-04
TFAP2B	8.050	3.253	1.269	2.562	1.04E-02	3.87E-02
GS1-304P7.2	18.649	3.249	0.856	3.795	1.48E-04	9.94E-04
PRDM8	45.636	3.247	0.554	5.860	4.62E-09	6.82E-08
CCDC80	13.734	3.246	0.984	3.301	9.65E-04	5.19E-03
PCDHGB3	28.859	3.246	0.691	4.698	2.63E-06	2.60E-05
GPR87	5.926	3.242	1.472	2.202	2.77E-02	8.64E-02
P3H3	35.062	3.241	0.635	5.107	3.28E-07	3.74E-06
RP11-434J24.4	46.893	3.240	0.574	5.642	1.68E-08	2.32E-07
CCDC184	15.895	3.239	0.909	3.564	3.65E-04	2.22E-03
MEIS1	79.586	3.238	0.427	7.578	3.50E-14	8.82E-13
FES	130.838	3.234	0.334	9.693	3.24E-22	1.38E-20
GNB3	7.845	3.226	1.295	2.490	1.28E-02	4.59E-02
RP11-381O6.1	12.252	3.225	1.043	3.092	1.99E-03	9.66E-03
SETP6	18.091	3.224	0.860	3.748	1.78E-04	1.17E-03
PLXNA2	9.733	3.221	1.155	2.790	5.27E-03	2.20E-02
ZNF300	13.659	3.218	0.978	3.289	1.00E-03	5.37E-03
LAMB4	29.657	3.218	0.688	4.676	2.93E-06	2.88E-05
RNU6-12P	10.641	3.218	1.186	2.713	6.66E-03	2.67E-02
RP11-214N1.1	6.203	3.217	1.460	2.203	2.76E-02	8.62E-02
MAGEA10	630.864	3.216	0.183	17.566	4.47E-69	1.05E-66
LINC01096	15.578	3.213	0.915	3.510	4.48E-04	2.66E-03
AC078899.3	13.813	3.210	0.971	3.307	9.44E-04	5.09E-03
LINC00261	74.945	3.208	0.432	7.421	1.16E-13	2.78E-12
CLIP3	54.268	3.205	0.500	6.405	1.50E-10	2.58E-09
RP11-489G11.5	6.086	3.204	1.460	2.194	2.82E-02	8.79E-02
LAMA4	7.733	3.199	1.292	2.476	1.33E-02	4.74E-02
ANKRD30BL	27.191	3.192	0.695	4.596	4.30E-06	4.08E-05
FRG1FP	241.126	3.192	0.265	12.048	2.00E-33	1.54E-31
SCN2A	51.093	3.190	0.515	6.195	5.83E-10	9.58E-09
ITGAX	480.729	3.188	0.208	15.349	3.59E-53	5.84E-51
KCNMB2	65.011	3.188	0.492	6.475	9.49E-11	1.67E-09
DNMT3B	11.454	3.184	1.063	2.996	2.73E-03	1.27E-02
SPEF2	26.628	3.181	0.713	4.460	8.19E-06	7.37E-05
CCDC74A	289.353	3.175	0.236	13.471	2.33E-41	2.42E-39
CH507-528H12.1	15.796	3.172	1.074	2.953	3.15E-03	1.43E-02
MEFV	7.287	3.172	1.390	2.282	2.25E-02	7.29E-02
PTPRU	11.731	3.171	1.053	3.011	2.60E-03	1.21E-02
MAPK10	1926.812	3.170	0.137	23.217	3.07E-119	1.96E-116
LINC02364	21.456	3.166	0.798	3.968	7.26E-05	5.23E-04
NYAP2	17.617	3.163	0.868	3.645	2.67E-04	1.68E-03
ECHDC2	125.219	3.160	0.342	9.238	2.52E-20	9.50E-19
IL23R	258.680	3.160	0.244	12.944	2.53E-38	2.40E-36
RP11-530N7.2	17.500	3.158	0.866	3.646	2.66E-04	1.68E-03
SMOC1	19.178	3.158	0.831	3.799	1.45E-04	9.79E-04
RP11-27G22.2	8.047	3.157	1.294	2.440	1.47E-02	5.14E-02
APBB1	9.335	3.151	1.168	2.697	7.01E-03	2.79E-02
NCR3LG1	11.137	3.147	1.073	2.932	3.37E-03	1.51E-02
PCDHGA11	9.094	3.147	1.200	2.623	8.72E-03	3.35E-02
RP11-40H19.1	17.388	3.145	0.877	3.587	3.35E-04	2.06E-03
G0S2	62.126	3.143	0.464	6.779	1.21E-11	2.31E-10
DCC	281.830	3.132	0.238	13.166	1.38E-39	1.37E-37
ODAD3	20.909	3.131	0.789	3.968	7.25E-05	5.23E-04
RP11-876N24.1	10.162	3.126	1.252	2.496	1.25E-02	4.52E-02
MORC1	11.568	3.126	1.080	2.894	3.80E-03	1.67E-02

ZNF470	64.384	3.123	0.459	6.805	1.01E-11	1.96E-10
LINC02326	45.377	3.122	0.546	5.714	1.11E-08	1.56E-07
STMN4	7.453	3.121	1.299	2.403	1.63E-02	5.60E-02
RGS6	959.959	3.120	0.151	20.639	1.23E-94	4.28E-92
LAMB1	16.466	3.119	0.885	3.524	4.26E-04	2.54E-03
NEUROG2	313.903	3.119	0.223	13.995	1.66E-44	1.94E-42
RP11-280F2.3	14.664	3.118	0.934	3.338	8.44E-04	4.61E-03
BAIAP2-DT	7.422	3.113	1.390	2.239	2.52E-02	8.01E-02
KCNK2	248.842	3.106	0.265	11.701	1.27E-31	8.84E-30
KIAA0513	270.773	3.104	0.244	12.710	5.19E-37	4.58E-35
GPR141	18.674	3.104	0.836	3.712	2.06E-04	1.33E-03
PCDHGA4	41.406	3.104	0.584	5.319	1.04E-07	1.28E-06
VSTM4	9.655	3.102	1.179	2.631	8.51E-03	3.28E-02
HTR7	16.508	3.101	0.878	3.531	4.14E-04	2.48E-03
RP11-314B1.2	23.997	3.099	0.733	4.231	2.33E-05	1.91E-04
SCG3	18.463	3.098	0.841	3.686	2.28E-04	1.46E-03
CDH12	74.733	3.095	0.423	7.309	2.68E-13	6.18E-12
SULT1C2P1	13.418	3.094	1.003	3.084	2.05E-03	9.90E-03
ELAPOR2	275.552	3.092	0.241	12.829	1.13E-37	1.04E-35
RP11-13A2.4	10.980	3.090	1.072	2.882	3.95E-03	1.73E-02
RP1-69D17.3	10.615	3.089	1.116	2.767	5.65E-03	2.33E-02
SLC12A1	12.664	3.089	0.999	3.091	2.00E-03	9.70E-03
AC009411.1	8.932	3.089	1.208	2.556	1.06E-02	3.92E-02
PLPPR2	93.407	3.088	0.411	7.518	5.55E-14	1.37E-12
RP11-575N24.1	47.026	3.081	0.540	5.702	1.18E-08	1.66E-07
ADM2	64.840	3.081	0.453	6.805	1.01E-11	1.97E-10
RP11-742B18.1	88.315	3.078	0.391	7.881	3.25E-15	8.79E-14
HSPA8P5	7.130	3.077	1.335	2.305	2.12E-02	6.95E-02
PGF	80.492	3.077	0.418	7.368	1.74E-13	4.07E-12
RP11-211C9.4	7.736	3.077	1.367	2.252	2.43E-02	7.79E-02
BBOX1-AS1	24.795	3.076	0.750	4.101	4.11E-05	3.18E-04
IL1R2	356.731	3.070	0.212	14.492	1.35E-47	1.80E-45
SH3PXD2B	28.927	3.068	0.668	4.596	4.32E-06	4.09E-05
RP11-116B13.1	7.377	3.068	1.326	2.314	2.07E-02	6.83E-02
SPARCL1	26.879	3.067	0.703	4.365	1.27E-05	1.10E-04
RP1	23.845	3.067	0.743	4.128	3.66E-05	2.87E-04
MCC	247.787	3.066	0.263	11.676	1.69E-31	1.17E-29
LINC00643	9.091	3.064	1.187	2.582	9.83E-03	3.69E-02
GRIK2	12.100	3.062	1.053	2.909	3.63E-03	1.61E-02
CCDC149	9.215	3.061	1.174	2.607	9.14E-03	3.48E-02
ZNF284	53.899	3.060	0.492	6.216	5.11E-10	8.41E-09
SBK1	19.360	3.059	0.813	3.761	1.69E-04	1.12E-03
PDZRN3	7.408	3.058	1.325	2.309	2.09E-02	6.89E-02
FBXO2	15.597	3.056	0.915	3.342	8.32E-04	4.55E-03
ZNF366	7.531	3.055	1.318	2.318	2.04E-02	6.75E-02
PCSK1N	7.259	3.055	1.345	2.271	2.31E-02	7.47E-02
ZNF793	110.801	3.051	0.360	8.464	2.57E-17	8.20E-16
EIF5AP2	78.584	3.050	0.411	7.420	1.17E-13	2.80E-12
LINC02752	32.415	3.046	0.634	4.808	1.52E-06	1.58E-05
NT5C1A	40.400	3.042	0.566	5.374	7.71E-08	9.68E-07
CKB	61.351	3.040	0.472	6.439	1.20E-10	2.09E-09
CTD-2288O8.1	62.374	3.040	0.467	6.512	7.40E-11	1.32E-09
LINC00560	7.049	3.040	1.351	2.250	2.45E-02	7.83E-02
LRRC32	598.835	3.035	0.178	17.077	2.22E-65	4.80E-63
IGLV6-57	22.329	3.033	0.763	3.973	7.09E-05	5.13E-04
IGSF21	6.931	3.028	1.349	2.244	2.48E-02	7.93E-02
GPRC5C	102.349	3.024	0.376	8.047	8.49E-16	2.42E-14
TRPC1	22.007	3.020	0.778	3.880	1.04E-04	7.27E-04

FAM189A1	55.627	3.020	0.488	6.194	5.87E-10	9.63E-09
DCDC2	201.703	3.019	0.275	10.969	5.38E-28	3.25E-26
CNTLN	42.882	3.019	0.560	5.390	7.06E-08	8.93E-07
CBARP	25.929	3.018	0.706	4.274	1.92E-05	1.60E-04
LINC02428	6.814	3.017	1.353	2.229	2.58E-02	8.18E-02
GPR158	72.134	3.016	0.432	6.986	2.83E-12	5.82E-11
KATNBL1P4	21.749	3.012	0.807	3.734	1.88E-04	1.23E-03
RNU6-1	8.534	3.010	1.230	2.446	1.44E-02	5.07E-02
BAIAP2	9.022	3.008	1.207	2.492	1.27E-02	4.57E-02
ROBO2	1451.158	3.008	0.137	21.961	6.73E-107	3.36E-104
RP11-546M4.1	10.618	3.007	1.090	2.759	5.80E-03	2.38E-02
NPAS2	6.696	3.006	1.364	2.204	2.76E-02	8.61E-02
RP1-134E15.3	6.696	3.006	1.364	2.204	2.76E-02	8.61E-02
RP11-531P20.2	35.595	3.004	0.612	4.907	9.25E-07	9.90E-06
PCDHGB2	41.725	3.003	0.555	5.410	6.31E-08	8.04E-07
RYR2	76.522	3.000	0.447	6.719	1.83E-11	3.45E-10
SHANK2	10.501	3.000	1.089	2.754	5.89E-03	2.40E-02
HOXC6	40.041	2.999	0.567	5.287	1.24E-07	1.52E-06
AZIN2	19.676	2.999	0.821	3.654	2.58E-04	1.63E-03
KCNC2	15.630	2.998	0.897	3.342	8.31E-04	4.55E-03
LINC01934	450.467	2.993	0.219	13.649	2.05E-42	2.25E-40
OVAAL	10.383	2.992	1.092	2.741	6.12E-03	2.49E-02
DPYD-AS1	24.571	2.991	0.725	4.127	3.67E-05	2.88E-04
DOK4	623.032	2.990	0.184	16.232	3.00E-59	5.65E-57
VASH1	65.525	2.989	0.459	6.516	7.23E-11	1.29E-09
CNGB3	13.310	2.986	0.979	3.050	2.29E-03	1.09E-02
CDH11	235.050	2.984	0.258	11.579	5.27E-31	3.58E-29
CCL17	15.247	2.983	0.934	3.196	1.39E-03	7.14E-03
FAM160A1	67.673	2.976	0.439	6.771	1.28E-11	2.43E-10
GRIK5	6.856	2.975	1.334	2.230	2.58E-02	8.17E-02
CLEC4A	11.750	2.970	1.026	2.896	3.78E-03	1.66E-02
RP11-260G13.2	6.738	2.964	1.345	2.204	2.75E-02	8.61E-02
PTGFR	13.476	2.963	0.961	3.085	2.04E-03	9.86E-03
PTPRN2	83.962	2.962	0.395	7.491	6.81E-14	1.67E-12
DEPTOR	32.154	2.957	0.627	4.714	2.42E-06	2.42E-05
SGCD	8.464	2.955	1.210	2.441	1.46E-02	5.13E-02
CALHM5	14.930	2.954	0.950	3.108	1.88E-03	9.22E-03
OBI1-AS1	32.339	2.953	0.650	4.541	5.60E-06	5.20E-05
LINC00504	44.820	2.952	0.543	5.434	5.52E-08	7.11E-07
APLP1	78.922	2.951	0.409	7.220	5.22E-13	1.16E-11
RP11-588P7.1	18.042	2.951	0.842	3.505	4.57E-04	2.71E-03
CRNDE	186.065	2.944	0.285	10.342	4.56E-25	2.34E-23
DNAH17	294.056	2.942	0.231	12.714	4.96E-37	4.40E-35
FAM155A	16.599	2.940	0.865	3.400	6.73E-04	3.79E-03
COL5A3	387.189	2.937	0.208	14.136	2.28E-45	2.77E-43
RP11-445F6.2	83.351	2.937	0.415	7.082	1.42E-12	3.01E-11
RP1-65P5.5	290.321	2.935	0.233	12.602	2.05E-36	1.76E-34
SLC16A9	66.426	2.931	0.450	6.515	7.27E-11	1.30E-09
SYTL5	11.192	2.928	1.057	2.770	5.61E-03	2.32E-02
CA13	336.680	2.927	0.219	13.365	9.66E-41	9.77E-39
LINC02082	12.949	2.920	0.993	2.939	3.29E-03	1.48E-02
RP11-361H10.5	17.160	2.920	0.878	3.324	8.89E-04	4.83E-03
EFCAB6	34.193	2.919	0.636	4.593	4.37E-06	4.14E-05
GAB3	105.964	2.915	0.367	7.942	1.99E-15	5.49E-14
ADHFE1	24.331	2.914	0.746	3.907	9.34E-05	6.57E-04
BEX2	75.701	2.911	0.454	6.406	1.49E-10	2.57E-09
RP11-426C22.1	24.343	2.903	0.715	4.058	4.94E-05	3.74E-04
NIM1K	61.410	2.901	0.456	6.357	2.05E-10	3.47E-09

RP5-851M4.1	9.508	2.900	1.135	2.556	1.06E-02	3.92E-02
SYCE1L	16.325	2.897	0.868	3.338	8.43E-04	4.61E-03
GABRA3	23.141	2.896	0.739	3.919	8.90E-05	6.30E-04
DCAF8L2	7.542	2.892	1.350	2.142	3.22E-02	9.78E-02
SNX18	3083.228	2.890	0.117	24.642	4.45E-134	3.65E-131
SOX2	34.717	2.890	0.623	4.641	3.46E-06	3.35E-05
NPDC1	122.557	2.886	0.334	8.646	5.33E-18	1.75E-16
IL12RB2	77.523	2.881	0.432	6.674	2.49E-11	4.63E-10
TXLNB	251.077	2.880	0.247	11.671	1.80E-31	1.25E-29
PCDH9	109.757	2.876	0.350	8.205	2.30E-16	6.80E-15
LINC01275	9.946	2.867	1.124	2.552	1.07E-02	3.97E-02
CPNE4	143.459	2.865	0.306	9.359	8.08E-21	3.15E-19
DENND2B	79.872	2.865	0.402	7.125	1.04E-12	2.24E-11
NBEAP1	35.812	2.864	0.605	4.734	2.20E-06	2.22E-05
A4GALT	20.375	2.863	0.786	3.641	2.72E-04	1.71E-03
OR51B5	68.201	2.863	0.432	6.626	3.45E-11	6.33E-10
ADGRF2	11.436	2.860	1.053	2.716	6.60E-03	2.65E-02
GBP1	519.536	2.857	0.190	15.067	2.69E-51	4.06E-49
THBS4	13.800	2.855	0.958	2.980	2.88E-03	1.32E-02
STOX2	38.193	2.854	0.572	4.986	6.15E-07	6.75E-06
CBS	10.128	2.853	1.282	2.225	2.61E-02	8.26E-02
DGKG	235.027	2.852	0.257	11.103	1.22E-28	7.51E-27
CABYR	15.686	2.848	0.882	3.231	1.24E-03	6.41E-03
RXFP1	69.237	2.848	0.433	6.582	4.65E-11	8.41E-10
FGFRL1	101.110	2.846	0.381	7.470	8.03E-14	1.95E-12
CCDC144B	8.102	2.846	1.227	2.318	2.04E-02	6.75E-02
LINC02871	258.707	2.845	0.241	11.821	3.04E-32	2.20E-30
SPRED1	236.528	2.843	0.252	11.300	1.31E-29	8.30E-28
NMRAL2P	9.469	2.843	1.127	2.523	1.16E-02	4.25E-02
ABCC9	15.450	2.838	0.887	3.198	1.38E-03	7.09E-03
AC083843.4	14.938	2.833	0.933	3.038	2.38E-03	1.13E-02
DSC3	263.317	2.832	0.236	12.025	2.63E-33	2.01E-31
KLF3-AS1	11.962	2.832	1.024	2.765	5.70E-03	2.35E-02
AP002856.4	32.915	2.832	0.629	4.505	6.63E-06	6.08E-05
RP11-640L9.2	9.623	2.830	1.140	2.484	1.30E-02	4.65E-02
LAMA5	12.481	2.829	0.984	2.876	4.02E-03	1.75E-02
ZNF385D-AS1	39.930	2.829	0.560	5.049	4.44E-07	4.97E-06
ZNF660	200.641	2.826	0.264	10.708	9.33E-27	5.24E-25
ARHGEF40	28.245	2.823	0.663	4.260	2.05E-05	1.70E-04
AC011288.2	115.086	2.822	0.357	7.906	2.67E-15	7.27E-14
PDE4D	427.088	2.811	0.206	13.653	1.93E-42	2.13E-40
RP11-755O11.2	11.032	2.804	1.053	2.662	7.77E-03	3.04E-02
ODF1	19.666	2.802	0.787	3.562	3.68E-04	2.23E-03
MMP2-AS1	21.947	2.801	0.756	3.706	2.10E-04	1.35E-03
TYRP1	8.026	2.800	1.256	2.230	2.57E-02	8.17E-02
PPP4R3C	43.505	2.799	0.543	5.153	2.56E-07	2.98E-06
RP11-554A11.11	158.939	2.798	0.296	9.448	3.45E-21	1.37E-19
RP11-122D13.1	63.479	2.797	0.452	6.187	6.12E-10	9.98E-09
CTC-260E6.4	95.999	2.792	0.379	7.362	1.81E-13	4.23E-12
RP11-468H14.2	17.092	2.787	0.851	3.274	1.06E-03	5.62E-03
FKBP10	25.614	2.785	0.692	4.022	5.76E-05	4.28E-04
FAM198B-AS1	25.639	2.784	0.699	3.980	6.88E-05	4.99E-04
SCML2P2	13.321	2.784	0.974	2.858	4.27E-03	1.84E-02
RP11-449H15.3	7.668	2.781	1.248	2.228	2.59E-02	8.20E-02
MIR3150BHG	288.744	2.780	0.234	11.868	1.74E-32	1.27E-30
PTPRF	159.681	2.776	0.296	9.376	6.85E-21	2.68E-19
LINC01699	7.939	2.776	1.270	2.185	2.89E-02	8.95E-02
ACBD7	16.708	2.776	0.878	3.161	1.57E-03	7.92E-03

TEKT5	8.429	2.774	1.282	2.164	3.05E-02	9.36E-02
RP11-179A10.2	9.065	2.774	1.165	2.381	1.72E-02	5.88E-02
KRT8P45	19.633	2.771	0.789	3.513	4.43E-04	2.63E-03
HES2	14.977	2.769	0.898	3.085	2.03E-03	9.86E-03
KREMEN2	119.166	2.768	0.337	8.214	2.13E-16	6.35E-15
C17orf99	322.631	2.765	0.228	12.107	9.70E-34	7.50E-32
NR2F1	32.489	2.762	0.622	4.438	9.08E-06	8.10E-05
RP11-492A10.1	8.830	2.756	1.162	2.372	1.77E-02	6.00E-02
RP11-361H10.3	10.475	2.755	1.068	2.580	9.87E-03	3.71E-02
ANKRD65	7.704	2.754	1.253	2.198	2.79E-02	8.72E-02
ARHGEF17	484.334	2.753	0.186	14.798	1.52E-49	2.18E-47
PRSS12	20.101	2.750	0.808	3.404	6.63E-04	3.74E-03
TUBB4A	48.673	2.749	0.529	5.196	2.03E-07	2.41E-06
RP11-15B24.5	33.110	2.747	0.615	4.470	7.81E-06	7.05E-05
NRXN3	1058.591	2.746	0.160	17.169	4.53E-66	1.00E-63
RAB3A	48.561	2.745	0.524	5.242	1.59E-07	1.90E-06
SPACA6	62.579	2.743	0.449	6.105	1.03E-09	1.63E-08
GABRB2	227.350	2.743	0.259	10.594	3.17E-26	1.73E-24
JAKMIP2	270.447	2.742	0.233	11.764	6.01E-32	4.28E-30
LINC02223	22.000	2.740	0.741	3.700	2.15E-04	1.39E-03
NMNAT3	80.418	2.740	0.398	6.889	5.62E-12	1.12E-10
GBE1	5612.874	2.737	0.112	24.331	9.30E-131	7.37E-128
MCMDC2	31.390	2.736	0.628	4.357	1.32E-05	1.14E-04
TPBG	81.351	2.735	0.397	6.886	5.72E-12	1.14E-10
RP11-513H8.2	11.914	2.732	1.030	2.651	8.01E-03	3.12E-02
PRR5L	191.284	2.732	0.273	9.999	1.53E-23	7.30E-22
RP11-369E15.3	30.939	2.728	0.649	4.206	2.60E-05	2.10E-04
HTR1B	13.354	2.721	1.026	2.653	7.97E-03	3.11E-02
CSRP2	25.008	2.717	0.699	3.885	1.02E-04	7.14E-04
CXCL16	15.128	2.713	0.920	2.947	3.21E-03	1.45E-02
LINC01687	97.395	2.707	0.378	7.156	8.29E-13	1.80E-11
OR51B4	30.062	2.699	0.677	3.989	6.64E-05	4.84E-04
PPM1H	1862.260	2.698	0.124	21.791	2.82E-105	1.22E-102
JPH2	8.914	2.696	1.163	2.319	2.04E-02	6.75E-02
BAALC-AS1	209.831	2.695	0.256	10.512	7.63E-26	4.10E-24
GRM7	18.719	2.692	0.803	3.354	7.96E-04	4.39E-03
LINC02732	23.448	2.692	0.725	3.714	2.04E-04	1.32E-03
CTC-260E6.6	85.196	2.691	0.387	6.947	3.74E-12	7.56E-11
RP11-114G22.1	14.657	2.690	0.909	2.960	3.07E-03	1.40E-02
IL1RN	8.278	2.687	1.200	2.240	2.51E-02	8.00E-02
SNX30	88.824	2.685	0.385	6.973	3.09E-12	6.32E-11
MTCO3P35	22.353	2.684	0.780	3.440	5.83E-04	3.34E-03
ARHGAP27	14.685	2.683	1.110	2.417	1.56E-02	5.41E-02
KCNK15-AS1	24.498	2.682	0.702	3.819	1.34E-04	9.12E-04
NCAM2	22.848	2.680	0.725	3.695	2.20E-04	1.41E-03
SHANK3	46.766	2.679	0.541	4.955	7.23E-07	7.88E-06
SCRIB	29.521	2.679	0.782	3.424	6.16E-04	3.51E-03
LOXL3	287.667	2.678	0.223	12.000	3.55E-33	2.65E-31
RP11-440D17.3	26.527	2.676	0.697	3.841	1.23E-04	8.42E-04
FGF2	31.415	2.674	0.626	4.273	1.93E-05	1.60E-04
HSF5	9.965	2.672	1.091	2.449	1.43E-02	5.04E-02
RNU7-181P	11.245	2.671	1.024	2.610	9.05E-03	3.45E-02
ZNF528	94.214	2.670	0.370	7.217	5.32E-13	1.18E-11
TREM1	38.999	2.668	0.571	4.673	2.96E-06	2.91E-05
NFIA	24.053	2.665	0.710	3.754	1.74E-04	1.15E-03
DDR2	678.664	2.660	0.170	15.623	5.05E-55	8.41E-53
RP11-386G21.2	12.808	2.659	0.967	2.750	5.95E-03	2.43E-02
RP11-542H15.1	8.197	2.655	1.195	2.222	2.63E-02	8.30E-02

RP11-29A19.2	41.463	2.654	0.588	4.515	6.33E-06	5.83E-05
LINC00375	16.270	2.654	0.870	3.052	2.27E-03	1.08E-02
AC010091.1	14.223	2.654	0.919	2.888	3.88E-03	1.70E-02
RP11-897M7.1	37.953	2.651	0.567	4.677	2.90E-06	2.86E-05
AP1S3	327.687	2.648	0.221	12.010	3.13E-33	2.38E-31
CRTC1P1	50.560	2.647	0.524	5.053	4.35E-07	4.87E-06
PTGR1	28.484	2.645	0.663	3.990	6.60E-05	4.82E-04
SYN1	141.923	2.640	0.303	8.715	2.91E-18	9.80E-17
AFP	14.778	2.639	0.955	2.762	5.74E-03	2.36E-02
LINC01979	28.915	2.638	0.657	4.016	5.92E-05	4.39E-04
AR	36.233	2.637	0.577	4.573	4.80E-06	4.52E-05
ENTHD1	22.764	2.636	0.749	3.521	4.29E-04	2.56E-03
MTCL1	10.805	2.630	1.056	2.492	1.27E-02	4.57E-02
RP11-561O4.1	31.801	2.630	0.642	4.099	4.15E-05	3.21E-04
CERCAM	92.175	2.629	0.385	6.825	8.77E-12	1.72E-10
RP11-90K6.1	12.374	2.618	0.971	2.695	7.04E-03	2.80E-02
RPS20P20	11.236	2.617	1.093	2.395	1.66E-02	5.70E-02
ABCA13	70.760	2.617	0.426	6.141	8.22E-10	1.32E-08
GCNT4	70.515	2.616	0.421	6.219	5.01E-10	8.27E-09
KCNK9	98.745	2.613	0.366	7.148	8.79E-13	1.90E-11
LINC01607	8.245	2.613	1.221	2.140	3.23E-02	9.81E-02
MAGEB6	31.395	2.600	0.630	4.129	3.65E-05	2.86E-04
ZNF385C	158.808	2.599	0.306	8.496	1.96E-17	6.30E-16
ARNT2	17.044	2.597	0.905	2.869	4.11E-03	1.79E-02
RP11-317N12.1	10.488	2.589	1.065	2.430	1.51E-02	5.25E-02
GGNBP2	22.189	2.586	0.937	2.758	5.81E-03	2.38E-02
GASK1B	124.585	2.582	0.319	8.088	6.06E-16	1.74E-14
RP11-567P19.1	11.438	2.581	1.118	2.309	2.10E-02	6.89E-02
PARM1-AS1	65.280	2.579	0.475	5.424	5.84E-08	7.49E-07
RP11-103J8.1	100.186	2.576	0.354	7.271	3.56E-13	8.09E-12
CTD-3006G17.2	98.057	2.572	0.359	7.160	8.08E-13	1.76E-11
NENFP2	75.161	2.570	0.431	5.959	2.54E-09	3.89E-08
MIR9-1HG	42.484	2.569	0.530	4.846	1.26E-06	1.32E-05
GAS6-AS1	124.229	2.562	0.322	7.948	1.90E-15	5.25E-14
LINC02763	9.244	2.556	1.114	2.295	2.18E-02	7.10E-02
LINC00494	159.142	2.556	0.307	8.313	9.35E-17	2.86E-15
PCDHGA6	49.106	2.555	0.500	5.106	3.29E-07	3.75E-06
KLHL35	23.074	2.550	0.728	3.500	4.65E-04	2.75E-03
LINC01630	36.501	2.549	0.572	4.460	8.19E-06	7.37E-05
MYO16	186.235	2.549	0.277	9.194	3.79E-20	1.42E-18
ANKRD6	10.566	2.545	1.057	2.408	1.61E-02	5.54E-02
RP11-347H15.7	61.603	2.544	0.460	5.527	3.26E-08	4.34E-07
PKIB	20.996	2.543	0.765	3.325	8.84E-04	4.81E-03
ADAMTS20	65.769	2.543	0.430	5.912	3.39E-09	5.08E-08
RP11-459O1.2	34.324	2.543	0.590	4.312	1.61E-05	1.37E-04
ANO3-AS1	35.770	2.541	0.580	4.380	1.19E-05	1.04E-04
SAMD12-AS1	82.117	2.541	0.392	6.484	8.95E-11	1.58E-09
KIRREL2	42.047	2.539	0.532	4.768	1.86E-06	1.91E-05
RP11-439H9.1	39.316	2.537	0.549	4.618	3.88E-06	3.71E-05
RP11-44F14.10	91.468	2.532	0.386	6.554	5.60E-11	1.01E-09
OLAH	16.362	2.527	0.865	2.920	3.50E-03	1.56E-02
RP11-44F21.2	11.133	2.519	1.100	2.289	2.21E-02	7.19E-02
MTATP6P22	19.528	2.516	0.882	2.852	4.34E-03	1.87E-02
RP3-383B8.1	94.802	2.516	0.364	6.904	5.07E-12	1.01E-10
RP11-106E15.1	103.845	2.515	0.348	7.230	4.83E-13	1.08E-11
EVC	1092.659	2.512	0.138	18.145	1.40E-73	3.48E-71
CREB3L1	365.697	2.507	0.201	12.443	1.52E-35	1.26E-33
RRN3P2	30.895	2.505	0.681	3.678	2.35E-04	1.50E-03

PRKACB	238.023	2.503	0.255	9.834	8.07E-23	3.59E-21
SNX19P1	11.448	2.502	1.067	2.344	1.91E-02	6.38E-02
REEP1	9.731	2.502	1.131	2.212	2.69E-02	8.47E-02
PCDHB9	25.242	2.500	0.710	3.522	4.28E-04	2.55E-03
MIR222HG	107.027	2.498	0.346	7.228	4.89E-13	1.09E-11
PSTPIP2	238.517	2.497	0.241	10.349	4.24E-25	2.18E-23
PXT1	50.641	2.497	0.489	5.108	3.26E-07	3.72E-06
RP11-646J21.7	14.345	2.495	0.922	2.706	6.80E-03	2.72E-02
UGT8	463.755	2.494	0.184	13.579	5.36E-42	5.80E-40
PLXND1	53.445	2.493	0.472	5.279	1.30E-07	1.58E-06
SHISA3	23.976	2.488	0.700	3.553	3.80E-04	2.30E-03
DNAH17-AS1	48.778	2.484	0.499	4.977	6.45E-07	7.07E-06
MIR193BHG	112.741	2.484	0.341	7.287	3.16E-13	7.23E-12
ZYG11AP1	8.964	2.484	1.134	2.191	2.85E-02	8.85E-02
SHISAL2A	133.806	2.481	0.318	7.810	5.72E-15	1.52E-13
MIR4533	10.569	2.471	1.077	2.294	2.18E-02	7.12E-02
LINC01487	12.020	2.471	1.030	2.399	1.64E-02	5.64E-02
FCGR2A	24.721	2.469	0.716	3.450	5.61E-04	3.24E-03
FABP5P7	51.573	2.466	0.485	5.085	3.67E-07	4.15E-06
GBP2	1474.386	2.462	0.130	18.876	1.78E-79	5.12E-77
BAHCC1	44.612	2.461	0.515	4.779	1.76E-06	1.82E-05
RP11-426C22.5	32.842	2.459	0.658	3.740	1.84E-04	1.20E-03
KMT2A	15418.576	2.459	0.126	19.474	1.81E-84	5.34E-82
GALNTL6	15.121	2.449	0.874	2.801	5.09E-03	2.14E-02
MXI1	283.074	2.448	0.239	10.232	1.42E-24	7.05E-23
TEX14	30.804	2.445	0.626	3.908	9.30E-05	6.55E-04
GRIK4	173.380	2.444	0.278	8.797	1.41E-18	4.80E-17
TP63	2299.327	2.438	0.133	18.325	5.24E-75	1.34E-72
SPIC	913.753	2.436	0.160	15.268	1.25E-52	2.00E-50
HTR2B	13.317	2.429	0.926	2.622	8.74E-03	3.35E-02
LINC02605	1293.024	2.426	0.417	5.820	5.88E-09	8.58E-08
ENTPD2	1518.624	2.425	0.131	18.515	1.57E-76	4.14E-74
PCDHGA10	13.594	2.423	0.920	2.633	8.47E-03	3.27E-02
DKK2	28.807	2.422	0.642	3.772	1.62E-04	1.08E-03
LRRK2-DT	131.529	2.421	0.323	7.491	6.83E-14	1.67E-12
PPP1R3A	19.468	2.421	0.774	3.129	1.76E-03	8.69E-03
REEP2	12.000	2.421	0.996	2.430	1.51E-02	5.25E-02
TUFT1	13.359	2.411	0.921	2.619	8.83E-03	3.38E-02
EGLN3	85.538	2.410	0.380	6.346	2.20E-10	3.71E-09
C2orf27A	213.534	2.407	0.252	9.552	1.27E-21	5.19E-20
ELK3	201.426	2.406	0.262	9.192	3.86E-20	1.44E-18
AXDND1	17.379	2.406	0.822	2.928	3.41E-03	1.53E-02
PTCHD4	44.254	2.401	0.574	4.182	2.89E-05	2.31E-04
LINC00954	146.166	2.397	0.362	6.620	3.60E-11	6.57E-10
ACOXL	97.540	2.397	0.361	6.633	3.28E-11	6.05E-10
SMIM38	104.771	2.396	0.346	6.927	4.31E-12	8.67E-11
PCSK4	30.286	2.395	0.638	3.756	1.73E-04	1.14E-03
BEX4	251.201	2.394	0.237	10.094	5.88E-24	2.85E-22
RP11-44F14.2	252.694	2.393	0.242	9.907	3.86E-23	1.76E-21
RP11-44F14.9	69.567	2.392	0.424	5.643	1.68E-08	2.31E-07
LINC02822	232.972	2.392	0.243	9.839	7.65E-23	3.41E-21
LINC02392	45.989	2.391	0.508	4.706	2.53E-06	2.51E-05
MIR138-1	14.087	2.390	0.902	2.649	8.08E-03	3.14E-02
LINC02653	42.963	2.386	0.540	4.419	9.93E-06	8.79E-05
DELEC1	917.521	2.385	0.166	14.378	7.10E-47	9.15E-45
RP11-138P22.1	20.804	2.384	0.753	3.167	1.54E-03	7.77E-03
HAVCR2	275.334	2.384	0.243	9.800	1.12E-22	4.97E-21
KIAA1522	20.286	2.382	0.750	3.176	1.49E-03	7.58E-03

RAG1	15.056	2.381	0.878	2.711	6.72E-03	2.69E-02
AARD	102.691	2.380	0.359	6.623	3.53E-11	6.46E-10
ABCA9	169.971	2.379	0.294	8.093	5.81E-16	1.68E-14
TNFAIP6	87.820	2.378	0.382	6.225	4.82E-10	7.96E-09
RHEX	22.860	2.375	0.711	3.342	8.32E-04	4.55E-03
COLEC10	710.907	2.375	0.157	15.138	9.06E-52	1.40E-49
HSPG2	52.921	2.370	0.477	4.972	6.64E-07	7.25E-06
FABP5	882.325	2.365	0.156	15.148	7.83E-52	1.22E-49
LINC02476	30.512	2.363	0.668	3.540	4.01E-04	2.41E-03
ELOVL7	99.503	2.362	0.368	6.425	1.32E-10	2.28E-09
SLC41A1	58.982	2.359	0.454	5.195	2.04E-07	2.43E-06
RPS6KA2	120.292	2.358	0.334	7.063	1.63E-12	3.43E-11
BEGAIN	29.991	2.354	0.625	3.764	1.67E-04	1.11E-03
IL2RA	643.597	2.351	0.161	14.560	5.07E-48	6.85E-46
RAPGEF4	38.510	2.349	0.569	4.127	3.67E-05	2.88E-04
RP4-781K5.6	29.336	2.348	0.635	3.695	2.20E-04	1.41E-03
PRSS51	1115.315	2.345	0.180	13.013	1.03E-38	9.99E-37
MICALL2	21.647	2.341	0.748	3.132	1.74E-03	8.62E-03
GBP3	181.168	2.341	0.266	8.802	1.35E-18	4.62E-17
CNTN3	11.509	2.340	1.002	2.335	1.95E-02	6.50E-02
MMADHCP2	30.638	2.337	0.628	3.723	1.97E-04	1.28E-03
XYLT1	1074.032	2.337	0.138	16.982	1.12E-64	2.41E-62
IL32	110.759	2.330	0.341	6.824	8.84E-12	1.73E-10
AC009237.8	20.905	2.327	0.749	3.109	1.88E-03	9.19E-03
ARG1	14.244	2.327	0.909	2.560	1.05E-02	3.88E-02
RP11-131L23.1	13.607	2.316	0.915	2.530	1.14E-02	4.18E-02
ADGRL1	640.278	2.315	0.163	14.243	4.98E-46	6.15E-44
BCL2L14	87.160	2.311	0.377	6.138	8.37E-10	1.35E-08
ALDH1L2	97.317	2.299	0.356	6.453	1.10E-10	1.92E-09
ITM2B	82.877	2.298	0.397	5.792	6.97E-09	1.01E-07
TUBBP5	25.384	2.297	0.702	3.274	1.06E-03	5.63E-03
RP11-44F14.8	253.399	2.296	0.234	9.796	1.17E-22	5.17E-21
TNNT3	20.087	2.289	0.785	2.915	3.56E-03	1.58E-02
PHLDB2	32.666	2.287	0.630	3.631	2.82E-04	1.77E-03
AC067959.1	15.347	2.284	0.868	2.632	8.48E-03	3.27E-02
EXT1	800.578	2.280	0.154	14.818	1.13E-49	1.63E-47
RP11-231C14.9	13.302	2.279	0.936	2.435	1.49E-02	5.20E-02
CSF2RB	459.612	2.279	0.183	12.428	1.85E-35	1.52E-33
ENPP6	47.908	2.276	0.512	4.441	8.95E-06	8.00E-05
SULT1B1	204.491	2.276	0.255	8.920	4.67E-19	1.63E-17
MIR1205	11.518	2.274	0.993	2.289	2.21E-02	7.19E-02
PKIA-AS1	10.425	2.268	1.054	2.152	3.14E-02	9.59E-02
LINC02865	22.103	2.265	0.749	3.026	2.48E-03	1.17E-02
RP1-79C4.4	578.855	2.264	0.222	10.198	2.02E-24	9.98E-23
IL10	19.542	2.263	0.767	2.949	3.19E-03	1.44E-02
SLCO2B1	38.355	2.263	0.557	4.066	4.78E-05	3.63E-04
LINC00877	158.324	2.262	0.287	7.886	3.13E-15	8.50E-14
PERP	405.609	2.257	0.194	11.610	3.68E-31	2.52E-29
TNFRSF9	743.526	2.257	0.158	14.324	1.55E-46	1.97E-44
PTPRR	21.511	2.254	0.749	3.011	2.60E-03	1.21E-02
HOXC-AS2	23.683	2.254	0.697	3.236	1.21E-03	6.31E-03
RP11-320N21.2	53.419	2.253	0.492	4.580	4.64E-06	4.38E-05
MMP7	1803.708	2.252	0.131	17.127	9.35E-66	2.05E-63
RAB11FIP5	16.671	2.251	0.828	2.718	6.57E-03	2.64E-02
C10orf99	11.030	2.248	1.035	2.172	2.99E-02	9.21E-02
TRIM29	26.187	2.247	0.684	3.286	1.01E-03	5.41E-03
OR52H1	11.308	2.245	1.049	2.140	3.24E-02	9.83E-02
PRELID2	19.343	2.244	0.770	2.915	3.56E-03	1.58E-02

EMX1	92.319	2.244	0.373	6.017	1.78E-09	2.75E-08
HORMAD1	12.856	2.242	0.937	2.394	1.67E-02	5.71E-02
LINC02539	34.951	2.242	0.589	3.804	1.43E-04	9.64E-04
SDK2	27.749	2.241	0.646	3.469	5.23E-04	3.05E-03
CCR12P	28.736	2.241	0.637	3.518	4.35E-04	2.59E-03
RP11-655C2.3	45.869	2.237	0.519	4.307	1.65E-05	1.40E-04
SYT17	99.748	2.234	0.350	6.389	1.67E-10	2.85E-09
DTNA	299.541	2.232	0.222	10.057	8.51E-24	4.08E-22
SLITRK5	23.817	2.232	0.688	3.243	1.18E-03	6.17E-03
FOXP2	1297.114	2.231	0.144	15.449	7.69E-54	1.26E-51
ACP3	78.091	2.231	0.390	5.719	1.07E-08	1.51E-07
LINC02051	385.827	2.230	0.227	9.844	7.26E-23	3.24E-21
NAPRT	14.529	2.230	0.990	2.253	2.43E-02	7.78E-02
PSD3	25.909	2.228	0.663	3.363	7.70E-04	4.27E-03
LRP1	435.510	2.228	0.203	10.975	5.05E-28	3.06E-26
NKX3-1	124.659	2.224	0.318	7.001	2.53E-12	5.23E-11
ETV5	962.379	2.223	0.142	15.666	2.59E-55	4.37E-53
AKAP6	604.625	2.223	0.166	13.362	1.01E-40	1.01E-38
PPP1R12B	1818.224	2.222	0.128	17.407	7.35E-68	1.69E-65
PHYHIPL	221.436	2.222	0.247	8.987	2.55E-19	9.07E-18
MTND3P6	12.195	2.222	1.015	2.190	2.85E-02	8.86E-02
LINC02175	119.175	2.220	0.324	6.857	7.03E-12	1.39E-10
BDH1	22.279	2.212	0.859	2.575	1.00E-02	3.75E-02
VNN1	16.131	2.212	0.850	2.603	9.25E-03	3.51E-02
LY96	257.177	2.212	0.228	9.691	3.30E-22	1.40E-20
CYP1B1-AS1	105.243	2.210	0.342	6.461	1.04E-10	1.82E-09
RP11-452E5.1	97.789	2.209	0.359	6.154	7.54E-10	1.22E-08
GBA3	19.914	2.208	0.762	2.899	3.74E-03	1.65E-02
RP11-48B3.4	25.301	2.207	0.675	3.268	1.08E-03	5.73E-03
KIT	128.462	2.207	0.311	7.102	1.23E-12	2.62E-11
EDN1	30.354	2.203	0.617	3.571	3.55E-04	2.17E-03
AC083843.1	258.587	2.202	0.233	9.463	3.00E-21	1.19E-19
SLFN5	682.788	2.201	0.162	13.612	3.40E-42	3.72E-40
SLC35G5	13.094	2.197	0.924	2.378	1.74E-02	5.92E-02
RRAD	86.495	2.195	0.369	5.943	2.79E-09	4.24E-08
RP11-325K19.1	272.928	2.192	0.222	9.886	4.78E-23	2.16E-21
MTND5P32	12.971	2.190	0.936	2.341	1.93E-02	6.43E-02
PLEKHA7	13.587	2.179	0.903	2.414	1.58E-02	5.45E-02
RP11-384J4.2	63.684	2.179	0.427	5.100	3.39E-07	3.86E-06
P4HA2	284.776	2.177	0.220	9.907	3.88E-23	1.76E-21
TMEM244	85.118	2.175	0.384	5.671	1.42E-08	1.98E-07
CH17-84K15.2	322.545	2.174	0.211	10.322	5.62E-25	2.87E-23
ZMIZ1	1255.930	2.173	0.149	14.535	7.30E-48	9.81E-46
LINC00461	142.080	2.172	0.300	7.251	4.13E-13	9.28E-12
LINC00862	14.999	2.171	0.866	2.507	1.22E-02	4.41E-02
OR5B21	15.271	2.167	0.871	2.489	1.28E-02	4.60E-02
SERPINE1	120.739	2.163	0.336	6.446	1.15E-10	2.00E-09
PRO1804	47.014	2.162	0.548	3.947	7.91E-05	5.67E-04
RP11-412P11.1	141.869	2.161	0.297	7.276	3.43E-13	7.82E-12
HIF1A-AS3	123.439	2.161	0.339	6.372	1.86E-10	3.16E-09
LINC01822	67.054	2.160	0.416	5.194	2.06E-07	2.44E-06
FCRL3	145.528	2.159	0.293	7.356	1.90E-13	4.44E-12
SLC1A3	60.259	2.158	0.458	4.717	2.40E-06	2.40E-05
OR5K3	17.850	2.157	0.809	2.665	7.69E-03	3.01E-02
CEND1	63.880	2.156	0.432	4.995	5.88E-07	6.47E-06
CGN	17.021	2.155	0.829	2.600	9.33E-03	3.54E-02
LIPH	669.377	2.155	0.159	13.559	7.06E-42	7.57E-40
RP1-300G12.2	679.254	2.155	0.163	13.180	1.15E-39	1.14E-37

PCDHGA5	29.157	2.152	0.622	3.462	5.36E-04	3.11E-03
SPATA3-AS1	20.175	2.151	0.767	2.804	5.05E-03	2.12E-02
PRKACB-DT	14.912	2.150	0.868	2.477	1.33E-02	4.73E-02
RP1-29C18.9	89.834	2.148	0.392	5.482	4.20E-08	5.53E-07
GPR146	95.832	2.148	0.353	6.082	1.19E-09	1.88E-08
ABCA1	20.284	2.146	0.760	2.823	4.76E-03	2.01E-02
RP11-512N21.1	127.086	2.146	0.331	6.492	8.45E-11	1.50E-09
RP11-178C10.4	109.271	2.139	0.331	6.466	1.01E-10	1.77E-09
TMEM45A	53.555	2.137	0.462	4.622	3.80E-06	3.64E-05
CNN2P6	50.693	2.136	0.511	4.177	2.96E-05	2.36E-04
NUDT4B	33.666	2.136	0.650	3.287	1.01E-03	5.41E-03
RRS1-AS1	21.494	2.135	0.721	2.962	3.06E-03	1.39E-02
CMTM8	18.075	2.133	0.830	2.570	1.02E-02	3.80E-02
P2RX5-TAX1BP3	160.154	2.130	0.302	7.057	1.70E-12	3.57E-11
FAT2	103.430	2.129	0.364	5.856	4.75E-09	7.00E-08
LPL	19.396	2.128	0.759	2.804	5.04E-03	2.12E-02
IL1B	130.795	2.127	0.311	6.847	7.52E-12	1.48E-10
HS3ST3B1	13.601	2.121	0.948	2.237	2.53E-02	8.05E-02
SIAE	454.387	2.119	0.182	11.647	2.37E-31	1.64E-29
SPRY1	11.215	2.118	0.986	2.148	3.17E-02	9.66E-02
AC026167.1	40.621	2.116	0.528	4.006	6.17E-05	4.55E-04
CTD-2541M15.3	17.463	2.114	0.794	2.662	7.77E-03	3.04E-02
LINC01679	52.858	2.113	0.476	4.436	9.16E-06	8.16E-05
FRMPD2B	22.595	2.112	0.711	2.970	2.98E-03	1.36E-02
PTPRG	1018.658	2.111	0.144	14.687	7.85E-49	1.10E-46
C17orf58	47.003	2.105	0.498	4.226	2.37E-05	1.94E-04
ANAPC10P1	12.775	2.103	0.965	2.180	2.92E-02	9.05E-02
MYOF	183.003	2.103	0.295	7.135	9.65E-13	2.08E-11
GS1-204I12.4	17.376	2.095	0.809	2.589	9.62E-03	3.62E-02
ZNF790-AS1	38.643	2.095	0.540	3.881	1.04E-04	7.25E-04
RASGRP1	1702.148	2.088	0.124	16.850	1.04E-63	2.20E-61
STK32A	293.907	2.087	0.215	9.695	3.18E-22	1.36E-20
RP11-103J8.2	52.140	2.077	0.474	4.385	1.16E-05	1.01E-04
ADGRL3	219.579	2.075	0.244	8.516	1.65E-17	5.33E-16
FAM43A	268.067	2.073	0.239	8.686	3.75E-18	1.26E-16
MUC19	2356.123	2.073	0.368	5.633	1.78E-08	2.44E-07
AC011294.3	18.188	2.071	0.785	2.638	8.33E-03	3.23E-02
MLF1	17.071	2.071	0.806	2.569	1.02E-02	3.81E-02
RP11-1D12.2	227.957	2.066	0.239	8.650	5.16E-18	1.70E-16
CTD-2516F10.2	672.487	2.064	0.172	12.036	2.29E-33	1.76E-31
VDR	58.732	2.064	0.449	4.602	4.19E-06	3.99E-05
CTD-2280E9.2	19.354	2.064	0.778	2.653	7.99E-03	3.11E-02
FFAR2	105.337	2.062	0.338	6.091	1.12E-09	1.78E-08
RNF152	79.235	2.061	0.393	5.249	1.53E-07	1.84E-06
INTU	27.838	2.060	0.666	3.091	1.99E-03	9.69E-03
SMO	228.528	2.058	0.239	8.599	8.04E-18	2.63E-16
RP11-554E23.4	25.817	2.057	0.719	2.861	4.22E-03	1.83E-02
TRIB1	1099.443	2.056	0.139	14.797	1.54E-49	2.20E-47
TNFRSF11B	171.548	2.054	0.277	7.409	1.27E-13	3.03E-12
HELLPAR	1113.483	2.047	0.430	4.763	1.91E-06	1.95E-05
SOX4	1767.726	2.046	0.134	15.305	7.13E-53	1.14E-50
PLEKHA4	298.836	2.046	0.215	9.531	1.56E-21	6.36E-20
RP11-96C13.1	14.122	2.044	0.887	2.305	2.12E-02	6.96E-02
HOXC9	31.036	2.039	0.611	3.336	8.50E-04	4.64E-03
AC069277.2	27.714	2.038	0.643	3.170	1.52E-03	7.71E-03
FBXO10	286.477	2.034	0.222	9.165	4.94E-20	1.84E-18
XKR9	43.564	2.029	0.532	3.815	1.36E-04	9.27E-04
RP5-1047A19.16	23.717	2.029	0.704	2.880	3.97E-03	1.74E-02

RP11-770J1.8	22.932	2.026	0.697	2.905	3.67E-03	1.62E-02
GNG8	36.431	2.023	0.591	3.424	6.16E-04	3.51E-03
PCDH1	17.289	2.023	0.816	2.478	1.32E-02	4.72E-02
RP11-485F13.1	34.648	2.018	0.600	3.361	7.76E-04	4.29E-03
RP11-159H10.3	247.541	2.018	0.241	8.364	6.08E-17	1.88E-15
CYP4F3	809.923	2.014	0.158	12.744	3.36E-37	3.02E-35
CITED2	486.045	2.013	0.178	11.293	1.42E-29	9.02E-28
RP11-95M15.1	105.145	2.010	0.339	5.933	2.97E-09	4.50E-08
FGL2	45.522	2.009	0.533	3.770	1.63E-04	1.09E-03
TLL2	197.669	2.008	0.254	7.920	2.37E-15	6.47E-14
DZIP1	51.742	2.006	0.498	4.031	5.55E-05	4.14E-04
CTB-157D17.2	23.887	2.004	0.704	2.849	4.39E-03	1.88E-02
NTNG1	264.620	2.001	0.231	8.659	4.77E-18	1.58E-16
GPR174	1453.838	-2.009	0.141	-14.207	8.28E-46	1.01E-43
ANKFN1	1062.920	-2.010	0.163	-12.311	7.94E-35	6.36E-33
RHOBTB2	1348.970	-2.014	0.149	-13.525	1.12E-41	1.18E-39
RP11-6G22.1	239.204	-2.017	0.253	-7.957	1.76E-15	4.88E-14
XK	25.062	-2.026	0.701	-2.889	3.86E-03	1.70E-02
HFE	80.767	-2.036	0.426	-4.775	1.80E-06	1.85E-05
NLRC3	296.937	-2.039	0.227	-8.991	2.44E-19	8.74E-18
MAPKAPK3	556.751	-2.040	0.175	-11.636	2.71E-31	1.87E-29
FBXO17	101.887	-2.046	0.371	-5.509	3.60E-08	4.79E-07
KLRC1	26.417	-2.052	0.685	-2.997	2.72E-03	1.26E-02
LDB3	15.843	-2.053	0.906	-2.266	2.34E-02	7.55E-02
RP11-552F3.9	17.368	-2.053	0.845	-2.431	1.50E-02	5.24E-02
DGKD	539.601	-2.059	0.178	-11.538	8.53E-31	5.76E-29
TEKT4	158.857	-2.061	0.291	-7.074	1.51E-12	3.18E-11
ARHGEF6	347.322	-2.090	0.209	-9.999	1.54E-23	7.32E-22
TMEM51	310.718	-2.091	0.218	-9.592	8.68E-22	3.59E-20
SPATS2L	1066.489	-2.106	0.142	-14.870	5.19E-50	7.59E-48
SELL	699.652	-2.113	0.166	-12.755	2.94E-37	2.66E-35
SYBU	107.118	-2.114	0.362	-5.846	5.02E-09	7.37E-08
PLEKHG3	165.610	-2.126	0.292	-7.285	3.21E-13	7.33E-12
HMOX1	369.207	-2.126	0.205	-10.354	4.01E-25	2.07E-23
RP11-566H8.3	126.424	-2.136	0.330	-6.478	9.31E-11	1.64E-09
SEPTIN10P1	14.256	-2.142	0.958	-2.237	2.53E-02	8.05E-02
CADPS2	31.957	-2.154	0.627	-3.437	5.88E-04	3.37E-03
MS4A7	314.989	-2.160	0.219	-9.880	5.09E-23	2.29E-21
CISH	49.744	-2.162	0.520	-4.154	3.27E-05	2.58E-04
CORO2A	15.160	-2.166	0.974	-2.223	2.62E-02	8.29E-02
L1TD1	66.277	-2.177	0.447	-4.869	1.12E-06	1.18E-05
RP11-876F14.1	13.542	-2.185	0.955	-2.288	2.22E-02	7.21E-02
NXPH1	187.413	-2.193	0.279	-7.861	3.82E-15	1.03E-13
BMP7	14.994	-2.203	0.906	-2.431	1.51E-02	5.25E-02
CH17-212P11.8	59.200	-2.206	0.480	-4.594	4.34E-06	4.11E-05
IGLL5	173.286	-2.208	0.306	-7.227	4.95E-13	1.10E-11
RP11-689B22.2	66.512	-2.211	0.451	-4.905	9.34E-07	9.97E-06
PYGL	97.722	-2.220	0.373	-5.951	2.67E-09	4.07E-08
AC002407.3	12.795	-2.224	0.979	-2.271	2.31E-02	7.48E-02
LINC02532	17.020	-2.225	0.890	-2.501	1.24E-02	4.48E-02
PRF1	144.373	-2.240	0.316	-7.091	1.33E-12	2.82E-11
CAPG	746.567	-2.248	0.187	-11.996	3.71E-33	2.77E-31
LINC01694	69.902	-2.269	0.439	-5.164	2.41E-07	2.82E-06
MKRN9P	67.423	-2.281	0.443	-5.148	2.64E-07	3.06E-06
XIRP2	15.775	-2.295	0.896	-2.563	1.04E-02	3.86E-02
CDCP1	226.210	-2.299	0.256	-8.990	2.46E-19	8.79E-18
GLIPR2	12.030	-2.306	1.025	-2.250	2.45E-02	7.83E-02
WNT9A	23.972	-2.328	0.734	-3.171	1.52E-03	7.69E-03

MCF2L	12.208	-2.335	1.012	-2.307	2.10E-02	6.91E-02
LINC00698	82.292	-2.335	0.405	-5.771	7.89E-09	1.13E-07
S100A11	359.937	-2.337	0.224	-10.451	1.45E-25	7.68E-24
RP11-542M13.4	12.339	-2.354	1.009	-2.334	1.96E-02	6.52E-02
LYL1	31.216	-2.354	0.645	-3.647	2.65E-04	1.67E-03
AC092835.2	17.784	-2.355	0.845	-2.788	5.31E-03	2.21E-02
CD27	320.281	-2.365	0.230	-10.261	1.06E-24	5.28E-23
CD101	73.495	-2.367	0.425	-5.570	2.55E-08	3.43E-07
SLC45A3	138.962	-2.373	0.319	-7.448	9.44E-14	2.29E-12
RASAL2	807.398	-2.377	0.163	-14.604	2.66E-48	3.66E-46
HRAS	20.876	-2.377	0.837	-2.842	4.48E-03	1.92E-02
BMP8B	91.488	-2.378	0.391	-6.076	1.23E-09	1.93E-08
CRIP3	53.063	-2.379	0.498	-4.778	1.77E-06	1.82E-05
CD99	168.610	-2.387	0.300	-7.945	1.95E-15	5.38E-14
CD9	157.402	-2.389	0.300	-7.978	1.49E-15	4.17E-14
XCL1	49.337	-2.391	0.516	-4.638	3.51E-06	3.39E-05
PDZD2	85.051	-2.401	0.399	-6.024	1.70E-09	2.64E-08
MGST2	201.553	-2.409	0.268	-8.975	2.83E-19	1.01E-17
PHYHIP	21.012	-2.412	0.786	-3.067	2.16E-03	1.04E-02
AC009133.17	19.168	-2.412	0.852	-2.831	4.64E-03	1.97E-02
RP11-61F12.1	21.493	-2.416	0.780	-3.097	1.96E-03	9.53E-03
ACRBP	36.579	-2.419	0.605	-3.999	6.36E-05	4.67E-04
SNX7	159.725	-2.419	0.322	-7.518	5.58E-14	1.38E-12
MUC15	163.583	-2.428	0.306	-7.938	2.06E-15	5.67E-14
GRIA4	81.074	-2.432	0.422	-5.764	8.19E-09	1.17E-07
THSD7B	137.302	-2.436	0.323	-7.536	4.85E-14	1.21E-12
CARD17	21.321	-2.439	0.784	-3.112	1.86E-03	9.11E-03
HMCES	975.764	-2.443	0.171	-14.327	1.48E-46	1.90E-44
FCER1G	24.557	-2.449	0.729	-3.359	7.83E-04	4.33E-03
PLBD1	47.322	-2.455	0.537	-4.577	4.73E-06	4.45E-05
NMNAT2	113.360	-2.456	0.378	-6.503	7.87E-11	1.40E-09
MARCHF3	267.685	-2.463	0.244	-10.074	7.22E-24	3.47E-22
PWWP2B	32.829	-2.463	0.650	-3.789	1.51E-04	1.01E-03
PHLPP1	1596.354	-2.482	0.132	-18.771	1.31E-78	3.63E-76
IL12A	31.817	-2.491	0.664	-3.752	1.75E-04	1.16E-03
TM6SF1	21.401	-2.500	0.788	-3.174	1.50E-03	7.62E-03
LCP2	882.077	-2.516	0.165	-15.228	2.31E-52	3.65E-50
ZNF205	79.730	-2.524	0.417	-6.049	1.46E-09	2.27E-08
ZBP1	48.519	-2.536	0.545	-4.650	3.31E-06	3.22E-05
CARD6	222.144	-2.540	0.263	-9.665	4.23E-22	1.79E-20
ZNF239	30.880	-2.540	0.711	-3.573	3.53E-04	2.16E-03
PMFBP1	20.716	-2.553	0.831	-3.074	2.11E-03	1.02E-02
LINC01322	200.432	-2.565	0.276	-9.279	1.71E-20	6.53E-19
TRDC	9.505	-2.566	1.175	-2.184	2.90E-02	8.98E-02
KLF2	55.169	-2.581	0.500	-5.166	2.40E-07	2.81E-06
MYO7B	116.961	-2.582	0.350	-7.377	1.62E-13	3.81E-12
ZNF462	557.008	-2.591	0.191	-13.552	7.69E-42	8.21E-40
SP3P	18.745	-2.592	0.843	-3.073	2.12E-03	1.02E-02
CLEC4M	9.688	-2.605	1.178	-2.211	2.70E-02	8.48E-02
MACROD1	33.809	-2.608	0.634	-4.116	3.85E-05	3.00E-04
RP11-1134I14.2	24.116	-2.609	0.767	-3.400	6.74E-04	3.79E-03
AOC1	124.633	-2.622	0.342	-7.674	1.66E-14	4.30E-13
CELSR1	1096.526	-2.625	0.153	-17.194	2.95E-66	6.57E-64
RP11-72L22.1	11.739	-2.651	1.070	-2.477	1.33E-02	4.73E-02
SH2D2A	117.938	-2.656	0.350	-7.597	3.04E-14	7.73E-13
ST3GAL4	13.976	-2.658	1.027	-2.588	9.66E-03	3.64E-02
ITPK1	91.646	-2.670	0.409	-6.530	6.59E-11	1.18E-09
IFNG-AS1	102.689	-2.677	0.374	-7.160	8.05E-13	1.75E-11

TLR2	25.085	-2.678	0.736	-3.636	2.77E-04	1.74E-03
RP11-542M13.5	11.379	-2.685	1.091	-2.462	1.38E-02	4.89E-02
PAGE2B	63.559	-2.690	0.502	-5.356	8.53E-08	1.06E-06
MAGI3	189.888	-2.700	0.293	-9.205	3.43E-20	1.29E-18
RPS15AP38	38.152	-2.714	0.643	-4.223	2.41E-05	1.96E-04
CFAP46	33.293	-2.729	0.650	-4.198	2.70E-05	2.18E-04
RHPN2P1	17.934	-2.736	0.904	-3.027	2.47E-03	1.16E-02
HDAC7	307.787	-2.750	0.232	-11.858	1.96E-32	1.43E-30
ACSS3	33.714	-2.751	0.656	-4.193	2.76E-05	2.22E-04
MGAT4A	975.462	-2.771	0.165	-16.843	1.19E-63	2.48E-61
VIM-AS1	66.393	-2.788	0.467	-5.972	2.35E-09	3.60E-08
CPB2	19.939	-2.797	0.835	-3.350	8.08E-04	4.44E-03
RGCC	16.785	-2.800	0.925	-3.026	2.48E-03	1.17E-02
RP11-356M20.1	619.859	-2.817	0.178	-15.823	2.17E-56	3.75E-54
ST14	10.320	-2.817	1.173	-2.402	1.63E-02	5.61E-02
PALD1	86.670	-2.823	0.418	-6.758	1.40E-11	2.66E-10
PCDH17	18.454	-2.841	0.876	-3.244	1.18E-03	6.15E-03
TMEM176A	91.114	-2.844	0.407	-6.982	2.91E-12	5.97E-11
TIE1	13.249	-2.844	1.031	-2.760	5.78E-03	2.37E-02
CCNI2	1100.738	-2.847	0.155	-18.418	9.37E-76	2.45E-73
AC009133.15	8.559	-2.848	1.322	-2.154	3.12E-02	9.56E-02
MYO5C	92.058	-2.860	0.408	-7.012	2.35E-12	4.87E-11
INAVA	381.576	-2.865	0.222	-12.882	5.71E-38	5.33E-36
RP11-511B23.2	30.932	-2.867	0.696	-4.122	3.76E-05	2.94E-04
TBX15	30.264	-2.874	0.724	-3.967	7.28E-05	5.24E-04
TCL1A	238.667	-2.889	0.269	-10.730	7.37E-27	4.15E-25
GRIA3	33.993	-2.892	0.650	-4.452	8.50E-06	7.62E-05
BIK	28.882	-2.909	0.706	-4.123	3.74E-05	2.93E-04
LCK	782.852	-2.930	0.165	-17.746	1.87E-70	4.51E-68
RP11-472K17.3	76.268	-2.956	0.447	-6.612	3.80E-11	6.92E-10
AFM	32.845	-2.962	0.676	-4.385	1.16E-05	1.01E-04
RP1-81D8.7	436.811	-2.984	0.246	-12.131	7.26E-34	5.63E-32
TSPAN5	178.445	-2.987	0.315	-9.474	2.69E-21	1.07E-19
TMEM176B	49.629	-3.016	0.556	-5.428	5.69E-08	7.31E-07
FCRL5	60.828	-3.020	0.523	-5.771	7.89E-09	1.13E-07
NAP1L3	45.112	-3.032	0.591	-5.132	2.86E-07	3.30E-06
CACNB2	136.437	-3.037	0.344	-8.824	1.11E-18	3.81E-17
LINC02336	28.543	-3.038	0.740	-4.105	4.05E-05	3.14E-04
LINC01036	78.575	-3.040	0.454	-6.698	2.12E-11	3.97E-10
AKT3	10.540	-3.048	1.310	-2.327	2.00E-02	6.62E-02
LDLRAP1	227.003	-3.050	0.272	-11.205	3.84E-29	2.41E-27
CTA-445C9.17	15.227	-3.060	0.986	-3.104	1.91E-03	9.32E-03
RP11-305F18.1	14.232	-3.066	1.028	-2.982	2.86E-03	1.32E-02
CSMD1	28.712	-3.077	0.728	-4.228	2.36E-05	1.93E-04
AP001596.6	19.367	-3.104	0.878	-3.535	4.08E-04	2.45E-03
MAL	17.097	-3.115	0.937	-3.324	8.86E-04	4.82E-03
LY6E	50.401	-3.130	1.407	-2.224	2.61E-02	8.27E-02
ENG	43.567	-3.146	0.596	-5.283	1.27E-07	1.55E-06
TPO	8.803	-3.160	1.314	-2.404	1.62E-02	5.58E-02
FRMD4B	216.112	-3.174	0.281	-11.289	1.48E-29	9.39E-28
ARHGAP42	205.793	-3.179	0.299	-10.620	2.42E-26	1.34E-24
TOM1L1	185.750	-3.241	0.303	-10.681	1.25E-26	6.98E-25
CUEDC1	142.775	-3.248	0.343	-9.479	2.57E-21	1.03E-19
RP1-111D6.3	9.322	-3.255	1.289	-2.525	1.16E-02	4.23E-02
IGHV1OR15-1	12.463	-3.322	1.124	-2.955	3.13E-03	1.42E-02
SLC9C1	7.009	-3.339	1.512	-2.208	2.72E-02	8.53E-02
IGLJ2	12.678	-3.348	1.118	-2.995	2.75E-03	1.27E-02
NFIB	158.667	-3.370	0.335	-10.074	7.19E-24	3.46E-22

TMEM51-AS1	13.290	-3.383	1.205	-2.807	5.01E-03	2.11E-02
TRIML2	36.656	-3.408	0.688	-4.954	7.27E-07	7.91E-06
LINC02377	14.627	-3.409	1.065	-3.201	1.37E-03	7.04E-03
MAP4K3-DT	7.360	-3.426	1.487	-2.304	2.12E-02	6.97E-02
CD180	134.516	-3.444	0.373	-9.238	2.51E-20	9.48E-19
OBSL1	12.062	-3.456	1.188	-2.910	3.61E-03	1.60E-02
PDLIM2	51.538	-3.463	0.571	-6.063	1.34E-09	2.09E-08
RP11-76C10.6	9.272	-3.487	1.347	-2.589	9.61E-03	3.62E-02
MMP14	281.006	-3.510	0.262	-13.383	7.57E-41	7.73E-39
KCNJ15	7.748	-3.512	1.469	-2.391	1.68E-02	5.75E-02
PLD5	23.367	-3.513	0.861	-4.080	4.50E-05	3.43E-04
MN1	9.609	-3.534	1.335	-2.647	8.13E-03	3.16E-02
HACD1	16.049	-3.562	1.043	-3.416	6.35E-04	3.60E-03
CCRL2	11.305	-3.563	1.228	-2.901	3.72E-03	1.64E-02
RP3-439F8.1	8.053	-3.576	1.459	-2.451	1.42E-02	5.01E-02
LINC00540	53.769	-3.579	0.593	-6.034	1.60E-09	2.48E-08
BIN1	114.677	-3.584	0.404	-8.875	6.98E-19	2.43E-17
NTRK2	794.959	-3.588	0.176	-20.339	5.85E-92	1.95E-89
FHAD1	345.737	-3.590	0.255	-14.067	6.02E-45	7.13E-43
CDC42BPA	133.942	-3.599	0.373	-9.660	4.46E-22	1.88E-20
CYBB	23.134	-3.601	0.866	-4.160	3.19E-05	2.53E-04
LIN7A	450.177	-3.603	0.222	-16.239	2.66E-59	5.04E-57
SLC37A2	72.956	-3.606	0.497	-7.255	4.02E-13	9.05E-12
ID3	388.433	-3.634	0.235	-15.488	4.18E-54	6.90E-52
RP11-566K19.5	8.394	-3.643	1.440	-2.530	1.14E-02	4.18E-02
MEI4	105.300	-3.661	0.423	-8.664	4.57E-18	1.52E-16
FBP2	7.137	-3.704	1.608	-2.303	2.13E-02	6.98E-02
PAFAH1B2P2	19.780	-3.722	0.950	-3.918	8.94E-05	6.33E-04
S100A9	50.768	-3.732	0.604	-6.178	6.51E-10	1.06E-08
PIK3R5	905.034	-3.752	0.171	-21.939	1.09E-106	5.35E-104
TBL1X	483.914	-3.783	0.216	-17.531	8.31E-69	1.93E-66
DOCK5	183.314	-3.787	0.331	-11.454	2.25E-30	1.50E-28
ZNF831	37.542	-3.789	0.701	-5.408	6.36E-08	8.09E-07
RP11-768B22.2	7.731	-3.802	1.536	-2.476	1.33E-02	4.74E-02
ALOX12P2	113.638	-3.811	0.417	-9.145	5.95E-20	2.20E-18
DSCAS	41.280	-3.813	0.679	-5.613	1.99E-08	2.72E-07
FRMD3	153.801	-3.827	0.367	-10.421	1.98E-25	1.04E-23
KRT18	7.988	-3.848	1.525	-2.523	1.16E-02	4.25E-02
CRIM1	251.677	-3.907	0.293	-13.326	1.62E-40	1.62E-38
RP11-526D8.12	8.334	-3.909	1.507	-2.594	9.48E-03	3.58E-02
ADGRD1-AS1	10.035	-3.935	1.384	-2.844	4.46E-03	1.91E-02
CD33	205.552	-3.956	0.331	-11.935	7.75E-33	5.70E-31
ANGPT2	88.371	-3.962	0.483	-8.197	2.46E-16	7.25E-15
CLEC20A	55.396	-3.974	0.600	-6.622	3.54E-11	6.48E-10
PHETA2	14.855	-3.997	1.150	-3.474	5.12E-04	2.99E-03
NRP1	43.757	-4.022	0.676	-5.950	2.69E-09	4.09E-08
LINC02820	15.154	-4.027	1.142	-3.527	4.20E-04	2.52E-03
PPM1J	5.077	-4.042	1.851	-2.184	2.90E-02	8.98E-02
DNAH9	395.005	-4.100	0.260	-15.772	4.85E-56	8.31E-54
C20orf197	6.296	-4.111	1.750	-2.349	1.88E-02	6.32E-02
CTB-88F18.5	5.334	-4.113	1.824	-2.255	2.41E-02	7.74E-02
PDCD1	5.366	-4.116	1.886	-2.182	2.91E-02	9.01E-02
LHFPL3-AS2	99.837	-4.140	0.468	-8.846	9.10E-19	3.14E-17
U2AF1L5	143.592	-4.145	1.278	-3.245	1.17E-03	6.14E-03
VIM	3489.836	-4.147	0.128	-32.486	1.70E-231	7.80E-228
CTB-41I6.2	5.549	-4.171	1.806	-2.309	2.09E-02	6.89E-02
TLR8	18.609	-4.191	1.087	-3.854	1.16E-04	8.02E-04
CASP1P2	16.875	-4.192	1.114	-3.761	1.69E-04	1.12E-03

UGT2A1	35.657	-4.199	0.783	-5.361	8.28E-08	1.03E-06
SOHLH2	10.280	-4.211	1.432	-2.940	3.28E-03	1.48E-02
GALNT5	607.880	-4.216	0.224	-18.791	8.91E-79	2.49E-76
CECR2	137.601	-4.217	0.411	-10.253	1.14E-24	5.70E-23
VWDE	63.024	-4.247	0.589	-7.209	5.63E-13	1.24E-11
RP11-274M17.3	10.794	-4.279	1.415	-3.024	2.50E-03	1.17E-02
PARD3B	28.666	-4.280	0.871	-4.911	9.06E-07	9.72E-06
NMB	28.792	-4.286	0.871	-4.923	8.52E-07	9.18E-06
IGF1R	242.640	-4.301	0.319	-13.498	1.60E-41	1.68E-39
TREML2	88.694	-4.331	0.514	-8.426	3.57E-17	1.12E-15
LINC02466	6.194	-4.331	1.762	-2.459	1.39E-02	4.93E-02
MIR194-2HG	20.807	-4.373	1.066	-4.102	4.09E-05	3.16E-04
NEO1	380.952	-4.406	0.264	-16.688	1.59E-62	3.26E-60
CXCR2P1	269.995	-4.406	0.321	-13.706	9.35E-43	1.04E-40
FERMT1	277.601	-4.411	0.308	-14.315	1.77E-46	2.23E-44
FAM9C	451.399	-4.439	0.247	-17.979	2.86E-72	7.05E-70
EDNRB	31.019	-4.482	0.880	-5.091	3.56E-07	4.03E-06
LINC00993	20.635	-4.501	1.073	-4.194	2.74E-05	2.21E-04
SNX18P7	7.018	-4.517	1.715	-2.633	8.45E-03	3.26E-02
PLAAT2	87.845	-4.594	0.540	-8.505	1.81E-17	5.84E-16
CCR6	7.658	-4.641	1.689	-2.748	6.00E-03	2.45E-02
PRH1	8.677	-4.643	1.649	-2.815	4.87E-03	2.06E-02
EGFL6	21.347	-4.673	1.094	-4.272	1.94E-05	1.61E-04
RNF144A	21.726	-4.698	1.098	-4.280	1.87E-05	1.56E-04
SELENOP	129.581	-4.776	0.463	-10.311	6.27E-25	3.20E-23
RP11-299A16.1	3.236	-4.780	2.228	-2.146	3.19E-02	9.72E-02
SIGLEC22P	15.368	-4.781	1.315	-3.637	2.76E-04	1.74E-03
NLRP11	311.846	-4.796	0.313	-15.305	7.11E-53	1.14E-50
RP11-180M15.4	3.320	-4.814	2.214	-2.175	2.96E-02	9.15E-02
ATXN7L1	8.650	-4.819	1.650	-2.920	3.50E-03	1.56E-02
LEF1	276.708	-4.831	0.331	-14.610	2.41E-48	3.33E-46
RP11-20J15.2	8.743	-4.838	1.641	-2.948	3.20E-03	1.45E-02
VN1R53P	3.409	-4.856	2.196	-2.212	2.70E-02	8.47E-02
LINC02627	36.121	-4.860	0.882	-5.507	3.65E-08	4.84E-07
RP11-707M1.1	18.369	-4.889	1.243	-3.932	8.42E-05	5.99E-04
ANKRD18B	55.678	-4.899	0.721	-6.795	1.08E-11	2.08E-10
RP11-80K21.4	3.536	-4.904	2.177	-2.253	2.43E-02	7.77E-02
RP11-690J15.1	3.582	-4.928	2.166	-2.275	2.29E-02	7.42E-02
SNCA	25.627	-4.935	1.059	-4.658	3.19E-06	3.11E-05
PTGES3P2	3.620	-4.935	2.179	-2.265	2.35E-02	7.57E-02
YAP1	151.312	-4.940	0.446	-11.080	1.56E-28	9.58E-27
CYP4F26P	9.520	-4.962	1.616	-3.071	2.13E-03	1.02E-02
RP11-105F19.1	3.709	-4.974	2.146	-2.318	2.04E-02	6.75E-02
LINC02882	77.281	-5.000	0.626	-7.986	1.39E-15	3.90E-14
TLDC2	29.652	-5.048	1.009	-5.003	5.65E-07	6.24E-06
RAB17	10.123	-5.051	1.598	-3.161	1.57E-03	7.92E-03
MTARC2	29.793	-5.056	1.017	-4.972	6.62E-07	7.24E-06
RP11-415I12.2	227.908	-5.072	0.377	-13.435	3.78E-41	3.89E-39
COX7B2	3.971	-5.076	2.106	-2.411	1.59E-02	5.50E-02
CYCSP6	10.464	-5.097	1.590	-3.207	1.34E-03	6.91E-03
RP11-417L14.1	10.904	-5.161	1.583	-3.260	1.11E-03	5.88E-03
PLOD2	64.640	-5.176	0.708	-7.313	2.61E-13	6.02E-12
CCHCR1	4.237	-5.177	2.170	-2.386	1.70E-02	5.82E-02
ZNF415	64.808	-5.179	0.708	-7.317	2.54E-13	5.87E-12
RP11-525K10.3	234.951	-5.244	0.386	-13.575	5.62E-42	6.06E-40
RP5-1028K7.2	4.485	-5.248	2.041	-2.572	1.01E-02	3.79E-02
CYP2B6	4.490	-5.255	2.044	-2.570	1.02E-02	3.80E-02
CNTN5	79.809	-5.272	0.653	-8.079	6.52E-16	1.87E-14

HOGA1	4.579	-5.285	2.052	-2.576	1.00E-02	3.75E-02
FOXO3	686.414	-5.313	0.245	-21.711	1.63E-104	6.92E-102
RP13-577H12.2	4.789	-5.345	2.005	-2.665	7.69E-03	3.01E-02
SPOCK1	34.404	-5.351	1.014	-5.277	1.31E-07	1.59E-06
CAVIN2	57.312	-5.355	0.789	-6.788	1.14E-11	2.18E-10
RP11-20D14.6	119.489	-5.363	0.548	-9.781	1.36E-22	5.96E-21
TLR8-AS1	25.352	-5.382	1.183	-4.549	5.39E-06	5.02E-05
LINC02561	4.962	-5.396	1.988	-2.714	6.65E-03	2.67E-02
TRBC2	5.014	-5.418	2.045	-2.650	8.05E-03	3.14E-02
RP11-3P22.2	5.130	-5.441	1.981	-2.747	6.01E-03	2.45E-02
HOXD4	5.177	-5.457	1.968	-2.773	5.56E-03	2.30E-02
LPA	103.859	-5.472	0.603	-9.080	1.09E-19	3.98E-18
RENBP	52.562	-5.493	0.852	-6.449	1.13E-10	1.96E-09
SLC9A2	27.433	-5.502	1.177	-4.672	2.98E-06	2.92E-05
ERBB4	1403.510	-5.575	0.204	-27.313	2.97E-164	3.59E-161
SPP1	14.870	-5.609	1.507	-3.721	1.98E-04	1.29E-03
LINC00397	43.406	-5.615	0.959	-5.856	4.73E-09	6.97E-08
TSPAN32	15.599	-5.677	1.498	-3.791	1.50E-04	1.01E-03
COL4A4	1315.031	-5.684	0.203	-28.057	3.27E-173	5.01E-170
NTAN1	36.572	-5.720	2.373	-2.411	1.59E-02	5.50E-02
RP11-391J13.2	6.342	-5.750	1.882	-3.055	2.25E-03	1.07E-02
ANKRD19P	6.510	-5.784	1.880	-3.077	2.09E-03	1.01E-02
RP11-471M2.4	6.477	-5.785	1.889	-3.063	2.19E-03	1.05E-02
NXF3	511.763	-5.788	0.308	-18.819	5.27E-79	1.49E-76
RP11-749H20.2	19.241	-5.895	1.453	-4.059	4.94E-05	3.74E-04
CTD-2535I10.1	130.452	-5.996	0.617	-9.717	2.56E-22	1.10E-20
CRYBA4	20.225	-6.056	1.456	-4.160	3.18E-05	2.53E-04
AC087499.7	37.928	-6.066	1.154	-5.255	1.48E-07	1.79E-06
RP11-318G21.4	8.535	-6.174	1.791	-3.446	5.68E-04	3.27E-03
QPCT	8.764	-6.220	1.780	-3.494	4.75E-04	2.80E-03
RP11-163F15.1	42.366	-6.223	1.143	-5.446	5.16E-08	6.68E-07
RP11-1299A16.3	9.148	-6.279	1.758	-3.571	3.56E-04	2.18E-03
ANKRD30A	154.830	-6.290	0.617	-10.191	2.17E-24	1.07E-22
NLRP4	72.421	-6.370	0.916	-6.956	3.50E-12	7.11E-11
LINC02027	25.261	-6.375	1.422	-4.483	7.34E-06	6.67E-05
CCDC198	173.202	-6.430	0.608	-10.569	4.16E-26	2.26E-24
TFPI2	10.658	-6.500	1.717	-3.785	1.54E-04	1.03E-03
RP11-471M2.3	189.176	-6.521	0.597	-10.929	8.36E-28	4.99E-26
RP11-197K6.1	57.917	-6.672	1.113	-5.995	2.03E-09	3.13E-08
LINC02611	12.248	-6.698	1.686	-3.974	7.08E-05	5.12E-04
LINC02726	33.566	-6.735	1.383	-4.869	1.12E-06	1.18E-05
RP11-20F24.2	12.809	-6.763	1.675	-4.037	5.41E-05	4.06E-04
WWC2	12.814	-6.765	1.674	-4.042	5.30E-05	3.98E-04
RP11-180C1.1	13.417	-6.831	1.664	-4.106	4.03E-05	3.13E-04
COL4A3	506.393	-6.849	0.409	-16.753	5.36E-63	1.11E-60
RP1-81D8.4	14.152	-6.908	1.653	-4.179	2.93E-05	2.34E-04
LINC02438	37.341	-6.939	1.380	-5.029	4.93E-07	5.47E-06
TLR3	14.661	-6.957	1.650	-4.215	2.50E-05	2.03E-04
IPCEF1	3013.000	-6.971	0.199	-35.105	5.58E-270	4.27E-266
PLAC4	16.046	-7.088	1.630	-4.347	1.38E-05	1.18E-04
AC126365.1	46.319	-7.211	1.359	-5.307	1.11E-07	1.37E-06
C11orf21	19.067	-7.337	1.602	-4.581	4.64E-06	4.38E-05
LINC02088	21.363	-7.504	1.588	-4.725	2.30E-06	2.31E-05
LINC01287	24.501	-7.699	1.569	-4.908	9.19E-07	9.84E-06
CD28	135.170	-7.886	1.064	-7.413	1.23E-13	2.94E-12
DNAJA4	73.660	-7.920	1.335	-5.931	3.02E-09	4.56E-08
NEBL	1406.024	-8.173	0.375	-21.801	2.26E-105	9.98E-103
RP11-643A5.2	93.545	-8.265	1.325	-6.236	4.50E-10	7.45E-09

CCDC120	69.168	-9.198	1.491	-6.170	6.81E-10	1.11E-08
LINC01807	82.707	-9.455	1.483	-6.376	1.82E-10	3.10E-09
MEC1 RNASEH2B Mono-KO Vs WT						
Gene Name	baseMean	log2FoldChange	lfcSE	stat	pvalue	padj
AC006042.6	1.294	4.065	2.013	2.019	4.35E-02	9.98E-02
NRIR	2.989	3.305	1.635	2.021	4.33E-02	9.94E-02
CPO	2.636	3.099	1.531	2.024	4.29E-02	9.87E-02
RN7SKP118	1.301	4.075	2.011	2.026	4.28E-02	9.83E-02
HOXA-AS2	5.197	2.293	1.131	2.028	4.26E-02	9.81E-02
RP11-2E11.9	4.235	2.314	1.141	2.029	4.25E-02	9.78E-02
MCIDAS	1.895	3.840	1.892	2.030	4.24E-02	9.77E-02
SLC35F4	1.817	3.851	1.894	2.033	4.20E-02	9.69E-02
POTEH	2.451	3.042	1.495	2.034	4.19E-02	9.67E-02
APOD	1.296	4.068	1.998	2.036	4.17E-02	9.63E-02
DCC	4.969	2.087	1.023	2.039	4.14E-02	9.56E-02
RP11-665J20.2	1.309	4.071	1.996	2.040	4.14E-02	9.56E-02
TRPC5OS	1.898	3.622	1.776	2.040	4.14E-02	9.56E-02
AR	1.918	3.625	1.776	2.041	4.12E-02	9.53E-02
TCEAL5	1.770	3.759	1.841	2.042	4.12E-02	9.52E-02
RP11-875O11.2	4.730	2.188	1.070	2.044	4.09E-02	9.47E-02
CPNE6	4.693	2.265	1.108	2.045	4.09E-02	9.46E-02
ROPN1B	2.404	3.582	1.748	2.050	4.04E-02	9.36E-02
PEAR1	5.343	2.097	1.022	2.051	4.03E-02	9.34E-02
SCG3	1.285	4.259	2.076	2.051	4.02E-02	9.33E-02
RP11-203M5.6	2.512	3.464	1.688	2.053	4.01E-02	9.31E-02
MT-TY	4.720	2.173	1.055	2.060	3.94E-02	9.17E-02
DGKB	1.756	3.883	1.885	2.060	3.94E-02	9.17E-02
CTA-363E19.2	2.854	3.107	1.507	2.061	3.93E-02	9.15E-02
CHI3L1	1.307	4.262	2.067	2.062	3.92E-02	9.13E-02
RP11-419C23.1	3.385	2.480	1.203	2.062	3.92E-02	9.13E-02
SLC7A3	1.677	3.847	1.866	2.062	3.92E-02	9.13E-02
PCDHB13	4.008	2.255	1.093	2.063	3.91E-02	9.12E-02
RP11-378J18.9	6.251	2.077	1.007	2.063	3.91E-02	9.11E-02
RP11-310I9.2	6.395	2.097	1.016	2.064	3.90E-02	9.09E-02
RP11-713M15.2	5.280	3.111	1.507	2.065	3.90E-02	9.08E-02
RP11-103C3.4	1.408	4.268	2.063	2.069	3.85E-02	8.99E-02
NPC1L1	4.564	2.300	1.111	2.071	3.83E-02	8.96E-02
LINC01852	3.334	2.745	1.325	2.072	3.82E-02	8.94E-02
RP11-16E18.3	4.985	2.189	1.056	2.074	3.81E-02	8.91E-02
RP11-697E2.12	1.534	4.253	2.050	2.074	3.80E-02	8.91E-02
FOXF1	2.146	3.618	1.742	2.076	3.79E-02	8.87E-02
CYCSP6	1.800	3.844	1.848	2.081	3.75E-02	8.79E-02
PLA2G4E	5.963	2.435	1.169	2.083	3.73E-02	8.75E-02
BRWD1P2	2.146	3.618	1.735	2.086	3.70E-02	8.70E-02
RP11-452J21.3	1.815	3.851	1.846	2.086	3.70E-02	8.70E-02
MRO	3.386	3.303	1.579	2.092	3.65E-02	8.59E-02
KCNQ2	1.793	3.847	1.839	2.092	3.64E-02	8.58E-02
LINC01151	5.424	2.009	0.960	2.093	3.63E-02	8.56E-02
IL27	2.539	3.472	1.656	2.097	3.60E-02	8.50E-02
AC012363.4	2.129	3.620	1.724	2.100	3.57E-02	8.44E-02
ZNF730	2.567	3.039	1.446	2.102	3.55E-02	8.40E-02
INHBA	4.674	2.155	1.024	2.104	3.54E-02	8.38E-02
CNBD1	2.038	3.761	1.788	2.104	3.54E-02	8.37E-02
RP11-647F2.2	2.586	3.275	1.552	2.110	3.48E-02	8.25E-02
AC004538.3	6.931	3.262	1.545	2.111	3.48E-02	8.24E-02
CATSPER1	3.341	3.579	1.694	2.113	3.46E-02	8.20E-02

RP11-274J16.5	2.624	3.469	1.641	2.115	3.45E-02	8.17E-02
DUOX1	5.376	2.497	1.180	2.115	3.44E-02	8.16E-02
SV2B	3.189	2.672	1.263	2.116	3.44E-02	8.16E-02
RP11-1094M14.5	6.824	3.262	1.540	2.119	3.41E-02	8.10E-02
EGLN3	2.508	3.284	1.548	2.122	3.38E-02	8.05E-02
DLX2	5.794	2.210	1.041	2.123	3.37E-02	8.03E-02
RAB42	2.893	3.469	1.632	2.125	3.36E-02	7.99E-02
HBE1	1.906	4.068	1.914	2.125	3.36E-02	7.99E-02
RET	1.892	3.757	1.765	2.128	3.33E-02	7.95E-02
GBA	12.528	5.973	2.807	2.128	3.33E-02	7.95E-02
RP11-158L12.6	3.123	3.128	1.469	2.130	3.32E-02	7.92E-02
CDC42-AS1	2.627	3.218	1.507	2.136	3.27E-02	7.81E-02
CDPF1P1	3.154	3.472	1.625	2.136	3.27E-02	7.81E-02
LIPN	3.490	2.561	1.199	2.137	3.26E-02	7.80E-02
CHRM3-AS2	1.280	4.725	2.202	2.146	3.19E-02	7.64E-02
AC073130.1	1.280	4.725	2.202	2.146	3.19E-02	7.64E-02
AC005394.1	1.282	4.579	2.129	2.151	3.15E-02	7.56E-02
C8orf31	3.621	2.659	1.236	2.151	3.15E-02	7.55E-02
ABALON	3.828	2.845	1.320	2.155	3.12E-02	7.49E-02
ZNF492	1.760	4.110	1.905	2.158	3.10E-02	7.45E-02
AC003991.3	5.715	2.305	1.068	2.158	3.09E-02	7.43E-02
RP11-348H3.5	1.685	4.068	1.883	2.160	3.08E-02	7.41E-02
ADGRF4	5.304	2.271	1.052	2.160	3.08E-02	7.41E-02
TEX37	1.286	4.431	2.051	2.160	3.07E-02	7.40E-02
CNTN5	1.275	4.582	2.121	2.160	3.07E-02	7.40E-02
IGLVI-56	3.221	3.186	1.473	2.163	3.05E-02	7.36E-02
S100A2	2.990	3.211	1.481	2.168	3.02E-02	7.28E-02
ANKRD35	3.144	3.467	1.598	2.170	3.00E-02	7.25E-02
SCN4B	2.410	3.854	1.776	2.170	3.00E-02	7.24E-02
MAMLD1	4.142	3.465	1.596	2.172	2.99E-02	7.22E-02
LAMA2	1.688	4.071	1.874	2.172	2.98E-02	7.21E-02
LINC01624	1.389	4.579	2.102	2.178	2.94E-02	7.12E-02
LINC01393	5.807	2.197	1.008	2.179	2.93E-02	7.10E-02
AC006460.2	5.725	2.089	0.958	2.181	2.92E-02	7.07E-02
C3AR1	4.597	2.649	1.213	2.183	2.90E-02	7.04E-02
CTD-2544D21.2	3.232	3.128	1.432	2.184	2.90E-02	7.03E-02
ITLN2	1.411	4.259	1.948	2.186	2.88E-02	7.00E-02
LGALS9C	3.569	3.126	1.425	2.194	2.82E-02	6.88E-02
CPA4	1.414	4.262	1.942	2.195	2.82E-02	6.87E-02
HOXC8	1.413	4.431	2.012	2.202	2.77E-02	6.76E-02
RP1-111C20.3	1.423	4.431	2.011	2.203	2.76E-02	6.74E-02
AC005616.1	1.424	4.434	2.011	2.205	2.75E-02	6.71E-02
RP11-11N7.4	5.010	2.518	1.140	2.209	2.72E-02	6.66E-02
ST8SIA1	10.660	2.739	1.239	2.211	2.70E-02	6.62E-02
RP4-744I24.5	3.862	3.084	1.394	2.212	2.70E-02	6.61E-02
RP11-91H12.1	2.267	3.763	1.700	2.214	2.68E-02	6.58E-02
CD93	2.748	3.287	1.483	2.216	2.67E-02	6.55E-02
RP11-149P24.2	2.411	3.844	1.733	2.218	2.65E-02	6.52E-02
HNF4G	1.550	4.434	1.986	2.233	2.56E-02	6.29E-02
RAB1AP1	2.500	3.882	1.735	2.237	2.53E-02	6.24E-02
TRAJ48	5.090	2.632	1.176	2.237	2.53E-02	6.24E-02
AB015752.3	4.933	2.291	1.024	2.238	2.52E-02	6.23E-02
ZNF90	3.111	3.046	1.361	2.239	2.52E-02	6.22E-02
AP002856.4	3.211	3.235	1.443	2.242	2.50E-02	6.17E-02
RP11-556I14.1	14.126	2.022	0.901	2.244	2.48E-02	6.14E-02
ACE	4.113	3.586	1.597	2.245	2.48E-02	6.13E-02
LINC02163	1.894	4.104	1.828	2.245	2.47E-02	6.12E-02
SYTL5	6.502	3.297	1.468	2.246	2.47E-02	6.12E-02

RP11-330H6.6	3.363	3.218	1.432	2.247	2.46E-02	6.10E-02
FGL2	6.213	3.304	1.465	2.256	2.41E-02	5.98E-02
LAD1	5.285	3.030	1.343	2.256	2.41E-02	5.98E-02
TMEM212	1.930	4.071	1.800	2.262	2.37E-02	5.89E-02
RYR3	7.083	2.264	1.001	2.263	2.36E-02	5.88E-02
LINC01579	1.388	4.843	2.140	2.263	2.36E-02	5.87E-02
APCDD1L-DT	7.374	2.326	1.027	2.265	2.35E-02	5.86E-02
RP11-568G11.5	4.627	3.103	1.368	2.268	2.34E-02	5.82E-02
ATP23	12.276	3.107	1.363	2.279	2.27E-02	5.67E-02
AC099552.4	5.074	2.219	0.974	2.279	2.27E-02	5.67E-02
LINC02875	3.023	3.841	1.685	2.280	2.26E-02	5.66E-02
FMO3	2.733	3.755	1.647	2.280	2.26E-02	5.65E-02
LINC02484	1.393	4.847	2.125	2.281	2.26E-02	5.65E-02
ASB4	6.370	2.174	0.953	2.282	2.25E-02	5.63E-02
FLJ12825	1.671	4.268	1.868	2.284	2.23E-02	5.60E-02
LINC02542	2.283	4.077	1.784	2.285	2.23E-02	5.58E-02
PAK3	1.399	4.718	2.058	2.293	2.18E-02	5.48E-02
MORC1	5.355	2.447	1.066	2.295	2.17E-02	5.45E-02
MEGF11	4.838	2.466	1.074	2.297	2.16E-02	5.43E-02
KCNJ2	4.071	2.860	1.243	2.301	2.14E-02	5.38E-02
AP000355.2	3.440	3.334	1.448	2.302	2.13E-02	5.36E-02
COPG2IT1	1.669	4.265	1.851	2.304	2.12E-02	5.34E-02
SNORD3B-1	2.583	3.516	1.524	2.307	2.11E-02	5.31E-02
USH1G	5.191	2.613	1.132	2.308	2.10E-02	5.29E-02
METTL21EP	3.689	2.931	1.269	2.309	2.09E-02	5.28E-02
RP11-44F14.8	1.801	4.260	1.839	2.317	2.05E-02	5.19E-02
RP11-703M24.5	3.592	3.618	1.561	2.317	2.05E-02	5.18E-02
PTPN21	3.542	3.028	1.306	2.318	2.05E-02	5.17E-02
RP11-119F7.5	4.542	2.875	1.239	2.321	2.03E-02	5.14E-02
RP11-686D22.10	5.815	3.588	1.543	2.325	2.01E-02	5.09E-02
MAGEB17	4.520	2.487	1.069	2.327	2.00E-02	5.06E-02
MIR550A2	4.043	2.971	1.275	2.331	1.98E-02	5.02E-02
FAM182A	3.146	3.850	1.651	2.332	1.97E-02	5.00E-02
LINC01554	4.186	2.925	1.254	2.332	1.97E-02	5.00E-02
AC083900.1	3.020	3.755	1.608	2.335	1.95E-02	4.97E-02
RP3-383B8.1	5.797	2.504	1.072	2.335	1.95E-02	4.97E-02
BARHL2	3.719	3.620	1.546	2.342	1.92E-02	4.89E-02
LINC02842	3.568	2.990	1.275	2.344	1.91E-02	4.86E-02
CRYM	6.511	2.203	0.939	2.346	1.90E-02	4.84E-02
RPSAP20	1.793	4.262	1.816	2.347	1.89E-02	4.83E-02
RP5-984P4.4	2.885	3.759	1.601	2.348	1.89E-02	4.82E-02
PCDH12	5.411	2.252	0.958	2.351	1.87E-02	4.78E-02
SVIL2P	2.244	4.000	1.700	2.353	1.86E-02	4.76E-02
ALDH3B2	5.774	3.473	1.475	2.355	1.85E-02	4.74E-02
RP11-226B15.1	1.899	4.434	1.883	2.355	1.85E-02	4.73E-02
RP11-362A9.3	3.989	3.408	1.446	2.357	1.84E-02	4.72E-02
SERTM2	2.404	4.068	1.726	2.357	1.84E-02	4.71E-02
RP11-301G19.1	3.120	3.761	1.594	2.359	1.83E-02	4.70E-02
PDZK1	2.956	3.880	1.645	2.359	1.83E-02	4.69E-02
GABRG1	4.559	2.451	1.038	2.361	1.82E-02	4.68E-02
RP11-416O18.4	2.752	4.071	1.721	2.366	1.80E-02	4.62E-02
PEAK3	5.576	2.733	1.154	2.367	1.79E-02	4.61E-02
RP11-115D19.3	2.054	4.260	1.799	2.368	1.79E-02	4.60E-02
UMODL1	5.724	2.458	1.034	2.378	1.74E-02	4.50E-02
AHNAK2	1.783	4.587	1.927	2.380	1.73E-02	4.47E-02
ADAMTSL2	3.619	3.403	1.429	2.382	1.72E-02	4.46E-02
RARRES2	1.660	4.436	1.862	2.382	1.72E-02	4.45E-02
DLK2	2.533	4.074	1.708	2.386	1.70E-02	4.41E-02

RP11-527L4.5	6.226	2.466	1.033	2.386	1.70E-02	4.41E-02
CYP2AB1P	2.415	4.071	1.705	2.388	1.69E-02	4.39E-02
PLCB1	3.052	3.185	1.332	2.391	1.68E-02	4.36E-02
RP11-24O17.2	1.917	4.428	1.848	2.396	1.66E-02	4.30E-02
HOXB8	3.645	3.131	1.305	2.399	1.64E-02	4.28E-02
SIGLEC22P	2.741	3.552	1.480	2.399	1.64E-02	4.27E-02
RP11-104H15.8	5.317	2.631	1.096	2.402	1.63E-02	4.25E-02
MIR1324	1.508	4.962	2.065	2.402	1.63E-02	4.24E-02
AMMECR1LP1	1.510	4.964	2.065	2.404	1.62E-02	4.22E-02
RP11-1109F11.3	2.271	4.254	1.769	2.405	1.62E-02	4.22E-02
INKA2-AS1	4.722	3.234	1.344	2.406	1.61E-02	4.20E-02
CTB-111H14.1	2.023	4.260	1.770	2.407	1.61E-02	4.20E-02
RP11-445O3.2	1.525	4.727	1.964	2.407	1.61E-02	4.19E-02
TEX13D	5.402	2.360	0.980	2.408	1.60E-02	4.18E-02
PDE3A	3.179	3.233	1.342	2.409	1.60E-02	4.17E-02
RP11-439E19.9	5.572	2.335	0.969	2.410	1.59E-02	4.16E-02
TINAG	2.530	4.068	1.687	2.411	1.59E-02	4.16E-02
RP11-217A12.2	4.970	2.400	0.994	2.415	1.57E-02	4.11E-02
GOLGA8Q	8.618	2.220	0.917	2.421	1.55E-02	4.06E-02
RP11-108L7.14	1.532	4.587	1.894	2.422	1.55E-02	4.05E-02
LINC01122	3.889	3.847	1.587	2.425	1.53E-02	4.02E-02
POU6F2-AS1	1.518	4.721	1.945	2.427	1.52E-02	4.00E-02
NEBL	2.746	3.997	1.646	2.427	1.52E-02	4.00E-02
SPINK13	5.966	2.242	0.923	2.428	1.52E-02	3.99E-02
XKR3	5.514	2.304	0.948	2.429	1.51E-02	3.98E-02
AC092155.4	2.096	4.299	1.770	2.429	1.51E-02	3.98E-02
SLCO3A1	2.238	4.110	1.690	2.432	1.50E-02	3.96E-02
RP11-187A9.3	6.679	2.121	0.872	2.432	1.50E-02	3.95E-02
RP11-433N2.1	2.173	4.265	1.752	2.434	1.49E-02	3.94E-02
RP11-252E2.1	1.885	4.428	1.818	2.436	1.48E-02	3.91E-02
RP11-379C1.2	2.328	4.205	1.725	2.437	1.48E-02	3.90E-02
LINC00431	5.409	2.840	1.165	2.438	1.48E-02	3.90E-02
SULF1	2.121	4.301	1.763	2.439	1.47E-02	3.88E-02
CTD-2008L17.1	1.630	4.851	1.988	2.440	1.47E-02	3.87E-02
TENM1	3.446	3.891	1.594	2.441	1.47E-02	3.87E-02
RP4-739H11.5	5.008	2.792	1.144	2.441	1.46E-02	3.87E-02
TRAJ10	7.024	2.280	0.933	2.443	1.46E-02	3.85E-02
NXPH1	1.746	4.851	1.983	2.447	1.44E-02	3.81E-02
LINC02201	4.499	2.880	1.172	2.458	1.40E-02	3.71E-02
RP11-736N17.12	1.637	4.723	1.916	2.464	1.37E-02	3.65E-02
CLMAT3	4.788	2.634	1.068	2.466	1.36E-02	3.63E-02
TRIM2	5.816	2.638	1.068	2.471	1.35E-02	3.59E-02
CADPS2	5.556	3.621	1.465	2.471	1.35E-02	3.59E-02
RP11-512N21.1	6.605	2.418	0.978	2.472	1.34E-02	3.58E-02
SPIC	2.114	4.587	1.853	2.475	1.33E-02	3.55E-02
RP11-1167A19.2	5.693	2.547	1.028	2.478	1.32E-02	3.52E-02
HR	3.247	3.887	1.568	2.479	1.32E-02	3.51E-02
RP11-811I7.2	4.486	3.070	1.238	2.480	1.31E-02	3.51E-02
RAPGEF5	7.213	2.387	0.962	2.482	1.31E-02	3.49E-02
MCF2	2.466	4.106	1.653	2.484	1.30E-02	3.48E-02
PRR20G	3.267	3.884	1.563	2.485	1.30E-02	3.47E-02
RP11-482M8.1	4.945	2.733	1.096	2.493	1.27E-02	3.40E-02
LINC01752	3.025	4.068	1.630	2.495	1.26E-02	3.38E-02
LINC01727	1.762	4.584	1.834	2.499	1.24E-02	3.35E-02
RNVU1-27	5.411	2.687	1.073	2.503	1.23E-02	3.31E-02
NFE2L3P1	7.066	2.390	0.954	2.506	1.22E-02	3.29E-02
RP11-560A15.7	3.348	3.301	1.316	2.509	1.21E-02	3.26E-02
AC009542.2	4.088	3.885	1.548	2.509	1.21E-02	3.26E-02

C11orf72	5.499	2.755	1.097	2.511	1.20E-02	3.25E-02
LINC02393	1.623	5.068	2.014	2.517	1.18E-02	3.20E-02
CACNG6	1.623	5.068	2.014	2.517	1.18E-02	3.20E-02
MOGAT2	5.673	2.535	1.007	2.518	1.18E-02	3.19E-02
PCDHB12	2.234	4.591	1.823	2.519	1.18E-02	3.19E-02
AC023669.1	7.977	2.274	0.902	2.520	1.17E-02	3.18E-02
LINC01419	1.627	5.072	2.012	2.521	1.17E-02	3.17E-02
IGHG4	8.774	2.494	0.989	2.521	1.17E-02	3.17E-02
RP11-286N22.10	2.970	3.998	1.585	2.523	1.16E-02	3.15E-02
RP11-409I10.2	12.171	3.471	1.375	2.525	1.16E-02	3.14E-02
EFL1P1	3.810	2.928	1.159	2.526	1.15E-02	3.13E-02
MUC3A	2.538	4.260	1.685	2.527	1.15E-02	3.12E-02
ANKRD19P	1.631	4.968	1.965	2.527	1.15E-02	3.12E-02
TMSB4XP2	5.452	3.312	1.310	2.528	1.15E-02	3.11E-02
AMBP	7.570	2.066	0.816	2.532	1.13E-02	3.08E-02
KCNMB1	2.612	4.108	1.621	2.534	1.13E-02	3.07E-02
IL1A	2.991	4.106	1.619	2.537	1.12E-02	3.05E-02
CTD-2012K14.2	5.120	2.593	1.022	2.538	1.12E-02	3.04E-02
LINC01666	2.919	4.429	1.745	2.538	1.11E-02	3.04E-02
SMARCA1	3.986	3.880	1.529	2.539	1.11E-02	3.04E-02
FAM230C	2.263	4.438	1.748	2.540	1.11E-02	3.03E-02
LINC02389	1.780	4.729	1.862	2.540	1.11E-02	3.02E-02
FAM90A1	4.110	2.942	1.157	2.543	1.10E-02	3.00E-02
TLL1	5.908	2.455	0.964	2.546	1.09E-02	2.98E-02
CUX2	8.387	2.106	0.827	2.548	1.08E-02	2.96E-02
NMRAL2P	3.986	3.882	1.522	2.550	1.08E-02	2.94E-02
PKD2L2	8.429	2.075	0.813	2.552	1.07E-02	2.93E-02
ADCY6-DT	2.019	4.725	1.849	2.555	1.06E-02	2.91E-02
SPATA41	7.584	2.105	0.823	2.558	1.05E-02	2.89E-02
WBP1LP2	2.960	4.113	1.605	2.562	1.04E-02	2.86E-02
PGLYRP2	5.173	3.430	1.336	2.567	1.03E-02	2.82E-02
CTTNBP2	12.044	2.167	0.844	2.567	1.03E-02	2.82E-02
FUT6	2.646	4.262	1.660	2.568	1.02E-02	2.81E-02
DUSP15	3.814	3.997	1.556	2.569	1.02E-02	2.80E-02
LINC01146	7.715	2.101	0.818	2.570	1.02E-02	2.80E-02
LUARIS	2.412	4.584	1.781	2.574	1.01E-02	2.77E-02
RP11-85G21.4	1.896	4.582	1.780	2.575	1.00E-02	2.76E-02
CYP27A1	6.077	2.854	1.108	2.577	9.98E-03	2.75E-02
ANKFN1	5.312	2.560	0.992	2.579	9.90E-03	2.73E-02
ZNF205	4.004	2.903	1.125	2.580	9.88E-03	2.73E-02
GPR156	5.068	2.840	1.100	2.582	9.83E-03	2.71E-02
C17orf114	3.440	4.108	1.591	2.582	9.82E-03	2.71E-02
RNU6-118P	4.171	3.513	1.358	2.587	9.67E-03	2.68E-02
CHST15	3.894	4.073	1.574	2.588	9.67E-03	2.67E-02
RP11-785J10.2	5.247	2.841	1.098	2.588	9.65E-03	2.67E-02
KLKP1	4.945	3.617	1.396	2.592	9.55E-03	2.65E-02
NENFP2	7.501	2.311	0.892	2.592	9.55E-03	2.65E-02
LINC00922	2.352	4.390	1.694	2.592	9.54E-03	2.64E-02
RP11-369E15.3	9.706	2.138	0.825	2.592	9.54E-03	2.64E-02
HPGDS	6.266	3.758	1.449	2.593	9.52E-03	2.64E-02
CYP3A4	2.375	4.433	1.709	2.594	9.48E-03	2.63E-02
FCER1G	5.431	2.894	1.114	2.599	9.36E-03	2.60E-02
RP11-465L8.1	4.206	4.068	1.564	2.602	9.28E-03	2.58E-02
FAM160A1-DT	10.381	2.214	0.851	2.603	9.23E-03	2.57E-02
FRG1FP	4.251	3.158	1.210	2.609	9.07E-03	2.53E-02
MS4A15	4.706	3.493	1.338	2.610	9.07E-03	2.53E-02
KCNK2	1.735	5.165	1.977	2.612	8.99E-03	2.51E-02
RP11-527D7.4	1.735	5.165	1.977	2.612	8.99E-03	2.51E-02

SYNPO2L	5.173	2.813	1.076	2.614	8.96E-03	2.50E-02
MEIOSIN	8.151	2.137	0.816	2.617	8.87E-03	2.48E-02
FOXN4	7.287	2.923	1.115	2.621	8.76E-03	2.45E-02
CTD-3247F14.2	1.894	4.727	1.803	2.622	8.75E-03	2.45E-02
RP11-34M7.1	7.243	2.100	0.801	2.622	8.75E-03	2.45E-02
RP1-288H2.2	3.552	3.346	1.276	2.623	8.71E-03	2.44E-02
AC006014.8	2.156	4.589	1.748	2.625	8.67E-03	2.43E-02
RP1-69D17.4	6.919	2.577	0.981	2.627	8.63E-03	2.42E-02
CRB1	5.192	2.704	1.029	2.628	8.59E-03	2.41E-02
RP11-190C22.9	6.144	2.594	0.987	2.629	8.57E-03	2.40E-02
GRB14	1.744	5.172	1.966	2.630	8.54E-03	2.39E-02
AC093843.1	1.744	5.172	1.966	2.630	8.54E-03	2.39E-02
GPRC5D	1.744	5.172	1.966	2.630	8.54E-03	2.39E-02
PCYT1B	6.895	3.758	1.427	2.633	8.47E-03	2.38E-02
FAM184B	5.017	2.897	1.099	2.635	8.42E-03	2.37E-02
APOL4	4.772	2.813	1.066	2.638	8.34E-03	2.34E-02
SERHL2	5.085	3.890	1.475	2.638	8.33E-03	2.34E-02
ARHGEF10L	3.927	3.143	1.190	2.640	8.28E-03	2.33E-02
CHST3	11.500	3.622	1.372	2.641	8.26E-03	2.33E-02
PPP4R4	2.969	4.293	1.624	2.643	8.21E-03	2.31E-02
CD1C	5.550	2.671	1.007	2.652	7.99E-03	2.26E-02
HRH1	2.149	4.721	1.779	2.653	7.98E-03	2.25E-02
RP11-22E12.1	3.246	4.260	1.604	2.656	7.91E-03	2.24E-02
GOLGA8R	5.947	3.411	1.284	2.658	7.87E-03	2.22E-02
TSPAN2	4.251	3.340	1.256	2.660	7.82E-03	2.21E-02
TRIM54	9.524	2.182	0.821	2.660	7.82E-03	2.21E-02
RP11-486O13.2	4.636	4.069	1.528	2.663	7.74E-03	2.19E-02
NGFR	10.598	2.010	0.754	2.665	7.70E-03	2.18E-02
RP11-757O6.6	3.336	3.779	1.418	2.666	7.69E-03	2.18E-02
ADIRF	7.531	2.327	0.872	2.669	7.62E-03	2.16E-02
CTNNA3	6.540	3.425	1.283	2.670	7.59E-03	2.15E-02
RP11-71L14.3	5.867	3.113	1.166	2.670	7.58E-03	2.15E-02
RPH3A	1.877	5.070	1.895	2.675	7.46E-03	2.12E-02
TEAD1	6.369	2.318	0.865	2.681	7.35E-03	2.09E-02
NACAD	3.924	4.267	1.589	2.685	7.25E-03	2.07E-02
WFDC21P	4.461	4.003	1.488	2.689	7.16E-03	2.04E-02
PAPPA2	2.714	4.390	1.629	2.696	7.03E-03	2.01E-02
PCSK1N	4.261	4.255	1.577	2.698	6.98E-03	2.00E-02
RP11-34P13.15	5.427	3.996	1.480	2.699	6.96E-03	1.99E-02
C3orf86	5.167	3.599	1.333	2.700	6.93E-03	1.99E-02
RPL32P9	2.271	4.716	1.744	2.704	6.86E-03	1.97E-02
LINC02257	5.768	3.100	1.146	2.705	6.84E-03	1.96E-02
HOXA2	2.399	4.589	1.696	2.706	6.82E-03	1.96E-02
RP11-578O24.2	8.766	2.055	0.758	2.712	6.69E-03	1.93E-02
SMAGP	8.908	2.007	0.740	2.713	6.67E-03	1.92E-02
RP13-415G19.2	3.562	4.208	1.549	2.716	6.61E-03	1.90E-02
DIAPH2-AS1	2.010	4.843	1.783	2.717	6.59E-03	1.90E-02
LINC01501	6.409	3.478	1.280	2.717	6.58E-03	1.90E-02
MAP3K19	3.080	4.296	1.580	2.719	6.55E-03	1.89E-02
LINC00937	5.062	3.148	1.158	2.719	6.55E-03	1.89E-02
ITGA2	3.880	4.265	1.567	2.721	6.51E-03	1.88E-02
RP11-121P12.1	3.210	4.296	1.577	2.725	6.43E-03	1.86E-02
IL20RA	3.295	3.888	1.427	2.725	6.43E-03	1.86E-02
FOXD1	5.449	3.548	1.302	2.726	6.41E-03	1.85E-02
KLRC3	5.060	3.186	1.167	2.729	6.35E-03	1.84E-02
LIPC	2.595	4.698	1.722	2.729	6.35E-03	1.84E-02
FA2H	10.340	2.055	0.752	2.733	6.28E-03	1.82E-02
CYP4X1	10.067	2.525	0.923	2.735	6.23E-03	1.81E-02

AC114765.1	1.851	5.165	1.883	2.742	6.10E-03	1.77E-02
RP11-326L17.1	6.795	3.473	1.266	2.743	6.10E-03	1.77E-02
RP11-528A4.5	5.775	2.600	0.946	2.747	6.01E-03	1.75E-02
CSTA	4.261	3.745	1.362	2.751	5.95E-03	1.73E-02
AC011288.2	2.567	4.691	1.705	2.751	5.95E-03	1.73E-02
IGLV11-55	2.013	5.077	1.846	2.751	5.95E-03	1.73E-02
SLITRK1	3.201	4.303	1.564	2.752	5.93E-03	1.73E-02
GPR153	10.049	2.113	0.767	2.755	5.88E-03	1.71E-02
LINC01068	8.807	2.192	0.795	2.757	5.84E-03	1.70E-02
RP11-56P9.4	4.446	4.258	1.544	2.757	5.83E-03	1.70E-02
RP11-406G20.1	1.873	5.066	1.837	2.758	5.82E-03	1.70E-02
TSLP	6.283	3.498	1.269	2.758	5.82E-03	1.70E-02
RAB27B	2.273	4.967	1.799	2.761	5.77E-03	1.69E-02
TMLHE-AS1	9.520	2.278	0.825	2.761	5.76E-03	1.68E-02
LINC01388	4.103	4.262	1.544	2.761	5.76E-03	1.68E-02
RP11-438N16.5	3.153	4.433	1.605	2.762	5.74E-03	1.68E-02
RP11-893F2.13	3.591	4.299	1.556	2.762	5.74E-03	1.68E-02
OTOA	4.821	3.271	1.183	2.765	5.69E-03	1.67E-02
FLJ30679	9.789	2.053	0.742	2.766	5.67E-03	1.66E-02
CTC-260E6.4	3.226	4.431	1.602	2.766	5.67E-03	1.66E-02
RP11-163F15.1	1.865	5.068	1.830	2.769	5.62E-03	1.65E-02
LIF	3.815	4.208	1.519	2.770	5.61E-03	1.65E-02
LINC00632	3.503	4.045	1.460	2.770	5.60E-03	1.64E-02
ADAMTS4	5.005	3.139	1.129	2.781	5.42E-03	1.60E-02
TRAV1-1	5.254	2.990	1.074	2.783	5.39E-03	1.59E-02
EGR4	4.992	3.075	1.105	2.783	5.38E-03	1.59E-02
SVEP1	5.757	4.000	1.437	2.784	5.37E-03	1.58E-02
RP11-280F2.3	5.996	3.173	1.139	2.785	5.36E-03	1.58E-02
IL1RN	10.720	2.057	0.738	2.785	5.35E-03	1.58E-02
TEKT4P2	7.014	6.126	2.194	2.793	5.23E-03	1.54E-02
PTPRD-AS1	4.960	4.105	1.466	2.800	5.11E-03	1.51E-02
DISC1FP1	15.950	2.067	0.738	2.800	5.11E-03	1.51E-02
RP11-737O24.1	7.004	3.138	1.120	2.802	5.08E-03	1.51E-02
RBPMS	2.956	4.549	1.622	2.805	5.04E-03	1.49E-02
RP11-763F8.1	8.622	2.391	0.852	2.805	5.03E-03	1.49E-02
RP11-876F14.1	4.445	4.205	1.498	2.808	4.99E-03	1.48E-02
ME3	10.092	2.428	0.865	2.808	4.99E-03	1.48E-02
EXOC3L4	5.128	3.792	1.346	2.816	4.86E-03	1.45E-02
RP11-363D14.1	7.421	2.518	0.893	2.820	4.81E-03	1.43E-02
BAALC	4.671	3.371	1.193	2.827	4.70E-03	1.40E-02
FBXO39	9.288	3.887	1.373	2.831	4.65E-03	1.39E-02
CLEC7A	6.947	2.609	0.919	2.840	4.52E-03	1.35E-02
CD3D	1.974	5.351	1.882	2.843	4.48E-03	1.34E-02
FERMT1	1.974	5.351	1.882	2.843	4.48E-03	1.34E-02
PKD1L2	6.558	2.669	0.939	2.843	4.46E-03	1.34E-02
RP1-72A23.4	5.420	3.265	1.148	2.844	4.46E-03	1.34E-02
PPP1R9A	2.847	4.548	1.598	2.845	4.44E-03	1.33E-02
CYSLTR2	13.992	2.506	0.880	2.847	4.41E-03	1.32E-02
HAP1	4.023	4.429	1.553	2.852	4.34E-03	1.31E-02
AC020743.2	5.046	3.459	1.213	2.853	4.34E-03	1.31E-02
MYL9	12.472	2.117	0.742	2.853	4.33E-03	1.30E-02
MAGEC2	1.977	5.165	1.809	2.855	4.30E-03	1.30E-02
DCHS2	6.280	2.921	1.023	2.856	4.29E-03	1.29E-02
CSAG4	1.978	5.259	1.841	2.857	4.28E-03	1.29E-02
LINC00475	9.174	3.519	1.229	2.864	4.18E-03	1.26E-02
NECTIN4	6.881	3.591	1.253	2.866	4.15E-03	1.26E-02
CTC-573N18.1	2.382	4.845	1.689	2.869	4.11E-03	1.24E-02
RP11-472K17.4	4.115	4.302	1.498	2.872	4.07E-03	1.23E-02

FKBP9P1	3.312	4.467	1.553	2.875	4.04E-03	1.22E-02
TRAJ45	8.352	3.085	1.072	2.876	4.02E-03	1.22E-02
RP5-1116C7.2	5.822	3.704	1.284	2.884	3.92E-03	1.19E-02
LINC00469	2.788	4.826	1.669	2.892	3.83E-03	1.17E-02
LRRC9	3.240	4.586	1.586	2.892	3.82E-03	1.16E-02
ANKRD20A3P	5.117	4.209	1.455	2.893	3.82E-03	1.16E-02
ZNF716	2.786	4.825	1.667	2.894	3.81E-03	1.16E-02
GBP5	3.682	4.389	1.515	2.897	3.77E-03	1.15E-02
NOMO3	20.597	4.531	1.564	2.897	3.77E-03	1.15E-02
RP11-214O1.3	2.847	4.964	1.712	2.899	3.74E-03	1.14E-02
CSAG2	2.817	4.760	1.639	2.904	3.68E-03	1.13E-02
SDR42E2	9.585	2.383	0.821	2.904	3.68E-03	1.13E-02
RP11-274H24.3	4.899	3.909	1.345	2.906	3.66E-03	1.12E-02
TOMM20P2	6.076	4.264	1.465	2.910	3.61E-03	1.11E-02
LINC01297	3.098	4.626	1.589	2.911	3.60E-03	1.10E-02
POMC	4.431	4.302	1.470	2.926	3.44E-03	1.06E-02
CTD-2288F12.1	7.896	2.728	0.932	2.928	3.41E-03	1.05E-02
STRA8	5.533	4.208	1.435	2.933	3.35E-03	1.03E-02
RP11-534J18.1	2.087	5.431	1.849	2.937	3.32E-03	1.02E-02
LINC01684	2.091	5.434	1.849	2.939	3.29E-03	1.02E-02
DIO2-AS1	2.753	4.849	1.647	2.945	3.23E-03	1.00E-02
LINC02273	6.073	2.857	0.968	2.951	3.17E-03	9.83E-03
CHL1-AS2	9.753	2.868	0.969	2.960	3.08E-03	9.58E-03
RP11-65N13.8	5.820	3.022	1.020	2.961	3.07E-03	9.54E-03
DNAJC5G	11.929	2.156	0.727	2.964	3.03E-03	9.44E-03
RP11-352B15.2	2.100	5.351	1.803	2.968	3.00E-03	9.35E-03
SPEG	3.586	4.550	1.531	2.972	2.96E-03	9.24E-03
AMER2	12.132	2.137	0.719	2.972	2.96E-03	9.24E-03
GREM2	2.481	5.170	1.736	2.978	2.90E-03	9.08E-03
CTB-131B5.5	8.584	2.572	0.863	2.981	2.87E-03	9.00E-03
HDGFL1	3.368	4.717	1.582	2.981	2.87E-03	9.00E-03
IL12B	8.448	2.952	0.989	2.983	2.85E-03	8.94E-03
RP11-657O9.1	2.211	5.259	1.761	2.987	2.82E-03	8.83E-03
AC004540.5	2.378	5.073	1.698	2.988	2.81E-03	8.80E-03
RBMS1P1	4.784	3.933	1.315	2.991	2.78E-03	8.73E-03
PXT1	15.171	2.114	0.707	2.991	2.78E-03	8.72E-03
WASH8P	46.401	3.747	1.251	2.994	2.75E-03	8.64E-03
POTEE	4.364	4.152	1.385	2.998	2.72E-03	8.55E-03
AMPH	3.371	4.719	1.571	3.004	2.67E-03	8.40E-03
RP11-386D6.2	2.487	5.261	1.750	3.006	2.65E-03	8.34E-03
ERICH2	7.537	3.269	1.087	3.008	2.63E-03	8.29E-03
UPK1A	7.612	4.208	1.398	3.009	2.62E-03	8.26E-03
ANXA3	11.786	3.124	1.038	3.010	2.62E-03	8.25E-03
CATIP-AS2	4.515	4.466	1.480	3.017	2.55E-03	8.07E-03
RP11-1166P10.1	5.039	4.590	1.519	3.021	2.52E-03	7.96E-03
BMERB1	6.847	4.297	1.419	3.027	2.47E-03	7.83E-03
IGHG2	14.437	2.247	0.742	3.029	2.45E-03	7.79E-03
AC007106.1	4.791	3.974	1.312	3.030	2.45E-03	7.77E-03
JAML	13.624	2.338	0.771	3.031	2.44E-03	7.74E-03
SOX18	13.407	2.602	0.858	3.033	2.42E-03	7.70E-03
CLCF1	8.475	3.364	1.108	3.035	2.40E-03	7.64E-03
MAGEC1	2.595	5.268	1.733	3.041	2.36E-03	7.51E-03
GOLGA8H	3.343	4.845	1.592	3.044	2.33E-03	7.43E-03
AXDND1	9.309	2.203	0.723	3.047	2.31E-03	7.39E-03
AC078842.3	3.111	4.971	1.630	3.050	2.29E-03	7.32E-03
AC067956.1	2.210	5.346	1.753	3.050	2.29E-03	7.30E-03
RP11-116B13.1	2.205	5.432	1.777	3.057	2.23E-03	7.14E-03
ENSG10010138034.1	3.002	4.969	1.624	3.059	2.22E-03	7.11E-03

CREB3L1	12.705	2.203	0.720	3.059	2.22E-03	7.10E-03
ITGBL1	4.502	3.631	1.187	3.060	2.22E-03	7.10E-03
RP11-306N14.1	15.844	2.022	0.659	3.068	2.16E-03	6.91E-03
RP11-485F13.1	2.326	5.346	1.739	3.073	2.12E-03	6.80E-03
RP13-20L14.11	7.508	2.646	0.860	3.076	2.10E-03	6.76E-03
RP11-731J8.4	10.260	2.411	0.783	3.078	2.09E-03	6.72E-03
KCNC2	3.179	4.882	1.586	3.079	2.08E-03	6.69E-03
RP11-552F3.9	4.270	4.144	1.345	3.082	2.06E-03	6.63E-03
FAM167B	12.047	2.154	0.698	3.086	2.03E-03	6.56E-03
KIAA1614	11.918	2.529	0.819	3.088	2.02E-03	6.51E-03
AC073043.1	12.842	2.043	0.661	3.088	2.02E-03	6.51E-03
TMEM72	3.239	4.957	1.604	3.090	2.00E-03	6.47E-03
RP5-1142A6.10	8.141	2.581	0.835	3.090	2.00E-03	6.47E-03
HLF	7.705	2.969	0.960	3.092	1.99E-03	6.43E-03
CES5A	3.187	4.825	1.559	3.094	1.97E-03	6.38E-03
SLFN12L	27.153	3.500	1.130	3.097	1.96E-03	6.33E-03
ANKRD20A7P	19.108	2.115	0.683	3.097	1.95E-03	6.33E-03
DHRSX	36.310	4.299	1.388	3.097	1.95E-03	6.33E-03
AC026150.8	4.488	4.692	1.511	3.106	1.90E-03	6.16E-03
IFITM3P1	3.495	4.851	1.560	3.109	1.87E-03	6.10E-03
BAGE2	2.317	5.582	1.793	3.113	1.85E-03	6.03E-03
CTD-2054N24.1	6.339	3.962	1.270	3.120	1.81E-03	5.91E-03
IGSF21	2.319	5.583	1.789	3.120	1.81E-03	5.89E-03
FAM133A	2.872	5.073	1.625	3.121	1.80E-03	5.88E-03
IL36G	5.756	4.584	1.467	3.125	1.78E-03	5.81E-03
GPR158	3.514	4.887	1.562	3.127	1.76E-03	5.77E-03
ITIH1	10.498	2.235	0.714	3.128	1.76E-03	5.76E-03
RP3-525N10.2	5.318	3.593	1.148	3.130	1.75E-03	5.72E-03
LINC02005	3.441	4.964	1.582	3.137	1.71E-03	5.61E-03
RP11-538D16.2	10.181	3.280	1.045	3.137	1.70E-03	5.59E-03
IKBKB-DT	9.032	2.701	0.860	3.140	1.69E-03	5.56E-03
NACAP8	4.269	4.621	1.472	3.140	1.69E-03	5.56E-03
SOX5	7.203	3.433	1.093	3.142	1.68E-03	5.51E-03
CIART	12.017	2.519	0.799	3.152	1.62E-03	5.34E-03
CH17-322D16.1	3.402	5.000	1.585	3.154	1.61E-03	5.32E-03
RP11-44F14.2	3.733	4.847	1.536	3.155	1.60E-03	5.29E-03
LHFPL3-AS2	4.218	4.282	1.356	3.158	1.59E-03	5.25E-03
PCDHB2	4.060	4.692	1.485	3.160	1.58E-03	5.21E-03
RP11-484L8.1	6.001	4.472	1.414	3.163	1.56E-03	5.16E-03
ARMCX1	5.578	4.147	1.310	3.166	1.55E-03	5.12E-03
C6orf58	7.391	3.223	1.018	3.166	1.55E-03	5.12E-03
LRIT3	10.209	2.169	0.685	3.168	1.54E-03	5.09E-03
RP11-219B17.3	8.781	3.415	1.078	3.169	1.53E-03	5.08E-03
FCAMR	5.030	4.618	1.456	3.171	1.52E-03	5.03E-03
TNFRSF21	2.343	5.351	1.687	3.172	1.52E-03	5.03E-03
LINC02754	9.097	2.454	0.773	3.176	1.49E-03	4.96E-03
RP11-439H9.1	2.689	5.342	1.682	3.176	1.49E-03	4.96E-03
RP11-103J8.1	4.835	4.719	1.484	3.179	1.48E-03	4.91E-03
TRIM29	2.956	5.170	1.622	3.188	1.44E-03	4.78E-03
LINC01451	32.410	2.746	0.859	3.195	1.40E-03	4.67E-03
BFAR	34.343	3.364	1.051	3.200	1.37E-03	4.59E-03
TMPRSS11A	3.102	5.071	1.583	3.204	1.36E-03	4.54E-03
CD160	7.477	3.197	0.995	3.212	1.32E-03	4.43E-03
MIR9-1HG	12.120	2.278	0.708	3.216	1.30E-03	4.36E-03
DUX4L26	4.367	4.457	1.384	3.220	1.28E-03	4.31E-03
RP11-350N15.6	4.323	4.847	1.505	3.221	1.28E-03	4.29E-03
DPEP1	5.343	4.272	1.326	3.223	1.27E-03	4.27E-03
COL6A6	4.278	4.758	1.476	3.224	1.26E-03	4.25E-03

RP11-384E22.1	6.350	3.588	1.108	3.237	1.21E-03	4.08E-03
HS6ST3	2.551	5.583	1.724	3.238	1.20E-03	4.07E-03
LCE1D	2.554	5.584	1.723	3.241	1.19E-03	4.03E-03
RP11-219E7.1	7.753	2.987	0.918	3.256	1.13E-03	3.84E-03
ZNF503-AS2	4.027	4.888	1.501	3.256	1.13E-03	3.84E-03
RP11-305F5.2	3.830	4.964	1.524	3.257	1.13E-03	3.83E-03
DYTN	3.840	4.964	1.523	3.260	1.12E-03	3.80E-03
CAMK2B	17.416	2.318	0.709	3.268	1.08E-03	3.69E-03
OCA2	7.080	3.159	0.966	3.270	1.07E-03	3.66E-03
KRT17	3.614	5.054	1.545	3.272	1.07E-03	3.65E-03
FBLN2	4.442	4.452	1.360	3.274	1.06E-03	3.62E-03
RP11-520E6.1	2.580	5.430	1.656	3.279	1.04E-03	3.56E-03
SMAD6	10.858	2.892	0.881	3.282	1.03E-03	3.52E-03
CLEC4C	2.549	5.719	1.742	3.283	1.03E-03	3.51E-03
HYAL4	2.959	5.259	1.601	3.285	1.02E-03	3.49E-03
CH17-353B19.1	6.439	3.184	0.964	3.304	9.53E-04	3.28E-03
CXCL13	11.545	2.657	0.804	3.304	9.52E-04	3.28E-03
RP11-88H10.2	4.995	4.758	1.438	3.309	9.36E-04	3.23E-03
RP11-424M21.1	4.324	4.964	1.499	3.310	9.32E-04	3.21E-03
CLLU1	2.569	5.582	1.683	3.316	9.13E-04	3.15E-03
PTN	7.198	4.121	1.242	3.318	9.07E-04	3.13E-03
RP1-309H15.3	9.569	3.988	1.200	3.322	8.93E-04	3.09E-03
ZNF98	2.561	5.583	1.679	3.325	8.84E-04	3.06E-03
LINC01914	5.023	3.983	1.198	3.326	8.81E-04	3.05E-03
AC006129.1	14.250	2.119	0.636	3.332	8.61E-04	2.99E-03
KALRN	7.524	3.126	0.936	3.339	8.41E-04	2.92E-03
PRAL	4.460	5.076	1.520	3.340	8.39E-04	2.92E-03
CNIH3-AS1	4.564	4.962	1.484	3.343	8.28E-04	2.88E-03
SLC4A3	3.470	5.170	1.546	3.344	8.26E-04	2.88E-03
SCN1A	4.424	4.555	1.361	3.346	8.19E-04	2.85E-03
RBFOX1	4.424	4.555	1.361	3.346	8.19E-04	2.85E-03
CTD-2410N18.5	8.411	2.767	0.826	3.349	8.12E-04	2.83E-03
NDRG2	33.189	2.312	0.687	3.364	7.68E-04	2.69E-03
AC084082.3	5.957	3.791	1.126	3.365	7.65E-04	2.68E-03
SUSD5	11.996	4.584	1.359	3.373	7.45E-04	2.61E-03
FAM135B	12.540	4.469	1.322	3.379	7.27E-04	2.56E-03
ASB9	19.359	2.454	0.725	3.383	7.16E-04	2.52E-03
FSCN1P1	8.603	4.159	1.229	3.384	7.15E-04	2.52E-03
PSMA8	10.917	2.812	0.831	3.385	7.12E-04	2.51E-03
CTD-2546F11.1	9.374	2.744	0.809	3.391	6.95E-04	2.46E-03
ZNF727	2.677	5.721	1.685	3.395	6.87E-04	2.43E-03
SNORD13	8.365	2.852	0.840	3.396	6.84E-04	2.42E-03
CRIP3	7.959	2.985	0.879	3.397	6.82E-04	2.42E-03
DNAH11	17.303	2.184	0.643	3.397	6.82E-04	2.41E-03
CTD-2314B22.4	3.081	5.350	1.574	3.399	6.77E-04	2.40E-03
PAGE5	2.824	5.659	1.665	3.399	6.75E-04	2.39E-03
CH17-174L20.1	5.295	4.946	1.446	3.420	6.27E-04	2.24E-03
NRP1	5.259	3.741	1.092	3.425	6.15E-04	2.20E-03
C2CD4D-AS1	3.602	5.353	1.562	3.426	6.12E-04	2.19E-03
RP11-823E8.3	5.700	4.966	1.449	3.428	6.08E-04	2.18E-03
GNAL	6.869	3.587	1.040	3.447	5.67E-04	2.04E-03
LCE1B	3.459	5.350	1.551	3.449	5.62E-04	2.02E-03
CLEC4D	3.427	5.349	1.550	3.452	5.57E-04	2.01E-03
CAVIN1	11.102	3.008	0.871	3.453	5.54E-04	1.99E-03
SPTA1	8.447	4.167	1.206	3.455	5.50E-04	1.98E-03
CCNYL2	2.790	5.783	1.671	3.460	5.40E-04	1.95E-03
AP000695.6	3.970	5.265	1.520	3.464	5.32E-04	1.92E-03
AOC1	4.444	5.166	1.488	3.471	5.18E-04	1.88E-03

CARD6	16.673	2.065	0.594	3.474	5.14E-04	1.86E-03
RP11-283G6.3	10.134	2.860	0.823	3.474	5.12E-04	1.86E-03
RP11-434C1.2	3.186	5.579	1.603	3.480	5.01E-04	1.82E-03
EGFEM1P	3.969	5.299	1.522	3.482	4.98E-04	1.81E-03
CXCR2	12.376	2.684	0.765	3.511	4.47E-04	1.63E-03
LINC00607	9.233	3.355	0.956	3.511	4.46E-04	1.63E-03
IFTAP	5.707	3.982	1.132	3.518	4.35E-04	1.60E-03
GPR150	19.474	2.845	0.805	3.533	4.11E-04	1.51E-03
XCR1	5.362	5.106	1.445	3.533	4.10E-04	1.51E-03
PCP4L1	6.957	5.075	1.431	3.548	3.89E-04	1.44E-03
SMPDL3B	18.120	3.159	0.889	3.552	3.82E-04	1.41E-03
RP13-314C10.5	3.823	5.430	1.523	3.566	3.63E-04	1.35E-03
CMA1	3.178	5.585	1.566	3.566	3.62E-04	1.35E-03
PIWIL4	8.944	3.580	1.004	3.567	3.61E-04	1.34E-03
RP11-305M3.6	12.062	2.940	0.824	3.568	3.59E-04	1.33E-03
MYO18B	4.656	5.384	1.505	3.577	3.48E-04	1.30E-03
MC4R	5.684	5.169	1.442	3.584	3.39E-04	1.26E-03
ZNF622P1	6.577	5.004	1.396	3.585	3.37E-04	1.26E-03
MAGEA6-DT	3.015	5.962	1.659	3.593	3.27E-04	1.22E-03
ANKRD30BP2	3.020	5.964	1.659	3.595	3.24E-04	1.21E-03
MIR3945HG	5.809	4.584	1.275	3.597	3.22E-04	1.21E-03
ADGRG7	8.428	3.523	0.974	3.615	3.00E-04	1.13E-03
ZNF682	13.011	3.695	1.022	3.616	2.99E-04	1.13E-03
RP11-455I9.1	16.007	2.018	0.558	3.618	2.97E-04	1.12E-03
NCAM2	4.463	5.302	1.465	3.619	2.96E-04	1.11E-03
RP11-253D19.3	7.923	3.879	1.072	3.619	2.96E-04	1.11E-03
RP11-111G13.1	17.851	4.124	1.138	3.623	2.92E-04	1.10E-03
IGFBP7	15.310	3.215	0.887	3.624	2.90E-04	1.09E-03
ST3GAL3-AS1	7.148	3.590	0.988	3.632	2.81E-04	1.06E-03
MISP	6.013	4.201	1.156	3.633	2.80E-04	1.06E-03
LINC00954	15.833	2.641	0.726	3.639	2.74E-04	1.04E-03
CDH11	5.531	4.183	1.149	3.641	2.71E-04	1.03E-03
RP11-681B3.4	6.433	4.618	1.266	3.647	2.66E-04	1.01E-03
CTD-2184D3.6	9.510	3.459	0.948	3.649	2.64E-04	1.00E-03
RP11-866E20.3	10.680	2.676	0.733	3.649	2.63E-04	9.98E-04
DNAH8	9.155	4.886	1.338	3.651	2.61E-04	9.93E-04
RP11-478I15.1	6.465	5.057	1.385	3.651	2.61E-04	9.92E-04
MARCOL	3.139	6.020	1.646	3.658	2.55E-04	9.69E-04
ZNF208	5.249	4.818	1.315	3.665	2.47E-04	9.43E-04
SLC45A1	13.819	3.042	0.830	3.667	2.45E-04	9.34E-04
KLHDC7B-DT	6.683	4.583	1.248	3.674	2.39E-04	9.14E-04
CLEC6A	12.007	3.412	0.925	3.690	2.24E-04	8.60E-04
CH17-343M10.2	7.779	5.113	1.385	3.692	2.22E-04	8.53E-04
NR5A1	5.916	5.264	1.423	3.699	2.16E-04	8.32E-04
RP11-76C10.6	16.420	2.591	0.699	3.704	2.12E-04	8.18E-04
CTA-109P11.4	3.419	5.723	1.544	3.707	2.10E-04	8.10E-04
AC005062.2	8.083	4.550	1.224	3.716	2.02E-04	7.82E-04
PTPRG	7.186	4.093	1.101	3.718	2.01E-04	7.78E-04
AC002407.3	3.779	5.792	1.556	3.722	1.98E-04	7.67E-04
SATL1	13.796	2.832	0.760	3.727	1.94E-04	7.51E-04
RP11-20F24.2	3.252	6.071	1.627	3.731	1.91E-04	7.40E-04
ERC2	17.998	2.024	0.542	3.736	1.87E-04	7.27E-04
LINC02471	8.748	4.488	1.200	3.742	1.83E-04	7.13E-04
CTC-340I23.2	6.265	4.110	1.098	3.743	1.81E-04	7.08E-04
LINC01518	5.183	5.344	1.427	3.744	1.81E-04	7.06E-04
PEX5L-AS2	12.519	2.543	0.677	3.759	1.71E-04	6.68E-04
SMIM18	6.201	5.301	1.409	3.763	1.68E-04	6.59E-04
NMUR2	6.328	3.994	1.061	3.764	1.67E-04	6.56E-04

EEF1A1P31	7.480	5.160	1.368	3.771	1.62E-04	6.38E-04
AACSP1	5.306	5.389	1.427	3.776	1.59E-04	6.26E-04
SNRK-AS1	13.056	2.544	0.673	3.778	1.58E-04	6.21E-04
STRA6	13.890	2.265	0.599	3.783	1.55E-04	6.09E-04
RP11-104H15.9	9.439	3.599	0.950	3.790	1.51E-04	5.96E-04
SOHLH2	3.776	5.722	1.509	3.791	1.50E-04	5.92E-04
DNM3OS	10.206	3.406	0.897	3.797	1.46E-04	5.79E-04
GCNT4	7.176	4.777	1.256	3.803	1.43E-04	5.66E-04
CRIM1	14.042	2.890	0.759	3.807	1.40E-04	5.57E-04
CACNA1G	14.234	2.506	0.657	3.816	1.36E-04	5.40E-04
RP11-517H2.7	7.910	5.257	1.374	3.826	1.30E-04	5.20E-04
ZDHHC22	29.239	4.825	1.261	3.827	1.30E-04	5.17E-04
MYOCOS	16.076	3.759	0.982	3.827	1.30E-04	5.17E-04
NR2F1	11.953	4.449	1.162	3.829	1.29E-04	5.15E-04
ACTG1P22	14.677	5.070	1.323	3.833	1.27E-04	5.06E-04
AC012354.6	4.391	5.656	1.475	3.834	1.26E-04	5.05E-04
BNC2	4.899	5.660	1.476	3.836	1.25E-04	5.01E-04
RP11-147L13.12	10.655	5.108	1.330	3.841	1.22E-04	4.91E-04
TENM2	13.607	2.192	0.570	3.845	1.20E-04	4.84E-04
KCNH5	4.917	5.622	1.461	3.849	1.19E-04	4.78E-04
GSPT2	27.900	2.793	0.725	3.851	1.18E-04	4.74E-04
CDC42BPA	9.713	3.363	0.873	3.851	1.18E-04	4.74E-04
SIX3-AS1	5.509	5.512	1.429	3.856	1.15E-04	4.64E-04
GFPT2	6.475	4.868	1.261	3.862	1.13E-04	4.55E-04
OPCML	6.481	4.868	1.261	3.862	1.13E-04	4.55E-04
MOCS1	3.515	5.964	1.544	3.862	1.12E-04	4.54E-04
CTC-546K23.2	6.493	5.430	1.405	3.865	1.11E-04	4.50E-04
ANO4	6.316	5.389	1.391	3.875	1.06E-04	4.32E-04
LINC02805	12.309	2.406	0.620	3.877	1.06E-04	4.29E-04
ESAM	19.341	2.072	0.534	3.877	1.06E-04	4.28E-04
RP11-305F18.1	3.493	6.121	1.578	3.879	1.05E-04	4.26E-04
IRS3P	18.491	2.093	0.539	3.879	1.05E-04	4.25E-04
RP11-223C24.1	11.545	5.110	1.317	3.881	1.04E-04	4.23E-04
FAR2P1	3.584	6.164	1.588	3.882	1.04E-04	4.21E-04
RP3-439F8.1	12.974	3.279	0.842	3.895	9.82E-05	4.00E-04
LINC02780	3.609	6.070	1.557	3.899	9.68E-05	3.95E-04
ZNF572	7.247	5.429	1.390	3.907	9.35E-05	3.82E-04
CTB-1I21.1	5.111	5.657	1.445	3.916	9.02E-05	3.69E-04
CTAG2	3.594	6.215	1.587	3.916	9.01E-05	3.69E-04
CYP4F35P	5.771	5.511	1.407	3.917	8.95E-05	3.67E-04
HTR2C	3.991	5.908	1.508	3.918	8.93E-05	3.66E-04
LRTM2	4.875	5.719	1.459	3.919	8.89E-05	3.65E-04
FAM242C	12.558	2.706	0.690	3.920	8.87E-05	3.64E-04
EPHB2	19.305	5.000	1.275	3.922	8.79E-05	3.61E-04
AC008079.10	7.167	5.387	1.373	3.925	8.68E-05	3.57E-04
MAGEB6	6.501	5.512	1.404	3.925	8.67E-05	3.57E-04
ELAVL2	3.606	6.168	1.567	3.937	8.26E-05	3.41E-04
CD209	8.799	3.383	0.859	3.940	8.16E-05	3.37E-04
ADGRB3	6.535	4.133	1.048	3.945	7.97E-05	3.30E-04
NHS	9.715	5.347	1.352	3.956	7.63E-05	3.17E-04
GAPT	8.479	4.734	1.196	3.957	7.60E-05	3.16E-04
MIR8089	7.394	5.428	1.371	3.958	7.55E-05	3.14E-04
MTARC2	16.249	2.532	0.639	3.965	7.34E-05	3.06E-04
RP11-439E19.10	20.896	2.104	0.530	3.967	7.27E-05	3.03E-04
RP11-707M1.1	5.198	5.784	1.454	3.979	6.93E-05	2.90E-04
MYO16	5.987	5.622	1.410	3.988	6.66E-05	2.79E-04
RP11-830F9.7	11.242	3.291	0.823	3.997	6.42E-05	2.70E-04
CALHM1	12.795	2.858	0.715	4.000	6.34E-05	2.67E-04

ROBO3	26.623	2.265	0.566	4.002	6.28E-05	2.64E-04
SAMD3	19.823	2.292	0.572	4.005	6.21E-05	2.61E-04
POTEF	7.819	3.511	0.877	4.005	6.20E-05	2.61E-04
S100A9	9.549	4.759	1.188	4.006	6.19E-05	2.61E-04
RP11-16K12.1	14.211	2.766	0.690	4.006	6.18E-05	2.60E-04
RP11-27J8.3	4.103	6.116	1.526	4.007	6.14E-05	2.59E-04
PI15	10.986	3.241	0.805	4.026	5.68E-05	2.40E-04
LINC02694	6.030	5.722	1.415	4.044	5.25E-05	2.23E-04
RP11-418J17.3	20.790	2.067	0.511	4.046	5.21E-05	2.21E-04
TMEM50B	24.117	2.475	0.611	4.052	5.07E-05	2.16E-04
CHRFAM7A	8.982	5.430	1.340	4.053	5.05E-05	2.15E-04
LINC00540	6.626	5.620	1.378	4.077	4.56E-05	1.95E-04
PTGER2	13.928	5.299	1.298	4.084	4.43E-05	1.90E-04
ATP6V1FNB	19.062	2.136	0.523	4.086	4.39E-05	1.88E-04
AC005307.5	4.220	6.070	1.485	4.089	4.34E-05	1.86E-04
CTD-2124B8.3	20.703	2.267	0.555	4.089	4.33E-05	1.86E-04
HOXB-AS1	10.153	3.440	0.840	4.093	4.25E-05	1.83E-04
FSTL5	7.976	3.834	0.934	4.105	4.04E-05	1.74E-04
HOXB2	7.755	5.547	1.351	4.107	4.01E-05	1.73E-04
NCKAP5	8.427	4.005	0.975	4.107	4.00E-05	1.73E-04
RP11-7F17.1	15.017	2.858	0.695	4.113	3.91E-05	1.69E-04
PTGFRN	18.088	5.351	1.300	4.117	3.85E-05	1.67E-04
LINC01135	16.576	2.480	0.602	4.117	3.84E-05	1.67E-04
SPOCK1	12.046	5.389	1.303	4.136	3.54E-05	1.54E-04
EDA2R	5.001	5.964	1.441	4.139	3.49E-05	1.52E-04
HS3ST3A1	8.886	5.725	1.380	4.150	3.32E-05	1.45E-04
AP001610.5	9.440	5.660	1.363	4.151	3.31E-05	1.45E-04
DUX4L37	4.199	6.350	1.529	4.153	3.28E-05	1.43E-04
HOXA4	12.615	3.495	0.841	4.156	3.24E-05	1.42E-04
SYT6	25.897	2.726	0.656	4.157	3.23E-05	1.41E-04
LINC01934	8.521	3.531	0.848	4.163	3.14E-05	1.38E-04
RP11-42I10.1	14.367	3.215	0.772	4.165	3.11E-05	1.37E-04
TMEM244	8.622	5.654	1.357	4.167	3.09E-05	1.36E-04
GAREM1	10.504	3.090	0.740	4.173	3.01E-05	1.32E-04
RP11-344L13.3	9.597	3.925	0.938	4.187	2.83E-05	1.25E-04
PDX1	17.219	5.434	1.297	4.189	2.80E-05	1.24E-04
PGM5	8.798	4.011	0.957	4.191	2.77E-05	1.23E-04
RP11-114H21.2	6.442	5.857	1.395	4.197	2.70E-05	1.20E-04
PTPRQ	14.040	3.010	0.717	4.200	2.67E-05	1.19E-04
RAPH1	8.143	3.853	0.915	4.210	2.56E-05	1.13E-04
MS4A4A	17.278	2.811	0.667	4.212	2.53E-05	1.12E-04
RP11-486O13.5	8.190	5.721	1.358	4.213	2.52E-05	1.12E-04
SKIDA1	21.396	2.192	0.519	4.227	2.37E-05	1.06E-04
OVOL1	19.035	2.763	0.652	4.234	2.29E-05	1.03E-04
BNIP5	19.526	2.511	0.593	4.236	2.27E-05	1.02E-04
RP1-153P14.5	11.939	3.262	0.768	4.249	2.14E-05	9.65E-05
P2RY6	12.121	3.897	0.911	4.278	1.89E-05	8.55E-05
LAMB3	16.896	2.325	0.543	4.279	1.88E-05	8.53E-05
KRT80	34.550	4.661	1.088	4.284	1.84E-05	8.36E-05
VWA5B2	16.428	2.926	0.682	4.291	1.78E-05	8.12E-05
AP000233.4	17.571	2.503	0.583	4.292	1.77E-05	8.07E-05
ATG9B	14.969	3.492	0.813	4.293	1.76E-05	8.03E-05
LINC00993	4.408	6.510	1.515	4.297	1.73E-05	7.92E-05
LPAR1	21.775	4.079	0.949	4.298	1.73E-05	7.89E-05
CALD1	12.614	4.961	1.152	4.305	1.67E-05	7.64E-05
BAMBI	7.339	4.732	1.094	4.323	1.54E-05	7.08E-05
CLSTN2	4.537	6.388	1.477	4.325	1.52E-05	7.03E-05
RP11-527B17.3	5.317	6.220	1.436	4.333	1.47E-05	6.81E-05

FXYD2	13.466	3.601	0.830	4.341	1.42E-05	6.58E-05
AC009262.2	4.523	6.547	1.507	4.344	1.40E-05	6.50E-05
RP11-248M19.2	22.414	2.322	0.534	4.344	1.40E-05	6.49E-05
MAGI2	19.610	2.593	0.596	4.351	1.35E-05	6.29E-05
KIF6	8.993	4.534	1.041	4.353	1.34E-05	6.24E-05
LPAR6	7.743	5.328	1.224	4.354	1.34E-05	6.22E-05
XIRP1	11.104	5.063	1.163	4.354	1.34E-05	6.22E-05
RP11-542M13.5	24.240	2.227	0.510	4.363	1.28E-05	5.98E-05
ABCC3	9.232	3.917	0.897	4.365	1.27E-05	5.93E-05
CACNG3	4.907	6.347	1.452	4.371	1.24E-05	5.79E-05
E2F3P2	16.410	2.778	0.635	4.375	1.22E-05	5.69E-05
POU2F3	9.582	5.852	1.335	4.383	1.17E-05	5.49E-05
RP11-320N7.1	16.547	2.696	0.614	4.388	1.14E-05	5.38E-05
RP11-567J20.3	5.604	6.432	1.465	4.390	1.13E-05	5.32E-05
CLYBL-AS2	6.737	6.107	1.391	4.391	1.13E-05	5.31E-05
MYO3A	6.732	6.134	1.396	4.393	1.12E-05	5.26E-05
RP11-554D15.1	12.130	3.431	0.778	4.409	1.04E-05	4.90E-05
CTD-2643I7.5	16.206	2.959	0.669	4.421	9.84E-06	4.66E-05
SCN1A-AS1	7.016	6.108	1.381	4.423	9.72E-06	4.60E-05
ARHGAP20	54.461	3.544	0.801	4.427	9.55E-06	4.53E-05
TBC1D30	15.130	5.023	1.133	4.432	9.35E-06	4.44E-05
LINC01181	11.557	3.691	0.830	4.445	8.79E-06	4.19E-05
RAMP2	10.389	3.681	0.828	4.447	8.72E-06	4.15E-05
ESRP1	26.733	2.010	0.452	4.451	8.55E-06	4.08E-05
EFNA1	19.565	2.598	0.582	4.461	8.16E-06	3.90E-05
LINC01239	4.865	6.652	1.489	4.468	7.90E-06	3.79E-05
HECW1	11.918	3.654	0.818	4.468	7.88E-06	3.78E-05
DLGAP1	7.485	6.081	1.360	4.470	7.80E-06	3.75E-05
AP003900.6	8.057	4.776	1.065	4.485	7.28E-06	3.51E-05
ULBP2	14.474	2.862	0.638	4.489	7.16E-06	3.46E-05
CAMKV	13.291	3.228	0.718	4.497	6.89E-06	3.34E-05
PDIA2	8.906	4.143	0.917	4.521	6.16E-06	3.01E-05
GTF2IP5	18.216	2.610	0.576	4.533	5.81E-06	2.84E-05
GPR87	9.139	6.072	1.339	4.533	5.80E-06	2.84E-05
AXL	11.718	5.964	1.315	4.537	5.72E-06	2.80E-05
CAV2	37.375	2.128	0.469	4.539	5.64E-06	2.76E-05
RP1-239B22.5	5.527	6.475	1.425	4.542	5.56E-06	2.72E-05
CSAG3	5.588	6.619	1.457	4.544	5.52E-06	2.71E-05
NCAPD2P1	9.216	6.055	1.331	4.548	5.40E-06	2.65E-05
NPAS3	8.630	5.596	1.229	4.554	5.27E-06	2.59E-05
RP11-146E13.9	10.201	6.082	1.334	4.558	5.17E-06	2.54E-05
S100A14	11.517	5.973	1.306	4.573	4.81E-06	2.38E-05
MALRD1	9.082	5.561	1.214	4.581	4.63E-06	2.29E-05
RP11-111A22.1	14.423	4.076	0.888	4.589	4.45E-06	2.21E-05
MUC15	10.643	4.041	0.879	4.596	4.30E-06	2.14E-05
TKTL1	15.992	2.878	0.626	4.601	4.21E-06	2.10E-05
CDA	5.862	6.509	1.412	4.608	4.06E-06	2.03E-05
IL6R	30.009	2.252	0.488	4.613	3.97E-06	1.99E-05
KSR2	62.110	5.723	1.239	4.617	3.89E-06	1.95E-05
OR7M1P	28.334	2.187	0.473	4.619	3.85E-06	1.93E-05
AGBL1	5.237	6.723	1.455	4.620	3.84E-06	1.93E-05
MDGA1	18.547	4.420	0.957	4.620	3.83E-06	1.92E-05
RP11-731J8.2	5.901	6.549	1.417	4.620	3.83E-06	1.92E-05
FAM222A-AS1	14.254	5.246	1.134	4.628	3.70E-06	1.86E-05
RANBP3L	28.093	2.407	0.520	4.629	3.67E-06	1.85E-05
LY6E	106.655	5.927	1.280	4.630	3.66E-06	1.84E-05
GBA3	6.399	6.432	1.389	4.632	3.62E-06	1.83E-05
RP11-539G18.4	11.039	5.445	1.175	4.636	3.55E-06	1.79E-05

LINC01426	9.428	5.607	1.208	4.642	3.44E-06	1.74E-05
DLX1	16.865	2.977	0.641	4.646	3.39E-06	1.71E-05
AC007743.1	102.928	5.722	1.231	4.649	3.34E-06	1.69E-05
RP11-473J6.1	9.482	6.231	1.335	4.666	3.07E-06	1.56E-05
LINC01077	8.543	6.346	1.359	4.669	3.02E-06	1.54E-05
HBG2	10.353	6.169	1.319	4.676	2.93E-06	1.49E-05
RP1-81D8.7	8.145	6.344	1.355	4.681	2.85E-06	1.45E-05
GPR84	19.102	2.897	0.618	4.688	2.75E-06	1.41E-05
RGS7	9.060	5.667	1.207	4.695	2.66E-06	1.36E-05
DHRS9	25.086	3.909	0.832	4.697	2.63E-06	1.35E-05
SLC6A8	31.527	4.315	0.918	4.698	2.62E-06	1.34E-05
LPAR3	18.312	2.771	0.588	4.710	2.47E-06	1.27E-05
RP11-167H9.4	7.263	6.509	1.379	4.720	2.36E-06	1.21E-05
DMRTA2	25.444	3.939	0.834	4.723	2.32E-06	1.20E-05
TMEM119	9.888	3.916	0.828	4.729	2.26E-06	1.17E-05
RP11-120K24.3	14.725	3.650	0.771	4.731	2.23E-06	1.16E-05
LINC01781	28.490	2.067	0.437	4.732	2.22E-06	1.15E-05
FCRL6	17.748	2.800	0.591	4.735	2.19E-06	1.14E-05
LINC02325	6.195	6.687	1.411	4.740	2.14E-06	1.11E-05
RP11-317N12.1	5.582	6.817	1.438	4.740	2.13E-06	1.11E-05
SEC24AP1	29.641	2.266	0.477	4.748	2.05E-06	1.07E-05
HCAR2	12.992	5.441	1.145	4.750	2.03E-06	1.06E-05
CYP2B6	7.506	6.471	1.361	4.753	2.00E-06	1.04E-05
CDH12	12.857	6.259	1.313	4.766	1.88E-06	9.85E-06
KIAA0319	27.922	2.239	0.468	4.779	1.76E-06	9.22E-06
ADTRP	26.575	2.208	0.461	4.785	1.71E-06	8.98E-06
PRICKLE2	9.539	4.913	1.026	4.788	1.69E-06	8.87E-06
MAPK4	240.723	5.847	1.221	4.790	1.66E-06	8.76E-06
COL27A1	23.337	2.396	0.500	4.794	1.63E-06	8.58E-06
LRRTM4-AS1	285.081	4.183	0.871	4.802	1.57E-06	8.28E-06
RP11-283G6.4	6.803	6.752	1.405	4.805	1.55E-06	8.18E-06
RP1-65P5.3	24.492	2.599	0.540	4.810	1.51E-06	7.99E-06
FSD2	21.912	2.456	0.510	4.812	1.50E-06	7.91E-06
CCN3	23.459	3.992	0.829	4.815	1.47E-06	7.80E-06
RP11-313J2.1	6.412	6.901	1.431	4.822	1.42E-06	7.52E-06
RP11-523H20.3	25.284	2.459	0.510	4.825	1.40E-06	7.42E-06
KCNA1	12.998	4.748	0.984	4.827	1.39E-06	7.37E-06
TNFRSF11B	14.860	6.217	1.288	4.828	1.38E-06	7.33E-06
RP11-32C20.1	5.918	6.935	1.432	4.842	1.29E-06	6.86E-06
EVC	5.936	6.908	1.426	4.845	1.26E-06	6.76E-06
CD300LB	11.472	6.300	1.300	4.846	1.26E-06	6.72E-06
DLL4	20.723	2.857	0.589	4.848	1.25E-06	6.69E-06
RASAL1	18.518	4.643	0.957	4.853	1.21E-06	6.51E-06
RP11-124N19.3	21.504	2.723	0.561	4.858	1.18E-06	6.36E-06
TSPAN18	12.502	4.779	0.982	4.867	1.13E-06	6.10E-06
SSPN	13.168	3.825	0.786	4.869	1.12E-06	6.04E-06
LINC02027	6.324	6.880	1.411	4.878	1.07E-06	5.79E-06
CASC15	20.432	3.390	0.694	4.882	1.05E-06	5.67E-06
DSC3	388.123	2.265	0.463	4.888	1.02E-06	5.52E-06
GATA3	14.350	3.123	0.636	4.909	9.16E-07	4.98E-06
LRP2	37.710	2.766	0.563	4.911	9.07E-07	4.93E-06
HOXA11-AS	17.497	4.228	0.859	4.924	8.50E-07	4.64E-06
TNN	30.964	2.503	0.508	4.930	8.22E-07	4.49E-06
CARMIL3	36.275	2.132	0.432	4.931	8.19E-07	4.48E-06
SLC5A5	12.774	3.929	0.797	4.931	8.17E-07	4.47E-06
ADD2	12.666	3.623	0.735	4.932	8.15E-07	4.46E-06
RP11-326C3.15	20.966	2.602	0.525	4.952	7.34E-07	4.04E-06
AFF2	19.228	6.354	1.282	4.956	7.18E-07	3.96E-06

ITIH5	14.276	3.710	0.748	4.962	6.96E-07	3.84E-06
LINC00500	19.611	2.824	0.568	4.971	6.66E-07	3.69E-06
CAPN6	6.413	6.935	1.394	4.975	6.53E-07	3.62E-06
LINC02703	25.821	2.251	0.452	4.976	6.50E-07	3.61E-06
RP11-283G6.5	11.304	5.059	1.017	4.976	6.50E-07	3.61E-06
SOWAHCP2	8.656	6.719	1.348	4.986	6.17E-07	3.44E-06
RP11-1055B8.2	31.327	2.344	0.469	4.995	5.88E-07	3.29E-06
C12orf54	17.371	5.556	1.111	5.001	5.70E-07	3.19E-06
KRT5	16.513	3.274	0.653	5.013	5.37E-07	3.01E-06
TCEAL2	12.426	4.101	0.815	5.033	4.84E-07	2.72E-06
ANKRD7	16.025	3.787	0.752	5.033	4.82E-07	2.71E-06
NR4A3	29.781	2.258	0.448	5.035	4.77E-07	2.69E-06
EDARADD	21.315	4.312	0.856	5.036	4.75E-07	2.68E-06
DOCK9-DT	18.732	2.806	0.557	5.036	4.74E-07	2.67E-06
FAM78B	10.457	5.101	1.011	5.046	4.51E-07	2.55E-06
CTD-2201E18.5	17.437	3.439	0.680	5.055	4.31E-07	2.43E-06
LINC01252	18.151	2.763	0.546	5.061	4.18E-07	2.36E-06
HOXA11	26.234	2.838	0.560	5.065	4.08E-07	2.31E-06
LNCTAM34A	32.147	3.761	0.741	5.074	3.90E-07	2.22E-06
PSD3	24.297	4.200	0.828	5.074	3.90E-07	2.22E-06
OR5K4	35.344	2.108	0.414	5.095	3.49E-07	1.99E-06
NUAK1	26.614	6.393	1.252	5.106	3.29E-07	1.89E-06
SUCNR1	21.142	4.786	0.936	5.112	3.19E-07	1.83E-06
DTNA	6.977	7.096	1.387	5.117	3.10E-07	1.79E-06
TCL1A	21.562	2.373	0.463	5.124	2.98E-07	1.72E-06
RP11-541P9.3	20.888	2.760	0.537	5.135	2.83E-07	1.64E-06
SDR42E1	14.255	5.838	1.136	5.139	2.77E-07	1.60E-06
CLLU1-AS1	14.656	3.391	0.658	5.150	2.61E-07	1.52E-06
RP11-132E11.2	10.839	6.809	1.314	5.180	2.22E-07	1.30E-06
DSCAML1	25.594	2.647	0.510	5.185	2.16E-07	1.27E-06
LINC01667	7.202	7.218	1.390	5.193	2.07E-07	1.22E-06
LONRF3	21.418	3.557	0.683	5.205	1.94E-07	1.15E-06
GRM8	33.346	2.383	0.456	5.225	1.74E-07	1.03E-06
PGLYRP4	16.878	6.604	1.262	5.235	1.65E-07	9.84E-07
RP11-22N19.2	40.324	2.005	0.383	5.235	1.65E-07	9.81E-07
RP11-25H12.1	11.335	6.817	1.302	5.236	1.64E-07	9.79E-07
LUCAT1	36.315	2.161	0.412	5.238	1.62E-07	9.67E-07
RAMP2-AS1	17.772	2.939	0.560	5.244	1.57E-07	9.37E-07
AC018462.2	12.981	4.004	0.763	5.244	1.57E-07	9.36E-07
CTD-2292N2.1	32.726	3.184	0.607	5.245	1.57E-07	9.34E-07
KCNB2	18.201	6.655	1.268	5.249	1.53E-07	9.15E-07
ZNF503	15.688	6.659	1.268	5.251	1.52E-07	9.06E-07
FTH1P22	22.953	5.779	1.100	5.252	1.51E-07	9.01E-07
LINC01139	7.564	7.218	1.374	5.255	1.48E-07	8.86E-07
MAGEA4	7.528	7.260	1.380	5.260	1.44E-07	8.64E-07
ACKR1	11.685	6.876	1.303	5.276	1.32E-07	7.95E-07
NLRP13	7.535	7.261	1.376	5.277	1.31E-07	7.90E-07
CXCR5	25.491	2.402	0.454	5.289	1.23E-07	7.44E-07
AQP9	12.163	6.876	1.300	5.291	1.22E-07	7.35E-07
RP11-331F4.5	15.187	4.014	0.755	5.315	1.07E-07	6.51E-07
AFAP1	17.164	3.172	0.596	5.319	1.04E-07	6.37E-07
TNFAIP6	14.107	5.133	0.965	5.319	1.04E-07	6.37E-07
RP11-386D6.1	13.645	5.241	0.985	5.324	1.02E-07	6.21E-07
RPS20P22	17.872	4.498	0.844	5.331	9.75E-08	5.97E-07
CYP4F29P	23.411	2.752	0.516	5.332	9.69E-08	5.93E-07
STAR	10.180	7.043	1.320	5.336	9.51E-08	5.83E-07
CEACAM16-AS1	15.692	3.861	0.722	5.347	8.95E-08	5.50E-07
RP11-21C4.1	31.487	2.257	0.422	5.350	8.80E-08	5.41E-07

RYR1	22.212	2.755	0.513	5.368	7.98E-08	4.93E-07
DCAF8L2	12.437	7.027	1.301	5.401	6.62E-08	4.12E-07
SEPTIN10	14.925	3.547	0.657	5.403	6.56E-08	4.08E-07
CH17-264B6.5	32.338	2.351	0.435	5.405	6.47E-08	4.03E-07
GNG4	44.643	6.604	1.219	5.415	6.12E-08	3.82E-07
SLC34A1	15.827	4.797	0.885	5.423	5.86E-08	3.66E-07
MTMR9LP	30.842	2.364	0.436	5.425	5.79E-08	3.62E-07
IL12RB2	23.831	2.609	0.481	5.426	5.78E-08	3.61E-07
NOL4	8.237	7.389	1.362	5.426	5.75E-08	3.60E-07
MTUS2	66.462	3.075	0.566	5.430	5.62E-08	3.52E-07
OR2V2	17.759	3.587	0.659	5.441	5.30E-08	3.33E-07
LGALS3BP	17.602	3.652	0.671	5.447	5.12E-08	3.22E-07
MAFIP	18.803	7.041	1.287	5.470	4.50E-08	2.85E-07
DMTN	19.262	5.151	0.939	5.484	4.16E-08	2.64E-07
RP11-327F22.6	24.632	2.968	0.541	5.488	4.07E-08	2.58E-07
OR51B4	20.144	6.905	1.256	5.497	3.86E-08	2.46E-07
DLGAP1-AS5	10.080	7.282	1.324	5.501	3.78E-08	2.41E-07
SAA2	25.721	3.076	0.559	5.506	3.66E-08	2.34E-07
PLAU	37.206	2.465	0.448	5.509	3.60E-08	2.30E-07
KLRC2	34.089	2.287	0.414	5.523	3.34E-08	2.14E-07
A2M	39.281	5.904	1.069	5.525	3.29E-08	2.11E-07
RP11-147L13.13	27.543	4.545	0.819	5.548	2.89E-08	1.87E-07
ADGRA3	14.902	4.289	0.772	5.558	2.73E-08	1.77E-07
ATP9A	17.040	3.497	0.629	5.559	2.72E-08	1.76E-07
GABRB1	18.254	7.029	1.264	5.562	2.67E-08	1.74E-07
RP11-54O7.17	16.053	7.097	1.273	5.575	2.47E-08	1.61E-07
TNK2-AS1	25.992	3.042	0.545	5.580	2.40E-08	1.57E-07
TSPAN11	31.739	2.562	0.459	5.583	2.37E-08	1.55E-07
GNAT2	23.246	2.809	0.502	5.592	2.24E-08	1.47E-07
ARHGAP23	57.404	2.733	0.488	5.600	2.14E-08	1.40E-07
FCHO2	36.327	3.221	0.574	5.609	2.03E-08	1.34E-07
RP11-511B23.2	19.159	4.114	0.733	5.613	1.99E-08	1.31E-07
PLXNA4	22.071	6.987	1.244	5.616	1.96E-08	1.29E-07
RP1-14D6.13	9.179	7.568	1.346	5.621	1.90E-08	1.25E-07
UTS2R	13.942	4.682	0.831	5.635	1.75E-08	1.16E-07
SGCZ	13.315	5.560	0.985	5.645	1.66E-08	1.10E-07
RP4-764O22.1	16.637	6.357	1.126	5.645	1.65E-08	1.10E-07
SHISA9	38.400	3.221	0.571	5.646	1.64E-08	1.09E-07
RNLS	24.465	4.319	0.764	5.652	1.59E-08	1.06E-07
LL22NC03-N14H11.1	18.573	4.218	0.746	5.653	1.58E-08	1.05E-07
TM4SF19	15.072	3.910	0.691	5.662	1.50E-08	9.99E-08
GDF15	23.372	2.858	0.504	5.670	1.43E-08	9.56E-08
SERPINA1	33.288	2.435	0.428	5.684	1.31E-08	8.81E-08
TPD52L1	24.066	3.325	0.584	5.691	1.26E-08	8.50E-08
ELF3-AS1	27.747	2.621	0.460	5.699	1.21E-08	8.14E-08
MAB21L1	55.838	2.770	0.486	5.704	1.17E-08	7.90E-08
POU6F2	15.106	7.313	1.282	5.707	1.15E-08	7.78E-08
CUEDC1	32.085	2.696	0.472	5.712	1.12E-08	7.57E-08
LINC01807	9.634	7.638	1.337	5.714	1.10E-08	7.46E-08
RP11-384F7.1	33.915	2.449	0.428	5.717	1.08E-08	7.33E-08
OFCC1	28.026	2.446	0.427	5.730	1.01E-08	6.84E-08
NAP1L3	43.845	3.340	0.580	5.763	8.29E-09	5.68E-08
LL21NC02-1C16.2	21.874	3.129	0.543	5.767	8.09E-09	5.55E-08
LINC02055	83.059	3.198	0.553	5.781	7.44E-09	5.13E-08
FAT2	20.424	7.264	1.255	5.786	7.19E-09	4.96E-08
LEF1-AS1	21.460	3.775	0.651	5.797	6.76E-09	4.68E-08
SPINT1-AS1	33.468	2.997	0.517	5.797	6.76E-09	4.68E-08
RP11-88H10.3	29.909	7.121	1.228	5.801	6.61E-09	4.58E-08

NR5A2	16.647	5.567	0.958	5.814	6.10E-09	4.24E-08
CCL19	12.847	7.491	1.287	5.820	5.88E-09	4.10E-08
WNT11	46.449	2.096	0.360	5.827	5.65E-09	3.94E-08
DSC1	28.501	3.098	0.531	5.838	5.27E-09	3.69E-08
IL4	40.502	2.361	0.404	5.841	5.19E-09	3.63E-08
SP3P	14.195	5.710	0.977	5.843	5.13E-09	3.60E-08
HPCAL4	86.425	2.322	0.397	5.847	5.01E-09	3.52E-08
LINC01758	22.667	3.302	0.563	5.860	4.62E-09	3.26E-08
RP4-742C19.12	42.282	2.396	0.407	5.883	4.04E-09	2.86E-08
FBN2	12.094	7.601	1.291	5.888	3.91E-09	2.77E-08
MKRN3	17.750	6.565	1.115	5.890	3.86E-09	2.74E-08
ABHD1	34.540	3.776	0.641	5.891	3.84E-09	2.72E-08
ACP5	37.642	2.199	0.373	5.898	3.69E-09	2.62E-08
AC007405.6	37.826	2.870	0.486	5.906	3.50E-09	2.49E-08
SLFN13	93.612	5.151	0.869	5.927	3.09E-09	2.21E-08
ALDH1A3	19.398	6.585	1.111	5.927	3.08E-09	2.20E-08
LINC01132	64.815	2.108	0.355	5.941	2.83E-09	2.03E-08
LINC02832	14.368	7.688	1.291	5.954	2.62E-09	1.89E-08
IFITM3P2	19.880	3.510	0.589	5.959	2.54E-09	1.83E-08
RAB3C	11.689	7.771	1.302	5.969	2.39E-09	1.73E-08
RP11-20J15.2	28.310	2.633	0.441	5.971	2.35E-09	1.70E-08
TRAJ49	34.229	2.937	0.492	5.973	2.33E-09	1.69E-08
LINC00839	11.367	7.847	1.313	5.977	2.28E-09	1.65E-08
H3C6	41.272	2.548	0.425	5.999	1.99E-09	1.45E-08
PECAM1	39.360	2.514	0.419	5.999	1.98E-09	1.45E-08
AC005537.2	23.518	3.189	0.531	6.006	1.90E-09	1.39E-08
RP3-431A14.7	19.100	3.897	0.648	6.013	1.83E-09	1.34E-08
RP11-67L14.2	24.270	5.509	0.914	6.026	1.68E-09	1.23E-08
HRAT92	74.174	2.227	0.369	6.031	1.63E-09	1.20E-08
ANKRD22	17.776	3.703	0.612	6.047	1.47E-09	1.09E-08
SELP	16.283	4.830	0.795	6.076	1.23E-09	9.20E-09
RP11-386M24.10	44.913	2.584	0.424	6.089	1.14E-09	8.51E-09
AC058791.1	32.075	2.666	0.437	6.095	1.10E-09	8.21E-09
CHRDL1	12.212	7.920	1.298	6.102	1.04E-09	7.85E-09
SYBU	48.710	2.164	0.354	6.107	1.02E-09	7.64E-09
IFNA2	26.591	7.528	1.232	6.109	1.00E-09	7.55E-09
KCNA2	16.000	4.199	0.687	6.110	9.95E-10	7.50E-09
NXF3	12.432	7.933	1.297	6.114	9.69E-10	7.31E-09
LRRN1	73.619	7.356	1.202	6.118	9.45E-10	7.14E-09
SOX2-OT	80.834	2.064	0.337	6.120	9.37E-10	7.08E-09
ISX	30.210	2.517	0.411	6.126	9.04E-10	6.84E-09
ABCA13	15.700	4.766	0.777	6.136	8.48E-10	6.43E-09
LDC1P	34.140	2.619	0.426	6.144	8.07E-10	6.13E-09
LINC02446	17.971	3.810	0.620	6.144	8.04E-10	6.11E-09
HNF1B	19.811	7.706	1.251	6.158	7.39E-10	5.64E-09
DNAJC5B	31.540	2.942	0.476	6.183	6.31E-10	4.85E-09
CACNB2	24.833	3.863	0.621	6.218	5.03E-10	3.89E-09
HS3ST1	70.961	2.133	0.343	6.224	4.84E-10	3.74E-09
FOXL1	13.109	8.082	1.296	6.238	4.42E-10	3.44E-09
ICOS	42.513	2.472	0.396	6.247	4.18E-10	3.26E-09
TMEM132D-AS1	15.894	5.434	0.870	6.248	4.16E-10	3.25E-09
SOCS2-AS1	54.134	2.801	0.448	6.252	4.05E-10	3.16E-09
SDC4	46.637	3.224	0.515	6.260	3.85E-10	3.02E-09
UGT2B7	17.546	7.907	1.263	6.260	3.84E-10	3.01E-09
PLK2	34.994	2.384	0.380	6.269	3.63E-10	2.85E-09
LINC00462	51.090	6.627	1.054	6.288	3.22E-10	2.55E-09
ULBP1	24.925	3.167	0.504	6.289	3.20E-10	2.53E-09
RP11-459O1.2	47.627	2.081	0.331	6.293	3.12E-10	2.47E-09

JAKMIP2	15.695	4.813	0.763	6.308	2.82E-10	2.24E-09
CCR4	21.530	5.229	0.828	6.313	2.75E-10	2.18E-09
F13A1	39.907	2.478	0.392	6.329	2.48E-10	1.97E-09
ACP3	32.645	2.799	0.440	6.356	2.07E-10	1.66E-09
SLC24A4	48.466	2.274	0.358	6.359	2.03E-10	1.63E-09
SPAG6	39.038	2.590	0.406	6.371	1.87E-10	1.51E-09
ARFGEF3	68.888	7.668	1.203	6.373	1.85E-10	1.49E-09
CR1L	64.479	2.665	0.417	6.388	1.68E-10	1.36E-09
LCE1E	16.430	8.106	1.267	6.397	1.59E-10	1.28E-09
ZNF618	16.616	4.825	0.754	6.403	1.52E-10	1.23E-09
NEURL3	50.218	7.744	1.209	6.403	1.52E-10	1.23E-09
LINC00355	14.628	8.228	1.282	6.418	1.38E-10	1.13E-09
RP11-215D10.3	31.907	5.147	0.801	6.427	1.30E-10	1.06E-09
UBE2QL1	128.108	2.992	0.464	6.453	1.10E-10	9.01E-10
OR51B5	58.065	6.796	1.053	6.455	1.08E-10	8.88E-10
IFNG	46.242	3.143	0.487	6.459	1.05E-10	8.66E-10
CD33	17.620	8.286	1.282	6.464	1.02E-10	8.40E-10
MERTK	25.777	3.914	0.606	6.465	1.02E-10	8.38E-10
C14orf132	68.950	7.801	1.207	6.465	1.01E-10	8.36E-10
TMEM100	28.735	6.975	1.076	6.482	9.03E-11	7.48E-10
SNCA	30.735	4.210	0.648	6.493	8.44E-11	7.01E-10
SLIT1	43.264	2.144	0.329	6.518	7.15E-11	5.97E-10
ANKRD20A11P	44.459	2.393	0.367	6.520	7.04E-11	5.89E-10
LINC01091	47.405	6.933	1.062	6.528	6.65E-11	5.57E-10
NGB	43.104	5.114	0.783	6.529	6.63E-11	5.56E-10
PTGS1	59.327	2.380	0.363	6.564	5.25E-11	4.43E-10
IGHG3	376.332	3.280	0.499	6.568	5.11E-11	4.31E-10
RP11-326C3.11	33.829	2.903	0.440	6.594	4.29E-11	3.64E-10
KLHL14	27.433	8.152	1.235	6.601	4.08E-11	3.47E-10
LINC00674	60.710	6.940	1.049	6.614	3.75E-11	3.20E-10
SPINK2	40.699	5.201	0.785	6.623	3.51E-11	3.01E-10
TDRD12	64.477	2.039	0.308	6.624	3.51E-11	3.01E-10
RP11-85O21.2	73.404	2.561	0.386	6.639	3.15E-11	2.71E-10
RP11-85O21.4	53.359	2.427	0.365	6.654	2.86E-11	2.47E-10
ASPHD1	40.517	3.202	0.480	6.670	2.56E-11	2.22E-10
KCNA3	59.169	2.016	0.302	6.687	2.28E-11	1.99E-10
COL5A3	30.539	4.928	0.736	6.694	2.17E-11	1.89E-10
BTBD19	29.615	3.319	0.494	6.713	1.91E-11	1.68E-10
RP11-334L9.2	55.730	5.880	0.874	6.727	1.73E-11	1.53E-10
FAM221A	44.134	4.017	0.597	6.729	1.71E-11	1.51E-10
HOXA3	37.331	6.020	0.895	6.729	1.71E-11	1.51E-10
NPSR1-AS1	31.740	7.234	1.075	6.731	1.69E-11	1.49E-10
CLDN16	28.921	3.142	0.466	6.743	1.55E-11	1.38E-10
ST14	21.800	5.650	0.837	6.748	1.50E-11	1.33E-10
FRMPD2B	29.537	4.756	0.703	6.766	1.33E-11	1.18E-10
RP11-168F16.1	36.856	2.544	0.375	6.780	1.20E-11	1.07E-10
LTBP2	30.637	3.867	0.570	6.783	1.18E-11	1.05E-10
GABRA3	18.463	8.567	1.262	6.791	1.11E-11	9.98E-11
OCLN	31.475	4.607	0.678	6.796	1.08E-11	9.67E-11
LINC02240	59.735	2.036	0.299	6.816	9.36E-12	8.42E-11
ARRB1	112.147	5.154	0.756	6.817	9.31E-12	8.38E-11
CRNDE	21.034	4.646	0.680	6.830	8.51E-12	7.68E-11
RP11-368I7.6	30.539	3.183	0.465	6.848	7.50E-12	6.80E-11
ANKRD30A	19.141	8.619	1.258	6.850	7.41E-12	6.72E-11
IGF2BP1	22.815	6.391	0.932	6.860	6.91E-12	6.28E-11
IL1R1	43.530	2.702	0.393	6.874	6.23E-12	5.68E-11
GIMAP7	38.781	2.765	0.401	6.888	5.65E-12	5.17E-11
MAGEA10	20.051	8.687	1.257	6.911	4.82E-12	4.43E-11

TGM2	43.932	2.431	0.352	6.912	4.78E-12	4.40E-11
RHOXF1	62.915	8.318	1.203	6.915	4.68E-12	4.31E-11
F5	108.378	2.866	0.413	6.933	4.13E-12	3.82E-11
CHRM3	32.341	7.460	1.075	6.939	3.94E-12	3.64E-11
CPS1	51.031	3.082	0.444	6.941	3.90E-12	3.61E-11
SNAI3	54.148	2.380	0.343	6.944	3.80E-12	3.53E-11
EPB41L3	31.452	8.510	1.225	6.949	3.68E-12	3.42E-11
NPTXR	79.451	3.380	0.486	6.952	3.59E-12	3.35E-11
RP11-214O1.2	63.658	8.371	1.203	6.958	3.46E-12	3.22E-11
GTSF1L	55.676	2.072	0.298	6.965	3.29E-12	3.08E-11
GGT6	33.209	3.962	0.568	6.981	2.92E-12	2.74E-11
CALHM3	37.483	3.121	0.447	6.989	2.77E-12	2.61E-11
KIRREL2	40.829	4.166	0.596	6.989	2.77E-12	2.61E-11
IRF6	75.601	2.191	0.313	6.995	2.66E-12	2.50E-11
STMN4	25.527	3.922	0.559	7.013	2.33E-12	2.20E-11
ATP6V0E2-AS1	31.219	3.653	0.519	7.034	2.01E-12	1.91E-11
RMST	159.574	2.770	0.393	7.042	1.89E-12	1.80E-11
CEBPD	46.115	4.205	0.597	7.043	1.88E-12	1.79E-11
LINC01629	40.197	2.818	0.399	7.063	1.62E-12	1.55E-11
DPYD-AS1	69.052	6.147	0.868	7.080	1.44E-12	1.38E-11
TNFRSF25	23.786	3.996	0.559	7.153	8.51E-13	8.29E-12
PHACTR2	66.056	2.081	0.290	7.187	6.63E-13	6.50E-12
CTC-546K23.1	84.233	6.212	0.864	7.188	6.56E-13	6.44E-12
RP11-488I20.9	24.505	8.984	1.243	7.230	4.82E-13	4.78E-12
DEPDC7	44.530	3.315	0.457	7.248	4.23E-13	4.22E-12
RP11-526D8.12	28.077	5.516	0.760	7.254	4.03E-13	4.03E-12
S100A6	55.578	2.546	0.351	7.258	3.93E-13	3.93E-12
LRRC36	29.859	4.322	0.592	7.305	2.77E-13	2.81E-12
PDGFRB	68.355	3.124	0.426	7.328	2.34E-13	2.38E-12
RASGRF1	71.695	2.123	0.290	7.329	2.31E-13	2.36E-12
HOXA10	57.752	8.840	1.205	7.338	2.17E-13	2.21E-12
SPOCK2	55.821	2.600	0.354	7.351	1.97E-13	2.01E-12
RP11-326C3.12	39.584	2.834	0.385	7.355	1.91E-13	1.96E-12
HMGA2	28.038	9.088	1.235	7.361	1.83E-13	1.88E-12
ABCA9	70.508	2.048	0.278	7.363	1.80E-13	1.85E-12
CCR8	50.136	5.686	0.770	7.383	1.55E-13	1.60E-12
TBX15	88.782	7.701	1.040	7.403	1.33E-13	1.38E-12
CLEC4M	31.572	3.406	0.458	7.431	1.07E-13	1.12E-12
WDR64	27.237	4.202	0.565	7.439	1.02E-13	1.06E-12
LINC02051	51.379	5.228	0.702	7.449	9.38E-14	9.81E-13
CASKIN2	74.412	2.288	0.307	7.450	9.33E-14	9.77E-13
WSCD1	105.977	7.766	1.039	7.473	7.81E-14	8.22E-13
SERPINB2	30.262	6.831	0.914	7.474	7.76E-14	8.17E-13
RP11-373N22.3	53.008	2.236	0.299	7.482	7.34E-14	7.74E-13
PRR5L	65.036	2.695	0.358	7.532	5.00E-14	5.33E-13
PPP4R3C	30.574	9.256	1.228	7.536	4.84E-14	5.16E-13
RP11-115D19.1	65.008	2.942	0.390	7.542	4.64E-14	4.96E-13
MCF2L	65.068	2.727	0.362	7.544	4.56E-14	4.88E-13
C15orf62	81.691	2.127	0.281	7.561	3.99E-14	4.28E-13
SIX3	72.245	9.094	1.201	7.573	3.64E-14	3.91E-13
GLIS3	84.797	2.235	0.295	7.574	3.62E-14	3.90E-13
RASSF8-AS1	53.678	4.639	0.612	7.577	3.55E-14	3.82E-13
DLG3	69.553	2.385	0.313	7.609	2.76E-14	3.00E-13
SULF2	63.661	3.073	0.403	7.620	2.54E-14	2.77E-13
SHOX2	67.464	2.371	0.311	7.635	2.25E-14	2.46E-13
NAV2	42.700	2.612	0.342	7.643	2.13E-14	2.33E-13
UNQ6494	54.723	3.162	0.413	7.651	1.99E-14	2.19E-13
KIF5A	78.528	2.718	0.355	7.667	1.76E-14	1.94E-13

RP11-87E22.2	46.918	2.961	0.384	7.706	1.30E-14	1.44E-13
CTNND2	58.623	2.279	0.295	7.722	1.14E-14	1.27E-13
ITGA5	71.166	8.086	1.044	7.744	9.63E-15	1.08E-13
RP11-791G22.3	38.791	3.644	0.469	7.775	7.56E-15	8.50E-14
TUBA8	75.061	2.153	0.276	7.799	6.25E-15	7.07E-14
RP11-163N15.2	66.796	3.202	0.410	7.805	5.94E-15	6.72E-14
ZNF257	30.988	6.296	0.807	7.806	5.91E-15	6.70E-14
ANO5	42.483	6.926	0.882	7.856	3.98E-15	4.54E-14
RORB	48.148	4.222	0.536	7.879	3.31E-15	3.79E-14
SNTB1	72.480	3.366	0.427	7.880	3.26E-15	3.74E-14
TNC	57.319	2.754	0.346	7.955	1.80E-15	2.09E-14
PLD4	82.779	5.067	0.634	7.996	1.28E-15	1.50E-14
LINC01446	42.069	9.717	1.214	8.001	1.23E-15	1.45E-14
COL4A6	227.635	9.525	1.188	8.020	1.06E-15	1.25E-14
RIMBP2	72.685	2.383	0.297	8.029	9.85E-16	1.16E-14
MAP7D2	33.069	4.013	0.493	8.146	3.75E-16	4.54E-15
LINC01402	44.550	5.039	0.618	8.154	3.51E-16	4.26E-15
NRXN3	35.832	3.361	0.409	8.211	2.20E-16	2.71E-15
PCDH15	30.520	5.598	0.678	8.253	1.54E-16	1.91E-15
RP5-1097P24.1	95.288	9.954	1.196	8.322	8.64E-17	1.09E-15
RP13-254B10.1	55.895	2.753	0.330	8.344	7.20E-17	9.07E-16
LINC01104	44.627	3.240	0.387	8.373	5.60E-17	7.10E-16
GPSM1	183.351	2.881	0.344	8.386	5.04E-17	6.41E-16
NLRP4	30.847	3.785	0.451	8.386	5.04E-17	6.40E-16
HNRNPA1P21	50.075	4.293	0.511	8.404	4.30E-17	5.49E-16
CCL17	82.242	2.173	0.258	8.413	3.99E-17	5.12E-16
LINC00461	151.966	2.526	0.300	8.414	3.97E-17	5.10E-16
RGL3	98.465	3.895	0.461	8.456	2.76E-17	3.57E-16
CH17-67K23.2	48.589	2.925	0.345	8.478	2.30E-17	2.99E-16
PTPRM	66.708	3.075	0.359	8.569	1.04E-17	1.39E-16
CSAG1	63.638	10.319	1.203	8.575	9.94E-18	1.32E-16
ADGRB2	92.638	2.505	0.292	8.586	8.98E-18	1.20E-16
LRG1	65.618	3.017	0.351	8.594	8.37E-18	1.12E-16
CNTLN	63.821	10.360	1.203	8.608	7.42E-18	9.94E-17
PRKAA2	232.499	10.216	1.187	8.609	7.35E-18	9.85E-17
DUSP6	75.267	3.812	0.442	8.616	6.95E-18	9.32E-17
SESN3	201.347	2.019	0.234	8.617	6.85E-18	9.21E-17
ST8SIA6	37.865	3.519	0.407	8.651	5.11E-18	6.89E-17
TNFSF12	50.902	4.587	0.530	8.659	4.74E-18	6.41E-17
WASH6P	43.256	4.131	0.475	8.690	3.64E-18	4.93E-17
SLC16A14	73.070	3.690	0.423	8.718	2.83E-18	3.87E-17
GTSF1	41.274	6.838	0.784	8.721	2.75E-18	3.77E-17
PIMREG	82.363	7.525	0.859	8.759	1.96E-18	2.71E-17
RHOXF1-AS1	198.352	10.412	1.187	8.773	1.74E-18	2.40E-17
RP11-88I21.3	62.111	3.897	0.443	8.790	1.50E-18	2.08E-17
HCAR3	47.123	5.724	0.650	8.800	1.37E-18	1.90E-17
LDLRAD2	90.549	2.037	0.230	8.839	9.62E-19	1.35E-17
SMPD3	142.113	2.018	0.227	8.873	7.09E-19	1.00E-17
CHODL	65.400	2.838	0.320	8.877	6.84E-19	9.67E-18
MMP7	177.556	9.169	1.032	8.885	6.37E-19	9.01E-18
HOXB6	47.464	4.579	0.513	8.923	4.53E-19	6.43E-18
NRXN1	66.574	7.778	0.872	8.925	4.45E-19	6.32E-18
RP11-57A1.1	87.570	2.232	0.250	8.927	4.39E-19	6.25E-18
ITGB8-AS1	88.292	5.611	0.627	8.949	3.60E-19	5.16E-18
LFNG	56.634	3.246	0.362	8.975	2.83E-19	4.08E-18
PRLR	65.878	5.353	0.595	8.996	2.33E-19	3.37E-18
OR2V1	53.140	3.301	0.365	9.034	1.65E-19	2.41E-18
VPREB3	87.050	2.144	0.236	9.098	9.21E-20	1.36E-18

TRIM47	47.897	3.662	0.402	9.103	8.78E-20	1.30E-18
STC1	40.542	6.517	0.714	9.128	6.98E-20	1.04E-18
DUXAP9	50.168	5.995	0.656	9.136	6.50E-20	9.68E-19
NCR3LG1	37.774	4.911	0.537	9.145	5.95E-20	8.88E-19
ANXA1	69.651	3.101	0.337	9.190	3.93E-20	5.93E-19
ABTB2	69.875	2.719	0.295	9.209	3.29E-20	4.98E-19
TCEAL9	161.884	6.812	0.740	9.211	3.24E-20	4.90E-19
ZNF853	83.862	5.117	0.555	9.224	2.87E-20	4.35E-19
ZG16B	80.683	2.654	0.285	9.306	1.32E-20	2.03E-19
PURPL	51.930	7.170	0.769	9.329	1.06E-20	1.64E-19
RBMS1	58.620	3.696	0.395	9.355	8.33E-21	1.29E-19
DIP2C	105.375	2.220	0.237	9.367	7.49E-21	1.17E-19
NBPF14	108.728	2.441	0.260	9.383	6.40E-21	9.99E-20
RP11-203B7.2	57.687	3.707	0.395	9.392	5.89E-21	9.22E-20
SLC30A3	117.757	2.531	0.269	9.394	5.76E-21	9.02E-20
CYS1	67.144	3.214	0.342	9.407	5.12E-21	8.03E-20
LINC02520	63.118	3.589	0.381	9.408	5.05E-21	7.92E-20
GRPR	44.953	3.693	0.392	9.409	5.00E-21	7.85E-20
PRSS51	43.087	5.314	0.561	9.471	2.78E-21	4.41E-20
ADGRE4P	75.260	7.159	0.755	9.482	2.49E-21	3.97E-20
A4GALT	74.436	3.167	0.333	9.509	1.92E-21	3.06E-20
C2orf91	51.644	3.536	0.372	9.512	1.87E-21	2.98E-20
LINC00997	59.637	3.068	0.322	9.532	1.54E-21	2.47E-20
GNAQ	39.764	5.965	0.625	9.544	1.38E-21	2.21E-20
GPAT3	89.862	3.606	0.377	9.569	1.08E-21	1.74E-20
MAGEA3	136.044	11.452	1.190	9.620	6.56E-22	1.06E-20
ANKRD29	121.599	2.104	0.218	9.639	5.50E-22	8.94E-21
BACE1	53.313	3.750	0.389	9.646	5.12E-22	8.34E-21
VPS37B	251.407	2.376	0.246	9.654	4.73E-22	7.70E-21
MCF2L-AS1	98.411	2.616	0.271	9.667	4.16E-22	6.80E-21
INKA1	117.493	2.308	0.239	9.669	4.09E-22	6.71E-21
ANKRD20A5P	53.653	3.193	0.330	9.670	4.05E-22	6.64E-21
RP11-648K4.2	39.462	5.527	0.571	9.674	3.90E-22	6.42E-21
CISH	105.067	2.429	0.251	9.678	3.76E-22	6.19E-21
FGF2	53.812	5.570	0.573	9.713	2.65E-22	4.41E-21
LINC01619	148.024	2.010	0.207	9.723	2.41E-22	4.02E-21
HOXA6	70.997	3.537	0.363	9.747	1.91E-22	3.19E-21
ZSWIM5	197.921	2.234	0.228	9.796	1.17E-22	1.97E-21
CACNA1D	65.777	4.882	0.498	9.806	1.06E-22	1.80E-21
BACE2	86.795	2.878	0.293	9.813	9.93E-23	1.68E-21
MAGEA12	160.741	11.676	1.189	9.817	9.52E-23	1.61E-21
LINC00884	143.128	2.372	0.242	9.818	9.41E-23	1.59E-21
PTPRG-AS1	69.016	4.464	0.453	9.849	6.95E-23	1.18E-21
CCL2	286.790	11.738	1.184	9.915	3.59E-23	6.20E-22
RP1-158P9.2	66.828	4.023	0.404	9.969	2.08E-23	3.61E-22
IFITM2	95.320	2.335	0.233	10.009	1.40E-23	2.45E-22
BCL11B	70.880	2.812	0.281	10.023	1.21E-23	2.13E-22
DLGAP3	98.608	2.953	0.295	10.026	1.17E-23	2.06E-22
KLRK1-AS1	59.708	4.059	0.402	10.097	5.72E-24	1.02E-22
DHRS2	53.590	4.070	0.401	10.144	3.51E-24	6.27E-23
RP11-191L9.4	46.093	5.500	0.540	10.178	2.50E-24	4.47E-23
CTA-384D8.34	93.861	2.924	0.287	10.183	2.36E-24	4.22E-23
CFAP57	112.276	2.715	0.267	10.186	2.28E-24	4.10E-23
FBXL16	154.956	2.349	0.230	10.200	1.98E-24	3.56E-23
RSAD2	111.714	6.365	0.620	10.261	1.05E-24	1.92E-23
MAGEA6	229.276	12.207	1.186	10.294	7.52E-25	1.38E-23
TRIM7	117.929	2.381	0.231	10.313	6.17E-25	1.13E-23
TMEM266	173.548	2.199	0.213	10.329	5.21E-25	9.63E-24

RP11-305F5.3	88.391	4.401	0.423	10.397	2.56E-25	4.79E-24
CHST7	173.108	2.132	0.205	10.415	2.13E-25	3.99E-24
LINC00958	374.802	5.863	0.561	10.449	1.48E-25	2.80E-24
ITGB8	125.394	6.014	0.575	10.462	1.28E-25	2.44E-24
P2RX5	83.919	2.742	0.262	10.484	1.02E-25	1.95E-24
HOXA5	94.816	3.098	0.295	10.498	8.86E-26	1.70E-24
CSGALNACT1	66.742	3.992	0.378	10.560	4.55E-26	8.77E-25
ASPH	72.985	3.005	0.283	10.600	2.99E-26	5.79E-25
SPTB	72.233	4.146	0.386	10.730	7.37E-27	1.46E-25
ADAMTS17	73.740	3.539	0.329	10.741	6.51E-27	1.30E-25
TRAT1	80.932	3.202	0.297	10.787	3.95E-27	7.96E-26
CSRNP3	84.939	2.991	0.276	10.825	2.62E-27	5.34E-26
FAM171A2	200.201	2.062	0.190	10.834	2.37E-27	4.83E-26
SAMD14	108.041	2.886	0.266	10.843	2.15E-27	4.39E-26
LINC01258	102.118	2.654	0.245	10.848	2.04E-27	4.17E-26
SELENON	108.665	3.066	0.282	10.858	1.83E-27	3.75E-26
CD84	159.262	2.127	0.196	10.865	1.69E-27	3.47E-26
IGLV6-57	89.864	3.068	0.282	10.866	1.67E-27	3.43E-26
LSAMP	90.229	2.606	0.240	10.872	1.57E-27	3.24E-26
IGSF9B	110.957	4.744	0.436	10.876	1.50E-27	3.08E-26
ADCY6	135.149	7.256	0.667	10.878	1.47E-27	3.03E-26
MAGEA1	193.610	9.231	0.845	10.928	8.51E-28	1.76E-26
C3	71.645	3.747	0.341	10.975	5.05E-28	1.06E-26
PRKAR2B	119.582	3.022	0.274	11.030	2.73E-28	5.76E-27
RP11-432J24.5	189.447	2.201	0.199	11.086	1.47E-28	3.13E-27
UPB1	101.293	2.887	0.260	11.106	1.17E-28	2.49E-27
ELF3	66.299	5.146	0.463	11.125	9.52E-29	2.05E-27
CCDC85A	312.396	5.092	0.457	11.137	8.30E-29	1.79E-27
ZSCAN31	141.848	2.410	0.216	11.140	8.06E-29	1.74E-27
GPC5	162.682	3.458	0.310	11.173	5.52E-29	1.20E-27
MIR34AHG	115.971	3.939	0.351	11.210	3.62E-29	7.92E-28
FOXA3	86.529	3.414	0.304	11.220	3.24E-29	7.10E-28
TMEM132D	104.448	3.308	0.295	11.227	3.02E-29	6.65E-28
BRSK1	156.370	2.763	0.245	11.278	1.69E-29	3.76E-28
BCL2L14	112.697	3.102	0.274	11.300	1.31E-29	2.91E-28
CNKSR2	116.123	2.417	0.213	11.321	1.03E-29	2.31E-28
PLS3	202.577	2.692	0.237	11.376	5.52E-30	1.24E-28
C1orf54	166.377	2.256	0.198	11.415	3.50E-30	7.94E-29
CERKL	82.811	3.311	0.290	11.436	2.76E-30	6.28E-29
AC005083.1	133.891	2.671	0.233	11.462	2.06E-30	4.70E-29
PTPRD	294.085	8.420	0.733	11.486	1.56E-30	3.58E-29
PHLDA3	171.341	4.178	0.364	11.491	1.46E-30	3.35E-29
SPTSSB	140.442	2.356	0.205	11.509	1.19E-30	2.76E-29
FOXC1	117.551	4.833	0.417	11.591	4.58E-31	1.08E-29
DGKG	166.772	2.928	0.252	11.603	3.98E-31	9.40E-30
ADAMTS3	97.742	4.450	0.382	11.635	2.72E-31	6.50E-30
CCDC198	131.384	6.674	0.572	11.664	1.95E-31	4.66E-30
CD101	75.431	4.027	0.341	11.793	4.25E-32	1.04E-30
SATB2-AS1	146.459	3.142	0.266	11.815	3.25E-32	7.92E-31
CD24	107.359	3.535	0.299	11.819	3.10E-32	7.58E-31
DELEC1	141.024	3.058	0.258	11.844	2.32E-32	5.71E-31
RP4-781K5.6	143.362	2.589	0.218	11.855	2.02E-32	4.99E-31
RP11-640F22.1	82.351	6.072	0.506	11.989	4.05E-33	1.03E-31
TGFBR3L	125.627	3.062	0.255	11.993	3.86E-33	9.80E-32
RP11-492E3.2	77.306	4.186	0.349	11.995	3.76E-33	9.54E-32
LINC01226	112.672	3.211	0.267	12.011	3.11E-33	7.93E-32
CMKLR1	188.092	3.816	0.317	12.020	2.80E-33	7.16E-32
CPNE4	79.134	4.234	0.350	12.095	1.12E-33	2.89E-32

NOTUM	130.038	3.110	0.255	12.177	4.11E-34	1.08E-32
ATP7B	164.886	2.384	0.195	12.208	2.81E-34	7.44E-33
NEUROG2-AS1	120.272	4.625	0.378	12.237	1.97E-34	5.26E-33
REC8	258.070	2.256	0.184	12.273	1.26E-34	3.39E-33
RHOB	246.505	2.548	0.206	12.373	3.68E-35	1.01E-33
PLEKHG6	124.592	3.533	0.285	12.415	2.16E-35	5.95E-34
FOSL1	115.633	4.270	0.343	12.430	1.80E-35	4.99E-34
MMP9	90.480	4.113	0.330	12.461	1.21E-35	3.38E-34
KCTD19	158.182	2.488	0.199	12.513	6.34E-36	1.79E-34
SLCO2B1	134.625	4.998	0.399	12.529	5.18E-36	1.47E-34
MOB3B	111.883	7.222	0.575	12.570	3.07E-36	8.74E-35
RASSF8	170.273	4.902	0.388	12.651	1.10E-36	3.17E-35
NRG2	194.671	2.262	0.178	12.697	6.18E-37	1.79E-35
TESK2	245.936	2.100	0.165	12.702	5.75E-37	1.67E-35
DTHD1	82.805	3.910	0.306	12.763	2.63E-37	7.75E-36
NT5DC4	106.067	3.857	0.301	12.802	1.60E-37	4.76E-36
NUS1P2	173.678	2.490	0.193	12.868	6.83E-38	2.04E-36
SPRED2	151.189	2.681	0.208	12.879	5.94E-38	1.78E-36
PWWP3B	108.803	5.032	0.390	12.903	4.31E-38	1.29E-36
SCNN1G	112.372	4.203	0.325	12.938	2.75E-38	8.28E-37
RUNDC3A-AS1	145.519	3.107	0.240	12.959	2.09E-38	6.31E-37
LINC00888	125.334	3.705	0.285	13.006	1.14E-38	3.46E-37
PTGIR	170.210	2.776	0.212	13.079	4.36E-39	1.34E-37
LGALS9	378.903	2.102	0.160	13.133	2.14E-39	6.65E-38
SIX4	126.685	4.642	0.353	13.158	1.53E-39	4.78E-38
EDN1	240.755	2.208	0.167	13.201	8.64E-40	2.72E-38
MEST	118.951	3.798	0.287	13.215	7.23E-40	2.29E-38
ACHE	158.176	3.445	0.260	13.251	4.46E-40	1.42E-38
RP11-472K17.3	362.093	9.674	0.730	13.261	3.92E-40	1.26E-38
RNF207	265.511	2.072	0.156	13.289	2.67E-40	8.58E-39
NEUROG2	211.509	3.413	0.255	13.380	7.90E-41	2.58E-39
MS4A6E	287.684	2.747	0.205	13.400	6.04E-41	1.98E-39
SLC35G2	157.400	4.534	0.335	13.519	1.21E-41	4.04E-40
RP11-356M20.1	131.653	6.895	0.510	13.527	1.08E-41	3.62E-40
FCRL4	88.481	4.371	0.322	13.582	5.15E-42	1.73E-40
AEBP1	330.219	7.588	0.558	13.595	4.30E-42	1.45E-40
LINC01320	239.231	4.575	0.336	13.609	3.56E-42	1.20E-40
SOCS2	251.452	2.852	0.209	13.673	1.47E-42	4.96E-41
SCN8A	139.495	3.988	0.290	13.734	6.33E-43	2.17E-41
INKA2	273.294	2.052	0.149	13.779	3.39E-43	1.18E-41
EFNB2	183.628	2.679	0.194	13.794	2.78E-43	9.67E-42
TIMP1	199.717	2.829	0.205	13.823	1.86E-43	6.48E-42
KLF7	147.034	5.354	0.387	13.829	1.71E-43	5.95E-42
DDX60L	202.858	2.526	0.182	13.844	1.38E-43	4.81E-42
PTPN14	137.316	4.625	0.331	13.978	2.12E-44	7.53E-43
LINC02341	205.105	2.667	0.190	14.006	1.43E-44	5.10E-43
APOBR	197.169	2.700	0.193	14.008	1.38E-44	4.94E-43
GHR	1055.518	11.734	0.836	14.030	1.02E-44	3.65E-43
GNAO1	334.692	2.125	0.150	14.126	2.62E-45	9.51E-44
MNDA	224.934	7.059	0.499	14.133	2.39E-45	8.68E-44
RNF43	113.047	3.863	0.273	14.140	2.15E-45	7.84E-44
PLXNB1	272.966	2.465	0.174	14.201	9.02E-46	3.33E-44
FUT4	140.751	3.826	0.268	14.254	4.22E-46	1.58E-44
COL4A5	848.215	9.366	0.650	14.401	5.14E-47	1.96E-45
EPCAM	320.087	2.323	0.161	14.414	4.24E-47	1.62E-45
JPH4	152.155	4.933	0.341	14.478	1.66E-47	6.40E-46
PLXND1	223.078	2.460	0.170	14.483	1.54E-47	5.97E-46
FBXO6	270.590	2.362	0.163	14.503	1.16E-47	4.52E-46

STXBP6	90.432	5.622	0.387	14.515	9.77E-48	3.80E-46
CYBB	121.865	5.804	0.399	14.538	6.93E-48	2.71E-46
OASL	210.946	2.834	0.192	14.797	1.54E-49	6.25E-48
LINC01206	252.300	4.090	0.275	14.854	6.59E-50	2.70E-48
PYGL	358.039	2.144	0.143	14.977	1.04E-50	4.29E-49
PLD1	611.345	9.768	0.652	14.989	8.61E-51	3.58E-49
SERPINB10	118.861	4.472	0.298	15.011	6.22E-51	2.61E-49
OXTR	197.074	3.181	0.211	15.061	2.91E-51	1.23E-49
EPHA3	822.164	10.960	0.726	15.098	1.68E-51	7.11E-50
TTC28	315.712	2.178	0.144	15.173	5.33E-52	2.28E-50
GCNT1	333.445	2.352	0.155	15.186	4.39E-52	1.88E-50
RP11-566H8.3	101.502	5.713	0.376	15.198	3.67E-52	1.58E-50
MYO3B	179.239	3.980	0.262	15.216	2.78E-52	1.20E-50
IL1B	308.753	6.892	0.452	15.258	1.46E-52	6.36E-51
EFR3B	380.680	3.393	0.222	15.301	7.54E-53	3.30E-51
PLAGL1	171.750	3.717	0.242	15.344	3.91E-53	1.73E-51
CCDC187	677.132	2.376	0.154	15.414	1.31E-53	5.90E-52
B3GALNT1	184.785	3.991	0.258	15.444	8.34E-54	3.78E-52
MARK1	296.254	6.700	0.433	15.474	5.23E-54	2.38E-52
CMPK2	224.477	6.202	0.397	15.634	4.28E-55	2.01E-53
ITGAM	153.865	4.055	0.258	15.705	1.41E-55	6.68E-54
SDC3	147.705	3.983	0.253	15.747	7.16E-56	3.45E-54
NOL4L	289.564	2.583	0.163	15.799	3.15E-56	1.53E-54
MYO5B	303.300	2.760	0.175	15.800	3.12E-56	1.52E-54
BHLHE41	200.093	3.137	0.197	15.911	5.35E-57	2.64E-55
EGR3	184.568	2.899	0.182	15.920	4.64E-57	2.30E-55
FRAS1	375.397	3.934	0.246	16.001	1.25E-57	6.30E-56
HES4	294.316	6.073	0.379	16.007	1.14E-57	5.73E-56
CD38	123.016	5.881	0.367	16.014	1.02E-57	5.15E-56
TMEM178B	512.656	2.252	0.140	16.038	6.90E-58	3.51E-56
LINC00944	401.664	2.340	0.145	16.087	3.16E-58	1.62E-56
TUSC3	109.422	5.560	0.345	16.113	2.05E-58	1.06E-56
PRR18	245.626	2.812	0.174	16.136	1.43E-58	7.42E-57
TRIM55	232.724	7.345	0.455	16.146	1.21E-58	6.32E-57
PTK7	600.869	4.922	0.304	16.180	6.95E-59	3.66E-57
ILDR1	294.864	2.850	0.175	16.318	7.40E-60	3.96E-58
UBASH3B	176.717	3.634	0.222	16.396	2.05E-60	1.11E-58
MORC4	297.631	5.007	0.304	16.468	6.22E-61	3.39E-59
TBXAS1	174.338	3.187	0.193	16.520	2.62E-61	1.43E-59
KATNAL2	334.301	2.474	0.150	16.551	1.56E-61	8.62E-60
IL23R	153.262	3.878	0.234	16.593	7.81E-62	4.32E-60
MAB21L3	294.834	7.504	0.451	16.653	2.89E-62	1.62E-60
CAMP	242.781	2.737	0.164	16.674	2.04E-62	1.15E-60
TLN2	270.747	2.705	0.161	16.770	4.04E-63	2.29E-61
RP11-328J6.1	242.388	6.108	0.364	16.800	2.44E-63	1.39E-61
LINC00327	277.813	2.511	0.149	16.841	1.22E-63	6.94E-62
HS3ST3B1	627.082	8.245	0.489	16.868	7.77E-64	4.45E-62
NLRP11	176.420	3.077	0.182	16.931	2.65E-64	1.54E-62
PLCL1	312.682	2.581	0.152	16.956	1.73E-64	1.01E-62
RASGRP1	487.062	2.086	0.122	17.039	4.22E-65	2.48E-63
CNIH3	316.329	2.795	0.164	17.064	2.73E-65	1.61E-63
FRK	367.362	2.323	0.136	17.092	1.70E-65	1.01E-63
KLHDC7B	222.425	3.684	0.215	17.119	1.07E-65	6.33E-64
TUBB2A	265.307	2.831	0.165	17.180	3.78E-66	2.26E-64
NRG4	324.383	2.917	0.169	17.212	2.14E-66	1.29E-64
KREMEN2	619.653	2.040	0.118	17.273	7.55E-67	4.57E-65
ABCA12	140.618	4.299	0.247	17.408	7.16E-68	4.44E-66
LINC00882	236.981	3.759	0.216	17.417	6.16E-68	3.83E-66

KLHL4	293.607	6.862	0.391	17.563	4.73E-69	2.99E-67
KL	315.062	3.251	0.184	17.633	1.38E-69	8.82E-68
GABRA4	157.340	4.376	0.246	17.794	7.80E-71	5.10E-69
RP11-307E17.8	222.237	4.071	0.228	17.842	3.34E-71	2.21E-69
TIAM1	771.111	2.060	0.115	17.936	6.22E-72	4.17E-70
NTRK2	209.456	4.583	0.255	17.974	3.13E-72	2.11E-70
LDB2	312.010	5.001	0.278	18.017	1.44E-72	9.77E-71
FILIP1	393.427	2.220	0.123	18.065	6.06E-73	4.18E-71
RP11-549D23.1	171.994	3.732	0.206	18.084	4.30E-73	2.98E-71
PERP	577.460	2.411	0.133	18.093	3.64E-73	2.53E-71
RPS6KA6	261.267	3.159	0.175	18.100	3.21E-73	2.24E-71
SPRY1	305.485	3.650	0.201	18.134	1.71E-73	1.21E-71
EXPH5	636.907	2.119	0.117	18.138	1.59E-73	1.13E-71
GGT4P	297.607	3.340	0.184	18.152	1.23E-73	8.74E-72
CHST6	291.614	2.672	0.147	18.175	8.07E-74	5.75E-72
SORD2P	562.213	2.019	0.111	18.220	3.59E-74	2.58E-72
YAP1	163.251	3.961	0.217	18.240	2.49E-74	1.80E-72
IVL	210.072	5.103	0.279	18.276	1.29E-74	9.49E-73
CACNA1E	288.937	3.123	0.171	18.286	1.06E-74	7.89E-73
AHNAK	599.395	2.650	0.145	18.330	4.76E-75	3.58E-73
KMO	290.372	2.882	0.156	18.494	2.30E-76	1.75E-74
C3orf14	259.283	5.037	0.271	18.577	4.90E-77	3.79E-75
CPLANE1	743.700	2.130	0.114	18.628	1.92E-77	1.49E-75
MAP7	298.658	3.543	0.190	18.683	6.80E-78	5.35E-76
KCNK5	158.046	5.490	0.293	18.710	4.07E-78	3.24E-76
HERC6	352.963	2.666	0.142	18.764	1.49E-78	1.19E-76
MRPS30-DT	445.807	2.404	0.128	18.844	3.28E-79	2.62E-77
FCRL5	510.212	2.367	0.124	19.074	4.19E-81	3.43E-79
TNFAIP2	507.684	2.575	0.135	19.133	1.33E-81	1.10E-79
COL1A1	320.237	3.486	0.180	19.352	1.97E-83	1.68E-81
PTPRN2	471.896	3.019	0.156	19.367	1.48E-83	1.26E-81
DUXAP10	224.401	4.849	0.250	19.380	1.15E-83	9.84E-82
SORT1	550.842	3.644	0.188	19.402	7.41E-84	6.38E-82
SGMS1	640.556	2.017	0.103	19.575	2.50E-85	2.20E-83
TMSB4XP8	709.744	2.107	0.108	19.588	1.95E-85	1.72E-83
CHDH	802.458	9.134	0.464	19.665	4.28E-86	3.81E-84
SPINT1	319.134	4.310	0.219	19.669	4.00E-86	3.57E-84
LINC02381	360.719	2.984	0.151	19.697	2.31E-86	2.07E-84
CBLN2	382.852	2.707	0.137	19.703	2.03E-86	1.83E-84
TBC1D8	326.160	2.635	0.133	19.776	4.77E-87	4.36E-85
CCNI2	321.788	4.231	0.213	19.871	7.31E-88	6.79E-86
IFI6	952.214	2.208	0.109	20.241	4.23E-91	4.04E-89
CTD-2184D3.5	621.619	2.478	0.122	20.327	7.38E-92	7.11E-90
IL17RB	590.444	8.666	0.426	20.339	5.79E-92	5.59E-90
RAB3B	574.210	2.191	0.107	20.435	8.12E-93	7.95E-91
RP11-1D12.2	335.834	3.065	0.149	20.541	9.30E-94	9.18E-92
KCP	743.517	2.444	0.119	20.594	3.10E-94	3.08E-92
QPRT	803.045	2.016	0.097	20.683	4.92E-95	4.93E-93
RP11-147L13.11	426.783	5.496	0.265	20.734	1.70E-95	1.74E-93
MS4A6A	1128.562	2.195	0.105	20.866	1.08E-96	1.12E-94
CLYBL	369.759	2.687	0.129	20.904	4.95E-97	5.14E-95
IFIT1	520.525	6.831	0.325	21.024	3.99E-98	4.22E-96
CRTAM	427.820	4.779	0.227	21.037	3.03E-98	3.23E-96
NFKBIZ	503.208	2.453	0.116	21.163	2.11E-99	2.29E-97
ANK1	423.987	3.069	0.145	21.192	1.14E-99	1.25E-97
CTTN	288.300	3.505	0.165	21.202	9.12E-100	1.01E-97
CYBRD1	729.330	2.201	0.101	21.693	2.41E-104	2.77E-102
PARP12	357.933	3.932	0.180	21.815	1.66E-105	1.98E-103

TLR7	853.116	2.255	0.103	21.915	1.87E-106	2.29E-104
POU3F1	686.630	3.958	0.180	22.020	1.84E-107	2.26E-105
TFPI2	540.468	2.886	0.131	22.087	4.22E-108	5.24E-106
MEOX1	662.510	3.183	0.144	22.154	9.58E-109	1.20E-106
LINC02137	311.006	4.272	0.192	22.241	1.39E-109	1.78E-107
DNAH7	416.615	3.694	0.165	22.364	8.84E-111	1.16E-108
PLEKHG1	275.961	4.634	0.205	22.576	7.54E-113	1.01E-110
FYB1	1281.508	10.495	0.462	22.714	3.28E-114	4.55E-112
SLC6A4	545.232	2.804	0.123	22.847	1.56E-115	2.21E-113
LINC01055	366.048	4.635	0.203	22.881	7.16E-116	1.02E-113
KCND2	360.834	3.866	0.169	22.937	1.98E-116	2.83E-114
DUXAP8	353.437	5.590	0.241	23.191	5.63E-119	8.40E-117
VCAM1	1024.842	2.123	0.090	23.625	2.15E-123	3.29E-121
PHLDA1	759.527	2.900	0.120	24.213	1.62E-129	2.61E-127
TNFSF13B	388.257	3.625	0.150	24.223	1.26E-129	2.05E-127
EEF1A2	606.207	2.820	0.116	24.275	3.60E-130	5.89E-128
TNFRSF9	565.288	3.146	0.129	24.391	2.11E-131	3.58E-129
DSE	630.177	3.181	0.130	24.431	8.11E-132	1.40E-129
EMX1	474.639	3.797	0.155	24.436	7.15E-132	1.24E-129
BCL2L10	489.327	4.792	0.194	24.716	7.23E-135	1.28E-132
INA	536.746	3.327	0.134	24.846	2.82E-136	5.16E-134
CLIC2	324.593	4.801	0.193	24.890	9.66E-137	1.78E-134
POF1B	882.450	2.432	0.097	24.983	9.38E-138	1.76E-135
SATB2	595.194	3.813	0.152	25.086	7.08E-139	1.34E-136
TSPAN12	1702.134	2.042	0.081	25.234	1.68E-140	3.19E-138
ADGRE1	400.834	5.277	0.209	25.250	1.13E-140	2.17E-138
FRMPD2	601.544	4.141	0.163	25.411	1.90E-142	3.68E-140
ZFHX3	571.692	3.479	0.134	25.964	1.25E-148	2.51E-146
ZNRF1	599.274	3.215	0.123	26.033	2.11E-149	4.30E-147
RP11-459E5.1	807.921	3.062	0.117	26.148	1.05E-150	2.15E-148
PLPP3	539.669	5.751	0.219	26.246	7.91E-152	1.64E-149
OTOGL	1591.685	2.558	0.097	26.494	1.14E-154	2.42E-152
SMAD1	504.841	4.960	0.187	26.584	1.04E-155	2.22E-153
CD86	1532.851	2.117	0.079	26.804	2.90E-158	6.32E-156
PLA1A	482.786	3.704	0.138	26.807	2.70E-158	5.94E-156
RORA	1214.719	2.613	0.097	26.810	2.46E-158	5.48E-156
CHST12	500.548	4.515	0.168	26.867	5.39E-159	1.21E-156
ALDH1L1	577.977	6.583	0.244	26.947	6.21E-160	1.42E-157
CHL1	771.548	2.887	0.107	27.093	1.19E-161	2.76E-159
LEF1	1105.779	2.690	0.099	27.133	3.99E-162	9.33E-160
EPS8	639.255	2.914	0.107	27.156	2.15E-162	5.06E-160
SOX4	764.841	4.899	0.180	27.258	1.32E-163	3.19E-161
SSTR3	674.595	3.209	0.116	27.719	4.15E-169	1.04E-166
SSTR2	1331.555	2.424	0.087	27.799	4.42E-170	1.12E-167
DUSP10	1098.231	2.566	0.092	27.844	1.28E-170	3.29E-168
SCCPDH	2227.442	2.161	0.077	27.944	7.76E-172	2.01E-169
LINC00996	1001.110	2.721	0.097	28.053	3.71E-173	9.73E-171
ENPP2	460.889	4.515	0.161	28.068	2.44E-173	6.47E-171
DDAH1	686.690	3.395	0.120	28.369	4.95E-177	1.34E-174
ISG15	2300.374	2.421	0.085	28.389	2.73E-177	7.50E-175
CMBL	1094.134	3.148	0.109	28.820	1.19E-182	3.34E-180
OAS1	2674.305	2.068	0.072	28.844	6.00E-183	1.71E-180
SCART1	3923.976	2.283	0.079	28.865	3.33E-183	9.59E-181
PACSIN1	453.226	4.315	0.148	29.088	5.13E-186	1.51E-183
CAV1	935.764	2.647	0.090	29.330	4.24E-189	1.27E-186
CTNNA2	706.142	3.444	0.116	29.790	5.33E-195	1.65E-192
CPNE5	827.456	2.895	0.097	29.840	1.19E-195	3.75E-193
HDGFL3	2761.878	2.067	0.069	29.846	9.83E-196	3.13E-193

EPSTI1	1033.839	2.774	0.092	30.096	5.44E-199	1.76E-196
GRIN2A	2265.161	9.260	0.307	30.118	2.81E-199	9.22E-197
NOD2	874.798	3.335	0.110	30.247	5.69E-201	1.89E-198
RASSF6	1547.144	2.823	0.092	30.596	1.39E-205	4.76E-203
SMIM30	982.730	4.320	0.141	30.715	3.54E-207	1.25E-204
H1-0	1467.821	4.239	0.137	30.909	8.93E-210	3.24E-207
F8	2220.870	2.392	0.077	31.159	3.88E-213	1.43E-210
ZNF711	1023.444	3.242	0.104	31.230	4.16E-214	1.56E-211
AC079466.1	1491.076	9.193	0.294	31.318	2.67E-215	1.02E-212
PTPRF	1571.965	3.163	0.100	31.567	1.05E-218	4.20E-216
CELSR1	2257.823	2.390	0.076	31.585	5.93E-219	2.41E-216
AFAP1-AS1	467.052	5.037	0.158	31.865	8.21E-223	3.40E-220
NOTCH2	742.275	3.553	0.111	31.895	3.11E-223	1.31E-220
ROBO2	800.433	7.791	0.243	32.092	5.71E-226	2.45E-223
FSCN1	1073.978	3.832	0.118	32.386	4.35E-230	1.94E-227
FAM174B	2310.733	2.269	0.069	32.798	6.36E-236	2.94E-233
USP18	867.873	4.429	0.133	33.369	3.84E-244	1.85E-241
PRXL2A	1453.373	3.040	0.087	34.855	3.58E-266	1.84E-263
DGKI	1239.603	3.556	0.101	35.086	1.11E-269	5.95E-267
RNF157	1639.343	3.157	0.089	35.345	1.21E-273	6.66E-271
PDGFA	1752.656	3.988	0.113	35.351	9.81E-274	5.51E-271
JAG1	1131.123	4.481	0.126	35.671	1.12E-278	6.44E-276
SLFN5	1573.559	3.411	0.095	35.764	4.07E-280	2.40E-277
TRIP6	1222.468	4.155	0.114	36.365	1.50E-289	9.54E-287
SAMD9L	3374.771	2.758	0.074	37.079	6.14E-301	4.14E-298
DDR2	864.541	4.118	0.110	37.326	6.14E-305	4.26E-302
KLRC1	957.625	4.400	0.118	37.352	2.36E-305	1.69E-302
IFI44L	8769.789	7.487	0.103	72.432	0.00E+00	0.00E+00
IFI44	2870.835	4.211	0.080	52.931	0.00E+00	0.00E+00
SDC1	3100.285	3.171	0.071	44.565	0.00E+00	0.00E+00
HNRNPLL	1374.947	4.657	0.103	45.203	0.00E+00	0.00E+00
STAT1	16457.261	2.872	0.048	60.166	0.00E+00	0.00E+00
CD28	926.441	5.935	0.139	42.777	0.00E+00	0.00E+00
SGPP2	2064.684	2.677	0.070	38.477	0.00E+00	0.00E+00
ITPR1	5020.023	2.552	0.060	42.216	0.00E+00	0.00E+00
EPHB1	1633.799	3.942	0.094	42.084	0.00E+00	0.00E+00
SHROOM3	1657.580	5.502	0.124	44.387	0.00E+00	0.00E+00
DDX60	1627.524	3.432	0.090	37.994	0.00E+00	0.00E+00
NRN1	3247.877	7.470	0.186	40.099	0.00E+00	0.00E+00
MACC1	1462.302	3.399	0.088	38.507	0.00E+00	0.00E+00
FGFR1	2343.573	3.748	0.082	45.663	0.00E+00	0.00E+00
TRIM22	3367.723	2.594	0.062	41.810	0.00E+00	0.00E+00
GSTP1	3058.884	3.453	0.069	50.333	0.00E+00	0.00E+00
GRAMD1B	1472.901	3.263	0.086	38.088	0.00E+00	0.00E+00
ERC1	2598.271	3.162	0.082	38.603	0.00E+00	0.00E+00
CCND2	1523.784	4.126	0.093	44.576	0.00E+00	0.00E+00
OAS3	2256.942	3.760	0.088	42.800	0.00E+00	0.00E+00
OAS2	6091.008	2.526	0.063	40.174	0.00E+00	0.00E+00
DOCK9	1218.908	5.447	0.113	48.351	0.00E+00	0.00E+00
DMXL2	2092.806	3.216	0.076	42.037	0.00E+00	0.00E+00
BCAR1	1645.938	3.489	0.087	40.223	0.00E+00	0.00E+00
XAF1	1351.105	4.445	0.113	39.386	0.00E+00	0.00E+00
IL4I1	1887.762	2.784	0.072	38.546	0.00E+00	0.00E+00
MX1	12039.907	5.045	0.066	76.874	0.00E+00	0.00E+00
LINC02656	2.541	-3.727	1.846	-2.019	4.35E-02	9.98E-02
ZNF415	2.647	-3.784	1.867	-2.027	4.26E-02	9.81E-02
ENSG10010139425.1	1.647	-4.195	2.064	-2.032	4.21E-02	9.71E-02
VWA5B1	3.157	-3.645	1.787	-2.040	4.14E-02	9.56E-02

SLC17A7	3.798	-3.597	1.756	-2.048	4.06E-02	9.39E-02
KIFC1	3.418	-3.578	1.746	-2.049	4.05E-02	9.38E-02
C16orf96	4.578	-2.765	1.347	-2.053	4.01E-02	9.30E-02
RP11-22E12.2	4.468	-2.797	1.360	-2.057	3.97E-02	9.23E-02
MYOM2	2.697	-3.836	1.864	-2.058	3.96E-02	9.21E-02
RP4-647C14.2	5.120	-2.182	1.058	-2.062	3.92E-02	9.13E-02
HMHB1	2.617	-3.831	1.857	-2.063	3.91E-02	9.11E-02
RP11-480I12.10	1.438	-4.489	2.175	-2.064	3.90E-02	9.09E-02
ARHGAP42-AS1	1.500	-4.541	2.184	-2.079	3.76E-02	8.82E-02
LRRC37A2	5.735	-2.723	1.307	-2.084	3.72E-02	8.73E-02
MIR4518	1.634	-4.324	2.074	-2.085	3.70E-02	8.70E-02
LXN	1.961	-4.241	2.009	-2.111	3.48E-02	8.24E-02
RP11-584P21.4	3.554	-3.734	1.765	-2.115	3.44E-02	8.17E-02
CLCN3P1	4.314	-2.893	1.366	-2.117	3.42E-02	8.13E-02
SEC1P	4.294	-3.581	1.688	-2.121	3.39E-02	8.07E-02
LRAT	2.593	-3.982	1.873	-2.126	3.35E-02	7.99E-02
L29074.3	1.566	-4.365	2.049	-2.130	3.32E-02	7.92E-02
LINC02586	3.624	-3.703	1.731	-2.139	3.24E-02	7.75E-02
RP11-713N11.4	5.898	-2.788	1.298	-2.148	3.17E-02	7.61E-02
RP11-669I1.2	4.103	-2.966	1.380	-2.150	3.16E-02	7.57E-02
LINC00304	1.903	-4.199	1.948	-2.155	3.12E-02	7.49E-02
RP11-90E9.1	5.437	-2.321	1.075	-2.159	3.08E-02	7.42E-02
RP1-159A19.4	3.738	-3.695	1.710	-2.160	3.08E-02	7.40E-02
RP3-347M6.3	1.649	-4.692	2.158	-2.174	2.97E-02	7.18E-02
RP11-395M19.1	3.890	-3.873	1.774	-2.183	2.90E-02	7.04E-02
RNY1P12	4.320	-2.909	1.326	-2.194	2.82E-02	6.88E-02
RP11-58O9.2	2.759	-4.027	1.832	-2.198	2.80E-02	6.83E-02
LINC02495	3.621	-3.056	1.386	-2.206	2.74E-02	6.70E-02
AC005789.9	5.835	-2.184	0.990	-2.206	2.74E-02	6.70E-02
RP11-227D13.2	6.389	-2.248	1.018	-2.208	2.72E-02	6.66E-02
TMEM52B	3.809	-3.029	1.370	-2.211	2.70E-02	6.62E-02
AC145124.2	3.289	-3.871	1.748	-2.214	2.68E-02	6.57E-02
BMPR1AP1	8.875	-2.072	0.925	-2.240	2.51E-02	6.20E-02
RP11-440G5.2	5.856	-2.439	1.085	-2.249	2.45E-02	6.08E-02
RP11-19J3.7	4.159	-3.812	1.691	-2.255	2.42E-02	6.00E-02
PYGO1	3.664	-3.132	1.388	-2.257	2.40E-02	5.97E-02
ITGB1-DT	4.906	-2.548	1.123	-2.269	2.33E-02	5.80E-02
RP11-693J15.6	3.361	-3.983	1.749	-2.277	2.28E-02	5.69E-02
SLC28A1	3.876	-3.121	1.369	-2.281	2.26E-02	5.64E-02
HMGB1P17	4.577	-3.844	1.671	-2.300	2.14E-02	5.39E-02
RP11-706F1.1	5.312	-2.392	1.039	-2.302	2.13E-02	5.37E-02
RP11-414H17.5	1.857	-4.528	1.957	-2.313	2.07E-02	5.23E-02
RP11-586D19.4	1.872	-4.539	1.956	-2.320	2.03E-02	5.15E-02
GRM3-AS1	3.097	-4.258	1.832	-2.325	2.01E-02	5.09E-02
RP11-463O9.9	5.330	-2.652	1.141	-2.325	2.01E-02	5.09E-02
NKAIN3	4.188	-3.150	1.354	-2.326	2.00E-02	5.07E-02
TOM1L1	2.037	-4.487	1.928	-2.328	1.99E-02	5.06E-02
RPS8P4	3.775	-3.350	1.437	-2.331	1.98E-02	5.02E-02
RP13-511M20.1	7.294	-3.982	1.707	-2.332	1.97E-02	5.00E-02
CALHM2	6.621	-2.250	0.963	-2.336	1.95E-02	4.95E-02
RP4-684F13.1	4.782	-3.956	1.685	-2.347	1.89E-02	4.82E-02
LINC02365	3.714	-4.087	1.723	-2.371	1.77E-02	4.56E-02
GRM7-AS3	7.134	-2.143	0.904	-2.372	1.77E-02	4.56E-02
RIPPLY3	5.670	-4.028	1.692	-2.381	1.73E-02	4.46E-02
KDM7A-DT	7.473	-2.089	0.877	-2.382	1.72E-02	4.46E-02
TSKS	3.532	-4.190	1.758	-2.383	1.72E-02	4.44E-02
RP11-622O11.6	4.804	-2.793	1.164	-2.399	1.64E-02	4.28E-02
CBR3-AS1	6.622	-3.891	1.611	-2.415	1.57E-02	4.11E-02

RP11-255M6.2	4.814	-2.831	1.169	-2.423	1.54E-02	4.04E-02
ATP2C2-AS1	7.694	-2.161	0.891	-2.426	1.53E-02	4.01E-02
TMEM71	6.430	-2.219	0.913	-2.429	1.51E-02	3.98E-02
CCER2	7.541	-2.211	0.908	-2.434	1.49E-02	3.94E-02
MEIS1	5.946	-2.381	0.976	-2.440	1.47E-02	3.87E-02
CTD-2509G16.3	3.839	-4.161	1.703	-2.444	1.45E-02	3.84E-02
CMB9-60A24.1	4.862	-4.061	1.658	-2.450	1.43E-02	3.78E-02
RP11-44N12.5	2.400	-4.607	1.874	-2.458	1.40E-02	3.70E-02
RP11-567P19.1	6.297	-2.562	1.034	-2.478	1.32E-02	3.52E-02
TNNC2	4.928	-3.215	1.295	-2.482	1.31E-02	3.49E-02
MAP1LC3A	2.052	-4.817	1.935	-2.490	1.28E-02	3.42E-02
RPSAP14	2.399	-4.699	1.882	-2.496	1.25E-02	3.37E-02
TYROBP	5.160	-2.920	1.168	-2.500	1.24E-02	3.34E-02
KCNJ16	2.034	-4.996	1.993	-2.507	1.22E-02	3.28E-02
DOK5	4.158	-3.438	1.370	-2.509	1.21E-02	3.26E-02
NUGGC	8.160	-2.448	0.970	-2.525	1.16E-02	3.14E-02
KIAA1217	6.121	-2.576	1.013	-2.542	1.10E-02	3.01E-02
AC156455.1	8.849	-2.173	0.848	-2.561	1.04E-02	2.86E-02
RP11-360N9.2	2.345	-4.969	1.935	-2.568	1.02E-02	2.81E-02
LINC02324	4.723	-4.288	1.664	-2.577	9.96E-03	2.74E-02
KRT18	4.682	-4.451	1.706	-2.609	9.07E-03	2.53E-02
SLC10A4	12.985	-2.104	0.805	-2.613	8.98E-03	2.51E-02
CA3-AS1	4.699	-4.375	1.671	-2.619	8.82E-03	2.47E-02
RP11-1396O13.23	2.482	-4.862	1.848	-2.631	8.51E-03	2.39E-02
RP11-875O11.5	5.824	-2.881	1.093	-2.637	8.36E-03	2.35E-02
BCAR3-AS1	6.490	-4.299	1.608	-2.673	7.51E-03	2.13E-02
CCDC154	9.524	-2.261	0.844	-2.678	7.41E-03	2.11E-02
PCSK6	6.424	-3.147	1.162	-2.708	6.77E-03	1.95E-02
PRKCZ-AS1	4.655	-4.494	1.659	-2.709	6.74E-03	1.94E-02
RP11-107N15.1	10.502	-2.219	0.794	-2.796	5.18E-03	1.53E-02
HNRNPA1P27	4.957	-4.718	1.664	-2.835	4.58E-03	1.37E-02
CXCL11	2.681	-5.317	1.874	-2.837	4.56E-03	1.36E-02
RP11-666O2.5	5.791	-3.608	1.271	-2.839	4.53E-03	1.36E-02
RP11-785D18.3	5.102	-4.685	1.648	-2.843	4.47E-03	1.34E-02
LRRC34	11.772	-2.086	0.731	-2.856	4.30E-03	1.29E-02
WWTR1-AS1	8.452	-2.481	0.864	-2.872	4.08E-03	1.23E-02
RP11-266N13.2	2.730	-5.274	1.822	-2.895	3.79E-03	1.15E-02
SYCP2L	2.976	-5.205	1.776	-2.931	3.38E-03	1.04E-02
RP11-141M1.3	9.118	-2.433	0.830	-2.931	3.37E-03	1.04E-02
ATP8A2	5.824	-3.766	1.283	-2.935	3.33E-03	1.03E-02
CTD-2313F11.1	5.587	-3.772	1.283	-2.941	3.28E-03	1.01E-02
ZNF625	9.510	-2.369	0.805	-2.941	3.27E-03	1.01E-02
RIC3	2.826	-5.457	1.852	-2.946	3.21E-03	9.95E-03
C19orf18	7.133	-3.691	1.251	-2.949	3.18E-03	9.86E-03
IGHV1OR15-1	6.457	-5.155	1.744	-2.956	3.12E-03	9.69E-03
HUS1B	11.807	-2.130	0.717	-2.972	2.96E-03	9.24E-03
HAAO	5.711	-4.864	1.634	-2.976	2.92E-03	9.13E-03
CCR5AS	12.415	-2.023	0.669	-3.022	2.51E-03	7.96E-03
PRSS16	3.153	-5.629	1.833	-3.072	2.13E-03	6.84E-03
CKLF-CMTM1	10.504	-2.471	0.804	-3.074	2.11E-03	6.79E-03
CADM4	9.564	-3.638	1.182	-3.078	2.09E-03	6.72E-03
RP11-706P11.2	11.330	-2.185	0.706	-3.095	1.97E-03	6.37E-03
CTD-2540F13.2	8.624	-4.874	1.574	-3.097	1.96E-03	6.33E-03
CTC-559E9.5	3.119	-5.548	1.790	-3.100	1.94E-03	6.28E-03
FAM86B2	13.168	-2.159	0.695	-3.105	1.90E-03	6.18E-03
AC133785.1	9.052	-2.528	0.801	-3.157	1.59E-03	5.26E-03
S100A11	8.000	-3.098	0.975	-3.177	1.49E-03	4.94E-03
RP11-508N22.12	7.170	-3.904	1.226	-3.185	1.45E-03	4.82E-03

IGLV3-1	6.942	-3.192	1.001	-3.188	1.43E-03	4.77E-03
VPS37D	10.394	-3.234	1.008	-3.209	1.33E-03	4.46E-03
PMEPA1	6.472	-3.982	1.237	-3.219	1.28E-03	4.32E-03
B3GNT4	11.685	-2.787	0.860	-3.243	1.18E-03	4.01E-03
RP11-566K19.6	7.415	-3.932	1.212	-3.245	1.17E-03	3.98E-03
TXNRD3	4.186	-5.518	1.697	-3.252	1.15E-03	3.89E-03
OCSTAMP	18.955	-2.272	0.698	-3.256	1.13E-03	3.84E-03
CHIT1	14.244	-2.174	0.665	-3.272	1.07E-03	3.65E-03
LINC01770	14.807	-2.586	0.779	-3.318	9.08E-04	3.13E-03
RP11-575N24.1	6.875	-4.133	1.239	-3.336	8.51E-04	2.96E-03
RP11-89F3.2	3.756	-5.877	1.754	-3.351	8.04E-04	2.81E-03
TNNT3	7.973	-5.298	1.581	-3.352	8.03E-04	2.81E-03
NDRG1	8.044	-5.326	1.586	-3.357	7.88E-04	2.76E-03
RP11-700A24.1	7.228	-3.585	1.066	-3.362	7.74E-04	2.71E-03
MYBPC2	16.689	-2.022	0.601	-3.365	7.67E-04	2.69E-03
JAKMIP1	10.584	-2.611	0.775	-3.370	7.53E-04	2.64E-03
RASGEF1B	13.904	-2.624	0.771	-3.402	6.70E-04	2.38E-03
ENSG10010138795.1	3.960	-5.948	1.745	-3.409	6.53E-04	2.32E-03
MMP25	16.003	-2.025	0.590	-3.433	5.97E-04	2.14E-03
LINC02090	16.197	-2.050	0.594	-3.450	5.61E-04	2.02E-03
MRC2	23.309	-3.307	0.943	-3.509	4.50E-04	1.65E-03
LINC02649	10.163	-2.907	0.828	-3.513	4.43E-04	1.62E-03
CTC-756D1.4	9.038	-3.599	1.024	-3.514	4.41E-04	1.62E-03
ZNF582-DT	9.428	-3.369	0.952	-3.540	4.00E-04	1.48E-03
RP11-46H11.12	4.327	-6.077	1.709	-3.555	3.78E-04	1.40E-03
RP11-46H11.11	4.409	-6.066	1.696	-3.577	3.48E-04	1.30E-03
RP4-768P8.2	5.816	-5.820	1.624	-3.584	3.39E-04	1.26E-03
FRMPD4	13.974	-2.275	0.634	-3.587	3.35E-04	1.25E-03
PPARGC1A	7.664	-4.373	1.216	-3.597	3.22E-04	1.21E-03
LINC00484	12.065	-2.784	0.773	-3.602	3.15E-04	1.18E-03
FZD4	19.422	-2.159	0.596	-3.619	2.95E-04	1.11E-03
RNU6-1069P	4.782	-6.070	1.661	-3.653	2.59E-04	9.84E-04
ASAP3	18.573	-2.220	0.602	-3.685	2.29E-04	8.76E-04
KCNG2	11.330	-4.469	1.177	-3.798	1.46E-04	5.78E-04
RYR2	11.163	-2.999	0.779	-3.849	1.19E-04	4.78E-04
JAG2	16.024	-2.468	0.639	-3.862	1.13E-04	4.55E-04
CTD-3037G24.3	10.628	-3.276	0.845	-3.875	1.06E-04	4.32E-04
LINC01422	14.042	-2.576	0.655	-3.934	8.36E-05	3.45E-04
RBFADN	20.044	-2.226	0.560	-3.975	7.05E-05	2.95E-04
MTSS1	22.031	-2.090	0.526	-3.976	7.02E-05	2.93E-04
ADCY1	6.013	-6.548	1.641	-3.990	6.61E-05	2.77E-04
PAPSS2	12.400	-6.142	1.536	-3.998	6.40E-05	2.69E-04
AVIL	24.153	-2.012	0.496	-4.057	4.97E-05	2.12E-04
GALNT18	9.930	-4.780	1.174	-4.073	4.64E-05	1.99E-04
MIR210HG	182.965	-5.111	1.254	-4.074	4.62E-05	1.98E-04
RP11-63C8.1	6.913	-6.622	1.608	-4.117	3.84E-05	1.67E-04
MUC1	11.511	-4.131	0.999	-4.137	3.52E-05	1.53E-04
RP11-20G13.1	13.721	-3.132	0.742	-4.222	2.42E-05	1.08E-04
PRKCQ-AS1	15.410	-6.410	1.517	-4.227	2.37E-05	1.06E-04
CXCL8	11.150	-3.884	0.917	-4.235	2.29E-05	1.03E-04
RTN4R	11.308	-3.826	0.902	-4.239	2.24E-05	1.01E-04
ZNF100	13.698	-3.212	0.754	-4.262	2.03E-05	9.15E-05
RIBC2	7.442	-6.842	1.601	-4.274	1.92E-05	8.72E-05
PRDM5	11.268	-4.971	1.163	-4.275	1.91E-05	8.65E-05
PLIN1	24.857	-2.274	0.528	-4.307	1.66E-05	7.60E-05
CST7	19.609	-2.443	0.566	-4.315	1.60E-05	7.34E-05
ACRBP	18.065	-2.686	0.619	-4.340	1.42E-05	6.58E-05
RP11-395I6.4	28.032	-2.035	0.468	-4.348	1.37E-05	6.38E-05

RP11-195F19.9	22.207	-2.509	0.574	-4.373	1.23E-05	5.74E-05
ARHGEF35	12.040	-3.947	0.902	-4.377	1.20E-05	5.64E-05
NUAK2	12.223	-3.948	0.892	-4.424	9.68E-06	4.59E-05
ZFP2	14.122	-3.221	0.727	-4.431	9.40E-06	4.46E-05
LPP-AS2	13.485	-3.480	0.781	-4.454	8.44E-06	4.03E-05
ZNF660	18.611	-6.736	1.507	-4.470	7.82E-06	3.75E-05
FAM86B1	25.533	-2.134	0.477	-4.475	7.63E-06	3.67E-05
LINC02367	15.999	-3.172	0.707	-4.485	7.28E-06	3.51E-05
GRM3	24.186	-2.719	0.603	-4.511	6.44E-06	3.13E-05
RNF112	14.991	-3.522	0.777	-4.533	5.82E-06	2.84E-05
MAPK8IP1	21.020	-2.505	0.548	-4.569	4.89E-06	2.41E-05
CTC-471J1.2	9.331	-7.170	1.567	-4.576	4.73E-06	2.34E-05
FAM66B	13.562	-5.222	1.141	-4.577	4.72E-06	2.34E-05
ZNF702P	21.229	-6.923	1.495	-4.630	3.66E-06	1.84E-05
RP11-316M20.3	22.144	-3.845	0.829	-4.639	3.50E-06	1.77E-05
CAMKK1	26.059	-2.294	0.491	-4.676	2.92E-06	1.49E-05
LINC00565	13.513	-4.546	0.969	-4.692	2.71E-06	1.38E-05
MLC1	15.501	-3.583	0.760	-4.714	2.42E-06	1.25E-05
RCN3	27.848	-2.315	0.488	-4.745	2.09E-06	1.08E-05
WASH5P	48.002	-2.137	0.450	-4.746	2.07E-06	1.08E-05
STK39	17.328	-3.062	0.636	-4.814	1.48E-06	7.80E-06
RTL3	37.052	-2.002	0.415	-4.825	1.40E-06	7.42E-06
AC020951.1	21.778	-2.862	0.592	-4.838	1.31E-06	6.99E-06
SARDH	25.294	-2.659	0.549	-4.844	1.27E-06	6.81E-06
LINC00629	23.424	-2.539	0.524	-4.848	1.25E-06	6.67E-06
ASIC3	31.175	-2.083	0.426	-4.885	1.03E-06	5.59E-06
CARD9	32.637	-2.012	0.411	-4.894	9.87E-07	5.35E-06
RP11-761I4.6	19.414	-2.907	0.591	-4.916	8.83E-07	4.81E-06
ZNF239	12.271	-7.585	1.543	-4.917	8.78E-07	4.79E-06
RP11-326C3.2	28.269	-7.329	1.484	-4.939	7.84E-07	4.30E-06
ADGRG6	37.634	-2.004	0.405	-4.945	7.60E-07	4.18E-06
XCL2	23.881	-3.038	0.611	-4.970	6.68E-07	3.70E-06
C1orf21-DT	21.353	-5.565	1.102	-5.052	4.38E-07	2.47E-06
ACOXL	18.423	-3.665	0.724	-5.059	4.21E-07	2.38E-06
RAB17	18.646	-3.391	0.669	-5.067	4.05E-07	2.30E-06
IGHM	15.598	-4.872	0.959	-5.081	3.75E-07	2.13E-06
CTD-2528L19.6	17.897	-3.692	0.723	-5.109	3.24E-07	1.86E-06
FGFR4	20.715	-3.736	0.728	-5.130	2.90E-07	1.68E-06
CTD-2509G16.5	19.648	-3.795	0.737	-5.147	2.64E-07	1.54E-06
LOXL2	23.159	-2.955	0.574	-5.148	2.63E-07	1.53E-06
DMBT1	19.336	-3.209	0.623	-5.154	2.55E-07	1.49E-06
TLR8-AS1	35.481	-7.650	1.475	-5.187	2.13E-07	1.25E-06
JAZF1	36.133	-2.104	0.406	-5.188	2.13E-07	1.25E-06
SH2D4A	15.986	-7.903	1.517	-5.210	1.89E-07	1.12E-06
CTD-2619J13.17	32.135	-2.451	0.466	-5.258	1.46E-07	8.73E-07
ST3GAL1-DT	21.295	-3.200	0.605	-5.286	1.25E-07	7.53E-07
ZNF528	20.710	-4.899	0.924	-5.302	1.15E-07	6.95E-07
CXCL9	21.220	-5.828	1.097	-5.312	1.08E-07	6.58E-07
RP11-46H11.3	16.997	-8.054	1.514	-5.318	1.05E-07	6.39E-07
ARSD	19.337	-8.239	1.504	-5.478	4.29E-08	2.72E-07
RP4-740C4.5	24.051	-3.220	0.585	-5.507	3.65E-08	2.33E-07
RIN2	33.654	-3.080	0.558	-5.523	3.33E-08	2.13E-07
GS1-53I10.2	28.249	-2.649	0.479	-5.530	3.21E-08	2.06E-07
NR2F2-AS1	40.082	-2.280	0.412	-5.537	3.08E-08	1.98E-07
NLRP6	27.360	-2.704	0.488	-5.545	2.94E-08	1.90E-07
MLF1	21.125	-8.348	1.498	-5.572	2.52E-08	1.64E-07
VILL	19.808	-4.007	0.718	-5.579	2.42E-08	1.58E-07
ADGRB1	22.644	-3.362	0.600	-5.608	2.05E-08	1.35E-07

ZNF595	373.163	-2.118	0.377	-5.625	1.86E-08	1.23E-07
MTARC1	28.118	-2.773	0.492	-5.634	1.76E-08	1.16E-07
ZNF287	22.592	-8.463	1.499	-5.647	1.63E-08	1.08E-07
LMCD1	55.383	-8.256	1.462	-5.649	1.62E-08	1.08E-07
HSBP1L1	27.396	-2.816	0.496	-5.672	1.41E-08	9.45E-08
LRRC3	21.683	-4.046	0.712	-5.681	1.34E-08	8.99E-08
XK	23.385	-8.506	1.494	-5.694	1.24E-08	8.37E-08
ZNF879	34.385	-2.614	0.454	-5.756	8.61E-09	5.89E-08
TPH1	32.256	-2.578	0.444	-5.806	6.39E-09	4.43E-08
LINC02870	33.764	-2.656	0.446	-5.952	2.66E-09	1.91E-08
GRASLND	30.975	-8.911	1.482	-6.013	1.83E-09	1.34E-08
ZNF573	45.481	-2.198	0.364	-6.043	1.51E-09	1.12E-08
RGS12	48.106	-2.233	0.369	-6.045	1.49E-09	1.10E-08
RP11-216B13.1	28.774	-3.224	0.526	-6.126	9.03E-10	6.84E-09
RP11-452E5.1	39.696	-2.335	0.379	-6.164	7.11E-10	5.43E-09
ARHGEF35-AS1	45.497	-2.242	0.363	-6.172	6.73E-10	5.15E-09
CDS1	36.407	-3.897	0.630	-6.187	6.11E-10	4.70E-09
WI2-87327B8.2	40.924	-2.463	0.394	-6.250	4.09E-10	3.20E-09
IGDCC4	32.571	-3.124	0.492	-6.345	2.22E-10	1.78E-09
ID1	42.689	-3.167	0.498	-6.353	2.11E-10	1.69E-09
ZNF284	33.760	-2.773	0.432	-6.415	1.40E-10	1.14E-09
ZNF69	54.239	-2.375	0.368	-6.460	1.05E-10	8.65E-10
C1orf115	47.249	-9.525	1.471	-6.477	9.37E-11	7.75E-10
ZKSCAN7	47.254	-9.530	1.470	-6.484	8.95E-11	7.42E-10
SPRED3	53.434	-2.144	0.330	-6.503	7.88E-11	6.56E-10
NRG3	44.388	-3.670	0.561	-6.545	5.95E-11	5.00E-10
GNAS-AS1	34.384	-3.171	0.479	-6.615	3.71E-11	3.17E-10
ZNF844	141.681	-9.662	1.449	-6.667	2.61E-11	2.26E-10
ZNF568	56.736	-9.786	1.467	-6.672	2.53E-11	2.19E-10
MICU3	56.062	-9.774	1.464	-6.674	2.49E-11	2.16E-10
PRSS12	64.505	-2.264	0.339	-6.680	2.38E-11	2.07E-10
GRIP1	58.081	-2.598	0.388	-6.701	2.07E-11	1.82E-10
BEX4	75.089	-10.159	1.459	-6.964	3.31E-12	3.09E-11
WWC2	40.329	-6.247	0.883	-7.071	1.53E-12	1.47E-11
MORC2-AS1	39.055	-4.510	0.631	-7.144	9.05E-13	8.81E-12
CYRIA	33.650	-5.233	0.722	-7.246	4.29E-13	4.28E-12
EEPD1	95.475	-2.006	0.274	-7.307	2.73E-13	2.77E-12
GIMAP5	53.060	-2.932	0.400	-7.337	2.19E-13	2.23E-12
ZNF585A	54.958	-2.535	0.345	-7.351	1.96E-13	2.01E-12
MICAL2	37.615	-3.471	0.471	-7.375	1.64E-13	1.69E-12
TNFRSF1A	50.481	-2.611	0.350	-7.466	8.28E-14	8.70E-13
PDE7B	42.206	-4.186	0.556	-7.527	5.18E-14	5.51E-13
FNBP1L	44.747	-4.354	0.575	-7.569	3.76E-14	4.04E-13
ITGB1P1	52.324	-2.756	0.364	-7.570	3.72E-14	4.00E-13
SSR4P1	49.896	-2.897	0.380	-7.620	2.53E-14	2.76E-13
HTR3A	44.633	-3.842	0.504	-7.631	2.33E-14	2.55E-13
GBP3	78.820	-2.306	0.301	-7.664	1.81E-14	1.99E-13
FUT8-AS1	87.692	-2.035	0.266	-7.666	1.77E-14	1.95E-13
MBOAT2	162.062	-11.304	1.451	-7.792	6.61E-15	7.45E-14
ZNF506	98.307	-8.111	1.039	-7.803	6.04E-15	6.83E-14
KIFC3	54.465	-2.919	0.367	-7.961	1.71E-15	2.00E-14
TMPRSS3	40.417	-4.064	0.505	-8.054	8.04E-16	9.56E-15
MAP9	209.498	-11.674	1.449	-8.055	7.96E-16	9.47E-15
ZNF665	74.494	-6.138	0.759	-8.089	6.04E-16	7.24E-15
LRFN1	74.182	-2.613	0.317	-8.235	1.79E-16	2.21E-15
CSTF3-DT	93.188	-2.095	0.254	-8.264	1.41E-16	1.75E-15
ZNF347	139.229	-8.569	1.035	-8.283	1.20E-16	1.49E-15
PTPRJ	60.864	-3.162	0.376	-8.401	4.43E-17	5.65E-16

CAPN12	52.914	-4.066	0.478	-8.514	1.68E-17	2.20E-16
KLF2	105.512	-2.119	0.249	-8.525	1.53E-17	2.01E-16
XKRX	45.393	-4.211	0.484	-8.693	3.53E-18	4.80E-17
RP11-16N11.2	75.263	-2.510	0.286	-8.779	1.65E-18	2.28E-17
MYO7B	108.169	-2.176	0.242	-8.987	2.53E-19	3.66E-18
RP11-203J24.9	88.516	-2.399	0.265	-9.056	1.35E-19	1.97E-18
ZNF829	118.120	-7.814	0.854	-9.155	5.45E-20	8.15E-19
AK1	63.430	-3.360	0.361	-9.311	1.27E-20	1.94E-19
MIR4435-2HG	69.274	-2.951	0.312	-9.448	3.44E-21	5.44E-20
TENT5C	118.071	-2.223	0.235	-9.476	2.65E-21	4.20E-20
MAST1	97.989	-2.656	0.279	-9.502	2.06E-21	3.28E-20
LTF	114.055	-3.154	0.331	-9.531	1.56E-21	2.50E-20
LNCOC1	122.076	-2.116	0.219	-9.655	4.68E-22	7.64E-21
LINC00173	70.183	-3.818	0.387	-9.868	5.72E-23	9.80E-22
TLR5	67.100	-3.326	0.331	-10.057	8.55E-24	1.51E-22
RP11-25K19.1	148.404	-2.462	0.242	-10.156	3.11E-24	5.55E-23
TLCD5	132.549	-7.565	0.742	-10.202	1.95E-24	3.51E-23
ZNF880	178.465	-2.055	0.200	-10.292	7.63E-25	1.40E-23
PLEKHH2	120.228	-2.555	0.248	-10.319	5.76E-25	1.06E-23
RHOBTB1	96.575	-3.162	0.306	-10.344	4.45E-25	8.25E-24
FRY	152.703	-2.277	0.218	-10.435	1.71E-25	3.22E-24
VWA5A	122.966	-2.353	0.225	-10.447	1.51E-25	2.85E-24
SYTL1	77.063	-5.570	0.529	-10.523	6.76E-26	1.30E-24
BCAN-AS1	101.986	-2.723	0.256	-10.624	2.31E-26	4.49E-25
PLCD1	142.651	-2.501	0.235	-10.628	2.21E-26	4.31E-25
ZNF433	86.620	-3.123	0.293	-10.654	1.67E-26	3.26E-25
SLC2A13	131.263	-2.336	0.217	-10.742	6.47E-27	1.29E-25
ZNF818P	87.265	-4.705	0.438	-10.752	5.77E-27	1.16E-25
ISYNA1	271.592	-2.282	0.209	-10.909	1.04E-27	2.15E-26
TSPAN9	169.589	-2.028	0.185	-10.964	5.67E-28	1.18E-26
ZNF888	87.385	-3.698	0.336	-11.014	3.26E-28	6.85E-27
ZNF585B	77.344	-3.846	0.349	-11.030	2.74E-28	5.78E-27
RAB31	106.640	-2.893	0.258	-11.213	3.52E-29	7.70E-28
GNLY	133.276	-2.577	0.227	-11.371	5.84E-30	1.31E-28
TANC2	135.429	-2.442	0.213	-11.469	1.90E-30	4.34E-29
ZDHHC11	95.265	-3.557	0.310	-11.490	1.49E-30	3.43E-29
TNFAIP8L2	84.846	-3.950	0.342	-11.539	8.35E-31	1.95E-29
ZNF841	180.627	-7.691	0.664	-11.591	4.58E-31	1.08E-29
C13orf46	123.915	-2.993	0.257	-11.661	2.01E-31	4.81E-30
PWWP2B	189.471	-2.330	0.199	-11.714	1.09E-31	2.61E-30
TESMIN	219.422	-2.110	0.180	-11.723	9.73E-32	2.34E-30
COX20P2	263.538	-2.080	0.174	-11.924	8.87E-33	2.22E-31
CA2	112.446	-3.866	0.324	-11.942	7.15E-33	1.79E-31
SPNS3	88.249	-4.255	0.356	-11.951	6.40E-33	1.61E-31
RP11-321P16.3	128.548	-3.320	0.276	-12.020	2.79E-33	7.16E-32
SH3PXD2B	94.249	-4.549	0.376	-12.099	1.07E-33	2.79E-32
BCL6	155.106	-6.948	0.569	-12.213	2.66E-34	7.06E-33
PNPLA7	175.889	-2.470	0.202	-12.215	2.60E-34	6.89E-33
SCN3A	143.303	-2.873	0.231	-12.451	1.38E-35	3.83E-34
ZNF607	126.396	-3.242	0.258	-12.549	4.04E-36	1.15E-34
CXCL10	153.590	-6.555	0.516	-12.696	6.20E-37	1.80E-35
PTPRVP	175.057	-2.495	0.195	-12.762	2.68E-37	7.90E-36
COL7A1	208.703	-2.662	0.205	-13.015	1.01E-38	3.07E-37
F2RL3	141.274	-2.941	0.225	-13.084	4.08E-39	1.26E-37
RP11-367L7.1	135.760	-3.122	0.236	-13.215	7.17E-40	2.27E-38
BCAR3	129.328	-4.141	0.312	-13.288	2.71E-40	8.70E-39
KLF9	116.615	-4.520	0.338	-13.379	7.97E-41	2.60E-39
AMPD3	193.520	-2.496	0.185	-13.486	1.88E-41	6.25E-40

RP11-284F21.7	222.721	-2.333	0.171	-13.623	2.93E-42	9.90E-41
IGLL5	223.633	-7.319	0.528	-13.866	1.02E-43	3.59E-42
RP11-466A19.1	142.720	-5.842	0.418	-13.973	2.27E-44	8.06E-43
RP11-515I12.1	249.137	-2.242	0.158	-14.172	1.36E-45	5.01E-44
CHFR	538.335	-9.261	0.652	-14.208	8.17E-46	3.02E-44
ARHGEF4	262.990	-2.385	0.168	-14.228	6.15E-46	2.28E-44
STAT4	262.430	-2.495	0.171	-14.549	5.93E-48	2.32E-46
KCNC3	554.731	-2.016	0.137	-14.760	2.63E-49	1.06E-47
GZMM	145.379	-3.894	0.261	-14.926	2.25E-50	9.25E-49
NLRP3	143.759	-4.461	0.297	-15.030	4.67E-51	1.96E-49
PRDM1	318.958	-2.269	0.149	-15.221	2.55E-52	1.10E-50
PRELID2	234.689	-2.987	0.196	-15.242	1.86E-52	8.08E-51
ODC1-DT	204.948	-2.963	0.194	-15.305	7.13E-53	3.13E-51
XCL1	382.960	-2.492	0.162	-15.354	3.34E-53	1.49E-51
CD96	204.900	-2.877	0.186	-15.460	6.50E-54	2.95E-52
RETREG1	295.123	-3.731	0.238	-15.695	1.63E-55	7.72E-54
TRIB1	526.918	-2.030	0.129	-15.737	8.43E-56	4.04E-54
ZIK1	169.063	-4.628	0.294	-15.743	7.72E-56	3.71E-54
ARL4C	285.993	-2.369	0.147	-16.156	1.04E-58	5.43E-57
RASGRP2	471.312	-2.004	0.124	-16.217	3.83E-59	2.02E-57
ZNF614	236.173	-6.044	0.369	-16.359	3.72E-60	2.00E-58
ZNF83	477.376	-2.011	0.121	-16.613	5.64E-62	3.13E-60
LINC00299	426.147	-2.360	0.140	-16.871	7.41E-64	4.25E-62
ADARB1	206.473	-5.027	0.292	-17.233	1.50E-66	9.05E-65
TNFRSF10A	292.649	-2.599	0.150	-17.363	1.57E-67	9.65E-66
PNMA2	217.347	-3.418	0.194	-17.657	9.04E-70	5.84E-68
RP11-588H23.3	203.180	-4.202	0.237	-17.704	3.88E-70	2.51E-68
KCNMB2	540.076	-2.101	0.118	-17.828	4.31E-71	2.83E-69
GZMK	241.322	-3.413	0.190	-17.987	2.46E-72	1.66E-70
TNFRSF10D	320.716	-2.986	0.166	-18.036	1.02E-72	6.92E-71
ZNF439	310.019	-3.249	0.179	-18.183	6.99E-74	5.00E-72
ZNF331	318.456	-4.831	0.265	-18.247	2.17E-74	1.58E-72
RNF144A	574.114	-2.040	0.112	-18.277	1.27E-74	9.33E-73
ZSCAN18	299.343	-3.794	0.205	-18.523	1.35E-76	1.04E-74
ZFP82	379.260	-2.564	0.138	-18.537	1.03E-76	7.91E-75
LINC02331	246.073	-5.404	0.290	-18.661	1.03E-77	8.09E-76
AF127936.3	476.703	-2.668	0.141	-18.975	2.72E-80	2.19E-78
PITX1	427.883	-2.814	0.148	-18.997	1.80E-80	1.46E-78
HDAC7	657.750	-2.244	0.117	-19.171	6.47E-82	5.35E-80
LINC00665	247.347	-4.454	0.232	-19.201	3.65E-82	3.05E-80
PRKCA	553.995	-2.224	0.113	-19.721	1.42E-86	1.29E-84
MYO1F	585.619	-2.206	0.110	-20.109	6.17E-90	5.82E-88
HHEX	370.736	-3.047	0.152	-20.111	5.94E-90	5.62E-88
CCDC152	362.513	-3.559	0.173	-20.519	1.47E-93	1.44E-91
CBR1	777.342	-2.291	0.108	-21.139	3.49E-99	3.76E-97
TOX	720.837	-2.618	0.122	-21.531	7.95E-103	8.92E-101
CA8	360.517	-4.037	0.187	-21.615	1.29E-103	1.46E-101
CLECL1	1144.909	-2.158	0.100	-21.664	4.48E-104	5.13E-102
TRPS1	405.285	-3.749	0.172	-21.795	2.56E-105	3.01E-103
CDH1	488.550	-2.997	0.137	-21.821	1.48E-105	1.77E-103
TP53INP1	1229.611	-2.022	0.092	-22.094	3.58E-108	4.47E-106
LPP	394.401	-4.084	0.184	-22.155	9.28E-109	1.17E-106
ZNF320	422.399	-3.987	0.176	-22.654	1.27E-113	1.71E-111
CMTM3	937.428	-2.033	0.090	-22.656	1.21E-113	1.64E-111
GPR160	1010.002	-2.433	0.107	-22.694	5.13E-114	7.04E-112
ERICH3	1251.751	-2.117	0.092	-22.977	7.99E-117	1.15E-114
CADM1	636.577	-2.657	0.115	-23.012	3.52E-117	5.09E-115
CDH17	1607.939	-2.027	0.088	-23.115	3.30E-118	4.81E-116

ST3GAL1	650.801	-2.527	0.106	-23.747	1.18E-124	1.84E-122
KLHL6	1898.028	-2.202	0.091	-24.311	1.50E-130	2.47E-128
TGFBR2	429.020	-4.250	0.174	-24.358	4.72E-131	7.89E-129
RP11-284F21.10	806.305	-2.598	0.101	-25.754	2.90E-146	5.70E-144
UGT8	552.273	-3.280	0.127	-25.766	2.15E-146	4.26E-144
PPP2R2C	655.607	-2.839	0.108	-26.252	6.78E-152	1.42E-149
SLC16A3	4103.625	-2.162	0.077	-28.168	1.43E-174	3.85E-172
JCHAIN	8038.816	-2.139	0.070	-30.597	1.34E-205	4.65E-203
ITGB1	1196.142	-2.733	0.089	-30.822	1.34E-208	4.80E-206
PITPNC1	865.736	-3.739	0.119	-31.340	1.34E-215	5.18E-213
RBPMS2	1270.793	-2.948	0.094	-31.391	2.72E-216	1.07E-213
LINC01694	1646.050	-2.730	0.085	-32.142	1.15E-226	5.01E-224
DTX1	2799.183	-2.401	0.072	-33.279	7.73E-243	3.65E-240
INPP5F	1740.306	-2.583	0.077	-33.450	2.56E-245	1.26E-242
C1orf21	1098.655	-4.705	0.136	-34.516	4.62E-261	2.32E-258
SERPINB6	1463.470	-3.207	0.092	-34.899	7.81E-267	4.09E-264
BASP1	4038.133	-2.250	0.063	-35.920	1.47E-282	8.86E-280
ZBED2	1115.397	-3.980	0.110	-36.227	2.28E-287	1.41E-284
MAP3K20	1612.210	-4.429	0.107	-41.520	0.00E+00	0.00E+00
ROBO1	3665.437	-3.700	0.082	-45.174	0.00E+00	0.00E+00
PPM1L	1889.303	-3.632	0.092	-39.270	0.00E+00	0.00E+00
PDE4D	1560.098	-3.386	0.085	-39.811	0.00E+00	0.00E+00
WWC3	3119.527	-3.163	0.072	-43.648	0.00E+00	0.00E+00
MEC1 RNASEH2B Bi-KO vs WT						
Gene Name	baseMean	log2FoldChange	lfcSE	stat	pvalue	padj
RP4-758J18.7	3.283	2.680	1.324	2.023	4.30E-02	9.96E-02
RP1-158P9.3	3.014	2.804	1.386	2.024	4.30E-02	9.95E-02
RP11-219B4.5	1.231	3.940	1.946	2.025	4.29E-02	9.94E-02
RP11-651L5.3	2.471	2.944	1.454	2.025	4.29E-02	9.94E-02
RP1-68D18.2	3.204	2.513	1.241	2.025	4.28E-02	9.93E-02
SYNPO2L	5.173	2.094	1.033	2.026	4.27E-02	9.91E-02
RP11-64K12.8	2.857	2.940	1.450	2.027	4.26E-02	9.89E-02
ZBTB8B	3.821	2.482	1.223	2.029	4.25E-02	9.85E-02
RP11-203M5.6	2.512	3.248	1.600	2.029	4.24E-02	9.85E-02
RP3-430N8.11	2.850	2.929	1.443	2.030	4.24E-02	9.84E-02
RP11-24O17.2	1.917	3.585	1.766	2.030	4.23E-02	9.83E-02
RP11-124N19.4	1.537	3.734	1.838	2.031	4.23E-02	9.82E-02
LINC02139	3.407	2.485	1.223	2.032	4.22E-02	9.80E-02
RP11-362A9.3	3.989	2.814	1.384	2.034	4.20E-02	9.76E-02
ZNF648	3.612	2.442	1.201	2.035	4.19E-02	9.75E-02
RP11-121P12.1	3.210	3.131	1.539	2.035	4.19E-02	9.75E-02
RP11-252E2.1	1.885	3.548	1.743	2.036	4.18E-02	9.72E-02
SLITRK1	3.201	3.116	1.529	2.037	4.16E-02	9.70E-02
UCA1	1.931	3.376	1.653	2.042	4.11E-02	9.59E-02
RP11-313J2.1	6.412	3.097	1.515	2.044	4.09E-02	9.55E-02
RP11-44F14.8	1.801	3.584	1.751	2.046	4.07E-02	9.52E-02
CSTA	4.261	2.719	1.327	2.049	4.04E-02	9.46E-02
CNTNAP2-AS1	1.350	3.940	1.921	2.052	4.02E-02	9.41E-02
RP11-369K17.1	1.938	3.384	1.648	2.053	4.01E-02	9.38E-02
LINC01389	2.790	2.983	1.453	2.054	4.00E-02	9.37E-02
FMO3	2.733	3.240	1.577	2.054	4.00E-02	9.36E-02
SELENOP	3.274	2.816	1.371	2.054	3.99E-02	9.36E-02
RP11-1E4.1	3.099	2.902	1.410	2.058	3.96E-02	9.29E-02
LINC02027	6.324	3.088	1.500	2.058	3.96E-02	9.28E-02
CHRM3	32.341	2.362	1.147	2.059	3.95E-02	9.27E-02
CTD-3065B20.2	5.193	2.025	0.984	2.059	3.95E-02	9.26E-02
FUNDC2P4	2.901	2.920	1.417	2.060	3.94E-02	9.25E-02

RPSAP20	1.793	3.572	1.733	2.061	3.93E-02	9.23E-02
DIS3L-AS1	3.977	2.314	1.121	2.063	3.91E-02	9.19E-02
RP11-307L14.1	2.421	3.263	1.581	2.064	3.90E-02	9.18E-02
RP11-310H4.2	1.585	3.780	1.831	2.064	3.90E-02	9.18E-02
RP11-486M23.1	1.952	3.503	1.696	2.065	3.89E-02	9.15E-02
FCER1G	5.431	2.199	1.063	2.068	3.86E-02	9.10E-02
GJB6	2.165	3.376	1.631	2.070	3.84E-02	9.07E-02
SLC6A12	2.075	3.384	1.633	2.072	3.83E-02	9.04E-02
LGALS9C	3.569	2.817	1.359	2.072	3.82E-02	9.02E-02
DPEP1	5.343	2.708	1.306	2.073	3.81E-02	9.01E-02
NPR1	2.090	3.384	1.631	2.074	3.81E-02	8.99E-02
IL27	2.539	3.263	1.573	2.074	3.80E-02	8.98E-02
PRKG2	1.855	3.494	1.684	2.075	3.80E-02	8.97E-02
SPEG	3.586	3.131	1.507	2.077	3.78E-02	8.94E-02
HOXB13	3.208	2.868	1.378	2.081	3.75E-02	8.86E-02
LINC02528	2.449	3.398	1.632	2.082	3.74E-02	8.85E-02
LA16c-352F7.1	1.318	3.908	1.877	2.082	3.73E-02	8.84E-02
TRAJ38	1.459	3.931	1.887	2.083	3.72E-02	8.82E-02
HMGB2P1	1.459	3.931	1.887	2.083	3.72E-02	8.82E-02
HRH1	2.149	3.582	1.719	2.084	3.72E-02	8.80E-02
RP11-217D23.1	1.970	3.494	1.676	2.085	3.71E-02	8.79E-02
TDH	2.805	3.025	1.449	2.087	3.69E-02	8.75E-02
RP11-350J20.9	2.895	2.919	1.398	2.088	3.68E-02	8.73E-02
RP11-785J10.2	5.247	2.192	1.049	2.089	3.67E-02	8.71E-02
ANKRD50	1.936	3.479	1.665	2.089	3.67E-02	8.71E-02
NPPC	2.293	3.391	1.622	2.091	3.65E-02	8.68E-02
GMPR	3.122	2.972	1.419	2.094	3.63E-02	8.62E-02
AC007106.1	4.791	2.700	1.289	2.095	3.62E-02	8.60E-02
ZNF385B	1.860	3.610	1.723	2.095	3.61E-02	8.60E-02
LINC02695	2.172	3.383	1.612	2.099	3.58E-02	8.53E-02
RP11-131L23.2	1.582	3.779	1.796	2.103	3.54E-02	8.44E-02
NCKAP5	8.427	2.046	0.973	2.104	3.54E-02	8.44E-02
AC084082.3	5.957	2.334	1.110	2.104	3.54E-02	8.44E-02
SPIC	2.114	3.724	1.768	2.106	3.52E-02	8.40E-02
SPATA18	4.155	2.313	1.097	2.109	3.50E-02	8.36E-02
DNAH14	2.034	3.479	1.650	2.109	3.50E-02	8.36E-02
EGF	3.037	2.905	1.376	2.111	3.47E-02	8.31E-02
LINC01801	3.279	2.935	1.384	2.120	3.40E-02	8.15E-02
RP11-286N22.10	2.970	3.255	1.532	2.124	3.36E-02	8.07E-02
KLF4	1.350	3.942	1.853	2.127	3.34E-02	8.03E-02
RP11-310H4.6	1.590	4.093	1.917	2.136	3.27E-02	7.88E-02
AATBC	2.407	3.472	1.625	2.137	3.26E-02	7.86E-02
LINC02398	1.361	4.228	1.977	2.138	3.25E-02	7.83E-02
PDZK1	2.956	3.368	1.574	2.140	3.24E-02	7.80E-02
GAS6	3.362	2.697	1.260	2.140	3.23E-02	7.80E-02
MAS1	3.817	2.727	1.270	2.147	3.18E-02	7.69E-02
RP11-27J8.3	4.103	3.354	1.558	2.152	3.14E-02	7.60E-02
SLC7A3	1.677	3.757	1.745	2.153	3.13E-02	7.59E-02
RP11-517H2.8	2.561	3.391	1.573	2.155	3.11E-02	7.55E-02
RP5-828H9.1	4.653	2.331	1.081	2.156	3.11E-02	7.54E-02
LINC02871	2.084	3.501	1.623	2.157	3.10E-02	7.52E-02
RP11-27G24.1	5.685	2.055	0.952	2.158	3.10E-02	7.51E-02
SPOCK3	2.425	3.488	1.616	2.158	3.09E-02	7.50E-02
TMEFF1	3.664	2.374	1.099	2.160	3.08E-02	7.47E-02
PTHLH	5.451	2.008	0.929	2.161	3.07E-02	7.46E-02
DZIP1L	1.474	3.951	1.829	2.161	3.07E-02	7.46E-02
AGTR2	1.340	4.075	1.883	2.164	3.05E-02	7.40E-02
NXF3	12.432	3.080	1.423	2.164	3.04E-02	7.40E-02

ST6GALNAC2	1.982	3.603	1.664	2.165	3.04E-02	7.39E-02
AC145343.2	3.118	2.998	1.385	2.165	3.04E-02	7.39E-02
LAMB4	2.307	3.507	1.620	2.165	3.04E-02	7.39E-02
RP11-243M5.2	1.446	3.920	1.810	2.166	3.03E-02	7.37E-02
LINC01518	5.183	3.116	1.437	2.168	3.01E-02	7.34E-02
RP11-274J16.5	2.624	3.376	1.556	2.170	3.00E-02	7.30E-02
GNAL	6.869	2.210	1.018	2.172	2.99E-02	7.28E-02
BTBD11	3.782	2.600	1.197	2.173	2.98E-02	7.26E-02
RP11-197M22.2	4.312	2.333	1.072	2.176	2.96E-02	7.22E-02
PHBP13	2.078	3.685	1.693	2.176	2.96E-02	7.21E-02
AACSP1	5.306	3.128	1.437	2.177	2.95E-02	7.20E-02
RAB34	5.169	2.200	1.010	2.179	2.93E-02	7.17E-02
MYO16	5.987	3.110	1.427	2.180	2.92E-02	7.15E-02
RP11-104H15.8	5.317	2.261	1.037	2.181	2.92E-02	7.14E-02
KLRC3	5.060	2.452	1.124	2.181	2.92E-02	7.13E-02
RCAN2	2.116	3.617	1.657	2.183	2.90E-02	7.11E-02
RP11-208N14.4	1.454	3.930	1.800	2.183	2.90E-02	7.10E-02
PDK4	2.188	3.704	1.696	2.184	2.90E-02	7.10E-02
HBE1	1.906	3.919	1.790	2.189	2.86E-02	7.01E-02
MXRA7P1	2.400	3.494	1.595	2.190	2.85E-02	7.00E-02
RBMS1P1	4.784	2.821	1.288	2.191	2.84E-02	6.99E-02
USH1G	5.191	2.337	1.067	2.191	2.84E-02	6.99E-02
PDE2A-AS2	1.473	4.095	1.863	2.198	2.80E-02	6.89E-02
RP11-523H20.6	4.741	2.278	1.034	2.203	2.76E-02	6.80E-02
RTL9	1.573	3.930	1.784	2.203	2.76E-02	6.80E-02
ALS2CL	5.410	2.043	0.927	2.204	2.75E-02	6.79E-02
UMODL1	5.724	2.148	0.974	2.205	2.74E-02	6.77E-02
RP5-984P4.4	2.885	3.384	1.533	2.208	2.73E-02	6.74E-02
RP11-26J3.1	1.669	3.910	1.771	2.208	2.72E-02	6.73E-02
SORCS3	1.540	4.047	1.828	2.214	2.68E-02	6.64E-02
HOXA7	1.561	3.920	1.769	2.215	2.67E-02	6.62E-02
TSIX	3.989	2.609	1.177	2.217	2.67E-02	6.60E-02
UPK1A-AS1	4.268	2.493	1.122	2.222	2.63E-02	6.51E-02
LINC02724	3.450	2.692	1.211	2.223	2.62E-02	6.51E-02
RP4-621F18.2	1.572	3.931	1.768	2.224	2.62E-02	6.50E-02
RNU6-118P	4.171	2.915	1.311	2.224	2.61E-02	6.49E-02
RP11-190C22.9	6.144	2.087	0.938	2.225	2.61E-02	6.48E-02
RP11-206F17.3	1.584	4.085	1.834	2.227	2.59E-02	6.45E-02
CDK6-AS1	5.531	2.069	0.929	2.228	2.59E-02	6.44E-02
RP11-337L12.1	3.128	3.121	1.401	2.228	2.59E-02	6.43E-02
RP11-119F7.5	4.542	2.624	1.173	2.236	2.53E-02	6.32E-02
SLC35F4	1.817	3.942	1.761	2.239	2.52E-02	6.28E-02
RP4-744I24.5	3.862	2.966	1.325	2.239	2.51E-02	6.28E-02
TTC39A	4.794	2.289	1.022	2.240	2.51E-02	6.26E-02
TMC1	4.649	2.245	1.002	2.241	2.51E-02	6.26E-02
RP11-681B3.4	6.433	2.820	1.258	2.241	2.50E-02	6.26E-02
PCDHB12	2.234	3.890	1.734	2.243	2.49E-02	6.23E-02
RP11-434C1.2	3.186	3.580	1.595	2.244	2.48E-02	6.21E-02
AC006014.8	2.156	3.768	1.678	2.245	2.47E-02	6.20E-02
OSMR-AS1	2.609	3.577	1.592	2.247	2.46E-02	6.17E-02
CHRNA7	1.678	3.920	1.742	2.250	2.45E-02	6.14E-02
RPL32P9	2.271	3.777	1.678	2.250	2.44E-02	6.13E-02
LINC02579	3.166	3.074	1.364	2.253	2.42E-02	6.08E-02
TRNP1	4.304	2.490	1.103	2.258	2.39E-02	6.01E-02
AARSD1P1	2.666	3.501	1.549	2.260	2.38E-02	5.99E-02
RP11-359B12.2	4.813	2.218	0.980	2.262	2.37E-02	5.96E-02
CDKL2	5.252	2.081	0.919	2.264	2.36E-02	5.94E-02
CTD-3092A11.3	1.741	4.374	1.926	2.271	2.32E-02	5.85E-02

CMA1	3.178	3.561	1.567	2.272	2.31E-02	5.83E-02
RP11-1191J2.5	1.498	4.244	1.867	2.274	2.30E-02	5.81E-02
IL37	2.308	3.610	1.583	2.281	2.26E-02	5.72E-02
AC083900.1	3.020	3.501	1.534	2.281	2.25E-02	5.71E-02
CYCSP6	1.800	3.930	1.721	2.284	2.24E-02	5.68E-02
KCNQ2	1.793	3.920	1.714	2.287	2.22E-02	5.64E-02
C11orf72	5.499	2.381	1.040	2.290	2.20E-02	5.60E-02
RP11-434D9.1	3.055	3.153	1.377	2.290	2.20E-02	5.59E-02
RP11-452J21.3	1.815	3.940	1.720	2.291	2.20E-02	5.58E-02
AC005281.1	3.705	2.739	1.194	2.294	2.18E-02	5.54E-02
CYP4F35P	5.771	3.250	1.416	2.295	2.17E-02	5.53E-02
ABI1P1	1.808	4.210	1.833	2.296	2.17E-02	5.52E-02
LINC02777	4.960	2.437	1.061	2.297	2.16E-02	5.51E-02
LINC01515	2.549	3.603	1.566	2.302	2.14E-02	5.45E-02
CTA-109P11.4	3.419	3.570	1.551	2.302	2.13E-02	5.45E-02
CTC-573N18.1	2.382	3.767	1.637	2.302	2.13E-02	5.45E-02
ST3GAL3-AS1	7.148	2.238	0.972	2.303	2.13E-02	5.44E-02
RP11-345F18.3	6.032	2.085	0.905	2.303	2.13E-02	5.43E-02
RP11-527L4.5	6.226	2.233	0.969	2.304	2.12E-02	5.42E-02
LIN28B	3.627	3.074	1.331	2.309	2.09E-02	5.36E-02
LINC00937	5.062	2.571	1.112	2.311	2.08E-02	5.33E-02
MCIDAS	1.895	4.058	1.753	2.314	2.06E-02	5.29E-02
PCDHB2	4.060	3.384	1.461	2.315	2.06E-02	5.28E-02
PDE11A	2.306	3.693	1.594	2.316	2.06E-02	5.27E-02
HAGLR	5.901	2.089	0.901	2.318	2.04E-02	5.25E-02
SCHIP1	2.339	3.713	1.599	2.321	2.03E-02	5.21E-02
RP11-115D19.3	2.054	3.950	1.699	2.325	2.01E-02	5.16E-02
RP11-274H24.3	4.899	3.040	1.307	2.327	2.00E-02	5.14E-02
TMEM212	1.930	3.940	1.691	2.329	1.98E-02	5.11E-02
RP11-893F2.13	3.591	3.513	1.507	2.332	1.97E-02	5.08E-02
RP11-7F3.1	1.486	4.354	1.865	2.334	1.96E-02	5.05E-02
ALOX5	5.480	5.076	2.173	2.336	1.95E-02	5.02E-02
C17orf114	3.440	3.572	1.528	2.338	1.94E-02	5.01E-02
RAB42	2.893	3.603	1.541	2.339	1.93E-02	5.00E-02
RP11-136B18.2	4.121	2.823	1.207	2.339	1.93E-02	5.00E-02
CTB-111H14.1	2.023	3.920	1.676	2.340	1.93E-02	4.99E-02
HOXA-AS2	5.197	2.457	1.050	2.340	1.93E-02	4.98E-02
RP11-366M4.12	2.540	3.704	1.580	2.345	1.90E-02	4.92E-02
CASC6	3.275	3.171	1.351	2.348	1.89E-02	4.89E-02
NFE2L3P1	7.066	2.106	0.895	2.353	1.86E-02	4.84E-02
RP11-1035L22.1	3.301	3.221	1.367	2.356	1.84E-02	4.79E-02
ASB4	6.370	2.104	0.889	2.366	1.80E-02	4.69E-02
PXDNL	5.986	2.025	0.856	2.366	1.80E-02	4.68E-02
RP11-301G19.1	3.120	3.598	1.520	2.368	1.79E-02	4.66E-02
GBP5	3.682	3.495	1.475	2.369	1.78E-02	4.64E-02
OR7E62P	1.810	4.085	1.724	2.370	1.78E-02	4.64E-02
THSD4	5.776	2.265	0.956	2.370	1.78E-02	4.64E-02
CSAG3	5.588	3.545	1.495	2.370	1.78E-02	4.64E-02
RP1-72A23.4	5.420	2.625	1.105	2.376	1.75E-02	4.57E-02
RP11-286B14.2	3.218	3.249	1.367	2.376	1.75E-02	4.57E-02
RP11-804H8.7	1.802	4.076	1.710	2.383	1.72E-02	4.49E-02
MAP6	1.814	4.085	1.714	2.383	1.72E-02	4.49E-02
TRAJ54	6.118	2.017	0.846	2.384	1.71E-02	4.49E-02
TMEM158	3.336	3.212	1.346	2.386	1.70E-02	4.46E-02
ROPN1L	6.575	2.066	0.866	2.386	1.70E-02	4.46E-02
RP5-1055C14.9	4.278	2.582	1.078	2.395	1.66E-02	4.36E-02
RP13-415G19.2	3.562	3.585	1.496	2.397	1.65E-02	4.34E-02
GOLGA8Q	8.618	2.041	0.851	2.398	1.65E-02	4.33E-02

AC004012.1	3.780	3.205	1.336	2.399	1.64E-02	4.32E-02
HR	3.247	3.604	1.501	2.401	1.64E-02	4.30E-02
C3AR1	4.597	2.736	1.139	2.402	1.63E-02	4.29E-02
COL6A6	4.278	3.489	1.451	2.405	1.62E-02	4.26E-02
RP11-560I19.1	4.924	2.612	1.084	2.409	1.60E-02	4.22E-02
DLX2	5.794	2.329	0.966	2.410	1.60E-02	4.21E-02
PRR20G	3.267	3.610	1.497	2.412	1.59E-02	4.19E-02
AC093110.3	4.192	2.951	1.217	2.424	1.53E-02	4.06E-02
MIR223HG	5.634	2.306	0.951	2.426	1.53E-02	4.05E-02
LUARIS	2.412	4.101	1.689	2.428	1.52E-02	4.02E-02
RP11-283G6.5	11.304	2.506	1.029	2.435	1.49E-02	3.95E-02
SCUBE3	2.357	3.895	1.598	2.437	1.48E-02	3.93E-02
CCL1	2.154	4.336	1.776	2.442	1.46E-02	3.88E-02
KALRN	7.524	2.214	0.904	2.448	1.44E-02	3.83E-02
CH17-360D5.2	1.706	4.346	1.773	2.451	1.42E-02	3.79E-02
PTPRG	7.186	2.655	1.083	2.453	1.42E-02	3.78E-02
FAM230C	2.263	4.067	1.657	2.454	1.41E-02	3.77E-02
OTOF	7.514	2.088	0.848	2.463	1.38E-02	3.69E-02
CLDN10-AS1	4.541	2.518	1.022	2.464	1.38E-02	3.68E-02
NRIR	2.989	3.783	1.530	2.473	1.34E-02	3.60E-02
GCNT4	7.176	3.077	1.244	2.473	1.34E-02	3.60E-02
RP11-433N2.1	2.173	4.093	1.653	2.476	1.33E-02	3.57E-02
EXOC3L4	5.128	3.214	1.297	2.477	1.33E-02	3.56E-02
C10orf55	2.795	3.789	1.526	2.482	1.31E-02	3.52E-02
CGNL1	3.696	3.286	1.323	2.483	1.30E-02	3.51E-02
MIR135A2	2.571	3.885	1.565	2.483	1.30E-02	3.51E-02
TMEM92	1.946	4.354	1.750	2.487	1.29E-02	3.47E-02
TENM1	3.446	3.778	1.518	2.489	1.28E-02	3.46E-02
RP11-564K10.1	4.767	2.535	1.018	2.490	1.28E-02	3.45E-02
ARMCX1	5.578	3.182	1.278	2.491	1.27E-02	3.44E-02
LCN10	4.095	2.929	1.175	2.492	1.27E-02	3.43E-02
CD2	4.954	2.554	1.025	2.492	1.27E-02	3.43E-02
CDPF1P1	3.154	3.813	1.528	2.495	1.26E-02	3.40E-02
BRDT	1.942	4.226	1.691	2.499	1.24E-02	3.37E-02
KLHDC7B-DT	6.683	3.088	1.234	2.502	1.23E-02	3.34E-02
AC005307.5	4.220	3.749	1.498	2.503	1.23E-02	3.34E-02
MIR221	5.997	2.227	0.889	2.505	1.22E-02	3.32E-02
HYAL4	2.959	3.930	1.567	2.508	1.21E-02	3.30E-02
LARGE2	2.647	3.873	1.543	2.511	1.20E-02	3.27E-02
RIPPLY3	5.670	2.150	0.856	2.513	1.20E-02	3.26E-02
MUC15	10.643	2.194	0.873	2.513	1.20E-02	3.26E-02
MS4A15	4.706	3.227	1.283	2.515	1.19E-02	3.24E-02
RP1-45C12.1	6.173	2.230	0.886	2.517	1.19E-02	3.23E-02
TRIM2	5.816	2.531	1.005	2.518	1.18E-02	3.22E-02
FIBCD1	2.472	3.974	1.577	2.520	1.17E-02	3.20E-02
BCO1	1.941	4.226	1.676	2.521	1.17E-02	3.19E-02
KLKP1	4.945	3.362	1.333	2.522	1.17E-02	3.19E-02
HOXA2	2.399	4.085	1.619	2.524	1.16E-02	3.17E-02
PGM5	8.798	2.391	0.947	2.524	1.16E-02	3.17E-02
ANKRD35	3.144	3.800	1.505	2.525	1.16E-02	3.17E-02
RP5-850O15.3	3.973	2.983	1.180	2.527	1.15E-02	3.15E-02
APCDD1	2.452	4.038	1.597	2.528	1.15E-02	3.14E-02
UGT3A2	6.288	2.272	0.898	2.529	1.14E-02	3.13E-02
ACTG1P25	6.211	2.293	0.904	2.536	1.12E-02	3.07E-02
CLU	3.088	3.941	1.553	2.537	1.12E-02	3.07E-02
RP11-1109F11.3	2.271	4.217	1.662	2.537	1.12E-02	3.07E-02
RP11-136L23.2	4.772	2.523	0.994	2.539	1.11E-02	3.06E-02
CTD-2314B22.4	3.081	3.930	1.547	2.540	1.11E-02	3.05E-02

CACNG3	4.907	3.750	1.476	2.541	1.11E-02	3.04E-02
TRAJ10	7.024	2.218	0.872	2.544	1.10E-02	3.01E-02
AC002407.3	3.779	3.922	1.541	2.545	1.09E-02	3.01E-02
CYP27A1	6.077	2.660	1.044	2.547	1.09E-02	2.99E-02
SLC8A3	2.574	3.958	1.553	2.549	1.08E-02	2.98E-02
LINC01833	2.791	3.889	1.526	2.549	1.08E-02	2.97E-02
LRIG3	2.792	3.959	1.550	2.554	1.07E-02	2.94E-02
RP11-307O13.1	1.708	4.558	1.784	2.554	1.06E-02	2.94E-02
LINC02598	1.826	4.346	1.698	2.560	1.05E-02	2.89E-02
SHH	2.901	3.884	1.517	2.561	1.05E-02	2.89E-02
RP11-214O1.3	2.847	4.208	1.639	2.567	1.02E-02	2.84E-02
AC026150.8	4.488	3.773	1.469	2.569	1.02E-02	2.83E-02
TRAJ44	3.889	3.365	1.309	2.570	1.02E-02	2.82E-02
LINC01709	5.018	2.763	1.074	2.573	1.01E-02	2.80E-02
LINC01476	2.720	4.063	1.579	2.573	1.01E-02	2.80E-02
NACAP8	4.269	3.700	1.438	2.574	1.01E-02	2.79E-02
PRUNE2	3.435	3.490	1.356	2.574	1.00E-02	2.79E-02
TMEM253	4.845	2.584	1.004	2.574	1.00E-02	2.79E-02
LINC02289	7.159	2.177	0.845	2.577	9.97E-03	2.77E-02
MSMP	4.550	2.682	1.041	2.577	9.97E-03	2.77E-02
ANGPT4	3.222	4.064	1.576	2.578	9.93E-03	2.76E-02
ADRA1B	5.032	2.606	1.011	2.579	9.91E-03	2.76E-02
C4orf19	1.920	4.330	1.677	2.582	9.83E-03	2.74E-02
TRIM29	2.956	4.069	1.575	2.583	9.78E-03	2.73E-02
LIF	3.815	3.784	1.465	2.584	9.77E-03	2.72E-02
DKFZP434A062	1.804	4.441	1.716	2.589	9.64E-03	2.69E-02
LINC02228	3.001	3.958	1.528	2.590	9.59E-03	2.68E-02
CYP3A4	2.375	4.201	1.619	2.595	9.45E-03	2.65E-02
CFAP46	4.966	2.665	1.026	2.597	9.40E-03	2.63E-02
RP1-69D17.4	6.919	2.398	0.923	2.598	9.37E-03	2.62E-02
SPARCL1	2.603	4.048	1.558	2.598	9.36E-03	2.62E-02
FAM133A	2.872	4.093	1.574	2.599	9.34E-03	2.62E-02
RASGRF2	5.837	2.467	0.948	2.602	9.28E-03	2.60E-02
DCHS2	6.280	2.537	0.975	2.602	9.27E-03	2.60E-02
HTR2C	3.991	3.914	1.505	2.602	9.28E-03	2.60E-02
RP11-386M24.5	4.981	2.686	1.031	2.605	9.18E-03	2.58E-02
LINC02542	2.283	4.337	1.662	2.610	9.06E-03	2.55E-02
KCNJ1	2.821	3.974	1.520	2.614	8.94E-03	2.52E-02
KIF6	8.993	2.720	1.037	2.624	8.70E-03	2.46E-02
HLF	7.705	2.414	0.915	2.639	8.31E-03	2.36E-02
CUX2	8.387	2.039	0.771	2.645	8.16E-03	2.32E-02
PWWP2AP1	2.903	4.110	1.548	2.655	7.93E-03	2.26E-02
RP3-383B8.1	5.797	2.666	1.002	2.662	7.77E-03	2.22E-02
RP11-568G11.5	4.627	3.436	1.291	2.662	7.77E-03	2.22E-02
RP11-384E22.1	6.350	2.858	1.073	2.664	7.73E-03	2.21E-02
PDCD1	4.856	3.416	1.281	2.667	7.66E-03	2.19E-02
DUSP15	3.814	3.959	1.484	2.668	7.62E-03	2.18E-02
LINC00543	1.856	4.675	1.750	2.671	7.56E-03	2.16E-02
CD4	1.941	4.456	1.667	2.672	7.53E-03	2.16E-02
DIO2-AS1	2.753	4.224	1.580	2.673	7.51E-03	2.15E-02
XCR1	5.362	3.799	1.421	2.674	7.50E-03	2.15E-02
RP11-378J18.9	6.251	2.484	0.927	2.680	7.35E-03	2.11E-02
RP4-764O22.1	16.637	3.095	1.152	2.687	7.21E-03	2.07E-02
LINC02607	2.251	4.531	1.685	2.688	7.19E-03	2.07E-02
RCAN3	6.118	2.429	0.903	2.690	7.15E-03	2.06E-02
LINC00540	6.626	3.705	1.376	2.692	7.10E-03	2.05E-02
TRAJ48	5.090	2.963	1.100	2.693	7.09E-03	2.04E-02
RP11-472K17.4	4.115	3.895	1.446	2.694	7.06E-03	2.03E-02

C3orf86	5.167	3.445	1.277	2.698	6.97E-03	2.01E-02
IKBKB-DT	9.032	2.200	0.815	2.699	6.96E-03	2.01E-02
UGT2B15	31.648	3.880	1.436	2.701	6.91E-03	2.00E-02
RP11-893F2.14	2.902	4.110	1.522	2.701	6.91E-03	2.00E-02
SMIM10L2A	6.418	2.291	0.846	2.706	6.80E-03	1.97E-02
INKA2-AS1	4.722	3.453	1.275	2.708	6.78E-03	1.96E-02
CTAGE3P	2.065	4.463	1.647	2.710	6.73E-03	1.95E-02
RP11-433O3.1	4.758	3.024	1.112	2.719	6.56E-03	1.90E-02
RP11-512N21.1	6.605	2.486	0.914	2.719	6.54E-03	1.90E-02
GFRA2	2.927	4.115	1.513	2.720	6.53E-03	1.90E-02
HOXB-AS1	10.153	2.227	0.819	2.721	6.51E-03	1.89E-02
RP11-1094M14.12	2.912	4.168	1.531	2.722	6.49E-03	1.89E-02
LINC02099	2.844	4.261	1.564	2.725	6.44E-03	1.87E-02
AC003991.3	5.715	2.697	0.990	2.725	6.43E-03	1.87E-02
OSBPL1A	8.119	2.066	0.758	2.725	6.43E-03	1.87E-02
CD9	4.181	3.171	1.162	2.728	6.38E-03	1.86E-02
SOHLH2	3.776	4.077	1.494	2.728	6.36E-03	1.85E-02
S100A8	2.067	4.660	1.707	2.729	6.35E-03	1.85E-02
CYP4F60P	2.959	4.129	1.513	2.730	6.34E-03	1.85E-02
LKAAEAR1	4.456	3.631	1.330	2.731	6.31E-03	1.84E-02
CTD-2369P2.8	7.611	2.055	0.750	2.739	6.16E-03	1.80E-02
SELP	16.283	2.219	0.810	2.740	6.14E-03	1.79E-02
SEPTIN4	6.281	2.431	0.887	2.740	6.14E-03	1.79E-02
RP11-703M24.5	3.592	4.039	1.473	2.741	6.12E-03	1.79E-02
ACCSL	2.194	4.471	1.629	2.744	6.06E-03	1.77E-02
TRIM54	9.524	2.095	0.763	2.744	6.06E-03	1.77E-02
MRO	3.386	4.048	1.474	2.745	6.04E-03	1.77E-02
GBA	12.528	7.030	2.558	2.748	6.00E-03	1.76E-02
RP11-7F17.10	4.508	3.548	1.291	2.749	5.99E-03	1.75E-02
ALDH1A3	19.398	3.138	1.137	2.759	5.79E-03	1.70E-02
OR51B2	2.265	4.545	1.646	2.762	5.75E-03	1.69E-02
LINC00431	5.409	3.030	1.097	2.764	5.72E-03	1.68E-02
GSTM3	1.959	4.667	1.687	2.766	5.67E-03	1.67E-02
SEZ6L2	5.787	2.576	0.930	2.770	5.60E-03	1.65E-02
RP11-310I9.2	6.395	2.588	0.933	2.773	5.55E-03	1.64E-02
SERTM2	2.404	4.457	1.607	2.774	5.54E-03	1.64E-02
SLC1A2-AS1	2.216	4.586	1.652	2.775	5.51E-03	1.63E-02
TEKT4P2	7.014	5.649	2.035	2.776	5.50E-03	1.63E-02
STARD13-IT1	7.959	2.180	0.784	2.779	5.45E-03	1.61E-02
SCN4B	2.410	4.560	1.635	2.789	5.29E-03	1.57E-02
ENSG10010138034.1	3.002	4.352	1.560	2.790	5.27E-03	1.56E-02
PGLYRP2	5.173	3.561	1.272	2.799	5.13E-03	1.53E-02
LINC02257	5.768	3.048	1.088	2.800	5.11E-03	1.52E-02
RP11-900F13.3	3.183	4.191	1.494	2.805	5.04E-03	1.50E-02
CYP2AB1P	2.415	4.463	1.589	2.809	4.97E-03	1.48E-02
RP11-763F8.1	8.622	2.246	0.799	2.811	4.94E-03	1.48E-02
CH17-174L20.1	5.295	3.981	1.414	2.816	4.86E-03	1.45E-02
RP11-331G2.10	5.704	2.659	0.944	2.817	4.85E-03	1.45E-02
HOXA13	6.875	2.472	0.877	2.817	4.84E-03	1.45E-02
BARHL2	3.719	4.114	1.459	2.821	4.79E-03	1.44E-02
CATIP-AS2	4.515	4.039	1.431	2.823	4.76E-03	1.43E-02
RP11-71L14.3	5.867	3.121	1.104	2.826	4.71E-03	1.42E-02
FOXD1	5.449	3.519	1.245	2.826	4.71E-03	1.42E-02
MUC3A	2.538	4.470	1.581	2.827	4.70E-03	1.41E-02
MPP3	2.068	4.661	1.647	2.830	4.65E-03	1.40E-02
RP11-146I2.1	7.863	2.310	0.816	2.831	4.65E-03	1.40E-02
DUOX1	5.376	3.097	1.094	2.831	4.65E-03	1.40E-02
ASS1P1	4.584	3.615	1.277	2.831	4.64E-03	1.40E-02

RP1-239B22.5	5.527	4.077	1.438	2.836	4.57E-03	1.38E-02
SMARCA1	3.986	4.124	1.453	2.838	4.54E-03	1.37E-02
PI15	10.986	2.208	0.778	2.840	4.51E-03	1.36E-02
TMPRSS11A	3.102	4.345	1.529	2.842	4.48E-03	1.35E-02
NMRAL2P	3.986	4.123	1.448	2.848	4.40E-03	1.33E-02
LGR5	3.315	4.326	1.518	2.849	4.39E-03	1.33E-02
LINC02325	6.195	4.071	1.428	2.850	4.37E-03	1.33E-02
RP11-314B1.2	2.172	4.655	1.632	2.852	4.34E-03	1.32E-02
PPP4R3C	30.574	3.761	1.318	2.853	4.33E-03	1.31E-02
AC009542.2	4.088	4.190	1.468	2.853	4.33E-03	1.31E-02
PDGFRL	9.108	2.073	0.726	2.853	4.32E-03	1.31E-02
AC078842.3	3.111	4.456	1.561	2.855	4.30E-03	1.31E-02
RP11-149P24.2	2.411	4.565	1.597	2.858	4.26E-03	1.29E-02
RP11-280F2.3	5.996	3.099	1.083	2.860	4.23E-03	1.29E-02
RP11-531A24.3	2.302	4.750	1.656	2.868	4.14E-03	1.26E-02
ZNF470	3.523	4.251	1.482	2.868	4.13E-03	1.26E-02
RP11-369E15.3	9.706	2.191	0.764	2.870	4.11E-03	1.25E-02
CLEC4D	3.427	4.332	1.509	2.871	4.09E-03	1.25E-02
RORB-AS1	2.088	4.762	1.659	2.871	4.09E-03	1.25E-02
LINC01666	2.919	4.689	1.632	2.872	4.08E-03	1.24E-02
DLK2	2.533	4.565	1.588	2.874	4.05E-03	1.23E-02
RP5-1097P24.1	95.288	3.602	1.253	2.875	4.04E-03	1.23E-02
LCE1B	3.459	4.351	1.509	2.884	3.93E-03	1.20E-02
RP11-88H10.2	4.995	4.044	1.402	2.884	3.92E-03	1.20E-02
C6orf58	7.391	2.804	0.972	2.885	3.91E-03	1.20E-02
ANO4	6.316	3.977	1.375	2.892	3.82E-03	1.17E-02
PEAK3	5.576	3.127	1.081	2.892	3.82E-03	1.17E-02
RAB3C	11.689	3.934	1.359	2.895	3.79E-03	1.16E-02
RP5-1116C7.2	5.822	3.581	1.233	2.905	3.68E-03	1.13E-02
POMC	4.431	4.119	1.417	2.907	3.65E-03	1.12E-02
TINAG	2.530	4.566	1.570	2.907	3.65E-03	1.12E-02
LINC00345	8.641	2.135	0.734	2.909	3.62E-03	1.12E-02
RP11-876F14.1	4.445	4.187	1.435	2.917	3.53E-03	1.09E-02
RP11-332H14.1	5.783	3.319	1.137	2.918	3.52E-03	1.09E-02
RP4-655C5.10	3.298	4.325	1.479	2.924	3.45E-03	1.07E-02
ATXN7L1	6.904	2.546	0.870	2.926	3.44E-03	1.06E-02
ROPN1B	2.404	4.655	1.590	2.928	3.41E-03	1.06E-02
SMIM18	6.201	4.060	1.386	2.928	3.41E-03	1.06E-02
CD160	7.477	2.789	0.952	2.930	3.39E-03	1.05E-02
FUT6	2.646	4.565	1.556	2.934	3.35E-03	1.04E-02
RP11-104L21.4	8.027	2.332	0.795	2.934	3.34E-03	1.04E-02
FGF7P6	7.107	2.562	0.871	2.940	3.28E-03	1.02E-02
TRIM6	2.444	4.853	1.651	2.940	3.28E-03	1.02E-02
GADD45G	4.321	3.776	1.284	2.941	3.28E-03	1.02E-02
MAMLD1	4.142	4.385	1.488	2.946	3.22E-03	1.00E-02
MYO1B	5.405	2.935	0.995	2.951	3.16E-03	9.88E-03
RP11-554D15.1	12.130	2.233	0.756	2.952	3.15E-03	9.85E-03
C2CD4D-AS1	3.602	4.476	1.514	2.957	3.10E-03	9.71E-03
RYR3	7.083	2.729	0.923	2.958	3.10E-03	9.71E-03
CTD-2546F11.1	9.374	2.280	0.771	2.958	3.10E-03	9.70E-03
RP11-567J20.3	5.604	4.314	1.458	2.959	3.09E-03	9.67E-03
GXYLT1P5	2.215	4.852	1.635	2.967	3.00E-03	9.43E-03
RP11-731J8.2	5.901	4.229	1.425	2.968	3.00E-03	9.42E-03
SFTPD	2.213	4.930	1.660	2.969	2.99E-03	9.38E-03
RAPGEF5	7.213	2.658	0.894	2.973	2.95E-03	9.28E-03
RP11-416O18.4	2.752	4.743	1.594	2.977	2.92E-03	9.18E-03
FCAMR	5.030	4.199	1.410	2.977	2.91E-03	9.17E-03
TMEM72	3.239	4.578	1.535	2.983	2.85E-03	9.00E-03

TMSB4XP2	5.452	3.712	1.242	2.988	2.81E-03	8.88E-03
ANKRD44-AS1	9.030	2.235	0.748	2.990	2.79E-03	8.82E-03
RP11-34P13.16	3.732	4.371	1.452	3.011	2.60E-03	8.26E-03
SLC6A14	4.276	3.873	1.285	3.013	2.58E-03	8.22E-03
RP11-473J6.1	9.482	4.029	1.337	3.014	2.58E-03	8.20E-03
RP11-208K4.1	6.135	2.819	0.933	3.020	2.52E-03	8.05E-03
LINC01181	11.557	2.447	0.809	3.025	2.48E-03	7.93E-03
RP11-539G18.4	11.039	3.548	1.170	3.033	2.42E-03	7.73E-03
ADGRG7	8.428	2.852	0.939	3.036	2.39E-03	7.66E-03
WFDC21P	4.461	4.317	1.419	3.043	2.34E-03	7.50E-03
MEF2C-AS2	7.549	2.571	0.845	3.044	2.34E-03	7.48E-03
EPHB6	8.330	2.253	0.740	3.045	2.33E-03	7.45E-03
RP11-347P5.1	5.960	3.004	0.986	3.045	2.32E-03	7.45E-03
AC023669.1	7.977	2.548	0.837	3.046	2.32E-03	7.42E-03
LAD1	5.285	3.839	1.260	3.047	2.31E-03	7.40E-03
CAMKV	13.291	2.120	0.696	3.048	2.31E-03	7.39E-03
CTD-2054N24.1	6.339	3.742	1.227	3.050	2.29E-03	7.34E-03
PTH1R	2.330	5.005	1.636	3.059	2.22E-03	7.14E-03
CDA	5.862	4.334	1.416	3.061	2.20E-03	7.09E-03
ZNF257	30.988	2.563	0.837	3.063	2.19E-03	7.06E-03
SLC4A3	3.470	4.571	1.492	3.063	2.19E-03	7.05E-03
RP11-344L13.3	9.597	2.811	0.916	3.068	2.15E-03	6.95E-03
RP11-520B13.8	10.881	2.054	0.666	3.085	2.03E-03	6.59E-03
TBL1Y	6.414	2.812	0.911	3.086	2.03E-03	6.58E-03
SLC5A5	12.774	2.420	0.784	3.086	2.03E-03	6.58E-03
PTGES	4.652	3.941	1.276	3.088	2.02E-03	6.54E-03
RP11-283G6.3	10.134	2.418	0.782	3.094	1.97E-03	6.41E-03
RP13-314C10.5	3.823	4.578	1.479	3.095	1.97E-03	6.39E-03
CTD-2288F12.1	7.896	2.718	0.878	3.096	1.96E-03	6.37E-03
LINC02562	8.690	2.257	0.729	3.098	1.95E-03	6.33E-03
TUBA5P	8.367	2.317	0.748	3.099	1.94E-03	6.31E-03
ADGRA3	14.902	2.396	0.769	3.118	1.82E-03	5.96E-03
NTS	5.194	3.939	1.261	3.124	1.79E-03	5.86E-03
MIR9-1HG	12.120	2.072	0.663	3.124	1.79E-03	5.86E-03
RP11-253D19.3	7.923	3.243	1.038	3.125	1.78E-03	5.84E-03
DOC2A	10.271	2.042	0.652	3.131	1.74E-03	5.74E-03
LINC02005	3.441	4.740	1.512	3.136	1.71E-03	5.64E-03
GOLGA8H	3.343	4.752	1.515	3.136	1.71E-03	5.64E-03
SLC7A8	2.445	5.005	1.595	3.137	1.70E-03	5.62E-03
FKBP1B	11.313	2.061	0.655	3.148	1.64E-03	5.43E-03
GPR153	10.049	2.247	0.711	3.159	1.58E-03	5.25E-03
RP11-347H15.7	4.162	4.505	1.425	3.161	1.57E-03	5.22E-03
FAM242C	12.558	2.086	0.660	3.162	1.57E-03	5.20E-03
RP11-283G6.4	6.803	4.456	1.407	3.166	1.54E-03	5.14E-03
GOLGA8R	5.947	3.868	1.220	3.169	1.53E-03	5.09E-03
RP11-386D6.1	13.645	3.133	0.985	3.181	1.47E-03	4.91E-03
IL1RN	10.720	2.178	0.684	3.183	1.46E-03	4.88E-03
RP11-463C8.7	2.614	5.101	1.600	3.189	1.43E-03	4.79E-03
PLA2G4E	5.963	3.442	1.075	3.200	1.37E-03	4.61E-03
GAPT	8.479	3.769	1.176	3.205	1.35E-03	4.55E-03
RP11-527B17.3	5.317	4.561	1.422	3.207	1.34E-03	4.51E-03
RP11-438N16.5	3.153	4.857	1.508	3.220	1.28E-03	4.34E-03
PTPRD-AS1	4.960	4.508	1.399	3.222	1.27E-03	4.31E-03
LINC02056	2.843	5.099	1.580	3.228	1.25E-03	4.23E-03
LRRC9	3.240	4.841	1.499	3.230	1.24E-03	4.20E-03
KRT86	10.288	2.097	0.649	3.231	1.23E-03	4.19E-03
AC005062.2	8.083	3.863	1.195	3.231	1.23E-03	4.19E-03
HDGFL1	3.368	4.851	1.500	3.234	1.22E-03	4.15E-03

BICDL2	9.593	2.300	0.711	3.234	1.22E-03	4.14E-03
ANKRD20A3P	5.117	4.508	1.393	3.237	1.21E-03	4.12E-03
RND3	5.760	3.183	0.982	3.240	1.20E-03	4.07E-03
CXCR2P1	2.796	5.005	1.544	3.240	1.19E-03	4.07E-03
SOX5	7.203	3.387	1.044	3.244	1.18E-03	4.02E-03
LINC02875	3.023	5.006	1.543	3.245	1.18E-03	4.01E-03
PIWIL4	8.944	3.122	0.961	3.249	1.16E-03	3.95E-03
RP4-607I7.1	11.732	2.025	0.623	3.251	1.15E-03	3.92E-03
AMPH	3.371	4.851	1.491	3.254	1.14E-03	3.89E-03
NCAPD2P1	9.216	4.314	1.325	3.256	1.13E-03	3.87E-03
RP11-737O24.1	7.004	3.443	1.057	3.256	1.13E-03	3.87E-03
CNTNAP3C	8.133	2.650	0.813	3.259	1.12E-03	3.83E-03
PTN	7.198	3.919	1.202	3.260	1.11E-03	3.82E-03
LINC01752	3.025	4.930	1.510	3.264	1.10E-03	3.77E-03
HECW1	11.918	2.592	0.794	3.264	1.10E-03	3.77E-03
IFITM3P1	3.495	4.851	1.486	3.265	1.10E-03	3.77E-03
RUNDC3A	11.935	2.046	0.627	3.266	1.09E-03	3.75E-03
RP11-731J8.4	10.260	2.396	0.733	3.268	1.08E-03	3.73E-03
LINC01501	6.409	3.975	1.216	3.268	1.08E-03	3.73E-03
CTC-260E6.4	3.226	4.915	1.504	3.268	1.08E-03	3.73E-03
TSLP	6.283	3.951	1.209	3.269	1.08E-03	3.72E-03
IGHG2	14.437	2.241	0.685	3.269	1.08E-03	3.72E-03
AC102953.4	6.602	3.185	0.974	3.270	1.07E-03	3.70E-03
RP11-16L9.5	4.258	4.649	1.419	3.276	1.05E-03	3.64E-03
DCSTAMP	8.645	2.441	0.743	3.284	1.02E-03	3.54E-03
LINC01446	42.069	4.218	1.281	3.292	9.96E-04	3.45E-03
AMER2	12.132	2.197	0.667	3.294	9.87E-04	3.42E-03
LINC00377	6.564	3.023	0.916	3.299	9.70E-04	3.37E-03
AC012354.6	4.391	4.752	1.439	3.302	9.60E-04	3.34E-03
CTC-235G5.3	4.247	4.699	1.423	3.302	9.59E-04	3.34E-03
AC008079.10	7.167	4.453	1.348	3.302	9.59E-04	3.34E-03
CDC42BPA	9.713	2.778	0.841	3.304	9.54E-04	3.32E-03
PPP1R1C	10.637	2.200	0.665	3.308	9.39E-04	3.27E-03
CALHM1	12.795	2.259	0.682	3.312	9.28E-04	3.23E-03
RP11-541G9.1	8.458	2.476	0.746	3.317	9.09E-04	3.17E-03
AP000695.6	3.970	4.857	1.464	3.317	9.09E-04	3.17E-03
CTC-260E6.6	5.992	3.587	1.079	3.324	8.89E-04	3.11E-03
RP11-478I15.1	6.465	4.498	1.353	3.325	8.85E-04	3.10E-03
SERHL2	5.085	4.652	1.397	3.331	8.65E-04	3.03E-03
RP11-22E12.1	3.246	5.000	1.496	3.343	8.30E-04	2.92E-03
MIR8089	7.394	4.507	1.347	3.346	8.20E-04	2.89E-03
FAM182A	3.146	5.077	1.512	3.358	7.86E-04	2.78E-03
CTNNA3	6.540	4.091	1.217	3.362	7.73E-04	2.74E-03
EDA2R	5.001	4.767	1.416	3.367	7.60E-04	2.69E-03
HOXB2	7.755	4.501	1.331	3.380	7.24E-04	2.57E-03
RP11-34P13.15	5.427	4.747	1.403	3.382	7.19E-04	2.56E-03
ZNF622P1	6.577	4.598	1.359	3.383	7.17E-04	2.55E-03
AC006129.1	14.250	2.010	0.593	3.388	7.04E-04	2.51E-03
NECTIN2	7.443	2.998	0.884	3.392	6.93E-04	2.47E-03
TRHDE	2.899	5.265	1.552	3.393	6.91E-04	2.47E-03
RP11-326L17.1	6.795	4.086	1.202	3.398	6.78E-04	2.42E-03
MS4A8	5.786	4.248	1.246	3.409	6.53E-04	2.34E-03
TSPAN1	5.879	4.161	1.221	3.409	6.52E-04	2.34E-03
AOAH	9.467	2.354	0.690	3.412	6.44E-04	2.31E-03
NR5A2	16.647	3.282	0.961	3.415	6.38E-04	2.29E-03
SLFN12	2.920	5.332	1.561	3.416	6.37E-04	2.29E-03
ERICH2	7.537	3.524	1.031	3.418	6.32E-04	2.27E-03
TRGV9	10.423	2.224	0.650	3.422	6.21E-04	2.24E-03

STRA8	5.533	4.696	1.372	3.422	6.21E-04	2.24E-03
RP11-44F14.2	3.733	5.010	1.462	3.428	6.09E-04	2.19E-03
RP11-305F5.2	3.830	5.001	1.455	3.436	5.90E-04	2.13E-03
RP1-153P14.5	11.939	2.541	0.739	3.437	5.89E-04	2.13E-03
DNAJC5G	11.929	2.319	0.674	3.441	5.80E-04	2.10E-03
DYTN	3.840	5.005	1.454	3.442	5.76E-04	2.09E-03
CATSPER1	3.341	5.257	1.527	3.443	5.75E-04	2.08E-03
IGHG4	8.774	3.144	0.913	3.445	5.71E-04	2.07E-03
RP11-109M17.2	2.952	5.287	1.534	3.447	5.66E-04	2.06E-03
SSPN	13.168	2.648	0.767	3.450	5.61E-04	2.04E-03
NECTIN4	6.881	4.127	1.196	3.452	5.57E-04	2.02E-03
RP3-359N14.3	12.653	2.085	0.602	3.466	5.29E-04	1.93E-03
SDR42E1	14.255	3.943	1.134	3.478	5.04E-04	1.85E-03
DNM3OS	10.206	2.986	0.858	3.480	5.02E-04	1.84E-03
CTD-2523D13.2	13.423	2.144	0.615	3.487	4.89E-04	1.80E-03
RP11-484L8.1	6.001	4.748	1.361	3.489	4.84E-04	1.78E-03
AC092657.2	3.294	5.283	1.511	3.496	4.73E-04	1.74E-03
PCDH15	30.520	2.447	0.699	3.499	4.67E-04	1.72E-03
PLEK2	3.078	5.291	1.512	3.500	4.65E-04	1.72E-03
ITIH5	14.276	2.550	0.728	3.502	4.61E-04	1.70E-03
APCDD1L-DT	7.374	3.301	0.942	3.504	4.59E-04	1.70E-03
ST14	21.800	2.971	0.848	3.505	4.57E-04	1.69E-03
LINC02471	8.748	4.098	1.169	3.507	4.53E-04	1.68E-03
RP11-104H15.9	9.439	3.206	0.913	3.510	4.49E-04	1.66E-03
FOXN4	7.287	3.663	1.043	3.511	4.46E-04	1.65E-03
RP11-830F9.7	11.242	2.774	0.789	3.517	4.36E-04	1.62E-03
TKTL1	15.992	2.114	0.600	3.522	4.29E-04	1.59E-03
S100A9	9.549	4.096	1.163	3.523	4.27E-04	1.59E-03
LRTM2	4.875	5.005	1.419	3.526	4.22E-04	1.57E-03
OR2V2	17.759	2.268	0.642	3.532	4.13E-04	1.54E-03
CH17-258A22.4	27.245	4.818	1.359	3.544	3.94E-04	1.47E-03
RP11-146E13.9	10.201	4.704	1.319	3.565	3.63E-04	1.37E-03
RP11-713M15.2	5.280	4.935	1.384	3.566	3.63E-04	1.37E-03
HMGA2	28.038	4.566	1.280	3.567	3.61E-04	1.36E-03
SVEP1	5.757	4.873	1.365	3.570	3.57E-04	1.35E-03
CADPS2	5.556	4.913	1.374	3.576	3.50E-04	1.32E-03
GAD1	3.375	5.329	1.489	3.580	3.44E-04	1.30E-03
RND2	7.361	3.389	0.946	3.583	3.40E-04	1.29E-03
LINC00607	9.233	3.266	0.911	3.583	3.39E-04	1.28E-03
C9orf57	11.866	2.453	0.684	3.584	3.38E-04	1.28E-03
GBA3	6.399	4.934	1.374	3.590	3.31E-04	1.26E-03
WNK2	3.578	5.420	1.509	3.592	3.28E-04	1.25E-03
CT66	11.637	2.464	0.685	3.599	3.20E-04	1.22E-03
EEF1A1P31	7.480	4.805	1.335	3.599	3.19E-04	1.22E-03
NEURL1B	11.317	2.440	0.677	3.603	3.15E-04	1.20E-03
IL12B	8.448	3.355	0.930	3.608	3.09E-04	1.18E-03
CLCF1	8.475	3.790	1.048	3.617	2.97E-04	1.14E-03
TNFAIP6	14.107	3.474	0.959	3.622	2.92E-04	1.12E-03
RP11-707M1.1	5.198	5.132	1.413	3.632	2.81E-04	1.08E-03
NACAD	3.924	5.361	1.475	3.634	2.79E-04	1.07E-03
FSCN1P1	8.603	4.315	1.185	3.642	2.70E-04	1.04E-03
CTD-2184D3.6	9.510	3.306	0.907	3.644	2.68E-04	1.04E-03
RAI14	6.437	4.403	1.208	3.645	2.67E-04	1.03E-03
PRAL	4.460	5.283	1.448	3.648	2.65E-04	1.02E-03
RP11-517H2.7	7.910	4.889	1.340	3.648	2.64E-04	1.02E-03
ALDH3B2	5.774	5.019	1.374	3.652	2.61E-04	1.01E-03
SPTA1	8.447	4.269	1.167	3.659	2.53E-04	9.84E-04
AOC1	4.444	5.221	1.426	3.662	2.50E-04	9.72E-04

ITGA2	3.880	5.345	1.457	3.669	2.43E-04	9.47E-04
POU2F3	9.582	4.830	1.316	3.670	2.42E-04	9.44E-04
NSUN7	6.616	3.526	0.960	3.673	2.40E-04	9.35E-04
CH17-343M10.2	7.779	4.954	1.345	3.682	2.32E-04	9.05E-04
PDE6B	7.402	3.537	0.959	3.690	2.24E-04	8.78E-04
HAP1	4.023	5.357	1.452	3.691	2.24E-04	8.76E-04
RP11-424M21.1	4.324	5.278	1.428	3.697	2.19E-04	8.58E-04
RP11-320N7.1	16.547	2.162	0.584	3.700	2.16E-04	8.47E-04
CD300LB	11.472	4.793	1.292	3.711	2.07E-04	8.15E-04
ZEB2	15.051	2.149	0.579	3.712	2.05E-04	8.10E-04
CSAG1	63.638	4.665	1.254	3.721	1.99E-04	7.86E-04
CHST15	3.894	5.406	1.451	3.725	1.95E-04	7.73E-04
XIRP1	11.104	4.275	1.144	3.737	1.86E-04	7.40E-04
HPGDS	6.266	5.096	1.363	3.738	1.86E-04	7.39E-04
RP11-350N15.6	4.323	5.337	1.427	3.739	1.85E-04	7.35E-04
CXCL13	11.545	2.823	0.752	3.755	1.74E-04	6.95E-04
RP3-431A14.7	19.100	2.397	0.638	3.757	1.72E-04	6.88E-04
BMERB1	6.847	5.097	1.356	3.759	1.70E-04	6.83E-04
RP11-219B17.3	8.781	3.848	1.022	3.765	1.67E-04	6.69E-04
TSPAN18	12.502	3.644	0.967	3.768	1.65E-04	6.61E-04
LINC01122	3.889	5.459	1.447	3.772	1.62E-04	6.51E-04
PCSK1N	4.261	5.522	1.461	3.779	1.58E-04	6.36E-04
LINC01388	4.103	5.453	1.434	3.803	1.43E-04	5.83E-04
CACNA1G	14.234	2.353	0.618	3.805	1.42E-04	5.78E-04
HCAR2	12.992	4.314	1.132	3.809	1.39E-04	5.69E-04
CNIH3-AS1	4.564	5.398	1.413	3.821	1.33E-04	5.43E-04
PPIC	9.340	2.900	0.758	3.825	1.31E-04	5.35E-04
KRT5	16.513	2.415	0.630	3.830	1.28E-04	5.25E-04
FGL2	6.213	5.191	1.355	3.831	1.28E-04	5.23E-04
PNPLA3	10.776	2.656	0.693	3.831	1.28E-04	5.23E-04
CHSY3	7.417	4.059	1.058	3.838	1.24E-04	5.11E-04
RP11-7F17.1	15.017	2.523	0.657	3.839	1.24E-04	5.09E-04
ME3	10.092	3.068	0.799	3.840	1.23E-04	5.06E-04
CEACAM16-AS1	15.692	2.715	0.706	3.848	1.19E-04	4.91E-04
PSMA8	10.917	3.007	0.780	3.854	1.16E-04	4.82E-04
TRAJ45	8.352	3.886	1.008	3.854	1.16E-04	4.80E-04
RP11-465L8.1	4.206	5.551	1.439	3.858	1.15E-04	4.74E-04
CHRFAM7A	8.982	5.086	1.311	3.879	1.05E-04	4.38E-04
DLGAP1-AS5	10.080	5.142	1.324	3.883	1.03E-04	4.32E-04
E2F3P2	16.410	2.341	0.603	3.884	1.03E-04	4.30E-04
SYTL5	6.502	5.275	1.356	3.890	1.00E-04	4.20E-04
RP11-167H9.4	7.263	5.294	1.358	3.897	9.72E-05	4.08E-04
ACE	4.113	5.607	1.435	3.908	9.29E-05	3.92E-04
RP11-56P9.4	4.446	5.604	1.432	3.915	9.05E-05	3.82E-04
LPAR3	18.312	2.199	0.561	3.921	8.83E-05	3.74E-04
CYP4X1	10.067	3.347	0.852	3.929	8.53E-05	3.62E-04
PCYT1B	6.895	5.285	1.342	3.937	8.26E-05	3.52E-04
RP11-331F4.5	15.187	2.911	0.739	3.939	8.19E-05	3.49E-04
TRERNA1	11.899	2.610	0.660	3.956	7.64E-05	3.27E-04
CD33	17.620	5.132	1.296	3.960	7.50E-05	3.21E-04
RP1-300G12.2	4.228	5.787	1.458	3.968	7.25E-05	3.11E-04
SLC34A1	15.827	3.461	0.869	3.981	6.85E-05	2.95E-04
TMEM144	6.218	5.434	1.363	3.986	6.71E-05	2.89E-04
TLX2	8.061	4.086	1.024	3.991	6.57E-05	2.84E-04
SIX3-AS1	5.509	5.509	1.379	3.994	6.48E-05	2.80E-04
KCNA1	12.998	3.861	0.965	4.000	6.33E-05	2.74E-04
NPSR1-AS1	31.740	4.336	1.083	4.002	6.28E-05	2.72E-04
UPK1A	7.612	5.335	1.333	4.004	6.23E-05	2.70E-04

RP1-309H15.3	9.569	4.622	1.153	4.008	6.12E-05	2.65E-04
RP11-103J8.1	4.835	5.617	1.400	4.011	6.03E-05	2.62E-04
FBN2	12.094	5.217	1.298	4.019	5.84E-05	2.54E-04
RTN1	4.324	5.814	1.443	4.028	5.62E-05	2.45E-04
RP11-553A21.3	8.165	3.776	0.936	4.032	5.53E-05	2.41E-04
RP11-1166P10.1	5.039	5.741	1.423	4.036	5.44E-05	2.38E-04
SMARCD3	12.047	2.753	0.680	4.047	5.18E-05	2.27E-04
CHL1-AS2	9.753	3.671	0.904	4.059	4.94E-05	2.17E-04
RP11-486O13.2	4.636	5.719	1.405	4.071	4.69E-05	2.07E-04
LINC02694	6.030	5.578	1.370	4.072	4.67E-05	2.06E-04
LL21NC02-1C16.2	21.874	2.141	0.526	4.072	4.67E-05	2.06E-04
CYP2B6	7.506	5.466	1.340	4.080	4.50E-05	1.99E-04
LINC00475	9.174	4.756	1.165	4.082	4.46E-05	1.98E-04
FOXP2	9.184	3.281	0.803	4.086	4.39E-05	1.95E-04
CTD-2643I7.5	16.206	2.596	0.635	4.086	4.39E-05	1.95E-04
MYL9	12.472	2.778	0.680	4.087	4.37E-05	1.94E-04
SEMA6A-AS2	13.249	2.581	0.631	4.091	4.29E-05	1.91E-04
FAM160A1-DT	10.381	3.183	0.778	4.093	4.26E-05	1.90E-04
RP11-345P4.12	15.922	2.174	0.531	4.094	4.24E-05	1.89E-04
P2RY6	12.121	3.600	0.878	4.100	4.14E-05	1.85E-04
S100A14	11.517	5.277	1.287	4.100	4.13E-05	1.84E-04
RP11-305M3.6	12.062	3.176	0.774	4.102	4.10E-05	1.83E-04
STUM	8.850	3.479	0.848	4.103	4.08E-05	1.83E-04
CIART	12.017	3.058	0.741	4.127	3.68E-05	1.66E-04
MAGEA12	160.741	5.081	1.230	4.132	3.60E-05	1.62E-04
SMAD6	10.858	3.411	0.825	4.132	3.59E-05	1.62E-04
CLDN23	15.955	2.341	0.566	4.138	3.50E-05	1.58E-04
RP11-16K12.1	14.211	2.711	0.652	4.160	3.19E-05	1.45E-04
CREB3L1	12.705	2.763	0.663	4.166	3.10E-05	1.41E-04
FAT4	11.591	2.945	0.706	4.174	2.99E-05	1.36E-04
RP11-405A12.2	10.759	3.009	0.719	4.182	2.89E-05	1.32E-04
NELL2	16.323	2.202	0.527	4.182	2.89E-05	1.32E-04
CALD1	12.614	4.717	1.128	4.182	2.89E-05	1.32E-04
PTPRQ	14.040	2.847	0.681	4.182	2.88E-05	1.32E-04
CAVIN1	11.102	3.431	0.820	4.185	2.85E-05	1.31E-04
MC4R	5.684	5.763	1.377	4.186	2.84E-05	1.30E-04
MIR3659HG	13.592	2.512	0.599	4.193	2.75E-05	1.26E-04
ULBP1	24.925	2.065	0.490	4.213	2.52E-05	1.17E-04
DNAH8	9.155	5.468	1.297	4.216	2.49E-05	1.15E-04
CXCR2	12.376	3.022	0.716	4.223	2.41E-05	1.12E-04
SOWAHCP2	8.656	5.617	1.328	4.228	2.35E-05	1.09E-04
LCE1E	16.430	5.409	1.277	4.236	2.28E-05	1.06E-04
RP11-823E8.3	5.700	5.849	1.375	4.254	2.10E-05	9.80E-05
RP11-538D16.2	10.181	4.198	0.986	4.257	2.07E-05	9.68E-05
GABRB1	18.254	5.358	1.258	4.258	2.06E-05	9.66E-05
NR5A1	5.916	5.804	1.362	4.260	2.04E-05	9.57E-05
TMEM100	28.735	4.601	1.079	4.263	2.02E-05	9.46E-05
STMN4	25.527	2.360	0.552	4.277	1.89E-05	8.91E-05
ADGRD1-AS1	13.344	2.779	0.647	4.295	1.74E-05	8.26E-05
HOXA4	12.615	3.454	0.804	4.296	1.74E-05	8.23E-05
U91319.1	13.046	2.712	0.631	4.300	1.70E-05	8.09E-05
ZNF503	15.688	5.417	1.259	4.301	1.70E-05	8.09E-05
SLC38A4	18.132	2.197	0.510	4.308	1.64E-05	7.83E-05
RP11-120K24.3	14.725	3.204	0.742	4.316	1.59E-05	7.57E-05
FAM222A-AS1	14.254	4.815	1.114	4.321	1.55E-05	7.41E-05
NR2F1	11.953	4.895	1.127	4.345	1.39E-05	6.70E-05
IL36G	5.756	5.981	1.374	4.353	1.34E-05	6.47E-05
MAGEB6	6.501	5.887	1.352	4.355	1.33E-05	6.43E-05

WNT16	13.700	2.742	0.628	4.366	1.26E-05	6.13E-05
STAR	10.180	5.711	1.307	4.369	1.25E-05	6.07E-05
SYT8	11.185	3.242	0.740	4.381	1.18E-05	5.78E-05
ATP6V0E2-AS1	31.219	2.212	0.505	4.384	1.17E-05	5.71E-05
CTC-546K23.2	6.493	5.926	1.350	4.390	1.14E-05	5.56E-05
RP11-147L13.12	10.655	5.692	1.291	4.407	1.05E-05	5.15E-05
FXYD2	13.466	3.504	0.795	4.409	1.04E-05	5.11E-05
LGALS3BP	17.602	2.874	0.650	4.421	9.84E-06	4.86E-05
CLEC6A	12.007	3.896	0.877	4.442	8.93E-06	4.45E-05
AC005537.2	23.518	2.284	0.514	4.447	8.70E-06	4.34E-05
KIAA1614	11.918	3.373	0.757	4.453	8.47E-06	4.23E-05
FRMPD1	9.794	3.960	0.889	4.455	8.39E-06	4.19E-05
SATL1	13.796	3.175	0.712	4.457	8.31E-06	4.16E-05
FBXO39	9.288	5.780	1.296	4.460	8.21E-06	4.11E-05
ELAPOR1	11.702	3.299	0.739	4.465	8.01E-06	4.01E-05
KDELR3	17.781	2.404	0.538	4.471	7.79E-06	3.91E-05
NCR3LG1	37.774	2.430	0.543	4.472	7.76E-06	3.90E-05
MTARC2	16.249	2.674	0.598	4.476	7.62E-06	3.83E-05
RP11-686D22.10	5.815	6.174	1.378	4.480	7.48E-06	3.76E-05
RP3-439F8.1	12.974	3.586	0.798	4.495	6.94E-06	3.51E-05
DLX1	16.865	2.742	0.609	4.499	6.83E-06	3.46E-05
LINC01077	8.543	5.993	1.327	4.515	6.32E-06	3.22E-05
ST8SIA1	10.660	5.149	1.139	4.519	6.20E-06	3.16E-05
CTD-2124B8.3	20.703	2.333	0.516	4.521	6.16E-06	3.14E-05
CRIM1	14.042	3.232	0.713	4.536	5.73E-06	2.93E-05
TOMM20P2	6.076	6.148	1.355	4.536	5.72E-06	2.93E-05
COL27A1	23.337	2.143	0.471	4.551	5.33E-06	2.74E-05
ANKRD7	16.025	3.307	0.726	4.554	5.27E-06	2.72E-05
WDR64	27.237	2.550	0.560	4.557	5.19E-06	2.68E-05
CCL19	12.847	5.840	1.281	4.557	5.19E-06	2.68E-05
PCP4L1	6.957	6.194	1.358	4.561	5.08E-06	2.63E-05
VWA5B2	16.428	2.937	0.643	4.566	4.96E-06	2.57E-05
SPOCK1	12.046	5.819	1.272	4.574	4.79E-06	2.48E-05
RP11-223C24.1	11.545	5.856	1.279	4.577	4.71E-06	2.44E-05
RP11-368I7.6	30.539	2.066	0.451	4.578	4.70E-06	2.43E-05
PGLYRP4	16.878	5.747	1.250	4.596	4.31E-06	2.24E-05
KLRK1	12.929	2.942	0.638	4.609	4.04E-06	2.11E-05
LINC02832	14.368	5.923	1.285	4.611	4.01E-06	2.10E-05
CTTNBP2	12.044	3.530	0.765	4.612	3.99E-06	2.09E-05
ZNF572	7.247	6.153	1.334	4.613	3.98E-06	2.08E-05
RP11-229P13.27	16.475	2.530	0.548	4.614	3.95E-06	2.07E-05
TBC1D30	15.130	5.131	1.109	4.627	3.70E-06	1.94E-05
C12orf54	17.371	5.072	1.095	4.630	3.66E-06	1.92E-05
ANXA3	11.786	4.498	0.971	4.631	3.64E-06	1.91E-05
LL22NC03-N14H11.1	18.573	3.361	0.726	4.631	3.63E-06	1.91E-05
RP11-111A22.1	14.423	3.974	0.857	4.636	3.55E-06	1.87E-05
LINC01315	17.669	2.559	0.552	4.638	3.51E-06	1.85E-05
AC007091.1	10.205	6.068	1.296	4.683	2.83E-06	1.50E-05
COL6A1	13.198	3.104	0.663	4.684	2.81E-06	1.49E-05
FAM160A1	12.922	3.243	0.691	4.691	2.72E-06	1.45E-05
RP11-443B7.2	21.835	2.095	0.445	4.706	2.52E-06	1.35E-05
RP11-712B9.2	18.954	2.341	0.497	4.707	2.52E-06	1.35E-05
LINC01096	13.207	3.006	0.638	4.708	2.50E-06	1.34E-05
ZNF682	13.011	4.581	0.972	4.711	2.46E-06	1.32E-05
CTD-2201E18.5	17.437	3.082	0.653	4.722	2.33E-06	1.25E-05
RP11-306N14.1	15.844	2.836	0.600	4.723	2.33E-06	1.25E-05
RP11-42I10.1	14.367	3.469	0.732	4.739	2.14E-06	1.16E-05
JAML	13.624	3.359	0.707	4.752	2.02E-06	1.10E-05

RP11-526D8.12	28.077	3.590	0.755	4.755	1.98E-06	1.08E-05
CCR4	21.530	3.912	0.819	4.777	1.78E-06	9.74E-06
RP11-486O13.5	8.190	6.280	1.312	4.786	1.70E-06	9.35E-06
MAP7D2	33.069	2.344	0.488	4.801	1.58E-06	8.70E-06
RP11-1094M14.5	6.824	6.454	1.341	4.814	1.48E-06	8.22E-06
AC004538.3	6.931	6.479	1.346	4.815	1.47E-06	8.18E-06
SAMD3	19.823	2.558	0.531	4.818	1.45E-06	8.04E-06
CHST3	11.500	6.177	1.281	4.822	1.42E-06	7.92E-06
PROS1	22.651	2.152	0.446	4.825	1.40E-06	7.81E-06
RP11-76C10.6	16.420	3.134	0.649	4.828	1.38E-06	7.70E-06
MAGI2	19.610	2.697	0.558	4.836	1.32E-06	7.42E-06
RP11-523H20.3	25.284	2.314	0.478	4.846	1.26E-06	7.08E-06
HS3ST3A1	8.886	6.448	1.329	4.853	1.21E-06	6.84E-06
LINC02610	23.021	2.191	0.451	4.856	1.20E-06	6.76E-06
GOLGA8O	35.002	2.029	0.417	4.862	1.16E-06	6.57E-06
GPR87	9.139	6.342	1.303	4.868	1.12E-06	6.37E-06
GPRIN3	11.492	3.746	0.769	4.869	1.12E-06	6.36E-06
PTGER2	13.928	6.158	1.264	4.872	1.11E-06	6.27E-06
LINC00954	15.833	3.285	0.674	4.876	1.08E-06	6.15E-06
FAM135B	12.540	6.190	1.268	4.880	1.06E-06	6.02E-06
IFNA2	26.591	6.006	1.229	4.889	1.02E-06	5.80E-06
RP11-327F22.6	24.632	2.516	0.514	4.896	9.77E-07	5.59E-06
TMEM244	8.622	6.411	1.309	4.899	9.65E-07	5.52E-06
CALHM3	37.483	2.108	0.428	4.921	8.61E-07	4.95E-06
RP11-409I10.2	12.171	6.282	1.276	4.924	8.46E-07	4.87E-06
BNIP5	19.526	2.726	0.553	4.927	8.34E-07	4.80E-06
EFNA1	19.565	2.700	0.546	4.944	7.67E-07	4.44E-06
RP11-25H12.1	11.335	6.341	1.281	4.949	7.45E-07	4.32E-06
AP000439.1	13.500	3.555	0.717	4.955	7.22E-07	4.20E-06
NT5C1A	21.378	2.232	0.450	4.956	7.21E-07	4.19E-06
SLC45A1	13.819	3.868	0.779	4.966	6.84E-07	3.99E-06
PXT1	15.171	3.191	0.642	4.967	6.81E-07	3.98E-06
ACKR1	11.685	6.371	1.283	4.967	6.80E-07	3.98E-06
GPR84	19.102	2.899	0.584	4.969	6.73E-07	3.94E-06
SOX18	13.407	3.930	0.790	4.973	6.59E-07	3.86E-06
PLXNA4	22.071	6.142	1.235	4.974	6.57E-07	3.86E-06
ATG9B	14.969	3.864	0.775	4.986	6.15E-07	3.63E-06
CC2D2A	16.210	2.841	0.569	4.997	5.84E-07	3.45E-06
DMTN	19.262	4.615	0.922	5.003	5.64E-07	3.34E-06
ADRB2	13.547	3.564	0.711	5.013	5.37E-07	3.19E-06
AP001610.5	9.440	6.590	1.312	5.022	5.12E-07	3.04E-06
RP11-511B23.2	19.159	3.572	0.711	5.024	5.05E-07	3.00E-06
DNAH11	17.303	2.968	0.589	5.040	4.66E-07	2.78E-06
UGT2B7	17.546	6.349	1.257	5.051	4.40E-07	2.63E-06
CYSLTR2	13.992	4.083	0.805	5.070	3.99E-07	2.40E-06
AQP9	12.163	6.482	1.278	5.071	3.95E-07	2.38E-06
RPS20P22	17.872	4.172	0.822	5.074	3.90E-07	2.35E-06
OR7M1P	28.334	2.233	0.440	5.077	3.83E-07	2.31E-06
RP11-124N19.3	21.504	2.685	0.528	5.082	3.74E-07	2.27E-06
MTMR9LP	30.842	2.086	0.410	5.082	3.73E-07	2.26E-06
CH17-264B6.5	32.338	2.085	0.408	5.106	3.29E-07	2.01E-06
HBG2	10.353	6.566	1.285	5.109	3.24E-07	1.98E-06
MS4A4A	17.278	3.197	0.626	5.110	3.22E-07	1.97E-06
KIAA1671	19.363	2.659	0.519	5.121	3.04E-07	1.86E-06
NRXN1	66.574	4.501	0.879	5.122	3.02E-07	1.85E-06
HLX	24.383	2.147	0.418	5.132	2.87E-07	1.77E-06
SERPINA1	33.288	2.086	0.404	5.165	2.41E-07	1.50E-06
NHS	9.715	6.738	1.294	5.207	1.92E-07	1.20E-06

DLL4	20.723	2.897	0.556	5.212	1.87E-07	1.18E-06
FTH1P22	22.953	5.664	1.085	5.220	1.79E-07	1.13E-06
RP11-556I14.1	14.126	4.194	0.803	5.223	1.76E-07	1.11E-06
HOXA11-AS	17.497	4.340	0.830	5.226	1.73E-07	1.09E-06
MYOCOS	16.076	4.919	0.936	5.256	1.47E-07	9.36E-07
KLRC2	34.089	2.046	0.389	5.261	1.44E-07	9.14E-07
DSCAML1	25.594	2.534	0.481	5.273	1.34E-07	8.56E-07
RASAL1	18.518	4.903	0.930	5.275	1.33E-07	8.50E-07
BTBD19	29.615	2.515	0.477	5.275	1.33E-07	8.49E-07
ANO5	42.483	4.678	0.883	5.299	1.16E-07	7.48E-07
RP11-111G13.1	17.851	5.813	1.095	5.307	1.12E-07	7.21E-07
DISC1FP1	15.950	3.539	0.666	5.317	1.06E-07	6.84E-07
OSBPL6	31.919	2.031	0.380	5.337	9.43E-08	6.14E-07
IGFBP7	15.310	4.460	0.835	5.344	9.12E-08	5.96E-07
RP11-211G23.2	15.023	6.711	1.255	5.347	8.94E-08	5.85E-07
ACOT11	28.304	2.158	0.403	5.359	8.37E-08	5.50E-07
RP11-326C3.11	33.829	2.261	0.421	5.373	7.76E-08	5.11E-07
IQCJ-SCHIP1	15.721	3.406	0.634	5.375	7.66E-08	5.05E-07
KIAA0319	27.922	2.345	0.436	5.381	7.42E-08	4.90E-07
LMO7-AS1	23.567	2.514	0.466	5.391	7.01E-08	4.64E-07
LEF1-AS1	21.460	3.387	0.628	5.391	7.00E-08	4.64E-07
ACP3	32.645	2.268	0.420	5.402	6.57E-08	4.37E-07
MDGA1	18.547	5.006	0.926	5.407	6.39E-08	4.26E-07
AXL	11.718	6.906	1.275	5.416	6.09E-08	4.06E-07
CDHR1	17.243	5.968	1.100	5.427	5.73E-08	3.83E-07
F13A1	39.907	2.012	0.370	5.434	5.51E-08	3.69E-07
RP11-238F2.1	14.633	3.632	0.667	5.444	5.21E-08	3.51E-07
LINC01358	32.112	2.137	0.393	5.444	5.20E-08	3.51E-07
RP11-67L14.2	24.270	4.916	0.901	5.455	4.90E-08	3.32E-07
CDH12	12.857	6.977	1.278	5.459	4.79E-08	3.25E-07
SEC24AP1	29.641	2.420	0.442	5.470	4.50E-08	3.06E-07
EPHB2	19.305	6.835	1.237	5.526	3.27E-08	2.26E-07
OVOL1	19.035	3.406	0.609	5.591	2.26E-08	1.58E-07
CAMK2B	17.416	3.622	0.647	5.595	2.21E-08	1.55E-07
RP11-54O7.17	16.053	7.022	1.254	5.601	2.13E-08	1.50E-07
SUCNR1	21.142	5.114	0.912	5.605	2.08E-08	1.47E-07
RP11-88H10.3	29.909	6.881	1.218	5.649	1.61E-08	1.15E-07
RP11-1055B8.2	31.327	2.474	0.436	5.674	1.39E-08	1.00E-07
TPD52L1	24.066	3.168	0.557	5.684	1.31E-08	9.50E-08
CASC17	17.684	3.296	0.580	5.686	1.30E-08	9.44E-08
SUSD5	11.996	7.221	1.270	5.686	1.30E-08	9.40E-08
HNF1B	19.811	7.064	1.240	5.696	1.22E-08	8.87E-08
PRSS51	43.087	3.203	0.562	5.700	1.20E-08	8.70E-08
EDARADD	21.315	4.721	0.825	5.720	1.06E-08	7.76E-08
CACNB2	24.833	3.428	0.599	5.721	1.06E-08	7.75E-08
RP11-384F7.1	33.915	2.305	0.402	5.730	1.01E-08	7.37E-08
CCL28	22.750	2.697	0.470	5.735	9.74E-09	7.14E-08
SMPDL3B	18.120	4.780	0.832	5.746	9.15E-09	6.73E-08
RP1-65P5.3	24.492	2.906	0.504	5.761	8.38E-09	6.18E-08
AARD	36.201	2.026	0.351	5.774	7.72E-09	5.72E-08
TNFRSF11B	14.860	7.279	1.254	5.804	6.49E-09	4.84E-08
RP1-65P5.5	25.214	2.659	0.458	5.809	6.29E-09	4.69E-08
SMKR1	36.135	2.086	0.359	5.812	6.17E-09	4.61E-08
VWCE	26.102	2.571	0.442	5.815	6.07E-09	4.54E-08
FGD4	25.928	2.691	0.463	5.819	5.94E-09	4.44E-08
LINC02470	36.322	2.162	0.371	5.833	5.44E-09	4.09E-08
CASC15	20.432	3.850	0.659	5.839	5.24E-09	3.95E-08
CARMIL3	36.275	2.331	0.399	5.841	5.18E-09	3.91E-08

MERTK	25.777	3.439	0.586	5.869	4.39E-09	3.34E-08
MAFIP	18.803	7.418	1.262	5.877	4.19E-09	3.19E-08
RP11-87E22.2	46.918	2.167	0.367	5.898	3.67E-09	2.82E-08
LONRF3	21.418	3.858	0.652	5.914	3.34E-09	2.57E-08
RP11-463O12.5	20.487	3.690	0.624	5.917	3.28E-09	2.53E-08
ANKRD20A7P	19.108	3.647	0.616	5.917	3.27E-09	2.52E-08
BIK	21.737	3.027	0.511	5.928	3.07E-09	2.37E-08
FGD1	22.061	3.104	0.521	5.961	2.50E-09	1.95E-08
ACTG1P22	14.677	7.490	1.256	5.963	2.48E-09	1.93E-08
LPAR1	21.775	5.442	0.912	5.969	2.38E-09	1.87E-08
CUEDC1	32.085	2.650	0.443	5.979	2.25E-09	1.76E-08
GPR171	32.452	2.410	0.403	5.980	2.23E-09	1.75E-08
LRRC36	29.859	3.466	0.578	6.000	1.97E-09	1.55E-08
SBK1	37.656	2.169	0.361	6.002	1.95E-09	1.54E-08
TNK2-AS1	25.992	3.116	0.516	6.039	1.55E-09	1.23E-08
FAT2	20.424	7.484	1.238	6.047	1.48E-09	1.18E-08
KCNB2	18.201	7.522	1.242	6.055	1.41E-09	1.12E-08
LINC01629	40.197	2.306	0.380	6.063	1.34E-09	1.07E-08
DNAJC5B	31.540	2.738	0.451	6.069	1.29E-09	1.03E-08
RP11-121A8.1	32.960	2.387	0.393	6.080	1.21E-09	9.70E-09
ASB9	19.359	4.033	0.663	6.082	1.19E-09	9.57E-09
TSPAN11	31.739	2.625	0.430	6.106	1.02E-09	8.28E-09
PECAM1	39.360	2.404	0.392	6.127	8.96E-10	7.28E-09
RNLS	24.465	4.529	0.738	6.134	8.58E-10	6.98E-09
GPR150	19.474	4.582	0.746	6.140	8.23E-10	6.70E-09
SLFN12L	27.153	6.573	1.069	6.149	7.78E-10	6.35E-09
FRMPD2B	29.537	4.214	0.684	6.157	7.41E-10	6.06E-09
GLYATL2	26.291	2.881	0.467	6.168	6.94E-10	5.68E-09
LGALS8-AS1	37.890	2.296	0.372	6.175	6.62E-10	5.44E-09
AFF2	19.228	7.716	1.249	6.177	6.53E-10	5.37E-09
OR51B4	20.144	7.628	1.235	6.178	6.49E-10	5.34E-09
ZDHHC22	29.239	7.546	1.219	6.189	6.04E-10	4.97E-09
PDX1	17.219	7.703	1.244	6.191	5.98E-10	4.93E-09
DSC1	28.501	3.115	0.502	6.201	5.61E-10	4.64E-09
MUC13	25.405	2.943	0.474	6.206	5.42E-10	4.49E-09
ITGA5	71.166	6.480	1.043	6.215	5.13E-10	4.26E-09
IL1R1	43.530	2.310	0.372	6.216	5.09E-10	4.24E-09
EPB41L3	31.452	7.575	1.218	6.217	5.07E-10	4.22E-09
SAA2	25.721	3.288	0.528	6.223	4.88E-10	4.07E-09
HOXA11	26.234	3.270	0.524	6.237	4.46E-10	3.73E-09
PTGFRN	18.088	7.794	1.244	6.266	3.70E-10	3.13E-09
LINC01091	47.405	6.626	1.054	6.286	3.26E-10	2.76E-09
TNN	30.964	2.970	0.470	6.317	2.66E-10	2.27E-09
ITPKA	38.596	2.246	0.355	6.331	2.43E-10	2.07E-09
CCN3	23.459	5.045	0.796	6.336	2.36E-10	2.01E-09
PSD3	24.297	5.065	0.798	6.344	2.24E-10	1.92E-09
RANBP3L	28.093	3.049	0.480	6.353	2.11E-10	1.81E-09
GRM8	33.346	2.696	0.423	6.372	1.86E-10	1.60E-09
CRIP2	20.293	4.039	0.632	6.390	1.66E-10	1.44E-09
AC008697.1	44.431	2.009	0.314	6.402	1.54E-10	1.33E-09
HOXA3	37.331	5.672	0.884	6.419	1.38E-10	1.20E-09
A2M	39.281	6.771	1.055	6.420	1.36E-10	1.18E-09
GPR161	29.573	2.869	0.447	6.422	1.34E-10	1.17E-09
NEURL3	50.218	7.724	1.203	6.423	1.34E-10	1.17E-09
IL6R	30.009	2.889	0.449	6.434	1.24E-10	1.09E-09
KRT80	34.550	6.834	1.058	6.458	1.06E-10	9.34E-10
ROBO3	26.623	3.356	0.517	6.497	8.20E-11	7.31E-10
ICOS	42.513	2.409	0.370	6.501	7.96E-11	7.10E-10

COL5A3	30.539	4.679	0.720	6.502	7.91E-11	7.06E-10
SPAG6	39.038	2.488	0.383	6.503	7.86E-11	7.01E-10
RP11-147L13.13	27.543	5.183	0.794	6.523	6.88E-11	6.17E-10
RP11-214O1.2	63.658	7.838	1.199	6.538	6.22E-11	5.60E-10
DHRS9	25.086	5.214	0.797	6.544	5.97E-11	5.38E-10
TRIM47	47.897	2.565	0.392	6.548	5.85E-11	5.29E-10
CNIH2	45.910	2.165	0.330	6.554	5.61E-11	5.08E-10
RHOXF1	62.915	7.855	1.199	6.554	5.60E-11	5.08E-10
DMRTA2	25.444	5.235	0.799	6.555	5.58E-11	5.06E-10
RP11-215D10.3	31.907	5.174	0.784	6.598	4.16E-11	3.81E-10
CROCCP3	55.314	2.027	0.307	6.603	4.03E-11	3.70E-10
GNG4	44.643	7.967	1.206	6.608	3.88E-11	3.57E-10
DUXAP9	50.168	4.331	0.651	6.650	2.92E-11	2.71E-10
LTBP2	30.637	3.655	0.550	6.651	2.91E-11	2.70E-10
RP11-810C16.2	37.588	2.355	0.354	6.656	2.82E-11	2.62E-10
RP11-791G22.3	38.791	3.014	0.452	6.673	2.50E-11	2.33E-10
LINC00462	51.090	6.996	1.045	6.693	2.19E-11	2.05E-10
IL4	40.502	2.532	0.376	6.730	1.69E-11	1.60E-10
SNPH	40.844	2.230	0.331	6.736	1.63E-11	1.54E-10
DHRS2	53.590	2.662	0.395	6.747	1.51E-11	1.43E-10
NUAK1	26.614	8.278	1.223	6.770	1.29E-11	1.23E-10
SLC6A8	31.527	6.040	0.887	6.812	9.64E-12	9.26E-11
ARLNC1	40.658	2.332	0.342	6.813	9.56E-12	9.19E-11
OCLN	31.475	4.511	0.660	6.830	8.50E-12	8.20E-11
OR51B5	58.065	7.200	1.045	6.891	5.53E-12	5.40E-11
IRS1	44.493	2.320	0.336	6.907	4.94E-12	4.84E-11
LINC00674	60.710	7.215	1.042	6.923	4.42E-12	4.35E-11
SNCA	30.735	4.349	0.627	6.941	3.89E-12	3.85E-11
C2orf88	23.492	3.881	0.558	6.959	3.44E-12	3.41E-11
GGT6	33.209	3.812	0.547	6.970	3.17E-12	3.16E-11
BACE1	53.313	2.663	0.379	7.033	2.02E-12	2.05E-11
SYT6	25.897	4.265	0.606	7.040	1.93E-12	1.95E-11
ARFGEF3	68.888	8.455	1.196	7.070	1.55E-12	1.58E-11
PTPRB	31.245	6.273	0.886	7.081	1.43E-12	1.46E-11
HCAR3	47.123	4.566	0.644	7.092	1.33E-12	1.36E-11
DTHD1	82.805	2.156	0.304	7.093	1.31E-12	1.34E-11
APLN	34.146	2.885	0.400	7.213	5.46E-13	5.73E-12
GNG11	53.066	2.132	0.294	7.253	4.09E-13	4.32E-12
KIAA1522	44.943	2.441	0.337	7.253	4.08E-13	4.31E-12
TRAJ49	34.229	3.358	0.462	7.270	3.61E-13	3.83E-12
LRRN1	73.619	8.681	1.194	7.270	3.59E-13	3.81E-12
CNTNAP3	54.292	2.173	0.298	7.282	3.30E-13	3.51E-12
GALNTL6	65.724	2.032	0.278	7.305	2.77E-13	2.96E-12
GSPT2	27.900	4.920	0.670	7.348	2.01E-13	2.17E-12
RP11-534K14.5	38.170	2.715	0.369	7.356	1.89E-13	2.05E-12
LINC00881	44.409	2.591	0.352	7.369	1.73E-13	1.88E-12
TBX15	88.782	7.637	1.036	7.372	1.68E-13	1.83E-12
SPINT1-AS1	33.468	3.583	0.485	7.384	1.54E-13	1.67E-12
SLC9A3R2	40.385	2.790	0.377	7.393	1.43E-13	1.56E-12
CD38	123.016	2.778	0.376	7.393	1.43E-13	1.56E-12
LINC01451	32.410	5.832	0.788	7.400	1.36E-13	1.49E-12
ADGRE4P	75.260	5.575	0.753	7.406	1.30E-13	1.42E-12
SPINK2	40.699	5.697	0.769	7.408	1.28E-13	1.41E-12
FGF2	53.812	4.218	0.568	7.430	1.09E-13	1.20E-12
HOXA10	57.752	8.938	1.199	7.456	8.91E-14	9.86E-13
FCRL4	88.481	2.394	0.321	7.458	8.77E-14	9.72E-13
LNCTAM34A	32.147	5.286	0.707	7.474	7.77E-14	8.63E-13
PIMREG	82.363	6.424	0.856	7.505	6.15E-14	6.88E-13

RHOXF1-AS1	198.352	8.947	1.186	7.545	4.53E-14	5.13E-13
RASGRF1	71.695	2.036	0.270	7.551	4.34E-14	4.91E-13
IGHG3	376.332	3.421	0.449	7.615	2.64E-14	3.03E-13
PLAU	37.206	3.153	0.414	7.615	2.63E-14	3.03E-13
SHOX2	67.464	2.215	0.290	7.627	2.41E-14	2.78E-13
GBP6	37.528	2.795	0.367	7.627	2.40E-14	2.77E-13
AC007405.6	37.826	3.465	0.454	7.635	2.26E-14	2.61E-13
CTD-2292N2.1	32.726	4.351	0.570	7.638	2.21E-14	2.55E-13
NGB	43.104	5.867	0.766	7.654	1.94E-14	2.26E-13
RP4-742C19.12	42.282	2.894	0.377	7.669	1.73E-14	2.02E-13
MOB3B	111.883	4.441	0.578	7.680	1.59E-14	1.86E-13
C10orf99	38.679	2.865	0.373	7.682	1.57E-14	1.84E-13
RBMS1	58.620	2.919	0.380	7.687	1.51E-14	1.77E-13
MAGEA1	193.610	6.513	0.846	7.700	1.36E-14	1.59E-13
CAV2	37.375	3.280	0.426	7.707	1.29E-14	1.51E-13
LRP4	35.717	3.357	0.435	7.709	1.27E-14	1.50E-13
FCHO2	36.327	4.153	0.538	7.713	1.23E-14	1.45E-13
RP11-334L9.2	55.730	6.664	0.862	7.728	1.09E-14	1.29E-13
RIMBP2	72.685	2.152	0.278	7.735	1.03E-14	1.22E-13
WSCD1	105.977	8.012	1.035	7.744	9.64E-15	1.14E-13
H3C6	41.272	3.058	0.395	7.749	9.24E-15	1.10E-13
LINC01402	44.550	4.705	0.605	7.773	7.68E-15	9.18E-14
GBP1	46.249	2.689	0.346	7.775	7.55E-15	9.03E-14
SIX3	72.245	9.301	1.196	7.779	7.29E-15	8.74E-14
NRTN	30.996	3.938	0.505	7.791	6.64E-15	7.99E-14
CCR8	50.136	5.913	0.759	7.793	6.55E-15	7.88E-14
CPM	66.729	2.014	0.258	7.814	5.53E-15	6.68E-14
CERKL	82.811	2.197	0.281	7.815	5.49E-15	6.65E-14
ABHD1	34.540	4.788	0.613	7.817	5.42E-15	6.56E-14
WNT7B	31.796	3.544	0.453	7.825	5.06E-15	6.14E-14
EPB41L4A	44.823	2.788	0.356	7.833	4.77E-15	5.79E-14
KRT7	63.903	2.307	0.294	7.850	4.17E-15	5.08E-14
LFNG	56.634	2.731	0.346	7.883	3.19E-15	3.92E-14
CD101	75.431	2.647	0.335	7.911	2.54E-15	3.13E-14
RP11-492E3.2	77.306	2.710	0.342	7.917	2.43E-15	3.00E-14
MMP7	177.556	8.198	1.030	7.958	1.75E-15	2.17E-14
TNC	57.319	2.604	0.327	7.971	1.57E-15	1.96E-14
HOXB6	47.464	4.000	0.501	7.981	1.46E-15	1.82E-14
LINC02539	52.464	2.503	0.313	7.989	1.36E-15	1.70E-14
TRAT1	80.932	2.299	0.286	8.043	8.76E-16	1.11E-14
C14orf132	68.950	9.647	1.195	8.070	7.01E-16	8.95E-15
KSR2	62.110	9.681	1.198	8.081	6.44E-16	8.23E-15
PLAAT3	68.120	2.154	0.266	8.083	6.33E-16	8.10E-15
RP11-640F22.1	82.351	4.083	0.505	8.086	6.17E-16	7.90E-15
NDRG2	33.189	5.006	0.618	8.095	5.72E-16	7.35E-15
DPYD-AS1	69.052	6.995	0.858	8.152	3.59E-16	4.63E-15
BDNF	64.898	2.129	0.261	8.165	3.23E-16	4.18E-15
KIRREL2	40.829	4.699	0.575	8.177	2.92E-16	3.79E-15
ROBO2	800.433	2.142	0.262	8.189	2.64E-16	3.44E-15
KCNN1	60.778	2.402	0.292	8.221	2.02E-16	2.66E-15
RP11-203B7.2	57.687	3.136	0.380	8.255	1.51E-16	2.01E-15
MCF2L2	56.559	2.577	0.312	8.263	1.42E-16	1.88E-15
ARHGAP23	57.404	3.701	0.448	8.269	1.36E-16	1.80E-15
ASPHD1	40.517	3.752	0.454	8.269	1.35E-16	1.79E-15
LINC02051	51.379	5.710	0.688	8.304	1.01E-16	1.35E-15
DAB2IP	56.950	2.462	0.296	8.325	8.44E-17	1.13E-15
KLRK1-AS1	59.708	3.251	0.391	8.325	8.41E-17	1.13E-15
CNFN	60.089	2.396	0.287	8.342	7.33E-17	9.88E-16

SHISA9	38.400	4.472	0.536	8.345	7.15E-17	9.65E-16
ELF3	66.299	3.818	0.457	8.352	6.71E-17	9.07E-16
RP11-85O21.4	53.359	2.830	0.338	8.365	6.03E-17	8.18E-16
CPNE4	79.134	2.872	0.343	8.377	5.43E-17	7.37E-16
DEPDC7	44.530	3.634	0.434	8.380	5.29E-17	7.19E-16
CASKIN2	74.412	2.388	0.285	8.384	5.12E-17	6.97E-16
CHODL	65.400	2.551	0.303	8.408	4.17E-17	5.69E-16
LRP2	37.710	4.380	0.520	8.418	3.83E-17	5.24E-16
FYB1	1281.508	4.005	0.474	8.453	2.84E-17	3.92E-16
RP11-556I14.2	64.431	2.208	0.261	8.473	2.40E-17	3.33E-16
DIRAS1	62.127	2.477	0.292	8.476	2.33E-17	3.24E-16
S100A6	55.578	2.790	0.328	8.513	1.70E-17	2.38E-16
ADAMTS17	73.740	2.712	0.318	8.530	1.46E-17	2.06E-16
CEBPD	46.115	4.945	0.575	8.604	7.68E-18	1.09E-16
SPOCK2	55.821	2.847	0.331	8.611	7.25E-18	1.03E-16
FAM221A	44.134	4.935	0.573	8.612	7.16E-18	1.02E-16
CTC-546K23.1	84.233	7.361	0.855	8.613	7.10E-18	1.01E-16
TNFSF12	50.902	4.443	0.516	8.618	6.80E-18	9.69E-17
PLCD3	67.319	2.457	0.284	8.661	4.66E-18	6.70E-17
RP11-386M24.10	44.913	3.411	0.393	8.675	4.14E-18	5.97E-17
ARHGAP20	54.461	6.579	0.758	8.679	3.98E-18	5.75E-17
AC007743.1	102.928	10.434	1.190	8.767	1.84E-18	2.70E-17
RORB	48.148	4.554	0.518	8.796	1.41E-18	2.09E-17
HRH2	42.275	3.335	0.378	8.815	1.19E-18	1.78E-17
HNRNPA1P21	50.075	4.374	0.495	8.838	9.76E-19	1.46E-17
CYS1	67.144	2.878	0.326	8.840	9.56E-19	1.43E-17
ABCA1	51.751	3.159	0.357	8.842	9.44E-19	1.42E-17
NAP1L3	43.845	4.867	0.546	8.916	4.85E-19	7.37E-18
CSGALNACT1	66.742	3.268	0.367	8.916	4.84E-19	7.36E-18
ANXA1	69.651	2.855	0.320	8.924	4.49E-19	6.85E-18
C3	71.645	2.957	0.331	8.933	4.16E-19	6.35E-18
CFAP58	61.754	2.690	0.300	8.955	3.40E-19	5.22E-18
PTGS1	59.327	2.993	0.334	8.957	3.34E-19	5.13E-18
RASSF8-AS1	53.678	5.361	0.595	9.014	1.99E-19	3.09E-18
ZG16B	80.683	2.433	0.269	9.041	1.55E-19	2.41E-18
CCL2	286.790	10.709	1.183	9.051	1.41E-19	2.21E-18
DIP2C	105.375	2.015	0.222	9.083	1.06E-19	1.67E-18
SLFN13	93.612	7.743	0.852	9.091	9.78E-20	1.54E-18
SERPINB10	118.861	2.671	0.294	9.098	9.19E-20	1.45E-18
CPS1	51.031	3.793	0.416	9.109	8.33E-20	1.32E-18
IL10RB-DT	95.370	2.013	0.221	9.120	7.49E-20	1.18E-18
ANO3	82.570	2.279	0.249	9.163	5.05E-20	8.07E-19
IFNG	46.242	4.199	0.457	9.187	4.04E-20	6.49E-19
GLIS3	84.797	2.511	0.272	9.228	2.76E-20	4.47E-19
FSTL1	46.094	3.506	0.380	9.237	2.54E-20	4.14E-19
SDC4	46.637	4.496	0.484	9.287	1.59E-20	2.61E-19
PRLR	65.878	5.448	0.584	9.325	1.11E-20	1.82E-19
SPINT2	64.105	2.937	0.314	9.362	7.86E-21	1.30E-19
C15orf62	81.691	2.432	0.260	9.367	7.47E-21	1.24E-19
LOXL4	61.827	2.741	0.292	9.376	6.85E-21	1.14E-19
DLG3	69.553	2.728	0.291	9.380	6.57E-21	1.09E-19
PRKAA2	232.499	11.236	1.184	9.489	2.34E-21	3.97E-20
RP11-613M5.5	79.588	2.330	0.245	9.496	2.18E-21	3.70E-20
UNQ6494	54.723	3.701	0.390	9.497	2.16E-21	3.67E-20
LINC02520	63.118	3.474	0.365	9.508	1.95E-21	3.31E-20
SMAD9	53.983	3.007	0.315	9.538	1.45E-21	2.49E-20
TRIM7	117.929	2.075	0.217	9.564	1.14E-21	1.95E-20
CACNA1D	65.777	4.653	0.486	9.568	1.09E-21	1.88E-20

UPB1	101.293	2.371	0.247	9.589	8.94E-22	1.55E-20
FOXA3	86.529	2.800	0.292	9.593	8.54E-22	1.48E-20
COL4A6	227.635	11.370	1.184	9.603	7.80E-22	1.35E-20
IGLV6-57	89.864	2.608	0.269	9.684	3.54E-22	6.23E-21
ULK2	57.440	2.946	0.304	9.690	3.33E-22	5.86E-21
RP11-88I21.3	62.111	4.109	0.424	9.690	3.32E-22	5.85E-21
GRB10	46.376	4.475	0.460	9.725	2.35E-22	4.17E-21
RP1-158P9.2	66.828	3.785	0.389	9.726	2.35E-22	4.16E-21
SPTB	72.233	3.640	0.374	9.729	2.28E-22	4.04E-21
RP11-76C10.2	80.272	2.485	0.255	9.742	1.99E-22	3.55E-21
RP11-356M20.1	131.653	4.964	0.509	9.755	1.76E-22	3.14E-21
FEZ1	110.822	2.154	0.221	9.757	1.72E-22	3.09E-21
RP11-472K17.3	362.093	7.188	0.730	9.850	6.85E-23	1.25E-21
C2orf72	57.410	3.148	0.319	9.866	5.84E-23	1.07E-21
MAPK4	240.723	11.679	1.184	9.867	5.80E-23	1.06E-21
HOXA6	70.997	3.419	0.346	9.871	5.58E-23	1.02E-21
A4GALT	74.436	3.144	0.316	9.961	2.25E-23	4.18E-22
LRG1	65.618	3.299	0.331	9.963	2.21E-23	4.10E-22
RP11-76C10.3	94.701	2.596	0.260	9.978	1.90E-23	3.55E-22
PTPRM	66.708	3.390	0.338	10.024	1.20E-23	2.25E-22
PRR5L	65.036	3.347	0.333	10.054	8.82E-24	1.67E-22
ADCY6	135.149	6.691	0.663	10.086	6.36E-24	1.21E-22
PTPRG-AS1	69.016	4.449	0.440	10.120	4.51E-24	8.63E-23
SOCS2-AS1	54.134	4.226	0.415	10.172	2.63E-24	5.10E-23
ARRB1	112.147	7.569	0.741	10.219	1.62E-24	3.15E-23
ITGB8-AS1	88.292	6.307	0.617	10.223	1.57E-24	3.05E-23
FRMPD3	51.116	4.541	0.442	10.262	1.04E-24	2.04E-23
PLD4	82.779	6.362	0.619	10.272	9.43E-25	1.85E-23
RP11-61G19.1	124.529	2.114	0.206	10.276	9.08E-25	1.78E-23
MAB21L1	55.838	4.634	0.448	10.341	4.62E-25	9.13E-24
MCF2L	65.068	3.486	0.336	10.364	3.62E-25	7.18E-24
CISH	105.067	2.433	0.235	10.374	3.25E-25	6.44E-24
GHR	1055.518	8.703	0.836	10.405	2.36E-25	4.71E-24
LINC01132	64.815	3.349	0.322	10.412	2.18E-25	4.37E-24
PODXL	67.722	3.141	0.301	10.433	1.75E-25	3.52E-24
CTA-384D8.34	93.861	2.832	0.271	10.462	1.29E-25	2.60E-24
RSAD2	111.714	6.440	0.614	10.493	9.32E-26	1.90E-24
MED12L	112.547	2.299	0.218	10.529	6.35E-26	1.31E-24
RNF43	113.047	2.803	0.266	10.529	6.33E-26	1.30E-24
FLVCR2	114.173	2.335	0.221	10.577	3.79E-26	7.87E-25
IRF6	75.601	3.032	0.287	10.582	3.63E-26	7.53E-25
WDFY3	82.634	2.681	0.253	10.583	3.56E-26	7.41E-25
MMP9	90.480	3.399	0.321	10.591	3.29E-26	6.86E-25
RP11-115D19.1	65.008	3.860	0.364	10.598	3.05E-26	6.38E-25
FNDC10	93.235	2.387	0.225	10.603	2.88E-26	6.04E-25
LINC01619	148.024	2.032	0.191	10.627	2.23E-26	4.70E-25
TGFBR3L	125.627	2.576	0.242	10.662	1.54E-26	3.27E-25
MTUS2	66.462	5.638	0.527	10.693	1.10E-26	2.36E-25
ZNF853	83.862	5.804	0.543	10.693	1.10E-26	2.36E-25
SULF2	63.661	4.045	0.378	10.693	1.09E-26	2.35E-25
TCEAL9	161.884	7.865	0.734	10.716	8.55E-27	1.84E-25
HOXA5	94.816	2.998	0.279	10.744	6.32E-27	1.37E-25
BACE2	86.795	2.977	0.276	10.770	4.78E-27	1.04E-25
GABRA4	157.340	2.644	0.244	10.859	1.81E-27	4.01E-26
RP11-163N15.2	66.796	4.190	0.386	10.865	1.70E-27	3.77E-26
RP11-76C10.4	99.392	2.534	0.233	10.888	1.31E-27	2.93E-26
CYBB	121.865	4.318	0.396	10.891	1.28E-27	2.85E-26
CHST7	173.108	2.063	0.189	10.896	1.20E-27	2.69E-26

EPHA3	822.164	7.920	0.726	10.906	1.08E-27	2.43E-26
SPRED2	151.189	2.160	0.197	10.942	7.28E-28	1.64E-26
PDGFRB	68.355	4.365	0.399	10.948	6.76E-28	1.52E-26
CCDC198	131.384	6.217	0.567	10.956	6.20E-28	1.40E-26
SLC16A14	73.070	4.419	0.403	10.978	4.87E-28	1.10E-26
HS3ST1	70.961	3.426	0.311	11.027	2.82E-28	6.43E-27
CR1L	64.479	4.286	0.384	11.155	6.79E-29	1.58E-27
ATP7B	164.886	2.052	0.184	11.178	5.22E-29	1.22E-27
MCF2L-AS1	98.411	2.835	0.253	11.213	3.53E-29	8.26E-28
DLGAP3	98.608	3.109	0.276	11.245	2.46E-29	5.79E-28
LRRTM4-AS1	285.081	9.477	0.840	11.279	1.66E-29	3.93E-28
TLL2	84.638	3.029	0.267	11.333	9.04E-30	2.16E-28
CD84	159.262	2.066	0.182	11.345	7.87E-30	1.89E-28
DUSP6	75.267	4.798	0.422	11.358	6.76E-30	1.62E-28
CFAP57	112.276	2.833	0.249	11.379	5.31E-30	1.28E-28
INKA1	117.493	2.525	0.221	11.398	4.28E-30	1.03E-28
SAMD14	108.041	2.870	0.251	11.450	2.35E-30	5.69E-29
FAM171A2	200.201	2.013	0.176	11.453	2.26E-30	5.50E-29
LINC02653	65.251	3.807	0.332	11.462	2.05E-30	5.00E-29
PTPRD	294.085	8.378	0.731	11.467	1.94E-30	4.71E-29
SNTB1	72.480	4.622	0.403	11.468	1.91E-30	4.65E-29
LINC02888	113.721	2.364	0.206	11.501	1.30E-30	3.18E-29
SLC2A9	73.729	3.545	0.308	11.515	1.11E-30	2.73E-29
ITGB8	125.394	6.539	0.567	11.523	1.01E-30	2.48E-29
IL23R	153.262	2.633	0.228	11.530	9.35E-31	2.31E-29
LINC02055	83.059	5.989	0.517	11.573	5.62E-31	1.39E-29
NBPF1	99.733	2.863	0.247	11.591	4.55E-31	1.13E-29
ICAM5	161.554	2.185	0.188	11.600	4.14E-31	1.03E-29
HRAT92	74.174	3.878	0.334	11.608	3.76E-31	9.40E-30
EFNB2	183.628	2.138	0.184	11.644	2.45E-31	6.18E-30
ENAH	167.969	2.112	0.181	11.649	2.31E-31	5.84E-30
ADCY9	80.462	3.503	0.301	11.652	2.23E-31	5.64E-30
RP11-305F5.3	88.391	4.770	0.409	11.660	2.05E-31	5.18E-30
PCDHGC3	101.533	2.903	0.247	11.764	5.97E-32	1.54E-30
SDC3	147.705	2.890	0.246	11.772	5.44E-32	1.41E-30
NPTXR	79.451	5.412	0.458	11.814	3.30E-32	8.59E-31
RP11-85O21.2	73.404	4.195	0.354	11.855	2.03E-32	5.33E-31
PWWP3B	108.803	4.544	0.382	11.905	1.11E-32	2.93E-31
ZSCAN31	141.848	2.406	0.202	11.910	1.05E-32	2.77E-31
ADAMTS3	97.742	4.439	0.370	11.981	4.45E-33	1.19E-31
NT5DC4	106.067	3.485	0.291	11.990	4.00E-33	1.07E-31
KIF5A	78.528	3.942	0.328	12.012	3.09E-33	8.32E-32
DDX60L	202.858	2.070	0.172	12.045	2.07E-33	5.62E-32
SCNN1G	112.372	3.791	0.313	12.094	1.14E-33	3.12E-32
ADGRB2	92.638	3.273	0.270	12.133	7.02E-34	1.93E-32
AC005083.1	133.891	2.686	0.218	12.298	9.24E-35	2.61E-33
TMEM132D	104.448	3.447	0.279	12.334	5.94E-35	1.68E-33
SOX2-OT	80.834	3.743	0.303	12.346	5.10E-35	1.45E-33
REC8	258.070	2.097	0.170	12.358	4.43E-35	1.26E-33
BCL2L14	112.697	3.211	0.259	12.391	2.92E-35	8.37E-34
TNFRSF18	177.815	2.046	0.165	12.419	2.06E-35	5.92E-34
GPAT3	89.862	4.456	0.358	12.443	1.53E-35	4.42E-34
RP4-781K5.6	143.362	2.550	0.205	12.449	1.41E-35	4.09E-34
B3GNT5	160.494	2.317	0.184	12.568	3.18E-36	9.39E-35
TRIM55	232.724	5.715	0.453	12.604	2.00E-36	5.91E-35
RGL3	98.465	5.558	0.440	12.633	1.39E-36	4.14E-35
STYK1	101.993	3.218	0.255	12.633	1.38E-36	4.13E-35
SV2C	105.035	3.151	0.248	12.686	7.09E-37	2.13E-35

SMPD3	142.113	2.635	0.208	12.697	6.18E-37	1.85E-35
IGSF9B	110.957	5.383	0.424	12.708	5.36E-37	1.62E-35
CD24	107.359	3.637	0.285	12.746	3.30E-37	9.97E-36
PROCA1	148.753	2.536	0.198	12.782	2.08E-37	6.31E-36
ITGAM	153.865	3.198	0.250	12.809	1.46E-37	4.45E-36
MEST	118.951	3.576	0.276	12.942	2.61E-38	8.11E-37
CEP170B	85.815	4.001	0.309	12.951	2.32E-38	7.22E-37
PLD1	611.345	8.458	0.651	12.996	1.29E-38	4.04E-37
SELENON	108.665	3.469	0.266	13.036	7.64E-39	2.40E-37
HPCAL4	86.425	4.677	0.358	13.049	6.46E-39	2.03E-37
FOXC1	117.551	5.307	0.406	13.070	4.90E-39	1.54E-37
BHLHE41	200.093	2.459	0.188	13.085	4.04E-39	1.28E-37
SEMA5A	85.517	4.710	0.360	13.101	3.27E-39	1.04E-37
NOTUM	130.038	3.182	0.241	13.193	9.68E-40	3.12E-38
PGF	151.668	2.616	0.197	13.246	4.77E-40	1.55E-38
RP11-432J24.5	189.447	2.425	0.183	13.253	4.34E-40	1.41E-38
C1orf54	166.377	2.447	0.183	13.343	1.30E-40	4.27E-39
FOSL1	115.633	4.431	0.332	13.352	1.16E-40	3.82E-39
EDN1	240.755	2.080	0.156	13.368	9.30E-41	3.09E-39
NUS1P2	173.678	2.430	0.181	13.400	6.02E-41	2.01E-39
MNDA	224.934	6.661	0.496	13.426	4.27E-41	1.43E-39
CKB	171.243	2.593	0.193	13.430	4.05E-41	1.36E-39
NEUROG2-AS1	120.272	4.947	0.367	13.477	2.14E-41	7.17E-40
PLXND1	223.078	2.153	0.160	13.483	1.96E-41	6.60E-40
LINC00888	125.334	3.711	0.273	13.608	3.58E-42	1.23E-40
BAIAP2	170.992	2.507	0.184	13.633	2.53E-42	8.74E-41
TESK2	245.936	2.092	0.153	13.673	1.48E-42	5.15E-41
SIX4	126.685	4.712	0.343	13.729	6.78E-43	2.37E-41
LINC02341	205.105	2.454	0.179	13.733	6.45E-43	2.26E-41
PTPN14	137.316	4.429	0.321	13.795	2.73E-43	9.64E-42
KLF7	147.034	5.245	0.380	13.809	2.26E-43	8.03E-42
SLCO2B1	134.625	5.395	0.390	13.841	1.44E-43	5.13E-42
PRKAR2B	119.582	3.563	0.257	13.845	1.36E-43	4.86E-42
PTGIR	170.210	2.759	0.199	13.856	1.17E-43	4.17E-42
PLEKHG6	124.592	3.762	0.271	13.884	7.92E-44	2.84E-42
MIR34AHG	115.971	4.679	0.337	13.904	6.00E-44	2.16E-42
F5	108.378	5.318	0.382	13.935	3.90E-44	1.41E-42
CLIC2	324.593	2.688	0.191	14.068	5.94E-45	2.16E-43
FBXL16	154.956	2.984	0.212	14.099	3.84E-45	1.41E-43
FUT4	140.751	3.644	0.258	14.126	2.62E-45	9.72E-44
AEBP1	330.219	7.854	0.555	14.147	1.95E-45	7.27E-44
SLC30A3	117.757	3.523	0.248	14.179	1.23E-45	4.63E-44
UBE2QL1	128.108	6.103	0.430	14.197	9.62E-46	3.63E-44
MAB21L3	294.834	6.371	0.449	14.200	9.22E-46	3.48E-44
DUXAP10	224.401	3.465	0.244	14.207	8.25E-46	3.12E-44
MPEG1	154.879	2.678	0.188	14.257	4.06E-46	1.55E-44
RUNDC3A-AS1	145.519	3.266	0.227	14.419	3.93E-47	1.52E-45
ECHDC3	238.480	2.120	0.147	14.429	3.39E-47	1.32E-45
APOBR	197.169	2.619	0.181	14.474	1.76E-47	6.88E-46
SCN8A	139.495	4.042	0.279	14.482	1.58E-47	6.18E-46
C9orf139	189.760	2.560	0.176	14.558	5.22E-48	2.06E-46
JPH4	152.155	4.868	0.333	14.627	1.88E-48	7.53E-47
UBASH3B	176.717	3.130	0.213	14.678	8.91E-49	3.61E-47
TMEM266	173.548	2.870	0.195	14.722	4.63E-49	1.88E-47
IRF9	333.897	2.014	0.137	14.724	4.52E-49	1.84E-47
EPHA10	229.572	2.187	0.148	14.794	1.59E-49	6.53E-48
KHDRBS3	246.974	2.055	0.137	14.985	9.22E-51	3.87E-49
COL4A5	848.215	9.741	0.649	15.004	6.93E-51	2.92E-49

LINC00884	143.128	3.341	0.222	15.075	2.36E-51	1.00E-49
IVL	210.072	4.110	0.273	15.077	2.28E-51	9.70E-50
EPB41L1	130.146	3.746	0.245	15.279	1.06E-52	4.58E-51
DELEC1	141.024	3.707	0.242	15.285	9.65E-53	4.20E-51
CMPK2	224.477	6.011	0.392	15.332	4.67E-53	2.04E-51
RASSF8	170.273	5.806	0.377	15.386	2.03E-53	8.92E-52
LINC00958	374.802	8.530	0.554	15.402	1.59E-53	6.99E-52
PLAGL1	171.750	3.602	0.232	15.532	2.10E-54	9.36E-53
SLC35G2	157.400	5.072	0.325	15.595	7.82E-55	3.52E-53
SATB2-AS1	146.459	3.916	0.250	15.681	2.04E-55	9.30E-54
IL17RB	590.444	6.706	0.425	15.760	5.85E-56	2.71E-54
IL1B	308.753	7.070	0.448	15.780	4.26E-56	1.98E-54
MYO3B	179.239	3.951	0.250	15.781	4.17E-56	1.94E-54
OASL	210.946	2.848	0.180	15.824	2.12E-56	9.95E-55
ACHE	158.176	3.904	0.246	15.851	1.39E-56	6.58E-55
PRR18	245.626	2.605	0.164	15.866	1.09E-56	5.20E-55
KLHL4	293.607	6.155	0.388	15.868	1.05E-56	5.02E-55
CLCN4	129.726	3.899	0.245	15.894	7.00E-57	3.36E-55
FBXO6	270.590	2.407	0.151	15.908	5.62E-57	2.70E-55
KATNAL2	334.301	2.237	0.140	16.025	8.48E-58	4.16E-56
MARK1	296.254	6.887	0.429	16.042	6.50E-58	3.21E-56
SPACA3	145.295	3.558	0.222	16.054	5.40E-58	2.68E-56
LGALS9	378.903	2.360	0.146	16.146	1.21E-58	6.12E-57
RP11-328J6.1	242.388	5.807	0.359	16.165	8.93E-59	4.51E-57
PLCL1	312.682	2.308	0.143	16.167	8.58E-59	4.34E-57
TUBB2A	265.307	2.535	0.156	16.275	1.49E-59	7.70E-58
RMST	159.574	5.880	0.361	16.287	1.22E-59	6.35E-58
PHLDA3	171.341	5.714	0.350	16.336	5.46E-60	2.86E-58
ZNF629	301.696	2.199	0.134	16.355	4.01E-60	2.12E-58
BRSK1	156.370	3.746	0.228	16.460	7.07E-61	3.81E-59
PLEKHG1	275.961	3.347	0.201	16.622	4.86E-62	2.69E-60
NTRK2	209.456	4.157	0.248	16.770	4.07E-63	2.26E-61
TNFSF13B	388.257	2.441	0.144	16.893	5.06E-64	2.85E-62
PYGL	358.039	2.234	0.132	16.912	3.65E-64	2.06E-62
LINC00461	151.966	4.638	0.274	16.947	2.04E-64	1.15E-62
OXTR	197.074	3.389	0.200	16.973	1.30E-64	7.39E-63
CCDC85A	312.396	7.595	0.447	16.980	1.16E-64	6.63E-63
HES4	294.316	6.315	0.371	17.005	7.53E-65	4.30E-63
GPC5	162.682	4.983	0.292	17.035	4.48E-65	2.57E-63
CHDH	802.458	7.894	0.463	17.038	4.31E-65	2.47E-63
DGKG	166.772	4.019	0.235	17.095	1.61E-65	9.40E-64
B3GALNT1	184.785	4.250	0.248	17.109	1.26E-65	7.41E-64
TIMP1	199.717	3.274	0.191	17.113	1.18E-65	6.96E-64
ANKRD65	179.101	3.226	0.188	17.128	9.16E-66	5.41E-64
KCNMA1	159.023	3.993	0.233	17.165	4.89E-66	2.90E-64
HS3ST3B1	627.082	8.363	0.487	17.169	4.56E-66	2.72E-64
RP11-1D12.2	335.834	2.457	0.142	17.286	6.00E-67	3.64E-65
TFPI2	540.468	2.124	0.123	17.296	5.06E-67	3.09E-65
FHL1	161.540	3.601	0.207	17.358	1.71E-67	1.05E-65
NOL4L	289.564	2.663	0.152	17.484	1.89E-68	1.18E-66
RP11-307E17.8	222.237	3.852	0.220	17.538	7.29E-69	4.60E-67
CMKLR1	188.092	5.358	0.303	17.704	3.91E-70	2.50E-68
LRP1	223.410	2.974	0.167	17.797	7.42E-71	4.83E-69
GPSM1	183.351	5.654	0.317	17.824	4.62E-71	3.03E-69
RPS6KA6	261.267	2.975	0.166	17.951	4.76E-72	3.19E-70
CAND2	260.737	2.685	0.149	18.010	1.62E-72	1.09E-70
ARHGEF40	168.912	3.724	0.207	18.029	1.16E-72	7.84E-71
MRPS30-DT	445.807	2.154	0.119	18.085	4.16E-73	2.85E-71

PLS3	202.577	3.944	0.218	18.100	3.19E-73	2.20E-71
LINC02137	311.006	3.369	0.186	18.129	1.88E-73	1.30E-71
KLHDC7B	222.425	3.744	0.206	18.200	5.20E-74	3.60E-72
OLFML2A	338.273	2.427	0.133	18.276	1.29E-74	9.01E-73
CACNA1E	288.937	2.951	0.161	18.277	1.25E-74	8.79E-73
LINC01320	239.231	5.967	0.325	18.343	3.79E-75	2.67E-73
LINC00882	236.981	3.789	0.206	18.390	1.58E-75	1.13E-73
ZNRF1	599.274	2.168	0.117	18.476	3.25E-76	2.34E-74
C3orf14	259.283	4.937	0.265	18.663	9.86E-78	7.25E-76
HERC6	352.963	2.494	0.133	18.684	6.67E-78	4.91E-76
COL1A1	320.237	3.202	0.171	18.778	1.15E-78	8.57E-77
ZSWIM5	197.921	3.892	0.206	18.859	2.46E-79	1.85E-77
ILDR1	294.864	3.076	0.163	18.870	1.99E-79	1.51E-77
AC079466.1	1491.076	5.563	0.294	18.927	6.88E-80	5.27E-78
DSC3	388.123	7.806	0.411	18.985	2.25E-80	1.75E-78
ACOT4	370.563	2.349	0.123	19.039	8.13E-81	6.37E-79
CBLN2	382.852	2.471	0.129	19.115	1.89E-81	1.49E-79
CD109	573.767	2.115	0.110	19.296	5.84E-83	4.68E-81
NEUROG2	211.509	4.680	0.241	19.431	4.21E-84	3.41E-82
VSIG10	494.654	2.115	0.109	19.481	1.59E-84	1.30E-82
NOTCH2	742.275	2.094	0.107	19.515	8.21E-85	6.77E-83
RNF208	531.295	2.057	0.104	19.727	1.27E-86	1.08E-84
SESN3	201.347	4.123	0.209	19.731	1.16E-86	9.94E-85
PLXNB1	272.966	3.167	0.160	19.783	4.15E-87	3.56E-85
LINC00944	401.664	2.660	0.134	19.862	8.66E-88	7.54E-86
PTPRR	201.863	5.337	0.268	19.929	2.27E-88	1.99E-86
LINC01206	252.300	5.264	0.264	19.961	1.21E-88	1.07E-86
ENPP2	460.889	3.137	0.157	20.015	4.04E-89	3.64E-87
DUXAP8	353.437	4.751	0.237	20.016	3.96E-89	3.58E-87
MORC4	297.631	5.951	0.297	20.061	1.60E-89	1.45E-87
RHOB	246.505	3.812	0.189	20.165	1.98E-90	1.81E-88
LINC02381	360.719	2.911	0.143	20.404	1.53E-92	1.44E-90
TMSB4XP8	709.744	2.028	0.099	20.465	4.42E-93	4.17E-91
EEF1A2	606.207	2.246	0.109	20.535	1.06E-93	1.01E-91
CNIH3	316.329	3.149	0.153	20.601	2.70E-94	2.59E-92
NCR2	302.527	2.983	0.144	20.644	1.11E-94	1.07E-92
GGT4P	297.607	3.603	0.174	20.720	2.26E-95	2.22E-93
NFATC4	445.609	2.416	0.116	20.803	4.05E-96	4.00E-94
LDB2	312.010	5.638	0.271	20.821	2.77E-96	2.74E-94
EXPH5	636.907	2.233	0.107	20.826	2.49E-96	2.49E-94
IFIT1	520.525	6.700	0.322	20.839	1.93E-96	1.94E-94
SORD2P	562.213	2.132	0.102	20.880	8.10E-97	8.17E-95
SOCS2	251.452	4.045	0.194	20.899	5.47E-97	5.56E-95
PLA1A	482.786	2.778	0.133	20.906	4.68E-97	4.77E-95
MYO5B	303.300	3.392	0.162	20.912	4.18E-97	4.29E-95
MAP7	298.658	3.769	0.180	20.939	2.35E-97	2.42E-95
EPCAM	320.087	3.101	0.148	20.978	1.04E-97	1.07E-95
GCNT1	333.445	3.006	0.142	21.097	8.45E-99	8.82E-97
PKIB	249.940	4.083	0.193	21.181	1.43E-99	1.50E-97
ADGRE1	400.834	4.353	0.205	21.249	3.35E-100	3.59E-98
KCND2	360.834	3.450	0.162	21.306	9.95E-101	1.07E-98
MLLT11	406.956	2.712	0.125	21.633	8.79E-104	9.64E-102
CCNI2	321.788	4.471	0.205	21.846	8.48E-106	9.57E-104
VPS37B	251.407	4.865	0.222	21.880	4.04E-106	4.58E-104
KCNIP2	361.867	2.827	0.129	21.900	2.58E-106	2.95E-104
CD200	478.252	2.515	0.115	21.902	2.48E-106	2.86E-104
KL	315.062	3.821	0.173	22.029	1.51E-107	1.75E-105
PARP12	357.933	3.805	0.173	22.056	8.35E-108	9.80E-106

DIPK1B	362.059	2.851	0.129	22.084	4.48E-108	5.29E-106
NRG4	324.383	3.518	0.158	22.228	1.86E-109	2.20E-107
LINC01055	366.048	4.377	0.196	22.279	5.85E-110	6.97E-108
SPINT1	319.134	4.720	0.212	22.319	2.44E-110	2.92E-108
SLC6A4	545.232	2.580	0.115	22.421	2.48E-111	3.00E-109
ALDH1L1	577.977	5.423	0.242	22.429	2.03E-111	2.47E-109
AHNAK	599.395	2.987	0.133	22.507	3.55E-112	4.34E-110
IFI6	952.214	2.249	0.100	22.552	1.30E-112	1.59E-110
DSE	630.177	2.761	0.122	22.626	2.39E-113	2.98E-111
SPRY1	305.485	4.337	0.192	22.642	1.68E-113	2.11E-111
RP11-147L13.11	426.783	5.956	0.260	22.905	4.15E-116	5.41E-114
SSTR3	674.595	2.532	0.110	23.091	5.73E-118	7.63E-116
MS4A6E	287.684	4.371	0.189	23.107	3.92E-118	5.25E-116
ANK1	423.987	3.167	0.136	23.241	1.75E-119	2.37E-117
TNFRSF9	565.288	2.912	0.121	23.986	3.88E-127	5.55E-125
FRAS1	375.397	5.639	0.234	24.053	7.86E-128	1.15E-125
TNFAIP2	507.684	2.992	0.124	24.067	5.55E-128	8.18E-126
RAB38	1098.694	2.067	0.086	24.155	6.61E-129	9.87E-127
CRTAM	427.820	5.358	0.220	24.363	4.18E-131	6.37E-129
PSTPIP2	700.073	2.245	0.092	24.385	2.45E-131	3.76E-129
POF1B	882.450	2.205	0.090	24.391	2.14E-131	3.29E-129
MS4A6A	1128.562	2.355	0.096	24.575	2.32E-133	3.60E-131
FAM171B	554.267	2.666	0.108	24.578	2.19E-133	3.42E-131
PTK7	600.869	7.281	0.296	24.582	1.97E-133	3.09E-131
ADGRD1	614.481	2.406	0.098	24.627	6.43E-134	1.02E-131
CTNNA2	706.142	2.714	0.110	24.674	2.04E-134	3.25E-132
VCAM1	1024.842	2.048	0.083	24.740	3.97E-135	6.51E-133
PLPP3	539.669	5.350	0.215	24.841	3.22E-136	5.35E-134
CHST12	500.548	4.048	0.162	24.941	2.70E-137	4.52E-135
DSG1	867.038	2.103	0.084	25.015	4.20E-138	7.08E-136
DNAH7	416.615	3.937	0.157	25.026	3.16E-138	5.36E-136
ZFHX3	571.692	3.208	0.127	25.282	5.10E-141	8.84E-139
CYBRD1	729.330	2.369	0.094	25.318	2.01E-141	3.55E-139
EFR3B	380.680	5.286	0.208	25.353	8.34E-142	1.49E-139
EMX1	474.639	3.764	0.148	25.399	2.56E-142	4.65E-140
BCL2L10	489.327	4.770	0.188	25.433	1.09E-142	2.00E-140
SMAD1	504.841	4.660	0.182	25.650	4.18E-145	7.71E-143
PPM1H	602.049	2.768	0.108	25.672	2.42E-145	4.49E-143
KREMEN2	619.653	2.779	0.107	25.884	1.01E-147	1.88E-145
FRMPD2	601.544	4.031	0.154	26.103	3.34E-150	6.31E-148
INA	536.746	3.327	0.127	26.273	3.91E-152	7.57E-150
FUT7	662.305	2.649	0.100	26.407	1.15E-153	2.28E-151
LINC00996	1001.110	2.395	0.090	26.509	7.70E-155	1.54E-152
NBEA	692.458	2.833	0.106	26.735	1.87E-157	3.80E-155
DDR2	864.541	2.875	0.107	26.917	1.40E-159	2.90E-157
ZNF462	626.671	2.811	0.104	27.129	4.50E-162	9.66E-160
PTPRN2	471.896	3.973	0.145	27.365	7.08E-165	1.55E-162
GRIN2A	2265.161	8.422	0.306	27.495	2.00E-166	4.49E-164
RP11-459E5.1	807.921	3.024	0.109	27.713	4.87E-169	1.11E-166
CD86	1532.851	2.028	0.072	27.977	3.07E-172	7.09E-170
CHL1	771.548	2.800	0.100	28.059	3.12E-173	7.36E-171
IGSF3	786.620	2.606	0.091	28.658	1.26E-180	3.12E-178
DDAH1	686.690	3.258	0.113	28.757	7.51E-182	1.88E-179
TMEM178B	512.656	3.669	0.127	28.803	2.00E-182	5.06E-180
ISG15	2300.374	2.253	0.078	28.994	7.82E-185	2.03E-182
SCCPDH	2227.442	2.062	0.071	29.233	7.46E-188	2.02E-185
APOL1	2521.278	2.260	0.077	29.252	4.18E-188	1.15E-185
BCAR1	1645.938	2.394	0.082	29.328	4.51E-189	1.27E-186

SFRP2	484.420	3.815	0.130	29.345	2.80E-189	7.96E-187
KCP	743.517	3.195	0.109	29.393	6.73E-190	1.94E-187
NOD2	874.798	3.064	0.104	29.525	1.39E-191	4.04E-189
TLR7	853.116	2.787	0.094	29.589	2.04E-192	6.02E-190
PERP	577.460	3.608	0.122	29.640	4.55E-193	1.36E-190
KLRC1	957.625	3.362	0.113	29.662	2.34E-193	7.08E-191
SMIM30	982.730	3.960	0.132	29.893	2.42E-196	7.43E-194
SORT1	550.842	5.348	0.178	30.063	1.48E-198	4.60E-196
PHLDA1	759.527	3.371	0.111	30.339	3.53E-202	1.13E-199
SATB2	595.194	4.422	0.145	30.564	3.66E-205	1.18E-202
USP18	867.873	3.945	0.127	31.052	1.06E-211	3.46E-209
CCND2	1523.784	2.758	0.088	31.182	1.86E-213	6.18E-211
DUSP10	1098.231	2.666	0.085	31.268	1.26E-214	4.26E-212
RORA	1214.719	2.822	0.090	31.480	1.61E-217	5.51E-215
IFIT3	2522.076	2.005	0.063	31.608	2.91E-219	1.01E-216
OTOGL	1591.685	2.800	0.088	31.758	2.46E-221	8.78E-219
NCS1	881.191	2.696	0.085	31.775	1.42E-221	5.24E-219
TIAM1	771.111	3.304	0.104	31.862	9.11E-223	3.41E-220
EPSTI1	1033.839	2.753	0.086	32.020	5.72E-225	2.18E-222
SOX4	764.841	5.606	0.174	32.155	7.56E-227	2.92E-224
LEF1	1105.779	2.944	0.091	32.181	3.27E-227	1.29E-224
POU3F1	686.630	5.575	0.171	32.517	6.05E-232	2.42E-229
TGFBR3	1787.286	2.159	0.065	32.993	1.02E-238	4.31E-236
MEOX1	662.510	4.457	0.134	33.204	9.55E-242	4.17E-239
ITM2C	1822.622	2.471	0.074	33.484	8.18E-246	3.64E-243
SCART1	3923.976	2.394	0.071	33.489	6.99E-246	3.17E-243
CCDC187	677.132	4.688	0.139	33.662	2.11E-248	9.78E-246
SGPP2	2064.684	2.192	0.065	33.887	1.05E-251	4.95E-249
CELSR1	2257.823	2.348	0.069	33.931	2.31E-252	1.11E-249
ERC1	2598.271	2.569	0.075	34.049	4.22E-254	2.07E-251
LHX2	1857.435	2.570	0.073	35.257	2.68E-272	1.37E-269
DDX60	1627.524	2.984	0.084	35.359	7.24E-274	3.79E-271
ZNF711	1023.444	3.511	0.097	36.078	5.07E-285	2.72E-282
CD44	2754.288	2.183	0.060	36.371	1.23E-289	6.72E-287
FSCN1	1073.978	4.138	0.112	37.048	1.91E-300	1.10E-297
SSTR2	1331.555	2.974	0.080	37.188	1.07E-302	6.32E-300
HNRNPLL	1374.947	3.710	0.100	37.285	2.83E-304	1.71E-301
OAS2	6091.008	2.134	0.057	37.378	9.04E-306	5.61E-303
PTPRF	1571.965	4.527	0.093	48.624	0.00E+00	0.00E+00
IFI44L	8769.789	7.122	0.101	70.630	0.00E+00	0.00E+00
IFI44	2870.835	4.030	0.075	53.716	0.00E+00	0.00E+00
STAT1	16457.261	2.693	0.043	62.374	0.00E+00	0.00E+00
ITPR1	5020.023	2.182	0.055	39.572	0.00E+00	0.00E+00
EPHB1	1633.799	3.905	0.089	44.023	0.00E+00	0.00E+00
RASSF6	1547.144	3.575	0.085	42.103	0.00E+00	0.00E+00
SHROOM3	1657.580	5.130	0.120	42.586	0.00E+00	0.00E+00
CMBL	1094.134	4.080	0.102	40.101	0.00E+00	0.00E+00
NRN1	3247.877	7.879	0.183	42.950	0.00E+00	0.00E+00
PDGFA	1752.656	5.339	0.107	49.905	0.00E+00	0.00E+00
MACC1	1462.302	3.241	0.083	39.073	0.00E+00	0.00E+00
SAMD9L	3374.771	2.568	0.068	37.813	0.00E+00	0.00E+00
TRIP6	1222.468	4.427	0.109	40.660	0.00E+00	0.00E+00
DGKI	1239.603	3.585	0.095	37.616	0.00E+00	0.00E+00
FGFR1	2343.573	3.992	0.077	51.838	0.00E+00	0.00E+00
NOTCH1	5299.072	2.386	0.061	39.188	0.00E+00	0.00E+00
PRXL2A	1453.373	3.272	0.081	40.296	0.00E+00	0.00E+00
GSTP1	3058.884	2.626	0.064	41.039	0.00E+00	0.00E+00
MYEOV	827.760	4.813	0.127	37.802	0.00E+00	0.00E+00

GRAMD1B	1472.901	3.076	0.080	38.269	0.00E+00	0.00E+00
OAS3	2256.942	3.308	0.082	40.424	0.00E+00	0.00E+00
DMXL2	2092.806	2.854	0.071	40.017	0.00E+00	0.00E+00
FAM174B	2310.733	2.557	0.063	40.455	0.00E+00	0.00E+00
XAF1	1351.105	4.255	0.108	39.530	0.00E+00	0.00E+00
SLFN5	1573.559	3.440	0.089	38.731	0.00E+00	0.00E+00
RNF157	1639.343	3.314	0.083	39.968	0.00E+00	0.00E+00
JAG1	1131.123	4.792	0.121	39.679	0.00E+00	0.00E+00
MACROD2	5119.718	2.685	0.067	39.950	0.00E+00	0.00E+00
MX1	12039.907	4.730	0.061	78.040	0.00E+00	0.00E+00
H1-0	1467.821	5.652	0.130	43.380	0.00E+00	0.00E+00
F8	2220.870	2.984	0.070	42.649	0.00E+00	0.00E+00
PLA2G2C	1.634	-3.780	1.865	-2.027	4.26E-02	9.88E-02
RP11-567P19.3	1.800	-3.448	1.697	-2.031	4.22E-02	9.81E-02
ZNF350-AS1	1.189	-3.979	1.957	-2.033	4.21E-02	9.78E-02
DLGAP1-AS1	1.880	-3.538	1.739	-2.035	4.19E-02	9.75E-02
ZNF528-AS1	1.879	-3.509	1.708	-2.055	3.99E-02	9.34E-02
TMEM132D-AS1	15.894	-2.970	1.443	-2.058	3.96E-02	9.29E-02
C1GALT1P1	3.266	-2.501	1.210	-2.066	3.88E-02	9.13E-02
AC004381.7	3.428	-2.393	1.157	-2.069	3.86E-02	9.09E-02
BFSP1	1.271	-3.939	1.895	-2.078	3.77E-02	8.91E-02
LAMC3	2.634	-3.045	1.450	-2.100	3.57E-02	8.51E-02
TERB1	1.853	-3.632	1.729	-2.101	3.57E-02	8.49E-02
LINC02365	3.714	-2.273	1.075	-2.114	3.45E-02	8.26E-02
CPLX1	4.577	-2.221	1.040	-2.136	3.27E-02	7.88E-02
HMGB1P21	3.280	-3.293	1.542	-2.136	3.27E-02	7.88E-02
TENM4	2.706	-3.164	1.481	-2.137	3.26E-02	7.85E-02
ZKSCAN7-AS1	3.008	-2.682	1.253	-2.140	3.24E-02	7.81E-02
RP11-70L8.5	5.338	-2.091	0.977	-2.140	3.24E-02	7.81E-02
RP13-198D9.5	2.618	-3.125	1.453	-2.152	3.14E-02	7.61E-02
RP11-693J15.6	3.361	-2.495	1.155	-2.160	3.08E-02	7.48E-02
KCNH8	3.720	-2.454	1.127	-2.177	2.95E-02	7.20E-02
ENSG00010137222.1	5.041	-2.078	0.951	-2.186	2.88E-02	7.06E-02
SLC28A1	3.876	-2.291	1.047	-2.189	2.86E-02	7.02E-02
PROX2	4.102	-2.243	1.016	-2.207	2.73E-02	6.74E-02
GUSBP5	1.338	-4.297	1.933	-2.223	2.62E-02	6.50E-02
LINC01082	1.338	-4.297	1.933	-2.223	2.62E-02	6.50E-02
CTD-2509G16.3	3.839	-2.347	1.048	-2.240	2.51E-02	6.27E-02
PARD3	3.796	-2.685	1.195	-2.248	2.46E-02	6.16E-02
RP11-622O11.6	4.804	-2.077	0.918	-2.263	2.37E-02	5.96E-02
AC002519.8	4.204	-2.446	1.080	-2.265	2.35E-02	5.93E-02
FAM241B	1.388	-4.364	1.919	-2.274	2.30E-02	5.81E-02
LINC02495	3.621	-2.567	1.116	-2.300	2.15E-02	5.47E-02
MDC1	5.665	-2.095	0.911	-2.300	2.14E-02	5.47E-02
RPL23AP58	2.326	-3.711	1.605	-2.312	2.08E-02	5.32E-02
KRT18	4.682	-2.349	1.013	-2.318	2.05E-02	5.25E-02
RP11-266N13.2	2.730	-3.322	1.430	-2.324	2.01E-02	5.17E-02
RP11-480I12.10	1.438	-4.407	1.883	-2.341	1.93E-02	4.98E-02
RP11-946P6.7	4.577	-2.348	1.001	-2.346	1.90E-02	4.92E-02
RP11-667K14.5	2.098	-4.109	1.750	-2.348	1.89E-02	4.88E-02
ARHGAP42-AS1	1.500	-4.458	1.891	-2.358	1.84E-02	4.77E-02
RP11-447M4.2	2.087	-3.944	1.669	-2.363	1.81E-02	4.71E-02
STC1	40.542	-3.269	1.369	-2.388	1.69E-02	4.44E-02
LINC01948	4.613	-2.480	1.037	-2.391	1.68E-02	4.41E-02
TYROBP	5.160	-2.214	0.922	-2.400	1.64E-02	4.31E-02
RP11-122K13.7	4.843	-2.428	0.997	-2.436	1.49E-02	3.94E-02
BORCS8-MEF2B	6.225	-2.108	0.856	-2.461	1.38E-02	3.70E-02
RP11-255M6.2	4.814	-2.344	0.950	-2.468	1.36E-02	3.64E-02

RP3-347M6.3	1.649	-4.610	1.866	-2.470	1.35E-02	3.62E-02
KCNA6	1.639	-4.496	1.785	-2.519	1.18E-02	3.21E-02
GLRA3	6.052	-2.216	0.879	-2.520	1.17E-02	3.20E-02
TF	4.875	-3.229	1.278	-2.526	1.15E-02	3.15E-02
RP4-806M20.4	4.832	-2.500	0.989	-2.528	1.15E-02	3.14E-02
SCG2	5.374	-2.374	0.934	-2.541	1.11E-02	3.04E-02
CD99	439.018	-3.802	1.488	-2.556	1.06E-02	2.93E-02
PYGO1	3.664	-3.050	1.192	-2.559	1.05E-02	2.90E-02
CH507-528H12.1	9.637	-2.110	0.823	-2.563	1.04E-02	2.87E-02
JAKMIP2	15.695	-3.548	1.382	-2.568	1.02E-02	2.83E-02
PCK1	1.781	-4.604	1.774	-2.596	9.45E-03	2.64E-02
AMPD1	8.534	-2.058	0.790	-2.604	9.21E-03	2.58E-02
LINC02656	2.541	-4.127	1.575	-2.620	8.79E-03	2.48E-02
TTBK1	7.376	-2.228	0.850	-2.620	8.78E-03	2.48E-02
ZNF415	2.647	-4.181	1.594	-2.624	8.70E-03	2.46E-02
RNU6-45P	1.937	-4.432	1.689	-2.624	8.68E-03	2.45E-02
MYOM2	2.697	-4.237	1.592	-2.661	7.78E-03	2.22E-02
PDXDC1	165.211	-2.018	0.757	-2.667	7.65E-03	2.19E-02
CXCL11	2.681	-4.273	1.598	-2.673	7.51E-03	2.15E-02
RP4-647C14.2	5.120	-2.681	0.996	-2.691	7.12E-03	2.05E-02
TSKS	3.532	-3.713	1.375	-2.701	6.91E-03	1.99E-02
PRKCZ-AS1	4.655	-2.668	0.986	-2.706	6.81E-03	1.97E-02
CALHM2	6.621	-2.343	0.858	-2.730	6.34E-03	1.85E-02
ATP8A2	5.824	-2.462	0.891	-2.762	5.75E-03	1.69E-02
UBXN10	5.419	-2.831	1.016	-2.788	5.30E-03	1.57E-02
MEIS1	5.946	-2.402	0.859	-2.795	5.19E-03	1.54E-02
RP11-360N9.3	2.050	-4.748	1.692	-2.806	5.02E-03	1.50E-02
GUSBP16	11.248	-2.525	0.899	-2.808	4.99E-03	1.49E-02
KCNJ16	2.034	-4.913	1.711	-2.872	4.08E-03	1.24E-02
RASAL2-AS1	2.329	-4.682	1.629	-2.873	4.06E-03	1.24E-02
GLB1L2	6.806	-4.007	1.373	-2.918	3.52E-03	1.09E-02
ABCC8	3.222	-4.379	1.491	-2.936	3.32E-03	1.03E-02
CTC-559E9.5	3.119	-4.503	1.518	-2.968	3.00E-03	9.43E-03
TMEM71	6.430	-2.505	0.837	-2.995	2.74E-03	8.69E-03
GZMA	4.677	-3.791	1.265	-2.997	2.73E-03	8.64E-03
PDPK2P	5.897	-3.269	1.089	-3.001	2.69E-03	8.53E-03
RNU6-1069P	4.782	-3.136	1.038	-3.020	2.53E-03	8.06E-03
ITGB1-DT	4.906	-3.453	1.138	-3.035	2.41E-03	7.69E-03
RP11-527D7.1	5.096	-3.377	1.106	-3.055	2.25E-03	7.23E-03
CTD-2313F11.1	5.587	-2.961	0.955	-3.099	1.94E-03	6.32E-03
RP11-785D18.3	5.102	-3.186	1.024	-3.113	1.85E-03	6.06E-03
RP11-883A18.3	7.981	-2.341	0.751	-3.116	1.83E-03	6.00E-03
ZNF341-AS1	4.851	-3.939	1.254	-3.142	1.68E-03	5.54E-03
LMNTD2	6.250	-3.134	0.994	-3.154	1.61E-03	5.33E-03
RP11-647K16.1	9.424	-2.421	0.760	-3.187	1.44E-03	4.82E-03
CTD-2325A15.5	2.611	-5.188	1.625	-3.192	1.41E-03	4.75E-03
NLRP4	30.847	-3.613	1.102	-3.278	1.05E-03	3.62E-03
NT5C3AP2	2.706	-5.190	1.565	-3.316	9.14E-04	3.19E-03
HNRNPA1P27	4.957	-4.214	1.267	-3.325	8.83E-04	3.09E-03
HAAO	5.711	-3.365	1.006	-3.347	8.18E-04	2.88E-03
PMEPA1	6.472	-2.899	0.865	-3.352	8.02E-04	2.83E-03
DOK5	4.158	-4.836	1.439	-3.360	7.78E-04	2.76E-03
RIC3	2.826	-5.375	1.577	-3.409	6.53E-04	2.34E-03
LINC02649	10.163	-2.287	0.661	-3.460	5.40E-04	1.97E-03
RP11-875O11.5	5.824	-4.370	1.258	-3.474	5.12E-04	1.88E-03
RP11-34M7.1	7.243	-4.785	1.376	-3.477	5.07E-04	1.86E-03
PKD1L1	5.152	-4.877	1.402	-3.478	5.04E-04	1.85E-03
KIAA1217	6.121	-3.803	1.090	-3.489	4.84E-04	1.78E-03

CEACAM1	14.856	-2.136	0.609	-3.509	4.50E-04	1.66E-03
MUC1	11.511	-2.142	0.610	-3.513	4.44E-04	1.64E-03
RP11-46H11.11	4.409	-5.021	1.427	-3.519	4.33E-04	1.61E-03
PRSS16	3.153	-5.547	1.558	-3.561	3.70E-04	1.39E-03
FOXO3	19.658	-2.257	0.631	-3.578	3.46E-04	1.31E-03
TNNT3	7.973	-2.798	0.781	-3.583	3.40E-04	1.29E-03
KDM7A-DT	7.473	-3.276	0.914	-3.585	3.37E-04	1.28E-03
AC133785.1	9.052	-2.514	0.700	-3.589	3.32E-04	1.26E-03
NDRG1	8.044	-2.843	0.792	-3.589	3.32E-04	1.26E-03
RP11-706F1.1	5.312	-5.114	1.389	-3.680	2.33E-04	9.09E-04
RP11-63C8.1	6.913	-3.370	0.912	-3.694	2.21E-04	8.67E-04
IGHV1OR15-1	6.457	-5.555	1.475	-3.767	1.65E-04	6.63E-04
CTD-3037G24.3	10.628	-2.403	0.637	-3.773	1.61E-04	6.49E-04
RP11-575N24.1	6.875	-3.637	0.962	-3.779	1.57E-04	6.35E-04
RP11-700A24.1	7.228	-3.346	0.882	-3.793	1.49E-04	6.05E-04
RP11-239E10.2	8.012	-3.313	0.870	-3.808	1.40E-04	5.71E-04
RPS8P4	3.775	-5.715	1.492	-3.831	1.28E-04	5.24E-04
TCL1A	21.562	-2.936	0.766	-3.832	1.27E-04	5.22E-04
IGHV4-61	3.840	-5.639	1.458	-3.867	1.10E-04	4.58E-04
LINC02090	16.197	-2.041	0.524	-3.896	9.80E-05	4.11E-04
ISX	30.210	-2.290	0.586	-3.906	9.37E-05	3.94E-04
RP11-89F3.2	3.756	-5.794	1.482	-3.909	9.26E-05	3.90E-04
ENSG10010138795.1	3.960	-5.865	1.474	-3.980	6.90E-05	2.97E-04
RP11-20G13.1	13.721	-2.272	0.568	-3.997	6.41E-05	2.77E-04
RP11-856M7.7	13.657	-2.903	0.725	-4.005	6.20E-05	2.68E-04
C1S	17.219	-2.094	0.521	-4.021	5.80E-05	2.52E-04
JAKMIP1	10.584	-2.939	0.714	-4.120	3.79E-05	1.70E-04
PPARGC1A	7.664	-4.879	1.183	-4.123	3.73E-05	1.68E-04
ASB2	10.252	-5.011	1.208	-4.148	3.35E-05	1.52E-04
WNT9A	6.965	-5.636	1.355	-4.159	3.20E-05	1.45E-04
RP11-46H11.12	4.327	-5.995	1.440	-4.164	3.13E-05	1.42E-04
CSMD1	19.167	-2.362	0.565	-4.177	2.96E-05	1.35E-04
RNF112	14.991	-2.365	0.565	-4.183	2.88E-05	1.32E-04
IGLV3-1	6.942	-5.591	1.335	-4.188	2.81E-05	1.29E-04
LINC02367	15.999	-2.273	0.543	-4.189	2.80E-05	1.29E-04
RIBC2	7.442	-5.798	1.334	-4.345	1.39E-05	6.70E-05
LRRC32	13.184	-2.769	0.637	-4.347	1.38E-05	6.64E-05
CTD-3037G24.4	12.622	-3.058	0.694	-4.405	1.06E-05	5.21E-05
MLC1	15.501	-2.429	0.547	-4.442	8.90E-06	4.43E-05
ZFP2	14.122	-2.540	0.566	-4.484	7.31E-06	3.69E-05
MIR210HG	182.965	-5.078	1.119	-4.539	5.65E-06	2.89E-05
ZNF100	13.698	-2.815	0.617	-4.563	5.03E-06	2.60E-05
LOXL2	23.159	-2.074	0.447	-4.640	3.49E-06	1.84E-05
GUCA1B	18.304	-2.273	0.490	-4.640	3.48E-06	1.83E-05
RTN4R	11.308	-3.333	0.708	-4.706	2.53E-06	1.35E-05
ADCY1	6.013	-6.465	1.373	-4.708	2.51E-06	1.34E-05
CTC-471J1.2	9.331	-6.125	1.301	-4.709	2.49E-06	1.33E-05
FRMPD4	13.974	-2.889	0.610	-4.739	2.15E-06	1.16E-05
GALNT18	9.930	-6.179	1.289	-4.792	1.65E-06	9.10E-06
ZFPM2-AS1	20.367	-2.592	0.540	-4.801	1.58E-06	8.73E-06
MAPK8IP1	21.020	-2.253	0.466	-4.836	1.32E-06	7.41E-06
MPP7	21.621	-2.972	0.611	-4.862	1.16E-06	6.58E-06
RYR2	11.163	-3.985	0.818	-4.872	1.10E-06	6.27E-06
CTB-92J24.2	15.481	-2.875	0.589	-4.879	1.07E-06	6.07E-06
LRRC3	21.683	-2.186	0.446	-4.901	9.54E-07	5.46E-06
MIX23P1	26.975	-2.418	0.492	-4.911	9.08E-07	5.21E-06
CXCL8	11.150	-4.808	0.979	-4.911	9.07E-07	5.20E-06
AXIN2	22.646	-2.296	0.465	-4.936	7.99E-07	4.62E-06

NUAK2	12.223	-3.450	0.697	-4.949	7.47E-07	4.34E-06
LINC01422	14.042	-3.074	0.620	-4.954	7.28E-07	4.23E-06
RP11-1O10.1	19.693	-4.114	0.830	-4.958	7.14E-07	4.16E-06
TMEM51-AS1	23.237	-2.169	0.437	-4.958	7.13E-07	4.15E-06
PRDM5	11.268	-6.367	1.281	-4.971	6.65E-07	3.90E-06
ARHGEF35	12.040	-3.647	0.733	-4.974	6.57E-07	3.85E-06
CST7	19.609	-2.492	0.501	-4.974	6.57E-07	3.85E-06
LPP-AS2	13.485	-3.390	0.668	-5.078	3.81E-07	2.30E-06
ADGRB1	22.644	-2.336	0.443	-5.271	1.35E-07	8.65E-07
NLRP6	27.360	-2.062	0.391	-5.276	1.32E-07	8.45E-07
LINC00565	13.513	-3.638	0.679	-5.357	8.45E-08	5.55E-07
FAM66B	13.562	-5.139	0.952	-5.399	6.71E-08	4.46E-07
RP11-761I4.6	19.414	-2.753	0.505	-5.457	4.84E-08	3.28E-07
ZNF43	33.696	-2.034	0.370	-5.500	3.79E-08	2.60E-07
PLCB2	28.494	-2.317	0.412	-5.621	1.90E-08	1.34E-07
STK39	17.328	-3.189	0.567	-5.626	1.84E-08	1.31E-07
LINC02043	29.915	-2.198	0.389	-5.648	1.62E-08	1.16E-07
DMBT1	19.336	-2.939	0.519	-5.668	1.45E-08	1.04E-07
VILL	19.808	-2.844	0.498	-5.713	1.11E-08	8.09E-08
RP11-299H22.4	22.464	-3.963	0.692	-5.726	1.03E-08	7.53E-08
LINC02870	33.764	-2.101	0.364	-5.769	7.96E-09	5.89E-08
RP11-168O16.1	37.056	-2.136	0.369	-5.795	6.83E-09	5.07E-08
PTPRO	28.185	-2.424	0.416	-5.832	5.47E-09	4.11E-08
PRKCQ-AS1	15.410	-4.916	0.841	-5.843	5.14E-09	3.88E-08
RP11-216B13.1	28.774	-2.368	0.404	-5.863	4.54E-09	3.45E-08
ZNF239	12.271	-7.503	1.277	-5.875	4.22E-09	3.22E-08
PAPSS2	12.400	-7.501	1.274	-5.888	3.91E-09	2.99E-08
MLF1	21.125	-6.410	1.084	-5.914	3.34E-09	2.57E-08
SH2D4A	15.986	-4.639	0.771	-6.016	1.79E-09	1.42E-08
CACHD1	26.523	-2.991	0.494	-6.058	1.37E-09	1.10E-08
XK	23.385	-7.462	1.229	-6.071	1.27E-09	1.02E-08
RAB17	18.646	-3.894	0.639	-6.098	1.08E-09	8.69E-09
IGHM	15.598	-7.816	1.253	-6.236	4.50E-10	3.76E-09
AC018634.9	31.179	-2.608	0.413	-6.320	2.62E-10	2.23E-09
ANKMY2	37.071	-2.245	0.355	-6.328	2.48E-10	2.11E-09
ASMTL	94.185	-3.914	0.618	-6.337	2.34E-10	2.00E-09
RP11-326C3.2	28.269	-6.835	1.072	-6.376	1.82E-10	1.56E-09
RP11-46H11.3	16.997	-7.972	1.249	-6.381	1.76E-10	1.52E-09
MTARC1	28.118	-2.773	0.431	-6.431	1.26E-10	1.10E-09
GRASLND	30.975	-7.867	1.217	-6.463	1.03E-10	9.07E-10
ZNF660	18.611	-8.096	1.245	-6.503	7.88E-11	7.03E-10
JAZF1	36.133	-2.456	0.373	-6.577	4.80E-11	4.38E-10
ARSD	19.337	-8.156	1.239	-6.584	4.58E-11	4.18E-10
ZNF702P	21.229	-8.283	1.234	-6.715	1.89E-11	1.77E-10
SNORA12	31.906	-2.756	0.407	-6.766	1.33E-11	1.26E-10
ZNF287	22.592	-8.381	1.234	-6.794	1.09E-11	1.04E-10
AC010149.4	44.091	-2.213	0.325	-6.806	1.01E-11	9.64E-11
CXCL9	21.220	-4.009	0.584	-6.863	6.72E-12	6.52E-11
FES	31.682	-3.327	0.483	-6.887	5.71E-12	5.57E-11
TRPM2	62.503	-2.146	0.306	-7.022	2.19E-12	2.21E-11
RP11-452E5.1	39.696	-2.341	0.333	-7.024	2.16E-12	2.18E-11
GNAS-AS1	34.384	-2.766	0.394	-7.029	2.08E-12	2.11E-11
MYADML2	32.145	-3.024	0.419	-7.211	5.55E-13	5.82E-12
IGDCC4	32.571	-3.106	0.429	-7.241	4.46E-13	4.70E-12
HSBP1L1	27.396	-3.564	0.492	-7.249	4.19E-13	4.42E-12
ZNF568	56.736	-8.742	1.202	-7.273	3.51E-13	3.73E-12
CYRIA	33.650	-6.471	0.882	-7.333	2.24E-13	2.42E-12
TLR8-AS1	35.481	-6.566	0.882	-7.448	9.47E-14	1.04E-12

AFAP1-AS1	467.052	-2.040	0.273	-7.483	7.28E-14	8.10E-13
KDM7A	54.437	-2.285	0.303	-7.530	5.08E-14	5.71E-13
SOAT2	42.398	-2.729	0.354	-7.707	1.29E-14	1.51E-13
WWC2	40.329	-6.752	0.875	-7.719	1.18E-14	1.39E-13
ARHGAP42	38.845	-2.885	0.370	-7.793	6.53E-15	7.86E-14
C1orf115	47.249	-9.442	1.206	-7.831	4.83E-15	5.87E-14
ZKSCAN7	47.254	-9.447	1.205	-7.840	4.49E-15	5.46E-14
AK1	63.430	-2.007	0.255	-7.874	3.43E-15	4.21E-14
SPRED3	53.434	-2.422	0.301	-8.047	8.51E-16	1.08E-14
MICU3	56.062	-9.692	1.200	-8.078	6.56E-16	8.38E-15
TMEM9B-AS1	74.450	-2.159	0.263	-8.216	2.11E-16	2.77E-15
ZNF829	118.120	-9.797	1.190	-8.234	1.81E-16	2.39E-15
FFAR2	88.979	-2.644	0.321	-8.239	1.73E-16	2.29E-15
ZNF284	33.760	-4.752	0.562	-8.453	2.85E-17	3.93E-16
MICAL2	37.615	-3.474	0.409	-8.488	2.09E-17	2.92E-16
RP11-64C12.3	95.694	-2.024	0.235	-8.597	8.22E-18	1.16E-16
NAALAD2	84.829	-2.053	0.238	-8.628	6.27E-18	8.96E-17
MBOAT2	162.062	-10.260	1.186	-8.651	5.11E-18	7.34E-17
TIGIT	74.584	-2.222	0.254	-8.743	2.26E-18	3.31E-17
LINC00173	70.183	-2.335	0.267	-8.753	2.08E-18	3.04E-17
ZNF841	180.627	-10.411	1.186	-8.777	1.68E-18	2.48E-17
TLCD5	132.549	-9.068	1.032	-8.788	1.52E-18	2.25E-17
ITGB1P1	52.324	-2.869	0.324	-8.846	9.09E-19	1.36E-17
MAP9	209.498	-10.630	1.185	-8.974	2.87E-19	4.42E-18
CNKSR2	116.123	-3.585	0.399	-8.990	2.48E-19	3.83E-18
RASAL2	56.702	-6.220	0.684	-9.093	9.68E-20	1.52E-18
TMPRSS3	40.417	-5.096	0.555	-9.179	4.34E-20	6.95E-19
IL7R	50.366	-3.756	0.396	-9.482	2.50E-21	4.22E-20
NLGN4X	70.283	-2.796	0.285	-9.819	9.33E-23	1.69E-21
TNFRSF1A	50.481	-3.631	0.363	-9.995	1.61E-23	3.02E-22
XKRX	45.393	-4.415	0.437	-10.100	5.51E-24	1.05E-22
LINC00683	54.999	-3.552	0.351	-10.120	4.49E-24	8.60E-23
ZNF844	141.681	-8.582	0.847	-10.128	4.16E-24	7.99E-23
ZNF681	59.027	-3.781	0.369	-10.242	1.29E-24	2.51E-23
PDE1B	88.369	-2.562	0.244	-10.483	1.04E-25	2.11E-24
TENT5C	118.071	-2.206	0.207	-10.680	1.26E-26	2.68E-25
RAB31	106.640	-2.201	0.205	-10.749	5.98E-27	1.30E-25
ZNF888	87.385	-2.680	0.248	-10.803	3.34E-27	7.32E-26
METRN	130.436	-2.080	0.192	-10.833	2.41E-27	5.30E-26
RP11-367L7.1	135.760	-7.999	0.738	-10.833	2.39E-27	5.28E-26
RP11-515I12.1	249.137	-9.211	0.841	-10.947	6.86E-28	1.55E-26
ZNF433	86.620	-2.597	0.236	-11.021	3.03E-28	6.89E-27
LMCD1	55.383	-4.758	0.428	-11.113	1.08E-28	2.50E-27
ZDHHC11	95.265	-2.581	0.231	-11.187	4.74E-29	1.11E-27
LNCOC1	122.076	-2.187	0.195	-11.220	3.24E-29	7.60E-28
BCAN-AS1	101.986	-2.440	0.216	-11.300	1.31E-29	3.12E-28
CYTOR	122.122	-2.252	0.195	-11.524	9.99E-31	2.46E-29
CTD-2134A5.3	114.058	-2.604	0.226	-11.546	7.77E-31	1.92E-29
MGST1	72.010	-3.738	0.316	-11.822	2.99E-32	7.80E-31
AOC3	109.462	-2.673	0.224	-11.918	9.48E-33	2.50E-31
MIR4435-2HG	69.274	-4.979	0.416	-11.972	4.97E-33	1.33E-31
TLR5	67.100	-4.959	0.413	-11.994	3.84E-33	1.03E-31
IGLL5	223.633	-8.822	0.732	-12.059	1.74E-33	4.72E-32
TNFAIP8L2	84.846	-3.002	0.247	-12.151	5.69E-34	1.57E-32
ZNF585B	77.344	-3.350	0.274	-12.234	2.04E-34	5.64E-33
TSPAN9	169.589	-2.000	0.163	-12.287	1.06E-34	2.99E-33
SLC2A13	131.263	-2.387	0.193	-12.387	3.06E-35	8.76E-34
SYTL1	77.063	-5.438	0.434	-12.516	6.10E-36	1.79E-34

SH3PXD2B	94.249	-2.950	0.234	-12.607	1.93E-36	5.72E-35
BEX4	75.089	-5.315	0.421	-12.624	1.56E-36	4.64E-35
SCN3A	143.303	-2.535	0.193	-13.103	3.16E-39	1.01E-37
MITF	142.426	-3.370	0.250	-13.490	1.80E-41	6.07E-40
ZNF506	98.307	-5.806	0.425	-13.649	2.04E-42	7.04E-41
SPNS3	88.249	-3.790	0.278	-13.654	1.92E-42	6.66E-41
F2RL3	141.274	-2.663	0.189	-14.119	2.90E-45	1.07E-43
RP11-466A19.1	142.720	-6.692	0.459	-14.590	3.24E-48	1.29E-46
KLF9	116.615	-3.403	0.232	-14.666	1.07E-48	4.32E-47
ARHGEF4	262.990	-2.107	0.144	-14.670	1.01E-48	4.07E-47
RP11-284F21.7	222.721	-2.231	0.149	-14.968	1.19E-50	5.01E-49
OSTN-AS1	220.257	-2.618	0.171	-15.336	4.38E-53	1.92E-51
GOLGA2P11	197.518	-4.052	0.258	-15.727	9.89E-56	4.54E-54
ALDH1A1	150.421	-3.655	0.231	-15.854	1.32E-56	6.28E-55
ZIK1	169.063	-2.950	0.184	-15.992	1.45E-57	7.04E-56
FCRL3	195.957	-2.779	0.171	-16.226	3.28E-59	1.67E-57
NLRP3	143.759	-3.254	0.199	-16.322	6.88E-60	3.60E-58
LINC01887	311.055	-2.412	0.146	-16.543	1.81E-61	9.86E-60
ZNF254	183.369	-3.055	0.178	-17.169	4.52E-66	2.70E-64
ARL4C	285.993	-2.156	0.126	-17.170	4.43E-66	2.65E-64
ZNF347	139.229	-4.292	0.249	-17.259	9.64E-67	5.83E-65
CXCL10	153.590	-4.871	0.282	-17.288	5.78E-67	3.51E-65
GZMM	145.379	-4.141	0.237	-17.438	4.28E-68	2.64E-66
RP11-1149O23.3	182.001	-3.279	0.184	-17.791	8.35E-71	5.42E-69
BCL6	155.106	-5.259	0.294	-17.887	1.48E-71	9.84E-70
ZNF614	236.173	-2.931	0.162	-18.048	8.21E-73	5.58E-71
ADARB1	206.473	-3.100	0.169	-18.390	1.59E-75	1.13E-73
TNFRSF10D	320.716	-2.533	0.138	-18.406	1.19E-75	8.48E-74
AF127936.3	476.703	-2.242	0.119	-18.804	7.03E-79	5.26E-77
EMSLR	190.974	-4.146	0.220	-18.878	1.74E-79	1.32E-77
AMPD3	193.520	-3.707	0.196	-18.951	4.29E-80	3.31E-78
TESC	531.183	-2.090	0.110	-18.969	3.09E-80	2.39E-78
ZFP82	379.260	-2.310	0.118	-19.555	3.73E-85	3.10E-83
FBP1	449.102	-2.261	0.115	-19.654	5.36E-86	4.50E-84
RP11-588H23.3	203.180	-3.704	0.185	-19.970	1.01E-88	8.93E-87
PNMA2	217.347	-5.721	0.286	-19.987	7.11E-89	6.36E-87
CD96	204.900	-5.113	0.254	-20.094	8.36E-90	7.64E-88
LINC00665	247.347	-3.212	0.158	-20.324	7.88E-92	7.35E-90
GZMK	241.322	-3.507	0.168	-20.883	7.61E-97	7.70E-95
UNC13D	249.556	-4.612	0.218	-21.181	1.43E-99	1.50E-97
LPP	394.401	-2.907	0.136	-21.410	1.08E-101	1.18E-99
LINC02331	246.073	-4.053	0.179	-22.587	5.82E-113	7.19E-111
HIC1	1105.905	-2.044	0.089	-22.912	3.54E-116	4.64E-114
RNF141	593.873	-2.302	0.099	-23.241	1.74E-119	2.37E-117
TNFRSF10A	292.649	-3.551	0.152	-23.306	3.86E-120	5.30E-118
NME8	364.860	-3.294	0.141	-23.413	3.17E-121	4.40E-119
UGT8	552.273	-2.309	0.098	-23.649	1.20E-123	1.70E-121
FIRRE	407.100	-3.615	0.146	-24.751	3.00E-135	4.94E-133
TGFBR2	429.020	-3.170	0.126	-25.134	2.11E-139	3.61E-137
CCDC152	362.513	-5.243	0.207	-25.294	3.74E-141	6.53E-139
CDH1	488.550	-3.254	0.125	-26.107	3.04E-150	5.79E-148
CHFR	538.335	-7.133	0.272	-26.195	3.05E-151	5.85E-149
PRKCA	553.995	-2.905	0.108	-26.980	2.52E-160	5.25E-158
RP11-299H22.3	626.745	-4.611	0.171	-27.031	6.45E-161	1.36E-158
KLHL6	1898.028	-2.213	0.081	-27.459	5.38E-166	1.19E-163
DNAH17-AS1	592.053	-6.433	0.234	-27.476	3.44E-166	7.66E-164
MED13L	1433.177	-2.136	0.077	-27.855	9.28E-171	2.12E-168
ST3GAL1	650.801	-2.698	0.096	-28.213	4.10E-175	9.76E-173

RP11-284F21.10	806.305	-2.476	0.088	-28.214	3.90E-175	9.38E-173
CREB5	3774.092	-2.002	0.070	-28.514	7.75E-179	1.90E-176
PITPNC1	865.736	-3.001	0.095	-31.656	6.22E-220	2.19E-217
PPP2R2C	655.607	-5.892	0.178	-33.123	1.38E-240	5.91E-238
ZBED2	1115.397	-5.625	0.132	-42.677	0.00E+00	0.00E+00
PPM1L	1889.303	-3.434	0.080	-43.018	0.00E+00	0.00E+00
JCHAIN	8038.816	-3.031	0.064	-47.645	0.00E+00	0.00E+00
PDE4D	1560.098	-3.375	0.074	-45.312	0.00E+00	0.00E+00
ITGB1	1196.142	-3.389	0.084	-40.227	0.00E+00	0.00E+00

REFERENCES

References

ADAM, M., ROBERT, F., LAROCHELLE, M. & GAUDREAU, L. 2001. H2A.Z is required for global chromatin integrity and for recruitment of RNA polymerase II under specific conditions. *Mol Cell Biol,* 21**,** 6270-9.

ADEN, K., BARTSCH, K., DAHL, J., REIJNS, M. A. M., ESSER, D., SHEIBANI-TEZERJI, R., SINHA, A., WOTTAWA, F., ITO, G., MISHRA, N., KNITTLER, K., BURKHOLDER, A., WELZ, L., VAN ES, J., TRAN, F., LIPINSKI, S., KAKAVAND, N., BOEGER, C., LUCIUS, R., VON SCHOENFELS, W., SCHAFMAYER, C., LENK, L., CHALARIS, A., CLEVERS, H., RÖCKEN, C., KALETA, C., ROSE-JOHN, S., SCHREIBER, S., KUNKEL, T., RABE, B. & ROSENSTIEL, P. 2019. Epithelial RNase H2 Maintains Genome Integrity and Prevents Intestinal Tumorigenesis in Mice. *Gastroenterology,* 156**,** 145-159.e19.

AGATHAGGELOU, A., MURINA, O., JACKSON, A. P., MOSS, P., PANEESHA, S., STEWART, G. S., TAYLOR, M. & STANKOVIC, T. 2018. Targeting an RNaseH2 Defect in Chronic Lymphocytic Leukaemia with PARP Inhibitors. *Blood,* 132**,** 1835.

AGATHANGELIDIS, A., DARZENTAS, N., HADZIDIMITRIOU, A., BROCHET, X., MURRAY, F., YAN, X. J., DAVIS, Z., VAN GASTEL-MOL, E. J., TRESOLDI, C., CHU, C. C., CAHILL, N., GIUDICELLI, V., TICHY, B., PEDERSEN, L. B., FORONI, L., BONELLO, L., JANUS, A., SMEDBY, K., ANAGNOSTOPOULOS, A., MERLE-BERAL, H., LAOUTARIS, N., JULIUSSON, G., DI CELLE, P. F., POSPISILOVA, S., JURLANDER, J., GEISLER, C., TSAFTARIS, A., LEFRANC, M. P., LANGERAK, A. W., OSCIER, D. G., CHIORAZZI, N., BELESSI, C., DAVI, F., ROSENQUIST, R., GHIA, P. & STAMATOPOULOS, K. 2012. Stereotyped B-cell receptors in one-third of chronic lymphocytic leukemia: a molecular classification with implications for targeted therapies. *Blood,* 119**,** 4467-75.

AGUILERA, A. & GARCÍA-MUSE, T. 2012. R loops: from transcription byproducts to threats to genome stability. *Mol Cell,* 46**,** 115-24.

AGUIRRE, A. J., MEYERS, R. M., WEIR, B. A., VAZQUEZ, F., ZHANG, C. Z., BEN-DAVID, U., COOK, A., HA, G., HARRINGTON, W. F., DOSHI, M. B., KOST-ALIMOVA, M., GILL, S., XU, H., ALI, L. D., JIANG, G., PANTEL, S., LEE, Y., GOODALE, A., CHERNIACK, A. D., OH, C., KRYUKOV, G., COWLEY, G. S., GARRAWAY, L. A., STEGMAIER, K., ROBERTS, C. W., GOLUB, T. R., MEYERSON, M., ROOT, D. E., TSHERNIAK, A. & HAHN, W. C. 2016. Genomic Copy Number Dictates a Gene-Independent Cell Response to CRISPR/Cas9 Targeting. *Cancer Discov,* 6**,** 914-29.

AHMADI, A., KAVIANI, S., YAGHMAIE, M., PASHAIEFAR, H., AHMADVAND, M., JALILI, M., ALIMOGHADDAM, K., ESLAMIJOUYBARI, M. & GHAVAMZADEH, A. 2018. Altered expression of. *Blood Res,* 53**,** 320-324.

AHN, I. E., UNDERBAYEV, C., ALBITAR, A., HERMAN, S. E., TIAN, X., MARIC, I., ARTHUR, D. C., WAKE, L., PITTALUGA, S., YUAN, C. M., STETLER-STEVENSON, M., SOTO, S., VALDEZ, J., NIERMAN, P., LOTTER, J., XI, L., RAFFELD, M., FAROOQUI, M., ALBITAR, M. & WIESTNER, A. 2017. Clonal evolution leading to ibrutinib resistance in chronic lymphocytic leukemia. *Blood,* 129**,** 1469-1479.

AI, L., VO, Q. N., ZUO, C., LI, L., LING, W., SUEN, J. Y., HANNA, E., BROWN, K. D. & FAN, C. Y. 2004. Ataxia-telangiectasia-mutated (ATM) gene in head and neck squamous cell carcinoma: promoter hypermethylation with clinical correlation in 100 cases. *Cancer Epidemiol Biomarkers Prev,* 13**,** 150-6.

AKHMANOVA, A. S., BINDELS, P. C., XU, J., MIEDEMA, K., KREMER, H. & HENNIG, W. 1995. Structure and expression of histone H3.3 genes in Drosophila melanogaster and Drosophila hydei. *Genome,* 38**,** 586-600.

AL-SAWAF, O., ROBRECHT, S., BAHLO, J., FINK, A. M., CRAMER, P., V TRESCKOW, J., LANGE, E., KIEHL, M., DREYLING, M., RITGEN, M., DÜRIG, J., TAUSCH, E., SCHNEIDER, C., STILGENBAUER, S.,

WENDTNER, C. M., FISCHER, K., GOEDE, HALLEK, M. & EICHHORST, B. 2021. Richter transformation in chronic lymphocytic leukemia (CLL)-a pooled analysis of German CLL Study Group (GCLLSG) front line treatment trials. *Leukemia,* 35**,** 169-176.

ALCALAY, M., MEANI, N., GELMETTI, V., FANTOZZI, A., FAGIOLI, M., ORLETH, A., RIGANELLI, D., SEBASTIANI, C., CAPPELLI, E., CASCIARI, C., SCIURPI, M. T., MARIANO, A. R., MINARDI, S. P., LUZI, L., MULLER, H., DI FIORE, P. P., FROSINA, G. & PELICCI, P. G. 2003. Acute myeloid leukemia fusion proteins deregulate genes involved in stem cell maintenance and DNA repair. *J Clin Invest,* 112**,** 1751-61.

ALLEN, F., BEHAN, F., KHODAK, A., IORIO, F., YUSA, K., GARNETT, M. & PARTS, L. 2019. JACKS: joint analysis of CRISPR/Cas9 knockout screens. *Genome Res,* 29**,** 464-471.

ALLEN-SOLTERO, S., MARTINEZ, S. L., PUTNAM, C. D. & KOLODNER, R. D. 2014. A saccharomyces cerevisiae RNase H2 interaction network functions to suppress genome instability. *Mol Cell Biol,* 34**,** 1521-34.

ANGELO AGATHAGGELOU AND OLGA MURINA AND ANDREW, P. J. A. P. M. A. S. P. A. G. S. S. A. M. T. A. T. S. 2018. Targeting an RNaseH2 Defect in Chronic Lymphocytic Leukaemia with PARP Inhibitors. *Blood,* 132**,** 1835.

ANTTILA, J. V., SHUBIN, M., CAIRNS, J., BORSE, F., GUO, Q., MONONEN, T., VÁZQUEZ-GARCÍA, I., PULKKINEN, O. & MUSTONEN, V. 2019. Contrasting the impact of cytotoxic and cytostatic drug therapies on tumour progression. *PLoS Comput Biol,* 15**,** e1007493.

ARIMOTO, K. I., LÖCHTE, S., STONER, S. A., BURKART, C., ZHANG, Y., MIYAUCHI, S., WILMES, S., FAN, J. B., HEINISCH, J. J., LI, Z., YAN, M., PELLEGRINI, S., COLLAND, F., PIEHLER, J. & ZHANG, D. E. 2017. STAT2 is an essential adaptor in USP18-mediated suppression of type I interferon signaling. *Nat Struct Mol Biol,* 24**,** 279-289.

ARRUGA, F., GYAU, B. B., IANNELLO, A., VITALE, N., VAISITTI, T. & DEAGLIO, S. 2020. Immune Response Dysfunction in Chronic Lymphocytic Leukemia: Dissecting Molecular Mechanisms and Microenvironmental Conditions. *Int J Mol Sci,* 21.

ASHWORTH, A. 2008. A synthetic lethal therapeutic approach: poly(ADP) ribose polymerase inhibitors for the treatment of cancers deficient in DNA double-strand break repair. *J Clin Oncol,* 26**,** 3785-90.

ASSI, S. A., IMPERATO, M. R., COLEMAN, D. J. L., PICKIN, A., POTLURI, S., PTASINSKA, A., CHIN, P. S., BLAIR, H., CAUCHY, P., JAMES, S. R., ZACARIAS-CABEZA, J., GILDING, L. N., BEGGS, A., CLOKIE, S., LOKE, J. C., JENKIN, P., UDDIN, A., DELWEL, R., RICHARDS, S. J., RAGHAVAN, M., GRIFFITHS, M. J., HEIDENREICH, O., COCKERILL, P. N. & BONIFER, C. 2019. Subtype-specific regulatory network rewiring in acute myeloid leukemia. *Nat Genet,* 51**,** 151-162.

ATSAVES, V., LEVENTAKI, V., RASSIDAKIS, G. Z. & CLARET, F. X. 2019. AP-1 Transcription Factors as Regulators of Immune Responses in Cancer. *Cancers (Basel),* 11.

ATSUMI, Y., MINAKAWA, Y., ONO, M., DOBASHI, S., SHINOHE, K., SHINOHARA, A., TAKEDA, S., TAKAGI, M., TAKAMATSU, N., NAKAGAMA, H., TERAOKA, H. & YOSHIOKA, K. 2015. ATM and SIRT6/SNF2H Mediate Transient H2AX Stabilization When DSBs Form by Blocking HUWE1 to Allow Efficient γH2AX Foci Formation. *Cell Rep,* 13**,** 2728-40.

AUDIA, J. E. & CAMPBELL, R. M. 2016. Histone Modifications and Cancer. *Cold Spring Harb Perspect Biol,* 8**,** a019521.

AUSTEN, B., POWELL, J. E., ALVI, A., EDWARDS, I., HOOPER, L., STARCZYNSKI, J., TAYLOR, A. M., FEGAN, C., MOSS, P. & STANKOVIC, T. 2005. Mutations in the ATM gene lead to impaired overall and treatment-free survival that is independent of IGVH mutation status in patients with B-CLL. *Blood,* 106**,** 3175-82.

AUSTEN, B., SKOWRONSKA, A., BAKER, C., POWELL, J. E., GARDINER, A., OSCIER, D., MAJID, A., DYER, M., SIEBERT, R., TAYLOR, A. M., MOSS, P. A. & STANKOVIC, T. 2007. Mutation status of the residual

ATM allele is an important determinant of the cellular response to chemotherapy and survival in patients with chronic lymphocytic leukemia containing an 11q deletion. *J Clin Oncol,* 25**,** 5448-57.
AWASTHI, P., FOIANI, M. & KUMAR, A. 2015. ATM and ATR signaling at a glance. *J Cell Sci,* 128**,** 4255-62.
BADRELDIN, A. A., BAGHERI, L., ZHANG, B., LARSON, A. N. & VAN WIJNEN, A. J. 2021. Relative mRNA and protein stability of epigenetic regulators in musculoskeletal cell culture models. *Gene,* 766**,** 145032.
BAKKENIST, C. J. & KASTAN, M. B. 2003. DNA damage activates ATM through intermolecular autophosphorylation and dimer dissociation. *Nature,* 421**,** 499-506.
BANERJEE, D. R., DECKARD, C. E., ZENG, Y. & SCZEPANSKI, J. T. 2019. Acetylation of the histone H3 tail domain regulates base excision repair on higher-order chromatin structures. *Sci Rep,* 9**,** 15972.
BANIN, S., MOYAL, L., SHIEH, S., TAYA, Y., ANDERSON, C. W., CHESSA, L., SMORODINSKY, N. I., PRIVES, C., REISS, Y., SHILOH, Y. & ZIV, Y. 1998. Enhanced phosphorylation of p53 by ATM in response to DNA damage. *Science,* 281**,** 1674-7.
BANNISTER, A. J. & KOUZARIDES, T. 2011. Regulation of chromatin by histone modifications. *Cell Res,* 21**,** 381-95.
BAO, Y. 2011. Chromatin response to DNA double-strand break damage. *Epigenomics,* 3**,** 307-21.
BARGHOUT, S. H., ZEPEDA, N., VINCENT, K., AZAD, A. K., XU, Z., YANG, C., STEED, H., POSTOVIT, L. M. & FU, Y. 2015. RUNX3 contributes to carboplatin resistance in epithelial ovarian cancer cells. *Gynecol Oncol,* 138**,** 647-55.
BARKESS, G. & WEST, A. G. 2012. Chromatin insulator elements: establishing barriers to set heterochromatin boundaries. *Epigenomics,* 4**,** 67-80.
BARLOW, C., BROWN, K. D., DENG, C. X., TAGLE, D. A. & WYNSHAW-BORIS, A. 1997. Atm selectively regulates distinct p53-dependent cell-cycle checkpoint and apoptotic pathways. *Nat Genet,* 17**,** 453-6.
BARRIO, S., SHANAFELT, T. D., OJHA, J., CHAFFEE, K. G., SECRETO, C., KORTÜM, K. M., PATHANGEY, S., VAN-DYKE, D. L., SLAGER, S. L., FONSECA, R., KAY, N. E. & BRAGGIO, E. 2017. Genomic characterization of high-count MBL cases indicates that early detection of driver mutations and subclonal expansion are predictors of adverse clinical outcome. *Leukemia,* 31**,** 170-176.
BARSKI, A., CUDDAPAH, S., CUI, K., ROH, T. Y., SCHONES, D. E., WANG, Z., WEI, G., CHEPELEV, I. & ZHAO, K. 2007. High-resolution profiling of histone methylations in the human genome. *Cell,* 129**,** 823-37.
BARTIK, M. M., WELKER, D. & KAY, N. E. 1998. Impairments in immune cell function in B cell chronic lymphocytic leukemia. *Semin Oncol,* 25**,** 27-33.
BARTKOVA, J., HAMERLIK, P., STOCKHAUSEN, M. T., EHRMANN, J., HLOBILKOVA, A., LAURSEN, H., KALITA, O., KOLAR, Z., POULSEN, H. S., BROHOLM, H., LUKAS, J. & BARTEK, J. 2010. Replication stress and oxidative damage contribute to aberrant constitutive activation of DNA damage signalling in human gliomas. *Oncogene,* 29**,** 5095-102.
BARTKOVA, J., HOREJSÍ, Z., KOED, K., KRÄMER, A., TORT, F., ZIEGER, K., GULDBERG, P., SEHESTED, M., NESLAND, J. M., LUKAS, C., ØRNTOFT, T., LUKAS, J. & BARTEK, J. 2005. DNA damage response as a candidate anti-cancer barrier in early human tumorigenesis. *Nature,* 434**,** 864-70.
BARTSCH, K., KNITTLER, K., BOROWSKI, C., RUDNIK, S., DAMME, M., ADEN, K., SPEHLMANN, M. E., FREY, N., SAFTIG, P., CHALARIS, A. & RABE, B. 2017. Absence of RNase H2 triggers generation of immunogenic micronuclei removed by autophagy. *Hum Mol Genet,* 26**,** 3960-3972.
BASEHOAR, A. D., ZANTON, S. J. & PUGH, B. F. 2004. Identification and distinct regulation of yeast TATA box-containing genes. *Cell,* 116**,** 699-709.
BAUMANN, T., MOIA, R., GAIDANO, G., DELGADO, J., CONDOLUCI, A., VILLAMOR, N., PAYEDIMARRI, A. B., COSTA, D., PATRIARCA, A., JIMÉNEZ-VICENTE, C., ROSSI, D. & MONTSERRAT, E. 2021.

Lymphocyte doubling time in chronic lymphocytic leukemia modern era: a real-life study in 848 unselected patients. *Leukemia,* 35**,** 2325-2331.

BAWAZIR, A., AL-ZAMEL, N., AMEN, A., AKIEL, M. A., ALHAWITI, N. M. & ALSHEHRI, A. 2019. The burden of leukemia in the Kingdom of Saudi Arabia: 15 years period (1999-2013). *BMC Cancer,* 19**,** 703.

BEAMISH, H., KEDAR, P., KANEKO, H., CHEN, P., FUKAO, T., PENG, C., BERESTEN, S., GUEVEN, N., PURDIE, D., LEES-MILLER, S., ELLIS, N., KONDO, N. & LAVIN, M. F. 2002. Functional link between BLM defective in Bloom's syndrome and the ataxia-telangiectasia-mutated protein, ATM. *J Biol Chem,* 277**,** 30515-23.

BEEKMAN, R., CHAPAPRIETA, V., RUSSIÑOL, N., VILARRASA-BLASI, R., VERDAGUER-DOT, N., MARTENS, J. H. A., DURAN-FERRER, M., KULIS, M., SERRA, F., JAVIERRE, B. M., WINGETT, S. W., CLOT, G., QUEIRÓS, A. C., CASTELLANO, G., BLANC, J., GUT, M., MERKEL, A., HEATH, S., VLASOVA, A., ULLRICH, S., PALUMBO, E., ENJUANES, A., MARTÍN-GARCÍA, D., BEÀ, S., PINYOL, M., AYMERICH, M., ROYO, R., PUIGGROS, M., TORRENTS, D., DATTA, A., LOWY, E., KOSTADIMA, M., ROLLER, M., CLARKE, L., FLICEK, P., AGIRRE, X., PROSPER, F., BAUMANN, T., DELGADO, J., LÓPEZ-GUILLERMO, A., FRASER, P., YASPO, M. L., GUIGÓ, R., SIEBERT, R., MARTÍ-RENOM, M. A., PUENTE, X. S., LÓPEZ-OTÍN, C., GUT, I., STUNNENBERG, H. G., CAMPO, E. & MARTIN-SUBERO, J. I. 2018. The reference epigenome and regulatory chromatin landscape of chronic lymphocytic leukemia. *Nat Med,* 24**,** 868-880.

BELLISSIMO, D. C. & SPECK, N. A. 2017. Mutations in Inherited and Sporadic Leukemia. *Front Cell Dev Biol,* 5**,** 111.

BELLOSILLO, B., VILLAMOR, N., COLOMER, D., PONS, G., MONTSERRAT, E. & GIL, J. 1999. In vitro evaluation of fludarabine in combination with cyclophosphamide and/or mitoxantrone in B-cell chronic lymphocytic leukemia. *Blood,* 94**,** 2836-43.

BELOTSERKOVSKAYA, R., OH, S., BONDARENKO, V. A., ORPHANIDES, G., STUDITSKY, V. M. & REINBERG, D. 2003. FACT facilitates transcription-dependent nucleosome alteration. *Science,* 301**,** 1090-3.

BERNDT, S. I., CAMP, N. J., SKIBOLA, C. F., VIJAI, J., WANG, Z., GU, J., NIETERS, A., KELLY, R. S., SMEDBY, K. E., MONNEREAU, A., COZEN, W., COX, A., WANG, S. S., LAN, Q., TERAS, L. R., MACHADO, M., YEAGER, M., BROOKS-WILSON, A. R., HARTGE, P., PURDUE, M. P., BIRMANN, B. M., VAJDIC, C. M., COCCO, P., ZHANG, Y., GILES, G. G., ZELENIUCH-JACQUOTTE, A., LAWRENCE, C., MONTALVAN, R., BURDETT, L., HUTCHINSON, A., YE, Y., CALL, T. G., SHANAFELT, T. D., NOVAK, A. J., KAY, N. E., LIEBOW, M., CUNNINGHAM, J. M., ALLMER, C., HJALGRIM, H., ADAMI, H. O., MELBYE, M., GLIMELIUS, B., CHANG, E. T., GLENN, M., CURTIN, K., CANNON-ALBRIGHT, L. A., DIVER, W. R., LINK, B. K., WEINER, G. J., CONDE, L., BRACCI, P. M., RIBY, J., ARNETT, D. K., ZHI, D., LEACH, J. M., HOLLY, E. A., JACKSON, R. D., TINKER, L. F., BENAVENTE, Y., SALA, N., CASABONNE, D., BECKER, N., BOFFETTA, P., BRENNAN, P., FORETOVA, L., MAYNADIE, M., MCKAY, J., STAINES, A., CHAFFEE, K. G., ACHENBACH, S. J., VACHON, C. M., GOLDIN, L. R., STROM, S. S., LEIS, J. F., WEINBERG, J. B., CAPORASO, N. E., NORMAN, A. D., DE ROOS, A. J., MORTON, L. M., SEVERSON, R. K., RIBOLI, E., VINEIS, P., KAAKS, R., MASALA, G., WEIDERPASS, E., CHIRLAQUE, M. D., VERMEULEN, R. C. H., TRAVIS, R. C., SOUTHEY, M. C., MILNE, R. L., ALBANES, D., VIRTAMO, J., WEINSTEIN, S., CLAVEL, J., ZHENG, T., HOLFORD, T. R., VILLANO, D. J., MARIA, A., SPINELLI, J. J., GASCOYNE, R. D., et al. 2016. Meta-analysis of genome-wide association studies discovers multiple loci for chronic lymphocytic leukemia. *Nat Commun,* 7**,** 10933.

BINET, J. L., AUQUIER, A., DIGHIERO, G., CHASTANG, C., PIGUET, H., GOASGUEN, J., VAUGIER, G., POTRON, G., COLONA, P., OBERLING, F., THOMAS, M., TCHERNIA, G., JACQUILLAT, C., BOIVIN, P., LESTY, C., DUAULT, M. T., MONCONDUIT, M., BELABBES, S. & GREMY, F. 1981. A new prognostic classification of chronic lymphocytic leukemia derived from a multivariate survival analysis. *Cancer,* 48**,** 198-206.

BIRNBAUM, R. Y., CLOWNEY, E. J., AGAMY, O., KIM, M. J., ZHAO, J., YAMANAKA, T., PAPPALARDO, Z., CLARKE, S. L., WENGER, A. M., NGUYEN, L., GURRIERI, F., EVERMAN, D. B., SCHWARTZ, C. E., BIRK, O. S., BEJERANO, G., LOMVARDAS, S. & AHITUV, N. 2012. Coding exons function as tissue-specific enhancers of nearby genes. *Genome Res,* 22**,** 1059-68.

BLOMBERY, P., ANDERSON, M. A., GONG, J. N., THIJSSEN, R., BIRKINSHAW, R. W., THOMPSON, E. R., TEH, C. E., NGUYEN, T., XU, Z., FLENSBURG, C., LEW, T. E., MAJEWSKI, I. J., GRAY, D. H. D., WESTERMAN, D. A., TAM, C. S., SEYMOUR, J. F., CZABOTAR, P. E., HUANG, D. C. S. & ROBERTS, A. W. 2019. Acquisition of the Recurrent Gly101Val Mutation in BCL2 Confers Resistance to Venetoclax in Patients with Progressive Chronic Lymphocytic Leukemia. *Cancer Discov,* 9**,** 342-353.

BLYTH, K., CAMERON, E. R. & NEIL, J. C. 2005. The RUNX genes: gain or loss of function in cancer. *Nat Rev Cancer,* 5**,** 376-87.

BLYTH, K., VAILLANT, F., JENKINS, A., MCDONALD, L., PRINGLE, M. A., HUSER, C., STEIN, T., NEIL, J. & CAMERON, E. R. 2010. Runx2 in normal tissues and cancer cells: A developing story. *Blood Cells Mol Dis,* 45**,** 117-23.

BOGUSLAWSKI, S. J., SMITH, D. E., MICHALAK, M. A., MICKELSON, K. E., YEHLE, C. O., PATTERSON, W. L. & CARRICO, R. J. 1986. Characterization of monoclonal antibody to DNA.RNA and its application to immunodetection of hybrids. *J Immunol Methods,* 89**,** 123-30.

BONNER, W. M., REDON, C. E., DICKEY, J. S., NAKAMURA, A. J., SEDELNIKOVA, O. A., SOLIER, S. & POMMIER, Y. 2008. GammaH2AX and cancer. *Nat Rev Cancer,* 8**,** 957-67.

BONNET, A., GROSSO, A. R., ELKAOUTARI, A., COLENO, E., PRESLE, A., SRIDHARA, S. C., JANBON, G., GÉLI, V., DE ALMEIDA, S. F. & PALANCADE, B. 2017. Introns Protect Eukaryotic Genomes from Transcription-Associated Genetic Instability. *Mol Cell,* 67**,** 608-621.e6.

BOSCH, F., FERRER, A., LÓPEZ-GUILLERMO, A., GINÉ, E., BELLOSILLO, B., VILLAMOR, N., COLOMER, D., COBO, F., PERALES, M., ESTEVE, J., ALTÉS, A., BESALDUCH, J., RIBERA, J. M., MONTSERRAT, E. & BALEARS), G. G. P. L. E. D. L. A. C. I. 2002. Fludarabine, cyclophosphamide and mitoxantrone in the treatment of resistant or relapsed chronic lymphocytic leukaemia. *Br J Haematol,* 119**,** 976-84.

BOTTONI, A., RIZZOTTO, L., LAI, T. H., LIU, C., SMITH, L. L., MANTEL, R., REIFF, S., EL-GAMAL, D., LARKIN, K., JOHNSON, A. J., LAPALOMBELLA, R., LEHMAN, A., PLUNKETT, W., BYRD, J. C., BLACHLY, J. S., WOYACH, J. A. & SAMPATH, D. 2016. Targeting BTK through microRNA in chronic lymphocytic leukemia. *Blood,* 128**,** 3101-3112.

BRASIER, A. R. 2006. The NF-kappaB regulatory network. *Cardiovasc Toxicol,* 6**,** 111-30.

BRAUNSCHWEIG, U., HOGAN, G. J., PAGIE, L. & VAN STEENSEL, B. 2009. Histone H1 binding is inhibited by histone variant H3.3. *EMBO J,* 28**,** 3635-45.

BREE, R. T., NEARY, C., SAMALI, A. & LOWNDES, N. F. 2004. The switch from survival responses to apoptosis after chromosomal breaks. *DNA Repair (Amst),* 3**,** 989-95.

BRZOSTEK-RACINE, S., GORDON, C., VAN SCOY, S. & REICH, N. C. 2011. The DNA damage response induces IFN. *J Immunol,* 187**,** 5336-45.

BURDA, P., LASLO, P. & STOPKA, T. 2010. The role of PU.1 and GATA-1 transcription factors during normal and leukemogenic hematopoiesis. *Leukemia,* 24**,** 1249-57.

BURGER, J. A. & O'BRIEN, S. 2018. Evolution of CLL treatment - from chemoimmunotherapy to targeted and individualized therapy. *Nat Rev Clin Oncol,* 15**,** 510-527.

BURKOVICS, P., HAJDÚ, I., SZUKACSOV, V., UNK, I. & HARACSKA, L. 2009. Role of PCNA-dependent stimulation of 3'-phosphodiesterase and 3'-5' exonuclease activities of human Ape2 in repair of oxidative DNA damage. *Nucleic Acids Res,* 37**,** 4247-55.

BUSCEMI, G., SAVIO, C., ZANNINI, L., MICCICHÈ, F., MASNADA, D., NAKANISHI, M., TAUCHI, H., KOMATSU, K., MIZUTANI, S., KHANNA, K., CHEN, P., CONCANNON, P., CHESSA, L. & DELIA, D. 2001. Chk2 activation dependence on Nbs1 after DNA damage. *Mol Cell Biol,* 21**,** 5214-22.

BUSHWELLER, J. H. 2019. Targeting transcription factors in cancer - from undruggable to reality. *Nat Rev Cancer,* 19**,** 611-624.

BÖNISCH, C. & HAKE, S. B. 2012. Histone H2A variants in nucleosomes and chromatin: more or less stable? *Nucleic Acids Res,* 40**,** 10719-41.

CAI, X., GAO, L., TENG, L., GE, J., OO, Z. M., KUMAR, A. R., GILLILAND, D. G., MASON, P. J., TAN, K. & SPECK, N. A. 2015. Runx1 Deficiency Decreases Ribosome Biogenesis and Confers Stress Resistance to Hematopoietic Stem and Progenitor Cells. *Cell Stem Cell,* 17**,** 165-77.

CALO, E. & WYSOCKA, J. 2013. Modification of enhancer chromatin: what, how, and why? *Mol Cell,* 49**,** 825-37.

CAMPBELL, S., ISMAIL, I. H., YOUNG, L. C., POIRIER, G. G. & HENDZEL, M. J. 2013. Polycomb repressive complex 2 contributes to DNA double-strand break repair. *Cell Cycle,* 12**,** 2675-83.

CAO, J., CUSANOVICH, D. A., RAMANI, V., AGHAMIRZAIE, D., PLINER, H. A., HILL, A. J., DAZA, R. M., MCFALINE-FIGUEROA, J. L., PACKER, J. S., CHRISTIANSEN, L., STEEMERS, F. J., ADEY, A. C., TRAPNELL, C. & SHENDURE, J. 2018. Joint profiling of chromatin accessibility and gene expression in thousands of single cells. *Science,* 361**,** 1380-1385.

CARCAGNO, A. L., OGARA, M. F., SONZOGNI, S. V., MARAZITA, M. C., SIRKIN, P. F., CERUTI, J. M. & CÁNEPA, E. T. 2009. E2F1 transcription is induced by genotoxic stress through ATM/ATR activation. *IUBMB Life,* 61**,** 537-43.

CARTER, D., CHAKALOVA, L., OSBORNE, C. S., DAI, Y. F. & FRASER, P. 2002. Long-range chromatin regulatory interactions in vivo. *Nat Genet,* 32**,** 623-6.

CASTILLO, J., LÓPEZ-RODAS, G. & FRANCO, L. 2017. Histone Post-Translational Modifications and Nucleosome Organisation in Transcriptional Regulation: Some Open Questions. *Adv Exp Med Biol,* 966**,** 65-92.

CAUCHY, P., JAMES, S. R., ZACARIAS-CABEZA, J., PTASINSKA, A., IMPERATO, M. R., ASSI, S. A., PIPER, J., CANESTRARO, M., HOOGENKAMP, M., RAGHAVAN, M., LOKE, J., AKIKI, S., CLOKIE, S. J., RICHARDS, S. J., WESTHEAD, D. R., GRIFFITHS, M. J., OTT, S., BONIFER, C. & COCKERILL, P. N. 2015. Chronic FLT3-ITD Signaling in Acute Myeloid Leukemia Is Connected to a Specific Chromatin Signature. *Cell Rep,* 12**,** 821-36.

CECCALDI, R., LIU, J. C., AMUNUGAMA, R., HAJDU, I., PRIMACK, B., PETALCORIN, M. I., O'CONNOR, K. W., KONSTANTINOPOULOS, P. A., ELLEDGE, S. J., BOULTON, S. J., YUSUFZAI, T. & D'ANDREA, A. D. 2015. Homologous-recombination-deficient tumours are dependent on Polθ-mediated repair. *Nature,* 518**,** 258-62.

CERRITELLI, S. M. & CROUCH, R. J. 2009. Ribonuclease H: the enzymes in eukaryotes. *FEBS J,* 276**,** 1494-505.

CHAO, D. T. & KORSMEYER, S. J. 1998. BCL-2 family: regulators of cell death. *Annu Rev Immunol,* 16**,** 395-419.

CHEN, G., YUAN, S. S., LIU, W., XU, Y., TRUJILLO, K., SONG, B., CONG, F., GOFF, S. P., WU, Y., ARLINGHAUS, R., BALTIMORE, D., GASSER, P. J., PARK, M. S., SUNG, P. & LEE, E. Y. 1999. Radiation-induced assembly of Rad51 and Rad52 recombination complex requires ATM and c-Abl. *J Biol Chem,* 274**,** 12748-52.

CHEN, J., MOORE, A. & RINGSHAUSEN, I. 2020. ZAP-70 Shapes the Immune Microenvironment in B Cell Malignancies. *Front Oncol,* 10**,** 595832.

CHEN, L., MORIO, T., MINEGISHI, Y., NAKADA, S., NAGASAWA, M., KOMATSU, K., CHESSA, L., VILLA, A., LECIS, D., DELIA, D. & MIZUTANI, S. 2005. Ataxia-telangiectasia-mutated dependent phosphorylation of Artemis in response to DNA damage. *Cancer Sci,* 96**,** 134-41.

CHEN, P., ZHAO, J., WANG, Y., WANG, M., LONG, H., LIANG, D., HUANG, L., WEN, Z., LI, W., LI, X., FENG, H., ZHAO, H., ZHU, P., LI, M., WANG, Q. F. & LI, G. 2013. H3.3 actively marks enhancers and primes gene transcription via opening higher-ordered chromatin. *Genes Dev,* 27**,** 2109-24.

CHEN, S., PAUL, P. & PRICE, B. D. 2003. ATM's leucine-rich domain and adjacent sequences are essential for ATM to regulate the DNA damage response. *Oncogene,* 22**,** 6332-9.

CHIORAZZI, N. 2007. Cell proliferation and death: forgotten features of chronic lymphocytic leukemia B cells. *Best Pract Res Clin Haematol,* 20**,** 399-413.

CHIORAZZI, N., CHEN, S. S. & RAI, K. R. 2021. Chronic Lymphocytic Leukemia. *Cold Spring Harb Perspect Med,* 11.

CHIORAZZI, N., RAI, K. R. & FERRARINI, M. 2005. Chronic lymphocytic leukemia. *N Engl J Med,* 352**,** 804-15.

CHO, J. E., KIM, N. & JINKS-ROBERTSON, S. 2015. Topoisomerase 1-dependent deletions initiated by incision at ribonucleotides are biased to the non-transcribed strand of a highly activated reporter. *Nucleic Acids Res,* 43**,** 9306-13.

CHOI, M., KIPPS, T. & KURZROCK, R. 2016. ATM Mutations in Cancer: Therapeutic Implications. *Mol Cancer Ther,* 15**,** 1781-91.

CHONG, S. Y., CUTLER, S., LIN, J. J., TSAI, C. H., TSAI, H. K., BIGGINS, S., TSUKIYAMA, T., LO, Y. C. & KAO, C. F. 2020. H3K4 methylation at active genes mitigates transcription-replication conflicts during replication stress. *Nat Commun,* 11**,** 809.

CHRISTMANN, M. & KAINA, B. 2013. Transcriptional regulation of human DNA repair genes following genotoxic stress: trigger mechanisms, inducible responses and genotoxic adaptation. *Nucleic Acids Res,* 41**,** 8403-20.

CHUNG, Y. M., PARK, S. H., TSAI, W. B., WANG, S. Y., IKEDA, M. A., BEREK, J. S., CHEN, D. J. & HU, M. C. 2012. FOXO3 signalling links ATM to the p53 apoptotic pathway following DNA damage. *Nat Commun,* 3**,** 1000.

COCKERILL, P. N. 2011. Structure and function of active chromatin and DNase I hypersensitive sites. *FEBS J,* 278**,** 2182-210.

CONNELLY, S. & MANLEY, J. L. 1988. A functional mRNA polyadenylation signal is required for transcription termination by RNA polymerase II. *Genes Dev,* 2**,** 440-52.

COQUEL, F., SILVA, M. J., TÉCHER, H., ZADOROZHNY, K., SHARMA, S., NIEMINUSZCZY, J., METTLING, C., DARDILLAC, E., BARTHE, A., SCHMITZ, A. L., PROMONET, A., CRIBIER, A., SARRAZIN, A., NIEDZWIEDZ, W., LOPEZ, B., COSTANZO, V., KREJCI, L., CHABES, A., BENKIRANE, M., LIN, Y. L. & PASERO, P. 2018. SAMHD1 acts at stalled replication forks to prevent interferon induction. *Nature,* 557**,** 57-61.

CORCES, M. R., TREVINO, A. E., HAMILTON, E. G., GREENSIDE, P. G., SINNOTT-ARMSTRONG, N. A., VESUNA, S., SATPATHY, A. T., RUBIN, A. J., MONTINE, K. S., WU, B., KATHIRIA, A., CHO, S. W., MUMBACH, M. R., CARTER, A. C., KASOWSKI, M., ORLOFF, L. A., RISCA, V. I., KUNDAJE, A., KHAVARI, P. A., MONTINE, T. J., GREENLEAF, W. J. & CHANG, H. Y. 2017. An improved ATAC-seq protocol reduces background and enables interrogation of frozen tissues. *Nat Methods,* 14**,** 959-962.

CRAIG, J. M. 2005. Heterochromatin--many flavours, common themes. *Bioessays,* 27**,** 17-28.

CREYGHTON, M. P., MARKOULAKI, S., LEVINE, S. S., HANNA, J., LODATO, M. A., SHA, K., YOUNG, R. A., JAENISCH, R. & BOYER, L. A. 2008. H2AZ is enriched at polycomb complex target genes in ES cells and is necessary for lineage commitment. *Cell,* 135**,** 649-61.

CROW, Y. J., LEITCH, A., HAYWARD, B. E., GARNER, A., PARMAR, R., GRIFFITH, E., ALI, M., SEMPLE, C., AICARDI, J., BABUL-HIRJI, R., BAUMANN, C., BAXTER, P., BERTINI, E., CHANDLER, K. E., CHITAYAT, D., CAU, D., DÉRY, C., FAZZI, E., GOIZET, C., KING, M. D., KLEPPER, J., LACOMBE, D., LANZI, G., LYALL, H., MARTÍNEZ-FRÍAS, M. L., MATHIEU, M., MCKEOWN, C., MONIER, A., OADE, Y.,

QUARRELL, O. W., RITTEY, C. D., ROGERS, R. C., SANCHIS, A., STEPHENSON, J. B., TACKE, U., TILL, M., TOLMIE, J. L., TOMLIN, P., VOIT, T., WESCHKE, B., WOODS, C. G., LEBON, P., BONTHRON, D. T., PONTING, C. P. & JACKSON, A. P. 2006. Mutations in genes encoding ribonuclease H2 subunits cause Aicardi-Goutières syndrome and mimic congenital viral brain infection. *Nat Genet,* 38**,** 910-6.

CURTIN, N. J. 2012. DNA repair dysregulation from cancer driver to therapeutic target. *Nat Rev Cancer,* 12**,** 801-17.

CUSABIO & TECHNOLOGY. 2019. *How Does Histone Modification Affect Gene Expression?* [Online]. [Accessed 2022].

CÔTÉ, J., QUINN, J., WORKMAN, J. L. & PETERSON, C. L. 1994. Stimulation of GAL4 derivative binding to nucleosomal DNA by the yeast SWI/SNF complex. *Science,* 265**,** 53-60.

DAMLE, R. N., WASIL, T., FAIS, F., GHIOTTO, F., VALETTO, A., ALLEN, S. L., BUCHBINDER, A., BUDMAN, D., DITTMAR, K., KOLITZ, J., LICHTMAN, S. M., SCHULMAN, P., VINCIGUERRA, V. P., RAI, K. R., FERRARINI, M. & CHIORAZZI, N. 1999. Ig V gene mutation status and CD38 expression as novel prognostic indicators in chronic lymphocytic leukemia. *Blood,* 94**,** 1840-7.

DAN, A. L. A. E. T. A. A. N. T.-W. A. C. S. A. J. G. R. A. J. B. A. S. K. A. I. B. A. M. L. 2015. Mutations driving CLL and their evolution in progression and relapse. *Nature,* 526**,** 525.

DANTZER, F., SCHREIBER, V., NIEDERGANG, C., TRUCCO, C., FLATTER, E., DE LA RUBIA, G., OLIVER, J., ROLLI, V., MÉNISSIER-DE MURCIA, J. & DE MURCIA, G. 1999. Involvement of poly(ADP-ribose) polymerase in base excision repair. *Biochimie,* 81**,** 69-75.

DARWICHE, W., GUBLER, B., MAROLLEAU, J. P. & GHAMLOUCH, H. 2018. Chronic Lymphocytic Leukemia B-Cell Normal Cellular Counterpart: Clues From a Functional Perspective. *Front Immunol,* 9**,** 683.

DAUB, H. 2012. DNA damage response: multilevel proteomics gains momentum. *Mol Cell,* 46**,** 113-4.

DAVIDS, M. S. & BROWN, J. R. 2012. Targeting the B cell receptor pathway in chronic lymphocytic leukemia. *Leuk Lymphoma,* 53**,** 2362-70.

DE SANTA, F., BAROZZI, I., MIETTON, F., GHISLETTI, S., POLLETTI, S., TUSI, B. K., MULLER, H., RAGOUSSIS, J., WEI, C. L. & NATOLI, G. 2010. A large fraction of extragenic RNA pol II transcription sites overlap enhancers. *PLoS Biol,* 8**,** e1000384.

DE TUTE, R., YUILLE, M., CATOVSKY, D., HOULSTON, R. S., HILLMEN, P. & RAWSTRON, A. C. 2006. Monoclonal B-cell lymphocytosis (MBL) in CLL families: substantial increase in relative risk for young adults. *Leukemia,* 20**,** 728-9.

DEATON, A. M. & BIRD, A. 2011. CpG islands and the regulation of transcription. *Genes Dev,* 25**,** 1010-22.

DELGADO, J., NADEU, F., COLOMER, D. & CAMPO, E. 2020. Chronic lymphocytic leukemia: from molecular pathogenesis to novel therapeutic strategies. *Haematologica,* 105**,** 2205-2217.

DENEBERG, S., KANDURI, M., ALI, D., BENGTZEN, S., KARIMI, M., QU, Y., KIMBY, E., MANSOURI, L., ROSENQUIST, R., LENNARTSSON, A. & LEHMANN, S. 2014. microRNA-34b/c on chromosome 11q23 is aberrantly methylated in chronic lymphocytic leukemia. *Epigenetics,* 9**,** 910-7.

DHANWANI, R., TAKAHASHI, M. & SHARMA, S. 2018. Cytosolic sensing of immuno-stimulatory DNA, the enemy within. *Curr Opin Immunol,* 50**,** 82-87.

DI VIRGILIO, M., YING, C. Y. & GAUTIER, J. 2009. PIKK-dependent phosphorylation of Mre11 induces MRN complex inactivation by disassembly from chromatin. *DNA Repair (Amst),* 8**,** 1311-20.

DICKEN, J., MILDNER, A., LESHKOWITZ, D., TOUW, I. P., HANTISTEANU, S., JUNG, S. & GRONER, Y. 2013. Transcriptional reprogramming of CD11b+Esam(hi) dendritic cell identity and function by loss of Runx3. *PLoS One,* 8**,** e77490.

DING, W., LAPLANT, B. R., CALL, T. G., PARIKH, S. A., LEIS, J. F., HE, R., SHANAFELT, T. D., SINHA, S., LE-RADEMACHER, J., FELDMAN, A. L., HABERMANN, T. M., WITZIG, T. E., WISEMAN, G. A., LIN, Y., ASMUS, E., NOWAKOWSKI, G. S., CONTE, M. J., BOWEN, D. A., AITKEN, C. N., VAN DYKE, D. L., GREIPP, P. T., LIU, X., WU, X., ZHANG, H., SECRETO, C. R., TIAN, S., BRAGGIO, E., WELLIK, L. E.,

MICALLEF, I., VISWANATHA, D. S., YAN, H., CHANAN-KHAN, A. A., KAY, N. E., DONG, H. & ANSELL, S. M. 2017. Pembrolizumab in patients with CLL and Richter transformation or with relapsed CLL. *Blood,* 129**,** 3419-3427.

DOBZHANSKY, T. 1946. Genetics of natural populations; recombination and variability in populations of Drosophila pseudoobscura. *Genetics,* 31**,** 269-90.

DRAKER, R., NG, M. K., SARCINELLA, E., IGNATCHENKO, V., KISLINGER, T. & CHEUNG, P. 2012. A combination of H2A.Z and H4 acetylation recruits Brd2 to chromatin during transcriptional activation. *PLoS Genet,* 8**,** e1003047.

DUNN, G. P., BRUCE, A. T., SHEEHAN, K. C., SHANKARAN, V., UPPALURI, R., BUI, J. D., DIAMOND, M. S., KOEBEL, C. M., ARTHUR, C., WHITE, J. M. & SCHREIBER, R. D. 2005. A critical function for type I interferons in cancer immunoediting. *Nat Immunol,* 6**,** 722-9.

DUNN, G. P., KOEBEL, C. M. & SCHREIBER, R. D. 2006. Interferons, immunity and cancer immunoediting. *Nat Rev Immunol,* 6**,** 836-48.

DUNN, K. & GRIFFITH, J. D. 1980. The presence of RNA in a double helix inhibits its interaction with histone protein. *Nucleic Acids Res,* 8**,** 555-66.

DÖHNER, H., STILGENBAUER, S., BENNER, A., LEUPOLT, E., KRÖBER, A., BULLINGER, L., DÖHNER, K., BENTZ, M. & LICHTER, P. 2000. Genomic aberrations and survival in chronic lymphocytic leukemia. *N Engl J Med,* 343**,** 1910-6.

EDELMANN, J., HOLZMANN, K., MILLER, F., WINKLER, D., BÜHLER, A., ZENZ, T., BULLINGER, L., KÜHN, M. W., GERHARDINGER, A., BLOEHDORN, J., RADTKE, I., SU, X., MA, J., POUNDS, S., HALLEK, M., LICHTER, P., KORBEL, J., BUSCH, R., MERTENS, D., DOWNING, J. R., STILGENBAUER, S. & DÖHNER, H. 2012. High-resolution genomic profiling of chronic lymphocytic leukemia reveals new recurrent genomic alterations. *Blood,* 120**,** 4783-94.

EDER, P. S. & WALDER, J. A. 1991. Ribonuclease H from K562 human erythroleukemia cells. Purification, characterization, and substrate specificity. *J Biol Chem,* 266**,** 6472-9.

EDER, P. S., WALDER, R. Y. & WALDER, J. A. 1993. Substrate specificity of human RNase H1 and its role in excision repair of ribose residues misincorporated in DNA. *Biochimie,* 75**,** 123-6.

EDGINTON-WHITE, B. & BONIFER, C. 2022. The transcriptional regulation of normal and malignant blood cell development. *FEBS J,* 289**,** 1240-1255.

EL HAGE, A., FRENCH, S. L., BEYER, A. L. & TOLLERVEY, D. 2010. Loss of Topoisomerase I leads to R-loop-mediated transcriptional blocks during ribosomal RNA synthesis. *Genes Dev,* 24**,** 1546-58.

EL HAGE, A., WEBB, S., KERR, A. & TOLLERVEY, D. 2014. Genome-wide distribution of RNA-DNA hybrids identifies RNase H targets in tRNA genes, retrotransposons and mitochondria. *PLoS Genet,* 10**,** e1004716.

ESTELLER, M., HAMILTON, S. R., BURGER, P. C., BAYLIN, S. B. & HERMAN, J. G. 1999. Inactivation of the DNA repair gene O6-methylguanine-DNA methyltransferase by promoter hypermethylation is a common event in primary human neoplasia. *Cancer Res,* 59**,** 793-7.

ESTELLER, M., LEVINE, R., BAYLIN, S. B., ELLENSON, L. H. & HERMAN, J. G. 1998. MLH1 promoter hypermethylation is associated with the microsatellite instability phenotype in sporadic endometrial carcinomas. *Oncogene,* 17**,** 2413-7.

FABBRI, G. & DALLA-FAVERA, R. 2016. The molecular pathogenesis of chronic lymphocytic leukaemia. *Nat Rev Cancer,* 16**,** 145-62.

FABBRI, G., RASI, S., ROSSI, D., TRIFONOV, V., KHIABANIAN, H., MA, J., GRUNN, A., FANGAZIO, M., CAPELLO, D., MONTI, S., CRESTA, S., GARGIULO, E., FORCONI, F., GUARINI, A., ARCAINI, L., PAULLI, M., LAURENTI, L., LAROCCA, L. M., MARASCA, R., GATTEI, V., OSCIER, D., BERTONI, F., MULLIGHAN, C. G., FOÁ, R., PASQUALUCCI, L., RABADAN, R., DALLA-FAVERA, R. & GAIDANO, G. 2011. Analysis of the chronic lymphocytic leukemia coding genome: role of NOTCH1 mutational activation. *J Exp Med,* 208**,** 1389-401.

FAINARU, O., WOOLF, E., LOTEM, J., YARMUS, M., BRENNER, O., GOLDENBERG, D., NEGREANU, V., BERNSTEIN, Y., LEVANON, D., JUNG, S. & GRONER, Y. 2004. Runx3 regulates mouse TGF-beta-mediated dendritic cell function and its absence results in airway inflammation. *EMBO J,* 23**,** 969-79.

FALCK, J., COATES, J. & JACKSON, S. P. 2005. Conserved modes of recruitment of ATM, ATR and DNA-PKcs to sites of DNA damage. *Nature,* 434**,** 605-11.

FALCK, J., PETRINI, J. H., WILLIAMS, B. R., LUKAS, J. & BARTEK, J. 2002. The DNA damage-dependent intra-S phase checkpoint is regulated by parallel pathways. *Nat Genet,* 30**,** 290-4.

FAN, J. Y., RANGASAMY, D., LUGER, K. & TREMETHICK, D. J. 2004. H2A.Z alters the nucleosome surface to promote HP1alpha-mediated chromatin fiber folding. *Mol Cell,* 16**,** 655-61.

FERNANDES, N., SUN, Y., CHEN, S., PAUL, P., SHAW, R. J., CANTLEY, L. C. & PRICE, B. D. 2005. DNA damage-induced association of ATM with its target proteins requires a protein interaction domain in the N terminus of ATM. *J Biol Chem,* 280**,** 15158-64.

FLAVAHAN, W. A., GASKELL, E. & BERNSTEIN, B. E. 2017. Epigenetic plasticity and the hallmarks of cancer. *Science,* 357.

FLEISHER, A. S., ESTELLER, M., WANG, S., TAMURA, G., SUZUKI, H., YIN, J., ZOU, T. T., ABRAHAM, J. M., KONG, D., SMOLINSKI, K. N., SHI, Y. Q., RHYU, M. G., POWELL, S. M., JAMES, S. P., WILSON, K. T., HERMAN, J. G. & MELTZER, S. J. 1999. Hypermethylation of the hMLH1 gene promoter in human gastric cancers with microsatellite instability. *Cancer Res,* 59**,** 1090-5.

FRANK, D., DOENECKE, D. & ALBIG, W. 2003. Differential expression of human replacement and cell cycle dependent H3 histone genes. *Gene,* 312**,** 135-43.

FRANK, P., BRAUNSHOFER-REITER, C., WINTERSBERGER, U., GRIMM, R. & BÜSEN, W. 1998. Cloning of the cDNA encoding the large subunit of human RNase HI, a homologue of the prokaryotic RNase HII. *Proc Natl Acad Sci U S A,* 95**,** 12872-7.

FRANKISH, A., DIEKHANS, M., FERREIRA, A. M., JOHNSON, R., JUNGREIS, I., LOVELAND, J., MUDGE, J. M., SISU, C., WRIGHT, J., ARMSTRONG, J., BARNES, I., BERRY, A., BIGNELL, A., CARBONELL SALA, S., CHRAST, J., CUNNINGHAM, F., DI DOMENICO, T., DONALDSON, S., FIDDES, I. T., GARCÍA GIRÓN, C., GONZALEZ, J. M., GREGO, T., HARDY, M., HOURLIER, T., HUNT, T., IZUOGU, O. G., LAGARDE, J., MARTIN, F. J., MARTÍNEZ, L., MOHANAN, S., MUIR, P., NAVARRO, F. C. P., PARKER, A., PEI, B., POZO, F., RUFFIER, M., SCHMITT, B. M., STAPLETON, E., SUNER, M. M., SYCHEVA, I., USZCZYNSKA-RATAJCZAK, B., XU, J., YATES, A., ZERBINO, D., ZHANG, Y., AKEN, B., CHOUDHARY, J. S., GERSTEIN, M., GUIGÓ, R., HUBBARD, T. J. P., KELLIS, M., PATEN, B., REYMOND, A., TRESS, M. L. & FLICEK, P. 2019. GENCODE reference annotation for the human and mouse genomes. *Nucleic Acids Res,* 47**,** D766-D773.

FRENCH, C. A., MIYOSHI, I., ASTER, J. C., KUBONISHI, I., KROLL, T. G., DAL CIN, P., VARGAS, S. O., PEREZ-ATAYDE, A. R. & FLETCHER, J. A. 2001. BRD4 bromodomain gene rearrangement in aggressive carcinoma with translocation t(15;19). *Am J Pathol,* 159**,** 1987-92.

FRENCH, C. A., RAMIREZ, C. L., KOLMAKOVA, J., HICKMAN, T. T., CAMERON, M. J., THYNE, M. E., KUTOK, J. L., TORETSKY, J. A., TADAVARTHY, A. K., KEES, U. R., FLETCHER, J. A. & ASTER, J. C. 2008. BRD-NUT oncoproteins: a family of closely related nuclear proteins that block epithelial differentiation and maintain the growth of carcinoma cells. *Oncogene,* 27**,** 2237-42.

FU, I., SMITH, D. J. & BROYDE, S. 2019. Rotational and translational positions determine the structural and dynamic impact of a single ribonucleotide incorporated in the nucleosome. *DNA Repair (Amst),* 73**,** 155-163.

FURMAN, R. R., SHARMAN, J. P., COUTRE, S. E., CHESON, B. D., PAGEL, J. M., HILLMEN, P., BARRIENTOS, J. C., ZELENETZ, A. D., KIPPS, T. J., FLINN, I., GHIA, P., ERADAT, H., ERVIN, T., LAMANNA, N., COIFFIER, B., PETTITT, A. R., MA, S., STILGENBAUER, S., CRAMER, P., AIELLO, M., JOHNSON, D.

M., MILLER, L. L., LI, D., JAHN, T. M., DANSEY, R. D., HALLEK, M. & O'BRIEN, S. M. 2014. Idelalisib and rituximab in relapsed chronic lymphocytic leukemia. *N Engl J Med,* 370**,** 997-1007.

GAILLARD, S., CHARASSON, V., RIBEYRE, C., SALIFOU, K., PILLAIRE, M. J., HOFFMANN, J. S., CONSTANTINOU, A., TROUCHE, D. & VANDROMME, M. 2021. KDM5A and KDM5B histone-demethylases contribute to HU-induced replication stress response and tolerance. *Biol Open,* 10.

GAITI, F., CHALIGNE, R., GU, H., BRAND, R. M., KOTHEN-HILL, S., SCHULMAN, R. C., GRIGOREV, K., RISSO, D., KIM, K. T., PASTORE, A., HUANG, K. Y., ALONSO, A., SHERIDAN, C., OMANS, N. D., BIEDERSTEDT, E., CLEMENT, K., WANG, L., FELSENFELD, J. A., BHAVSAR, E. B., ARYEE, M. J., ALLAN, J. N., FURMAN, R., GNIRKE, A., WU, C. J., MEISSNER, A. & LANDAU, D. A. 2019. Epigenetic evolution and lineage histories of chronic lymphocytic leukaemia. *Nature,* 569**,** 576-580.

GALE, R. P. & RAI, K. R. 1987. Chronic Lymphocytic Leukemia: Recent Progress and Future Direction: Proceedings of a Hyland Laboratories-UCLA Symposium Held in Napa, California, December 2-5, 1986.

GARCÍA-MUSE, T. & AGUILERA, A. 2016. Transcription-replication conflicts: how they occur and how they are resolved. *Nat Rev Mol Cell Biol,* 17**,** 553-63.

GARG, R., WIERDA, W., FERRAJOLI, A., ABRUZZO, L., PIERCE, S., LERNER, S., KEATING, M. & O'BRIEN, S. 2012. The prognostic difference of monoallelic versus biallelic deletion of 13q in chronic lymphocytic leukemia. *Cancer,* 118**,** 3531-7.

GASSER, S. & RAULET, D. H. 2006. The DNA damage response arouses the immune system. *Cancer Res,* 66**,** 3959-62.

GASSER, S., ZHANG, W. Y. L., TAN, N. Y. J., TRIPATHI, S., SUTER, M. A., CHEW, Z. H., KHATOO, M., NGEOW, J. & CHEUNG, F. S. G. 2017. Sensing of dangerous DNA. *Mech Ageing Dev,* 165**,** 33-46.

GATEI, M., JAKOB, B., CHEN, P., KIJAS, A. W., BECHEREL, O. J., GUEVEN, N., BIRRELL, G., LEE, J. H., PAULL, T. T., LERENTHAL, Y., FAZRY, S., TAUCHER-SCHOLZ, G., KALB, R., SCHINDLER, D., WALTES, R., DÖRK, T. & LAVIN, M. F. 2011. ATM protein-dependent phosphorylation of Rad50 protein regulates DNA repair and cell cycle control. *J Biol Chem,* 286**,** 31542-56.

GHAMLOUCH, H., NGUYEN-KHAC, F. & BERNARD, O. A. 2017. Chronic lymphocytic leukaemia genomics and the precision medicine era. *Br J Haematol,* 178**,** 852-870.

GHANDI, M., HUANG, F. W., JANÉ-VALBUENA, J., KRYUKOV, G. V., LO, C. C., MCDONALD, E. R., BARRETINA, J., GELFAND, E. T., BIELSKI, C. M., LI, H., HU, K., ANDREEV-DRAKHLIN, A. Y., KIM, J., HESS, J. M., HAAS, B. J., AGUET, F., WEIR, B. A., ROTHBERG, M. V., PAOLELLA, B. R., LAWRENCE, M. S., AKBANI, R., LU, Y., TIV, H. L., GOKHALE, P. C., DE WECK, A., MANSOUR, A. A., OH, C., SHIH, J., HADI, K., ROSEN, Y., BISTLINE, J., VENKATESAN, K., REDDY, A., SONKIN, D., LIU, M., LEHAR, J., KORN, J. M., PORTER, D. A., JONES, M. D., GOLJI, J., CAPONIGRO, G., TAYLOR, J. E., DUNNING, C. M., CREECH, A. L., WARREN, A. C., MCFARLAND, J. M., ZAMANIGHOMI, M., KAUFFMANN, A., STRANSKY, N., IMIELINSKI, M., MARUVKA, Y. E., CHERNIACK, A. D., TSHERNIAK, A., VAZQUEZ, F., JAFFE, J. D., LANE, A. A., WEINSTOCK, D. M., JOHANNESSEN, C. M., MORRISSEY, M. P., STEGMEIER, F., SCHLEGEL, R., HAHN, W. C., GETZ, G., MILLS, G. B., BOEHM, J. S., GOLUB, T. R., GARRAWAY, L. A. & SELLERS, W. R. 2019. Next-generation characterization of the Cancer Cell Line Encyclopedia. *Nature,* 569**,** 503-508.

GHIA, P., STAMATOPOULOS, K., BELESSI, C., MORENO, C., STELLA, S., GUIDA, G., MICHEL, A., CRESPO, M., LAOUTARIS, N., MONTSERRAT, E., ANAGNOSTOPOULOS, A., DIGHIERO, G., FASSAS, A., CALIGARIS-CAPPIO, F. & DAVI, F. 2005. Geographic patterns and pathogenetic implications of IGHV gene usage in chronic lymphocytic leukemia: the lesson of the IGHV3-21 gene. *Blood,* 105**,** 1678-85.

GILMOUR, J., ASSI, S. A., NOAILLES, L., LICHTINGER, M., OBIER, N. & BONIFER, C. 2018. The Co-operation of RUNX1 with LDB1, CDK9 and BRD4 Drives Transcription Factor Complex Relocation During Haematopoietic Specification. *Sci Rep,* 8**,** 10410.

GINNO, P. A., LOTT, P. L., CHRISTENSEN, H. C., KORF, I. & CHÉDIN, F. 2012. R-loop formation is a distinctive characteristic of unmethylated human CpG island promoters. *Mol Cell,* 45**,** 814-25.

GOEDE, V., FISCHER, K., BUSCH, R., ENGELKE, A., EICHHORST, B., WENDTNER, C. M., CHAGOROVA, T., DE LA SERNA, J., DILHUYDY, M. S., ILLMER, T., OPAT, S., OWEN, C. J., SAMOYLOVA, O., KREUZER, K. A., STILGENBAUER, S., DÖHNER, H., LANGERAK, A. W., RITGEN, M., KNEBA, M., ASIKANIUS, E., HUMPHREY, K., WENGER, M. & HALLEK, M. 2014. Obinutuzumab plus chlorambucil in patients with CLL and coexisting conditions. *N Engl J Med,* 370**,** 1101-10.

GOLDIN, L. R., PFEIFFER, R. M., LI, X. & HEMMINKI, K. 2004. Familial risk of lymphoproliferative tumors in families of patients with chronic lymphocytic leukemia: results from the Swedish Family-Cancer Database. *Blood,* 104**,** 1850-4.

GONG, F., CLOUAIRE, T., AGUIRREBENGOA, M., LEGUBE, G. & MILLER, K. M. 2017. Histone demethylase KDM5A regulates the ZMYND8-NuRD chromatin remodeler to promote DNA repair. *J Cell Biol,* 216**,** 1959-1974.

GOODARZI, A. A., JONNALAGADDA, J. C., DOUGLAS, P., YOUNG, D., YE, R., MOORHEAD, G. B., LEES-MILLER, S. P. & KHANNA, K. K. 2004. Autophosphorylation of ataxia-telangiectasia mutated is regulated by protein phosphatase 2A. *EMBO J,* 23**,** 4451-61.

GOODARZI, A. A., NOON, A. T., DECKBAR, D., ZIV, Y., SHILOH, Y., LÖBRICH, M. & JEGGO, P. A. 2008. ATM signaling facilitates repair of DNA double-strand breaks associated with heterochromatin. *Mol Cell,* 31**,** 167-77.

GORGOULIS, V. G., VASSILIOU, L. V., KARAKAIDOS, P., ZACHARATOS, P., KOTSINAS, A., LILOGLOU, T., VENERE, M., DITULLIO, R. A., KASTRINAKIS, N. G., LEVY, B., KLETSAS, D., YONETA, A., HERLYN, M., KITTAS, C. & HALAZONETIS, T. D. 2005. Activation of the DNA damage checkpoint and genomic instability in human precancerous lesions. *Nature,* 434**,** 907-13.

GREAVES, I. K., RANGASAMY, D., RIDGWAY, P. & TREMETHICK, D. J. 2007. H2A.Z contributes to the unique 3D structure of the centromere. *Proc Natl Acad Sci U S A,* 104**,** 525-30.

GREENBERG, M. V. C. & BOURC'HIS, D. 2019. The diverse roles of DNA methylation in mammalian development and disease. *Nat Rev Mol Cell Biol,* 20**,** 590-607.

GREWAL, S. I. & ELGIN, S. C. 2002. Heterochromatin: new possibilities for the inheritance of structure. *Curr Opin Genet Dev,* 12**,** 178-87.

GRUBER, M., BOZIC, I., LESHCHINER, I., LIVITZ, D., STEVENSON, K., RASSENTI, L., ROSEBROCK, D., TAYLOR-WEINER, A., OLIVE, O., GOYETCHE, R., FERNANDES, S. M., SUN, J., STEWART, C., WONG, A., CIBULSKIS, C., ZHANG, W., REITER, J. G., GEROLD, J. M., GRIBBEN, J. G., RAI, K. R., KEATING, M. J., BROWN, J. R., NEUBERG, D., KIPPS, T. J., NOWAK, M. A., GETZ, G. & WU, C. J. 2019. Growth dynamics in naturally progressing chronic lymphocytic leukaemia. *Nature,* 570**,** 474-479.

GRÜNBERG, S., WARFIELD, L. & HAHN, S. 2012. Architecture of the RNA polymerase II preinitiation complex and mechanism of ATP-dependent promoter opening. *Nat Struct Mol Biol,* 19**,** 788-96.

GU, Z., EILS, R. & SCHLESNER, M. 2016. Complex heatmaps reveal patterns and correlations in multidimensional genomic data. *Bioinformatics,* 32**,** 2847-9.

GUENTHER, M. G., LEVINE, S. S., BOYER, L. A., JAENISCH, R. & YOUNG, R. A. 2007. A chromatin landmark and transcription initiation at most promoters in human cells. *Cell,* 130**,** 77-88.

GUI, X., YANG, H., LI, T., TAN, X., SHI, P., LI, M., DU, F. & CHEN, Z. J. 2019. Autophagy induction via STING trafficking is a primordial function of the cGAS pathway. *Nature,* 567**,** 262-266.

GUO, Z., KOZLOV, S., LAVIN, M. F., PERSON, M. D. & PAULL, T. T. 2010. ATM activation by oxidative stress. *Science,* 330**,** 517-21.

HABERLE, V. & STARK, A. 2018. Eukaryotic core promoters and the functional basis of transcription initiation. *Nat Rev Mol Cell Biol,* 19**,** 621-637.
HALAZONETIS, T. D., GORGOULIS, V. G. & BARTEK, J. 2008. An oncogene-induced DNA damage model for cancer development. *Science,* 319**,** 1352-5.
HALKIDOU, K., GAUGHAN, L., COOK, S., LEUNG, H. Y., NEAL, D. E. & ROBSON, C. N. 2004. Upregulation and nuclear recruitment of HDAC1 in hormone refractory prostate cancer. *Prostate,* 59**,** 177-89.
HALLEK, M. 2019. Chronic lymphocytic leukemia: 2020 update on diagnosis, risk stratification and treatment. *Am J Hematol,* 94**,** 1266-1287.
HALLEK, M., CHESON, B. D., CATOVSKY, D., CALIGARIS-CAPPIO, F., DIGHIERO, G., DÖHNER, H., HILLMEN, P., KEATING, M., MONTSERRAT, E., CHIORAZZI, N., STILGENBAUER, S., RAI, K. R., BYRD, J. C., EICHHORST, B., O'BRIEN, S., ROBAK, T., SEYMOUR, J. F. & KIPPS, T. J. 2018. iwCLL guidelines for diagnosis, indications for treatment, response assessment, and supportive management of CLL. *Blood,* 131**,** 2745-2760.
HAMBLIN, T. J., DAVIS, Z., GARDINER, A., OSCIER, D. G. & STEVENSON, F. K. 1999. Unmutated Ig V(H) genes are associated with a more aggressive form of chronic lymphocytic leukemia. *Blood,* 94**,** 1848-54.
HAMID, O., ROBERT, C., DAUD, A., HODI, F. S., HWU, W. J., KEFFORD, R., WOLCHOK, J. D., HERSEY, P., JOSEPH, R. W., WEBER, J. S., DRONCA, R., GANGADHAR, T. C., PATNAIK, A., ZAROUR, H., JOSHUA, A. M., GERGICH, K., ELASSAISS-SCHAAP, J., ALGAZI, A., MATEUS, C., BOASBERG, P., TUMEH, P. C., CHMIELOWSKI, B., EBBINGHAUS, S. W., LI, X. N., KANG, S. P. & RIBAS, A. 2013. Safety and tumor responses with lambrolizumab (anti-PD-1) in melanoma. *N Engl J Med,* 369**,** 134-44.
HARDY, S., JACQUES, P. E., GÉVRY, N., FOREST, A., FORTIN, M. E., LAFLAMME, L., GAUDREAU, L. & ROBERT, F. 2009. The euchromatic and heterochromatic landscapes are shaped by antagonizing effects of transcription on H2A.Z deposition. *PLoS Genet,* 5**,** e1000687.
HART, T., TONG, A. H. Y., CHAN, K., VAN LEEUWEN, J., SEETHARAMAN, A., AREGGER, M., CHANDRASHEKHAR, M., HUSTEDT, N., SETH, S., NOONAN, A., HABSID, A., SIZOVA, O., NEDYALKOVA, L., CLIMIE, R., TWORZYANSKI, L., LAWSON, K., SARTORI, M. A., ALIBEH, S., TIEU, D., MASUD, S., MERO, P., WEISS, A., BROWN, K. R., USAJ, M., BILLMANN, M., RAHMAN, M., CONSTANZO, M., MYERS, C. L., ANDREWS, B. J., BOONE, C., DUROCHER, D. & MOFFAT, J. 2017. Evaluation and Design of Genome-Wide CRISPR/SpCas9 Knockout Screens. *G3 (Bethesda),* 7**,** 2719-2727.
HE, R. & KIDDER, B. L. 2017. H3K4 demethylase KDM5B regulates global dynamics of transcription elongation and alternative splicing in embryonic stem cells. *Nucleic Acids Res,* 45**,** 6427-6441.
HEINZ, S., BENNER, C., SPANN, N., BERTOLINO, E., LIN, Y. C., LASLO, P., CHENG, J. X., MURRE, C., SINGH, H. & GLASS, C. K. 2010. Simple combinations of lineage-determining transcription factors prime cis-regulatory elements required for macrophage and B cell identities. *Mol Cell,* 38**,** 576-89.
HELSEN, J., VOORDECKERS, K., VANDERWAEREN, L., SANTERMANS, T., TSONTAKI, M., VERSTREPEN, K. J. & JELIER, R. 2020. Gene Loss Predictably Drives Evolutionary Adaptation. *Mol Biol Evol,* 37**,** 2989-3002.
HERFARTH, K. K., BRENT, T. P., DANAM, R. P., REMACK, J. S., KODNER, I. J., WELLS, S. A. & GOODFELLOW, P. J. 1999. A specific CpG methylation pattern of the MGMT promoter region associated with reduced MGMT expression in primary colorectal cancers. *Mol Carcinog,* 24**,** 90-8.
HERISHANU, Y. & POLLIACK, A. 2013. B-cell receptor signaling in chronic lymphocytic leukemia leans on Lyn. *Leuk Lymphoma,* 54**,** 1125-6.
HERMAN, J. G., UMAR, A., POLYAK, K., GRAFF, J. R., AHUJA, N., ISSA, J. P., MARKOWITZ, S., WILLSON, J. K., HAMILTON, S. R., KINZLER, K. W., KANE, M. F., KOLODNER, R. D., VOGELSTEIN, B., KUNKEL, T. A. & BAYLIN, S. B. 1998. Incidence and functional consequences of hMLH1 promoter hypermethylation in colorectal carcinoma. *Proc Natl Acad Sci U S A,* 95**,** 6870-5.

HERZ, H. M., HU, D. & SHILATIFARD, A. 2014. Enhancer malfunction in cancer. *Mol Cell,* 53**,** 859-66.
HEWISH, D. R. & BURGOYNE, L. A. 1973. Chromatin sub-structure. The digestion of chromatin DNA at regularly spaced sites by a nuclear deoxyribonuclease. *Biochem Biophys Res Commun,* 52**,** 504-10.
HIGGS, M. R., SATO, K., REYNOLDS, J. J., BEGUM, S., BAYLEY, R., GOULA, A., VERNET, A., PAQUIN, K. L., SKALNIK, D. G., KOBAYASHI, W., TAKATA, M., HOWLETT, N. G., KURUMIZAKA, H., KIMURA, H. & STEWART, G. S. 2018. Histone Methylation by SETD1A Protects Nascent DNA through the Nucleosome Chaperone Activity of FANCD2. *Mol Cell,* 71**,** 25-41.e6.
HILLMEN, P., ROBAK, T., JANSSENS, A., BABU, K. G., KLOCZKO, J., GROSICKI, S., DOUBEK, M., PANAGIOTIDIS, P., KIMBY, E., SCHUH, A., PETTITT, A. R., BOYD, T., MONTILLO, M., GUPTA, I. V., WRIGHT, O., DIXON, I., CAREY, J. L., CHANG, C. N., LISBY, S., MCKEOWN, A., OFFNER, F. & INVESTIGATORS, C. S. 2015. Chlorambucil plus ofatumumab versus chlorambucil alone in previously untreated patients with chronic lymphocytic leukaemia (COMPLEMENT 1): a randomised, multicentre, open-label phase 3 trial. *Lancet,* 385**,** 1873-83.
HINOHARA, K., WU, H. J., SÉBASTIEN VIGNEAU, MCDONALD, T. O., IGARASHI, K. J., YAMAMOTO, K. N., MADSEN, T., FASSL, A., EGRI, S. B., PAPANASTASIOU, M., DING, L., PELUFFO, G., COHEN, O., KALES, S. C., LAL-NAG, M., RAI, G., MALONEY, D. J., JADHAV, A., SIMEONOV, A., WAGLE, N., BROWN, M., MEISSNER, A., SICINSKI, P., JAFFE, J. D., JESELSOHN, R., GIMELBRANT, A. A., MICHOR, F. & POLYAK, K. 2019. KDM5 Histone Demethylase Activity Links Cellular Transcriptomic Heterogeneity to Therapeutic Resistance. *Cancer Cell,* 35**,** 330-332.
HINOHARA, K., WU, H. J., VIGNEAU, S., MCDONALD, T. O., IGARASHI, K. J., YAMAMOTO, K. N., MADSEN, T., FASSL, A., EGRI, S. B., PAPANASTASIOU, M., DING, L., PELUFFO, G., COHEN, O., KALES, S. C., LAL-NAG, M., RAI, G., MALONEY, D. J., JADHAV, A., SIMEONOV, A., WAGLE, N., BROWN, M., MEISSNER, A., SICINSKI, P., JAFFE, J. D., JESELSOHN, R., GIMELBRANT, A. A., MICHOR, F. & POLYAK, K. 2018. KDM5 Histone Demethylase Activity Links Cellular Transcriptomic Heterogeneity to Therapeutic Resistance. *Cancer Cell,* 34**,** 939-953.e9.
HNISZ, D., WEINTRAUB, A. S., DAY, D. S., VALTON, A. L., BAK, R. O., LI, C. H., GOLDMANN, J., LAJOIE, B. R., FAN, Z. P., SIGOVA, A. A., REDDY, J., BORGES-RIVERA, D., LEE, T. I., JAENISCH, R., PORTEUS, M. H., DEKKER, J. & YOUNG, R. A. 2016. Activation of proto-oncogenes by disruption of chromosome neighborhoods. *Science,* 351**,** 1454-1458.
HO, G. P., MARGOSSIAN, S., TANIGUCHI, T. & D'ANDREA, A. D. 2006. Phosphorylation of FANCD2 on two novel sites is required for mitomycin C resistance. *Mol Cell Biol,* 26**,** 7005-15.
HOFFMAN, G. R., RAHAL, R., BUXTON, F., XIANG, K., MCALLISTER, G., FRIAS, E., BAGDASARIAN, L., HUBER, J., LINDEMAN, A., CHEN, D., ROMERO, R., RAMADAN, N., PHADKE, T., HAAS, K., JASKELIOFF, M., WILSON, B. G., MEYER, M. J., SAENZ-VASH, V., ZHAI, H., MYER, V. E., PORTER, J. A., KEEN, N., MCLAUGHLIN, M. E., MICKANIN, C., ROBERTS, C. W., STEGMEIER, F. & JAGANI, Z. 2014. Functional epigenetics approach identifies BRM/SMARCA2 as a critical synthetic lethal target in BRG1-deficient cancers. *Proc Natl Acad Sci U S A,* 111**,** 3128-33.
HOLDT, L. M., HOFFMANN, S., SASS, K., LANGENBERGER, D., SCHOLZ, M., KROHN, K., FINSTERMEIER, K., STAHRINGER, A., WILFERT, W., BEUTNER, F., GIELEN, S., SCHULER, G., GÄBEL, G., BERGERT, H., BECHMANN, I., STADLER, P. F., THIERY, J. & TEUPSER, D. 2013. Alu elements in ANRIL non-coding RNA at chromosome 9p21 modulate atherogenic cell functions through trans-regulation of gene networks. *PLoS Genet,* 9**,** e1003588.
HONDELE, M., STUWE, T., HASSLER, M., HALBACH, F., BOWMAN, A., ZHANG, E. T., NIJMEIJER, B., KOTTHOFF, C., RYBIN, V., AMLACHER, S., HURT, E. & LADURNER, A. G. 2013. Structural basis of histone H2A-H2B recognition by the essential chaperone FACT. *Nature,* 499**,** 111-4.
HONG, C., TIJHUIS, A. E. & FOIJER, F. 2019. The cGAS Paradox: Contrasting Roles for cGAS-STING Pathway in Chromosomal Instability. *Cells,* 8.

HOPFNER, K. P., KARCHER, A., CRAIG, L., WOO, T. T., CARNEY, J. P. & TAINER, J. A. 2001. Structural biochemistry and interaction architecture of the DNA double-strand break repair Mre11 nuclease and Rad50-ATPase. *Cell,* 105**,** 473-85.

HOUSE, N. C., KOCH, M. R. & FREUDENREICH, C. H. 2014. Chromatin modifications and DNA repair: beyond double-strand breaks. *Front Genet,* 5**,** 296.

HOVATTER, K. R. & MARTINSON, H. G. 1987. Ribonucleotide-induced helical alteration in DNA prevents nucleosome formation. *Proc Natl Acad Sci U S A,* 84**,** 1162-6.

HSIEH, F. K., KULAEVA, O. I., PATEL, S. S., DYER, P. N., LUGER, K., REINBERG, D. & STUDITSKY, V. M. 2013. Histone chaperone FACT action during transcription through chromatin by RNA polymerase II. *Proc Natl Acad Sci U S A,* 110**,** 7654-9.

HU, H., MIAO, Y. R., JIA, L. H., YU, Q. Y., ZHANG, Q. & GUO, A. Y. 2019. AnimalTFDB 3.0: a comprehensive resource for annotation and prediction of animal transcription factors. *Nucleic Acids Res,* 47**,** D33-D38.

HUANG, A., GARRAWAY, L. A., ASHWORTH, A. & WEBER, B. 2020. Synthetic lethality as an engine for cancer drug target discovery. *Nat Rev Drug Discov,* 19**,** 23-38.

HUANG, S. Y., GHOSH, S. & POMMIER, Y. 2015. Topoisomerase I alone is sufficient to produce short DNA deletions and can also reverse nicks at ribonucleotide sites. *J Biol Chem,* 290**,** 14068-76.

HYJEK, M., FIGIEL, M. & NOWOTNY, M. 2019. RNases H: Structure and mechanism. *DNA Repair (Amst),* 84**,** 102672.

HÄRTLOVA, A., ERTTMANN, S. F., RAFFI, F. A., SCHMALZ, A. M., RESCH, U., ANUGULA, S., LIENENKLAUS, S., NILSSON, L. M., KRÖGER, A., NILSSON, J. A., EK, T., WEISS, S. & GEKARA, N. O. 2015. DNA damage primes the type I interferon system via the cytosolic DNA sensor STING to promote anti-microbial innate immunity. *Immunity,* 42**,** 332-343.

HØJFELDT, J. W., AGGER, K. & HELIN, K. 2013. Histone lysine demethylases as targets for anticancer therapy. *Nat Rev Drug Discov,* 12**,** 917-30.

II, M., II, T., MIRONOVA, L. I. & BRILL, S. J. 2011. Epistasis analysis between homologous recombination genes in Saccharomyces cerevisiae identifies multiple repair pathways for Sgs1, Mus81-Mms4 and RNase H2. *Mutat Res,* 714**,** 33-43.

IMPROGO, M. R., TESAR, B., KLITGAARD, J. L., MAGORI-COHEN, R., YU, L., KASAR, S., CHAUDHARY, D., MIAO, W., FERNANDES, S. M., HOANG, K., WESTLIN, W. F., KIM, H. T. & BROWN, J. R. 2019. MYD88 L265P mutations identify a prognostic gene expression signature and a pathway for targeted inhibition in CLL. *Br J Haematol,* 184**,** 925-936.

ISHIBE, N., SGAMBATI, M. T., FONTAINE, L., GOLDIN, L. R., JAIN, N., WEISSMAN, N., MARTI, G. E. & CAPORASO, N. E. 2001. Clinical characteristics of familial B-CLL in the National Cancer Institute Familial Registry. *Leuk Lymphoma,* 42**,** 99-108.

JACKSON, S. P. & BARTEK, J. 2009. The DNA-damage response in human biology and disease. *Nature,* 461**,** 1071-8.

JAIN, N., KEATING, M., THOMPSON, P., FERRAJOLI, A., BURGER, J., BORTHAKUR, G., TAKAHASHI, K., ESTROV, Z., FOWLER, N., KADIA, T., KONOPLEVA, M., ALVARADO, Y., YILMAZ, M., DINARDO, C., BOSE, P., OHANIAN, M., PEMMARAJU, N., JABBOUR, E., SASAKI, K., KANAGAL-SHAMANNA, R., PATEL, K., JORGENSEN, J., GARG, N., WANG, X., SONDERMANN, K., CRUZ, N., WEI, C., AYALA, A., PLUNKETT, W., KANTARJIAN, H., GANDHI, V. & WIERDA, W. 2019. Ibrutinib and Venetoclax for First-Line Treatment of CLL. *N Engl J Med,* 380**,** 2095-2103.

JAIN, P., KEATING, M. J., WIERDA, W. G., SIVINA, M., THOMPSON, P. A., FERRAJOLI, A., ESTROV, Z., KANTARJIAN, H., O'BRIEN, S. & BURGER, J. A. 2017. Long-term Follow-up of Treatment with Ibrutinib and Rituximab in Patients with High-Risk Chronic Lymphocytic Leukemia. *Clin Cancer Res,* 23**,** 2154-2158.

JAMAI, A., PUGLISI, A. & STRUBIN, M. 2009. Histone chaperone spt16 promotes redeposition of the original h3-h4 histones evicted by elongating RNA polymerase. *Mol Cell,* 35**,** 377-83.

JARAMILLO, S., AGATHANGELIDIS, A., SCHNEIDER, C., BAHLO, J., ROBRECHT, S., TAUSCH, E., BLOEHDORN, J., HOECHSTETTER, M., FISCHER, K., EICHHORST, B., GOEDE, V., HALLEK, M., DÖHNER, H., ROSENQUIST, R., GHIA, P., STAMATOPOULOS, K. & STILGENBAUER, S. 2020. Prognostic impact of prevalent chronic lymphocytic leukemia stereotyped subsets: analysis within prospective clinical trials of the German CLL Study Group (GCLLSG). *Haematologica,* 105**,** 2598-2607.

JASSAL, B., MATTHEWS, L., VITERI, G., GONG, C., LORENTE, P., FABREGAT, A., SIDIROPOULOS, K., COOK, J., GILLESPIE, M., HAW, R., LONEY, F., MAY, B., MILACIC, M., ROTHFELS, K., SEVILLA, C., SHAMOVSKY, V., SHORSER, S., VARUSAI, T., WEISER, J., WU, G., STEIN, L., HERMJAKOB, H. & D'EUSTACHIO, P. 2020. The reactome pathway knowledgebase. *Nucleic Acids Res,* 48**,** D498-D503.

JIANG, X., ZHOU, J., GIOBBIE-HURDER, A., WARGO, J. & HODI, F. S. 2013. The activation of MAPK in melanoma cells resistant to BRAF inhibition promotes PD-L1 expression that is reversible by MEK and PI3K inhibition. *Clin Cancer Res,* 19**,** 598-609.

JIN, C. & FELSENFELD, G. 2007. Nucleosome stability mediated by histone variants H3.3 and H2A.Z. *Genes Dev,* 21**,** 1519-29.

JIN, C., ZANG, C., WEI, G., CUI, K., PENG, W., ZHAO, K. & FELSENFELD, G. 2009. H3.3/H2A.Z double variant-containing nucleosomes mark 'nucleosome-free regions' of active promoters and other regulatory regions. *Nat Genet,* 41**,** 941-5.

JOERGER, A. C. & FERSHT, A. R. 2016. The p53 Pathway: Origins, Inactivation in Cancer, and Emerging Therapeutic Approaches. *Annu Rev Biochem,* 85**,** 375-404.

JOHN, S. A., CLEMENTS, J. L., RUSSELL, L. M. & GARRETT-SINHA, L. A. 2008. Ets-1 regulates plasma cell differentiation by interfering with the activity of the transcription factor Blimp-1. *J Biol Chem,* 283**,** 951-62.

JOHNSON, T. A., CHEREJI, R. V., STAVREVA, D. A., MORRIS, S. A., HAGER, G. L. & CLARK, D. J. 2018. Conventional and pioneer modes of glucocorticoid receptor interaction with enhancer chromatin in vivo. *Nucleic Acids Res,* 46**,** 203-214.

KAISER, V. B. & SEMPLE, C. A. 2017. When TADs go bad: chromatin structure and nuclear organisation in human disease. *F1000Res,* 6.

KAKAROUGKAS, A., ISMAIL, A., CHAMBERS, A. L., RIBALLO, E., HERBERT, A. D., KÜNZEL, J., LÖBRICH, M., JEGGO, P. A. & DOWNS, J. A. 2014. Requirement for PBAF in transcriptional repression and repair at DNA breaks in actively transcribed regions of chromatin. *Mol Cell,* 55**,** 723-32.

KALOCSAY, M., HILLER, N. J. & JENTSCH, S. 2009. Chromosome-wide Rad51 spreading and SUMO-H2A.Z-dependent chromosome fixation in response to a persistent DNA double-strand break. *Mol Cell,* 33**,** 335-43.

KANAGAL-SHAMANNA, R., JAIN, P., PATEL, K. P., ROUTBORT, M., BUESO-RAMOS, C., ALHALOULI, T., KHOURY, J. D., LUTHRA, R., FERRAJOLI, A., KEATING, M., JAIN, N., BURGER, J., ESTROV, Z., WIERDA, W., KANTARJIAN, H. M. & MEDEIROS, L. J. 2019. Targeted multigene deep sequencing of Bruton tyrosine kinase inhibitor-resistant chronic lymphocytic leukemia with disease progression and Richter transformation. *Cancer,* 125**,** 559-574.

KANE, M. F., LODA, M., GAIDA, G. M., LIPMAN, J., MISHRA, R., GOLDMAN, H., JESSUP, J. M. & KOLODNER, R. 1997. Methylation of the hMLH1 promoter correlates with lack of expression of hMLH1 in sporadic colon tumors and mismatch repair-defective human tumor cell lines. *Cancer Res,* 57**,** 808-11.

KANG, C., XU, Q., MARTIN, T. D., LI, M. Z., DEMARIA, M., ARON, L., LU, T., YANKNER, B. A., CAMPISI, J. & ELLEDGE, S. J. 2015. The DNA damage response induces inflammation and senescence by inhibiting autophagy of GATA4. *Science,* 349**,** aaa5612.

KARAKAIDOS, P., KARAGIANNIS, D. & RAMPIAS, T. 2020. Resolving DNA Damage: Epigenetic Regulation of DNA Repair. *Molecules,* 25.

KARANDE, A., FIALKOW, P. J., NILSSON, K., POVEY, S., KLEIN, G., NAJFELD, V. & PENFOLD, G. 1980. Establishment of a lymphoid cell line from leukemic cells of a patient with chronic lymphocytic leukemia. *Int J Cancer,* 26**,** 551-6.

KARDAVA, L., YANG, Q., ST LEGER, A., FOON, K. A., LENTZSCH, S., VALLEJO, A. N., MILCAREK, C. & BORGHESI, L. 2011. The B lineage transcription factor E2A regulates apoptosis in chronic lymphocytic leukemia (CLL) cells. *Int Immunol,* 23**,** 375-84.

KARIN, M. 1995. The regulation of AP-1 activity by mitogen-activated protein kinases. *J Biol Chem,* 270**,** 16483-6.

KELLAWAY, S. G., KEANE, P., EDGINTON-WHITE, B., REGHA, K., KENNETT, E. & BONIFER, C. 2021. Different mutant RUNX1 oncoproteins program alternate haematopoietic differentiation trajectories. *Life Sci Alliance,* 4.

KELLNER, V. & LUKE, B. 2020. Molecular and physiological consequences of faulty eukaryotic ribonucleotide excision repair. *EMBO J,* 39**,** e102309.

KENT, T., CHANDRAMOULY, G., MCDEVITT, S. M., OZDEMIR, A. Y. & POMERANTZ, R. T. 2015. Mechanism of microhomology-mediated end-joining promoted by human DNA polymerase θ. *Nat Struct Mol Biol,* 22**,** 230-7.

KIM, D., PAGGI, J. M., PARK, C., BENNETT, C. & SALZBERG, S. L. 2019. Graph-based genome alignment and genotyping with HISAT2 and HISAT-genotype. *Nat Biotechnol,* 37**,** 907-915.

KIM, E. & HART, T. 2021. Improved analysis of CRISPR fitness screens and reduced off-target effects with the BAGEL2 gene essentiality classifier. *Genome Med,* 13**,** 2.

KIM, K., PUNJ, V., CHOI, J., HEO, K., KIM, J. M., LAIRD, P. W. & AN, W. 2013. Gene dysregulation by histone variant H2A.Z in bladder cancer. *Epigenetics Chromatin,* 6**,** 34.

KIM, N., HUANG, S. N., WILLIAMS, J. S., LI, Y. C., CLARK, A. B., CHO, J. E., KUNKEL, T. A., POMMIER, Y. & JINKS-ROBERTSON, S. 2011. Mutagenic processing of ribonucleotides in DNA by yeast topoisomerase I. *Science,* 332**,** 1561-4.

KIM, T. K., HEMBERG, M., GRAY, J. M., COSTA, A. M., BEAR, D. M., WU, J., HARMIN, D. A., LAPTEWICZ, M., BARBARA-HALEY, K., KUERSTEN, S., MARKENSCOFF-PAPADIMITRIOU, E., KUHL, D., BITO, H., WORLEY, P. F., KREIMAN, G. & GREENBERG, M. E. 2010. Widespread transcription at neuronal activity-regulated enhancers. *Nature,* 465**,** 182-7.

KINNER, A., WU, W., STAUDT, C. & ILIAKIS, G. 2008. Gamma-H2AX in recognition and signaling of DNA double-strand breaks in the context of chromatin. *Nucleic Acids Res,* 36**,** 5678-94.

KINNEY, J. S., VISCIDI, R. P., VONDERFECHT, S. L., EIDEN, J. J. & YOLKEN, R. H. 1989. Monoclonal antibody assay for detection of double-stranded RNA and application for detection of group A and non-group A rotaviruses. *J Clin Microbiol,* 27**,** 6-12.

KINNEY, S. R. & PRADHAN, S. 2013. Ten eleven translocation enzymes and 5-hydroxymethylation in mammalian development and cancer. *Adv Exp Med Biol,* 754**,** 57-79.

KLEIN DOUWEL, D., BOONEN, R. A., LONG, D. T., SZYPOWSKA, A. A., RÄSCHLE, M., WALTER, J. C. & KNIPSCHEER, P. 2014. XPF-ERCC1 acts in Unhooking DNA interstrand crosslinks in cooperation with FANCD2 and FANCP/SLX4. *Mol Cell,* 54**,** 460-71.

KLEIN, U., LIA, M., CRESPO, M., SIEGEL, R., SHEN, Q., MO, T., AMBESI-IMPIOMBATO, A., CALIFANO, A., MIGLIAZZA, A., BHAGAT, G. & DALLA-FAVERA, R. 2010. The DLEU2/miR-15a/16-1 cluster controls B cell proliferation and its deletion leads to chronic lymphocytic leukemia. *Cancer Cell,* 17**,** 28-40.

KLEMENT, K., LUIJSTERBURG, M. S., PINDER, J. B., CENA, C. S., DEL NERO, V., WINTERSINGER, C. M., DELLAIRE, G., VAN ATTIKUM, H. & GOODARZI, A. A. 2014. Opposing ISWI- and CHD-class chromatin remodeling activities orchestrate heterochromatic DNA repair. *J Cell Biol,* 207**,** 717-33.

KLEMM, S. L., SHIPONY, Z. & GREENLEAF, W. J. 2019. Chromatin accessibility and the regulatory epigenome. *Nat Rev Genet,* 20**,** 207-220.

KOLOVOS, P., KNOCH, T. A., GROSVELD, F. G., COOK, P. R. & PAPANTONIS, A. 2012. Enhancers and silencers: an integrated and simple model for their function. *Epigenetics Chromatin,* 5**,** 1.

KORNBERG, R. D. 1974. Chromatin structure: a repeating unit of histones and DNA. *Science,* 184**,** 868-71.

KORNBERG, R. D. & LORCH, Y. 1999. Twenty-five years of the nucleosome, fundamental particle of the eukaryote chromosome. *Cell,* 98**,** 285-94.

KOSALAI, S. T., MORSY, M. H. A., PAPAKONSTANTINOU, N., MANSOURI, L., STAVROYIANNI, N., KANDURI, C., STAMATOPOULOS, K., ROSENQUIST, R. & KANDURI, M. 2019. EZH2 upregulates the PI3K/AKT pathway through IGF1R and MYC in clinically aggressive chronic lymphocytic leukaemia. *Epigenetics,* 14**,** 1125-1140.

KOSTREWA, D., ZELLER, M. E., ARMACHE, K. J., SEIZL, M., LEIKE, K., THOMM, M. & CRAMER, P. 2009. RNA polymerase II-TFIIB structure and mechanism of transcription initiation. *Nature,* 462**,** 323-30.

KOUZARIDES, T. 2007. Chromatin modifications and their function. *Cell,* 128**,** 693-705.

KOZLOV, S. V., GRAHAM, M. E., JAKOB, B., TOBIAS, F., KIJAS, A. W., TANUJI, M., CHEN, P., ROBINSON, P. J., TAUCHER-SCHOLZ, G., SUZUKI, K., SO, S., CHEN, D. & LAVIN, M. F. 2011. Autophosphorylation and ATM activation: additional sites add to the complexity. *J Biol Chem,* 286**,** 9107-19.

KRUHLAK, M., CROUCH, E. E., ORLOV, M., MONTAÑO, C., GORSKI, S. A., NUSSENZWEIG, A., MISTELI, T., PHAIR, R. D. & CASELLAS, R. 2007. The ATM repair pathway inhibits RNA polymerase I transcription in response to chromosome breaks. *Nature,* 447**,** 730-4.

KRYUKOV, G. V., WILSON, F. H., RUTH, J. R., PAULK, J., TSHERNIAK, A., MARLOW, S. E., VAZQUEZ, F., WEIR, B. A., FITZGERALD, M. E., TANAKA, M., BIELSKI, C. M., SCOTT, J. M., DENNIS, C., COWLEY, G. S., BOEHM, J. S., ROOT, D. E., GOLUB, T. R., CLISH, C. B., BRADNER, J. E., HAHN, W. C. & GARRAWAY, L. A. 2016. MTAP deletion confers enhanced dependency on the PRMT5 arginine methyltransferase in cancer cells. *Science,* 351**,** 1214-8.

KU, M., JAFFE, J. D., KOCHE, R. P., RHEINBAY, E., ENDOH, M., KOSEKI, H., CARR, S. A. & BERNSTEIN, B. E. 2012. H2A.Z landscapes and dual modifications in pluripotent and multipotent stem cells underlie complex genome regulatory functions. *Genome Biol,* 13**,** R85.

KULIS, M., HEATH, S., BIBIKOVA, M., QUEIRÓS, A. C., NAVARRO, A., CLOT, G., MARTÍNEZ-TRILLOS, A., CASTELLANO, G., BRUN-HEATH, I., PINYOL, M., BARBERÁN-SOLER, S., PAPASAIKAS, P., JARES, P., BEÀ, S., RICO, D., ECKER, S., RUBIO, M., ROYO, R., HO, V., KLOTZLE, B., HERNÁNDEZ, L., CONDE, L., LÓPEZ-GUERRA, M., COLOMER, D., VILLAMOR, N., AYMERICH, M., ROZMAN, M., BAYES, M., GUT, M., GELPÍ, J. L., OROZCO, M., FAN, J. B., QUESADA, V., PUENTE, X. S., PISANO, D. G., VALENCIA, A., LÓPEZ-GUILLERMO, A., GUT, I., LÓPEZ-OTÍN, C., CAMPO, E. & MARTÍN-SUBERO, J. I. 2012. Epigenomic analysis detects widespread gene-body DNA hypomethylation in chronic lymphocytic leukemia. *Nat Genet,* 44**,** 1236-42.

KWAK, H. & LIS, J. T. 2013. Control of transcriptional elongation. *Annu Rev Genet,* 47**,** 483-508.

KWOK, M., DAVIES, N., AGATHANGGELOU, A., SMITH, E., OLDREIVE, C., PETERMANN, E., STEWART, G., BROWN, J., LAU, A., PRATT, G., PARRY, H., TAYLOR, M., MOSS, P., HILLMEN, P. & STANKOVIC, T. 2016. ATR inhibition induces synthetic lethality and overcomes chemoresistance in TP53- or ATM-defective chronic lymphocytic leukemia cells. *Blood,* 127**,** 582-95.

KWON, S. J., PARK, J. H., PARK, E. J., LEE, S. A., LEE, H. S., KANG, S. W. & KWON, J. 2015. ATM-mediated phosphorylation of the chromatin remodeling enzyme BRG1 modulates DNA double-strand break repair. *Oncogene,* 34**,** 303-13.

KÖNIG, F., SCHUBERT, T. & LÄNGST, G. 2017. The monoclonal S9.6 antibody exhibits highly variable binding affinities towards different R-loop sequences. *PLoS One,* 12**,** e0178875.

LAHTZ, C. & PFEIFER, G. P. 2011. Epigenetic changes of DNA repair genes in cancer. *J Mol Cell Biol,* 3**,** 51-8.

LANDAU, D. A., CARTER, S. L., STOJANOV, P., MCKENNA, A., STEVENSON, K., LAWRENCE, M. S., SOUGNEZ, C., STEWART, C., SIVACHENKO, A., WANG, L., WAN, Y., ZHANG, W., SHUKLA, S. A., VARTANOV, A., FERNANDES, S. M., SAKSENA, G., CIBULSKIS, K., TESAR, B., GABRIEL, S., HACOHEN, N., MEYERSON, M., LANDER, E. S., NEUBERG, D., BROWN, J. R., GETZ, G. & WU, C. J. 2013. Evolution and impact of subclonal mutations in chronic lymphocytic leukemia. *Cell,* 152**,** 714-26.

LANDAU, D. A., CLEMENT, K., ZILLER, M. J., BOYLE, P., FAN, J., GU, H., STEVENSON, K., SOUGNEZ, C., WANG, L., LI, S., KOTLIAR, D., ZHANG, W., GHANDI, M., GARRAWAY, L., FERNANDES, S. M., LIVAK, K. J., GABRIEL, S., GNIRKE, A., LANDER, E. S., BROWN, J. R., NEUBERG, D., KHARCHENKO, P. V., HACOHEN, N., GETZ, G., MEISSNER, A. & WU, C. J. 2014. Locally disordered methylation forms the basis of intratumor methylome variation in chronic lymphocytic leukemia. *Cancer Cell,* 26**,** 813-825.

LANDAU, D. A., TAUSCH, E., TAYLOR-WEINER, A. N., STEWART, C., REITER, J. G., BAHLO, J., KLUTH, S., BOZIC, I., LAWRENCE, M., BÖTTCHER, S., CARTER, S. L., CIBULSKIS, K., MERTENS, D., SOUGNEZ, C. L., ROSENBERG, M., HESS, J. M., EDELMANN, J., KLESS, S., KNEBA, M., RITGEN, M., FINK, A., FISCHER, K., GABRIEL, S., LANDER, E. S., NOWAK, M. A., DÖHNER, H., HALLEK, M., NEUBERG, D., GETZ, G., STILGENBAUER, S. & WU, C. J. 2015. Mutations driving CLL and their evolution in progression and relapse. *Nature,* 526**,** 525-30.

LANEMO MYHRINDER, A., HELLQVIST, E., BERGH, A. C., JANSSON, M., NILSSON, K., HULTMAN, P., JONASSON, J., BUHL, A. M., BREDO PEDERSEN, L., JURLANDER, J., KLEIN, E., WEIT, N., HERLING, M., ROSENQUIST, R. & ROSÉN, A. 2013. Molecular characterization of neoplastic and normal "sister" lymphoblastoid B-cell lines from chronic lymphocytic leukemia. *Leuk Lymphoma,* 54**,** 1769-79.

LANGMEAD, B. & SALZBERG, S. L. 2012. Fast gapped-read alignment with Bowtie 2. *Nat Methods,* 9**,** 357-9.

LASHGARI, A., MILLAU, J. F., JACQUES, P. & GAUDREAU, L. 2017. Global inhibition of transcription causes an increase in histone H2A.Z incorporation within gene bodies. *Nucleic Acids Res,* 45**,** 12715-12722.

LAW, P. J., BERNDT, S. I., SPEEDY, H. E., CAMP, N. J., SAVA, G. P., SKIBOLA, C. F., HOLROYD, A., JOSEPH, V., SUNTER, N. J., NIETERS, A., BEA, S., MONNEREAU, A., MARTIN-GARCIA, D., GOLDIN, L. R., CLOT, G., TERAS, L. R., QUINTELA, I., BIRMANN, B. M., JAYNE, S., COZEN, W., MAJID, A., SMEDBY, K. E., LAN, Q., DEARDEN, C., BROOKS-WILSON, A. R., HALL, A. G., PURDUE, M. P., MAINOU-FOWLER, T., VAJDIC, C. M., JACKSON, G. H., COCCO, P., MARR, H., ZHANG, Y., ZHENG, T., GILES, G. G., LAWRENCE, C., CALL, T. G., LIEBOW, M., MELBYE, M., GLIMELIUS, B., MANSOURI, L., GLENN, M., CURTIN, K., DIVER, W. R., LINK, B. K., CONDE, L., BRACCI, P. M., HOLLY, E. A., JACKSON, R. D., TINKER, L. F., BENAVENTE, Y., BOFFETTA, P., BRENNAN, P., MAYNADIE, M., MCKAY, J., ALBANES, D., WEINSTEIN, S., WANG, Z., CAPORASO, N. E., MORTON, L. M., SEVERSON, R. K., RIBOLI, E., VINEIS, P., VERMEULEN, R. C., SOUTHEY, M. C., MILNE, R. L., CLAVEL, J., TOPKA, S., SPINELLI, J. J., KRAFT, P., ENNAS, M. G., SUMMERFIELD, G., FERRI, G. M., HARRIS, R. J., MILIGI, L., PETTITT, A. R., NORTH, K. E., ALLSUP, D. J., FRAUMENI, J. F., BAILEY, J. R., OFFIT, K., PRATT, G., HJALGRIM, H., PEPPER, C., CHANOCK, S. J., FEGAN, C., ROSENQUIST, R., DE SANJOSE, S., CARRACEDO, A., DYER, M. J., CATOVSKY, D., CAMPO, E., CERHAN, J. R., ALLAN, J. M., ROTHMAN, N., HOULSTON, R. & SLAGER, S. 2017. Genome-wide association analysis implicates dysregulation of immunity genes in chronic lymphocytic leukaemia. *Nat Commun,* 8**,** 14175.

LAWRENCE, M., DAUJAT, S. & SCHNEIDER, R. 2016. Lateral Thinking: How Histone Modifications Regulate Gene Expression. *Trends Genet,* 32**,** 42-56.

LAZARIAN, G., GUIÈZE, R. & WU, C. J. 2017. Clinical Implications of Novel Genomic Discoveries in Chronic Lymphocytic Leukemia. *J Clin Oncol,* 35**,** 984-993.

LEE, D. H., GOODARZI, A. A., ADELMANT, G. O., PAN, Y., JEGGO, P. A., MARTO, J. A. & CHOWDHURY, D. 2012. Phosphoproteomic analysis reveals that PP4 dephosphorylates KAP-1 impacting the DNA damage response. *EMBO J,* 31**,** 2403-15.

LEE, J. H. & PAULL, T. T. 2005. ATM activation by DNA double-strand breaks through the Mre11-Rad50-Nbs1 complex. *Science,* 308**,** 551-4.

LEE, M. N., TSENG, R. C., HSU, H. S., CHEN, J. Y., TZAO, C., HO, W. L. & WANG, Y. C. 2007. Epigenetic inactivation of the chromosomal stability control genes BRCA1, BRCA2, and XRCC5 in non-small cell lung cancer. *Clin Cancer Res,* 13**,** 832-8.

LEVANON, D. & GRONER, Y. 2004. Structure and regulated expression of mammalian RUNX genes. *Oncogene,* 23**,** 4211-9.

LEVANON, D., NEGREANU, V., LOTEM, J., BONE, K. R., BRENNER, O., LESHKOWITZ, D. & GRONER, Y. 2014. Transcription factor Runx3 regulates interleukin-15-dependent natural killer cell activation. *Mol Cell Biol,* 34**,** 1158-69.

LI, B., BRADY, S. W., MA, X., SHEN, S., ZHANG, Y., LI, Y., SZLACHTA, K., DONG, L., LIU, Y., YANG, F., WANG, N., FLASCH, D. A., MYERS, M. A., MULDER, H. L., DING, L., TIAN, L., HAGIWARA, K., XU, K., ZHOU, X., SIOSON, E., WANG, T., YANG, L., ZHAO, J., ZHANG, H., SHAO, Y., SUN, H., SUN, L., CAI, J., SUN, H. Y., LIN, T. N., DU, L., LI, H., RUSCH, M., EDMONSON, M. N., EASTON, J., ZHU, X., ZHANG, J., CHENG, C., RAPHAEL, B. J., TANG, J., DOWNING, J. R., ALEXANDROV, L. B., ZHOU, B. S., PUI, C. H. & YANG, J. J. 2020a. Therapy-induced mutations drive the genomic landscape of relapsed acute lymphoblastic leukemia. *Blood,* 135**,** 41-55.

LI, G., KANAGASABAI, T., LU, W., ZOU, M. R., ZHANG, S. M., CELADA, S. I., IZBAN, M. G., LIU, Q., LU, T., BALLARD, B. R., ZHOU, X., ADUNYAH, S. E., MATUSIK, R. J., YAN, Q. & CHEN, Z. 2020b. KDM5B Is Essential for the Hyperactivation of PI3K/AKT Signaling in Prostate Tumorigenesis. *Cancer Res,* 80**,** 4633-4643.

LI, H., HANDSAKER, B., WYSOKER, A., FENNELL, T., RUAN, J., HOMER, N., MARTH, G., ABECASIS, G., DURBIN, R. & SUBGROUP, G. P. D. P. 2009. The Sequence Alignment/Map format and SAMtools. *Bioinformatics,* 25**,** 2078-9.

LI, Q., ZOU, J., WANG, M., DING, X., CHEPELEV, I., ZHOU, X., ZHAO, W., WEI, G., CUI, J., ZHAO, K., WANG, H. Y. & WANG, R. F. 2014a. Critical role of histone demethylase Jmjd3 in the regulation of CD4+ T-cell differentiation. *Nat Commun,* 5**,** 5780.

LI, X., LIU, L., YANG, S., SONG, N., ZHOU, X., GAO, J., YU, N., SHAN, L., WANG, Q., LIANG, J., XUAN, C., WANG, Y., SHANG, Y. & SHI, L. 2014b. Histone demethylase KDM5B is a key regulator of genome stability. *Proc Natl Acad Sci U S A,* 111**,** 7096-101.

LI, Y. & BREAKER, R. R. 1999. Kinetics of RNA degradation by specific base catalysis of transesterification involving the 2 ‘-hydroxyl group. *Journal of the American Chemical society,* 121**,** 5364-5372.

LIAO, Y., SMYTH, G. K. & SHI, W. 2014. featureCounts: an efficient general purpose program for assigning sequence reads to genomic features. *Bioinformatics,* 30**,** 923-30.

LIBERZON, A., BIRGER, C., THORVALDSDÓTTIR, H., GHANDI, M., MESIROV, J. P. & TAMAYO, P. 2015. The Molecular Signatures Database (MSigDB) hallmark gene set collection. *Cell Syst,* 1**,** 417-425.

LILLY, A. J., COSTA, G., LARGEOT, A., FADLULLAH, M. Z., LIE-A-LING, M., LACAUD, G. & KOUSKOFF, V. 2016. Interplay between SOX7 and RUNX1 regulates hemogenic endothelial fate in the yolk sac. *Development,* 143**,** 4341-4351.

LIM, M., ZHONG, C., YANG, S., BELL, A. M., COHEN, M. B. & ROY-BURMAN, P. 2010. Runx2 regulates survivin expression in prostate cancer cells. *Lab Invest,* 90**,** 222-33.

LIN, K. I., TAM, C. S., KEATING, M. J., WIERDA, W. G., O'BRIEN, S., LERNER, S., COOMBES, K. R., SCHLETTE, E., FERRAJOLI, A., BARRON, L. L., KIPPS, T. J., RASSENTI, L., FADERL, S., KANTARJIAN, H. & ABRUZZO, L. V. 2009. Relevance of the immunoglobulin VH somatic mutation status in patients with chronic lymphocytic leukemia treated with fludarabine, cyclophosphamide, and rituximab (FCR) or related chemoimmunotherapy regimens. *Blood,* 113**,** 3168-71.

LIN, Y., BAI, L., CUPELLO, S., HOSSAIN, M. A., DEEM, B., MCLEOD, M., RAJ, J. & YAN, S. 2018. APE2 promotes DNA damage response pathway from a single-strand break. *Nucleic Acids Res,* 46**,** 2479-2494.

LIU, C., PENG, W., XU, C., LOU, Y., ZHANG, M., WARGO, J. A., CHEN, J. Q., LI, H. S., WATOWICH, S. S., YANG, Y., TOMPERS FREDERICK, D., COOPER, Z. A., MBOFUNG, R. M., WHITTINGTON, M., FLAHERTY, K. T., WOODMAN, S. E., DAVIES, M. A., RADVANYI, L. G., OVERWIJK, W. W., LIZÉE, G. & HWU, P. 2013a. BRAF inhibition increases tumor infiltration by T cells and enhances the antitumor activity of adoptive immunotherapy in mice. *Clin Cancer Res,* 19**,** 393-403.

LIU, X., BUSHNELL, D. A. & KORNBERG, R. D. 2013b. RNA polymerase II transcription: structure and mechanism. *Biochim Biophys Acta,* 1829**,** 2-8.

LIU, X., ZHANG, S. M., MCGEARY, M. K., KRYKBAEVA, I., LAI, L., JANSEN, D. J., KALES, S. C., SIMEONOV, A., HALL, M. D., KELLY, D. P., BOSENBERG, M. W. & YAN, Q. 2019. KDM5B Promotes Drug Resistance by Regulating Melanoma-Propagating Cell Subpopulations. *Mol Cancer Ther,* 18**,** 706-717.

LIVAK, K. J. & SCHMITTGEN, T. D. 2001. Analysis of relative gene expression data using real-time quantitative PCR and the 2(-Delta Delta C(T)) Method. *Methods,* 25**,** 402-8.

LJUNGSTRÖM, V., CORTESE, D., YOUNG, E., PANDZIC, T., MANSOURI, L., PLEVOVA, K., NTOUFA, S., BALIAKAS, P., CLIFFORD, R., SUTTON, L. A., BLAKEMORE, S. J., STAVROYIANNI, N., AGATHANGELIDIS, A., ROSSI, D., HÖGLUND, M., KOTASKOVA, J., JULIUSSON, G., BELESSI, C., CHIORAZZI, N., PANAGIOTIDIS, P., LANGERAK, A. W., SMEDBY, K. E., OSCIER, D., GAIDANO, G., SCHUH, A., DAVI, F., POTT, C., STREFFORD, J. C., TRENTIN, L., POSPISILOVA, S., GHIA, P., STAMATOPOULOS, K., SJÖBLOM, T. & ROSENQUIST, R. 2016. Whole-exome sequencing in relapsing chronic lymphocytic leukemia: clinical impact of recurrent RPS15 mutations. *Blood,* 127**,** 1007-16.

LLORCA, O., RIVERA-CALZADA, A., GRANTHAM, J. & WILLISON, K. R. 2003. Electron microscopy and 3D reconstructions reveal that human ATM kinase uses an arm-like domain to clamp around double-stranded DNA. *Oncogene,* 22**,** 3867-74.

LOGAN, J., FALCK-PEDERSEN, E., DARNELL, J. E. & SHENK, T. 1987. A poly(A) addition site and a downstream termination region are required for efficient cessation of transcription by RNA polymerase II in the mouse beta maj-globin gene. *Proc Natl Acad Sci U S A,* 84**,** 8306-10.

LONGO, P. G., LAURENTI, L., GOBESSI, S., PETLICKOVSKI, A., PELOSI, M., CHIUSOLO, P., SICA, S., LEONE, G. & EFREMOV, D. G. 2007. The Akt signaling pathway determines the different proliferative capacity of chronic lymphocytic leukemia B-cells from patients with progressive and stable disease. *Leukemia,* 21**,** 110-20.

LOOK, A. T. 1997. Oncogenic transcription factors in the human acute leukemias. *Science,* 278**,** 1059-64.

LORD, C. J. & ASHWORTH, A. 2017. PARP inhibitors: Synthetic lethality in the clinic. *Science,* 355**,** 1152-1158.

LOTEM, J., LEVANON, D., NEGREANU, V., BAUER, O., HANTISTEANU, S., DICKEN, J. & GRONER, Y. 2015. Runx3 at the interface of immunity, inflammation and cancer. *Biochim Biophys Acta,* 1855**,** 131-43.

LOVE, M. I., HUBER, W. & ANDERS, S. 2014. Moderated estimation of fold change and dispersion for RNA-seq data with DESeq2. *Genome Biol,* 15**,** 550.

LU, Y., LIU, Y., OECK, S. & GLAZER, P. M. 2018. Hypoxia Promotes Resistance to EGFR Inhibition in NSCLC Cells via the Histone Demethylases, LSD1 and PLU-1. *Mol Cancer Res,* 16**,** 1458-1469.

LU, Z., HOFMEISTER, B. T., VOLLMERS, C., DUBOIS, R. M. & SCHMITZ, R. J. 2017. Combining ATAC-seq with nuclei sorting for discovery of cis-regulatory regions in plant genomes. *Nucleic Acids Res,* 45**,** e41.

LUO, H., ZHU, G., XU, J., LAI, Q., YAN, B., GUO, Y., FUNG, T. K., ZEISIG, B. B., CUI, Y., ZHA, J., COGLE, C., WANG, F., XU, B., YANG, F. C., LI, W., SO, C. W. E., QIU, Y., XU, M. & HUANG, S. 2019. HOTTIP lncRNA Promotes Hematopoietic Stem Cell Self-Renewal Leading to AML-like Disease in Mice. *Cancer Cell,* 36**,** 645-659.e8.

MACKENZIE, K. J., CARROLL, P., LETTICE, L., TARNAUSKAITĖ, Ž., REDDY, K., DIX, F., REVUELTA, A., ABBONDATI, E., RIGBY, R. E., RABE, B., KILANOWSKI, F., GRIMES, G., FLUTEAU, A., DEVENNEY, P. S., HILL, R. E., REIJNS, M. A. & JACKSON, A. P. 2016. Ribonuclease H2 mutations induce a cGAS/STING-dependent innate immune response. *EMBO J,* 35**,** 831-44.

MACKENZIE, K. J., CARROLL, P., MARTIN, C. A., MURINA, O., FLUTEAU, A., SIMPSON, D. J., OLOVA, N., SUTCLIFFE, H., RAINGER, J. K., LEITCH, A., OSBORN, R. T., WHEELER, A. P., NOWOTNY, M., GILBERT, N., CHANDRA, T., REIJNS, M. A. M. & JACKSON, A. P. 2017. cGAS surveillance of micronuclei links genome instability to innate immunity. *Nature,* 548**,** 461-465.

MAHARAJ, K., POWERS, J. J., ACHILLE, A., DENG, S., FONSECA, R., PABON-SALDANA, M., QUAYLE, S. N., JONES, S. S., VILLAGRA, A., SOTOMAYOR, E. M., SAHAKIAN, E. & PINILLA-IBARZ, J. 2018. Silencing of HDAC6 as a therapeutic target in chronic lymphocytic leukemia. *Blood Adv,* 2**,** 3012-3024.

MAILAND, N., BEKKER-JENSEN, S., FAUSTRUP, H., MELANDER, F., BARTEK, J., LUKAS, C. & LUKAS, J. 2007. RNF8 ubiquitylates histones at DNA double-strand breaks and promotes assembly of repair proteins. *Cell,* 131**,** 887-900.

MAIR, B., TOMIC, J., MASUD, S. N., TONGE, P., WEISS, A., USAJ, M., TONG, A. H. Y., KWAN, J. J., BROWN, K. R., TITUS, E., ATKINS, M., CHAN, K. S. K., MUNSIE, L., HABSID, A., HAN, H., KENNEDY, M., COHEN, B., KELLER, G. & MOFFAT, J. 2019. Essential Gene Profiles for Human Pluripotent Stem Cells Identify Uncharacterized Genes and Substrate Dependencies. *Cell Rep,* 27**,** 599-615.e12.

MALLM, J. P., ISKAR, M., ISHAQUE, N., KLETT, L. C., KUGLER, S. J., MUINO, J. M., TEIF, V. B., POOS, A. M., GROßMANN, S., ERDEL, F., TAVERNARI, D., KOSER, S. D., SCHUMACHER, S., BRORS, B., KÖNIG, R., REMONDINI, D., VINGRON, M., STILGENBAUER, S., LICHTER, P., ZAPATKA, M., MERTENS, D. & RIPPE, K. 2019. Linking aberrant chromatin features in chronic lymphocytic leukemia to transcription factor networks. *Mol Syst Biol,* 15**,** e8339.

MARSHALL, N. F. & PRICE, D. H. 1995. Purification of P-TEFb, a transcription factor required for the transition into productive elongation. *J Biol Chem,* 270**,** 12335-8.

MARTINEZ-SORIA, N., MCKENZIE, L., DRAPER, J., PTASINSKA, A., ISSA, H., POTLURI, S., BLAIR, H. J., PICKIN, A., ISA, A., CHIN, P. S., TIRTAKUSUMA, R., COLEMAN, D., NAKJANG, S., ASSI, S., FORSTER, V., REZA, M., LAW, E., BERRY, P., MUELLER, D., OSBORNE, C., ELDER, A., BOMKEN, S. N., PAL, D., ALLAN, J. M., VEAL, G. J., COCKERILL, P. N., WICHMANN, C., VORMOOR, J., LACAUD, G., BONIFER, C. & HEIDENREICH, O. 2018. The Oncogenic Transcription Factor RUNX1/ETO Corrupts Cell Cycle Regulation to Drive Leukemic Transformation. *Cancer Cell,* 34**,** 626-642.e8.

MARTÍNEZ-TRILLOS, A., NAVARRO, A., AYMERICH, M., DELGADO, J., LÓPEZ-GUILLERMO, A., CAMPO, E. & VILLAMOR, N. 2016. Clinical impact of MYD88 mutations in chronic lymphocytic leukemia. *Blood,* 127**,** 1611-3.

MATEOS-GOMEZ, P. A., GONG, F., NAIR, N., MILLER, K. M., LAZZERINI-DENCHI, E. & SFEIR, A. 2015. Mammalian polymerase θ promotes alternative NHEJ and suppresses recombination. *Nature,* 518**,** 254-7.

MAVRAKIS, K. J., MCDONALD, E. R., SCHLABACH, M. R., BILLY, E., HOFFMAN, G. R., DEWECK, A., RUDDY, D. A., VENKATESAN, K., YU, J., MCALLISTER, G., STUMP, M., DEBEAUMONT, R., HO, S., YUE, Y., LIU, Y., YAN-NEALE, Y., YANG, G., LIN, F., YIN, H., GAO, H., KIPP, D. R., ZHAO, S., MCNAMARA, J. T., SPRAGUE, E. R., ZHENG, B., LIN, Y., CHO, Y. S., GU, J., CRAWFORD, K., CICCONE, D., VITARI, A.

C., LAI, A., CAPKA, V., HUROV, K., PORTER, J. A., TALLARICO, J., MICKANIN, C., LEES, E., PAGLIARINI, R., KEEN, N., SCHMELZLE, T., HOFMANN, F., STEGMEIER, F. & SELLERS, W. R. 2016. Disordered methionine metabolism in MTAP/CDKN2A-deleted cancers leads to dependence on PRMT5. *Science,* 351**,** 1208-13.

MCARTHUR, E. & CAPRA, J. A. 2021. Topologically associating domain boundaries that are stable across diverse cell types are evolutionarily constrained and enriched for heritability. *Am J Hum Genet,* 108**,** 269-283.

MCCLELAND, M. L., MESH, K., LORENZANA, E., CHOPRA, V. S., SEGAL, E., WATANABE, C., HALEY, B., MAYBA, O., YAYLAOGLU, M., GNAD, F. & FIRESTEIN, R. 2016. CCAT1 is an enhancer-templated RNA that predicts BET sensitivity in colorectal cancer. *J Clin Invest,* 126**,** 639-52.

MENDOZA-VILLANUEVA, D., DENG, W., LOPEZ-CAMACHO, C. & SHORE, P. 2010. The Runx transcriptional co-activator, CBFbeta, is essential for invasion of breast cancer cells. *Mol Cancer,* 9**,** 171.

MENEGHINI, M. D., WU, M. & MADHANI, H. D. 2003. Conserved histone variant H2A.Z protects euchromatin from the ectopic spread of silent heterochromatin. *Cell,* 112**,** 725-36.

MERONI, A., MENTEGARI, E., CRESPAN, E., MUZI-FALCONI, M., LAZZARO, F. & PODESTÀ, A. 2017. The Incorporation of Ribonucleotides Induces Structural and Conformational Changes in DNA. *Biophys J,* 113**,** 1373-1382.

MEUWISSEN, M. E., SCHOT, R., BUTA, S., OUDESLUIJS, G., TINSCHERT, S., SPEER, S. D., LI, Z., VAN UNEN, L., HEIJSMAN, D., GOLDMANN, T., LEQUIN, M. H., KROS, J. M., STAM, W., HERMANN, M., WILLEMSEN, R., BROUWER, R. W., VAN IJCKEN, W. F., MARTIN-FERNANDEZ, M., DE COO, I., DUDINK, J., DE VRIES, F. A., BERTOLI AVELLA, A., PRINZ, M., CROW, Y. J., VERHEIJEN, F. W., PELLEGRINI, S., BOGUNOVIC, D. & MANCINI, G. M. 2016. Human USP18 deficiency underlies type 1 interferonopathy leading to severe pseudo-TORCH syndrome. *J Exp Med,* 213**,** 1163-74.

MICHAL ZIMMERMANN AND OLGA MURINA AND MARTIN, A. M. R. A. A. A. A. R. C. A. Ž. T. A. M. M. A. A. F. A. M. A. A. A. 2018. CRISPR screens identify genomic ribonucleotides as a source of PARP-trapping lesions. *Nature,* 559**,** 285-289.

MICHAUD, J., WU, F., OSATO, M., COTTLES, G. M., YANAGIDA, M., ASOU, N., SHIGESADA, K., ITO, Y., BENSON, K. F., RASKIND, W. H., ROSSIER, C., ANTONARAKIS, S. E., ISRAELS, S., MCNICOL, A., WEISS, H., HORWITZ, M. & SCOTT, H. S. 2002. In vitro analyses of known and novel RUNX1/AML1 mutations in dominant familial platelet disorder with predisposition to acute myelogenous leukemia: implications for mechanisms of pathogenesis. *Blood,* 99**,** 1364-72.

MICHELINI, F., PITCHIAYA, S., VITELLI, V., SHARMA, S., GIOIA, U., PESSINA, F., CABRINI, M., WANG, Y., CAPOZZO, I., IANNELLI, F., MATTI, V., FRANCIA, S., SHIVASHANKAR, G. V., WALTER, N. G. & D'ADDA DI FAGAGNA, F. 2017. Damage-induced lncRNAs control the DNA damage response through interaction with DDRNAs at individual double-strand breaks. *Nat Cell Biol,* 19**,** 1400-1411.

MIN, S., JO, S., LEE, H. S., CHAE, S., LEE, J. S., JI, J. H. & CHO, H. 2014. ATM-dependent chromatin remodeler Rsf-1 facilitates DNA damage checkpoints and homologous recombination repair. *Cell Cycle,* 13**,** 666-77.

MITSUI, E., YOSHIDA, S., SHINODA, Y., MATSUMORI, Y., TSUJII, H., TSUCHIDA, M., WADA, S., HASEGAWA, M., ITO, A., MINO, K., ONUKI, T., YOSHIDA, M., SASAKI, R. & MIZUKAMI, T. 2019. Identification of ryuvidine as a KDM5A inhibitor. *Sci Rep,* 9**,** 9952.

MOLICA, S. & ALBERTI, A. 1987. Prognostic value of the lymphocyte doubling time in chronic lymphocytic leukemia. *Cancer,* 60**,** 2712-6.

MORRILL, S. A. & AMON, A. 2019. Why haploinsufficiency persists. *Proc Natl Acad Sci U S A,* 116**,** 11866-11871.

MUGGEN, A. F., SINGH, S. P., HENDRIKS, R. W. & LANGERAK, A. W. 2016. Targeting Signaling Pathways in Chronic Lymphocytic Leukemia. *Curr Cancer Drug Targets,* 16**,** 669-688.

MUNOZ, D. M., CASSIANI, P. J., LI, L., BILLY, E., KORN, J. M., JONES, M. D., GOLJI, J., RUDDY, D. A., YU, K., MCALLISTER, G., DEWECK, A., ABRAMOWSKI, D., WAN, J., SHIRLEY, M. D., NESHAT, S. Y., RAKIEC, D., DE BEAUMONT, R., WEBER, O., KAUFFMANN, A., MCDONALD, E. R., KEEN, N., HOFMANN, F., SELLERS, W. R., SCHMELZLE, T., STEGMEIER, F. & SCHLABACH, M. R. 2016. CRISPR Screens Provide a Comprehensive Assessment of Cancer Vulnerabilities but Generate False-Positive Hits for Highly Amplified Genomic Regions. *Cancer Discov,* 6**,** 900-13.

NADEU, F., CLOT, G., DELGADO, J., MARTÍN-GARCÍA, D., BAUMANN, T., SALAVERRIA, I., BEÀ, S., PINYOL, M., JARES, P., NAVARRO, A., SUÁREZ-CISNEROS, H., AYMERICH, M., ROZMAN, M., VILLAMOR, N., COLOMER, D., GONZÁLEZ, M., ALCOCEBA, M., TEROL, M. J., NAVARRO, B., COLADO, E., PAYER, Á., PUENTE, X. S., LÓPEZ-OTÍN, C., LÓPEZ-GUILLERMO, A., ENJUANES, A. & CAMPO, E. 2018. Clinical impact of the subclonal architecture and mutational complexity in chronic lymphocytic leukemia. *Leukemia,* 32**,** 645-653.

NAFRIA, M., KEANE, P., NG, E. S., STANLEY, E. G., ELEFANTY, A. G. & BONIFER, C. 2020. Expression of RUNX1-ETO Rapidly Alters the Chromatin Landscape and Growth of Early Human Myeloid Precursor Cells. *Cell Rep,* 31**,** 107691.

NEVADUNSKY, N. S., BARBIERI, J. S., KWONG, J., MERRITT, M. A., WELCH, W. R., BERKOWITZ, R. S. & MOK, S. C. 2009. RUNX3 protein is overexpressed in human epithelial ovarian cancer. *Gynecol Oncol,* 112**,** 325-30.

NICK MCELHINNY, S. A., KUMAR, D., CLARK, A. B., WATT, D. L., WATTS, B. E., LUNDSTRÖM, E. B., JOHANSSON, E., CHABES, A. & KUNKEL, T. A. 2010. Genome instability due to ribonucleotide incorporation into DNA. *Nat Chem Biol,* 6**,** 774-81.

NISHIBUCHI, I., SUZUKI, H., KINOMURA, A., SUN, J., LIU, N. A., HORIKOSHI, Y., SHIMA, H., KUSAKABE, M., HARATA, M., FUKAGAWA, T., IKURA, T., ISHIDA, T., NAGATA, Y. & TASHIRO, S. 2014. Reorganization of damaged chromatin by the exchange of histone variant H2A.Z-2. *Int J Radiat Oncol Biol Phys,* 89**,** 736-44.

NOGUEIRA, V. & HAY, N. 2013. Molecular pathways: reactive oxygen species homeostasis in cancer cells and implications for cancer therapy. *Clin Cancer Res,* 19**,** 4309-14.

NORA, E. P., GOLOBORODKO, A., VALTON, A. L., GIBCUS, J. H., UEBERSOHN, A., ABDENNUR, N., DEKKER, J., MIRNY, L. A. & BRUNEAU, B. G. 2017. Targeted Degradation of CTCF Decouples Local Insulation of Chromosome Domains from Genomic Compartmentalization. *Cell,* 169**,** 930-944.e22.

O'CONNOR, M. J. 2015. Targeting the DNA Damage Response in Cancer. *Mol Cell,* 60**,** 547-60.

O'NEIL, N. J., BAILEY, M. L. & HIETER, P. 2017. Synthetic lethality and cancer. *Nat Rev Genet,* 18**,** 613-623.

OAKES, C. C., CLAUS, R., GU, L., ASSENOV, Y., HÜLLEIN, J., ZUCKNICK, M., BIEG, M., BROCKS, D., BOGATYROVA, O., SCHMIDT, C. R., RASSENTI, L., KIPPS, T. J., MERTENS, D., LICHTER, P., DÖHNER, H., STILGENBAUER, S., BYRD, J. C., ZENZ, T. & PLASS, C. 2014. Evolution of DNA methylation is linked to genetic aberrations in chronic lymphocytic leukemia. *Cancer Discov,* 4**,** 348-61.

OAKES, C. C. & MARTIN-SUBERO, J. I. 2018. Insight into origins, mechanisms, and utility of DNA methylation in B-cell malignancies. *Blood,* 132**,** 999-1006.

OAKES, C. C., SEIFERT, M., ASSENOV, Y., GU, L., PRZEKOPOWITZ, M., RUPPERT, A. S., WANG, Q., IMBUSCH, C. D., SERVA, A., KOSER, S. D., BROCKS, D., LIPKA, D. B., BOGATYROVA, O., WEICHENHAN, D., BRORS, B., RASSENTI, L., KIPPS, T. J., MERTENS, D., ZAPATKA, M., LICHTER, P., DÖHNER, H., KÜPPERS, R., ZENZ, T., STILGENBAUER, S., BYRD, J. C. & PLASS, C. 2016. DNA methylation dynamics during B cell maturation underlie a continuum of disease phenotypes in chronic lymphocytic leukemia. *Nat Genet,* 48**,** 253-64.

OBIER, N., CAUCHY, P., ASSI, S. A., GILMOUR, J., LIE-A-LING, M., LICHTINGER, M., HOOGENKAMP, M., NOAILLES, L., COCKERILL, P. N., LACAUD, G., KOUSKOFF, V. & BONIFER, C. 2016. Cooperative

binding of AP-1 and TEAD4 modulates the balance between vascular smooth muscle and hemogenic cell fate. *Development,* 143**,** 4324-4340.

OKAMOTO, Y., IWASAKI, W. M., KUGOU, K., TAKAHASHI, K. K., ODA, A., SATO, K., KOBAYASHI, W., KAWAI, H., SAKASAI, R., TAKAORI-KONDO, A., YAMAMOTO, T., KANEMAKI, M. T., TAOKA, M., ISOBE, T., KURUMIZAKA, H., INNAN, H., OHTA, K., ISHIAI, M. & TAKATA, M. 2018. Replication stress induces accumulation of FANCD2 at central region of large fragile genes. *Nucleic Acids Res,* 46**,** 2932-2944.

OLUWADARE, O., HIGHSMITH, M. & CHENG, J. 2019. An Overview of Methods for Reconstructing 3-D Chromosome and Genome Structures from Hi-C Data. *Biol Proced Online,* 21**,** 7.

OPPEZZO, P., VUILLIER, F., VASCONCELOS, Y., DUMAS, G., MAGNAC, C., PAYELLE-BROGARD, B., PRITSCH, O. & DIGHIERO, G. 2003. Chronic lymphocytic leukemia B cells expressing AID display dissociation between class switch recombination and somatic hypermutation. *Blood,* 101**,** 4029-32.

OTT, C. J., FEDERATION, A. J., KASAR, S., KLITGAARD, J. L., FERNANDES, S. M., BROWN, J. R. & BRADNER, J. E. 2015. Enhancer landscapes reveal transcription factor network dependencies in chronic lymphocytic leukemia. American Society of Hematology Washington, DC.

OTT, C. J., FEDERATION, A. J., SCHWARTZ, L. S., KASAR, S., KLITGAARD, J. L., LENCI, R., LI, Q., LAWLOR, M., FERNANDES, S. M., SOUZA, A., POLASKI, D., GADI, D., FREEDMAN, M. L., BROWN, J. R. & BRADNER, J. E. 2018. Enhancer Architecture and Essential Core Regulatory Circuitry of Chronic Lymphocytic Leukemia. *Cancer Cell,* 34**,** 982-995.e7.

OUE, N., SHIGEISHI, H., KUNIYASU, H., YOKOZAKI, H., KURAOKA, K., ITO, R. & YASUI, W. 2001. Promoter hypermethylation of MGMT is associated with protein loss in gastric carcinoma. *Int J Cancer,* 93**,** 805-9.

OZAKI, T., WU, D., SUGIMOTO, H., NAGASE, H. & NAKAGAWARA, A. 2013. Runt-related transcription factor 2 (RUNX2) inhibits p53-dependent apoptosis through the collaboration with HDAC6 in response to DNA damage. *Cell Death Dis,* 4**,** e610.

PASTORE, A., GAITI, F., LU, S. X., ABDEL-WAHAB, O. & LANDAU, D. A. 2017. Integrative Epigenomics Reveals Novel Chronic Lymphocytic Leukemia-Specific Chromatin States Associated with Epigenetic and Transcriptional Heterogeneity. American Society of Hematology Washington, DC.

PAULL, T. T. 2015. Mechanisms of ATM Activation. *Annu Rev Biochem,* 84**,** 711-38.

PEI, Y. & SHUMAN, S. 2002. Interactions between fission yeast mRNA capping enzymes and elongation factor Spt5. *J Biol Chem,* 277**,** 19639-48.

PETERSEN, A. J., RIMKUS, S. A. & WASSARMAN, D. A. 2012. ATM kinase inhibition in glial cells activates the innate immune response and causes neurodegeneration in Drosophila. *Proc Natl Acad Sci U S A,* 109**,** E656-64.

PILKA, E. S., JAMES, T. & LISZTWAN, J. H. 2015. Structural definitions of Jumonji family demethylase selectivity. *Drug Discov Today,* 20**,** 743-9.

PIPPA, S., MANNIRONI, C., LICURSI, V., BOMBARDI, L., COLOTTI, G., CUNDARI, E., MOLLICA, A., COLUCCIA, A., NACCARATO, V., LA REGINA, G., SILVESTRI, R. & NEGRI, R. 2019. Small Molecule Inhibitors of KDM5 Histone Demethylases Increase the Radiosensitivity of Breast Cancer Cells Overexpressing JARID1B. *Molecules,* 24.

PIZZI, S., SERTIC, S., ORCESI, S., CEREDA, C., BIANCHI, M., JACKSON, A. P., LAZZARO, F., PLEVANI, P. & MUZI-FALCONI, M. 2015. Reduction of hRNase H2 activity in Aicardi-Goutières syndrome cells leads to replication stress and genome instability. *Hum Mol Genet,* 24**,** 649-58.

PLCH, J., HRABETA, J. & ECKSCHLAGER, T. 2019. KDM5 demethylases and their role in cancer cell chemoresistance. *Int J Cancer,* 144**,** 221-231.

POKHOLOK, D. K., HARBISON, C. T., LEVINE, S., COLE, M., HANNETT, N. M., LEE, T. I., BELL, G. W., WALKER, K., ROLFE, P. A., HERBOLSHEIMER, E., ZEITLINGER, J., LEWITTER, F., GIFFORD, D. K. &

YOUNG, R. A. 2005. Genome-wide map of nucleosome acetylation and methylation in yeast. *Cell,* 122**,** 517-27.

POMMIER, Y., SUN, Y., HUANG, S. N. & NITISS, J. L. 2016. Roles of eukaryotic topoisomerases in transcription, replication and genomic stability. *Nat Rev Mol Cell Biol,* 17**,** 703-721.

PORTER, D. L., LEVINE, B. L., KALOS, M., BAGG, A. & JUNE, C. H. 2011. Chimeric antigen receptor-modified T cells in chronic lymphoid leukemia. *N Engl J Med,* 365**,** 725-33.

POTENSKI, C. J., NIU, H., SUNG, P. & KLEIN, H. L. 2014. Avoidance of ribonucleotide-induced mutations by RNase H2 and Srs2-Exo1 mechanisms. *Nature,* 511**,** 251-4.

POWELL, W. T., COULSON, R. L., GONZALES, M. L., CRARY, F. K., WONG, S. S., ADAMS, S., ACH, R. A., TSANG, P., YAMADA, N. A., YASUI, D. H., CHÉDIN, F. & LASALLE, J. M. 2013. R-loop formation at Snord116 mediates topotecan inhibition of Ube3a-antisense and allele-specific chromatin decondensation. *Proc Natl Acad Sci U S A,* 110**,** 13938-43.

POZZO, F., BITTOLO, T., ARRUGA, F., BULIAN, P., MACOR, P., TISSINO, E., GIZDIC, B., ROSSI, F. M., BOMBEN, R., ZUCCHETTO, A., BENEDETTI, D., DEGAN, M., D'ARENA, G., CHIARENZA, A., ZAJA, F., POZZATO, G., ROSSI, D., GAIDANO, G., DEL POETA, G., DEAGLIO, S., GATTEI, V. & DAL BO, M. 2016. NOTCH1 mutations associate with low CD20 level in chronic lymphocytic leukemia: evidence for a NOTCH1 mutation-driven epigenetic dysregulation. *Leukemia,* 30**,** 182-9.

PRICE, B. D. & D'ANDREA, A. D. 2013. Chromatin remodeling at DNA double-strand breaks. *Cell,* 152**,** 1344-54.

PUENTE, X. S., BEÀ, S., VALDÉS-MAS, R., VILLAMOR, N., GUTIÉRREZ-ABRIL, J., MARTÍN-SUBERO, J. I., MUNAR, M., RUBIO-PÉREZ, C., JARES, P., AYMERICH, M., BAUMANN, T., BEEKMAN, R., BELVER, L., CARRIO, A., CASTELLANO, G., CLOT, G., COLADO, E., COLOMER, D., COSTA, D., DELGADO, J., ENJUANES, A., ESTIVILL, X., FERRANDO, A. A., GELPÍ, J. L., GONZÁLEZ, B., GONZÁLEZ, S., GONZÁLEZ, M., GUT, M., HERNÁNDEZ-RIVAS, J. M., LÓPEZ-GUERRA, M., MARTÍN-GARCÍA, D., NAVARRO, A., NICOLÁS, P., OROZCO, M., PAYER, Á., PINYOL, M., PISANO, D. G., PUENTE, D. A., QUEIRÓS, A. C., QUESADA, V., ROMEO-CASABONA, C. M., ROYO, C., ROYO, R., ROZMAN, M., RUSSIÑOL, N., SALAVERRÍA, I., STAMATOPOULOS, K., STUNNENBERG, H. G., TAMBORERO, D., TEROL, M. J., VALENCIA, A., LÓPEZ-BIGAS, N., TORRENTS, D., GUT, I., LÓPEZ-GUILLERMO, A., LÓPEZ-OTÍN, C. & CAMPO, E. 2015. Non-coding recurrent mutations in chronic lymphocytic leukaemia. *Nature,* 526**,** 519-24.

QIN, Y., VASILATOS, S. N., CHEN, L., WU, H., CAO, Z., FU, Y., HUANG, M., VLAD, A. M., LU, B., OESTERREICH, S., DAVIDSON, N. E. & HUANG, Y. 2019. Inhibition of histone lysine-specific demethylase 1 elicits breast tumor immunity and enhances antitumor efficacy of immune checkpoint blockade. *Oncogene,* 38**,** 390-405.

QUEK, H., LUFF, J., CHEUNG, K., KOZLOV, S., GATEI, M., LEE, C. S., BELLINGHAM, M. C., NOAKES, P. G., LIM, Y. C., BARNETT, N. L., DINGWALL, S., WOLVETANG, E., MASHIMO, T., ROBERTS, T. L. & LAVIN, M. F. 2017. A rat model of ataxia-telangiectasia: evidence for a neurodegenerative phenotype. *Hum Mol Genet,* 26**,** 109-123.

QUESADA, V., CONDE, L., VILLAMOR, N., ORDÓÑEZ, G. R., JARES, P., BASSAGANYAS, L., RAMSAY, A. J., BEÀ, S., PINYOL, M., MARTÍNEZ-TRILLOS, A., LÓPEZ-GUERRA, M., COLOMER, D., NAVARRO, A., BAUMANN, T., AYMERICH, M., ROZMAN, M., DELGADO, J., GINÉ, E., HERNÁNDEZ, J. M., GONZÁLEZ-DÍAZ, M., PUENTE, D. A., VELASCO, G., FREIJE, J. M., TUBÍO, J. M., ROYO, R., GELPÍ, J. L., OROZCO, M., PISANO, D. G., ZAMORA, J., VÁZQUEZ, M., VALENCIA, A., HIMMELBAUER, H., BAYÉS, M., HEATH, S., GUT, M., GUT, I., ESTIVILL, X., LÓPEZ-GUILLERMO, A., PUENTE, X. S., CAMPO, E. & LÓPEZ-OTÍN, C. 2011. Exome sequencing identifies recurrent mutations of the splicing factor SF3B1 gene in chronic lymphocytic leukemia. *Nat Genet,* 44**,** 47-52.

QUINLAN, A. R. & HALL, I. M. 2010. BEDTools: a flexible suite of utilities for comparing genomic features. *Bioinformatics,* 26**,** 841-2.

RAMANA, C. V., GIL, M. P., SCHREIBER, R. D. & STARK, G. R. 2002. Stat1-dependent and -independent pathways in IFN-gamma-dependent signaling. *Trends Immunol,* 23**,** 96-101.
RAMÍREZ, F., DÜNDAR, F., DIEHL, S., GRÜNING, B. A. & MANKE, T. 2014. deepTools: a flexible platform for exploring deep-sequencing data. *Nucleic Acids Res,* 42**,** W187-91.
RANGASAMY, D., BERVEN, L., RIDGWAY, P. & TREMETHICK, D. J. 2003. Pericentric heterochromatin becomes enriched with H2A.Z during early mammalian development. *EMBO J,* 22**,** 1599-607.
REIJNS, M. A. & JACKSON, A. P. 2014. Ribonuclease H2 in health and disease. *Biochem Soc Trans,* 42**,** 717-25.
RENDEIRO, A. F., KRAUSGRUBER, T., FORTELNY, N., ZHAO, F., PENZ, T., FARLIK, M., SCHUSTER, L. C., NEMC, A., TASNÁDY, S., RÉTI, M., MÁTRAI, Z., ALPÁR, D., BÖDÖR, C., SCHMIDL, C. & BOCK, C. 2020. Chromatin mapping and single-cell immune profiling define the temporal dynamics of ibrutinib response in CLL. *Nat Commun,* 11**,** 577.
RENDEIRO, A. F., SCHMIDL, C., STREFFORD, J. C., WALEWSKA, R., DAVIS, Z., FARLIK, M., OSCIER, D. & BOCK, C. 2016. Chromatin accessibility maps of chronic lymphocytic leukaemia identify subtype-specific epigenome signatures and transcription regulatory networks. *Nat Commun,* 7**,** 11938.
RENNERT, J., COFFMAN, J. A., MUSHEGIAN, A. R. & ROBERTSON, A. J. 2003. The evolution of Runx genes I. A comparative study of sequences from phylogenetically diverse model organisms. *BMC Evol Biol,* 3**,** 4.
RICHARD, P. & MANLEY, J. L. 2009. Transcription termination by nuclear RNA polymerases. *Genes Dev,* 23**,** 1247-69.
RICHES, J. C., DAVIES, J. K., MCCLANAHAN, F., FATAH, R., IQBAL, S., AGRAWAL, S., RAMSAY, A. G. & GRIBBEN, J. G. 2013. T cells from CLL patients exhibit features of T-cell exhaustion but retain capacity for cytokine production. *Blood,* 121**,** 1612-21.
ROBINSON, M. D., MCCARTHY, D. J. & SMYTH, G. K. 2010. edgeR: a Bioconductor package for differential expression analysis of digital gene expression data. *Bioinformatics,* 26**,** 139-40.
ROESCH, A., VULTUR, A., BOGESKI, I., WANG, H., ZIMMERMANN, K. M., SPEICHER, D., KÖRBEL, C., LASCHKE, M. W., GIMOTTY, P. A., PHILIPP, S. E., KRAUSE, E., PÄTZOLD, S., VILLANUEVA, J., KREPLER, C., FUKUNAGA-KALABIS, M., HOTH, M., BASTIAN, B. C., VOGT, T. & HERLYN, M. 2013. Overcoming intrinsic multidrug resistance in melanoma by blocking the mitochondrial respiratory chain of slow-cycling JARID1B(high) cells. *Cancer Cell,* 23**,** 811-25.
RONCHETTI, D., MANZONI, M., AGNELLI, L., VINCI, C., FABRIS, S., CUTRONA, G., MATIS, S., COLOMBO, M., GALLETTI, S., TAIANA, E., RECCHIA, A. G., BOSSIO, S., GENTILE, M., MUSOLINO, C., DI RAIMONDO, F., GRILLI, A., BICCIATO, S., CORTELEZZI, A., TASSONE, P., MORABITO, F., FERRARINI, M. & NERI, A. 2016. lncRNA profiling in early-stage chronic lymphocytic leukemia identifies transcriptional fingerprints with relevance in clinical outcome. *Blood Cancer J,* 6**,** e468.
RONDINELLI, B., SCHWERER, H., ANTONINI, E., GAVIRAGHI, M., LUPI, A., FRENQUELLI, M., CITTARO, D., SEGALLA, S., LEMAITRE, J. M. & TONON, G. 2015. H3K4me3 demethylation by the histone demethylase KDM5C/JARID1C promotes DNA replication origin firing. *Nucleic Acids Res,* 43**,** 2560-74.
ROOS, W. P., THOMAS, A. D. & KAINA, B. 2016. DNA damage and the balance between survival and death in cancer biology. *Nat Rev Cancer,* 16**,** 20-33.
ROSSI, D., SPINA, V. & GAIDANO, G. 2018. Biology and treatment of Richter syndrome. *Blood,* 131**,** 2761-2772.
ROTHER, M. B. & VAN ATTIKUM, H. 2017. DNA repair goes hip-hop: SMARCA and CHD chromatin remodellers join the break dance. *Philos Trans R Soc Lond B Biol Sci,* 372.
ROUILLARD, A. D., GUNDERSEN, G. W., FERNANDEZ, N. F., WANG, Z., MONTEIRO, C. D., MCDERMOTT, M. G. & MA'AYAN, A. 2016. The harmonizome: a collection of processed datasets gathered to serve and mine knowledge about genes and proteins. *Database (Oxford),* 2016.

ROZOVSKI, U., KEATING, M. J. & ESTROV, Z. 2013. Targeting inflammatory pathways in chronic lymphocytic leukemia. *Crit Rev Oncol Hematol,* 88**,** 655-66.
RUDNIZKY, S., BAVLY, A., MALIK, O., PNUELI, L., MELAMED, P. & KAPLAN, A. 2016. H2A.Z controls the stability and mobility of nucleosomes to regulate expression of the LH genes. *Nat Commun,* 7**,** 12958.
RYDBERG, B. & GAME, J. 2002. Excision of misincorporated ribonucleotides in DNA by RNase H (type 2) and FEN-1 in cell-free extracts. *Proc Natl Acad Sci U S A,* 99**,** 16654-9.
SAINSBURY, S., BERNECKY, C. & CRAMER, P. 2015. Structural basis of transcription initiation by RNA polymerase II. *Nat Rev Mol Cell Biol,* 16**,** 129-43.
SAKSOUK, N., SIMBOECK, E. & DÉJARDIN, J. 2015. Constitutive heterochromatin formation and transcription in mammals. *Epigenetics Chromatin,* 8**,** 3.
SALDANHA, A. J. 2004. Java Treeview--extensible visualization of microarray data. *Bioinformatics,* 20**,** 3246-8.
SALEM, D. A. & STETLER-STEVENSON, M. 2019. Clinical Flow-Cytometric Testing in Chronic Lymphocytic Leukemia. *Methods Mol Biol,* 2032**,** 311-321.
SAMARAKKODY, A. S., SHIN, N. Y. & CANTOR, A. B. 2020. Role of RUNX Family Transcription Factors in DNA Damage Response. *Mol Cells,* 43**,** 99-106.
SANZ, L. A., HARTONO, S. R., LIM, Y. W., STEYAERT, S., RAJPURKAR, A., GINNO, P. A., XU, X. & CHÉDIN, F. 2016. Prevalent, Dynamic, and Conserved R-Loop Structures Associate with Specific Epigenomic Signatures in Mammals. *Mol Cell,* 63**,** 167-78.
SAVITSKY, K., BAR-SHIRA, A., GILAD, S., ROTMAN, G., ZIV, Y., VANAGAITE, L., TAGLE, D. A., SMITH, S., UZIEL, T., SFEZ, S., ASHKENAZI, M., PECKER, I., FRYDMAN, M., HARNIK, R., PATANJALI, S. R., SIMMONS, A., CLINES, G. A., SARTIEL, A., GATTI, R. A., CHESSA, L., SANAL, O., LAVIN, M. F., JASPERS, N. G., TAYLOR, A. M., ARLETT, C. F., MIKI, T., WEISSMAN, S. M., LOVETT, M., COLLINS, F. S. & SHILOH, Y. 1995. A single ataxia telangiectasia gene with a product similar to PI-3 kinase. *Science,* 268**,** 1749-53.
SAYEGH, J., CAO, J., ZOU, M. R., MORALES, A., BLAIR, L. P., NORCIA, M., HOYER, D., TACKETT, A. J., MERKEL, J. S. & YAN, Q. 2013. Identification of small molecule inhibitors of Jumonji AT-rich interactive domain 1B (JARID1B) histone demethylase by a sensitive high throughput screen. *J Biol Chem,* 288**,** 9408-17.
SCHEITZ, C. J., LEE, T. S., MCDERMITT, D. J. & TUMBAR, T. 2012. Defining a tissue stem cell-driven Runx1/Stat3 signalling axis in epithelial cancer. *EMBO J,* 31**,** 4124-39.
SCHICK, S., FOURNIER, D., THAKURELA, S., SAHU, S. K., GARDING, A. & TIWARI, V. K. 2015. Dynamics of chromatin accessibility and epigenetic state in response to UV damage. *J Cell Sci,* 128**,** 4380-94.
SCHIER, A. C. & TAATJES, D. J. 2020. Structure and mechanism of the RNA polymerase II transcription machinery. *Genes Dev,* 34**,** 465-488.
SCHMIDL, C., VLADIMER, G. I., RENDEIRO, A. F., SCHNABL, S., KRAUSGRUBER, T., TAUBERT, C., KRALL, N., PEMOVSKA, T., ARAGHI, M., SNIJDER, B., HUBMANN, R., RINGLER, A., RUNGGATSCHER, K., DEMIRTAS, D., DE LA FUENTE, O. L., HILGARTH, M., SKRABS, C., PORPACZY, E., GRUBER, M., HOERMANN, G., KUBICEK, S., STABER, P. B., SHEHATA, M., SUPERTI-FURGA, G., JÄGER, U. & BOCK, C. 2019. Combined chemosensitivity and chromatin profiling prioritizes drug combinations in CLL. *Nat Chem Biol,* 15**,** 232-240.
SCHONES, D. E., CUI, K., CUDDAPAH, S., ROH, T. Y., BARSKI, A., WANG, Z., WEI, G. & ZHAO, K. 2008. Dynamic regulation of nucleosome positioning in the human genome. *Cell,* 132**,** 887-98.
SCHUETTENGRUBER, B., CHOURROUT, D., VERVOORT, M., LEBLANC, B. & CAVALLI, G. 2007. Genome regulation by polycomb and trithorax proteins. *Cell,* 128**,** 735-45.
SCHULZ, H., KLEIN, S. K., REHWALD, U., REISER, M., HINKE, A., KNAUF, W. U., AULITZKY, W. E., HENSEL, M., HEROLD, M., HUHN, D., HALLEK, M., DIEHL, V., ENGERT, A. & GROUP, G. C. S. 2002. Phase 2

study of a combined immunochemotherapy using rituximab and fludarabine in patients with chronic lymphocytic leukemia. *Blood,* 100**,** 3115-20.
SCHWABISH, M. A. & STRUHL, K. 2004. Evidence for eviction and rapid deposition of histones upon transcriptional elongation by RNA polymerase II. *Mol Cell Biol,* 24**,** 10111-7.
SEGERT, J. A., GISSELBRECHT, S. S. & BULYK, M. L. 2021. Transcriptional Silencers: Driving Gene Expression with the Brakes On. *Trends Genet,* 37**,** 514-527.
SEIDEL, J. J., ANDERSON, C. M. & BLACKBURN, E. H. 2008. A novel Tel1/ATM N-terminal motif, TAN, is essential for telomere length maintenance and a DNA damage response. *Mol Cell Biol,* 28**,** 5736-46.
SELIGSON, D. B., HORVATH, S., SHI, T., YU, H., TZE, S., GRUNSTEIN, M. & KURDISTANI, S. K. 2005. Global histone modification patterns predict risk of prostate cancer recurrence. *Nature,* 435**,** 1262-6.
SEO, W., IKAWA, T., KAWAMOTO, H. & TANIUCHI, I. 2012. Runx1-Cbfβ facilitates early B lymphocyte development by regulating expression of Ebf1. *J Exp Med,* 209**,** 1255-62.
SERGUSHICHEV, A. A. 2016. An algorithm for fast preranked gene set enrichment analysis using cumulative statistic calculation. *bioRxiv***,** 060012.
SEYMOUR, J. F., KIPPS, T. J., EICHHORST, B., HILLMEN, P., D'ROZARIO, J., ASSOULINE, S., OWEN, C., GERECITANO, J., ROBAK, T., DE LA SERNA, J., JAEGER, U., CARTRON, G., MONTILLO, M., HUMERICKHOUSE, R., PUNNOOSE, E. A., LI, Y., BOYER, M., HUMPHREY, K., MOBASHER, M. & KATER, A. P. 2018. Venetoclax-Rituximab in Relapsed or Refractory Chronic Lymphocytic Leukemia. *N Engl J Med,* 378**,** 1107-1120.
SHABAN, N. M., HARVEY, S., PERRINO, F. W. & HOLLIS, T. 2010. The structure of the mammalian RNase H2 complex provides insight into RNA.NA hybrid processing to prevent immune dysfunction. *J Biol Chem,* 285**,** 3617-3624.
SHAFMAN, T., KHANNA, K. K., KEDAR, P., SPRING, K., KOZLOV, S., YEN, T., HOBSON, K., GATEI, M., ZHANG, N., WATTERS, D., EGERTON, M., SHILOH, Y., KHARBANDA, S., KUFE, D. & LAVIN, M. F. 1997. Interaction between ATM protein and c-Abl in response to DNA damage. *Nature,* 387**,** 520-3.
SHANAFELT, T. D., GEYER, S. M., BONE, N. D., TSCHUMPER, R. C., WITZIG, T. E., NOWAKOWSKI, G. S., ZENT, C. S., CALL, T. G., LAPLANT, B., DEWALD, G. W., JELINEK, D. F. & KAY, N. E. 2008. CD49d expression is an independent predictor of overall survival in patients with chronic lymphocytic leukaemia: a prognostic parameter with therapeutic potential. *Br J Haematol,* 140**,** 537-46.
SHANNON, P., MARKIEL, A., OZIER, O., BALIGA, N. S., WANG, J. T., RAMAGE, D., AMIN, N., SCHWIKOWSKI, B. & IDEKER, T. 2003. Cytoscape: a software environment for integrated models of biomolecular interaction networks. *Genome Res,* 13**,** 2498-504.
SHARMA, N. 2016. Regulation of RNA polymerase II-mediated transcriptional elongation: Implications in human disease. *IUBMB Life,* 68**,** 709-16.
SHEN, H. & LAIRD, P. W. 2013. Interplay between the cancer genome and epigenome. *Cell,* 153**,** 38-55.
SHIGEKAWA, Y., HAYAMI, S., UENO, M., MIYAMOTO, A., SUZAKI, N., KAWAI, M., HIRONO, S., OKADA, K. I., HAMAMOTO, R. & YAMAUE, H. 2018. Overexpression of KDM5B/JARID1B is associated with poor prognosis in hepatocellular carcinoma. *Oncotarget,* 9**,** 34320-34335.
SHILOH, Y. & ZIV, Y. 2013. The ATM protein kinase: regulating the cellular response to genotoxic stress, and more. *Nat Rev Mol Cell Biol,* 14**,** 197-210.
SIMS, R. J., MILLHOUSE, S., CHEN, C. F., LEWIS, B. A., ERDJUMENT-BROMAGE, H., TEMPST, P., MANLEY, J. L. & REINBERG, D. 2007. Recognition of trimethylated histone H3 lysine 4 facilitates the recruitment of transcription postinitiation factors and pre-mRNA splicing. *Mol Cell,* 28**,** 665-76.
SKOWRONSKA, A., AUSTEN, B., POWELL, J. E., WESTON, V., OSCIER, D. G., DYER, M. J., MATUTES, E., PRATT, G., FEGAN, C., MOSS, P., TAYLOR, M. A. & STANKOVIC, T. 2012. ATM germline

heterozygosity does not play a role in chronic lymphocytic leukemia initiation but influences rapid disease progression through loss of the remaining ATM allele. *Haematologica,* 97**,** 142-6.
SLAGER, S. L. & KAY, N. E. 2009. Familial chronic lymphocytic leukemia: what does it mean to me? *Clin Lymphoma Myeloma,* 9 Suppl 3**,** S194-7.
SMITH, E. & SHILATIFARD, A. 2014. Enhancer biology and enhanceropathies. *Nat Struct Mol Biol,* 21**,** 210-9.
SMITH, E. N., GHIA, E. M., DEBOEVER, C. M., RASSENTI, L. Z., JEPSEN, K., YOON, K. A., MATSUI, H., ROZENZHAK, S., ALAKUS, H., SHEPARD, P. J., DAI, Y., KHOSROHEIDARI, M., BINA, M., GUNDERSON, K. L., MESSER, K., MUTHUSWAMY, L., HUDSON, T. J., HARISMENDY, O., BARRETT, C. L., JAMIESON, C. H., CARSON, D. A., KIPPS, T. J. & FRAZER, K. A. 2015. Genetic and epigenetic profiling of CLL disease progression reveals limited somatic evolution and suggests a relationship to memory-cell development. *Blood Cancer J,* 5**,** e303.
SONG, J., NOH, J. H., LEE, J. H., EUN, J. W., AHN, Y. M., KIM, S. Y., LEE, S. H., PARK, W. S., YOO, N. J., LEE, J. Y. & NAM, S. W. 2005. Increased expression of histone deacetylase 2 is found in human gastric cancer. *APMIS,* 113**,** 264-8.
SPARKS, J. L. & BURGERS, P. M. 2015. Error-free and mutagenic processing of topoisomerase 1-provoked damage at genomic ribonucleotides. *EMBO J,* 34**,** 1259-69.
SPARKS, J. L., CHON, H., CERRITELLI, S. M., KUNKEL, T. A., JOHANSSON, E., CROUCH, R. J. & BURGERS, P. M. 2012. RNase H2-initiated ribonucleotide excision repair. *Mol Cell,* 47**,** 980-6.
SPEEDY, H. E., DI BERNARDO, M. C., SAVA, G. P., DYER, M. J., HOLROYD, A., WANG, Y., SUNTER, N. J., MANSOURI, L., JULIUSSON, G., SMEDBY, K. E., ROOS, G., JAYNE, S., MAJID, A., DEARDEN, C., HALL, A. G., MAINOU-FOWLER, T., JACKSON, G. H., SUMMERFIELD, G., HARRIS, R. J., PETTITT, A. R., ALLSUP, D. J., BAILEY, J. R., PRATT, G., PEPPER, C., FEGAN, C., ROSENQUIST, R., CATOVSKY, D., ALLAN, J. M. & HOULSTON, R. S. 2014. A genome-wide association study identifies multiple susceptibility loci for chronic lymphocytic leukemia. *Nat Genet,* 46**,** 56-60.
SPITZ, F. & FURLONG, E. E. 2012. Transcription factors: from enhancer binding to developmental control. *Nat Rev Genet,* 13**,** 613-26.
STACCHINI, A., ARAGNO, M., VALLARIO, A., ALFARANO, A., CIRCOSTA, P., GOTTARDI, D., FALDELLA, A., REGE-CAMBRIN, G., THUNBERG, U., NILSSON, K. & CALIGARIS-CAPPIO, F. 1999. MEC1 and MEC2: two new cell lines derived from B-chronic lymphocytic leukaemia in prolymphocytoid transformation. *Leuk Res,* 23**,** 127-36.
STANKOVIC, T., STEWART, G. S., FEGAN, C., BIGGS, P., LAST, J., BYRD, P. J., KEENAN, R. D., MOSS, P. A. & TAYLOR, A. M. 2002. Ataxia telangiectasia mutated-deficient B-cell chronic lymphocytic leukemia occurs in pregerminal center cells and results in defective damage response and unrepaired chromosome damage. *Blood,* 99**,** 300-9.
STATELLO, L., GUO, C. J., CHEN, L. L. & HUARTE, M. 2021. Gene regulation by long non-coding RNAs and its biological functions. *Nat Rev Mol Cell Biol,* 22**,** 96-118.
STERNER, R. C. & STERNER, R. M. 2021. CAR-T cell therapy: current limitations and potential strategies. *Blood Cancer J,* 11**,** 69.
STEWART, G. S., LAST, J. I., STANKOVIC, T., HAITES, N., KIDD, A. M., BYRD, P. J. & TAYLOR, A. M. 2001. Residual ataxia telangiectasia mutated protein function in cells from ataxia telangiectasia patients, with 5762ins137 and 7271T-->G mutations, showing a less severe phenotype. *J Biol Chem,* 276**,** 30133-41.
STILGENBAUER, S., SCHNAITER, A., PASCHKA, P., ZENZ, T., ROSSI, M., DÖHNER, K., BÜHLER, A., BÖTTCHER, S., RITGEN, M., KNEBA, M., WINKLER, D., TAUSCH, E., HOTH, P., EDELMANN, J., MERTENS, D., BULLINGER, L., BERGMANN, M., KLESS, S., MACK, S., JÄGER, U., PATTEN, N., WU, L., WENGER, M. K., FINGERLE-ROWSON, G., LICHTER, P., CAZZOLA, M., WENDTNER, C. M., FINK,

A. M., FISCHER, K., BUSCH, R., HALLEK, M. & DÖHNER, H. 2014. Gene mutations and treatment outcome in chronic lymphocytic leukemia: results from the CLL8 trial. *Blood,* 123**,** 3247-54.
STOVNER, E. B. & SÆTROM, P. 2019. epic2 efficiently finds diffuse domains in ChIP-seq data. *Bioinformatics,* 35**,** 4392-4393.
STRATI, P. & SHANAFELT, T. D. 2015. Monoclonal B-cell lymphocytosis and early-stage chronic lymphocytic leukemia: diagnosis, natural history, and risk stratification. *Blood,* 126**,** 454-62.
SUMIMOTO, H., TAKANO, A., TERAMOTO, K. & DAIGO, Y. 2016. RAS-Mitogen-Activated Protein Kinase Signal Is Required for Enhanced PD-L1 Expression in Human Lung Cancers. *PLoS One,* 11**,** e0166626.
SUN, Y., XU, Y., ROY, K. & PRICE, B. D. 2007. DNA damage-induced acetylation of lysine 3016 of ATM activates ATM kinase activity. *Mol Cell Biol,* 27**,** 8502-9.
TAGAMI, H., RAY-GALLET, D., ALMOUZNI, G. & NAKATANI, Y. 2004. Histone H3.1 and H3.3 complexes mediate nucleosome assembly pathways dependent or independent of DNA synthesis. *Cell,* 116**,** 51-61.
TAN, M., LUO, H., LEE, S., JIN, F., YANG, J. S., MONTELLIER, E., BUCHOU, T., CHENG, Z., ROUSSEAUX, S., RAJAGOPAL, N., LU, Z., YE, Z., ZHU, Q., WYSOCKA, J., YE, Y., KHOCHBIN, S., REN, B. & ZHAO, Y. 2011. Identification of 67 histone marks and histone lysine crotonylation as a new type of histone modification. *Cell,* 146**,** 1016-28.
TAN, S. H., SAPARI, N. S., MIAO, H., HARTMAN, M., LOH, M., CHNG, W. J., IAU, P., BUHARI, S. A., SOONG, R. & LEE, S. C. 2015. High-Throughput Mutation Profiling Changes before and 3 Weeks after Chemotherapy in Newly Diagnosed Breast Cancer Patients. *PLoS One,* 10**,** e0142466.
TAUSCH, E., CLOSE, W., DOLNIK, A., BLOEHDORN, J., CHYLA, B., BULLINGER, L., DÖHNER, H., MERTENS, D. & STILGENBAUER, S. 2019. Venetoclax resistance and acquired. *Haematologica,* 104**,** e434-e437.
TAY, L. S., KRISHNAN, V., SANKAR, H., CHONG, Y. L., CHUANG, L. S. H., TAN, T. Z., KOLINJIVADI, A. M., KAPPEI, D. & ITO, Y. 2018. RUNX Poly(ADP-Ribosyl)ation and BLM Interaction Facilitate the Fanconi Anemia Pathway of DNA Repair. *Cell Rep,* 24**,** 1747-1755.
TAYLOR, A. M., METCALFE, J. A., THICK, J. & MAK, Y. F. 1996. Leukemia and lymphoma in ataxia telangiectasia. *Blood,* 87**,** 423-38.
TECHNOLOGY, C. S. 2022. *Histone Modification Table* [Online]. Cell Signalling Technology. Available: https://www.cellsignal.com/learn-and-support/reference-tables/histone-modification-table [Accessed 20 Feb 2022 2022].
THORSÉLIUS, M., KRÖBER, A., MURRAY, F., THUNBERG, U., TOBIN, G., BÜHLER, A., KIENLE, D., ALBESIANO, E., MAFFEI, R., DAO-UNG, L. P., WILEY, J., VILPO, J., LAURELL, A., MERUP, M., ROOS, G., KARLSSON, K., CHIORAZZI, N., MARASCA, R., DÖHNER, H., STILGENBAUER, S. & ROSENQUIST, R. 2006. Strikingly homologous immunoglobulin gene rearrangements and poor outcome in VH3-21-using chronic lymphocytic leukemia patients independent of geographic origin and mutational status. *Blood,* 107**,** 2889-94.
TICCHIONI, M., ESSAFI, M., JEANDEL, P. Y., DAVI, F., CASSUTO, J. P., DECKERT, M. & BERNARD, A. 2007. Homeostatic chemokines increase survival of B-chronic lymphocytic leukemia cells through inactivation of transcription factor FOXO3a. *Oncogene,* 26**,** 7081-91.
TIJCHON, E., HAVINGA, J., VAN LEEUWEN, F. N. & SCHEIJEN, B. 2013. B-lineage transcription factors and cooperating gene lesions required for leukemia development. *Leukemia,* 27**,** 541-52.
TOYOTA, M. & SUZUKI, H. 2010. Epigenetic drivers of genetic alterations. *Adv Genet,* 70**,** 309-23.
TRAPNELL, C., WILLIAMS, B. A., PERTEA, G., MORTAZAVI, A., KWAN, G., VAN BAREN, M. J., SALZBERG, S. L., WOLD, B. J. & PACHTER, L. 2010. Transcript assembly and quantification by RNA-Seq reveals unannotated transcripts and isoform switching during cell differentiation. *Nat Biotechnol,* 28**,** 511-5.

TSUKIYAMA, T., BECKER, P. B. & WU, C. 1994. ATP-dependent nucleosome disruption at a heat-shock promoter mediated by binding of GAGA transcription factor. *Nature,* 367**,** 525-32.

TSUNEMATSU, T., KUDO, Y., IIZUKA, S., OGAWA, I., FUJITA, T., KURIHARA, H., ABIKO, Y. & TAKATA, T. 2009. RUNX3 has an oncogenic role in head and neck cancer. *PLoS One,* 4**,** e5892.

TUBBS, A. & NUSSENZWEIG, A. 2017. Endogenous DNA Damage as a Source of Genomic Instability in Cancer. *Cell,* 168**,** 644-656.

TURTLE, C. J., HAY, K. A., HANAFI, L. A., LI, D., CHERIAN, S., CHEN, X., WOOD, B., LOZANSKI, A., BYRD, J. C., HEIMFELD, S., RIDDELL, S. R. & MALONEY, D. G. 2017. Durable Molecular Remissions in Chronic Lymphocytic Leukemia Treated With CD19-Specific Chimeric Antigen Receptor-Modified T Cells After Failure of Ibrutinib. *J Clin Oncol,* 35**,** 3010-3020.

VARDABASSO, C., GASPAR-MAIA, A., HASSON, D., PÜNZELER, S., VALLE-GARCIA, D., STRAUB, T., KEILHAUER, E. C., STRUB, T., DONG, J., PANDA, T., CHUNG, C. Y., YAO, J. L., SINGH, R., SEGURA, M. F., FONTANALS-CIRERA, B., VERMA, A., MANN, M., HERNANDO, E., HAKE, S. B. & BERNSTEIN, E. 2015. Histone Variant H2A.Z.2 Mediates Proliferation and Drug Sensitivity of Malignant Melanoma. *Mol Cell,* 59**,** 75-88.

VENKATESH, S. & WORKMAN, J. L. 2015. Histone exchange, chromatin structure and the regulation of transcription. *Nat Rev Mol Cell Biol,* 16**,** 178-89.

WALLACE, B. D., BERMAN, Z., MUELLER, G. A., LIN, Y., CHANG, T., ANDRES, S. N., WOJTASZEK, J. L., DEROSE, E. F., APPEL, C. D., LONDON, R. E., YAN, S. & WILLIAMS, R. S. 2017. APE2 Zf-GRF facilitates 3'-5' resection of DNA damage following oxidative stress. *Proc Natl Acad Sci U S A,* 114**,** 304-309.

WANG, B., WANG, M., ZHANG, W., XIAO, T., CHEN, C. H., WU, A., WU, F., TRAUGH, N., WANG, X., LI, Z., MEI, S., CUI, Y., SHI, S., LIPP, J. J., HINTERNDORFER, M., ZUBER, J., BROWN, M., LI, W. & LIU, X. S. 2019a. Integrative analysis of pooled CRISPR genetic screens using MAGeCKFlute. *Nat Protoc,* 14**,** 756-780.

WANG, C., WANG, G., FENG, X., SHEPHERD, P., ZHANG, J., TANG, M., CHEN, Z., SRIVASTAVA, M., MCLAUGHLIN, M. E., NAVONE, N. M., HART, G. T. & CHEN, J. 2019b. Genome-wide CRISPR screens reveal synthetic lethality of RNASEH2 deficiency and ATR inhibition. *Oncogene,* 38**,** 2451-2463.

WANG, C. Q., KRISHNAN, V., TAY, L. S., CHIN, D. W., KOH, C. P., CHOOI, J. Y., NAH, G. S., DU, L., JACOB, B., YAMASHITA, N., LAI, S. K., TAN, T. Z., MORI, S., TANUICHI, I., TERGAONKAR, V., ITO, Y. & OSATO, M. 2014. Disruption of Runx1 and Runx3 leads to bone marrow failure and leukemia predisposition due to transcriptional and DNA repair defects. *Cell Rep,* 8**,** 767-82.

WANG, D., JOHN, S. A., CLEMENTS, J. L., PERCY, D. H., BARTON, K. P. & GARRETT-SINHA, L. A. 2005. Ets-1 deficiency leads to altered B cell differentiation, hyperresponsiveness to TLR9 and autoimmune disease. *Int Immunol,* 17**,** 1179-91.

WANG, H., SONG, C., DING, Y., PAN, X., GE, Z., TAN, B. H., GOWDA, C., SACHDEV, M., MUTHUSAMI, S., OUYANG, H., LAI, L., FRANCIS, O. L., MORRIS, C. L., ABDEL-AZIM, H., DORSAM, G., XIANG, M., PAYNE, K. J. & DOVAT, S. 2016. Transcriptional Regulation of JARID1B/KDM5B Histone Demethylase by Ikaros, Histone Deacetylase 1 (HDAC1), and Casein Kinase 2 (CK2) in B-cell Acute Lymphoblastic Leukemia. *J Biol Chem,* 291**,** 4004-18.

WANG, J. C., KAFEEL, M. I., AVEZBAKIYEV, B., CHEN, C., SUN, Y., RATHNASABAPATHY, C., KALAVAR, M., HE, Z., BURTON, J. & LICHTER, S. 2011a. Histone deacetylase in chronic lymphocytic leukemia. *Oncology,* 81**,** 325-9.

WANG, K. C., YANG, Y. W., LIU, B., SANYAL, A., CORCES-ZIMMERMAN, R., CHEN, Y., LAJOIE, B. R., PROTACIO, A., FLYNN, R. A., GUPTA, R. A., WYSOCKA, J., LEI, M., DEKKER, J., HELMS, J. A. & CHANG, H. Y. 2011b. A long noncoding RNA maintains active chromatin to coordinate homeotic gene expression. *Nature,* 472**,** 120-4.

WANG, Q., FRANKS, H. A., LAX, S. J., EL REFAEE, M., MALECKA, A., SHAH, S., SPENDLOVE, I., GOUGH, M. J., SEEDHOUSE, C., MADHUSUDAN, S., PATEL, P. M. & JACKSON, A. M. 2013. The ataxia telangiectasia mutated kinase pathway regulates IL-23 expression by human dendritic cells. *J Immunol,* 190**,** 3246-55.

WANG, S. W. & SPECK, N. A. 1992. Purification of core-binding factor, a protein that binds the conserved core site in murine leukemia virus enhancers. *Mol Cell Biol,* 12**,** 89-102.

WATLING, D., CARMO, C. R., KERR, I. M. & COSTA-PEREIRA, A. P. 2008. Multiple kinases in the interferon-gamma response. *Proc Natl Acad Sci U S A,* 105**,** 6051-6.

WEINREB, J. T., GHAZALE, N., PRADHAN, K., GUPTA, V., POTTS, K. S., TRICOMI, B., DANIELS, N. J., PADGETT, R. A., DE OLIVEIRA, S., VERMA, A. & BOWMAN, T. V. 2021. Excessive R-loops trigger an inflammatory cascade leading to increased HSPC production. *Dev Cell,* 56**,** 627-640.e5.

WEINTRAUB, H. & GROUDINE, M. 1976. Chromosomal subunits in active genes have an altered conformation. *Science,* 193**,** 848-56.

WEIZMAN, N., SHILOH, Y. & BARZILAI, A. 2003. Contribution of the Atm protein to maintaining cellular homeostasis evidenced by continuous activation of the AP-1 pathway in Atm-deficient brains. *J Biol Chem,* 278**,** 6741-7.

WEN, Z., ZHANG, L., RUAN, H. & LI, G. 2020. Histone variant H2A.Z regulates nucleosome unwrapping and CTCF binding in mouse ES cells. *Nucleic Acids Res,* 48**,** 5939-5952.

WEST, S., PROUDFOOT, N. J. & DYE, M. J. 2008. Molecular dissection of mammalian RNA polymerase II transcriptional termination. *Mol Cell,* 29**,** 600-10.

WESTBROOK, A. M. & SCHIESTL, R. H. 2010. Atm-deficient mice exhibit increased sensitivity to dextran sulfate sodium-induced colitis characterized by elevated DNA damage and persistent immune activation. *Cancer Res,* 70**,** 1875-84.

WESTON, V. J., OLDREIVE, C. E., SKOWRONSKA, A., OSCIER, D. G., PRATT, G., DYER, M. J., SMITH, G., POWELL, J. E., RUDZKI, Z., KEARNS, P., MOSS, P. A., TAYLOR, A. M. & STANKOVIC, T. 2010. The PARP inhibitor olaparib induces significant killing of ATM-deficient lymphoid tumor cells in vitro and in vivo. *Blood,* 116**,** 4578-87.

WILLEMS, P., CLAES, K., BAEYENS, A., VANDERSICKEL, V., WERBROUCK, J., DE RUYCK, K., POPPE, B., VAN DEN BROECKE, R., MAKAR, A., MARRAS, E., PERLETTI, G., THIERENS, H. & VRAL, A. 2008. Polymorphisms in nonhomologous end-joining genes associated with breast cancer risk and chromosomal radiosensitivity. *Genes Chromosomes Cancer,* 47**,** 137-48.

WILLIAMS, J. S., GEHLE, D. B. & KUNKEL, T. A. 2017. The role of RNase H2 in processing ribonucleotides incorporated during DNA replication. *DNA Repair (Amst),* 53**,** 52-58.

WILLIAMS, J. S., LUJAN, S. A. & KUNKEL, T. A. 2016. Processing ribonucleotides incorporated during eukaryotic DNA replication. *Nat Rev Mol Cell Biol,* 17**,** 350-63.

WILLIAMS, J. S., SMITH, D. J., MARJAVAARA, L., LUJAN, S. A., CHABES, A. & KUNKEL, T. A. 2013. Topoisomerase 1-mediated removal of ribonucleotides from nascent leading-strand DNA. *Mol Cell,* 49**,** 1010-5.

WILLIAMS, R. S., MONCALIAN, G., WILLIAMS, J. S., YAMADA, Y., LIMBO, O., SHIN, D. S., GROOCOCK, L. M., CAHILL, D., HITOMI, C., GUENTHER, G., MOIANI, D., CARNEY, J. P., RUSSELL, P. & TAINER, J. A. 2008. Mre11 dimers coordinate DNA end bridging and nuclease processing in double-strand-break repair. *Cell,* 135**,** 97-109.

WINKELMANN, N., ROSE-ZERILLI, M., FORSTER, J., PARRY, M., PARKER, A., GARDINER, A., DAVIES, Z., STEELE, A. J., PARKER, H., CROSS, N. C., OSCIER, D. G. & STREFFORD, J. C. 2015. Low frequency mutations independently predict poor treatment-free survival in early stage chronic lymphocytic leukemia and monoclonal B-cell lymphocytosis. *Haematologica,* 100**,** e237-9.

WOJDACZ, T. K., AMARASINGHE, H. E., KADALAYIL, L., BEATTIE, A., FORSTER, J., BLAKEMORE, S. J., PARKER, H., BRYANT, D., LARRAYOZ, M., CLIFFORD, R., ROBBE, P., DAVIS, Z. A., ELSE, M.,

HOWARD, D. R., STAMATOPOULOS, B., STEELE, A. J., ROSENQUIST, R., COLLINS, A., PETTITT, A. R., HILLMEN, P., PLASS, C., SCHUH, A., CATOVSKY, D., OSCIER, D. G., ROSE-ZERILLI, M. J. J., OAKES, C. C. & STREFFORD, J. C. 2019. Clinical significance of DNA methylation in chronic lymphocytic leukemia patients: results from 3 UK clinical trials. *Blood Adv,* 3**,** 2474-2481.

WU, J., ZHANG, X., ZHANG, L., WU, C. Y., REZAEIAN, A. H., CHAN, C. H., LI, J. M., WANG, J., GAO, Y., HAN, F., JEONG, Y. S., YUAN, X., KHANNA, K. K., JIN, J., ZENG, Y. X. & LIN, H. K. 2012. Skp2 E3 ligase integrates ATM activation and homologous recombination repair by ubiquitinating NBS1. *Mol Cell,* 46**,** 351-61.

WU, L., CAO, J., CAI, W. L., LANG, S. M., HORTON, J. R., JANSEN, D. J., LIU, Z. Z., CHEN, J. F., ZHANG, M., MOTT, B. T., POHIDA, K., RAI, G., KALES, S. C., HENDERSON, M. J., HU, X., JADHAV, A., MALONEY, D. J., SIMEONOV, A., ZHU, S., IWASAKI, A., HALL, M. D., CHENG, X., SHADEL, G. S. & YAN, Q. 2018. KDM5 histone demethylases repress immune response via suppression of STING. *PLoS Biol,* 16**,** e2006134.

XANTHOPOULOS, C. & KOSTARELI, E. 2019. Advances in epigenetics and epigenomics in chronic lymphocytic leukemia. *Current Genetic Medicine Reports,* 7**,** 214-226.

XIAO, A., LI, H., SHECHTER, D., AHN, S. H., FABRIZIO, L. A., ERDJUMENT-BROMAGE, H., ISHIBE-MURAKAMI, S., WANG, B., TEMPST, P., HOFMANN, K., PATEL, D. J., ELLEDGE, S. J. & ALLIS, C. D. 2009. WSTF regulates the H2A.X DNA damage response via a novel tyrosine kinase activity. *Nature,* 457**,** 57-62.

XOCHELLI, A., BALIAKAS, P., KAVAKIOTIS, I., AGATHANGELIDIS, A., SUTTON, L. A., MINGA, E., NTOUFA, S., TAUSCH, E., YAN, X. J., SHANAFELT, T., PLEVOVA, K., BOUDJOGRA, M., ROSSI, D., DAVIS, Z., NAVARRO, A., SANDBERG, Y., VOJDEMAN, F. J., SCARFO, L., STAVROYIANNI, N., SUDARIKOV, A., VERONESE, S., TZENOU, T., KARAN-DJURASEVIC, T., CATHERWOOD, M., KIENLE, D., CHATZOULI, M., FACCO, M., BAHLO, J., POTT, C., PEDERSEN, L. B., MANSOURI, L., SMEDBY, K. E., CHU, C. C., GIUDICELLI, V., LEFRANC, M. P., PANAGIOTIDIS, P., JULIUSSON, G., ANAGNOSTOPOULOS, A., VLAHAVAS, I., ANTIC, D., TRENTIN, L., MONTILLO, M., NIEMANN, C., DÖHNER, H., LANGERAK, A. W., POSPISILOVA, S., HALLEK, M., CAMPO, E., CHIORAZZI, N., MAGLAVERAS, N., OSCIER, D., GAIDANO, G., JELINEK, D. F., STILGENBAUER, S., CHOUVARDA, I., DARZENTAS, N., BELESSI, C., DAVI, F., HADZIDIMITRIOU, A., ROSENQUIST, R., GHIA, P. & STAMATOPOULOS, K. 2017. Chronic Lymphocytic Leukemia with Mutated IGHV4-34 Receptors: Shared and Distinct Immunogenetic Features and Clinical Outcomes. *Clin Cancer Res,* 23**,** 5292-5301.

XOSE, S. P. A. S. B. A. R. V. S.-M. A. N. V. A. J. S. G. R.-A. A. J. I. M. N.-S. A. M. M. 2015. Non-coding recurrent mutations in chronic lymphocytic leukaemia. *Nature,* 526**,** 519.

XU, B., O'DONNELL, A. H., KIM, S. T. & KASTAN, M. B. 2002. Phosphorylation of serine 1387 in Brca1 is specifically required for the Atm-mediated S-phase checkpoint after ionizing irradiation. *Cancer Res,* 62**,** 4588-91.

XU, H. & EL-GEWELY, M. R. 2003. Differentially expressed downstream genes in cells with normal or mutated p53. *Oncol Res,* 13**,** 429-36.

XU, W., ZHOU, B., ZHAO, X., ZHU, L., XU, J., JIANG, Z., CHEN, D., WEI, Q., HAN, M., FENG, L., WANG, S., WANG, X., ZHOU, J. & JIN, H. 2018. KDM5B demethylates H3K4 to recruit XRCC1 and promote chemoresistance. *Int J Biol Sci,* 14**,** 1122-1132.

XU, Y., AYRAPETOV, M. K., XU, C., GURSOY-YUZUGULLU, O., HU, Y. & PRICE, B. D. 2012. Histone H2A.Z controls a critical chromatin remodeling step required for DNA double-strand break repair. *Mol Cell,* 48**,** 723-33.

XUE, S., LAM, Y. M., HE, Z., ZHENG, Y., LI, L., ZHANG, Y., LI, C., MBADHI, M. N., ZHENG, L., CHENG, Z., LIU, Y., WANG, X., CHAN, L. C., NG, R. K. & ZHANG, J. 2020. Histone lysine demethylase KDM5B maintains chronic myeloid leukemia via multiple epigenetic actions. *Exp Hematol,* 82**,** 53-65.

YAMAGUCHI, Y., SHIBATA, H. & HANDA, H. 2013. Transcription elongation factors DSIF and NELF: promoter-proximal pausing and beyond. *Biochim Biophys Acta,* 1829**,** 98-104.
YAMAMOTO, S., WU, Z., RUSSNES, H. G., TAKAGI, S., PELUFFO, G., VASKE, C., ZHAO, X., MOEN VOLLAN, H. K., MARUYAMA, R., EKRAM, M. B., SUN, H., KIM, J. H., CARVER, K., ZUCCA, M., FENG, J., ALMENDRO, V., BESSARABOVA, M., RUEDA, O. M., NIKOLSKY, Y., CALDAS, C., LIU, X. S. & POLYAK, K. 2014. JARID1B is a luminal lineage-driving oncogene in breast cancer. *Cancer Cell,* 25**,** 762-77.
YAMANE, A., RESCH, W., KUO, N., KUCHEN, S., LI, Z., SUN, H. W., ROBBIANI, D. F., MCBRIDE, K., NUSSENZWEIG, M. C. & CASELLAS, R. 2011. Deep-sequencing identification of the genomic targets of the cytidine deaminase AID and its cofactor RPA in B lymphocytes. *Nat Immunol,* 12**,** 62-9.
YANG, Y., HUI, C. W., LI, J. & HERRUP, K. 2014. The interaction of the atm genotype with inflammation and oxidative stress. *PLoS One,* 9**,** e85863.
YAP, K. L., LI, S., MUÑOZ-CABELLO, A. M., RAGUZ, S., ZENG, L., MUJTABA, S., GIL, J., WALSH, M. J. & ZHOU, M. M. 2010. Molecular interplay of the noncoding RNA ANRIL and methylated histone H3 lysine 27 by polycomb CBX7 in transcriptional silencing of INK4a. *Mol Cell,* 38**,** 662-74.
YAZDI, P. T., WANG, Y., ZHAO, S., PATEL, N., LEE, E. Y. & QIN, J. 2002. SMC1 is a downstream effector in the ATM/NBS1 branch of the human S-phase checkpoint. *Genes Dev,* 16**,** 571-82.
YE, Z., SHI, Y., LEES-MILLER, S. P. & TAINER, J. A. 2021. Function and Molecular Mechanism of the DNA Damage Response in Immunity and Cancer Immunotherapy. *Front Immunol,* 12**,** 797880.
YOKOYAMA, A., WANG, Z., WYSOCKA, J., SANYAL, M., AUFIERO, D. J., KITABAYASHI, I., HERR, W. & CLEARY, M. L. 2004. Leukemia proto-oncoprotein MLL forms a SET1-like histone methyltransferase complex with menin to regulate Hox gene expression. *Mol Cell Biol,* 24**,** 5639-49.
YOSHIDA, K., OZAKI, T., FURUYA, K., NAKANISHI, M., KIKUCHI, H., YAMAMOTO, H., ONO, S., KODA, T., OMURA, K. & NAKAGAWARA, A. 2008. ATM-dependent nuclear accumulation of IKK-alpha plays an important role in the regulation of p73-mediated apoptosis in response to cisplatin. *Oncogene,* 27**,** 1183-8.
YOUNG, D. B., JONNALAGADDA, J., GATEI, M., JANS, D. A., MEYN, S. & KHANNA, K. K. 2005. Identification of domains of ataxia-telangiectasia mutated required for nuclear localization and chromatin association. *J Biol Chem,* 280**,** 27587-94.
YOUNG, L. C. & HENDZEL, M. J. 2013. The oncogenic potential of Jumonji D2 (JMJD2/KDM4) histone demethylase overexpression. *Biochem Cell Biol,* 91**,** 369-77.
YU, G., WANG, L. G., HAN, Y. & HE, Q. Y. 2012. clusterProfiler: an R package for comparing biological themes among gene clusters. *OMICS,* 16**,** 284-7.
YU, G., WANG, L. G. & HE, Q. Y. 2015a. ChIPseeker: an R/Bioconductor package for ChIP peak annotation, comparison and visualization. *Bioinformatics,* 31**,** 2382-3.
YU, G., WANG, L. G., YAN, G. R. & HE, Q. Y. 2015b. DOSE: an R/Bioconductor package for disease ontology semantic and enrichment analysis. *Bioinformatics,* 31**,** 608-9.
YU, Y., DENG, Y., REED, S. H., MILLAR, C. B. & WATERS, R. 2013. Histone variant Htz1 promotes histone H3 acetylation to enhance nucleotide excision repair in Htz1 nucleosomes. *Nucleic Acids Res,* 41**,** 9006-19.
YU, Y., TENG, Y., LIU, H., REED, S. H. & WATERS, R. 2005. UV irradiation stimulates histone acetylation and chromatin remodeling at a repressed yeast locus. *Proc Natl Acad Sci U S A,* 102**,** 8650-5.
YUN, X., ZHANG, Y. & WANG, X. 2020. Recent progress of prognostic biomarkers and risk scoring systems in chronic lymphocytic leukemia. *Biomarker research,* 8**,** 1-11.
ZAHAVI, D. & WEINER, L. 2020. Monoclonal Antibodies in Cancer Therapy. *Antibodies (Basel),* 9.

ZENTNER, G. E. & HENIKOFF, S. 2013. Regulation of nucleosome dynamics by histone modifications. *Nat Struct Mol Biol,* 20**,** 259-66.

ZHANG, J., DEWAR, J. M., BUDZOWSKA, M., MOTNENKO, A., COHN, M. A. & WALTER, J. C. 2015a. DNA interstrand cross-link repair requires replication-fork convergence. *Nat Struct Mol Biol,* 22**,** 242-7.

ZHANG, J., WILLERS, H., FENG, Z., GHOSH, J. C., KIM, S., WEAVER, D. T., CHUNG, J. H., POWELL, S. N. & XIA, F. 2004. Chk2 phosphorylation of BRCA1 regulates DNA double-strand break repair. *Mol Cell Biol,* 24**,** 708-18.

ZHANG, Q., GREEN, M. D., LANG, X., LAZARUS, J., PARSELS, J. D., WEI, S., PARSELS, L. A., SHI, J., RAMNATH, N., WAHL, D. R., PASCA DI MAGLIANO, M., FRANKEL, T. L., KRYCZEK, I., LEI, Y. L., LAWRENCE, T. S., ZOU, W. & MORGAN, M. A. 2019. Inhibition of ATM Increases Interferon Signaling and Sensitizes Pancreatic Cancer to Immune Checkpoint Blockade Therapy. *Cancer Res,* 79**,** 3940-3951.

ZHANG, S. M., CAI, W. L., LIU, X., THAKRAL, D., LUO, J., CHAN, L. H., MCGEARY, M. K., SONG, E., BLENMAN, K. R. M., MICEVIC, G., JESSEL, S., ZHANG, Y., YIN, M., BOOTH, C. J., JILAVEANU, L. B., DAMSKY, W., SZNOL, M., KLUGER, H. M., IWASAKI, A., BOSENBERG, M. W. & YAN, Q. 2021. KDM5B promotes immune evasion by recruiting SETDB1 to silence retroelements. *Nature,* 598**,** 682-687.

ZHANG, T., COOPER, S. & BROCKDORFF, N. 2015b. The interplay of histone modifications - writers that read. *EMBO Rep,* 16**,** 1467-81.

ZHANG, Y., LIANG, J. & LI, Q. 2014. Coordinated regulation of retinoic acid signaling pathway by KDM5B and polycomb repressive complex 2. *J Cell Biochem,* 115**,** 1528-38.

ZHANG, Y., LIU, T., MEYER, C. A., EECKHOUTE, J., JOHNSON, D. S., BERNSTEIN, B. E., NUSBAUM, C., MYERS, R. M., BROWN, M., LI, W. & LIU, X. S. 2008. Model-based analysis of ChIP-Seq (MACS). *Genome Biol,* 9**,** R137.

ZHANG, Z. Z., PANNUNZIO, N. R., HSIEH, C. L., YU, K. & LIEBER, M. R. 2015c. Complexities due to single-stranded RNA during antibody detection of genomic rna:dna hybrids. *BMC Res Notes,* 8**,** 127.

ZHAO, S., ALLIS, C. D. & WANG, G. G. 2021. The language of chromatin modification in human cancers. *Nat Rev Cancer,* 21**,** 413-430.

ZHAO, Y. & GARCIA, B. A. 2015. Comprehensive Catalog of Currently Documented Histone Modifications. *Cold Spring Harb Perspect Biol,* 7**,** a025064.

ZHOU, K., ZHANG, Q., LIU, Y., XIONG, Y., WU, S., YANG, J., ZHOU, H., LIU, X., WEI, X. & SONG, Y. 2017. Aberrant histone modification in CD19. *Onco Targets Ther,* 10**,** 1173-1179.

ZHOU, Q., LI, T. & PRICE, D. H. 2012. RNA polymerase II elongation control. *Annu Rev Biochem,* 81**,** 119-43.

ZHOU, Y., HILEMAN, E. O., PLUNKETT, W., KEATING, M. J. & HUANG, P. 2003. Free radical stress in chronic lymphocytic leukemia cells and its role in cellular sensitivity to ROS-generating anticancer agents. *Blood,* 101**,** 4098-104.

ZHU, L. J., GAZIN, C., LAWSON, N. D., PAGÈS, H., LIN, S. M., LAPOINTE, D. S. & GREEN, M. R. 2010. ChIPpeakAnno: a Bioconductor package to annotate ChIP-seq and ChIP-chip data. *BMC Bioinformatics,* 11**,** 237.

ZIMMERMANN, M., MURINA, O., REIJNS, M. A. M., AGATHANGGELOU, A., CHALLIS, R., TARNAUSKAITĖ, Ž., MUIR, M., FLUTEAU, A., AREGGER, M., MCEWAN, A., YUAN, W., CLARKE, M., LAMBROS, M. B., PANEESHA, S., MOSS, P., CHANDRASHEKHAR, M., ANGERS, S., MOFFAT, J., BRUNTON, V. G., HART, T., DE BONO, J., STANKOVIC, T., JACKSON, A. P. & DUROCHER, D. 2018. CRISPR screens identify genomic ribonucleotides as a source of PARP-trapping lesions. *Nature,* 559**,** 285-289.

ZIV, Y., BIELOPOLSKI, D., GALANTY, Y., LUKAS, C., TAYA, Y., SCHULTZ, D. C., LUKAS, J., BEKKER-JENSEN, S., BARTEK, J. & SHILOH, Y. 2006. Chromatin relaxation in response to DNA double-strand breaks is modulated by a novel ATM- and KAP-1 dependent pathway. *Nat Cell Biol,* 8**,** 870-6.

ÁLVAREZ-QUILÓN, A., WOJTASZEK, J. L., MATHIEU, M. C., PATEL, T., APPEL, C. D., HUSTEDT, N., ROSSI, S. E., WALLACE, B. D., SETIAPUTRA, D., ADAM, S., OHASHI, Y., MELO, H., CHO, T., GERVAIS, C., MUÑOZ, I. M., GRAZZINI, E., YOUNG, J. T. F., ROUSE, J., ZINDA, M., WILLIAMS, R. S. & DUROCHER, D. 2020. Endogenous DNA 3' Blocks Are Vulnerabilities for BRCA1 and BRCA2 Deficiency and Are Reversed by the APE2 Nuclease. *Mol Cell,* 78**,** 1152-1165.e8.

ČABART, P., ÚJVÁRI, A., PAL, M. & LUSE, D. S. 2011. Transcription factor TFIIF is not required for initiation by RNA polymerase II, but it is essential to stabilize transcription factor TFIIB in early elongation complexes. *Proc Natl Acad Sci U S A,* 108**,** 15786-91.